# *iDod*

## *Development of a generic inflatable de-orbit device for CubeSats*

Part 1 of 2

D.C. Maessen

9-5-2007

Design and Production of Composite Structures
Space Systems Engineering

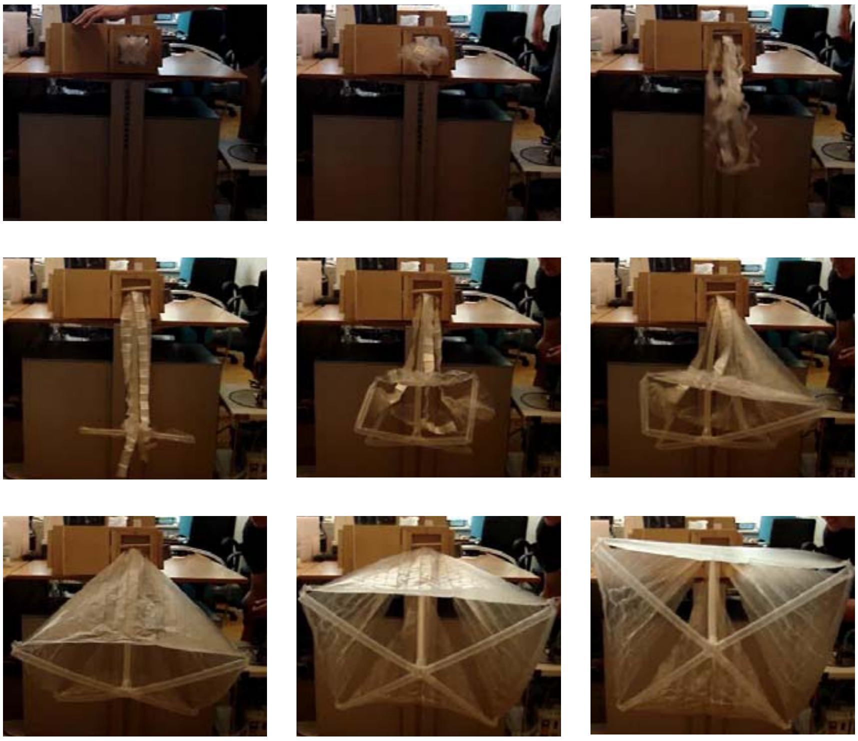

Faculty of Aerospace Engineering

Delft University of Technology

# PREFACE

Inflatable space structures have a long standing record of being a very promising technology but failing in being applied in space missions. At this point in time, they are however beginning to pop up in various missions. One example is the Genesis I vehicle, which is a technology demonstrator for an expandable space station module.
In this master thesis a study is made of inflatable space structures with emphasis on the development of a drag augmentation device for CubeSats named iDod (inflatable De-orbit device). The thesis work has been performed at the chair of Design and Production of Composite Structures (DPCS) and at the chair of Space Systems Engineering (SSE). In consultation with the project supervisors and the customer, E.D. van Breukelen on behalf of ISIS – Innovative Solutions In Space B.V., it has been chosen to generate a thesis work with maximum heritability for future research into this and related topics. The result is not a "standard" master thesis report, but a collection of all technical reports produced and a technical paper which is to be presented at the 58th International Astronautical Congress in Hyderabad, India.

When regarding this as one report, the technical paper should be regarded as the main body of the report while all technical reports act as appendices. Therefore, the technical reports are arranged in order of their appearance in the paper. All technical reports are coded as (ISIS.)iDod.xx.xxx. The second pair of digits represents the type of report: technical note (TN), design description (DD), construction manual (CM), trade-off (TO), or work plan (WP). The work plan also contains the thesis assignment. The third pair of digits is a number indicating the chronology of that type of technical report.
It is noted that reports iDod.TN.001 till iDod.TN.005, iDod.DD.001, and iDod.WP.001 have a different layout than the other reports. Cause of this is a switch to a more "professional" layout in the course of the thesis.

Concluding, I would like to thank my supervisors, O.K. Bergsma, B.T.C. Zandbergen, and E.D. van Breukelen for their discussions with me and their comments to my work, resulting in a better result than possible without them. I appreciate the information and suggestions provided by Laurens van Vliet of TNO Defense & Security regarding cool gas generators. I would also like to thank Peter de Regt of the adhesion institute for his help and advice in adhering polyethylene foil using adhesive. Furthermore, I would like to thank RUPLO Lijmtechniek B.V. for supplying adhesives free of charge. Last but not least, I would like to thank my parents and my girlfriend for trying to understand me when I was explaining with hand and feet and everything else in reach what on Earth I was doing the past year.

Daan Maessen

Delft, 9-3-2007

## TABLE OF CONTENTS

IAC-07-A6.3.06

# DEVELOPMENT OF A GENERIC INFLATABLE DE-ORBIT DEVICE FOR CUBESATS


**D.C. Maessen, BSc**
Faculty of Aerospace Engineering, Chair of Space Systems Engineering, Delft University of Technology, the Netherlands (NL)
D.C.Maessen@student.tudelft.nl

**E.D. van Breukelen, MSc**
ISIS - Innovative Solutions In Space B.V., Delft (NL)
E.D.vanbreukelen@isispace.nl

**ir. B.T.C. Zandbergen**
Faculty of Aerospace Engineering, Chair of Space Systems Engineering, Delft University of Technology, the Netherlands (NL)
B.T.C.Zandbergen@lr.tudelft.nl

**dr.ir. O.K. Bergsma**
Faculty of Aerospace Engineering, Chair of Space Systems Engineering, Delft University of Technology, the Netherlands (NL)
O.K.Bergsma@lr.tudelft.nl



## ABSTRACT

New space debris mitigation guidelines require satellites in low Earth orbit to de-orbit within 25 years after end of life. This effectively limits the orbital altitude of conventional CubeSat satellites, with a ballistic coefficient in the range of 33-150 kg/m$^2$, to 400-700 km. For CubeSats employing the generic inflatable de-orbit device discussed here, this range is extended to 910 km by reducing the ballistic coefficient by a factor 10-45.
This paper outlines the concept and preliminary design of a generic inflatable de-orbit device, which reduces the ballistic coefficient by increasing the frontal surface area of the satellite. The device essentially is of the attached ballute type and consists of a thin membrane covering an inflatable structure, which is chemically rigidized after deployment. Coatings are applied to the structure to provide protection against the hostile low Earth orbit environment and to manipulate the temperature of the inflatable. The inflation gas is stored in solid form inside a so-called Cool Gas Generator, developed by The Netherlands Organisation for Applied Scientific Research (TNO) in the Netherlands.

Three different geometrical concepts for the ballute are analyzed. A pyramid-like structure is selected as the best overall concept based on mass, stowed volume, flexibility, manufacturing, and deployment control. A preliminary design of the device is performed for a 1-unit CubeSat of 1 kg mass, with focus on ease of integration.

Initial results of the physical development of the structure are shown. A development model of a flexible connector piece is constructed to which five inflatable tubes, made from polyethylene foil, are attached at right angles in a leak-tight manner. The method used to bond the tubes to the connector piece as well as attachment of the membranes to the inflatable structure is outlined. Lastly, stowage and deployment of the inflatable structure are discussed. The results indicate that the mass and stowed volume of the complete de-orbit system remain within 9.4% and 10.3% of the CubeSats' total mass and volume.

## INTRODUCTION

The CubeSat satellite standard, developed by California Polytechnic State University and Stanford University [1], is becoming very popular as a cheap and standardized means to gain access to space. The width and depth of a CubeSat are 10 cm and its height can be 10, 20, or 30 cm. Depending on the height, a CubeSat can have a maximum mass of 1, 2, or 3 kg [2].
When launched into a circular orbit with an altitude higher than 700 km, a CubeSat will not re-enter Earth's atmosphere within 25 years after end of life (EOL) [3]. This 25 year time span is advised by international space debris mitigation guidelines [4, 5, 6] as the time in which a LEO satellite should de-orbit after EOL.

Decreasing the time to de-orbit a LEO satellite can be achieved by either of the following means:

- Propulsion system
- Electrodynamic tether
- Aerodynamic drag augmentation

Literature references for the propulsion system option are [4] and [7]. For the tether option, references are [8, 9, 10, 11, 12].
This study focuses on drag augmentation. The development of a baseline system, called iDod (**i**nflatable **D**e-**o**rbit **d**evice), is presented. The system utilizes an inflatable drag device that enables de-orbiting of a CubeSat within 25 years after EOL from an initial orbit higher than 700 km. This baseline design is performed for a 1-unit CubeSat (10x10x10 $cm^3$) in a circular orbit with an inclination of 90°. Initially, the desired starting altitude is set at 1000 km.

The following topics are treated in the coming sections:

- Design process
- Requirements
- Aerodynamic drag augmentation
- Attitude stability
- Concept generation and selection
- Rigidization and thermal design
- Stowage and deployment
- Space environment protection
- Physical development
- Results
- Conclusions and recommendations

## DESIGN PROCESS

The iDod design process up to the definition of the preliminary design is depicted in a figure on the next page. In each design step, the reference documents dealing with that step are indicated.
When a design step performed for the drag device or for the storage device results in a solution that does not fulfil all the requirements, an iteration loop needs to be performed. Depending on the specific problem, the iteration loop can start at a different point in the design process. The iteration can also, in consultation with the customer, result in new or adjusted requirements.

The steps in the design process are treated in this paper in the order I would follow with my current experience. Although the physical development step is treated at the end, I would perform this step in parallel with other design steps and start with it as early as possible. This has also been done for the current design and provides very useful inputs and feedback for the design process.
During the actual design, the order of the design steps was to a large extent similar to the order in which they are presented in this paper. Yet, now I would do two things differently: The need for rigidization has been analysed in the last week and the influence of the space environment on materials has been determined in the first few weeks. Now, I would reverse this order since rigidizing a structure has a significant complicating effect on its development and space environment effects do not influence the overall design to a large extent.

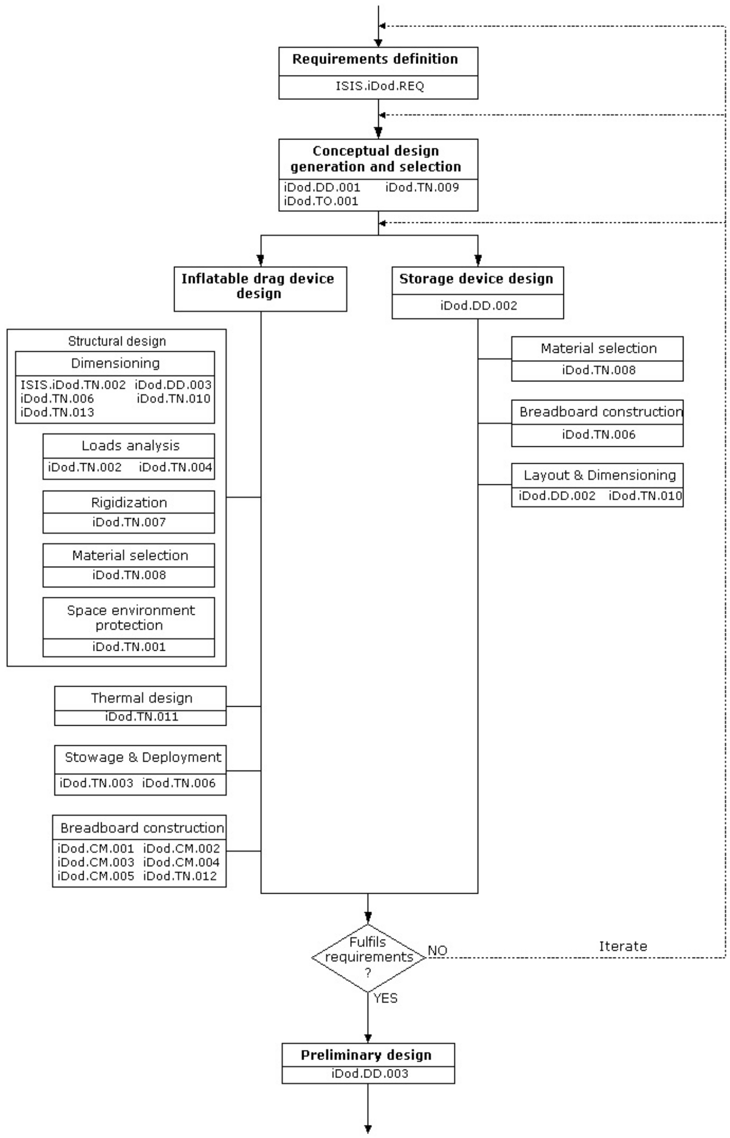


*Figure 1 iDod design process*

## REQUIREMENTS

The prime requirements for the iDod system are defined in [13] and are:

1. The iDod shall de-orbit a 1-unit CubeSat within 25 years from a baseline altitude of 1000 km.
2. The iDod shall use an inflatable structure to achieve the de-orbit requirement.
3. The envelope of the inflatable structure shall be as small as possible to minimize the risk of hitting protruding satellite components when deployed.
4. The mass difference between a CubeSat with iDod and the same CubeSat without iDod shall be equal or less than 100 grams.
5. The stowage volume of the iDod system shall be equal or less than 103 $cm^3$.
6. The system shall allow for easy integration in various CubeSat configurations.
7. The inflatable structure shall survive the complete de-orbit manoeuvre.

## AERODYNAMIC DRAG AUGMENTATION

Increasing the drag encountered by the CubeSat results in an increased deceleration, leading to a relatively fast orbit decay.

Drag increase is obtained by increasing the frontal surface area (A) of the satellite. This leads to a decrease of the ballistic coefficient ($C_B$) of the satellite which is defined as [14]:

$$C_B = \frac{m}{C_D A}$$

The variable $C_D$ is the drag coefficient of the satellite and assumed to be equal to 2. The variable m is the mass of the satellite and equal to 1 kg. The average frontal surface area of a 1-unit CubeSat is 0.015 $m^2$ [3], resulting in $C_B$ = 33.3 kg/$m^2$.

An orbit lifetime analysis performed with Satellite Tool Kit (STK) 7.0.1 indicates that a 1-unit CubeSat de-orbits within 24.6 years from an altitude of 700 km if the orbit epoch is set to 1 July 2007 (solar minimum) [3].
When the frontal surface area is increased tenfold, the de-orbit time reduces to 2.7 years, clearly showing the effect of drag augmentation.

For the baseline altitude of 1000 km, the $C_B$ required for the CubeSat to de-orbit within 25 years is 1.6 kg/$m^2$.

## ATTITUDE STABILITY

For maximum material efficiency, the inflatable structure should be a flat plate oriented perpendicular to the velocity vector of the CubeSat. However, there are several natural causes that result in disturbance torques which affect the orientation of the satellite [14]:

- Aerodynamic drag
- Solar radiation pressure
- Magnetic field Earth
- Gravity gradient

Ideally, the orientation of the satellite with deployed inflatable is passively stabilized and dictated by aerodynamic drag.
Unfortunately, a first order attitude stability analysis performed in [15] indicates that it is not possible to attain a stable orientation utilizing aerodynamic drag above an altitude of 450-650 km. Main reason for this is that the torque generated by solar radiation pressure above this altitude range is substantially larger than the torque generated by aerodynamic drag. The precise altitude at which aerodynamic drag torque becomes dominant depends on the level of solar activity.

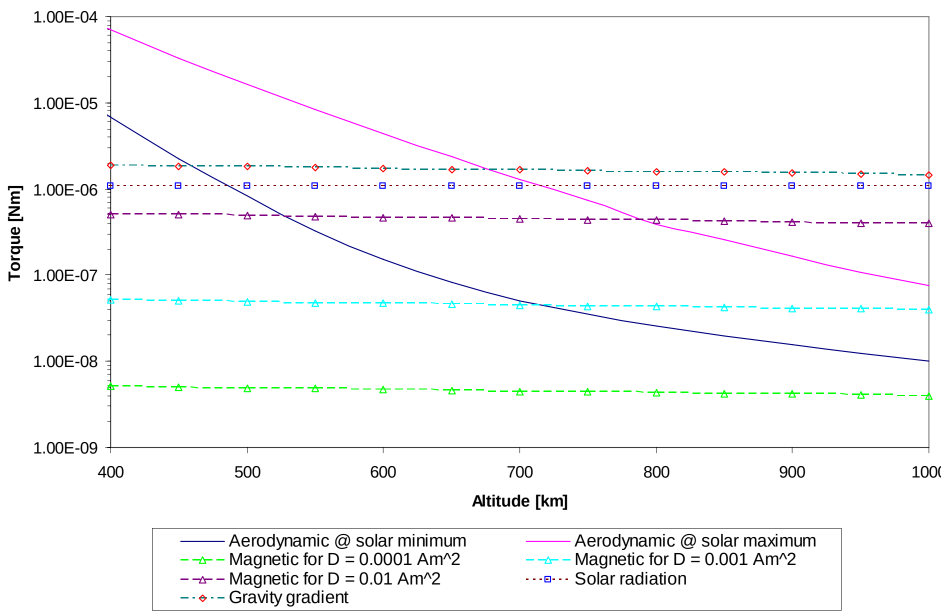


*Figure 2 Torques acting on the CubeSat with deployed inflatable structure [adapted from 15]*

A stable, passively obtained orientation above 450-650 km can be achieved by utilizing the gravity gradient effect, but then the residual dipole moment of the CubeSat (abbreviated with D in the legend of the previous figure) needs to be relatively small. Unfortunately, ensuring this results in unfeasible dimensions for the inflatable structure and is therefore not possible.

The above results lead to the conclusion that the orientation of the CubeSat with deployed inflatable has to be assumed to be random above 450-650 km.

## CONCEPT GENERATION AND SELECTION

Based on experience gained in analysing a straw man concept [16], three geometrical concepts are generated for the inflatable structure [17]: planar, pyramid, and sphere. All are of the attached ballute type.

The performance of all concepts with respect to the following criteria is determined:

- Stowed volume
- Mass
- Deployment control
- Manufacturing
- Flexibility

The flexibility criterion is a bit vague. It is used to indicate how likely it is that a particularly shaped inflatable can be used on a CubeSat. A measure for this is the clearance of the inflatable with respect to other protruding components likely to be present on a CubeSat such as antennas.

A pyramid with one long inflatable central tube and four smaller inflatable tubes (or spokes) is the best overall concept. Main causes for this are its small mass and stowed volume.

When the attitude of the pyramid concept is stabilized, it will behave like a shuttlecock. Then, the required frontal surface area of the inflatable is provided by the base of the pyramid.
When the attitude is not stable, the dimensions of the pyramid have to be such that its frontal surface area for a random orientation is equal to the desired frontal surface area.

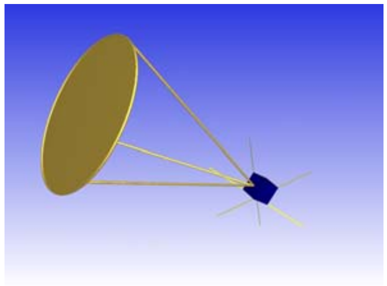

*Figure 3 Planar concept [17]*

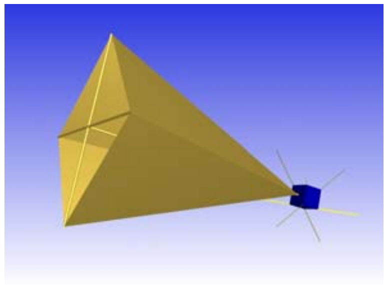

*Figure 4 Pyramid concept [17]*

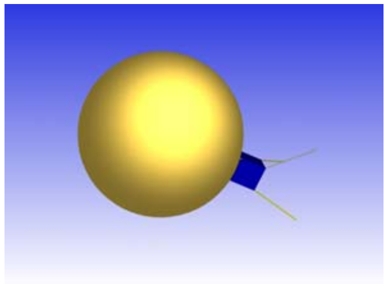

*Figure 5 Spherical concept [17]*

## RIGIDIZATION AND THERMAL DESIGN

Rigidization of space inflatables increases their stiffness and is usually done to provide increased dimensional stability [18]. However, the required dimensional stability for the present inflatable is not high and would not justify rigidization.
An analysis performed in [19] shows that rigidization is only required when the risk of micrometeoroids and orbital debris (MMOD) impacting on the inflatable tubes is considered to be too high. This risk has not been quantified yet, but for the present it is assumed that rigidization is required.

To increase the stiffness of the inflatable tubes they can be either chemically or mechanically rigidized after deployment [18]. A number of rigidization methods for the current inflatable structure are explored in [19]. There, thermal cure of a thermosetting fibre composite by means of

solar radiation is selected as the best method.
The fibre composite is situated in the inflatable tubes and encapsulated between two layers of foil material:

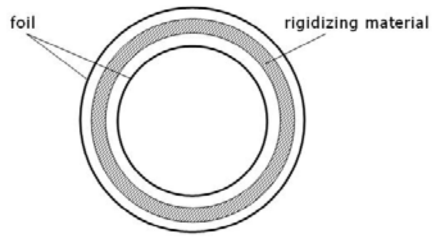


*Figure 6 Tube cross-section [20]*

The fibre material selected is Technora®, an aramid fibre. Reasons for its selection are its good folding properties, its large temperature range, and its small available thickness. The fibre is woven into a 4H satin weave with a thickness of 70 μm [20].
A thermosetting cyanate ester resin forms the other part of the composite material. An important requirement for the resin is that its out life (the period during which a resin stays 'unrigidized' after having been removed from storage) has to be in the order of years, which is very uncommon.

For thermal cure, the thermosetting resin needs to attain a temperature of 120°C [21]. Analysis with a single node model indicates that achieving this temperature is possible [21].
In the analysis, the triangular membranes of the drag device are given a thermo-optical coating at the side facing space. This coating has an absorption/emission ($\alpha/\varepsilon$) ratio larger than 1. This results in the membranes heating up to a high (>100°C) temperature when exposed to sunlight. The tubes are now assumed to be coated with the same material and the inside of the membranes is assumed to have a $\alpha/\varepsilon$ ratio smaller than 1 to channel heat from the membranes towards the tubes. The last effect and possible direct illumination by the Sun are assumed to heat up the tubes to a temperature close to that of the membranes.

Depending on the orbit and orientation of the satellite, the required $\alpha/\varepsilon$ ratio of the coating is between 2 and 7.
Vapour deposited aluminium (VDA) is selected as thermo-optical coating for the membranes and the tubes [21]. According to [22], the $\alpha/\varepsilon$ ratio of VDA coated Kapton® is 5 to 6 at the side of the VDA coating. At the Kapton® side, the $\alpha/\varepsilon$ ratio is ~0.6.

An extra benefit of having a large metallic surface is an increased visibility on radar. This makes tracking of the satellite easier, thereby reducing the chance of it colliding with an active satellite.

Channelling heat towards the inflatable tubes is a complicated method to increase their temperature. Another option is to use transparent membranes without thermo-optical coating and to apply VDA on the tubes. An analysis for this situation has not yet been performed, but two downsides with respect to the analyzed option are already evident: The membranes will get very cold and the tubes will get very hot, resulting in thermal expansion issues at the points where the membranes are connected to the tubes. In addition, the radar signature of the satellite is now much smaller.

Which one of the two coating options is best needs to be determined at a later stage. For now, the analyzed option is adopted.

## STOWAGE AND DEPLOYMENT

A standard CubeSat is built up out of a 100x100x100 $mm^3$ aluminium frame with L-shaped ribs. The flanges of these ribs are maximally 8.5 mm wide. The ribs are covered with aluminium shear panels onto which solar panels and antennas can be mounted. Commonly, the electronic hardware of a CubeSat consists out of a stack of printed circuit boards (PCBs).

*Figure 7 Standard 1-unit CubeSat chassis [23]*

The inflatable drag device is stowed inside an 83x83x15 $mm^3$ aluminium storage device. Flanges at the top of the storage device extend to a width of 100x100 $mm^2$. These flanges and the lid of the storage device replace a standard CubeSat shear panel. The dimensions of the storage device allow it to be slid inside standard CubeSat frames. The small height of the storage device leaves ~8 cm of height for PCBs and other components to be stacked inside the CubeSat.

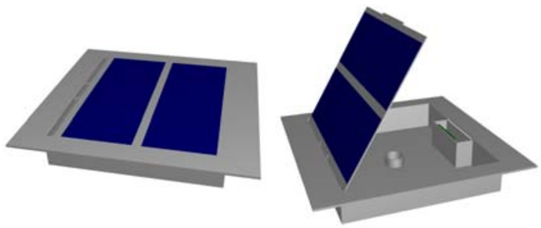

*Figure 8 iDod storage device [24]*

The lid of the storage device is rotated around an axle by means of helical torsion springs. A Dyneema® wire holds down the lid and is melted through by means of a resistor once the lid needs to be opened [24].

The membranes and tubes of the inflatable structure are folded separately. Once folded, the membranes are connected to the tubes. Separate folding allows the membranes to be folded into small packages, which results in a high packing efficiency.

Deployment of the inflatable structure is achieved by pressurizing the tubes of the inflatable using nitrogen gas. This gas is stored in solid form and produced at ambient temperature by means of a Cool Gas Generator (CGG). Production of all inflation gas, 0.12 normal litres, is performed in one second [25]. This is very fast and its influence on the deployment of the inflatable needs to be determined. Depending on the temperature, 0-225°C, the resulting internal pressure of the inflatable tubes is 0.97–1.76 bar [26, 27].

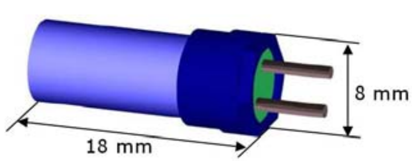


*Figure 9 CGG with dimensions [25]*

SPACE ENVIRONMENT PROTECTION

In LEO, there are several phenomena that cause degradation in material performance (i.e. optical, thermal, mechanical, and electrical) [18]:

- Atomic oxygen (AO)
- micrometeoroids and orbital debris (MMOD)
- vacuum ultra-violet radiation (VUV)
- charged particles

AO is a major cause for concern when designing an inflatable structure for LEO operation since it causes rapid erosion of most unprotected polymer materials [18]. In [28], an analysis is performed to determine the erosion of pristine Kapton® during a 25-year de-orbit from a starting altitude of 1000 km. The most optimistic erosion depth estimation in this analysis, 30 μm, already indicates that some form of protection is required in order to keep the mass and volume of the inflatable at an acceptable level.
The material degradation caused by the remaining three phenomena has not been investigated.

In [20], $SiO_2$ is selected as protective coating for the foil material that is exposed to AO. There, it is also advised to mix $SiO_2$ with 10% PTFE for increased flexibility, minimising the formation of cracks in the coating due to thermal cycling.

In [20], a polyimide film called Upilex-S® is selected as foil material. Reasons for its selection are that it retains its properties over a large temperature range and its resistance to the space environment. In addition, Upilex-S® can be readily ordered with VDA and $SiO_2$ coatings from the manufacturer.

A membrane of the inflatable structure is now composed out of the following layers:

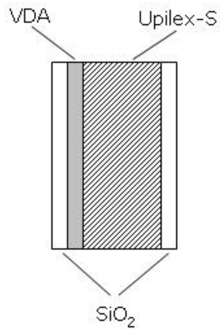


*Figure 10 Membrane cross-section [adapted from 21]*

PHYSICAL DEVELOPMENT

The physical development of the iDod system has been focussed on the inflatable structure. The next figure indicates the different parts of the inflatable structure.

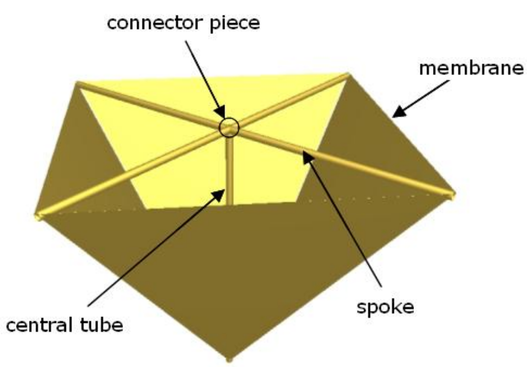


*Figure 11 Complete inflatable structure [26]*

A connector piece is required and has been developed for the point where the five inflatable tubes meet. This connector piece is flexible, resulting in a reduced mass and stowed volume compared to a rigid connector piece.

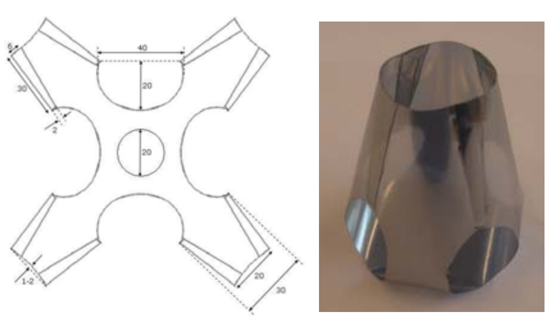

*Figure 12 Connector piece for 20 mm tubes [2928]*

Breadboard tubular structures have been produced from polyethylene (PE) tubes. These tubes are constructed by heat welding polyethylene foil and have a diameter of 20 mm [30].

The tubes are bonded to a PE connector piece using silicone sealant [31]. The connector piece itself is constructed by bonding it together using cyanoacrylate adhesive [29]. The adhesives are selected in [32].

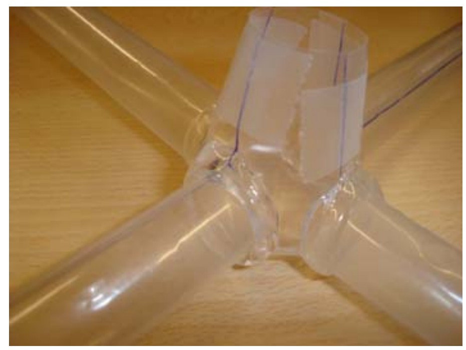

*Figure 13 Close-up of early connector piece-tube interface*

The membranes of the breadboard models are made from 20 μm thick foil and are attached to the spokes and the storage device using a 'loop and slit' method. This method requires no adhesive and results in a flexible, detachable joint.

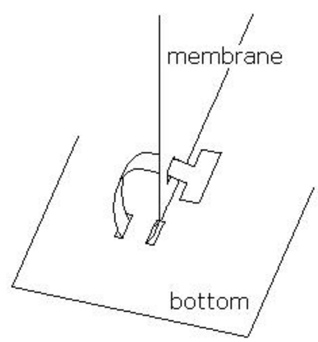


*Figure 14 Membrane attachment to the bottom of the storage device using the loop and slit method [33]*

*Figure 15 Breadboard inflatable structure*

Production of a structure always results in small misalignments of components. When too severe, misalignments can negatively influence the average frontal surface area of the inflatable. For the breadboard models produced, the measured angular misalignments of the inflatable tubes are ~3° [34]. This is too small to have any significant effect on the resulting average frontal surface area of the inflatable and indicates that the current production method is already accurate enough for construction of future breadboard models.

The breadboard inflatable structures are stowed and deployed from a breadboard storage device. The internal volume of this storage device is reduced stepwise using inserts to determine the maximum packing efficiency for the inflatable.

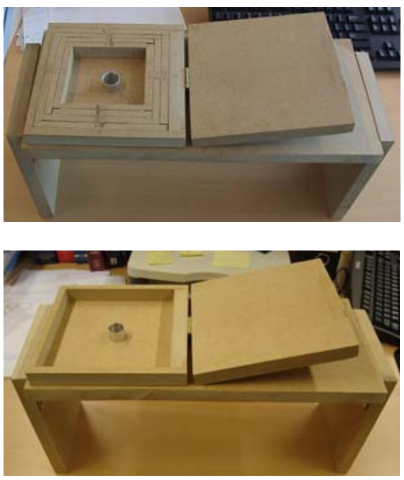

*Figure 16 Breadboard storage device with and without inserts*

## RESULTS

This section discusses the results obtained thus far and shortly compares the performance of the current design with a propulsion system and an electrodynamic tether.

### Stowage

Stowage tests of breadboard inflatable structures indicate that a packing efficiency of 20-25% is achievable for the inflatable structure.
Stowage of the inflatable is achieved as follows. First, the membranes are folded into square packages using interleaved folding and zigzag folding patterns [25]. Next, air is evacuated from the inflatable tubes and the central tube is zigzag folded over the width of the storage device. The connector piece is positioned in the middle of the storage device. After that, the membranes are connected to the ends of the spokes. Finally, the spokes are zigzag folded between the centre and a corner of the storage device.

*Figure 17 Membranes folded in 3x3 cm squares (left) and complete inflatable structure folded (right) [25]*

### Mass and volume

A conservative packing efficiency of 20% translates into a central tube length of 40 cm and spoke lengths of 30 cm [26]. The diameter of the tubes is 1 cm and their wall thickness is 120 μm (70 μm fibre composite and two times 25 μm Upilex-S® foil). The thickness of the triangular Upilex-S® membranes is 25 μm [35].

The mass of the inflatable structure is 30 grams. The mass of the complete iDod system is 94 grams [26]. The mass difference between a CubeSat with iDod and the same CubeSat without iDod is 70 grams.
The material volume of the inflatable structure is 15 $cm^3$. The volume occupied by the complete iDod system in stowed configuration is 103 $cm^3$ [26].

### Deployment

Deployment tests for breadboard inflatable structures indicate that deployment occurs in three steps: First, the central tube fully deploys. Then, the spokes deploy up to approximately half their length and the membranes are deployed in length-direction. Finally, the remaining half of the spokes inflates and the membranes deploy in width-direction.
The next page depicts a figure with nine frames taken from a deployment video that exemplifies the deployment scheme. No form of gravity offloading is applied, resulting in the inflatable being pulled towards the ground.

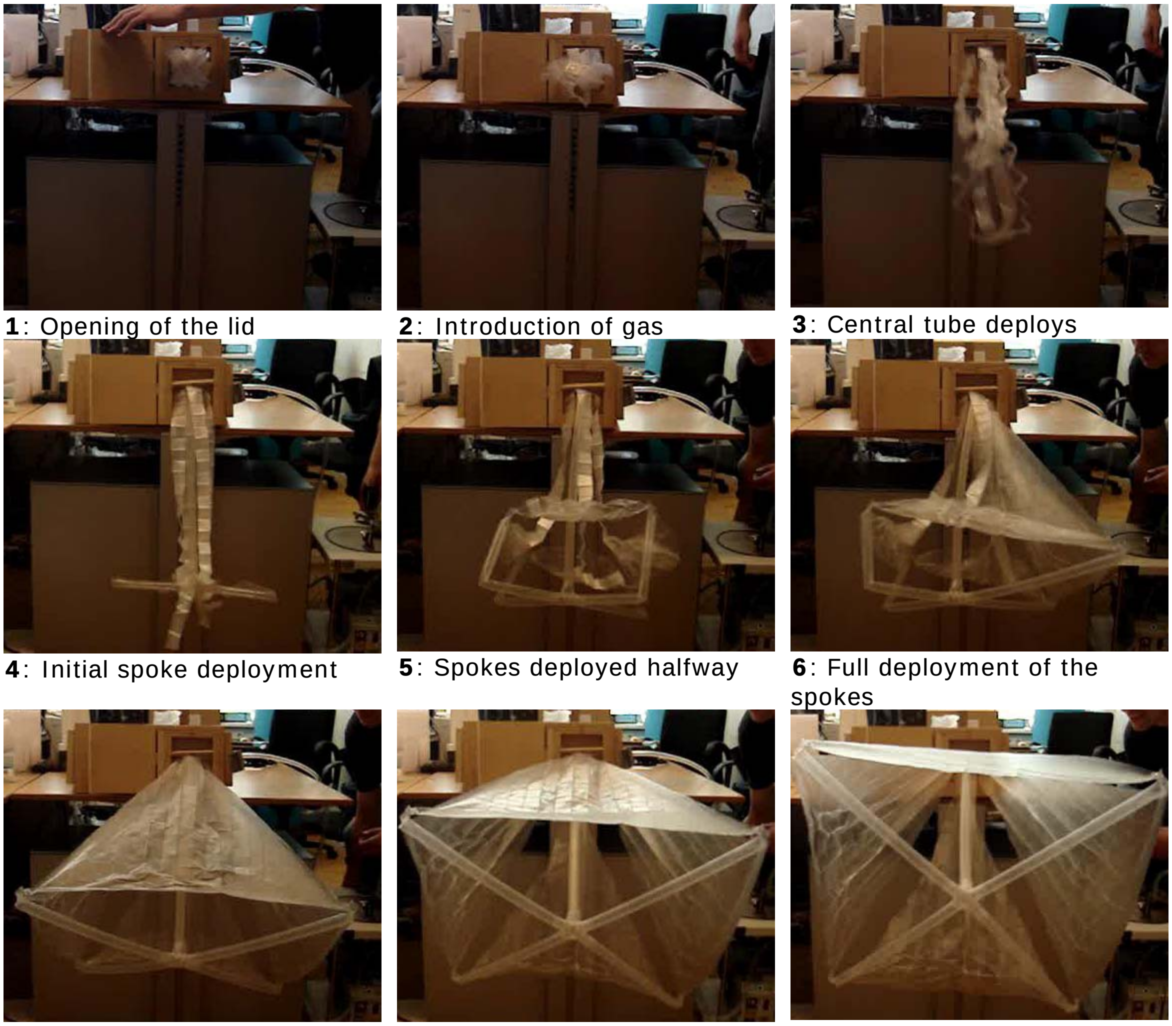

**1**: Opening of the lid
**2**: Introduction of gas
**3**: Central tube deploys
**4**: Initial spoke deployment
**5**: Spokes deployed halfway
**6**: Full deployment of the spokes
**7**: Deployment achieved
**8**: Internal pressure increases
**9**: Internal pressure maximal

*Figure 18 Inflatable structure deployment test [25]*

The above frames suggest that the deployment envelope of the inflatable is small, approximately the same as the envelope for the fully deployed structure. This is beneficial since it reduces the likelihood of the structure coming into contact with protruding CubeSat elements during deployment

De-orbit performance

The average frontal surface area of the inflatable structure is 1500 $cm^2$, resulting in a ballistic coefficient of 3.33 $kg/m^2$ [26]. A lifetime analysis performed using STK 7 in the manner described in [3] indicates that this area enables a 1-unit CubeSat to be de-orbited within 25 years from a maximum altitude of 910 km [26]. Without iDod system, de-orbiting will take 197 years.

In [4], it is stated that drag augmentation should not be applied when this results in an increased area-time product (a measure for the probability that space debris impacts on a satellite). With drag device, the area-time product for the CubeSat is 3.7 $yr{\cdot}m^2$ for an initial altitude of 910 km. Without iDod, the product is 3.0 $yr{\cdot}m^2$. Following the reasoning in [4], the iDod should not be used. However, drag augmentation using an inflatable structure has three major benefits:

- The satellite is removed from the current population, making room for new satellites.
- When the inflatable structure is metallized, it is clearly visible on

radar, reducing the probability of impact with operational satellites since these can take evasive action when required.

– When the satellite is hit by debris, there is a large chance that the inflatable structure is hit, resulting in a hole in the membrane and not in many new long-lived debris objects.

Because of the above reasons, drag augmentation is preferred over natural orbit decay.

The figure below shows that the orbit decay increases in an exponential manner: The first 200 km take ~23 years while the remaining 700 km only take two years.

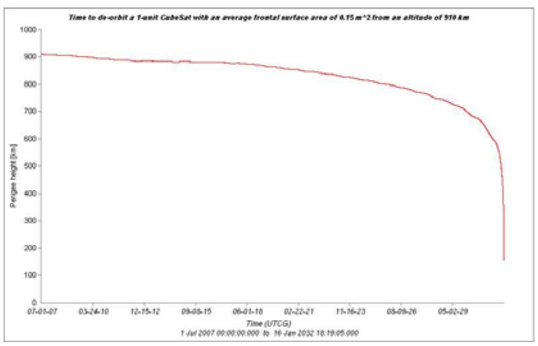


*Figure 19 STK de-orbit prediction for a 1-unit CubeSat with 0.15 $m^2$ drag device from an initial altitude of 910 km*

The increase in orbit decay rate is logical since the atmospheric density, the factor influencing orbit decay rate the most, decreases exponentially with increasing altitude [14]. The effect of increased solar activity shortly after solar minimum in 2007 and 2018 is visible by a temporary 'extra' increase in orbit decay rate.

<u>Comparison with alternative methods</u>

The introduction already mentioned that a propulsion system or an electrodynamic tether can also be used to accelerate the orbit decay of a CubeSat. Here, a short analysis is performed to compare these methods to drag augmentation.

A propulsion system can be used to force a direct re-entry of the CubeSat. Assuming a 1000 km high circular starting orbit, this requires a velocity change ($\Delta V$) of at least 230 m/s [7].

A second option, requiring much less $\Delta V$, is to change the previous starting orbit into an elliptical orbit with a perigee low enough for the satellite to eventually re-enter Earth's atmosphere 25 years after the manoeuvre. This requires a $\Delta V$ of ~100 m/s for a satellite with a mass comparable to that of a CubeSat [7].
Adopting the second, least demanding, option results in a required propellant mass of 33 grams when assuming a specific impulse ($I_{sp}$) of 300 seconds and a pointing accuracy and thrust efficiency of 100%. The best propulsion system for a CubeSat-like satellite is a solid propellant system [7]. Assuming a titanium motor casing and performing an optimistic calculation, the total propulsion system mass is roughly twice the propellant mass.
There are two important downsides of using a propellant system to de-orbit a small satellite. Firstly, there is the need for some means of attitude control (spin stabilisation or 3-axis stabilization [7]), requiring the presence of torque devices and sensors on the satellite. Secondly, creation of any torque around the centre of mass (c.o.m.) of the satellite causes the satellite to rotate around its c.o.m., leading to ill pointing of the thrust vector (assuming the attitude control system cannot compensate quickly enough) and a different than intended orbit alteration.

An electrodynamic tether functions by rolling out a long (up to several km [8]) conducting cable which at one end collects and at the other end emits ions into the ionospheric plasma around Earth to generate an electrical current in the cable. This current interacts with the Earth's magnetic field, resulting in a small Lorentz force that decelerates the satellite [9].
The nanoTerminator™ [10] is an existing electrodynamic tether system that can be installed on CubeSats. Its mass is 56 grams and its height and diameter are 54.5 mm and 38.0 mm respectively.
For CubeSats, the nanoTerminator™ is considered to be unpractical. Reason for this is that both its height and width are approximately half the width of a CubeSat. Installing it implies that the available volume for other systems gets very small and unpractical, especially for 1-unit CubeSats. Furthermore, the long, thin cable is vulnerable to space debris impact, which can lead to severing of the cable and total failure of the system [8].

A selection of properties and downsides of each method is listed in the next table.

| Drag augmentation | |
|---|---|
| Mass [g] | 70 |
| Start altitude [km] | 910 |
| Downsides | - Unproven<br>- Lower starting altitude than other options<br>- Partial failure at MMOD impact in tubes |
| **Propulsion system** | |
| Mass [g] | > 60 |
| Start altitude [km] | 1000 |
| Downsides | - Attitude control required<br>- Very precise thrust vector alignment |
| **nanoTerminator™** | |
| Mass [g] | 56 |
| Start altitude [km] | 1000 |
| Downsides | - Unproven<br>- Unpractical dimensions<br>- Total failure at MMOD impact in tether |

*Table 1 De-orbit method comparison*

Determining which method is best requires a more detailed comparison. Yet, two significant observations can be made: The iDod system is heavily penalized by the exponential decrease in atmospheric density, limiting its practical altitude range. The other methods do not have this disadvantage, but both have a much larger impact on the total CubeSat system than the iDod system.

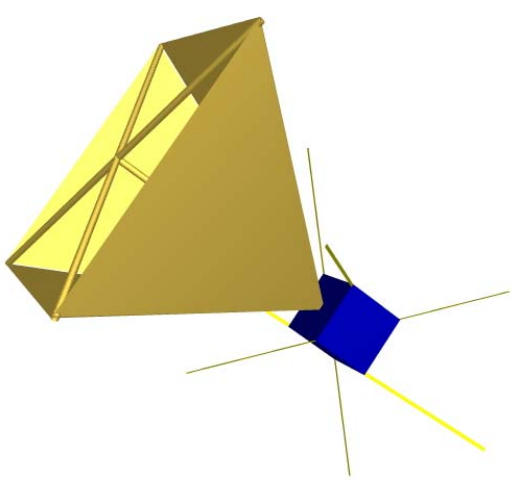

*Figure 20 Deployed inflatable attached to 1-unit CubeSat [26]*

## CONCLUSIONS AND RECOMMENDATIONS

De-orbiting a 1-unit CubeSat from an initial orbit height of 1000 km, an original top level requirement, is not possible using the iDod. Currently, the maximum initial orbit height is 910 km.

The total iDod mass is currently 94 grams and the total iDod volume in stowed configuration is 103 $cm^3$. The mass difference between a CubeSat with iDod and the same CubeSat without iDod is 70 grams.

For the inflatable drag device, a packing efficiency of 20% is feasible. The resulting inflatable structure is pyramid-shaped with a height of 40 cm and a diameter of the base of 60 cm. The ballistic coefficient for a 1-unit CubeSat with deployed drag device is 3.33 $kg/m^2$.

For further development of the iDod system, it is recommended to perform the following steps. These are listed in order of importance and start at the most important one.

- Determine whether rigidization of the drag device is required
- When the drag device needs to be rigidized, determine the achievable temperatures for the components that need to be rigidized using thermal cure in a more detailed thermal analysis.
- Perform a detailed attitude and orbit analysis to determine the influence of the Sun on the orbit decay of a CubeSat with deployed drag device.
- Design the storage device and its components in more detail
- Devise test and qualification plans for the complete iDod system
- Determine the precise packing efficiency for the drag device.
- Perform deployment tests either utilizing gravity offloading or in zero-g to confirm the observation that the drag device has a small deployment envelope.
- Determine the influence of space environment effects other than atomic oxygen on the materials of the iDod system, especially for the drag device.

REFERENCES

1. Puig-Suari, J., et. al., *CubeSat: The Development and Launch Support Infrastructure for Eighteen Different Satellite Customers on One Launch*, 15th Annual AIAA/USU Conference on Small Satellites, Utah State University, Logan, USA, 13-16 August 2001
2. Toorian, A., *CubeSat Design Specification*, Revision 9, 15 May 2005
3. Breukelen, E.D. van, *Determination of scenario for iDod baseline conceptual design and range of required inflatable drag surface sizes*, iDod document ISIS.iDod.TN.002, issue 1.1, Delft, The Netherlands (NL), 12 July 2006
4. Klinkrad, H., *Space Debris - Models and Risk Analysis*, Praxis Publishing Ltd., Chichester, UK, 2006
5. IADC, *Space Debris Mitigation Guidelines*, 15 October 2002
6. Anselmo, et. al., *European Code of Conduct for Space Debris Mitigation*, Issue 1.0, 28 June 2004
7. Janovsky, R., et. al., *End-Of-Life De-Orbiting Strategies for Satellites*, Deutscher Luft- und Raumfahrtkongress, Stuttgart, Germany, 23-26 September 2006
8. Pardini, C., et. al., *Benefits and risks of using electrodynamic tethers to de-orbit spacecraft*, 57th International Astronautical Congress, Valencia, Spain, 2-6 October 2006
9. Cosmo, M.L., Lorenzini, E.C., et. al., *Tethers in Space Handbook*, Smithsonian Astrophysical Observatory, 3rd Edition, 1997
10. Tethers Unlimited Inc., *nanoTerminator™*, Technical datasheet, [http://www.tethers.com/SpecSheets/nanoTerminator.pdf](http://www.tethers.com/SpecSheets/nanoTerminator.pdf), viewed April 2007
11. Wijnans, A.S., et. al., *Bare Electrodynamic Tape Tether Experiment Onboard the Delfi-1 University Satellite*, 4th International Spacecraft Propulsion Conference, Cagliari, Italy, 2-9 June 2004
12. Heijning, S.P.A. van de, Zandbergen, B.T.C., *Design of an Electro-Dynamic Tape-Tether Deployment System*, 56th International Astronautical Congress, Fukuoka, Japan, 17-21 October 2005
13. Breukelen, E.D. van and Maessen, D.C., *Top level requirements for inflatable De-orbit device (iDod)*, iDod document ISIS.iDod.REQ, Revision 2.1, Delft, NL, 7 May 2007
14. Wertz, J.R. and Larson, W.J., *Space Mission Analysis and Design*, Third Edition, Kluwer Academic Publishers, Dordrecht, NL, 1999
15. Maessen, D.C., *iDod attitude stability analysis*, iDod document iDod.TN.009, Version 1.0, Faculty of Aerospace Engineering, Delft, NL, 16 January 2007
16. Maessen, D.C., *Straw man concept design description*, iDod document iDod.DD.001, Version 1.0, Faculty of Aerospace Engineering, Delft, NL, 25 September 2006
17. Maessen, D.C., *inflatable structure conceptual design trade-off*, iDod document iDod.TO.001, Version 1.1, Faculty of Aerospace Engineering, Delft, NL, 28 February 2007
18. Jenkins, C.H.M., *Gossamer Spacecraft: Membrane and Inflatable Structures and Technology for Space Applications*, AIAA, Reston (USA), 2001.
19. Maessen, D.C., *iDod rigidization*, iDod document iDod.TN.007, Version 1.1, Faculty of Aerospace Engineering, Delft, NL, 2 May 2007
20. Maessen, D.C., *Material selection*, iDod document iDod.TN.008, Version 1.0, Faculty of Aerospace Engineering, Delft, NL, 13 March 2007
21. Maessen, D.C., *Thermal design*, iDod document iDod.TN.011, Version 1.2, Faculty of Aerospace Engineering, Delft, NL, 21 March 2007
22. Scialdone, J.J. and Clatterbuck, C.H., *Four Space Application Material coatings on the Long-Duration Exposure Flight*, NASA Technical Memorandum 104574, Goddard Space Flight Center, Greenbelt (USA), November 1992.
23. Pumpkin, Inc., *CubeSat Kit*, [http://www.cubesatkit.com/](http://www.cubesatkit.com/) Viewed January 2007
24. Maessen, D.C., *iDod storage device,* iDod document iDod.DD.002, Version 1.2, Faculty of Aerospace Engineering, Delft University of Technology, NL, 2 April 2007
25. Maessen, D.C., *iDod stowage and deployment,* iDod document iDod.TN.006, Version 1.1, Faculty of Aerospace Engineering, Delft University of Technology, NL, 19 April 2007
26. Maessen, D.C., *iDod preliminary design description*, iDod document iDod.DD.003, Version 1.0, Faculty of Aerospace Engineering, Delft University of Technology, NL, 3 May 2007
27. Maessen, D.C., *Required amount of inflation gas for tripod,* iDod document iDod.TN.003, Version 1.0, Faculty of

Aerospace Engineering, Delft University of Technology, NL, 5 October 2006
28. Maessen, D.C., *Effects of atomic oxygen on space inflatable materials,* iDod document iDod.TN.001, Version 1.0, Faculty of Aerospace Engineering, Delft University of Technology, NL, 2 October 2006
29. Maessen, D.C., *Connector piece design and construction,* iDod document iDod.CM.002, Draft, Faculty of Aerospace Engineering, Delft University of Technology, NL, 2 March 2007
30. Maessen, D.C., *Creating flexible tubes,* iDod document iDod.CM.001, Version 0.1, Faculty of Aerospace Engineering, Delft University of Technology, NL, 10 April 2007
31. Maessen, D.C., *Connecting tubes to a connector piece,* iDod document iDod.CM.004, Version 0.1, Faculty of Aerospace Engineering, Delft University of Technology, NL, 11 April 2007
32. Maessen, D.C., *PE adhesives testing,* iDod document iDod.CM.003, Version 0.1, Faculty of Aerospace Engineering, Delft University of Technology, NL, 10 April 2007
33. Maessen, D.C., *Membrane attachment,* iDod document iDod.CM.005, Draft, Faculty of Aerospace Engineering, Delft University of Technology, NL, 12 April 2007
34. Maessen, D.C., *Misalignments inflatable structure,* iDod document iDod.TN.012, Draft, Faculty of Aerospace Engineering, Delft University of Technology, NL, 30 March 2007
35. Maessen, D.C., *iDod mass and volume breakdown,* iDod document iDod.TN.010, Version 1.1, Faculty of Aerospace Engineering, Delft University of Technology, NL, 19 April 2007

# Top Level Requirements for inflatable De-orbit device (iDod)

**Document-ID: ISIS.iDod.REQ**
Issue: r2.1
Date: 7 May 2007

| | |
|---|---|
| Prepared: | E.D. van Breukelen |
| Revised: | D.C. Maessen |
| Checked: | |
| Approved: | |

# Parent Requirement Specifications

| *Doc Code* | *Title* | *Comment* |
|---|---|---|
| *n/a* | | |

# Change Record

| *Date* | *Responsible* | *Changes* |
|---|---|---|
| 17-1-2007 | EB | |
| 18-1-2007 | DM | Added approximate volume in description of SYS.C.02 |
| | DM | Changed mass from 84 g to 100 g in description of SYS.C.03 |
| 1-3-2007 | DM | SYS.F.02.01 added |
| | DM | Added that required stiffness (requirement SYS.F.02.01) is TBD |
| | DM | SYS.F.01.01 added |
| | DM | Added that connector type (requirement SYS.I.01) is TBD |
| | DM | SYS.F.02.02 added |
| | DM | SYS.C.04 added |
| 17-3-2007 | DM | Test Requirements added (SYS.T.XX) |
| | DM | Description of SYS.C.03 changed |
| 1-5-2007 | DM | Changed SYS.C.04 into SYS.C.05 and added SYS.C.04 |
| | DM | Added SYS.C.01.01 and SYS.C.01.02 |
| | DM | Volume in SYS.C.02 changed from 104 $cm^3$ to 103 $cm^3$ and changed figure 1 belonging to SYS.C.02 |
| | DM | Expanded list of TBD's/TBC's with SYS.C.01.01, SYS.C.01.02, and SYS.R.01.03 |
| | DM | Expanded description SYS.F.01 and removed SYS.F.01.01 |
| | DM | Expanded description and rationale SYS.F.03 |
| | DM | Added SYS.I.03 |
| | DM | Added SYS.R.01.01 till SYS.R.01.05 |
| | DM | Added SYS.O.01 |
| | DM | Added SYS.T.01 till SYS.T.14 |
| 7-5-2007 | DM | Added in SYS.C.01.02 that current CGG ignition power is 13 Watts during 2 seconds |
| | DM | SYS.F.02 is child of SYS.P.01 |
| | DM | Removed previous change (1-5-2007) in description and rationale SYS.F.03 |

| *Date* | *Responsible* | *Changes* |
|---|---|---|
| | DM | Connector type in SYS.I.01 no longer TBD |
| | DM | Deleted SYS.R.01.01 till SYS.R.01.05 because they are an implementation of SYS.R.01 and not requirements in themselves |

List of TBD's / TBC's

| *Requirement* | *TBD / TBC Action* | *Responsible* | *Deadline* |
|---|---|---|---|
| SYS.C.01 | TBC 2 W max power for ignition. short survey of 1-unit CubeSat EPS systems | TBD | TBD |
| SYS.C.01.01 | TBD wire melt through power | TBD | TBD |
| SYS.C.01.02 | TBC CGG ignition power of 13 Watts for 2 seconds | EB (TNO) | TBD |
| SYS.F.02.01 | TBD Required stiffness of inflatable structure | TBD | TBD |
| SYS.I.01 | TBD Determine Voltage/Current required for ignition of a CGG. Determine power required for cogex cgg ignition, Determine power required for Nico Rackemans adapted cgg ignition. (related to SYS.C.01 TBC) | EB (TNO) | TBD |

| Constraints | | | | | |
|---|---|---|---|---|---|
| ***Number*** | ***Title*** | ***Description*** | ***Rationale / Comment*** | ***Parent Trace*** | ***Child Trace*** |
| SYS.C.01 | Power | The system shall need no more than 2 W (TBC) for ignition. | Maximum available power while other systems can keep functioning in a typical CubeSat. | - | SYS.C.01.01 SYS.C.01.02 |
| SYS.C.01.01 | Wire melt through power | The system shall need no more than TBD W for melting through the wire that restrains the lid of the storage device | Required power (voltage/current) is unknown at this point | SYS.C.01 | - |
| SYS.C.01.02 | CGG ignition power | The system shall need no more than 13 Watts during 2 seconds for ignition of the CGG | Power required to ignite CGG (TBC) is still being optimised by TNO | SYS.C.01 | - |
| SYS.C.02 | Dimensions | The system shall not protrude outside the envelope as defined in Figure 1 (~103 $cm^3$) | Envelope that fits inside a CubeSat frame and leaves room for at least four stacked PCBs in the remaining CubeSat volume | - | - |
| SYS.C.03 | Mass | The mass difference between a CubeSat with iDod and the same CubeSat without iDod shall be less than 100 g | Mass of nanoterminator approximately times 2. 10% of CubeSat mass. | - | - |
| SYS.C.04 | Inflatable structure | The system shall use an inflatable structure to meet SYS.P.01 | An inflatable structure is lightweight and requires little stowage volume | - | - |
| SYS.C.05 | (Deployment) Envelope | The envelope of the inflatable shall be as small as possible while still meeting SYS.P.01 | A small envelope reduces the chances of coming into contact with protruding elements on the CubeSat upon inflation, leading to the risk of severely damaging the inflatable or failure to completely deploy the inflatable | - | - |

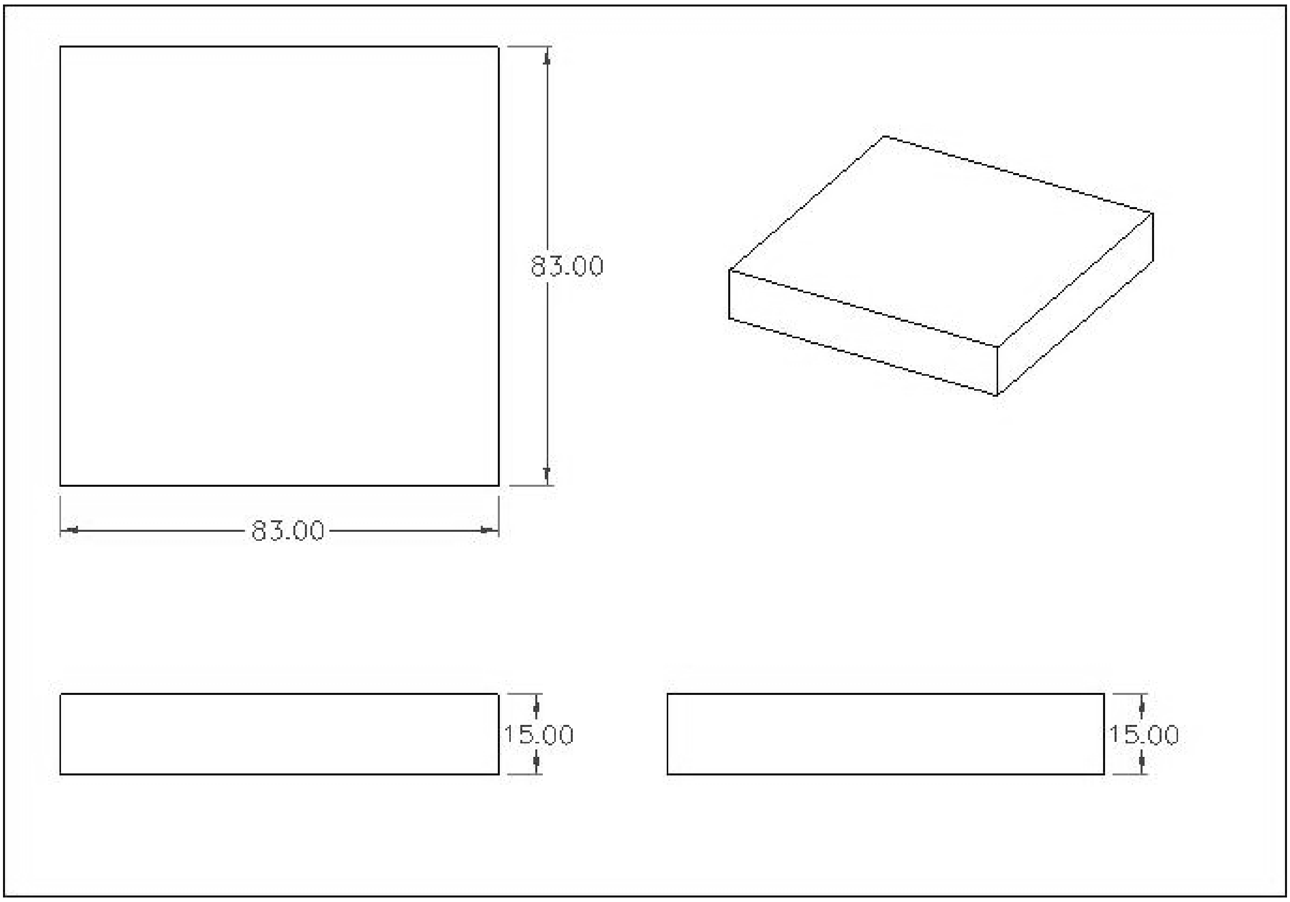


*Figure 1 Bounding envelope*

| Functional Requirements | | | | | |
|---|---|---|---|---|---|
| ***Number*** | ***Title*** | ***Description*** | ***Rationale / Comment*** | ***Parent Trace*** | ***Child Trace*** |
| SYS.F.01 | Decrease ballistic coefficient | Upon activation, the system shall decrease the ballistic coefficient of the satellite by increasing its frontal surface area | Operating principle | - | - |
| SYS.F.02 | Structural integrity | The system shall retain its general shape over its lifetime | Orbital debris, solar radiation and increased aerodynamic pressure, etc. should be assessed | SYS.P.01 | SYS.F.02.01 SYS.F.02.02 |
| SYS.F.02.01 | Stiffness | The stiffness of the system shall be sufficient to prevent shape deformation leading to failure in meeting SYS.P.01 | Forces and (mainly) thermal influences likely to be encountered may not result in major geometrical changes of the inflatable | SYS.F.02 | - |
| SYS.F.02.02 | Material integrity | The materials of the iDod shall enable meeting requirement SYS.P.01 | The space environment causes material degradation. Materials have to be selected that degrade at a very slow rate. | SYS.F.02 | - |
| SYS.F.03 | Aerodynamic stability | The satellite with inflated system shall be passively stabilized when possible | Only applicable if attitude influences the ballistic coefficient | - | - |

| Performance Requirements | | | | | |
|---|---|---|---|---|---|
| ***Number*** | ***Title*** | ***Description*** | ***Rationale / Comment*** | ***Parent Trace*** | ***Child Trace*** |
| SYS.P.01 | Limit orbital lifetime | The system shall limit orbital lifetime after operational lifetime to 25 years | European Code of Conduct for Space Debris Mitigation, SD-OP-03 | EcoCfSDM, SD-OP-03 | SYS.F.02 |
| SYS.P.02 | Satellite characteristics | The system shall achieve SYS.P.01 for a 1 unit CubeSat | 1-unit CubeSat chosen for straw man concept (1-3 unit eventually) | - | - |
| SYS.P.03 | Increase maximum altitude to 1000 km | The system shall achieve SYS.P.01 for satellites in circular orbits at altitudes of up to 1000 km | Double practical altitude range from 400-700 km to 400-1000 km | - | - |

| Interface Requirements | | | | | |
|---|---|---|---|---|---|
| ***Number*** | ***Title*** | ***Description*** | ***Rationale / Comment*** | ***Parent Trace*** | ***Child Trace*** |
| SYS.I.01 | Electrical interface | The system is activated upon provision of sufficient (TBD) electrical power on a PC/104 connector | To keep the electrical interface as simple as possible. The customer can implement safe/arm/test circuitry as desired on the satellite side of the system boundary | - | - |
| SYS.I.02 | Integration | The system shall allow for -easy- integration in various CubeSat configurations | Apologies for the fuzzy wording of the requirement. Assess using mock-ups and common sense. Think of testability, mounting provisions, etc., it probably needs to be removed from the satellite several times | - | - |
| SYS.I.03 | Component integration | System components should be easy to install and remove | Easy installation reduces the likelihood of failures to occur and reduces costs (time, equipment) | - | - |

| RAMS Requirements | | | | | |
|---|---|---|---|---|---|
| ***Number*** | ***Title*** | ***Description*** | ***Rationale / Comment*** | ***Parent Trace*** | ***Child Trace*** |
| SYS.R.01 | Lifetime limitation success probability | The probability of successful limitation of the orbit life should be 0.9 or higher, assuming that the satellite can still be operated at the time of activation. | European Code of Conduct for Space Debris Mitigation, SD-OP-05. Please notice the **should** which is also used in that document. | - | SYS.R.01.01<br>SYS.R.01.02<br>SYS.R.01.03<br>SYS.R.01.04<br>SYS.R.01.05 |

| Operational Requirements | | | | | |
|---|---|---|---|---|---|
| ***Number*** | ***Title*** | ***Description*** | ***Rationale / Comment*** | ***Parent Trace*** | ***Child Trace*** |
| SYS.O.01 | Passive operation | After deployment of the inflatable structure, SYS.P.01 shall be achieved in a passive manner | The de-orbit manoeuvre is uncontrolled and cannot be influenced from the ground | - | - |

| Test Requirements | | | | | |
|---|---|---|---|---|---|
| ***Number*** | ***Title*** | ***Description*** | ***Rationale / Comment*** | ***Parent Trace*** | ***Child Trace*** |
| SYS.T.01 | (Zero-g) Deployment | The deployment envelope of the inflatable structure has to be determined and optimised | A small deployment envelope reduces the chances of coming into contact with protruding satellite elements. Deployment in zero-g (parabolic flight) approaches deployment in space the most | - | - |
| SYS.T.02 | Leak rate | The rate at which the inflation gas escapes from the inflatable has to be determined | Proper inflation of the inflatable with the available amount of inflation gas has to be guaranteed | - | - |
| SYS.T.03 | Adhesive strength | The strength at the expected operating temperatures of the adhesive(s) used to construct the inflatable structure needs to be known | A too high pressure and too weak adhesive lead to failure of the bond and immediate evacuation of all inflation gas from the structure, possibly resulting in incomplete deployment | - | - |
| SYS.T.04 | Adhesive endurance | The endurance of the adhesive under space conditions has to be determined | Charged particles, high or low temperatures, a vacuum environment, and (V)UV radiation can lead to chemical changes in the adhesive and a decrease in its adhering properties | - | - |
| SYS.T.05 | Ultimate pressure | The burst pressure of the inflatable structure has to be determined | A CGG delivers a fixed amount of inflation gas. The smallest CGG available may not deliver an amount of gas that, in combination with a high temperature, can result in bursting of the inflatable structure | - | - |
| SYS.T.06 | Thermal cycling | The iDod with deployed inflatable is subjected to many cycles of alternating high and low temperatures | This test is used to verify workmanship. In addition, the response of the iDod materials and coatings to many thermal cycles can be determined | - | - |
| SYS.T.07 | Thermal balance | The thermal environment in space is simulated | This test is used to validate thermal models of the iDod and to determine the temperatures obtained by the iDod system | - | - |

| Test Requirements | | | | | |
|---|---|---|---|---|---|
| ***Number*** | ***Title*** | ***Description*** | ***Rationale / Comment*** | ***Parent Trace*** | ***Child Trace*** |
| SYS.T.08 | Reliability membrane connections | The likelihood of failure of the connections of the membranes to the storage device and to the inflatable tubes has to be determined | The reliability has to be determined by performing many deployment tests | - | - |
| SYS.T.09 | CubeSat integration | Integration of the iDod system into a CubeSat structure has to be tested | This integration test is needed to verify that no unforeseen problems arise during iDod integration | - | - |
| SYS.T.10 | Inflation with CGG | Inflation of the inflatable structure by means of inflation gas delivered by a CGG | Up to now, inflation has been performed using pumps. It has to be determined whether the fast gas production of a CGG does not result in inflation problems | - | - |
| SYS.T.11 | Hinge rotation | Determine the chance that a helical torsion spring cold welds to the axle it is positioned over. | The helical torsion springs used to rotate the lid of the storage device can cold weld to the axle around which the lid rotates, thereby losing their function. | - | - |
| SYS.T.12 | Wire melt | Melting of a Dyneema wire by means of heating up a resistor | Determine the power and length of time required to melt through a Dyneema wire under the expected operating conditions (low temperature, vacuum) | - | - |
| SYS.T.13 | Random vibration | The iDod is subjected to a representative spectrum of random vibrations likely to be encountered during launch | These test results provide the CubeSat integrator with knowledge about the responses of the iDod as a result of vibrations. This has an impact on the design of the total CubeSat system.<br>The test also serves as a design check and as a check for workmanship. | - | - |
| SYS.T.14 | Pressure decrease | Simulate the pressure decrease that occurs during launch | Air present in the closed storage device will expand and will be sucked out. This can lead to unexpected issues (e.g. failure of the hold down wire) | - | - |

# iDod attitude stability analysis

## SUMMARY

The purpose of this document is to find out whether a specific orientation can be achieved for the CubeSat with deployed iDod in a passive manner for the complete de-orbit maneuver. This has to be achieved under influence of the following four disturbance torques:

1. aerodynamic drag
2. solar radiation pressure
3. magnetic field Earth
4. gravity gradient

A first-order analysis of the disturbance torques acting on the CubeSat with deployed iDod learns that this is only possible for the complete de-orbit maneuver when the gravity gradient effect is utilized. Below an altitude of ~ 450 - 650 km, this is also possible by making use of aerodynamic drag.
However, when the gravity gradient effect is utilized, the length of the required inflatable boom needs to be roughly 3 meters and the required tip mass needs to be roughly 100 grams. In addition, the residual dipole moment of the CubeSat may not be larger than ~ 0.05 $Am^2$. The required length of the inflatable boom does not seem feasible at this point of the design. Furthermore, the residual dipole requirement will reduce the potential market for the iDod considerably, adding to the unattractiveness of a concept utilizing gravity gradient stabilization.

These results lead to the conclusion that it is not possible to achieve a single orientation of the satellite for the complete de-orbit maneuver. Therefore, it is recommended to create an inflatable structure for the iDod that will, on average, have a frontal surface area of 0.315 $m^2$. This way, the de-orbit performance of the iDod is not sensitive to the orientation of the spacecraft, which makes it in principle applicable on every 1-unit CubeSat.

## KEYWORDS

Passive attitude control, iDod, disturbance torque

## DISTRIBUTION

| | Name | | Company / Institution |
|---|---|---|---|
| 1 | E.D. van Breukelen | Project leader | ISIS B.V. |
| 2 | B.T.C. Zandbergen | Reviewer | TU Delft |

## APPROVAL

| | Name | Company / Institution | Date | Signature |
|---|---|---|---|---|
| *Written* | D.C. Maessen | TU Delft | 1/16/2007 | |
| *Checked* | | | | |
| *Approved* | | | | |

## REVISION RECORD

| Issue | Date | Total pages | Affected pages | Brief description of change |
|---|---|---|---|---|
| Draft | 11/1/2006 | 15 | | |
| Version 1 | 1/16/2007 | 15 | 1,9,10 | 400-500 km changed in 450-650 km |

## LIST OF TBD'S AND TBC'S

| TBD / TBC | Paragraph | Subject | Due date | Action by |
|---|---|---|---|---|
| TBD | Chapter 4 | Average frontal surface area inflatable structure for random orientation of spacecraft | TBD | D.C. Maessen |
| TBD | Chapter 4 | Influence solar radiation pressure on orbit height | TBD | E.D. van Breukelen |
| | | | | |

## TABLE OF CONTENTS

# 1 INTRODUCTION

This document assesses the attitude (in)stability of the CubeSat with inflated iDod. Since the function of the iDod is to facilitate a de-orbiting maneuver of the satellite by means of a decrease in its ballistic coefficient [Maessen, iDod.DD.001], the orientation of the spacecraft during the de-orbit period is very important. This orientation is required to be achieved in a passive manner (requirement SYS.F.03, [van Breukelen, 2006]). The purpose of this document is to find out whether a specific orientation can be achieved for the CubeSat with deployed iDod in a passive manner for the complete de-orbit maneuver.

The next chapter treats the four main disturbance torques encountered. First, the general equations with which the magnitude of the torques can be assessed are provided. Paragraphs 2.1 till 2.4 will then discuss each effect briefly, focusing on the current application. In paragraph 2.5 the variation in magnitude of all torques is plotted against height, resulting in several important conclusions which are treated in the third chapter. Lastly, it is indicated what further work needs to be performed for this element of the design of the iDod.

# 2 DISTURBANCE TORQUES

In space, there are four main external influences present that result in disturbance torques on satellites:

1. aerodynamic drag
2. solar radiation pressure
3. magnetic field Earth
4. gravity gradient

The magnitude of these torques can be determined using the following (simplified) formulas [Wertz, 1999]:

$$T_{drag} = F_{drag}\left(c_{pa} - c_m\right) = \frac{1}{2}\rho C_D A_{drag} V^2 \left(c_{pa} - c_m\right) \tag{1}$$

$$T_{sp} = F_{sp}\left(c_{ps} - c_m\right) = \frac{F_s}{c} A_{sp}\left(1+q\right)\cos\left(i\right)\left(c_{ps} - c_m\right) \tag{2}$$

$$T_m = DB = D\frac{2M}{R^3} \tag{3}$$

$$T_{gg} = \frac{3\mu}{2R^3}\left|I_z - I_y\right|\sin\left(2\theta\right) \tag{4}$$

An explanation of the symbols used in the above formulas is provided in table 1 (values are obtained from [Wertz, 1999]):

| Symbol | Description | Value | Units |
|---|---|---|---|
| $A_{drag}$ | Drag surface area | | $m^2$ |
| $A_{sp}$ | Solar pressure surface area | | $m^2$ |
| B | Earth's magnetic field strength | | T |
| c | Speed of light | $3*10^8$ | m/s |
| $c_m$ | Center of mass | | m |
| $c_{pa}$ | Center of aerodynamic pressure | | m |

| | | | |
|---|---|---|---|
| $c_{ps}$ | Center of solar radiation pressure | | m |
| $C_D$ | Drag coefficient | ~2 – 2.5 | - |
| D | Residual dipole spacecraft | | $Am^2$ |
| i | Sun incidence angle | | deg |
| $I_y$ | Mass moment of inertia around y-axis spacecraft | | $kgm^2$ |
| $I_z$ | Mass moment of inertia around z-axis spacecraft | | $kgm^2$ |
| $F_{drag}$ | Force due to aerodynamic drag | | N |
| $F_{sp}$ | Force due to solar radiation pressure | | N |
| $F_s$ | Solar constant | 1367 | $W/m^2$ |
| M | Magnetic moment Earth | $7.96*10^{15}$ | $Tm^3$ |
| R | Orbit radius spacecraft | | m |
| $T_{drag}$ | Torque due to aerodynamic drag | | Nm |
| $T_{gg}$ | Torque due to gravity gradient | | Nm |
| $T_{sp}$ | Torque due to solar radiation pressure | | Nm |
| $T_m$ | Torque due to magnetic field Earth | | Nm |
| q | Reflectance factor | 0 - 1 | - |
| V | Spacecraft velocity | | m/s |
| $\mu$ | Earth's gravity constant | $3.986*10^{14}$ | $m^3/s^2$ |
| $\theta$ | Deviation of z-axis from local vertical | | deg |
| $\rho$ | Density atmosphere | | $kg/m^3$ |

*Table 1 Symbol description*

All four disturbance torques are discussed in the coming paragraphs. It is explained how they can be manipulated by relatively easy means. Rough estimations of the disturbance torques generated by each effect are determined for various orbital altitudes in paragraph 2.5. This is done to find out whether a specific orientation can be achieved for the CubeSat with deployed iDod in a passive manner for the complete de-orbit maneuver. The ideal situation would namely be to have the attitude of the spacecraft be determined by the aerodynamic drag torque. This way, the geometry of the inflatable structure can be made such that the frontal surface area, which determines the amount of deceleration, is always maximal during the de-orbit maneuver.

It is noted that various effects such as solar eclipse and variations in the gravitational and magnetic field strength of the Earth (etc.) are not taken into consideration for the determination of the various torques. Thus, the current analysis is regarded as a conservative first-order estimation of the disturbance torques encountered.

## 2.1 Aerodynamic drag torque

The aerodynamic drag torque and the solar radiation pressure torque can basically be manipulated in the same manner. The following explanation thus also applies to the paragraph in which solar radiation pressure torque is discussed (paragraph 2.2).

In equation (1), it is shown that the torque is determined by multiplying a certain force ($F_{drag}$) with a moment arm ($c_{pa}$-$c_m$). This force is the summation of all individual pressure forces acting on the surface under consideration and acts at the so-called center of pressure of that surface. The center of pressure of a surface roughly coincides with the geometrical center of that surface. When one now strives to either maximize or minimize the drag torque, this can be done by manipulating the surface area (larger, smaller, other angle with respect to the pressure source, etc.) or by manipulating the moment arm (other center of mass or other center of pressure).
For the inflatable structure, the moment arm can for instance be manipulated by changing the geometry of the inflated surface. This is visualized in the next figure where a front view of the CubeSat-iDod combination is provided for a pyramid-shaped inflatable structure.

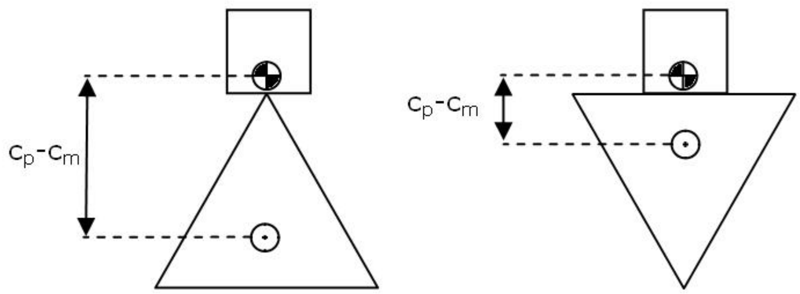


*Figure 1 Manipulation of moment arm by change in geometry*

Thus, a simple change in geometry can result in a significant change of the induced torque.

However, since the density of the atmosphere decreases with altitude, the magnitude of the aerodynamic drag torque will also decrease with altitude. This is depicted in figure 4 in paragraph 2.5. Above altitudes of roughly 450 – 700 km, the other disturbance torques can easily be larger than the aerodynamic disturbance torque.

## 2.2 Solar radiation pressure torque

Since the iDod has to be applicable on as much CubeSats as possible, it has to work for every type of orbit (ideally). This means that the position of the sun with respect to the spacecraft should not influence the practicality of the device. Therefore, the position of the sun has to be assumed to be unknown and has to be assumed to cause a worst-case effect. This translates into the solar pressure area ($A_{sp}$) being equal to the drag surface area ($A_{drag}$) and in ($c_{ps}$ – $c_m$) being equal to ($c_{pa}$ - $c_m$), see equations (1) and (2). Now, the altitude for which the solar radiation pressure torque is larger than the aerodynamic torque can be roughly determined for both solar minimum and solar maximum conditions:

$$T_{sp} > T_{drag}$$

$$\frac{F_s}{c} A_{sp} (1+q) \cos(i) (c_{ps} - c_m) > \frac{1}{2} \rho C_D A_{drag} V^2 (c_{pa} - c_m)$$

$$\frac{F_s}{c} (1+q) \cos(i) > \frac{1}{2} \rho C_D V^2$$

$$\frac{2F_s}{cC_D} (1+q) \cos(i) > \rho V^2$$

With q = 1, i = 0, and $C_D$ = 2, the left hand side of the above equation is equal to $9.11 \cdot 10^{-6}$ N/m$^2$. Using the values for the atmospheric density and the orbital velocity at various altitudes from the back cover of [Wertz, 1999], the altitudes for which $T_{sp}$ is larger than $T_{drag}$ are determined. For solar minimum conditions, $T_{sp}$ is larger at altitudes above ~450 km ($\rho$ = $2.47 \cdot 10^{-13}$ kg/m$^3$ and V = 7640 m/s). For solar maximum conditions, the discriminating altitude is ~700 km ($\rho$ = $1.47 \cdot 10^{-13}$ kg/m$^3$ and V = 7504 m/s).

The above analysis shows that in the region between 700 and 1000 km, the attitude of the spacecraft with deployed iDod cannot be assumed to be determined by the aerodynamic drag. Between 450 and 700 km altitude, the amount of solar activity determines which of the two effects will dominate. This is further visualized in figure 4 in paragraph 2.5.

## 2.3 Magnetic field interaction torque

The attitude problem is increased even more since the torque due to the interaction of the spacecraft with the magnetic field of the Earth is unknown. The cause of this is that the magnetic properties of the spacecraft are unknown, which in turn causes the size of the residual magnetic dipole moment of the spacecraft to be unknown. This residual dipole moment is created by the magnetization of certain parts of the satellite due to dipole moments created during its life or by incorporation of permanent magnets in the CubeSat. The artificially created dipole moments are often obtained by creating a current loop (multiplying the current with the area enclosed by the loop gives the magnetic dipole thus created).

The dipole moment actually has a certain direction and can thus be visualized as a vector with a certain magnitude. The same applies to the magnetic field of the Earth; this can also be seen as a vector with a certain strength and direction (which is different for every position around Earth). In equation (3) however, both vectors are assumed to be scalars. Multiplying these with each other only results in a new scalar and not in a new vector. Thus, only the magnitude of the resulting torque is determined and not the direction. Normally, this is not desired, but since it is unknown what direction the residual magnetic dipole of the CubeSat will have, the only useful thing that can be determined is the magnitude of the torque. In addition, equation (3) actually signifies a worst-case moment where the two vectors are perpendicular to each other (the cross product then results in a product of scalar values) and the spacecraft is situated above one of the magnetic poles of the Earth (there, the magnetic field strength is at its peak).

As said earlier, the residual magnetic dipole moment of the CubeSat is unknown. In fact, no literature has been found in which this dipole moment has been determined for a CubeSat (excluding cases where permanent magnets are used). A small survey of papers concerning CubeSats where this dipole moment is briefly assessed learns that only rough guesses have been made. These guesses range between 0.0001 $Am^2$ and 0.01 $Am^2$ [Carroll, Fauske, Fong, Scholz].

In paragraph 2.5, the variation in disturbance torque on the spacecraft with altitude (for various effects) is determined using estimated guesses for the properties of the spacecraft. The resulting graph shows that a residual dipole moment higher than 0.001 $Am^2$ will cause the magnetic torque to be larger than the aerodynamic drag torque for certain conditions. A residual dipole moment of 0.01 $Am^2$ will make it a bit smaller than the solar radiation pressure torque.

## 2.4 Gravity gradient torque

The gravity gradient torque is created by the tendency of the satellite's axis of minimum mass moment of inertia to be aligned with the nadir vector (vector pointing from the center of mass of the satellite to the center of the Earth) of the satellite. In figure 2, this is explained graphically using a body consisting of two equal masses $m_1$ and $m_2$. Both masses are attracted to the Earth by gravity, but since mass $m_1$ is a little bit closer to Earth than mass $m_2$, gravity pulls harder on mass $m_1$ (since gravity depends on the inverse square of the distance between two objects). This is the gravity gradient effect. The resulting force $F_1$ is a little bit larger than force $F_2$, resulting in a counter-clockwise rotation around the body's center of mass. The resulting motion is very similar to that of a pendulum. When this motion is not damped and not disturbed, the body will oscillate around its rest position (where the two masses are exactly aligned with the nadir vector) indefinitely. In case of a damped motion, the oscillation will eventually grind to a halt with the body being aligned exactly with the nadir vector. This effect can thus be used when it is desired to have one axis of the body constantly pointing towards Earth.

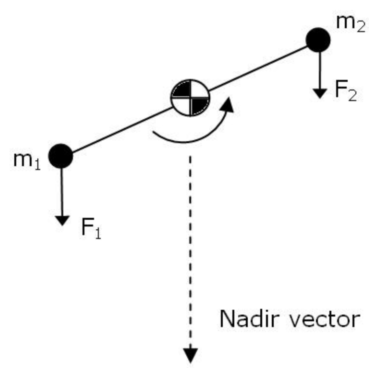


*Figure 2 Gravity gradient effect*

When this effect is utilized in practice for attitude control, it is customary to use a relatively small mass attached to the end of a long boom. Gravity now pulls less hard on the small mass, but the large arm compensates for this, resulting in a considerable torque.

For a normal 1-unit CubeSat, the gravity gradient effect is negligibly small since the satellite's shape is cubic and its center of mass is close to its geometric center. However, the gravity gradient effect can be enhanced by employing a small deployable boom with a tip mass. Since in this case the satellite needs to be de-orbited using aerodynamic drag, a large frontal surface area is still required. This can be achieved by using thin membranes with which a pyramid shape is created. The deployed boom now can be seen as a central column of the pyramid.

Figure 3 shows a conceptual front view of the complete spacecraft for which the gravity gradient effect is used (dimensions are not to scale!). Since the gravity gradient torque can only be determined when the mass moments of inertia of the spacecraft are known (see equation (4)), it helps to assume for those calculations that the triangular membranes of the pyramid are rectangular and aligned with the z-axis of the spacecraft. This will introduce a minor error (since the mass of the membranes is very low), but simplifies the required calculations significantly. Figure 3 also depicts the orientation of the coordinate system; the x-axis is the axis in the direction of flight.

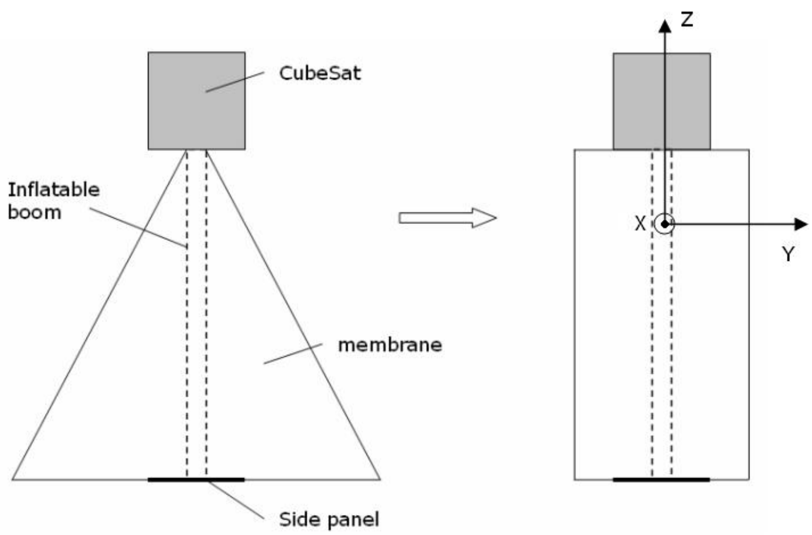


*Figure 3 Simplification of geometry*

In appendix A, the complete calculation for the determination of the moments of inertia can be found for a boom length of 2 meters and a side panel mass of 50 grams. This result is used in paragraph 2.5 to determine the disturbance torque caused by the gravity gradient effect.

## 2.5 Disturbance torque evaluation

This paragraph deals with the determination of the disturbance torques created by the four effects discussed earlier. Equations (1) till (4) are used to calculate the torque due to a particular effect at a certain orbital altitude. The manner in which this is done is quite straightforward and is not treated. First, the values that are used for the various variables are given and then the result is provided in figure 4.

The atmospheric density and the orbital velocity are used to determine the aerodynamic drag torque for various cases. The below table provides these for various altitudes during either solar minimum or solar maximum conditions.

| **Altitude [km]** | **Atm. Density @ solar min. [kg/m$^3$]** | **Atm. Density @ solar max. [kg/m$^3$]** | **Circular velocity [km/s]** |
|---|---|---|---|
| 100 | 4.61E-07 | 5.10E-07 | 7.844 |
| 150 | 1.65E-09 | 2.04E-09 | 7.814 |
| 200 | 1.78E-10 | 3.52E-10 | 7.784 |
| 250 | 3.35E-11 | 1.06E-10 | 7.755 |
| 300 | 8.19E-12 | 3.96E-11 | 7.726 |
| 350 | 2.34E-12 | 1.66E-11 | 7.697 |
| 400 | 7.32E-13 | 7.55E-12 | 7.669 |
| 450 | 2.47E-13 | 3.61E-12 | 7.640 |
| 500 | 8.98E-14 | 1.80E-12 | 7.613 |
| 550 | 3.63E-14 | 9.25E-13 | 7.585 |
| 600 | 1.68E-14 | 4.89E-13 | 7.558 |
| 650 | 9.14E-15 | 2.64E-13 | 7.531 |
| 700 | 5.74E-15 | 1.47E-13 | 7.504 |
| 750 | 3.99E-15 | 8.37E-14 | 7.478 |
| 800 | 2.96E-15 | 4.39E-14 | 7.452 |
| 850 | 2.28E-15 | 3.00E-14 | 7.426 |
| 900 | 1.80E-15 | 1.91E-14 | 7.400 |
| 950 | 1.44E-15 | 1.27E-14 | 7.375 |
| 1000 | 1.17E-15 | 8.84E-15 | 7.350 |

*Table 2 Atmospheric density and orbital velocity [Wertz, 1999]*

The next table provides the values that are used for the variables in equations (1) till (4) in order to create the graph of figure 4. For the solar radiation pressure torque, worst-case values are assumed for all variables for reasons discussed in paragraph 2.2. For the magnetic field interaction torque, three different values for D are used: 0.0001, 0.001, and 0.01 Am$^2$. This is done to visualize the effect of (relatively) small and large residual magnetic dipoles. For the gravity gradient torque, the mass moments of inertia as determined in appendix A are used. In addition, the angle $\theta$ is set at 45 degrees in order to obtain the maximum torque caused by this effect (since $T_{gg} \propto \sin(2\theta)$).

| **Aerodynamic drag torque** | | |
|---|---|---|
| $C_D$ | 2 | - |
| $A_{drag}$ | 0.315 | m$^2$ |
| $c_{pa} - c_m$ | 0.5 | m |
| **Solar radiation pressure torque** | | |
| $F_s$ | 1367 | W/m$^2$ |
| c | $3.0*10^8$ | m/s |
| $A_{sp}$ | 0.315 | m$^2$ |
| q | 1 | - |
| i | 0 | deg |
| $c_{ps} - c_m$ | 0.5 | m |

| Magnetic field interaction torque | | |
|---|---|---|
| D | 0.0001 - 0.01 | $Am^2$ |
| M | $7.96*10^{15}$ | $Tm^3$ |
| **Gravity gradient torque** | | |
| $\mu$ | $3.986*10^{14}$ | $m^3/s^2$ |
| $I_z$ | 0.2765 | $kgm^2$ |
| $I_y$ | 0.0017 | $kgm^2$ |
| $\theta$ | 45 | deg |

*Table 3 Values used to determine torques*

The first thing that is clear from the results in figure 4 is that the aerodynamic drag torque varies about one order of magnitude between solar minimum and solar maximum conditions. It is also much larger than the other disturbance torques at altitudes below ~ 450 - 650 km. Furthermore, the magnitude of all disturbance torques except the aerodynamic drag torque is virtually independent of altitude.

A bit unclear in the figure is the torque caused by the gravity gradient effect. Due to chance, this torque is very close to the torque created with a residual magnetic dipole moment of 0.01 $Am^2$.

In order to have a gravity gradient torque close to the solar radiation pressure torque (which is equal to $1.44*10^{-6}$ Nm), the offset between the side panel and the CubeSat needs to be increased to about 3 meters resulting in $I_y$ = 0.63 $kgm^2$ and $T_{gg}$ ~ $1.1*10^{-6}$ Nm. In order to get the gravity gradient torque to be larger than the solar radiation pressure torque, also the mass of the side panel has to be increased to 100 grams instead of 50 grams resulting in $I_y$ = 0.98 $kgm^2$ and $T_{gg}$ ~ $2*10^{-6}$ Nm (for clarity: the offset here is still 3 meters).

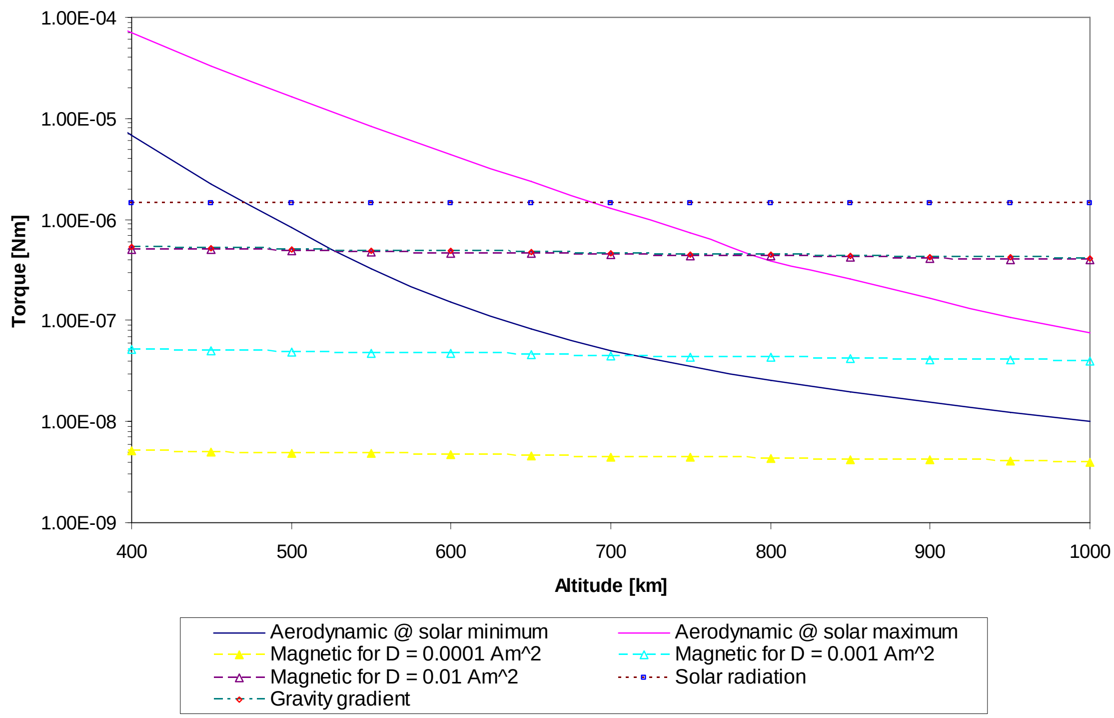


*Figure 4 Disturbance torques due to various effects*

From the above figure it is immediately clear that the ideal situation, to have the attitude of the CubeSat be determined by aerodynamic drag, is impossible for the entire de-orbit maneuver. This is only possible at altitudes below ~ 450 - 650 km.

Since the position of the sun (and therefore the direction of the solar radiation) varies over one orbit, this effect cannot be used to generate a constant attitude for the satellite (during eclipse there is even no torque due to solar radiation pressure!).
A similar argumentation holds for the magnetic field interaction torque; its direction and magnitude are not constant over one orbit and can therefore not be used to obtain a specific orientation in a passive manner. It is even not desired at all to use magnetic fields for attitude control for this application because they either require a power source with a lifetime of 25 years or it is required to use permanent magnets that can very well interfere with normal spacecraft operations.
This leaves only the gravity gradient effect as a candidate for passive attitude control. However, for it to be larger than all other torques (above ~ 450 - 650 km), the required inflatable boom has to be very long (~ 3 m) and the tip mass has to be large (~ 100 grams). Especially the boom length does not seem feasible. In addition, the residual magnetic dipole moment of the CubeSat may not be very large either (smaller than ~ 0.05 $Am^2$).

# 3 CONCLUSIONS & RECOMMENDATIONS

As stated in the introduction, the purpose of this document is to find out whether a specific stable orientation can be achieved for a CubeSat with deployed iDod in a passive manner for the entire de-orbit maneuver. The foregoing analysis has shown that this is only possible when the gravity gradient effect is utilized. However, below an altitude of ~ 450 - 650 km, the aerodynamic drag torque is thus large that it will easily be larger than the gravity gradient torque. But this is not undesired; the satellite will now also assume a stable orientation, only now due to aerodynamic drag and not due to the gravity gradient effect. This can be incorporated into the design of the iDod.

Yet, the gravity gradient effect can only be utilized when the residual magnetic dipole of the CubeSat is not too large (smaller than ~ 0.05 $Am^2$). This virtually rules out application on CubeSats with permanent magnets, reducing the potential market for the device. In addition, to be sure that the gravity gradient torque is close to or larger than the solar radiation pressure torque, the offset of the side panel from the CubeSat needs to be roughly 3 meters. This boom length does not seem to be feasible.

Therefore, it is concluded that it is not possible to achieve a stable orientation for the satellite using the gravity gradient effect for all possible CubeSat designs. Thus, since the gravity gradient effect was the only possible way to achieve a stable orientation above an altitude of ~ 450 - 650 km, it is not possible to achieve a stable orientation above this altitude in a passive manner.

It is now recommended to create an inflatable structure for the iDod that will, on average, have a frontal surface area of 0.315 $m^2$. This way, the de-orbit performance of the iDod is not sensitive to the orientation of the spacecraft, which makes it in principle applicable on every 1-unit CubeSat.

# 4 FURTHER WORK

Since it has been recommended to use a configuration for the iDod that does not depend on the orientation of the satellite, it is not foreseen that a more detailed attitude dynamics analysis is performed in the future.

However, it has to be determined for the configuration that will be chosen for the inflatable structure what its dimensions need to be in order for it to have a frontal surface area of about 0.315 $m^2$ irrespective of its attitude.

Although not being completely within the scope of this technical note, it needs to be determined whether the solar radiation pressure does not push the satellite with deployed iDod into a higher orbit instead of a lower orbit.

## REFERENCES

1. Breukelen, E.D. van, *iDod Requirements Specification*, draft, iDod document ISIS.iDod.REQ, Innovative Solutions In Space, Delft, 10 July 2006.

2. Carroll, K.A., et. al., *Arc-Minute Nanosatellite Attitude Control: Enabling Technology for the BRITE Stellar Photometry Mission*, 18th Annual AIAA/USU Conference on Small Satellites, SSC04-V-2.

3. Fauske, K.M., *NCUBE Attitude Control*, http://www.unik.no/personer/fauske/publications/ncubeattctrl.pdf , 2003-05-06.

4. Fong, Chen-Joe, et. al., *Lessons learned of NSPO's Picosatellite Mission: YamSat – 1A, 1B & 1C,* 16th Annual AIAA/USU Conference on Small Satellites, SSC02-X-6.

5. Maessen, D.C., *iDod Straw man concept design description,* version 1, iDod document iDod.DD.001, Faculty of Aerospace Engineering, Delft University of Technology, 25 September 2006.

6. Scholz, A., et. al., *COMPASS-1, Phase A Study*, Hochschule Aachen, 06 November 2003.

7. Wertz, J.R., Larson, W.J., *Space Mission Analysis and Design*, Third Edition, Kluwer Academic Publishers, Dordrecht (NL), 1999.

## APPENDIX A: DETERMINATION OF MASS MOMENTS OF INERTIA IN CASE OF GRAVITY GRADIENT STABILIZATION

Using information from [Maessen, iDod.DD.001], the various mass moments of inertia for an iDod utilizing the gravity gradient effect are estimated.

The mass of an inflatable boom with a radius of 5 mm is roughly 15 grams per meter with a Kapton thickness of 25 microns and a composite thickness of 0.25 mm. Since the satellite has to be de-orbited by means of drag, membranes are needed to create a large frontal surface area. Assuming these membranes are positioned such that a pyramid shape is created and assuming that each membrane needs to have a surface area of 3150 $cm^2$, this results in a mass of ~11.25 grams for each membrane when made from 25 microns thick Kapton (the mass of all membranes combined is ~ 45 grams). For ease of calculation, the membranes are assumed to be rectangular and are assumed to run parallel to the z-axis of the satellite. For the tip mass, a complete side panel of the CubeSat can be used. Its mass is estimated at 50 grams.

For easy reference, the figure describing the simplification of geometry from a pyramid-shape to a rectangular shape from paragraph 2.4 is again given below.

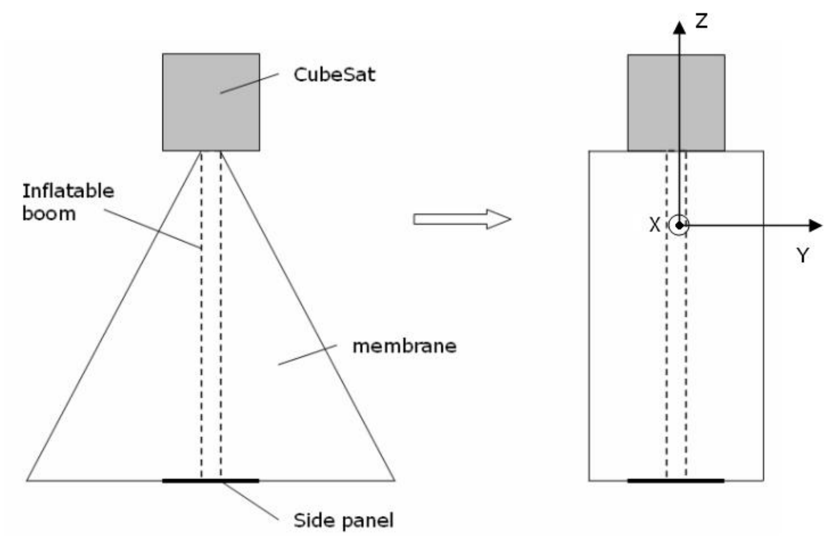


For a rectangular solid and for a thin-walled cylinder, the mass moments of inertia are:

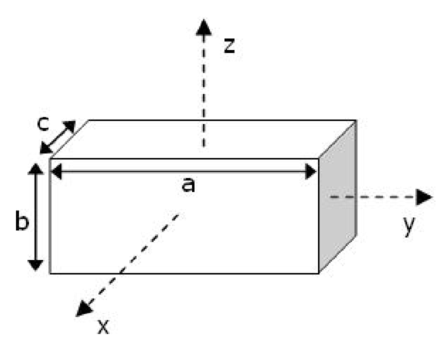


$$I_{xx} = \frac{1}{12} m\left(a^2 + b^2\right)$$

$$I_{yy} = \frac{1}{12} m\left(b^2 + c^2\right)$$

$$I_{zz} = \frac{1}{12} m\left(a^2 + c^2\right)$$

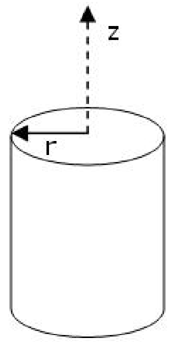


$$I_{xx} = I_{yy} = 0$$
$$I_{zz} = mr^2$$

*Figure 5 Mass moments of inertia*

For all individual components, the mass moments of inertia around their central axes can now be obtained:

| Component | Mass moments of inertia |
|---|---|
| CubeSat | $I_{xx} = \frac{1}{12} m_{cubesat} \left(a^2 + b^2\right) = \frac{a^2}{6} m_{cubesat}$<br>$I_{yy} = \frac{1}{12} m_{cubesat} \left(b^2 + c^2\right) = \frac{a^2}{6} m_{cubesat}$<br>$I_{zz} = \frac{1}{12} m_{cubesat} \left(a^2 + c^2\right) = \frac{a^2}{6} m_{cubesat}$ |
| Inflatable boom | $I_{xx} = 0$<br>$I_{yy} = 0$<br>$I_{zz} = m_{boom} r^2$ |
| Membrane | $I_{xx} = \frac{1}{12} m_{membrane} \left(w^2 + l^2\right)$ or $I_{xx} = \frac{l^2}{12} m_{membrane}$<br>$I_{yy} = \frac{l^2}{12} m_{membrane}$ or $I_{yy} = \frac{1}{12} m_{membrane} \left(w^2 + l^2\right)$<br>$I_{zz} = \frac{w^2}{12} m_{membrane}$ |
| Side panel | $I_{xx} = \frac{a^2}{12} m_{panel}$<br>$I_{yy} = \frac{a^2}{12} m_{panel}$<br>$I_{zz} = \frac{1}{12} m_{panel} \left(a^2 + c^2\right) = \frac{a^2}{6} m_{panel}$ |

*Table 4 Mass moments of inertia for different components*

For clarity: the x-axis is parallel to the direction of flight of the satellite, the y-axis lies in the orbital plane of the satellite, and the z-axis is in nadir direction. The variables a, b, and c denote the lengths of the sides of the CubeSat (0.1 m each). The variable m denotes the mass of the component under consideration. Each membrane has a length l and a width w. The moments of inertia in x-direction and in y-direction can be calculated in two ways for a membrane since there are two possible orientations for a membrane: parallel to the xz-plane or parallel to the yz-plane.

Before the moments of inertia of the complete spacecraft can be determined, the location of the center of mass must be known. It is assumed that it lies somewhere on the z-axis of the spacecraft. To determine its location on the z-axis, the distance of the center of mass with respect to the upper panel of the CubeSat is determined in the following manner:

$$c.o.m._{satellite} = \frac{m_{cubesat} * \frac{1}{2} a + m_{boom} * \left( a + \frac{l}{2} \right) + m_{membranes} * \left( a + \frac{l}{2} \right) + m_{panel} * (a + l)}{m_{cubesat} + m_{boom} + m_{membranes} + m_{panel}} \tag{5}$$

The parallel axis theorem provides the contribution of each component to the total mass moment of inertia around the x-axis or the y-axis of the satellite (this is not required for the z-axis). The origin of these axes is the center of mass of the satellite.

$$I_{\overline{xx},component} = I_{xx,component} + m_{component} \left| c.o.m._{component} - c.o.m._{satellite} \right|^2 \tag{6}$$

The next table provides the values for the variables that are required to determine the moments of inertia and the location of the center of mass of the satellite. The mass of the CubeSat is determined by subtracting the other masses (4 times the mass of one membrane!) from 1 kg, which is the maximum mass for a CubeSat.

| **Variable** | **Description** | **Value** | **Units** |
|---|---|---|---|
| a | Length of one side of the CubeSat | 0.1 | m |
| b | Length of one side of the CubeSat | 0.1 | m |
| c | Length of one side of the CubeSat | 0.1 | m |
| l | Length of the inflatable boom | 2 | m |
| r | Radius of the inflatable boom | 0.005 | m |
| w | Width of the membranes | 0.1575 | m |
| | | | |
| $m_{cubesat}$ | Mass CubeSat | 0.875 | kg |
| $m_{boom}$ | Mass inflatable boom | 0.03 | kg |
| $m_{membrane}$ | Mass of a membrane | 0.01125 | kg |
| $m_{panel}$ | Mass of the side panel | 0.05 | kg |

*Table 5 Variables used for determination of mass moments of inertia*

Using the equations in table 4 and the values for the variables in table 5, the mass moments of inertia for the different components are determined:

| **Component** | **$I_{xx}$ [kgm$^2$]** | **$I_{yy}$ [kgm$^2$]** | **$I_{zz}$ [kgm$^2$]** |
|---|---|---|---|
| CubeSat | 1.46E-03 | 1.46E-03 | 1.46E-03 |
| Inflatable boom | 0 | 0 | 7.50E-07 |
| Membrane | 3.77E-03 or 3.75E-03 | 3.75E-03 or 3.77E-03 | 2.33E-05 |
| Side panel | 4.17E-05 | 4.17E-05 | 8.33E-05 |

*Table 6 Mass moments of inertia of individual components*

The center of mass of the satellite is determined by filling in equation (5):

$$c.o.m._{satellite} = \frac{0.875*\frac{1}{2}*0.1+0.03*\left(0.1+\frac{2}{2}\right)+(4*0.01125)*\left(0.1+\frac{2}{2}\right)+0.05*(0.1+2)}{0.875+0.03+(4*0.01125)+0.05} =$$

$$= 0.23125\text{ m}$$

Now that the location of the center of mass is known, the parallel axis theorem can be applied to all moments of inertia around the x-axis or y-axis (it is not required to do this for the z-axis):

| Component | Mass moment of inertia around central axes satellite [kgm$^2$] |
|---|---|
| CubeSat | $I_{\overline{xx},cubesat} = 1.46*10^{-3} + 0.875*\left|0.05-0.23125\right|^2 = 1.46*10^{-3} + 0.0287 = 0.0302$ |
| | $I_{\overline{yy},cubesat} = 1.46*10^{-3} + 0.875*\left|0.05-0.23125\right|^2 = 1.46*10^{-3} + 0.0287 = 0.0302$ |
| Inflatable boom | $I_{\overline{xx},boom} = 0 + 0.03*\left|1.1-0.23125\right|^2 = 0.0226$ |
| | $I_{\overline{yy},boom} = 0 + 0.03*\left|1.1-0.23125\right|^2 = 0.0226$ |
| Membrane | $I_{\overline{xx},membrane} = 3.77*10^{-3} + 0.01125*\left|1.1-0.23125\right|^2 = 3.77*10^{-3} + 8.49*10^{-3} = 0.0123$ |
| | $I_{\overline{yy},membrane} = 3.75*10^{-3} + 0.01125*\left|1.1-0.23125\right|^2 = 3.75*10^{-3} + 8.49*10^{-3} = 0.0122$ |
| Side panel | $I_{\overline{xx},panel} = 4.17*10^{-5} + 0.05*\left|2.1-0.23125\right|^2 = 4.17*10^{-5} + 0.1746 = 0.1747$ |
| | $I_{\overline{yy},panel} = 4.17*10^{-5} + 0.05*\left|2.1-0.23125\right|^2 = 4.17*10^{-5} + 0.1746 = 0.1747$ |

*Table 7 Mass moments of inertia around the central axes of the complete satellite*

The last thing that has to be done is to add all individual moments of inertia for all axes. Since the membranes can have two possible orientations, it is allowed to add the moment of inertia of a membrane around the y-axis to the other moments of inertia around the x-axis. This way, the contribution of the membranes perpendicular to the x-axis to the total moment of inertia around the x-axis is simulated. It is further important not to forget that there are two membranes per axis and thus this moment of inertia has to be multiplied by 2!

$$\begin{aligned} I_{\overline{xx},satellite} &= I_{\overline{xx},cubesat} + I_{\overline{xx},boom} + 2I_{\overline{xx},membrane} + 2I_{\overline{yy},membrane} + I_{\overline{xx},panel} = \\ &= 0.0302 + 0.0226 + 2*0.0123 + 2*0.0122 + 0.1747 = \\ &= 0.2765\text{ kgm}^2 \\ I_{\overline{yy},satellite} &= I_{\overline{yy},cubesat} + I_{\overline{yy},boom} + 2I_{\overline{yy},membrane} + 2I_{\overline{xx},membrane} + I_{\overline{yy},panel} = \\ &= 0.0302 + 0.0226 + 2*0.0122 + 2*0.0123 + 0.1747 = \\ &= 0.2765\text{ kgm}^2 \\ I_{\overline{zz},satellite} &= I_{zz,cubesat} + I_{zz,boom} + 4I_{zz,membrane} + I_{zz,panel} = \\ &= 1.46*10^{-3} + 7.50*10^{-5} + 4*2.33*10^{-5} + 8.33*10^{-5} = \\ &= 0.0017\text{ kgm}^2 \end{aligned}$$

## Straw man concept design description

### Introduction

In this document, the main features of the straw man concept of the iDod are discussed. As the name already implies, this concept is a first design for the iDod structure and can be used as baseline for future designs.

The main function of the iDod is to decelerate a satellite in such a way that the satellite loses altitude and eventually burns up in the Earth's atmosphere. This de-orbit maneuver has to be completed within 25 years after the operational life of the satellite has ended. This deceleration is to be accomplished by inflating a structure that increases the frontal surface area of the satellite in the direction of flight. This will result in a larger drag force on the satellite and hence will decrease the velocity of the satellite, which in turn results in a decrease in altitude. The inflation gas has to be delivered by a so-called cold gas generator (CGG), provided by TNO.

The required size of the iDod structure will vary with satellite mass and initial altitude. Therefore, a baseline design of the iDod is made that can be adapted such that it can be applied on non-baseline satellites in non-baseline orbits. For the straw man concept, the following structure is taken (the dark gray box is the satellite):

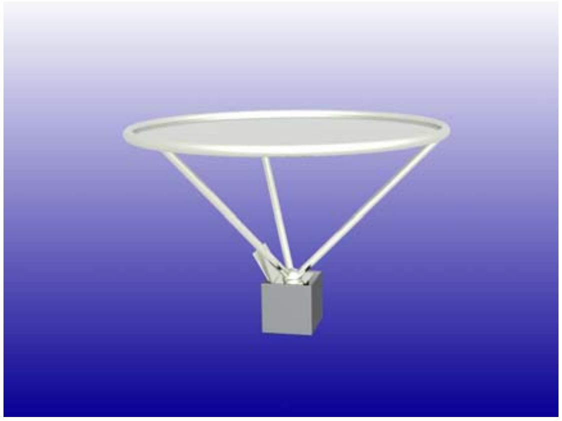

*Figure 1 iDod straw man structure in deployed state*

### Baseline orbit

The required frontal surface area of the baseline iDod design can only be determined when the baseline orbit of the satellite is specified. This orbit is defined as follows:

- Circular polar orbit (90° inclination)
- Altitude is 1000 km

### Satellite characteristics

The baseline satellite is a 1-unit CubeSat (10x10x10 cm, mass is 1.0 kg).

Simulations performed using Satellite Tool Kit (STK) 7.0.1 indicate that for the baseline design a frontal surface area of 0.315 $m^2$ is required in order to de-orbit the satellite within 25 years [van Breukelen, 2006].

The atmospheric model used for these simulations was NRLMSISE-2000. The simulations were started at Solar Minimum conditions in order to obtain the longest de-orbit time (worst-case scenario). During Solar Minimum, the activity of the sun is relatively low, which results in less heating (and thus expansion) of the Earth's atmosphere and hence a lower density at a certain altitude. This obviously results in less drag and thus a longer de-orbit time. Since the density of the atmosphere decreases exponentially with altitude, it is important to take this effect into account. When the simulation is started at Solar Maximum conditions, the de-orbit time is 24 years instead of 25 years.

An important design parameter for the iDod is the ballistic coefficient ($C_B$) of the satellite. This is a measure for how susceptive the satellite is to aerodynamic drag. A low ballistic coefficient indicates high susceptibility and therefore faster orbit decay than a high ballistic coefficient.
In order to determine the required ballistic coefficient, the frontal surface area, the mass, and the drag coefficient of the satellite have to be known. The mass is set at 1 kg and the drag coefficient ($C_D$) is set at 2.0. The mass of 1 kg is the maximum mass of a 1-unit CubeSat and the value 2.0 for the $C_D$ is a standard estimate (values are usually in the range 1.5 – 2.5). The ballistic coefficient is now equal to:

$$C_B = \frac{m}{C_D S} = \frac{1}{2*0.315} = 1.59\ kg/m^2$$

In comparison, the ballistic coefficient of a standard 1-unit cubesat is about 50 kg/m$^2$. The difference between the two ballistic coefficients is also roughly the difference in de-orbit time. Thus, when the inflatable structure is used, the satellite will de-orbit ~30 (50/1.59) times faster than the satellite without inflatable structure.

System breakdown

The entire system that will be designed can be broken down into several distinct subsystems as is depicted below.

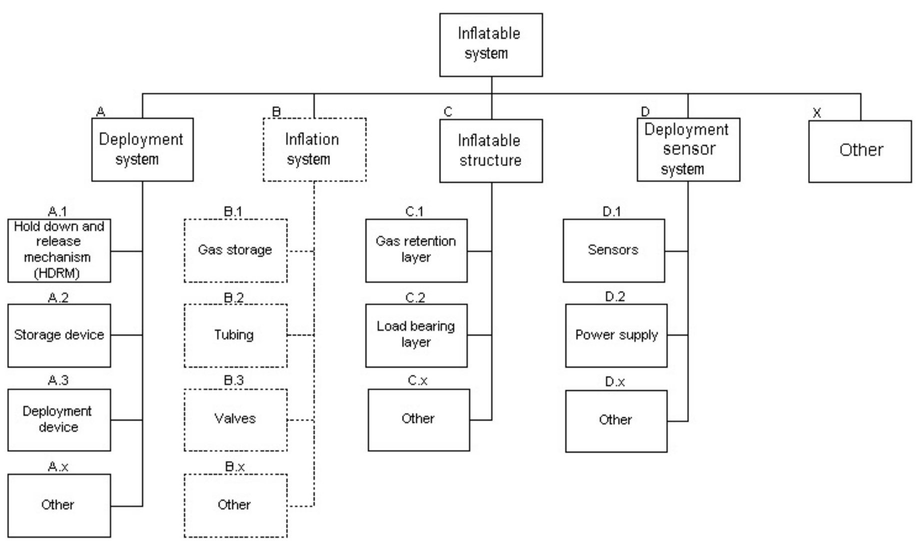


*Figure 2 Inflatable system breakdown*

For the straw man concept, the inflatable structure is studied and the required amount of inflation gas is roughly determined. All other items are left TBD.

Structural design

For the straw man concept, the frontal surface area of the satellite is increased by inflating a so-called tripod structure. This tripod has a large circular base that is connected via three inflatable struts to the CubeSat. At the base, a membrane is used to provide the required surface area. Below, the structure is depicted including some definitions and dimensions.

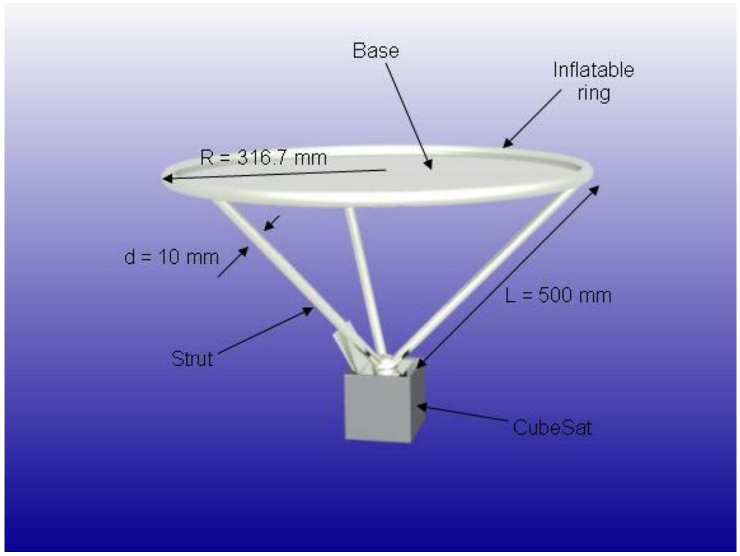


*Figure 3 Deployed iDod with definitions and dimensions*

The struts and the large inflatable ring consist out of three layers of material: two layers of Kapton HN foil with one layer of fiber/epoxy composite in between. The membrane at the base of the tripod consists out of one layer of Kapton HN.

| Property | Temperature | |
|---|---|---|
| | **23°C** | **200°C** |
| Ultimate tensile strength [MPa] | 231 | 139 |
| 3% Yield stress [MPa] | 69 | 41 |
| Young's modulus [GPa] | 2.5 | 2.0 |
| Thermal coefficient of linear expansion [ppm/°C] | 20 | 32 |
| Poisson's ratio [-] | 0.34 | 0.34 |
| Density [kg/m$^3$] | 1.42 | 1.42 |

*Table 1 Kapton HN properties [DuPont, 2006]*

The main reason for creating the offset between the CubeSat and the large membrane is the possible presence of protruding elements on the CubeSat like antennas and small solar panels. Since the actual end product should be applicable on various CubeSat designs, these protruding elements have to be avoided in order to minimize the chance of punctures or ruptures due to collision with these protruding elements during deployment. Furthermore, creating an offset between the CubeSat and the membrane has a stabilizing effect on the attitude of the satellite.

A proper material choice has not yet been made. The Kapton HN foil has been selected since it is a quite common material for space applications. The fiber/epoxy composite is as yet undefined, but for its properties (density, thickness) values from [de Groot, 2002] are used. There, the fiber/epoxy composite is a Kevlar 49 4H satin prepreg weave with a density of ~1300 kg/m$^3$ and a thickness of 0.25 mm.

| | | | |
|---|---|---|---|
| Manufacturer | | Ten Cate | |
| Fiber | | Kevlar 49, DuPont | |
| Resin system | | 8497 (epoxy) | |
| Weave | | 4H satin | |
| Cure temperature | | 125 °C | |
| Resin content | | ± 53% | |
| **Property** | | **Measured** | **Predicted** |
| Density | [kg/m$^3$] | 1293 | 1320 |
| Young's modulus | [GPa] | 21.6 | 28.1 |
| Tensile strength | [MPa] | 340 | 1340 |
| Compressive strength | [MPa] | 50 | 190 |
| Thickness | [mm] | - | 0.25 |

*Table 2 Properties of Kevlar 49 4H satin prepreg weave [de Groot, 2002]*

The dimensions of the various items of the straw man concept are as follows.

- Strut length ~500 mm
- Radius ring = 316.7 mm
- Strut diameter = inflatable ring diameter = 10 mm

The allowable mass of the entire system has for now been set to maximally 84 g. This is 50% more than the mass of a competing product, the nanoTerminator™ [Tethers Unlimited, 2006]. For the straw man concept, only the mass of the inflatable structure is estimated.

| Component | Mass determined for straw man concept? |
|---|---|
| Inflatable structure | YES |
| Inflation system | NO |
| Deployment system | NO |
| Deployment sensor system | NO |

*Table 3 Mass determination*

Inflation and rigidization

For inflation, a certain amount of gas is required. This gas is for now assumed to be $N_2$ and is delivered by a CGG. The inflation pressure is for now chosen to be constant an equal to 0.2 bar, which is a value commonly found in literature. The entire inflation procedure and control of the inflation are considered to be beyond the scope of this first design and are left TBD.

The gas that is used to inflate and support the structure will eventually be lost due to the permeability of the materials used and due to small punctures caused by space debris or small meteorites. Since there is no gas available to replenish the gas lost in this way and since the structure has to function properly during 25 years in space, it is necessary to rigidize the structure after deployment. This rigidization can be done in various ways, but none of them is easy. The rigidization method is left TBD.

Non-deployed system

The system in its non-deployed configuration is not considered for the straw man concept and left TBD.

References


1. Breukelen, E.D. van, *Determination of scenario for iDod baseline conceptual design and range of required inflatable drag surface sizes*. ISIS internal document, July 2006.

2. DuPont*, Technical Data Sheet Kapton HN,* *http://www2.dupont.com/Kapton/en_US/assets/downloads/pdf/HN_datasheet.pdf* , March 2006.

3. Groot, B.C.H. de, *Delfi-1 Inflatable Gravity Gradient Boom*, TZ report (internal document), Faculty of Aerospace Engineering, Delft University of Technology, October 2002.

4. Tethers Unlimited, Inc, *nanoTeminator$^{TM}$, End-of-Mission Deorbit Module for Nanosatellites.* *http://www.tethers.com/SpecSheets/nanoTerminator.pdf* . Viewed August 2006.

# iDod inflatable structure conceptual design trade-off


## SUMMARY

In this document, a trade-off is performed to select the most promising conceptual design for the inflatable structure of the iDod. Three different geometrical concepts are looked at: planar, pyramid, and spherical. The performance of all concepts with respect to the following criteria is determined:

1. Stowed volume
2. Mass
3. Deployment control
4. Manufacturing
5. Flexibility (ease of integration into standard CubeSat designs)

A trade-off is performed between the three concepts. This leads to the selection of a pyramid-shaped inflatable structure since it offers the best compromise between the various criteria.



## KEYWORDS

Inflatable structure, conceptual designs, trade-off, planar, pyramid, sphere


## DISTRIBUTION

| | Name | | Company/ Institution |
|---|---|---|---|
| 1 | E.D. van Breukelen | Customer | ISIS B.V. |
| 2 | B.T.C. Zandbergen | Project supervisor | TU Delft |
| 3 | O.K. Bergsma | Project supervisor | TU Delft |

## APPROVAL

| | Name | Company/ Institution | Date | Signature |
|---|---|---|---|---|
| *Written* | D.C. Maessen | TU Delft | 2/28/2007 | |
| *Checked* | | | | |
| *Approved* | | | | |

## REVISION RECORD

| Issue | Date | Total pages | Affected pages | Brief description of change |
|---|---|---|---|---|
| Draft | 11/7/2006 | 24 | | |
| Version 1.0 | 1/11/2007 | 24 | 1 | Summary shortened |
| | | | many | Document buildup changed |
| Version 1.1 | 2/28/2007 | 25 | 1 | Summary changed textually |
| | | | 4 | Instability of planar concept discussed |
| | | | 11 | Indicated that the mass and volume calculations in appendix A are incorrect |
| | | | 11, 12 | “a”, “e”, and “s” added in figure 12 |
| | | | 13 | Indicated that the stowage factor and the contingency are TBC |
| | | | 14, 15, 18 | Mass and volume of pyramid concepts multiplied by 1.5 to take into account shadowing |
| | | | 14, 18 | Table with CBE of masses and volumes added |
| | | | 15 | Indicated that the trade-off, in concurrence with the customer, is performed with no weight factors |
| | | | 16-19 | Appendix B changed into a fifth section in the body of the document |
| | | | 17 | Typing errors in formulas for volume of aluminum option corrected (factor 1.15 was missing) |
| | | | 19 | Section 6 extended. Contents of section 7 added as recommendation in section 6. |

## LIST OF TBD’S AND TBC’S

| TBD / TBC | Paragraph | Subject | Due date | Action by |
|---|---|---|---|---|
| TBC | Section 3 | Stowage factor of 3 | TBD | TBD |
| TBC | Section 3 | Contingency of 10% for adhesives | TBD | TBD |
| TBD | Section 3, section 7 | Exact size inflatable structure | TBD | E.D. van Breukelen |

## TABLE OF CONTENTS

# 1 INTRODUCTION

The current document presents a trade-off that is made between several conceptual designs for the inflatable structure of the iDod. In section 2, each design is shortly highlighted and some of its pro's and con's are assessed. In section 3 it is determined what size the inflatable structures need to be in order to have an average frontal surface area of 0.315 $m^2$ for a random orientation. Section 4 deals with the trade-off between the various options. In section 5 it is shown which mass and volume gains can be obtained by using a thinner or different rigidizing material. Conclusions and recommendations are given in section 6 and further work on this subject is shortly discussed in section 7.

# 2 CONCEPTUAL DESIGNS

In this chapter, three conceptual designs for the inflatable structure are discussed. Their main difference lies in their geometrical shape. Within each concept, several sub-concepts are possible. The three concepts are:

1. planar
2. pyramid
3. sphere

All concepts are in principle of the "attached" ballute type. A ballute is a hybrid of a parachute and a balloon (hence the name: balloon and parachute) designed to increase the aerodynamic drag of the vehicle it is attached to [Hall, 2000]. For completeness, the three basic ballute concepts are shown below.

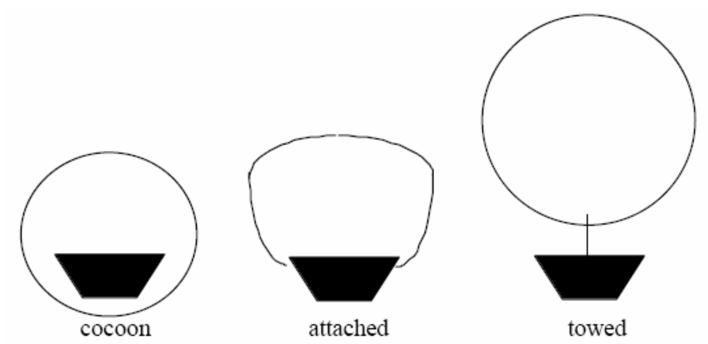


*Figure 1 The three basic ballute configurations [Hall, 2000]*

For the current application, the cocoon and the towed configuration are considered to be unpractical and are therefore not investigated. The cocoon option is simply unfeasible for an off the shelf device which the iDod is meant to be; it has to be incorporated in the entire design of the spacecraft to be feasible. The towed ballute option is not considered since the attainable shape of a towed ballute is not that much more practical than in the case of an attached ballute: it is for instance easier to obtain a spherical shape (no clearance problems), which is the most desired, but deployment issues are introduced since one or more ropes are used to create an offset between the sphere and the CubeSat. In case of a tumbling satellite, the rope can be wrapped around the structure of the satellite after deployment, introducing a high risk of cutting of the rope and of the rope getting stuck behind something. If the rope(s) fail(s) for some reason during the operational life of the de-orbit device, the ballute is severed from the CubeSat. It is far less risky to use a rigid attachment, resulting in an attached ballute.

The discussion of the concepts will focus mainly on their performance with respect to the following trade-off criteria:

- Stowed volume
- Mass
- Deployment control
- Manufacturing
- Flexibility (ease of integration into standard CubeSat designs)

It is noted that only the functionality of the geometry of the inflatable structure is assessed. Thus, deployment methods, inflation methods, rigidization methods, etc. do not come into play for this trade-off. Materials do come into play, but only to assess the mass and the stowage volume of the concepts.

## 2.1 Planar concept

For the current concept, altitude reduction is obtained by exposing a large planar surface to atmospheric drag. Within this concept, two options are possible: the original straw man concept and a revised straw man concept.

A disadvantage of this concept over the other two concepts is that it is not stable. It will thus not assume a constant orientation even at relatively low altitudes (< ~600 km). In appendix A, it is determined that this concept needs to have a planar surface area of 7772 $cm^2$ in case of random orientation. If the current concept would be stable at lower altitudes, it would have a much larger frontal surface area than the other two concepts and would therefore de-orbit faster, which is an advantage. However, since it is not stable, it will continue to rotate "randomly", as discussed in [Maessen, iDod.TN.009] and will therefore still have an average frontal surface area of 3150 $cm^2$, which is equal to the frontal surface area of the other two concepts at low altitudes.

### *2.1.1 Straw man concept*

The first concept is the original straw man concept, extensively treated in [Maessen, iDod.DD.001]. It features three inflatable struts and a large inflatable torus that supports a Kapton membrane.

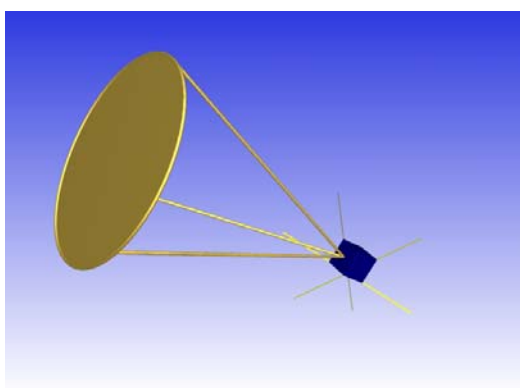

*Figure 2 Straw man concept*

*Manufacturing*

Manufacturing of the structure is rather complicated since it is not possible to construct a perfectly round inflatable torus from non-stretchable materials like Kapton without excessive wrinkling and deformation in the inflated state. A larger tube radius for the ring will alleviate this problem, but is not desired for obvious reasons (larger mass, volume, more gas required, etc.). To avoid wrinkling, the torus has to be built up out of multiple straight sections leading to a multi-cornered shape. However, this is very time-consuming work and all bonds between the straight sections need to be airtight, which introduces a quality issue.

*Deployment control*

The deployment of this structure will be quite straight if the three struts are inflated at the same pace. They will then restrain each other's sideway movement. Contact with protruding elements on the CubeSat during deployment is thus not likely.

*Flexibility*

The flexibility of this structure depends on the angle of the struts with respect to the surface normal vector of the side of the CubeSat they are attached to. The larger this angle, the more chance of interference with a protruding element and therefore the less flexible the structure is. The analysis in chapter 3 shows that the membrane radius needs to be 49.8 cm, which leads to a strut length of 44.9 cm for an angle of 29°, indicating reasonably good flexibility.

### 2.1.2 Revised straw man concept

The original straw man concept has a big disadvantage when it comes to manufacturing of the inflatable torus. In light of this drawback, it is better to replace the torus by a square or a triangle, leading to the structures depicted below.

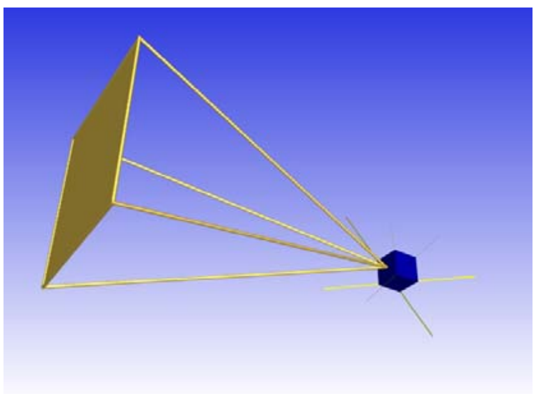

*Figure 3 Square straw man concept*

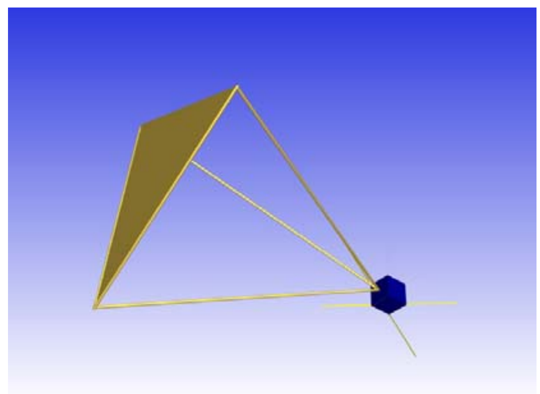

*Figure 4 Triangular straw man concept*

*Manufacturing*

For both options, the structure that caries the large membrane now consists entirely out of a few simple straight tubes, which is much simpler to produce than the many segmented torus. This concept therefore scores better than the original straw man concept with respect to manufacturing.

*Deployment control*

Deployment control of this concept is considered just as good as that of the straw man concept.

*Flexibility*

The flexibility of this concept is considered just as good as that of the straw man concept.

## 2.2 Pyramid concept

This concept utilizes a pyramid-shaped structure. It is very similar to the previous concept; the only difference is that the membrane is in this case not situated at the base of the pyramid, but at its sides.

### 2.2.1 Hollow

In the first option for the pyramid concept, the sides of the pyramid are utilized for structural support ánd for generation of the required frontal surface area. The interior of the pyramid is empty. Structural support is provided by inflatable struts that are positioned at the ribs of the pyramid. The required frontal surface area is provided by a Kapton membrane that is spanned between the inflatable ribs. The next figures depict examples of this concept.

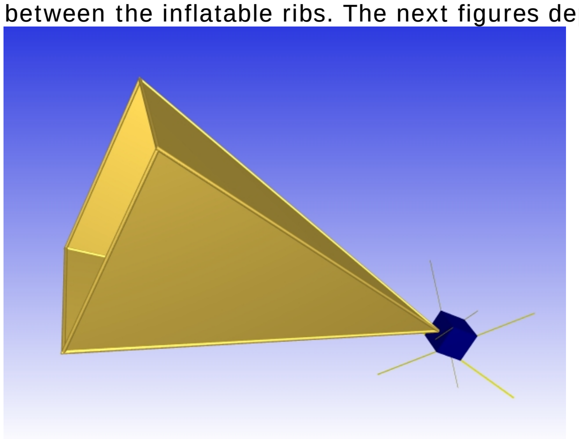

*Figure 5 Square pyramid*

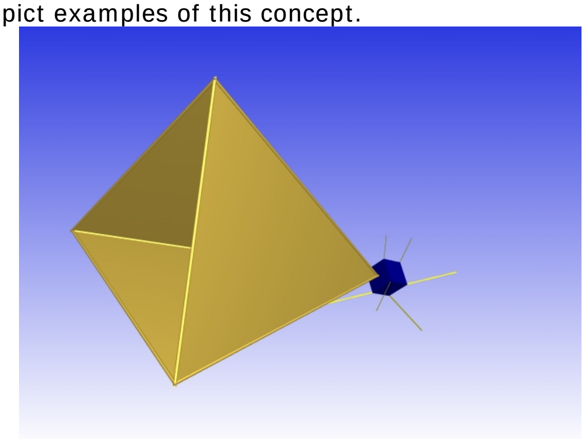

*Figure 6 Triangular pyramid*

The advantage of placing the membrane at the sides of the pyramid is that the frontal surface area of the entire satellite is now substantial for every possible attitude. Thus, the attitude of the spacecraft is now less important in terms of de-orbit performance than for the planar concepts. This design is therefore largely in accordance with the recommendation done in [Maessen, iDod.TN.009] that the frontal surface area of the satellite should be insensitive to the attitude of the satellite since passive attitude control is impossible to achieve at high altitudes for the current application.

*Manufacturing*

Like the revised straw man concept, this concept is regarded to outperform the original straw man concept with respect to manufacturability.

*Deployment control*

Deployment control might be less good than that of the planar concepts since the Kapton membranes now restrict the way in which the inflatable tubes can be folded and stowed. However, nothing definitive can be said about this since folding and stowage has not yet been investigated thoroughly.

*Flexibility*

The flexibility of this concept is regarded equally good as that of the planar concepts.

### 2.2.2 Gravity gradient

The underlying thought for this concept is: don't fight it, use it! The gravity gradient effect is caused by the Earth's gravity and, when large enough, results in the axis of minimum mass moment of inertia of a satellite to be aligned with the nadir vector. In other words: it will cause that axis to always be pointed towards the center of the Earth. This is beneficial since then the attitude of the spacecraft is more or less fixed, making a more efficient inflatable structure design possible. The workings of this concept are explained in more detail in [Maessen, iDod.TN.009].

The concept is shown in the next figure. It employs one central inflatable boom that pushes one side panel of the CubeSat away from the rest of the CubeSat. This mass offset is required to enhance the gravity gradient effect. At the panel, four more inflatable tubes (in the shape of a cross) are situated. Between these four tubes, membranes are spanned such that a frontal surface area of 0.315 $m^2$ is created once the torque due to atmospheric drag overcomes the gravity gradient torque (below ~400 - 500 km) and the spacecraft starts to behave like a shuttlecock. To provide enough frontal surface area before this happens, membranes are spanned between the central strut and the four tubes.

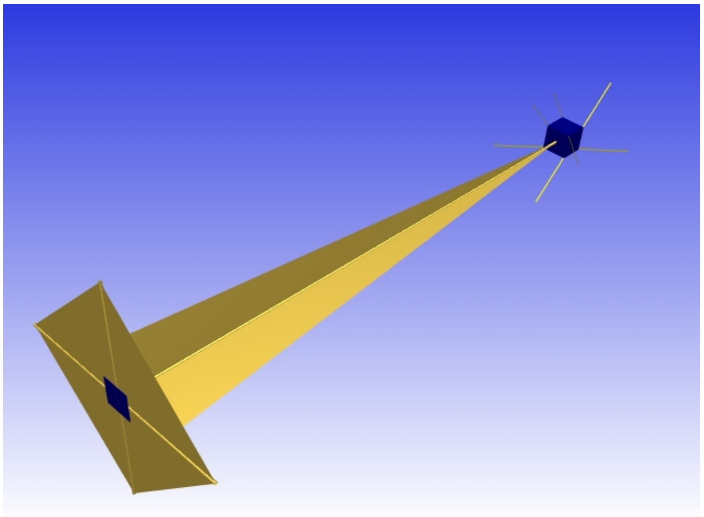

*Figure 7 Gravity gradient concept*

Unfortunately for this concept, the analysis performed in [Maessen, iDod.TN.009] points out that this concept is impossible to create under the requirements imposed on it. The length of the inflatable boom would need to be roughly 3 meters with a side panel mass of 100 grams. This results in a total mass that is much larger than the total allowable system mass of 100 grams. With respect to stowage the problems are comparable to other concepts, since they use multiple struts that are in total also several meters long. However, manufacturing a 3 meter long tube with a diameter of 1 cm is regarded as being problematic at the very least. Furthermore, even if it can be made light and small enough, it would still not be applicable on CubeSats that employ permanent magnets for attitude control (see [Maessen, iDod.TN.009]). Therefore, this concept is not feasible.

### *2.2.3 Hybrid*

Although unfeasible, the gravity gradient concept does have a feature which is beneficial with respect to mass and volume. It namely employs only one central strut and four smaller ‘spokes’ to create a pyramid shape. The hollow pyramid concept requires four long struts, which leads to a much larger mass and volume for the same pyramid height. Therefore, a hybrid between these two concepts is created that utilizes one central strut and four inflatable spokes for structural support. The gravity gradient effect is not utilized. The frontal surface area is provided by membranes which are situated at the sides of the pyramid and are attached to the spokes and the CubeSat.

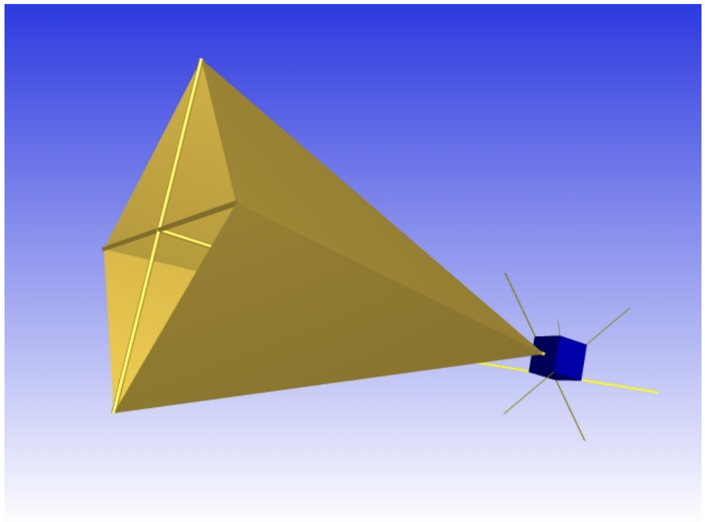

*Figure 8 Hybrid pyramid*

*Manufacturing*

The biggest manufacturing problem for this concept is the point where the five inflatable tubes meet. Here, a connector needs to be created that provides and airtight connection between these tubes. This connector is preferred to be flexible since that reduces the required stowage volume of the structure. However, manufacturing of this concept is not deemed to be more complex than manufacturing of the other concepts since there also connector pieces are required to link tubes. The number of connections per connector is less for the other concepts, but the total number of connectors is larger. Therefore, manufacturing of this concept is considered equally difficult as manufacturing of the revised straw man concept or the hollow pyramid. It might even be less difficult, since only one connection point is required here whereas there are at least three connector points required for the other concepts.

*Deployment control*

Controlling the deployment of this concept is more challenging than controlling the deployment of the other concepts. This is due to the presence of only one central strut instead of three or four struts. Multiple struts can restrict each other's movement, but this is not the case for the current concept. Standard methods to ensure straight deployment of a tube are considered impractical for the current application and thus this structure is expected to impair a large amount of lateral displacement during deployment. This negative aspect is alleviated to some degree since the width of the structure during initial deployment will be relatively small, since the spokes are not yet inflated, and therefore the chance of hitting protruding elements will remain small.

*Flexibility*

The flexibility is this concept is considered equally good as that of all the previous concepts.

## 2.3 Spherical concept

The great advantage of using an inflatable spherical balloon is that its frontal surface area is always 0.315 $m^2$, irrespective of the attitude of the spacecraft. In order to reduce the amount of mass required for inflating the balloon and in order for the structure to be rigidizable, inflatable tubes are used. These tubes are exactly the same (diameter, materials) as the ones used for the other concepts.

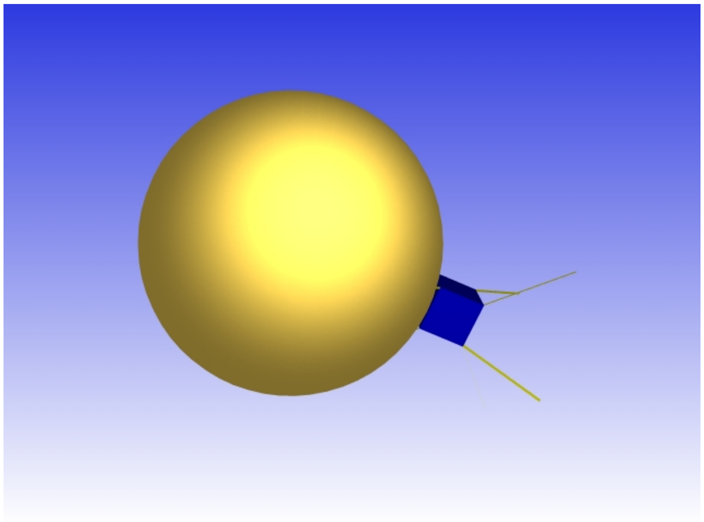

*Figure 9 Spherical concept*

*Manufacturing*

Manufacturing of this structure is more involved than the other concepts since round shapes need to be created from tubes and flat membranes. For structural support, two circular tubes can be used that are positioned perpendicular to each other. This requires the least amount of mass and volume. However, the inflatable tubes need to be held in place in some way in order to achieve a proper spherical shape. This is not required for the other concepts.
When a tube is used that spirals upwards along the surface of the sphere, manufacturing and shape control is somewhat easier, but the required tube length is likely to be larger than in case two circular tubes are used (albeit not very much).
The next figure depicts an early conceptual drawing for the so-called "Inflate-A-Brake" de-orbit device [Cowan, 2004] which is very similar to the current concept. The number of ribs that are depicted there is far larger than what is assumed for this concept.

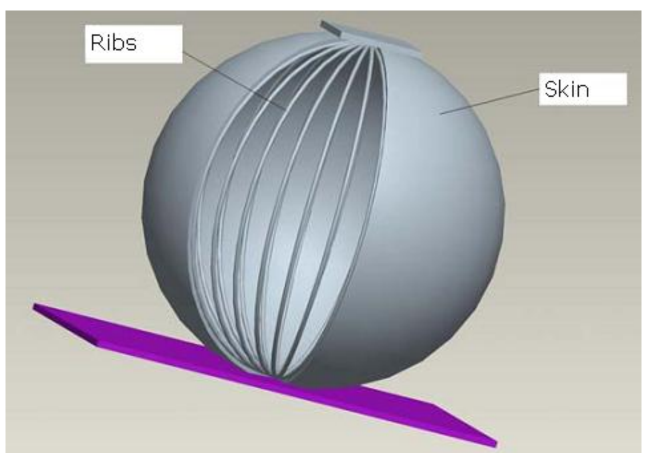


*Figure 10 Inflate-A-Brake balloon concept [Cowan, 2004]*

*Deployment control*

The deployment characteristics of this concept will be good since the inflatable tubes constrain each other's movement, resulting in a deployment envelope that is close to the size of the structure itself.

*Flexibility*

As is obvious from figure 9, the amount of clearance with respect to protruding elements of the CubeSat is bad for this concept. This results in an inflexible product that cannot be applied on as much CubeSats as the other concepts.

# 3 REQUIRED SIZE OF EACH CONCEPT

The performance of each concept with respect to mass and stowed volume can only be known when the required size of the concept is determined.
Since passive attitude control is not feasible above an altitude of ~ 450-650 km [Maessen, iDod.TN.009], it is assumed that the spacecraft has a random orientation above this altitude range. The spacecraft is thus free to rotate around all three of its body axes (assuming a body fixed Cartesian coordinate system).
For each concept, it is determined what its size should be in order for it to present an average frontal surface area of 3150 $m^2$ in the direction of flight when the satellite is rotated around the vectors perpendicular to its velocity vector.

## 3.1 Method

Using trigonometry, the dimensions of the various concepts can be determined such that their average frontal surface area is approximately 3150 $cm^2$, as required. In the calculations, the frontal surface area of the CubeSat is neglected. This will not lead to large errors since the maximum frontal surface area of the CubeSat is about 6% of the required 3150 $cm^2$.

The dimensions of the concepts are determined by calculating the average frontal surface areas of the shapes out of which the concept exists. These are in essence squares, triangles and circles. When these 2D shapes are rotated around an in-plane axis, their projected surface area varies as a function of the rotation angle and can be described by analytical functions. Integrating these functions over the total rotation angle and dividing this by the total rotation angle results in the average projected area. When the results for the 2D shapes are properly combined, the dimensions for the 3D concepts can be distilled.

Since the calculations are too long to present here, they are described in appendix A. It is noted that in those calculations, shadowing is NOT taken into account. This leads to underestimations for the required size of the pyramid concepts. Therefore, the mass and volume calculated for those concepts is multiplied by a factor 1.5 later on in this section. The dimensions that are calculated are not altered. Instead, this is left TBD in a more exact way in a later stage.

## 3.2 Results

The results obtained by using the method described in the previous subsection are now given. First, the required dimensions of each concept (as determined in appendix A) are provided. After that, the implications on mass and stowed volume are determined.

### *3.2.1 Required size*

In appendix A, it is determined that the membranes for the planar concepts need to have a total area of 7772 $cm^2$. This information can be used to determine the size of the various membrane shapes, but cannot be used to determine the offset of the membranes from the CubeSat. To determine the required offset for the planar concepts, the half angle of the pyramid concepts is used. The half angle is the angle between the line perpendicular to the upper face of the CubeSat and one side of the pyramid. The definition for the half angle and for the height (h) of the pyramid is graphically shown in the next figures. The edges of the base of the pyramid have length “a”, the sides of the pyramid have a *slant height* “s”, and the skewed edges of the pyramid have an *edge length* “e”.

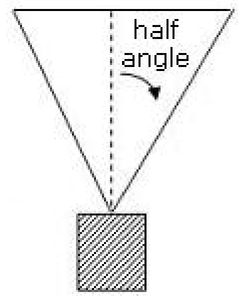


Figure 11 Half angle

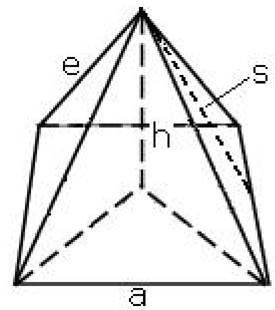


Figure 12 Pyramid with length definitions

The slant height s of the sides of the pyramid is determined using [Weisstein, 2006]:

$$s_{square} = \sqrt{h^2 + \frac{1}{4}a^2}$$

$$s_{triangle} = \sqrt{h^2 + \frac{1}{12}a^2}$$

The half angle $\theta$ is computed using the following equation:

$$\theta = a\cos\left(\frac{h}{s}\right)$$

In appendix A, the height and base side length of the square pyramid are determined to be 50 cm and 56.12 cm respectively. For the triangular pyramid, the values are 45 cm and 85.29 cm. This leads to slant heights of 57.34 cm and 51.30 cm for the square and triangular pyramid respectively. For the square pyramid and the triangular pyramid, the half angles are now computed to be 29.3° and 28.7° respectively.
Since both angles are roughly the same, an angle of 29° is assumed for the planar concepts. Using the goal seek routine in Microsoft Excel, the height of the planar concepts is determined. For the straw man concept, it is assumed that its struts are positioned such that their connection points with the circular membrane lie on the corners of an equilateral triangle that fits precisely inside the circular membrane. The length of a side "a" of this triangle is computed using the following formula [Weisstein, 2005]:

$$R_{circle} = \frac{1}{3}\sqrt{3}a$$

Where $R_{circle}$ is the radius of the circular membrane. The length of a side of this equilateral triangle is thus 86.15 cm. Knowing this value allows calculation of the height for the straw man concept.

The results for all concepts (except the hybrid pyramid, its result is the same as that of the square pyramid) are given in table 1:

| Concept | | Size |
|---|---|---|
| **Planar** | Straw man | Height = 44.87 cm, base diameter = 99.5 cm |
| | Revised straw man (square) | Height = 79.56 cm, base side length = 88.2 cm |
| | Revised straw man (triangle) | Height = 69.78 cm, base side length = 134.0 cm |
| **Pyramid** | Square | Height = 50 cm, base side length = 56.1 cm |
| | Triangle | Height = 45 cm, base side length = 85.3 cm |
| **Sphere** | Balloon | Diameter = 63.3 cm |

*Table 1 Required size of each concept*

### *3.2.2 Mass and stowed volume*

Using material data from [Maessen, iDod.DD.001], the inflatable tube mass and volume per meter tube length and the membrane mass and volume per $cm^2$ can be calculated. Assuming a thickness of 0.25 mm for the fiber/epoxy composite layer and a thickness of 25 microns for the Kapton layers, the mass per meter length of an inflatable tube with a radius of 5 mm is 12.78 grams (assuming 15% overlap to create a lap joint for the Kapton layers). The volume per meter tube length is 9.66 $cm^3$. The membrane mass per $cm^2$, assuming a Kapton thickness of 25 microns, is 0.00355 grams. The volume per $cm^2$ is $2.5*10^{-3}$ $cm^3$. The stowed volume is estimated by multiplying the physical volume of the structure by a factor 3 (TBC).
It is noted that in the coming calculations, the mass of connections and adhesives is *not* taken into account. Instead, a contingency of 10% (TBC) is added to the obtained masses and volumes.

| | |
|---|---|
| Tube mass per meter [g] | 12.78 |
| Tube volume per meter [$cm^3$] | 9.66 |
| Membrane mass per $cm^2$ [g] | 0.00355 |
| Membrane volume per $cm^2$ [$cm^3$] | $2.5*10^{-3}$ |
| Packing factor [-] | 3 |

*Table 2 Assumptions made for mass and volume calculations*

For the pyramid concepts, the membrane area per side of the pyramid is determined using the following equation:

$$A_{side} = \frac{1}{2}as$$

The length of the struts of the hollow pyramids and the planar concepts is the same as the *edge length* e (see figure 12) of a pyramid and is determined using [Weisstein, 2006]:

$$e_{square} = \sqrt{h^2 + \frac{1}{2}a^2}$$

$$e_{triangle} = \sqrt{h^2 + \frac{1}{3}a^2}$$

Now, all necessary information is available to determine the total tube length and the total membrane area for all concepts. These are provided in the next table:

| Concept | | Total tube length [m] | Total membrane area [$cm^2$] |
|---|---|---|---|
| **Planar** | Straw man | 5.13 | 7772 |
| | Revised straw man (square) | 7.57 | 7772 |
| | Revised straw man (triangle) | 7.14 | 7772 |
| **Pyramid** | Hollow (square) | 4.80 | 6435 |
| | Hollow (triangle) | 4.56 | 6562 |
| | Hybrid | 2.09 | 6435 |
| **Sphere** | Balloon | 3.98 | 12600 |

*Table 3 Tube length and membrane area for each concept*

Knowing the total tube length and membrane area for each concept allows calculation of its mass and volume using the information from table 2.
As example, the mass of the straw man concept and the stowed volume of the straw man concept are calculated below:

- The radius "r" of the base of the structure is 49.74 cm, the required membrane area "A" is A = 7772 $cm^2$. This weighs 0.00355*7772 = 27.59 grams.
- The circumference "c" of the base of the structure is $2\pi r$ = 312.53 cm, which is equal to the length of the circular inflatable tube at the base.
- The height "h" of the structure is 44.87 cm, this leads to a strut length "L" of $\sqrt{(44.87^2 + 49.74^2)}$ = 66.99 cm. Three struts then have a total length of 3*66.99 = 201 cm.
- The total length of all inflatable tubes is 312.53 + 201 = 513.49 cm, thus they weigh in total 513.49/100*12.78 = 65.62 grams.
- The total mass "$m_{total}$" of the structure is then 27.59 + 65.62 = 93.21 grams.
- With 10% contingency, the total mass is: 93.21*1.1 = 102.53 grams.

- The volume "$V_{membrane}$" of the circular membrane is $7772*2.5*10^{-3}$ = 19.43 $cm^3$.
- The volume "$V_{tubes}$" of all tubes combined is 513.49/100*9.66 = 49.60 $cm^3$
- The stowed volume "$V_{total}$" of the complete structure is then: 3*(19.43 + 49.60) = 207.1 $cm^3$
- With 10% contingency, the stowed volume is: 207.1*1.1 = 227.81 $cm^3$

The "*Current Best Estimate*" (CBE) of the masses and volumes (thus without contingency) for all concepts are depicted in the next table. It is noted that for the pyramid concepts, the mass and volume are multiplied by 1.5 to take into account the underestimation of their size as determined in appendix A.

| Concept | | Volume [$cm^3$] | Stowed volume [$cm^3$] | Mass [g] |
|---|---|---|---|---|
| **Planar** | Straw man | 69 | 207 | 93 |
| | Revised straw man (square) | 93 | 278 | 124 |
| | Revised straw man (triangle) | 88 | 265 | 119 |
| **Pyramid** | Hollow (square) | 93 | 279 | 126 |
| | Hollow (triangle) | 90 | 270 | 123 |
| | Hybrid (square) | 55 | 164 | 75 |
| **Sphere** | Balloon | 70 | 210 | 96 |

*Table 4 Required stowed volume and mass per concept (CBE)*

The masses and volumes, including 10% contingency, for all concepts are depicted in the below table:

| Concept | | Volume [$cm^3$] | Stowed volume [$cm^3$] | Mass [g] |
|---|---|---|---|---|
| **Planar** | Straw man | 76 | 228 | 103 |
| | Revised straw man (square) | 102 | 305 | 137 |
| | Revised straw man (triangle) | 97 | 292 | 131 |
| **Pyramid** | Hollow (square) | 102 | 307 | 139 |
| | Hollow (triangle) | 99 | 297 | 135 |
| | Hybrid (square) | 60 | 180 | 82 |
| **Sphere** | Balloon | 77 | 231 | 105 |

*Table 5 Required stowed volume and mass per concept (10% contingency)*

The table shows that a triangular structure is slightly more efficient in terms of mass and stowed volume than a square structure. However, manufacturing of a square structure is deemed easier because of the nice 90° angles and because of the shorter tubes required. Furthermore, although the half angle for both structures is almost the same, the square structure is considered to perform better with respect to clearance. This is explained by not looking to the half angle, but at the angle between the central axis of the pyramid shape and a strut on an edge of the pyramid shape. For the square option, this angle is 38.4° ($\tan^{-1}(½\sqrt{2}*56.1/50)$) while it is 47.6° for the triangular option ($\tan^{-1}(1/3\sqrt{3}*85.3/45)$).
Therefore, the trade-off in the next chapter will treat the square version of the revised straw man concept and the square version of the hollow pyramid concept.

It is already visible that the hybrid pyramid outperforms all other concepts with respect to mass and volume and is close to meeting the requirements. However, it is believed to be possible to reduce the thickness of the fiber/epoxy layer to 0.1 mm instead of 0.25 mm. The influence of this reduction in thickness on the mass and volume of the hybrid concept is explored in section 6. There, also the effect of using an aluminum foil instead of composite material is investigated.

# 4 TRADE-OFF

The trade-off criteria on which the concepts are judged are:

- Stowed volume
- Mass
- Deployment control
- Manufacturing
- Flexibility (ease of integration into standard CubeSat designs)

Throughout the previous chapters, the performance of each concept with respect to these criteria has been discussed. The result of these discussions is summarized in the next table where each concept is awarded a score for each criterion. The scores are either their calculated performance with respect to a criterion or are of the form: --, -, 0, +, or ++ with –- meaning very poor performance and ++ meaning excellent performance.

It is noted that, in concurrence with the customer, in this trade-off no weight factors are applied. For clarity, it is repeated that the square versions of the concepts are used in trade-off. The trade-off is conducted in a similar fashion as discussed in [Hamann, 2004].

| Concept | | Volume | Mass | Manufacturing | Deployment | Flexibility |
|---|---|---|---|---|---|---|
| **Planar** | Straw man | 76 | 103 | - | + | + |
| | Revised straw man | 102 | 137 | + | + | + |
| **Pyramid** | Hollow | 102 | 139 | + | 0 | + |
| | Hybrid | 60 | 82 | + | 0 | + |
| **Sphere** | Balloon | 77 | 105 | - | ++ | - |

*Table 6 Trade-off*

From the trade-off table, it is clear that the hybrid pyramid concept outperforms all other concepts with respect to mass and volume. With respect to manufacturing, deployment, and flexibility it is second only to the square version of the revised straw man concept. Therefore, the hybrid pyramid concept is selected as being the best concept.

# 5 ANALYSIS FOR REDUCED MATERIAL THICKNESS

In light of the foregoing conclusions, it is investigated what the effect will be of using a thinner composite layer of 0.1 mm thickness or of using an aluminum foil of 25 microns thickness (assumed density of 2700 kg/m$^3$) for the tubes. This is done for the hybrid pyramid concept. Structural integrity will not be in jeopardy by reducing the wall thickness since the forces on the structure are extremely small [Maessen, iDod.TN.002 & iDod.TN.004].

The table below provides an overview of the symbols and their properties used in the coming calculations.

| Symbol | Description | Value | Unit |
|---|---|---|---|
| $\rho_{alu}$ | Aluminum density | 2.7 | g/cm$^3$ |
| $\rho_{comp}$ | Composite density | 1.3 | g/cm$^3$ |
| $\rho_{Kapton}$ | Kapton density | 1.42 | g/cm$^3$ |
| | | | |
| $t_{alu}$ | Aluminum thickness | 2.5E-3 | cm |
| $t_{comp1}$ | Composite thickness 1 | 0.025 | cm |
| $t_{comp2}$ | Composite thickness 2 | 0.01 | cm |
| $t_{Kapton}$ | Kapton thickness | 2.5E-3 | cm |
| | | | |
| A | Area | | cm$^2$ |
| a | Base width | 56.12 | cm |
| h | Height | 50 | cm |
| L | Length | 100 | cm |
| M | Mass per cm$^2$ | | g/cm$^2$ |
| m | Mass | | g |
| r | Tube radius | 0.5 | cm |
| s | Slant height | | cm |
| V | volume | | cm$^3$ |

*Table 7 Symbols used in this section and their values*

Knowing the density of the materials and the thickness of the materials, their mass per cm$^2$ of surface area is determined in the following manner:

$$M = \rho \cdot t$$

The total area of material used (per meter tube) for the composite or aluminum layer is:

$$A = 2\pi \cdot r \cdot L$$

Since two layers of Kapton are used in a tube [Maessen, iDod.DD.001], the total Kapton area is:

$$A_{Kapton} = 2A$$

The mass of a layer per meter tube length is now:

$$m_{comp} = A \cdot M_{comp}$$
$$m_{alu} = A \cdot M_{alu}$$
$$m_{Kapton} = 2A \cdot M_{Kapton}$$

Including a 15% contingency for bond overlap for the Kapton and the aluminum:

$$m_{alu} = 1.15 \cdot A \cdot M_{alu}$$
$$m_{Kapton} = 1.15 \cdot 2A \cdot M_{Kapton} = 2.3 \cdot A \cdot M_{Kapton}$$

The total mass per meter tube length is now:

$$m_{total,comp} = m_{comp} + m_{Kapton} = AM_{comp} + 2.3AM_{Kapton} = A\left(M_{comp} + 2.3M_{Kapton}\right)$$
$$m_{total,alu} = m_{alu} + m_{Kapton} = AM_{alu} + 2.3AM_{Kapton} = A\left(M_{alu} + 2.3M_{Kapton}\right)$$

The volume of a layer of material is (including the 15% contingency for the Kapton layer):

$$V_{comp} = A \cdot t_{comp}$$
$$V_{alu} = 1.15 \cdot A \cdot t_{alu}$$
$$V_{Kapton} = 1.15 \cdot 2A \cdot t_{Kapton} = 2.3At_{Kapton}$$

The total volume per meter tube length:

$$V_{total,comp} = V_{comp} + V_{Kapton} = A\left(t_{comp} + 2.3t_{Kapton}\right)$$
$$V_{total,alu} = V_{alu} + V_{Kapton} = A\left(1.15t_{alu} + 2.3t_{Kapton}\right)$$

The below table presents the mass, area, and volume for each separate material per meter tube length:

| **Material** | **M [g/cm$^2$]** | **A [cm$^2$]** | **m [g]** | **V [cm$^3$]** |
|---|---|---|---|---|
| Kapton | 0.00355 | 628.32 | 2.23 | 1.81 |
| Aluminum | 0.00675 | 314.16 | 2.12 | 0.90 |
| 0.25 mm comp | 0.0325 | 314.16 | 10.21 | 7.85 |
| 0.1 mm comp | 0.0130 | 314.16 | 4.08 | 3.14 |

*Table 8 Mass, area and volume for each material*

Now, the mass and volume for the three different tubes is determined by combining the values found in the above table (tube 1 has a composite thickness of 0.25 mm, tube 2 has a composite thickness of 0.1 mm, and tube 3 has aluminum foil instead of a composite layer):

| | Mass [g] | Volume [cm$^3$] | Stowed volume [cm$^3$] |
|---|---|---|---|
| Tube 1 ($t_{comp}$ = 0.25 mm) | 12.78 | 9.66 | 29.27 |
| Tube 2 ($t_{comp}$ = 0.1 mm) | 6.65 | 4.95 | 14.99 |
| Tube 3 (aluminum) | 5.00 | 2.71 | 8.21 |

*Table 9 Mass and volume per meter tube length*

The total area of the Kapton membrane at the sides of the inflatable structure is:

$$A_{membranes} = 4A_{side} = 4\cdot\frac{1}{2}as = 2a\sqrt{h^2+\frac{1}{4}a^2} = 2\cdot 56.12\cdot\sqrt{50^2+\frac{56.12^2}{4}} = 6435.34\text{ cm}^2$$

Since it is expected that only a very small amount of material is required to connect the membranes to the tubes and the CubeSat (in comparison to the area determined above), a contingency of 1% is taken into account on top of the calculated membrane area for connections:

$$A_{membranes} = 1.01\cdot 6435.34 = 6500\text{ cm}^2$$

Knowing that the total tube length is 2.09 m, the mass and volume of the hybrid pyramid is determined for the three different tube configurations:

$$m_{pyramid} = 2.09m_{tube} + A_{membranes}\cdot t_{Kapton}\cdot\rho_{Kapton}$$
$$V_{pyramid} = 2.09V_{tube} + A_{membranes}\cdot t_{Kapton}$$

The result for the three different configurations, with no contingency on mass and volume, is:

| | Mass [g] | Volume [cm$^3$] | Stowed volume [cm$^3$] |
|---|---|---|---|
| $t_{comp}$ = 0.25 mm | 49.78 | 36.44 | 109.32 |
| $t_{comp}$ = 0.1 mm | 36.97 | 24.18 | 72.54 |
| Aluminum | 30.48 | 19.92 | 59.76 |

*Table 10 Hybrid pyramid mass and volume*

Multiplying all masses and volumes by 1.5 results in the following CBEs:

| | Mass [g] | Volume [cm$^3$] | Stowed volume [cm$^3$] |
|---|---|---|---|
| $t_{comp}$ = 0.25 mm | 74.67 | 54.66 | 163.98 |
| $t_{comp}$ = 0.1 mm | 55.46 | 36.27 | 108.81 |
| Aluminum | 45.72 | 29.88 | 89.64 |

*Table 11 CBE for hybrid pyramid mass and volume*

The final result for the three different configurations, including a 10% contingency on mass and volume, is:

| | Mass [g] | Volume [cm$^3$] | Stowed volume [cm$^3$] |
|---|---|---|---|
| $t_{comp}$ = 0.25 mm | 82.14 | 60.13 | 180.38 |
| $t_{comp}$ = 0.1 mm | 61.01 | 39.90 | 119.69 |
| Aluminum | 50.29 | 32.87 | 98.60 |

*Table 12 Hybrid pyramid mass and volume (10% contingency on CBE)*

In percentages:

| | Mass [%] | Volume [%] |
|---|---|---|
| $t_{comp}$ = 0.25 mm | 100 | 100 |
| $t_{comp}$ = 0.1 mm | 74.3 | 66.4 |
| Aluminum | 61.2 | 54.7 |

*Table 13 Differences between configurations in %*

The obvious winner here is the aluminum layer, but it is also clear that it pays to reduce the thickness of the composite layer.

# 6 CONCLUSIONS & RECOMMENDATIONS

From the foregoing, it is concluded that a hybrid between the square pyramid concept and the gravity gradient concept is the best solution. This concept is however too massive (82 g) and too voluminous (stowed volume of 180 $cm^3$) when the materials selected for the straw man concept are used and the required average frontal surface area is 3150 $cm^2$.

The hybrid pyramid is built up as follows. One central inflatable tube creates the required height, while inflatable “spokes”, extending from the central tube, are used to shape the base of the pyramid. The pyramid is attached at its top to the CubeSat. The sides of the pyramid consist out of Kapton membranes in order to provide the required surface area. The membranes are attached to the inflatable “spokes” and to the CubeSat.

It is recommended to reduce the wall thickness of the inflatable tubes in any case. This results in less mass and volume for the inflatable structure and can be done by reducing the thickness of the rigidizing material. Structural integrity will not be in jeopardy by reducing the wall thickness since the forces on the structure are extremely small [Maessen, iDod.TN.002 & iDod.TN.004].

It is recommended that the rough determination of the average frontal surface area performed analytically in appendix A, is performed in a graphical manner using special software. This will allow for a more exact determination of the average frontal area.

When the exact dimensions of the inflatable structure have been determined and when reducing the wall thickness of the tubes still results in a too large mass or volume, then it is recommended to reduce the starting altitude for the de-orbit maneuver. This results in a smaller required frontal surface area and thus in even less mass and volume.

# 7 FURTHER WORK

No further work on this trade-off is foreseen during this thesis.

# REFERENCES

1. Breukelen, E.D. van, *Top Level Requirements for inflatable De-orbit device (iDod),* ISIS document ISIS.iDod.REQ, July 2006.

2. Cowan, T., et. al., *Inflate-A-Brake – A Gossamer Structures Technology Demonstrator for De-orbiting Pico-satellites*, University of Florida (USA), submitted to the FUNSAT design competition, December 13, 2004.

3. Hall, J.L., *A review of ballute technology for planetary aerocapture*, Jet Propulsion Laboratory, California (USA), presented at the 4th AIAA Conference on Low Cost Planetary Missions, May 2-5, 2000.

4. Hamann, R.J., Tooren, M.J.L. van, *Systems Engineering & Technical Management Techniques,* Lecture notes issue 1, Delft University Press, Delft (NL), January 2004.

5. Maessen, D.C., *External forces on the iDod,* Version 1, iDod document iDod.TN.002, Faculty of Aerospace Engineering, Delft University of Technology, 9 October 2006.

6. Maessen, D.C., *iDod attitude stability analysis,* Draft, iDod document iDod.TN.009, Faculty of Aerospace Engineering, Delft University of Technology, 1 November 2006.

7. Maessen, D.C., *iDod Straw man concept design description,* Version 1, iDod document iDod.DD.001, Faculty of Aerospace Engineering, Delft University of Technology, 25 September 2006.

8. Maessen, D.C., *Simplified load case to assess the importance of structural strength,* Version 1, iDod document iDod.TN.004, Faculty of Aerospace Engineering, Delft University of Technology, 9 October 2006.

9. Maessen, D.C., *Tripod mass estimate,* iDod document iDod.TN.005, Draft, Faculty of Aerospace Engineering, Delft University of Technology, 5 September 2006.

10. Weisstein, E.W., *Equilateral Triangle*, From Mathworld—A Wolfram Web Resource, http://mathworld.wolfram.com/EquilateralTriangle.html , Last modified on 8 November 2005.

11. Weisstein, E.W., *Square Pyramid*, From Mathworld—A Wolfram Web Resource, http://mathworld.wolfram.com/SquarePyramid.html , Last modified on 10 February 2006.

12. Weisstein, E.W., *Triangular Pyramid*, From Mathworld—A Wolfram Web Resource, http://mathworld.wolfram.com/TriangularPyramid.html , Last modified on 23 December 2006.

# APPENDIX A: METHOD FOR DETERMINING THE DIMENSIONS OF EACH CONCEPT

In this section, an analytical estimate is given for the dimensions of the planar concepts, the pyramid concepts, and the spherical concept in order for them to have an average frontal surface area of 3150 $cm^2$. **The geometry of the pyramids leads to a complication in the calculation of their average frontal surface area due to shadowing. Taking shadowing into account is beyond the scope of this estimation. Instead, the masses and volumes calculated for the pyramids are multiplied by a factor 1.5 in the body of the report.** It is noted that the mass and volume increase must lead to an increase in the dimensions of the base of the pyramids in order to keep the height of the pyramids to an acceptable level (< 1 m).

*Arbitrarily shaped plane*

The frontal surface area of a plane changes with the cosine of the angle the plane makes with the direction of view. Thus, an arbitrarily shaped plate with an area of 1 $m^2$ under an angle of 30 degrees has a frontal surface area of just 0.866 $m^2$. When the angle is varied between 0 and 90 degrees, the average frontal surface area of the 1 $m^2$ plate is the average of the cosine function between 0 and $\pi/2$, which is:

$$\mathrm{A}_{\mathrm{average}} = \frac{\int_0^{\pi/2} \cos\alpha \, d\alpha}{\pi/2} = \frac{\sin\alpha\big|_0^{\pi/2}}{\pi/2} = \frac{1-0}{\pi/2} = \frac{2}{\pi} \ \mathrm{m}^2$$

This is roughly equal to the value at an angle of 50°. When rotated around 360°, the average frontal surface area of the plate is also equal to $2/\pi$ $m^2$. Rotating the plate around an axis perpendicular to the previous one has the same effect. Therefore, when the plate is rotated around two axes at the same time the average frontal surface area is $2/\pi * 2/\pi \approx 0.405$ $m^2$. Applying this knowledge to each concept, its average frontal surface area for a certain dimension can be roughly determined.

*Planar concepts*

For the planar concepts, determination of the required total surface area is easy:

$$A_{planar,average} = \left(\frac{2}{\pi}\right)^2 A_{plane} \quad \Rightarrow \quad A_{plane} = \frac{\pi^2}{4} A_{planar,average} = \frac{\pi^2}{4} 3150 = 7772 \ \mathrm{cm}^2$$

*Pyramid concepts*

For the pyramid concepts, two geometries have to be looked at: square and triangle. What needs to be determined first is the average width of a square or triangle with unit length ribs when it is rotated 360°.

<u>Square</u>

Using the below picture, the width (w) of a square is equal to $w = x\cos\alpha + x\sin\alpha$ .

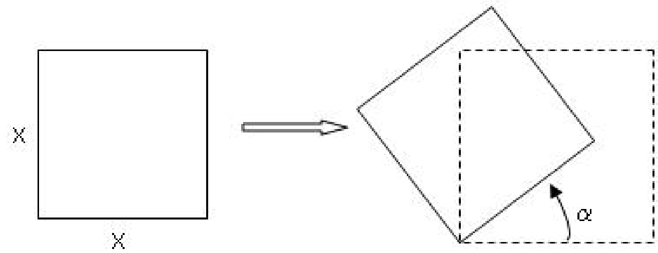


*Figure 13 Rotation of a square*

This simple formula leads to a variation in width for increasing angle:

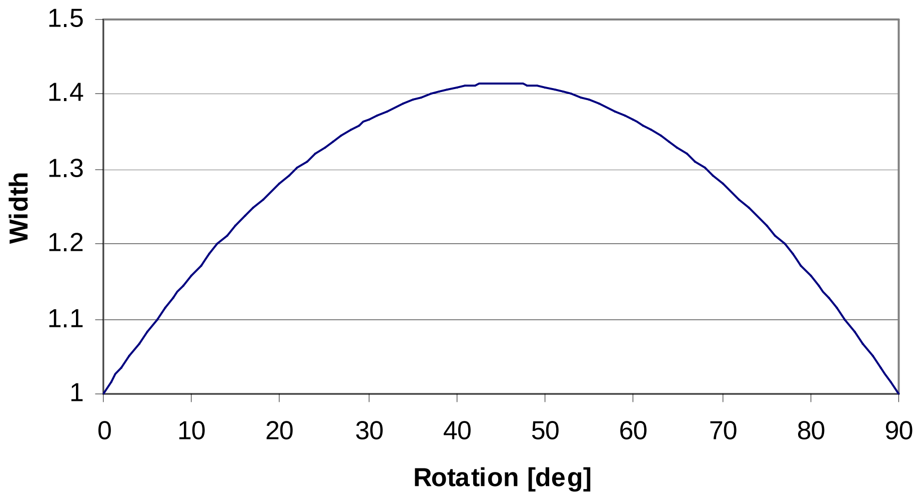


*Figure 14 Variation in width of square*

The average width of the square when rotated 90° is:

$$w_{\text{average}} = \frac{\int_0^{\pi/2} \left( x\cos\alpha + x\sin\alpha \right) d\alpha}{\pi/2} = \frac{\left( x\sin\alpha - x\cos\alpha \right)\Big|_0^{\pi/2}}{\pi/2} = \frac{x - -x}{\pi/2} = \frac{4x}{\pi}$$

This is roughly equal to the width of the square when it is rotated 19°.

The average frontal surface area of the square pyramid when rotated around its central axis is now equal to the total surface area of a triangle with base width $4x/\pi$ and a height equal to that of the pyramid. When the pyramid is now rotated around two axes, the surface area of the triangle needs to be multiplied by $2/\pi$ to obtain the average frontal surface area of the triangle.
The average frontal surface area of the pyramid is that of the triangle plus the base of the pyramid. When the length of one rib of the base of the pyramid is called x, the average frontal surface area of the base of the pyramid is equal to $2/\pi * x^2$ (a rotation around the central axis of the pyramid has got no effect on the frontal surface area of the base, therefore only a multiplication by $2/\pi$ is required). When the height of the pyramid is called h, a relationship between h and x is found:

$$A_{\text{square pyrmid, average}} = A_{triangle} \cdot \frac{2}{\pi} + A_{square} \cdot \frac{2}{\pi} = \frac{1}{2} w_{average} h \cdot \frac{2}{\pi} + \frac{2}{\pi} x^2 = \frac{1}{2}\frac{4}{\pi} xh \cdot \frac{2}{\pi} + \frac{2}{\pi} x^2 = \frac{2x}{\pi}\left(\frac{2}{\pi} h + x\right)$$

$$3150 = \frac{2x}{\pi}\left(\frac{2}{\pi} h + x\right)$$

$$h = \frac{3150\pi^2}{4x} - \frac{\pi}{2} x$$

This relationship results in the following figure:

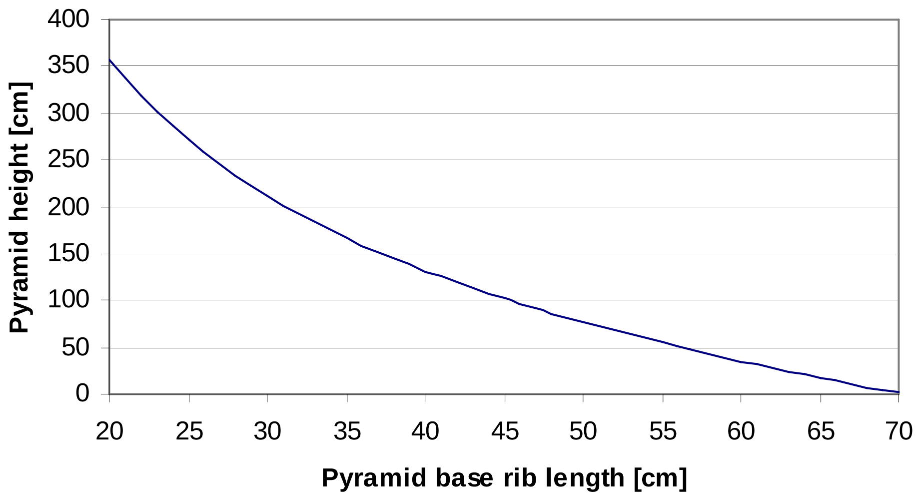


*Figure 15 Relation between square pyramid height and base rib length for $A_{average}$ = 3150 cm$^2$*

When the orientation of the satellite is determined by aerodynamic drag, the satellite is expected to behave like a shuttlecock. This effectively results in the surface area of the base of the pyramid to be equal to the frontal surface area of the satellite. Since this area is required to be 3150 cm$^2$, the length of the sides of the base needs to be about 56 cm. From figure 15 now follows a required pyramid height of about 50 cm.

Triangle

For the triangular pyramid, matters are a bit more complicated. The width of an equilateral triangle width rib length 1 varies between ½√3 and 1, with the average being 3/π. Determining this requires some more calculation than is necessary for the square. First, a picture of the rotation in question is given below for easy reference:

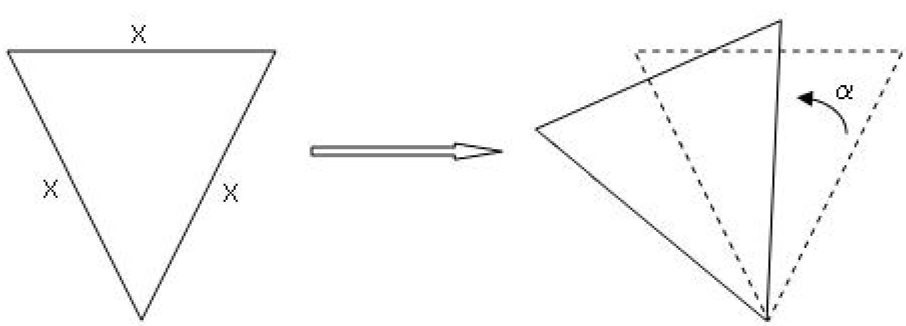


*Figure 16 Rotation of an equilateral triangle*

Rotating the triangle such that its orientation at the end of the rotation is the same as at the start requires a rotation of 120°. The width of the triangle needs to be determined using three different formulas:

$$0^\circ < \alpha \le 30^\circ \quad \Rightarrow \quad w = x\cos\left(60^\circ + \alpha\right) + x\cos\left(60^\circ - \alpha\right)$$

$$30^\circ < \alpha \le 90^\circ \quad \Rightarrow \quad w = x\cos\left(60^\circ - \alpha\right)$$

$$90^\circ < \alpha \le 120^\circ \quad \Rightarrow \quad w = x\cos\left(180^\circ - \alpha\right) + x\cos\left(60^\circ - \alpha\right)$$

The resulting variation in width looks as follows:

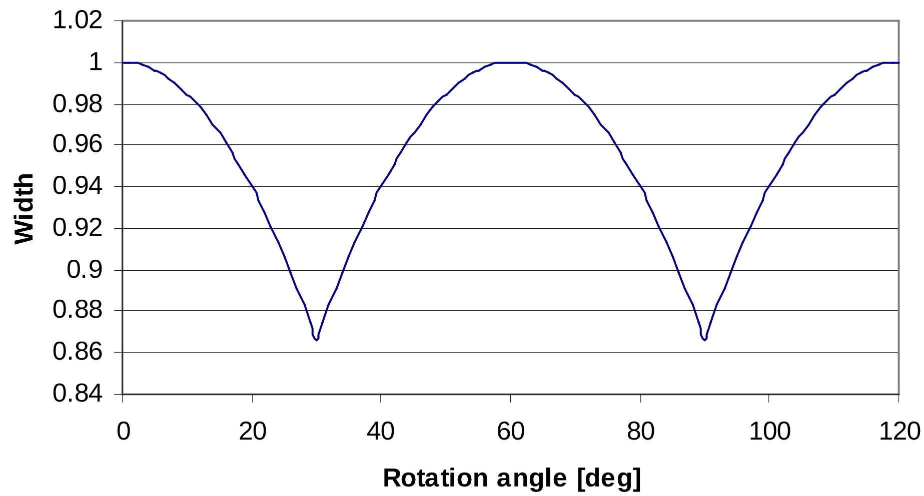


*Figure 17 Variation in width of equilateral triangle*

The average width is determined using the formula required to determine the width between 30° and 90°:

$$w_{average} = \frac{\int_{\alpha=30^\circ}^{\alpha=90^\circ} x\cos\left(60^\circ - \alpha\right) d\alpha}{\pi/2 - \pi/6} = \frac{\left[-x\sin\left(60^\circ - \alpha\right)\right]_{30^\circ}^{90^\circ}}{\pi/3} = \frac{\frac{x}{2} - -\frac{x}{2}}{\pi/3} = \frac{3x}{\pi}$$

Knowing the average width, the approach to determine the average frontal surface area of the triangular pyramid is the same as for the square pyramid:

$$A_{\text{triangular pyrmid, average}} = A_{triangle} \cdot \frac{2}{\pi} + A_{\text{equilateral triangle}} \cdot \frac{2}{\pi} = \frac{1}{2} w_{average} h \cdot \frac{2}{\pi} + \frac{2}{\pi}\frac{1}{4}\sqrt{3}x^2 =$$

$$= \frac{1}{2}\frac{3}{\pi} xh \cdot \frac{2}{\pi} + \frac{\sqrt{3}}{2\pi}x^2 = \frac{\sqrt{3}x}{\pi}\left(\frac{\sqrt{3}}{\pi}h + \frac{x}{2}\right)$$

$$3150 = \frac{\sqrt{3}x}{\pi}\left(\frac{\sqrt{3}}{\pi}h + \frac{x}{2}\right)$$

$$h = \frac{3150\pi^2}{3x} - \frac{\pi}{2\sqrt{3}}x$$

The resulting graph is depicted on the next page:

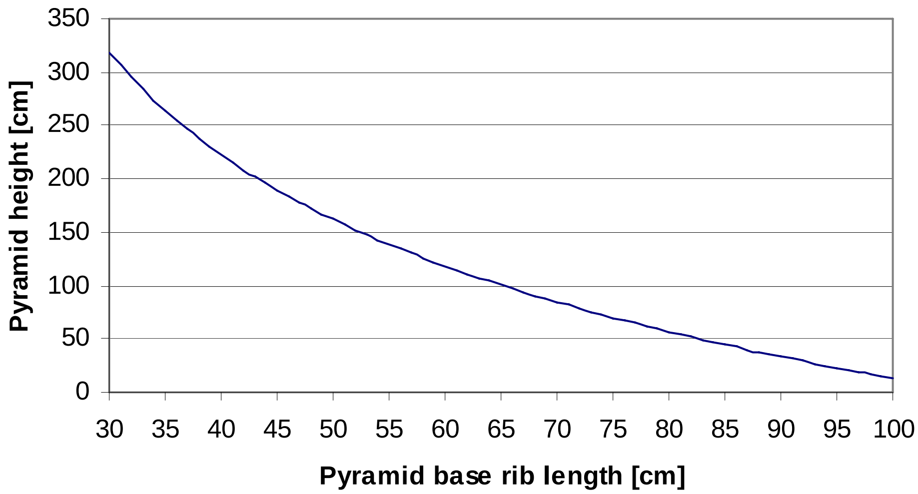


*Figure 18 Relation between triangular pyramid height and base rib length for $A_{average}$ = 3150 $cm^2$*

The requirement that the area of the base of the pyramid must be 3150 $cm^2$ results in a length of 85 cm for the ribs of the base, which in turn results in a pyramid height of about 45 cm. The length of the ribs of the base is determined using the following equation from [Weisstein, 2005]:

$$A_{base} = \frac{1}{4}\sqrt{3}x^2$$

*Sphere*

For the spherical concept the calculations are easy since its frontal surface area is constant for all possible orientations. To obtain a frontal surface area of 3150 $cm^2$, the radius of the sphere has to be 31.67 cm ($\sqrt{(3150/\pi)}$).

# iDod rigidization


## SUMMARY

Several chemical and one mechanical rigidization method for the tubes of the inflatable structure of the iDod are discussed. Selection of the most suited option is difficult since sufficient knowledge regarding all the various technologies is not available at this faculty. The simplest one, thermal cure, is finally selected. This is partly due to the fact that this technology is already well known at this faculty.
However, it needs to be confirmed that rigidization is really required for this structure before this method is put into practice.



## KEYWORDS

Rigidization, inflatable structure, chemical, mechanical


## DISTRIBUTION

| | Name | | Company / Institution |
|---|---|---|---|
| 1 | E.D. van Breukelen | Customer | ISIS B.V. |
| 2 | O.K. Bergsma | Project supervisor | TU Delft |

## APPROVAL

| | Name | Company / Institution | Date | Signature |
|---|---|---|---|---|
| *Written* | D.C. Maessen | TU Delft | 5/2/2007 | |
| *Checked* | | | | |
| *Approved* | | | | |

## REVISION RECORD

| Issue | Date | Total pages | Affected pages | Brief description of change |
|---|---|---|---|---|
| Draft | 1/16/2007 | 13 | | |
| Version 1.0 | 3/28/2007 | 13 | 1 | |
| | | | 11 | Required amount of rigidization time indicated for thermal cure option |
| | | | 11 | Noted that eclipses have no adverse affect on thermal cure |
| | | | 11 | Small textual change in paragraph after second summation |
| | | | 11 | Table added with major drawbacks of rejected options instead of third summation |
| Version 1.1 | 5/2/2007 | 18 | 3 | Changed second paragraph of section 1 |
| | | | 12 | Slightly changed 1st recommendation in section 3 |
| | | | 12 | Removed section 4 (further work) since the work indicated to be performed in that section has been performed |
| | | | 14 | Added appendix A |

## LIST OF TBD'S AND TBC'S

| TBD / TBC | Paragraph | Subject | Due date | Action by |
|---|---|---|---|---|
| TBD | Section 1 | Risk of impact meteoroid with an inflatable tube (determines whether rigidization is required) | TBD | TBD |
| TBC | 2.8 | Attainable temperature inflatable tubes | TBD | TBD |

## TABLE OF CONTENTS

# 1 INTRODUCTION

This document treats the various ways known in which the stiffness of a flexible, inflatable structure can be increased without applying any internal pressure for an extended period of time. This "rigidization" of the structure can be required since it has to maintain its shape under influence of external forces for 25 years. When gas is used for this purpose, an unacceptably large amount of spare gas is required to compensate for gas loss due to material permeability or due to puncturing of the material by small objects (micrometeoroids or space debris).

It is noted that rigidization of the structure might not be necessary if the stiffness of inflatable tubes with only a gas retention membrane is high enough to ensure no large structural deformations occur during the 25-year de-orbit maneuver. No other requirements exist for the stiffness of the structure.
An analysis performed in appendix A results in the conclusion that rigidization of the inflatable tubes of the iDod is only required when the risk (the probability times the impact of the result!) of impacts of micrometeoroids and orbital debris on the inflatable tubes is considered by the customer to be too high. Since no risk analysis regarding micrometeoroids and space debris (MMOD) has been performed yet, it is for now assumed rigidization is necessary and the risk is left TBD.

The next chapter discusses known rigidization methods and provides tables in which the most important properties of the methods are summarized. At the end of the chapter, the most suitable rigidization methods for this application are given as well as the reason why they are the most suitable. From the most suitable methods, one method is finally chosen. Chapter 3 provides the conclusions and recommendations that are drawn from this study.

# 2 AVAILABLE RIGIDIZATION METHODS

Due to the limited gas supply available, the structure has to be a rigidized inflation (RI) device. This means that inflation gas is required for the initial deployment of the structure and that the structure will rigidize in some manner, removing the need of inflation gas for structural support upon rigidization. Several methods for in-orbit rigidization exist [Jenkins, 2001]:

1. Thermally cured thermoset composites
2. UV-cured thermoset composites
3. Inflation gas reaction thermoset composites
4. Second-order transition change and shape memory polymer thermoplastic composites
5. Plasticizer or solvent boil-off thermoplastic composites
6. Foam rigidization
7. Aluminum laminates

All seven methods are described in the comings sections. If not explicitly stated otherwise, the information in those sections is obtained from [Jenkins, 2001].
In each section, a table with the most important positive and negative properties of the method under consideration is provided. Cells with bold letters are deemed more important than cells with normal letters.

## 2.1 Thermally cured thermoset composites

This method utilizes heat to cure a thermoset composite, thereby rigidizing the inflatable structure. The required heat can be supplied by solar radiation or by embedded heaters in the structure. The thermoset composite is typically encased on both sides by polymeric material which acts as pressure barrier and which prevents blocking of the material in packed state (uncured resin in a fold sticking to uncured resin in an adjacent fold). Cure time is typically between one and several hours. Various fibers can be applied in the composite. Due to the negative CTE (coefficient of thermal expansion) of some fibers, the complete composite can have a near-zero CTE. This is beneficial, since it will prevent or at the least slow the onset of cracks forming in the structure (especially in the coating) due to thermal cycling.

The most important positive and negative aspects of utilizing this method of rigidization are listed in the next table.

<table>
<tr><th>Pro's</th><th>Con's</th></tr>
<tr><td>When embedded heaters are used, curing of the composite can be done in a very controlled manner. In addition, the structure can be pre-heated before deployment in order to increase the flexibility of the material (it stiffens when it is cold)</td><td rowspan="3">Embedded heaters require power. For graphite / epoxy composites, cure energies lower than 15 $W/m^2$ have been recorded. However, when no MLI (multi-layer insulation) is used to contain the heat, it will rapidly leak away to space. Using MLI is not possible for the current application due to mass and volume constraints.</td></tr>
<tr><td>Laminates hardly degrade due to packaging and deployment.</td></tr>
<tr><td>Excellent structural properties.</td></tr>
<tr><td rowspan="2">The use of a fiber-matrix laminate can lead to a near-zero CTE. If the polymeric outer tube layer is coated and also has a very small CTE, this reduces the amount of micro-cracks due to thermal cycling in the coating. This is good for environmental resistance.</td><td>Shadowing can lead to unequal cure times when solar radiation is used to cure the composite. This can cause deformations and internal strains in the structure.</td></tr>
<tr><td>Special epoxies are required to obtain long enough shelf-life (order of years)</td></tr>
<tr><td>Solar energy can be used for rigidization, making the rigidization process passive.</td><td>Rigidization is irreversible, thus testing of the flight model can only be done for inflation.</td></tr>
<tr><td>Outgassing of volatile components is very low due to the confinement of outgassing products between the layers of polymer film.</td><td></td></tr>
</table>

*Table 1 Positive and negative aspects of thermal cure*

The power requirement of embedded heaters, in combination with not using MLI, is a killer for the embedded heater option for this method. Thus, only passive heating by the sun can be used to rigidize the structure using this method.

## 2.2 UV-cured thermoset composites

For this method, internal or external UV-radiation is used to rigidize the structure. The specific wavelength at which the resin rigidizes (typically between 250 and 380 nm) can be manipulated by means of a photoinitiated cationic catalyst. Premature rigidization can be prevented in a controlled environment. Structural performance is limited since only UV-transparent materials can be used for reinforcement (glass fiber of quartz). Cure times can vary from several minutes to several hours, depending on resin chemistry and temperature of the composite during rigidization. The temperature of the resin greatly affects curing kinetics (a higher temperature leads to faster curing).

An important downside of this form of curing is that UV radiation is absorbed by polyimide materials such as Kapton. UV curing is then not possible at short wavelengths, leaving only a very small portion, if any at all, of the UV-part of the electromagnetic spectrum available for resin curing. In addition, protective coatings can also absorb a part of the UV radiation. This therefore limits the amount of options for materials and coatings that can be used when this curing method is applied.

The absorption of UV radiation by PET and polyimide film is shown in figure 1 (in the picture, "A" refers to absorption). Clearly, PET performs better in this respect, since it absorbs all radiation below ~300 nm while polyimides absorb all radiation below ~450 nm. However, PET has clear disadvantages over polyimides in other areas (sensitivity to atomic oxygen, smaller temperature range, less radiation resistance, higher permeability, etc.).

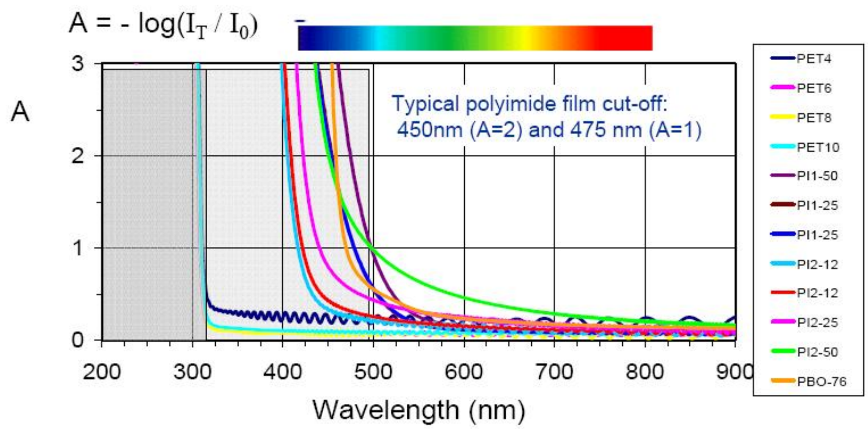


*Figure 1 Absorption of UV radiation by PET and polyimide film [Defoort, 2006]*

The effect on the amount of cross linking of resin when a Kapton filter is applied between the UV source and the resin is shown in figure 2. Clearly, the conversion rate is decreased dramatically resulting in extremely poor performance of the composite.

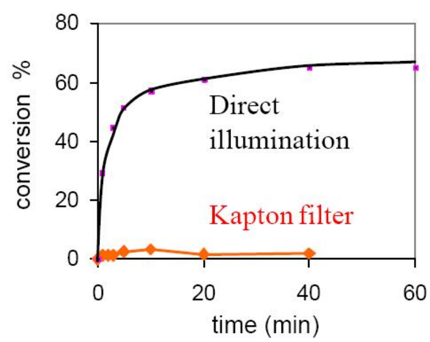


*Figure 2 Effect of a Kapton filter on resin cross linking [Defoort,2004]*

The most important positive and negative aspects of utilizing this method of rigidization are listed in the next table.

| Pro's | Con's |
|---|---|
| Rigidization can be controlled by using internal UV-sources. MLI blankets can be used on the outside of the structure for thermal stability. | **Estimated lamp power when utilizing internal UV-sources is 25 W/m$^2$.** |
| **The use of a fiber-matrix laminate can lead to a near-zero CTE. If the polymeric outer tube layer is coated and also has a very small CTE, this reduces the amount of micro-cracks due to thermal cycling in the coating. This is good for environmental resistance.** | **Premature rigidization (on Earth) has to be prevented by controlling the UV wavelengths the material is exposed to.**<br>Only UV-transparent reinforcements can be used (glass fiber or quartz). |
| **Laminates hardly degrade due to packaging and deployment.** | Rigidization is irreversible, thus testing of the flight model can only be done for inflation. |
| **Solar UV radiation can be used for rigidization, making the rigidization process passive.** | **Shadowing can lead to unequal cure times when solar UV radiation is used to cure the composite.** |
| Outgassing is very low due to confinement of outgassing products between the layers of | Special epoxies are required (photoinitiated) and the epoxy has to have a long enough |

| | |
|---|---|
| polymer film. | shelf-life (order of years). |
| Cure continues even when the structure is in the shadow (albeit at a much slower pace). | **Restraint layers and coatings have to be UV transparent.** |

*Table 2 Positive and negative aspects of UV-cure*

The power requirement of lamps is a killer for the internal UV-source option for this method. In addition, lamps are likely to be too bulky for the current application.

## 2.3 Inflation gas reaction thermoset composites

The thermoset resin of the composite is in this method rigidized by means of a catalyst introduced by the inflation gas. A high temperature increases the reaction rate and is therefore beneficial. The buildup of the laminate is the same as for thermal/UV cured thermoset composites, but the inner layer of polymer has to be highly permeable and the thickness of the resin has to be small in order for the catalyst to be able to penetrate the resin completely. Catalysts used in the past are a.o. water vapor, amines, triphenylphosphine, stannic chloride, and $BF_3$.

| Pro's | Con's |
|---|---|
| **No onboard power is required to initiate and sustain rigidization.** | **Control of the rigidization-rate throughout the structure is a problem (keeping the rate of rigidization the same everywhere)** |
| **No restrictions on fiber types (as with UV rigidization).** | Laminate thickness is limited. |
| **Separating reactants can lengthen storage life.** | Rigidization is irreversible, thus testing of the flight model can only be done for inflation. |
| **Laminates hardly degrade due to packaging and deployment.** | Outgassing of unreacted inflation gas (spacecraft contamination) is an issue. |
| **The use of a fiber-matrix laminate can lead to a near-zero CTE. If the polymeric outer tube layer is coated and also has a very small CTE, this reduces the amount of micro-cracks due to thermal cycling in the coating. This is good for environmental resistance.** | State of cure on orbit cannot be easily monitored. |
| | Premature rigidization (on Earth) can be an issue when the selected catalyst is for instance water vapor. |
| | **The catalyst has to be mixed with the gas used for inflation.** |

*Table 3 Positive and negative aspects of inflation gas reaction*

The last negative aspect is normally not that much of an issue, but when the inflation gas is stored in solid form, matters are different. This is especially true when the stowage volume is critically small, making incorporation of a second gas supply next to the inflation gas not a trivial matter. The most convenient solution to this problem is to let the inflation gas also be the catalyst. Whether this is possible is TBD.

## 2.4 Sub-$T_g$ rigidized and shape memory polymer thermoplastic composites

Here, the structure consists of a thermoplastic coated fibrous reinforcement that may or may not be encased in barrier films for gas containment or blocking prevention. Prior to deployment, the thermoplastic composite is heated above its glass transition temperature ($T_g$) which causes it to become flexible. After deployment, the structure cools to a temperature below the $T_g$ and the structure becomes rigid. Heat can come from spacecraft radiant energy, solar heating of the packed assembly, or from heaters. MLI blankets can be used to control the rate of cooling.

Shape memory polymer (SMP) can also be used and is similar in use as the thermoplastic. This polymer exhibits a natural shape restoring force when heated above its $T_g$.

The advantages and disadvantages of using thermoplastic composites are listed in the below table.

| Pro's | Con's |
|---|---|
| **When heated, SMP forms into the correct shape automatically (but the generated force is low, thus no other mass objects can be deployed using this force).** | **The temperature of the stowed structure has to be above its $T_g$ before deployment. This might necessitate the use of heaters or low-$T_g$ thermoplastics in order to make the structure universally applicable.** |
| **The use of a fiber-matrix laminate can lead to a near-zero CTE. If the polymeric outer tube layer is coated and also has a very small CTE, this reduces the amount of micro-cracks due to thermal cycling in the coating. This is good for environmental resistance.** | Thermoplastic materials are outperformed by thermoset materials in strength, stiffness, and dimensional and thermal stability. |
| | **Care must be taken that, once deployed and rigidized, (part of) the structure cannot be heated above its $T_g$.** |
| **The used materials are inert, allowing long storage life.** | Creep (time-dependent distortion under static load) may be an issue for thermoplastic materials. However, with the extremely small expected loads, this is only a minor issue. |
| **The rigidization process is reversible, allowing flight model rigidization testing on ground.** | |
| **The amount of outgassing of the used materials is very low.** | Shape accuracy might be an issue, since some thermoplastics exhibit a lower degree of flexibility when heated and cannot eliminate distortions from packaging. |
| The state of rigidization can be monitored using thermistors. | |

*Table 4 Positive and negative aspects of thermoplastic composite rigidization through temperature control*

Unfortunately, both methods are not an option for the current application. This is caused by the impossibility to control the temperature of the material in stowed or deployed configuration.

## 2.5 Plasticizer or solvent boil-off thermoplastic composites

With this method, the structure becomes rigid as the matrix-softening component of the thermoplastic evaporates upon exposure to the space environment. In stowed state, the material has to be kept in a controlled environment to prevent boil-off (high humidity, high ambient pressure, etc.). When the matrix is encased between two membranes, the outer membrane has to be permeable to the softening agent to facilitate slow release of the agent into space. Mass loss due to outgassing can be significant, even more than 20%. Examples of materials that have been studied for this goal are gelatin, PVA, and Hydron. The positive and negative aspects of this method are listed below.

| Pro's | Con's |
|---|---|
| **All composite materials have good resistance with respect to UV, IR, and gamma radiation.** | **In stowed state, the pressure and humidity of the package has to be controlled.** |
| **Simple rigidization method.** | Large mass loss upon rigidization, this is inefficient with respect to mass. |
| **The rigidization process is reversible, allowing flight model rigidization testing on ground.** | **Shrinkage during rigidization due to boil-off. This leads to bad shape accuracy and undesired laminate stresses.** |
| **The material packages very well and has good flexibility which results in few packing wrinkles and accurate patterned shape.** | **The temperature of the material must be higher than 15°C in order to prevent stiffening of the material.** |
| | **In packed state, the resin can be able to flow, resulting in dry spots in the** |

| | |
|---|---|
| | **laminate and consequential loss of structural integrity in the deployed state** |
| | Not all matrix-fiber combinations are possible |
| | **The material needs to be stored under special conditions (frozen, dry, high humidity, etc.)** |

*Table 5 Positive and negative aspects of thermoplastic composite rigidization through boil-off*

Like the previous option, this form of rigidization is not deemed possible for the current application. This is due to the lack of temperature control, pressure control, and humidity control in stowed state.

## 2.6 Foam rigidization

With this rigidization method, the foam can serve multiple purposes. It can be used to fill interior cavities and it can be used as the inflation medium. Foam can be injected or can be applied to the wall of the structure as a film that foams upon exposure to vacuum (for instance solvent-expanded polystyrene or polyurethane). Foam can be used as structural material alone or in combination with composite laminate materials. There also exist foam types which can be collapsed and stowed, leading to self-deployment because of the nature of the strain in the foam cell structure.

Foam can also be applied in the form of cold hibernated elastic memory (CHEM) foam structures. The structure is manufactured from open-cell foam made from shape-memory thermoplastic polyurethane materials. By heating the material above its $T_g$, the structure can be folded and packaged. Subsequent cooling of the material below its $T_g$ ensures that the material remains in the packed state. Before deployment, the material is again heated above its $T_g$ and will retain its original shape due to its shape memory properties.

The (dis)advantages of the current rigidization method are provided below.

| Pro's | Con's |
|---|---|
| **Foam can be used to inflate the structure AND to provide structural support (although its physical properties are rather low)** | **The cell structure of the foam may collapse under very low pressures.** |
| | **The system tends to have a high mass.** |
| Rigidization can be reversible, depending on the chosen materials | **Deployment reliability and repeatability are points of concern.** |
| **Can be combined with composites in order to increase strength and stiffness of the structure** | Outgassing can be a problem. |
| | Foams can have limited storage life. |
| | Rigidization of the structure can be a slow process. |
| | **For the foaming film option, the canister in which the structure is stowed has to be air tight.** |

*Table 6 Positive and negative aspects of foam rigidization*

For the current application, the collapsible foam option is simply too bulky. Utilizing CHEM is also not possible due to the already mentioned lack of temperature control. However, a film that foams upon exposure to vacuum remains an option.

## 2.7 Aluminum laminates

For this method, polyimide film is laminated to aluminum using an adhesive. The polymeric film is used as pressure barrier since the aluminum is susceptible to pin hole formation when flexed. Generally, the laminate is stretched to the approximate work-hardening stress of the aluminum used. At that stress, the polymer is still in its elastic range. By doing this, the structural properties of the laminate are slightly elevated and wrinkles are removed. When this phase is completed, the gas pressure is removed. Upon removal of the internal pressure, the polymer wants to shrink back to its original size. This leads to the aluminum being loaded in compression and therefore being prestressed. The downside of this prestressing of the aluminum is that it reduces the overall load-carrying properties of the laminate. This effect can be minimized by having a high ratio of aluminum/polymer or by stretching the aluminum just beyond its yield point.

Two laminate variants can be used with this method:

1. film – aluminum - film
2. aluminum – film – aluminum

The latter option is the stronger option. The type of aluminum used is typically 1100-O, 1145-O or 3003-O. The index "O" refers to that type being in its softest state.

The next table lists the most important features of this rigidization method.

| Pro's | Con's |
|---|---|
| **Most simple rigidization mechanism next to thermal cure (no power required, rapid, predictable, long storage life).**<br>Low outgassing (only the adhesive) | Limited beam performance capability caused by thickness limitations (the aluminum has to be very thin in order to reduce the required pressure) |
| Storage effects on the packed system have little to no effect on the structural properties. | The beam has to be of constant thickness and diameter |
| Radiation has little or no effect on the structure due to the aluminum. | **Wrinkles may not be completely removed during rigidization due to insufficient wall stress). This results in shape deformation.** |
| **The rigidization is reversible to a certain extent, but laminate properties degrade with each deployment** | **The rigidization pressure is very close to the burst pressure of laminate. This is a high system risk.** |
| | **Aluminum has a high CTE. The use of MLI is required to prevent thermal deformations.** |

*Table 7 Positive and negative aspects of aluminum laminate rigidization*

In the below table, the properties of Kapton HN and aluminum 1145-O are listed (the properties of aluminum 1100-O and 3003-O are very similar).

| Property | Aluminum 1145-O (foil) | Kapton HN |
|---|---|---|
| Yield stress [MPa] | 35 | 69 @ 23°C (3% elongation)<br>41 @ 200°C (3% elongation) |
| Ultimate stress [MPa] | 75 | 231 @ 23°C<br>139 @ 200°C |
| Elongation at break [%] | 2.4 | 72 @ 23°C (25 μm thickness)<br>83 @ 200°C |
| CTE [μm/m/K] | 23.6 @ 20 to 100°C<br>25.5 @ 20 to 300°C | 17 @ 30 to 100°C<br>40 @ 200 to 300°C |
| Young's modulus [GPa] | 69 | 2.5 @ 23°C<br>2.0 @ 200°C |
| Thermal conductivity [W/m/K] | 230 | 0.12 |
| Specific heat capacity [J/g/K] | 0.904 | 1.09 |

*Table 8 Properties of Aluminum and Kapton [Matweb, Dupont]*

From table 8, assuming that 20 μm thick 1145-O aluminum can be obtained, the following inflation pressure is deduced for the iDod:

$$\sigma_{hoop} = \frac{pr}{t} \quad \Rightarrow \quad p = \frac{\sigma_{0.2} t}{r} = \frac{35 \cdot 10^6 * 20 \cdot 10^{-6}}{5 \cdot 10^{-3}} = 140 \text{ kPa} = 1.4 \text{ bar}$$

Reducing this pressure can be done by either increasing the radius of the tubes or by decreasing the aluminum thickness. Both options are not desired since increasing the tube radius increases the internal volume quadratically and reducing the aluminum thickness eventually results in problems with handling of the fragile material (and possibly even problems with procurement).
A point of serious concern for this rigidization method is the small room for allowable pressure variation. Since the temperature of the structure cannot be controlled by for instance MLI, the real temperature of the structure upon deployment can vary some tens of degrees Kelvin from the estimated temperature. Since the amount of gas delivered is fixed, the internal pressure of the structure depends on its temperature (provided no pressure relieving devices such as valves are applied).
A quick calculation learns the following. Assuming an internal volume of $2.5 \cdot 10^{-4}$ $m^3$, a nominal inflation temperature of 300 K, and a pressure of 1.4 bar, the required amount of moles of inflation gas is:

$$n = \frac{pV}{R_a T} = \frac{140000 \cdot 2.5 \cdot 10^{-4}}{8.3145 \cdot 300} = 0.014 \text{ moles}$$

When using this amount of inflation gas, every 10 degrees of variation in temperature results in a variation in internal pressure of 4.6 kPa. Looking at the first formula, a hoop stress of 37.5 MPa equals 150 kPa of internal pressure. This now translates to a temperature of 322 K. The stress in length direction is twice the stress in hoop direction, thus the stress in length direction is 75 MPa, which is already equal to the ultimate stress of this type of aluminum (see table 8)! Going beyond this pressure will lead to rupture of the aluminum foil and likely to bursting of the complete tube.
The above problem can be circumvented by assuming a relatively high ambient temperature upon deployment. Then, there is not much chance for the temperature to be higher than the assumed temperature. It is likely to be lower, resulting in lower pressures and thus no concern for bursting of the tube. However, the problem now is that the pressure can become too low for even work-hardening to occur, also resulting in a failure to rigidize.

There are at least three ways out of this predicament:

1. Using a pressure relieve valve.
2. Deliberately making a hole in the tube through which gas can escape with the same mass flow as with which gas is introduced in the tube at the required pressure of 1.4 bar. This of course requires a gas supply much larger than required without a hole.
3. Helically wrapping a fiber (usually PBO) along the tube.

The first option is the “dumbest” one, only marginally increasing the mass and stowed volume of the structure.
The second option has the same effect, but no extra parts are required. Only the amount of gas delivered needs to be increased. When the mass flow is not too high, the propelling effect of this gas jet is negligible.
Unlike the first two options, the last option does not strive to keep the inflation pressure at the desired value, but it increases the safety margin between rigidization and bursting. The fiber will take up most of the stress in hoop direction, thereby reducing the hoop stress in the aluminum. Manufacturing of the tubes will be more complicated and the mass of the tubes will be higher, but this is not necessarily a show stopper.

## 2.8 Most promising methods

From the preceding discussion, five rigidization methods come out as being the most promising methods currently available for this application:

1. Inflation gas reaction cured thermoset composite,
2. UV-cured thermoset composite,
3. Aluminum laminate,
4. Foam rigidization with a film that foams when exposed to vacuum.
5. Thermally cured thermoset composite.

However, all methods have serious drawbacks and unanswered questions:

1. *Inflation gas reaction:* How is the catalyst mixed with the inflation gas when a CGG is used? A separate gas supply is not desired. Can the catalyst perhaps also be the inflation gas? High temperature increases cure kinetics. How can a higher temperature be assured when the orientation of the spacecraft is unknown?
2. *UV-cure:* The material choice is limited due to requirement of UV-transparency. Cure kinetics are enhanced by higher temperature, but the temperature is difficult to increase when UV-transparent materials have to be used and when the orientation of the spacecraft is unknown.
3. *Aluminum laminate:* Methods exist with which the chance of tube failure due to the high pressure is significantly reduced, but which method is the best to use? Since no fiber/composite is used, thermal cycling is an issue. But how important is this issue?
4. *Foam rigidization:* The requirement to have an airtight canister is an issue. Furthermore, little is known about the foam itself.
5. *Thermal cure:* For this method, the temperature of the structure has to be ~100-120°C for a prolonged amount of time (~1 to 5 hours, depending on resin type, resin thickness, and temperature). How can this temperature be guaranteed when the orientation of the spacecraft is unknown and no MLI or internal heaters can be applied? It is noted that eclipses have no serious adverse affect on the rigidization process (they only cause it to be longer).

Choosing between the five options is difficult since sufficient knowledge regarding all the various technologies is not available at this faculty. Because of this lack of knownledge, the safest option to choose is the least difficult one, which is thermal cure. In [Maessen, iDod.TN.011] it is indicated that the temperature required for thermal cure is attainable (TBC). Furthermore, this method utilizes thermoplastic composites, a technology in which this faculty has got a lot of experience. Lastly, the shape accuracy of the structure does not need to be very high, allowing possible shape deficiencies due to unequal cure, which is a real possibility for this method.

The reason that thermal cure is chosen is because of the following major draw backs for the other options:

| Rigidization option | Draw back |
|---|---|
| Inflation gas reaction | Very limited choice for inflation gas |
| UV-cure | Limited material choice (especially for (protective) coatings) |
| Aluminum laminate | High pressure (close to burst pressure, introduces problems at the point where all tubes meet) and many unknowns |
| Foam rigidization | Very little knowledge about foaming films available |

*Table 9 Draw backs of rejected options*

# 3 CONCLUSIONS & RECOMMENDATIONS

From the foregoing discussion it is concluded that selecting a rigidization method is not trivial. Many options are possible, but when it comes down to it, the least difficult option is the best choice when experience with this technology is lacking. Therefore, thermal cure is regarded the best option. The downside of this option is that there is no control over the rigidization process in space.

As already stated in the introduction, it is not known whether rigidization is really required for the inflatable structure. It is therefore strongly recommended to determine whether inflatable tubes consisting only out of a polyimide gas retention layer are stiff enough to prevent large structural deformation as a result of micrometeoroid impact.

It is further recommended to obtain more knowledge about at least the five promising rigidization methods of section 2.8. This knowledge should not only be theoretical, but also practical.

## REFERENCES


1. Bousquet, P.W., et. al., *De-orbiting Microscope spacecraft by drag enhancement,* IAC-06-B6.4.5.

2. Cadogan, D.P. & Scarborough, S.E., *Rigidizable Materials for use in Gossamer Space Inflatable Structures*, AIAA 2001-1417, April 2001.

3. Defoort, B., et. al., *Recent Advances and Perspectives in the Rigidization of Gossamer Structures*, presentation during the 2nd European Workshop on Inflatable Space Structures, Tivoli (It), June 21-23, 2004.

4. Defoort, B., et. al., *Polymerisation of Composite Structures in Free Space Conditions*, presentation during the 3rd European Workshop on Inflatable Space Structures, Noordwijk (NL), 10 October, 2006.

5. Dupont, *Summary of Kapton properties,* http://www2.dupont.com/Kapton/en_US/assets/downloads/pdf/summaryofprop.pdf , viewed September 2006.

6. Gere, J.M., Timoshenko, S.P., *Mechanics of Materials,* Fourth SI edition, Stanley Thornes (Publishers) Ltd., Cheltenham (UK), 1999.

7. Jenkins, C.H.M., *Gossamer Spacecraft: Membrane and Inflatable Structures and Technology for Space Applications*, AIAA, Reston (USA), 2001.

8. Maessen, D.C., *iDod preliminary design description,* iDod document iDod.DD.003, Version 0.1, Faculty of Aerospace Engineering, Delft University of Technology, 25 April 2007.

9. Maessen, D.C., *External forces on the iDod,* iDod document iDod.TN.002, Version 1.0, Faculty of Aerospace Engineering, Delft University of Technology, 9 October 2006.

10. Maessen, D.C., *Material selection,* iDod document iDod.TN.008, Version 1.0, Faculty of Aerospace Engineering, Delft University of Technology, 13 March 2007.

11. Maessen, D.C., *Required amount of inflation gas for tripod,* iDod document iDod.TN.003, Version 1, Faculty of Aerospace Engineering, Delft University of Technology, 5 October 2006.

12. Maessen, D.C., *Thermal design,* iDod document iDod.TN.011, Draft, Faculty of Aerospace Engineering, Delft University of Technology, 16 January 2007.

*13.* Matweb, *Aluminum 1145-0*, http://www.matweb.com/search/SpecificMaterial.asp?bassnum=MA1145O , viewed October 2006.

*14.* Matweb, *Aluminum 1145-H18*, http://www.matweb.com/search/SpecificMaterial.asp?bassnum=MA1145H18 , viewed October 2006.

*15.* Wertz, J.R., Larson, W.J., *Space Mission Analysis and Design*, Third Edition, Kluwer Academic Publishers, Dordrecht (NL), 1999.

*16.* Wijker, J.J., *Spacecraft Structures*, Lecture notes, Delft University Press, September 2004.

# APPENDIX A: DETERMINATION OF THE NEED FOR RIGIDIZATION

Throughout the design performed for the inflatable structure of the iDod thus far, it has been assumed that rigidization of the inflatable tubes after deployment is required. Rigidization increases the stiffness of the inflatable tubes and increases the chance that the inflatable structure retains its shape during the entire de-orbit period of 25 years.
In this section a first analysis is performed to determine whether rigidization is really required. There are four factors that determine the required stiffness of the inflatable:

1. Allowable stresses and deflections due to external forces (aerodynamic drag, solar radiation pressure)
2. Allowable temperature gradient over the tubes
3. Vibrations due to instantaneous forces
4. Impact of micrometeoroids and orbital debris (MMOD)

The above factors are discussed in separate subsections. After these discussions, a conclusion regarding the need for rigidization is formulated.

The inflatable structure and a cross-section of an inflatable tube (if rigidization is applied) are shown below.

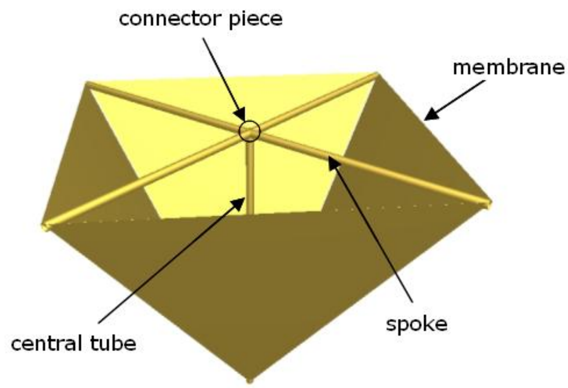


*Figure 3 Inflatable structure [Maessen, iDod.DD.003]*

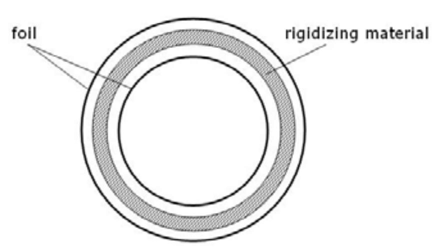


*Figure 4 Tube cross-section [Maessen, iDod.TN.008]*

The following table lists all symbols that are used in the coming subsections. Values are obtained from [Maessen, iDod.DD.003][Maessen, iDod.TN.008][Wertz, 1999].

| Symbol | Description | Value | Units |
|---|---|---|---|
| A | cross-sectional area | | $m^2$ |
| a | Semi-major axis at 200 km altitude | 6578 | km |
| $C_d$ | Drag coefficient | 2.0 | - |
| d | Tube diameter | 0.01 | m |
| E | Young's modulus Upilex-S foil | $9 \cdot 10^9$ | $N/m^2$ |
| F | Resulting tensile force on the central tube | | N |

| | | | |
|---|---|---|---|
| L | Central tube length | 0.4 | m |
| $L_{spoke}$ | Spoke length | 0.3 | m |
| M | Moment on the central tube | | Nm |
| m | Mass | | kg |
| r | Tube radius | 0.005 | m |
| T | Temperature | | K |
| t | tube wall thickness | $120 \cdot 10^{-6}$ | m |
| $\ddot{x}$ | Deceleration | | $m/s^2$ |
| | | | |
| $\alpha$ | Coefficient of thermal expansion Upilex-S | 12 | ppm/K |
| $\Delta$ | Difference | | - |
| $\delta$ | Deflection of the end of the central tube | | m |
| $\rho$ | Atmospheric density at 200 km altitude | $3.52 \cdot 10^{-10}$ | $kg/m^3$ |
| $\sigma$ | Stress | | $N/m^2$ |
| $\upsilon$ | Poisson's ratio Upilex-S foil | 0.3 (assumed) | - |
| $\omega$ | Orbit angular velocity at 200 km altitude | $1.1833 \cdot 10^{-3}$ | rad/s |

*Table 10 Symbol description*

External forces

In [Maessen, iDod.TN.002] it is determined that aerodynamic drag is the largest external force acting on the inflatable structure. This force is proportional to the frontal surface and mass of the object considered and only acts in the direction of flight. With the inflatable structure deployed, the complete satellite can be regarded to consist out of two objects: the original cubesat and the inflatable. The maximum deceleration experienced by both objects occurs at the orbit with maximum atmospheric density during solar maximum. Of course, this is the lowest orbit attained and is assumed to be at a height of 200 km. In reality, the lowest orbit height before the satellite burns up is much smaller (<100 km), but a CubeSat without iDod will de-orbit within a day once below 200 km. Thus, below 200 km the iDod is no longer required and is allowed to fail.
The next figure schematically depicts the aerodynamic force acting on the membranes of the inflatable. The x-axis of the satellite is parallel to the velocity vector. The aerodynamic force is symmetrically distributed over the inflatable structure, leading to a single resulting force exactly at the center of the inflatable.

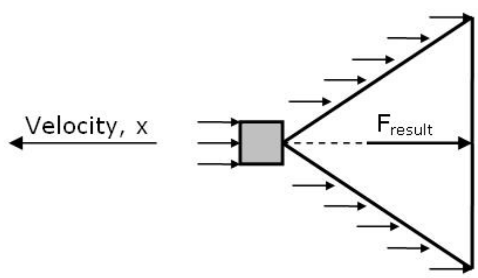


*Figure 5 Resulting force on central tube inflatable due to aerodynamic load*

The mass of the iDod is 0.03 kg [Maessen, iDod.DD.003], which leads to a CubeSat mass of 0.97 kg. The deceleration of both objects is now determined in the same manner as in [Maessen, iDod.TN.002]:

$$\ddot{x}_{cubesat} = \frac{1}{2}\frac{C_d A_{cubesat}}{m_{cubesat}}\rho a^2\omega^2 = \frac{1}{2}\frac{2*0.01}{0.97}3.52*10^{-10}*6578000^2*\left(1.1833*10^{-3}\right)^2 =$$
$$= 2.199*10^{-4}\ \text{m/s}^2$$

$$\ddot{x}_{iDod} = \frac{1}{2}\frac{C_d A_{iDod}}{m_{iDod}}\rho a^2\omega^2 = \frac{1}{2}\frac{2*0.18}{0.03}3.52*10^{-10}*6578000^2*\left(1.1833*10^{-3}\right)^2 =$$
$$= 0.1280 = 1280*10^{-4}\ \text{m/s}^2$$

The force on both objects is easily determined:

$$F_{cubesat} = m_{cubesat}\ddot{x}_{cubesat} = 0.97*2.245*10^{-4} = 2.1*10^{-4}\ \text{N}$$

$$F_{iDod} = m_{iDod}\ddot{x}_{iDod} = 0.03*1280*10^{-4} = 38.4*10^{-4}\ \text{N}$$

Since the iDod experiences a larger force than the CubeSat, it is concluded that the central tube of the inflatable is loaded in tension with a force equal to $3.6*10^{-3}$ N when it is assumed that this tube takes up the entire load. The stress in the tube due to this force is equal to [Gere, 1999]:

$$\sigma = \frac{F}{A} = \frac{F}{2\pi rt} = \frac{3.6\cdot10^{-3}}{2\pi\cdot0.005\cdot120\cdot10^{-6}} = 962\ \text{Pa}$$

It is assumed that there is no rigidizing material present in the tube. The tensile stress at 5% elongation for Upilex-S, the foil material selected for the inflatable, at 25°C is 255 MPa [Maessen, iDod.TN.008]. Clearly, the resulting stress poses absolutely no problems. The foil thickness can even be as small as $4.5\cdot10^{-4}$ μm.

When assuming that the resulting force F does not act exactly at the center of the inflatable but on a spoke end (for whatever reason), a moment is generated that acts on the central tube. This moment is equal to $F\cdot L_{spoke} = 1.08\cdot10^{-3}$ Nm. A too large moment can lead to failure of the central tube through flexural buckling. The Upilex-S foil thickness required to prevent this is determined using a formula for the collapse bending moment for a tube clamped at one end from [Veldman, 2005]:

$$M = \frac{2\sqrt{2}}{9}\frac{\pi E r t^2}{\sqrt{1-\upsilon^2}} \Rightarrow t = \sqrt{\frac{9}{2\sqrt{2}}\frac{\sqrt{1-\upsilon^2}M}{\pi E r}} = \sqrt{\frac{9}{2\sqrt{2}}\frac{\sqrt{1-0.3^2}\cdot1.08\cdot10^{-3}}{\pi\cdot9\cdot10^9\cdot0.005}} = 4.8\cdot10^{-6}\text{m} = 4.8\mu\text{m}$$

This thickness is much smaller than the thickness of 120 μm assumed thus far. Therefore, flexural buckling is not an issue.

With respect to the external forces encountered in space, rigidization of the inflatable structure is not required.

Temperature gradient

The lack of convection in space and shadowing effects will result in temperature gradients over the inflatable tubes. When the temperature of a tube at its 'upper' side ($T_1$) is lower than at its 'lower' side ($T_2$), the tube will bend upwards due to the expansion of material at the lower side. The deflection of the end of the tube is equal to δ.

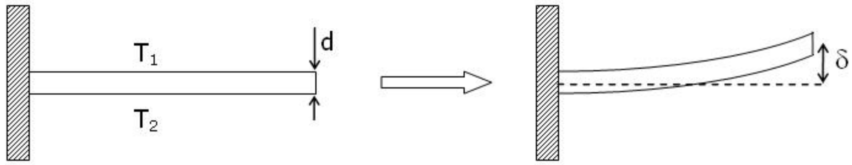


*Figure 6 Deflection of tube end due to thermal gradient*

The deflection of the end of the tube is determined using the following formula [Gere, 1999]

$$\delta_{\Delta T} = \frac{\alpha L^2 \left(T_2 - T_1\right)}{2d} = \frac{\alpha L^2 \Delta T}{4r}$$

Earlier, the formula for the collapse bending moment of a clamped beam has been given:

$$M_{\text{collapse}} = \frac{2\sqrt{2}}{9} \frac{\pi E r t^2}{\sqrt{1-\upsilon^2}}$$

The myosotis formulae [Wijker, 2004] describe the deflection (angle) of a clamped beam as a result of a force, a moment, or a distributed load acting on it. In case of a moment acting on a thin walled tube, the deflection is:

$$\delta_M = \frac{ML^2}{2EI} = \frac{ML^2}{2E\pi r^3 t}$$

In the formula, L is the length of the tube, r is its radius, and t is its wall thickness. Combining the above formulas leads to a prediction for the temperature gradient required to cause collapse of the central tube:

$$\left.\begin{array}{l} \delta_{\Delta T} = \dfrac{\alpha L^2 \left(T_2 - T_1\right)}{2d} = \dfrac{\alpha L^2 \Delta T}{4r} \\ \left.\begin{array}{l} \delta_M = \dfrac{ML^2}{2EI} = \dfrac{ML^2}{2E\pi r^3 t} \\ M_{\text{collapse}} = \dfrac{2\sqrt{2}}{9} \dfrac{\pi E r t^2}{\sqrt{1-\upsilon^2}} \end{array}\right\} \Rightarrow \delta_{\text{collapse}} = \dfrac{\sqrt{2}}{9} \dfrac{tL^2}{\sqrt{1-\upsilon^2}\, r^2} \end{array}\right\} \Rightarrow \delta_{\Delta T} = \delta_{\text{collapse}} \Rightarrow$$

$$\Rightarrow \frac{\alpha L^2 \Delta T}{4r} = \frac{\sqrt{2}}{9} \frac{tL^2}{\sqrt{1-\upsilon^2}\, r^2} \Rightarrow$$

$$\Rightarrow \Delta T = \frac{4\sqrt{2}}{9} \frac{t}{\alpha \sqrt{1-\upsilon^2}\, r} = \frac{4\sqrt{2}}{9} \frac{120 \cdot 10^{-6}}{12 \cdot 10^{-6} \cdot \sqrt{1-0.3^2} \cdot 0.005} = 1318^{\circ}\mathrm{C}$$

This temperature gradient is enormous and will not occur. Even a small deflection of 1 mm requires a temperature gradient of 10 °C (the deflection at collapse is 127 mm).

In the final formula, the Young's modulus, the material property that is enhanced by means of rigidization, is not present! Thus, rigidization will not aid in preventing collapse of the inflatable tubes due to thermal gradients and is therefore not required for this case.

## Vibrations

Since the CubeSat is no longer operational when the inflatable structure has deployed, there will not occur any instantaneous forces that are a result of satellite operations (firing of a thruster for instance). Thus, the satellite and inflatable structure will not vibrate as a result of their own actions exception for the vibrations resulting from the deployment of the inflatable. Due to the vacuum environment, these vibrations are only marginally damped. However, rigidization of the structure will not do anything to prevent this from occurring. Therefore, in this case vibrations induced by the satellite itself cannot be used as criterion whether or not to rigidize the inflatable structure.

## Impacts

Impacts from micrometeoroids and orbital debris are likely to cause structural problems when they impact on the inflatable tubes. The energy of such impacts is very high and can very well lead to an immediate collapse of the tube or to violent vibrations that ultimately lead to collapse when the tubes are not rigidized. This knowledge has been obtained during a discussion on 2 May 2007 with J.M.A.M. Hol. For which cases (size, mass, velocity, and impact angle of the particle) the inflatable tubes will collapse remains TBD. When determined, these cases have to be cross-checked with the probability of these cases occurring during the service life of the inflatable structure. When the customer decides that the risk (the probability times the impact of the result!) of collapse is too high, rigidization is required.

## Conclusion

Rigidization of the inflatable tubes of the iDod is only required when the risk of impacts of micrometeoroids and orbital debris on the inflatable tubes is considered by the customer to be too high.

# Material selection

## SUMMARY

The main materials for the storage device and the inflatable structure of the iDod are selected based on the properties that are important for the function(s) the materials have to perform. The selected materials are listed in the table below.

| | **Material** |
|---|---|
| **Storage device** | Aluminum 6061-T6 |
| **Inflatable structure** | Upilex-S |
| | Technora/cyanate composite |
| | VDA |
| | $SiO_2$<br>90% $SiO_2$ + 10% PTFE |

Upilex-S is a polyimide foil used as gas barrier in the inflatable structure. Technora is an aramid fiber; it is used in a composite material together with a thermally cured cyanate resin to provide enhanced stiffness for the inflatable structure. VDA and $SiO_2$ are coatings that have to be applied on the inflatable structure.

## KEYWORDS

Inflatable structure, storage device, foil, fiber, resin, coating

## DISTRIBUTION

| | **Name** | | **Company/ Institution** |
|---|---|---|---|
| 1 | E.D. van Breukelen | Customer | ISIS B.V. |
| 2 | O.K. Bergsma | Project supervisor | TU Delft |

## APPROVAL

| | **Name** | **Company/ Institution** | **Date** | **Signature** |
|---|---|---|---|---|
| *Written* | D.C. Maessen | TU Delft | 3/13/2007 | |
| *Checked* | | | | |
| *Approved* | | | | |

## REVISION RECORD

| Issue | Date | Total pages | Affected pages | Brief description of change |
|---|---|---|---|---|
| Draft | 3/1/2007 | 21 | | |
| Version 1.0 | 3/13/2007 | 23 | 10 | Row with out-life added in table 5 |
| | | | 10 | Discussion about out-life added |
| | | | 11 | Added that there are resins with low cure temperature (<120°C) |
| | | | 11 | Added that there is an epoxy resin available with an out-life of one year |
| | | | 12 | First requirement for fiber changed from low Young's modulus to high strain/thickness ratio |
| | | | 12 | Fold resistance requirement added for fiber |
| | | | 12-15 | Subsection 4.4 changed due to above changes on page 12 |
| | | | 16 | Units for $t_{ply}$ indicated in formula |
| | | | 17 | Ply thickness and Young's modulus composite adapted following the changes in subsection 4.4 |
| | | | 19 | Indicated that coating of a fiber does not necessarily mean more UV resistance |

## LIST OF TBD'S AND TBC'S

| TBD / TBC | Paragraph | Subject | Due date | Action by |
|---|---|---|---|---|
| TBD | 4.2 | Resin selection | TBD | TBD |
| TBC | 4.2 | Properties of resins with a low cure temperature | TBD | TBD |
| TBC | 4.2 | Properties ATK's TCR resin | TBD | TBD |
| TBD | 4.4 | Impact of the bad UV-resistance of Technora on its selection as preferred fiber | TBD | TBD |
| TBC | 5.2.1 | Performance of siloxane coating compared to $SiO_2$ | TBD | TBD |
| TBD | 5.2.1 | Availability of Kapton AOR | TBD | TBD |

## TABLE OF CONTENTS

# 1 INTRODUCTION

The iDod has two main structural components: the storage device and the inflatable structure. The inflatable structure is made out of two separate materials: a polymeric foil and a rigidizing material.

The material selection for the storage device is briefly addressed in section 2. Selection of the type of foil and rigidizing material is done in section 3 and 4 respectively. Section 5 treats the coatings that have to be applied on the material of the inflatable structure.

# 2 STORAGE DEVICE

The layout and design of the storage device is discussed in detail in [Maessen, iDod.DD.002].

Information from [Pumpkin, 2007] leads to the selection of aluminum 6061-T6 sheet for the lid of the storage device and extruded aluminum 6061-T6 for the machined container of the storage device. The density of this type of aluminum is 2.7 g/cc and its coefficient of thermal expansion (CTE) is 23.6 μm/m/K at 20°C [Matweb, 2007].
The printed circuit board (PCB) on which to mount the required resistors to burn through the wire restraining the lid of the storage device is made from FR-4 PCB laminate, which is also standard in a CubeSat kit. The wire that has to be burned through is made from a polyethylene fiber such as Dyneema.

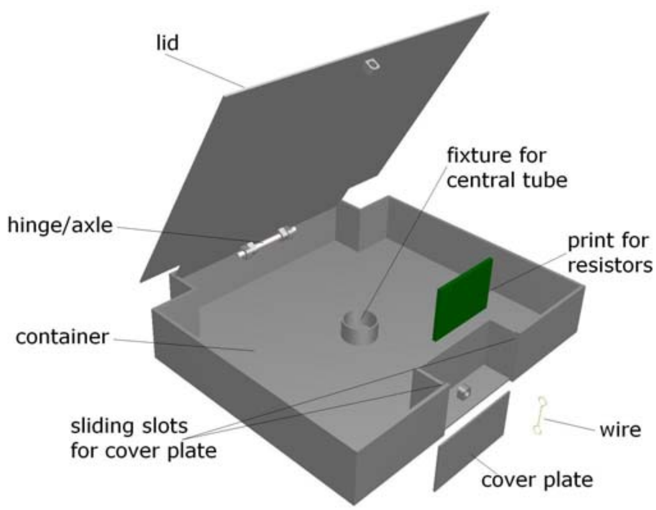


*Figure 1 Storage device [Maessen, iDod.DD.002]*

# 3 FOIL

Polymeric foil is used in the inflatable structure of the iDod as gas barrier and restraint layer for the inflatable tubes, to provide the required surface area in the form of membranes, and as substrate for thermal and protective coatings.

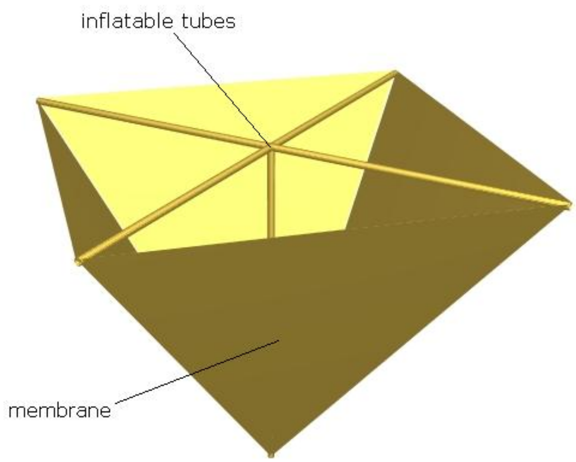


*Figure 2 Inflatable structure of the iDod*

Selecting a foil that can be used for all four functions is desirable. However, the foil also needs to be available as thin film, have a large operational temperature range (-50°C - 200°C), excellent radiation resistance, and preferably good atomic oxygen resistance.
The large temperature range is caused by the selection of a heat curable thermosetting resin as part of the rigidization material [Maessen, iDod.TN.007] and the uncertainty over the orbit and the attitude of the satellite [Maessen, iDod.TN.009 and iDod.TN.011].

Typical engineering polymers that comply with (most of) the above requirements are [Bernasconi, 2006]:

| Polymer type | Trade name |
|---|---|
| Polyamides | Capran, Emblem, Combitherm |
| Polycarbonates | Lexan, Calibre, Zelux |
| Polyolefins | LDPE, PMP, PP |
| PET (poly(ethylene terepthalate))<br>PEN (poly(ethylene 2,6-naphthalate))<br>PBT (poly(butylene terepthalate)) | Mylar, Teonex |
| Polyimides | Kapton, Upilex, Aurum, CP-1 & CP-2 |
| PAE (polyarylether)<br>PAEK (polyaryletherketone) | COR, TOR |
| PAR (polyarylate) | Victrex, Ultem, Ardel, Vectran |
| Fluorocarbons | Teflon PFA, Hyflon MFA, Tefzel ETFE, Dyneon THV |
| Fluorocarbon halides | Aclar PCTFE, Halar, Neoflon, Saran, Tedlar, Kynar |
| Sulfone-based resins | Udel, Radel, Ultrason, Torelina |

*Table 1 Available polymer types*

For all above polymers, the required temperature range of -50°C - 200°C is a very demanding requirement. In addition, several American high-tech polymers (CP-1, CP-2, COR, TOR) are not or very difficult to obtain and are therefore no option.

From the above options, polyimides are the best candidate foil material. This is not only because of their broad temperature range, but also because of their space heritage. This heritage ensures that much information about their resistance to the space environment is available, something that is very expensive and time-consuming to determine.
Of the polyimides, Kapton and Upilex have got the most space heritage and are readily available as thin film. Therefore, these two materials are analyzed in more detail.

Upilex is used on most Japanese satellites and is a product of UBE Industries, Ltd. There are three different types of Upilex available: the standard Upilex-R, the high temperature Upilex-S, and the heat sealable Upilex-VT.

Kapton is the 'standard' polyimide film used in many of today's spacecraft and is a product of DuPont. Many different types of Kapton are available; types H and HN are most commonly found in spacecraft application and are used as benchmark to rate the performance of other polymers.

The next table, copied from [de Groot, 2003], shows some general characteristics for Upilex and Kapton.

| **Material** | **Tensile strength [MPa]** | **Tensile modulus [GPa]** | **Radiation** | **Outgassing [%]** | **CTE [$10^{-6}$m/K]** | **Density [$g/cm^3$]** |
|---|---|---|---|---|---|---|
| Kapton | 231 | 2.5 | insensitive | 1 | 20 | 1.42 |
| Upilex | 245-290 | 3.7-8.8 | insensitive | - | 12-32 | 1.40 |

*Table 2 General properties Upilex and Kapton*

In the above table, the specific type of Kapton listed is Kapton HN. For Upilex, it is Upilex-R.

A literature survey indicates that Upilex has better overall properties than Kapton:

- Test results in [Semprimoschnig, 2002] indicate a higher degree of thermal stability (i.e. less mass loss) for Upilex foil compared to Kapton foil in a vacuum environment. In addition, Upilex shows less thermo-optical degradation than Kapton. It is unknown for which specific types of Kapton and Upilex this data was obtained.

- With respect to atomic oxygen resistance, Upilex also performs better than Kapton. This is shown by the MISSE 2 (Materials International Space Station Experiment 2) results in table 3. The table shows that the erosion yield for Upilex-S (serial# 2-E5-32 in the table) is much less than for Kapton HN (9.22E-25 $cm^3$/atom versus 2.81E-24 $cm^3$/atom). Striking in the table is that the reported density of Upilex-S is 1.3866 g/cc. Various other literature claim a density of 1.47 g/cc (a.o. [MatWeb, 2007 and UBE Europe GmbH, 2005])! However, the density of the Kapton samples is close to 1.42 g/cc in the table, which is the same value as commonly found in literature. It is unknown what the cause for this discrepancy is. For now, a density of 1.47 g/cc is assumed for Upilex-S.

- According to [Iwata, 2001], the chemical thermal stability of Upilex-S is better than for Kapton-H and Upilex-R.

Upilex-S performs better than Upilex-R, but has the drawback of a higher density: 1.47 g/cc versus 1.40 g/cc. For a total weight of the inflatable structure of the iDod of ~50 grams, this results in a mass increase of 2.5 grams when Upilex-S is used instead of Upilex-R. Since it is expected that a part of the inflatable structure will consist out of a fiber composite material (~20 g), the mass increase of 2.5 grams will not be reached and is more likely to be 1.5 grams.
Since the structure has to function in the hostile space environment for 25 years, using the most resilient material available is of paramount importance. The small mass increase when using Upilex-S instead of Upilex-R or Kapton HN does not weigh up against this observation. Therefore, Upilex-S is selected as foil material for the inflatable structure of the iDod.

It is noted that Upilex-S can be purchased off the shelf with a variety of coatings on one or both sides of the foil [UBE Industries, 2007]: vapor deposited aluminum (VDA), germanium, indium tin oxide (ITO), and silicon dioxide ($SiO_2$).

Some properties of 25 $\mu$m thick Upilex-S at 25°C are listed in table 4.

| MISSE Serial # | Material | Polymer Abbrev. | MISSE 2 Mass Loss (g) | Density (g/cm$^3$) | Area (cm$^2$) | MISSE 2 Erosion Yield (cm$^3$/atom) |
|---|---|---|---|---|---|---|
| 2-E5-6 | Acrylonitrile butadiene styrene | ABS | 0.033861 | 1.0500 | 3.4944 | 1.09E-24 |
| 2-E5-7 | Cellulose acetate | CA | 0.191482 | 1.2911 | 3.4831 | 5.05E-24 |
| 2-E5-8 | Poly-(p-phenylene terephthalamide) | PPD-T (Kevlar) | 0.026790 | 1.4422 | 3.5099 | 6.28E-25 |
| 2-E5-9 | Polyethylene | PE | 0.102760 | 0.9180 | 3.5489 | > 3.74E-24 |
| 2-E5-10 | Polyvinyl fluoride | PVF (Tedlar) | 0.132537 | 1.3792 | 3.5737 | 3.19E-24 |
| 2-E5-11 | Crystalline polyvinylfluoride w/white pigment | PVF (White Tedlar) | 0.004714 | 1.6241 | 3.4176 | 1.01E-25 |
| 2-E5-12 | Polyoxymethylene; acetal; polyformaldehyde | POM (Delrin) | 0.378378 | 1.3984 | 3.5119 | 9.14E-24 |
| 2-E5-13 | Polyacrylonitrile | PAN | 0.047281 | 1.1435 | 3.4768 | 1.41E-24 |
| 2-E5-14 | Allyl diglycol carbonate | ADC (CR-39) | 0.267295 | 1.3173 | 3.5392 | > 6.80E-24 |
| 2-E5-15 | Polystyrene | PS | 0.115947 | 1.0503 | 3.5043 | 3.74E-24 |
| 2-E5-16 | Polymethyl methacrylate | PMMA | 0.194588 | 1.1628 | 3.5456 | > 5.60E-24 |
| 2-E5-17 | Polyethylene oxide | PEO | 0.066395 | 1.1470 | 3.5591 | 1.93E-24 |
| 2-E5-18 | Poly(p-phenylene-2 6-benzobisoxazole) | PBO (Zylon) | 0.056778 | 1.3976 | 3.5526 | 1.36E-24 |
| 2-E5-19 | Epoxide or epoxy | EP | 0.140720 | 1.1150 | 3.5576 | 4.21E-24 |
| 2-E5-20 | Polypropylene | PP | 0.072357 | 0.9065 | 3.5336 | 2.68E-24 |
| 2-E5-21 | Polybutylene terephthalate | PBT | 0.036429 | 1.3318 | 3.5619 | 9.11E-25 |
| 2-E5-22 | Polysulphone | PSU | 0.105948 | 1.2199 | 3.5010 | 2.94E-24 |
| 2-E5-23 | Polyeurethane | PU | 0.057227 | 1.2345 | 3.5182 | 1.56E-24 |
| 2-E5-24 | Polyphenylene isophthalate | PPPA (Nomex) | 0.030549 | 0.7200 | 3.5626 | 1.41E-24 |
| 2-E5-25 | Graphite | PG | 0.02773 | 2.2200 | 3.5703 | 4.15E-25 |
| 2-E5-26 | Polyetherimide | PEI | 0.126853 | 1.2873 | 3.5352 | > 3.31E-24 |
| 2-E5-27 | Polyamide 6 or nylon 6 | PA 6 | 0.118376 | 1.1233 | 3.5646 | 3.51E-24 |
| 2-E5-28 | Polyamide 66 or nylon 66 | PA 66 | 0.065562 | 1.2252 | 3.5249 | 1.80E-24 |
| 2-E5-29 | Polyimide | PI (CP1) | 0.080648 | 1.4193 | 3.5316 | 1.91E-24 |
| 2-E5-30 | Polyimide (PMDA) | PI (Kapton H) | 0.124780 | 1.4273 | 3.4590 | 3.00E-24 |
| 2-E5-31 | Polyimide (PMDA) | PI (Kapton HN) | 0.121315 | 1.4345 | 3.5676 | 2.81E-24 |
| 2-E5-32 | Polyimide (BPDA) | PI (Upilex-S) | 0.038127 | 1.3866 | 3.5382 | 9.22E-25 |
| 2-E5-33 | Polyimide (PMDA) | PI (Kapton H) | 0.129250 | 1.4273 | 3.5773 | 3.00E-24 |
| 2-E5-34 | High temperature polyimide resin | PI (PMR-15) | 0.118887 | 1.3232 | 3.5256 | > 3.02E-24 |
| 2-E5-35 | Polybenzimidazole | PBI | 0.082708 | 1.2758 | 3.4762 | > 2.21E-24 |
| 2-E5-36 | Polycarbonate | PC | 0.142287 | 1.1231 | 3.5010 | 4.29E-24 |
| 2-E5-37 | Polyetheretherkeytone | PEEK | 0.107764 | 1.2259 | 3.4821 | 2.99E-24 |
| 2-E5-38 | Polyethylene terephthalate | PET (Mylar) | 0.125187 | 1.3925 | 3.5432 | 3.01E-24 |
| 2-E5-39 | Chlorotrifluoroethylene | CTFE (Kel-f) | 0.052949 | 2.1327 | 3.5452 | 8.31E-25 |
| 2-E5-40 | Halar ethylene-chlorotrifluoroethylene | ECTFE (Halar) | 0.088869 | 1.6761 | 3.5103 | 1.79E-24 |
| 2-E5-41 | Tetrafluorethylene-ethylene copolymer | ETFE (Tefzel) | 0.049108 | 1.7397 | 3.4854 | 9.61E-25 |
| 2-E5-42 | Fluorinated ethylene propylene | FEP | 0.012479 | 2.1443 | 3.4468 | 2.00E-25 |
| 2-E5-43 | Polytetrafluoroethylene | PTFE | 0.008938 | 2.1503 | 3.4841 | 1.42E-25 |
| 2-E5-44 | Perfluoroalkoxy copolymer resin | PFA | 0.010785 | 2.1383 | 3.4570 | 1.73E-25 |
| 2-E5-45 | Amorphous Fluoropolymer | AF | 0.012352 | 2.1463 | 3.4544 | 1.98E-25 |
| 2-E5-46 | Polyvinylidene fluoride | PVDF (Kynar) | 0.066860 | 1.7623 | 3.4993 | 1.29E-24 |

*Table 3 Atomic oxygen results MISSE 2 [de Groh, 2006]*

| Property | Value | Unit |
|---|---|---|
| Tensile strength | 520 | MPa |
| Stress @ 5% elongation | 255 | MPa |
| Elongation | 42 | % |
| Tensile modulus | 9.121 | GPa |
| Tear strength - initiation | 226 | N |
| Tear strength – propagation | 3.24 | N |
| Folding endurance | >100000 | cycles |
| Density | 1.47 | g/cm$^3$ |
| Coefficient of Thermal Expansion (between 20 - 200°C) | 12 | ppm/K |
| Specific heat | 1.13 | J/g/K |
| Thermal conductivity | 0.29 | W/m/K |
| Gas permeability (oxygen @ 30°C, 1 bar for 24 h) | 0.8 | ml/m$^2$ |

*Table 4 Properties of Upilex-25S at 25°C [UBE Europe GmbH, 2005]*

# 4 RIGIDIZING MATERIAL

The tubular structure of the iDod not only consists out of flexible foil, but also out of a rigidizable material. A cross-section of a tube looks as follows:

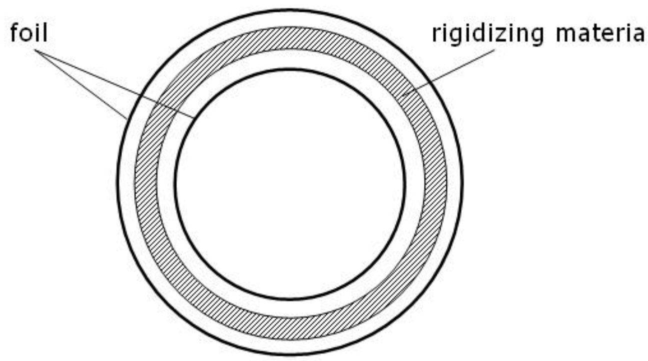


*Figure 3 Tube cross-section*

The inflatable tubes can be chemically rigidized or mechanically rigidized by stretching aluminum sheet. In [Maessen, iDod.TN.007], the latter option was discarded. The favored option is a heat curable thermosetting fiber composite.

Subsection 4.1 will treat a number of terms commonly used when working with fiber composites. Subsection 4.2 deals with the selection of the resin for the composite. The third subsection discusses which type of weave is preferred. In subsection 4.4, a fiber selection is made. Subsection 4.5 treats a suggestion for a possible fiber composite.

## 4.1 Glossary

Below, a number of terms and abbreviations [Fiberset Inc., 1999] commonly encountered when dealing with fiber composites are briefly explained. Some of these will return in the coming subsections.

- *AS:* as spun (e.g. Carbon AS)
- *Decitex (dtex):* (Metric) unit of measuring the thickness/weight of a fiber, the linear density. The weight in grams of 10000 m of a fiber filament. The lower the decitex number, the finer the yarn. Sometimes, tex is used instead of dtex, this is the weight in grams of 1000 m of a fiber filament.
- *Denier:* (Imperial) unit of measuring the thickness/weight of a fiber. The weight in grams of 9000 m of a fiber filament. The lower the denier number, the finer the yarn.
- *Filament:* Smallest unit of a fibrous material. The basic units formed during spinning and which are gathered into strands of fiber for use in composites. Filaments usually are of extreme length and of very small diameter.
- *Flex strength:* Ability of a fiber to retain its strength after being folded back and forth
- *HM:* high modulus (e.g. Carbon HM)
- *Strand:* Primary bundle of continuous filaments combined in a single compact unit without twist. These filaments (usually 51, 102 or 204) are gathered together in the forming operations.
- *Tack:* Stickiness of a filament reinforced resin prepreg material.

- *Tow size:* An untwisted bundle of continuous filaments, usually designated by a number and followed by “K”, indicating multiplication by 1000 (e.g. 12K tow has 12000 filaments).
- *Warp:* Fibers in length direction of a weave.
- *Weft:* Fibers in width direction of a weave.
- *Woven fabric:* A material constructed of interlaced yarns, fibers, or filaments.
- *Yarn:* Continuously twisted fibers or strands suitable for use in weaving into fabrics.

## 4.2 Resin selection

In [Maessen, iDod.TN.009], it is decided to rigidize the inflatable structure of the iDod by means of a heat curable fiber reinforced thermosetting resin. Typical thermosetting resin systems are epoxies (or polyepoxides) and cyanates. Most common epoxy resins are produced from a reaction between bisphenol-A and epichlorohydrin [Wikipedia, 2007]. Bisphenol-A is the primary monomer while epichlorohydrin is the hardening agent.

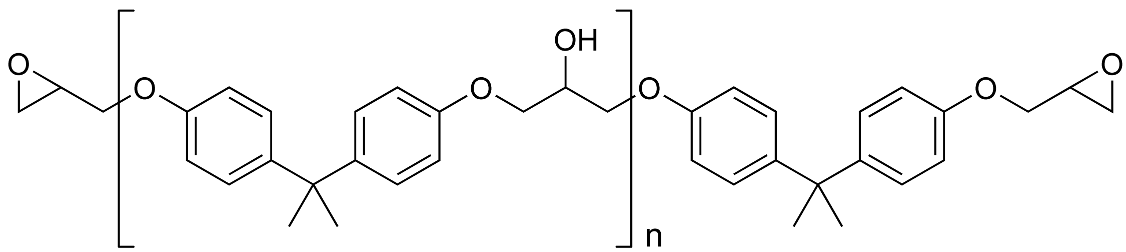

*Figure 4 Epoxy prepolymer chemical structure [Wikipedia, 2007]*

Cyanate resin systems are much less sensitive to moisture absorption (leading to less outgassing), have better microcrack resistance, and have better radiation resistance than epoxies [Smithsonian/NASA ADS, 2007]. According to [Lefevre, 2002], cyanates (O-C=N) are used in thermally cured structures. Cyanate esters cure via a “ter-molecular” reaction (a reaction in which three molecules collide at the same instant) to form thermally stable triazine rings [Myslinski, 1997]:

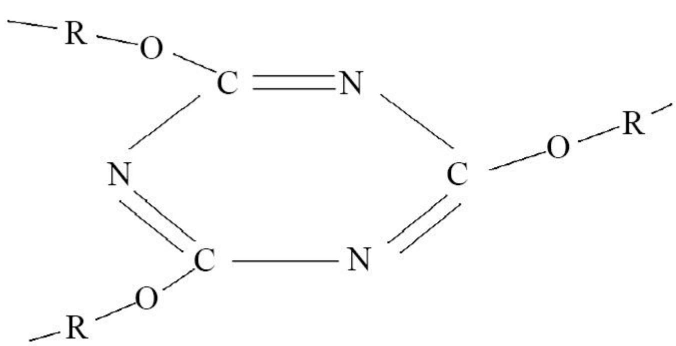

*Figure 5 Chemical structure of cyanate ester resin [Myslinski, 1997]*

Generally, cyanate esters have a minimal cure time of 3 hours at their cure temperature (either ~120°C or ~180°C). Their density is around 1.2 g/cm$^3$. Possible resin candidates for the iDod are:

- HexPly prepreg 954 or 996 series [Hexcel, 2007]

- Ten Cate Bryte Technologies EX-1515 [Ten Cate, 2007]
- YLA RS-3 and RS-12 [YLA, 2007]
- Cytec Cycom 5575-1 [Cytec, 2002]

| | | HexPly 954-6 | HexPly 996 | Ten Cate EX-1515 | YLA RS-3 | YLA RS-12 | Cytec Cycom 5575-1 |
|---|---|---|---|---|---|---|---|
| Cure temperature [°C] | | 121 | 177 | 107-121 | 177 | 129 | 175 |
| Density [g/cm$^3$] | | 1.25 | 1.15 | 1.17 | 1.19 | 1.21 | 1.21 |
| Out-life @ 25°C [days] | | - | - | 7 | - | - | 14 |
| Young's modulus [GPa] | | 3.7 | 3.0 | - | 2.96 | 3.45 | 3.7 |
| Flexural modulus [GPa] | | 3.9 | 3.2 | - | 3.32 | 3.52 | 4.2 |
| CTE [ppm/K] | | - | 58 | 61 | 43 | 52 | 48 |
| Moisture absorption [%] | | 0.25 | 0.2 | 0.04 | 0.69 | 0.91 | < 0.4 |
| CME [ppm/%m] | | - | - | - | 1364 | 1410 | 1170 |
| Outgassing [%] | TML | 0.07 | 0.17 | 0.18 | - | 0.24 | 0.21 |
| | CVCM | 0.00 | 0.01 | 0.01 | - | 0.00 | 0.01 |
| | WVR | 0.06 | 0.1 | - | - | 0.11 | - |

*Table 5 Properties of selected cyanate resins*

In the table, several abbreviations are used: CME stands for “coefficient of moisture expansion”, TML stands for “total mass loss”, CVCM stands for “collected volatile condensable materials”, and WVR stands for “water vapor regained”. All properties are for room temperature conditions. Cells without value indicate that no immediate information is available for these properties.
According to [Hexcel, 2007], NASA limits for outgassing are: TML = 1.0%, CVCM = 0.1% (no limit for WVR). Clearly, the resins for which this information is available are all well below these limits.
From the data that is available, it is clear that the out-life of the selected resins is only a few weeks. The out-life of a resin is the time it can be stored at room temperature. This should not be confused with the self-life, which is the storage time at a temperature of -18°C. When the out-life of a resin has been passed, it is no longer possible to cure it properly. This is due to the fact that the resin will already form crosslinks, albeit very slowly, at room temperature. For the current application the out-life needs to be years! This is amongst others caused by the satellite being exposed to room temperature conditions on Earth for at least a week. However, the main cause for this long out-life is the temperatures the CubeSat will attain in space. This of course depends on many parameters, but it has to be assumed that this temperature can be at or above room temperature for an extended period of time.
It is noted that the HexPly 996 resin is a cyanate siloxane resin. As will be discussed in subsection 5.2.1, this is an advantageous property with respect to protection against atomic oxygen.

At the present time, too little information is available to assess which specific resin type is best suited for the current application. A resin with a low curing temperature is preferred; therefore the HexPly 954-6, the Ten Cate EX-1515, and the YLA RS-12 resins are initially selected. Selecting the best resin remains TBD. It is certain that, when one of the above resins is selected, it needs to be modified to create a long out-life. For now, it is assumed that the resin is a cyanate ester with the following properties:

- Cure temperature of 120°C
- Density of 1.2 g/cm$^3$
- Young's modulus of 3.5 GPa
- Flexural modulus of 3.7 GPa
- CTE of 55 ppm/K

- 0.5% moisture absorption
- CME of 1400 ppm/%m
- TML of 0.2%, CVCM of 0.01%, WVR of 0.1%

It is noted that there are resins available that have a lower cure temperature than 120°C [Advanced Composites Group, 2007]. It however remains TBC whether the properties of these resins, possibly after modification, can meet the stringent requirements posed on them (low outgassing, long out-life, high resistance to thermal cycling, slow crack formation, good adherence to the fiber, etc.).
Lastly, it is noted that there is at least one commercial epoxy resin available, ATK's TCR resin, with an out-life of one year at room temperature [ATK, 2007]. Whether this resin can meet the requirements also remains TBC.

### 4.3 Weave type

Before selecting a specific fiber, a look is taken at the preferred type of weave in which the fiber should be woven. Several common weave styles are depicted on the next page.

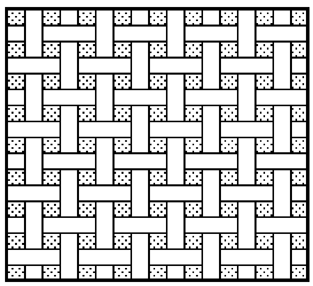

Plain Weave

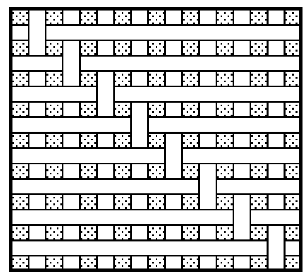

8 Harness Satin

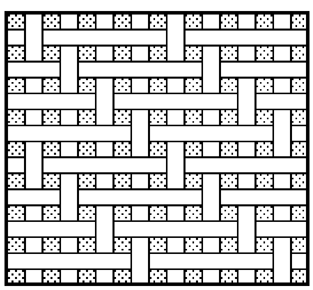

4 Harness Satin (or *crowfoot*)

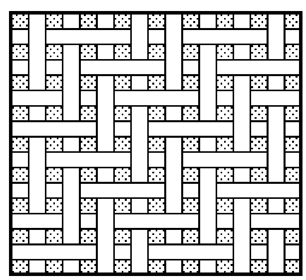

2 x 2 Twill

*Figure 6 Weaves styles [The Composites Store, 2007]*

The main requirement for the weave is that it has to be easy to deform since that will allow for a high packing efficiency for the inflatable structure. From the above styles, the 8H satin weave is the easiest one to deform. The explanation for this is that the individual fibers are less hindered by other fibers when they want to buckle or shear than in for instance a plain weave.
Although the 8H satin weave will allow more deformation than the 4H satin weave, it is not as common as the latter one. Therefore, when an off the shelf product is preferred, a 4H satin weave will do as well. In fact, since the fiber thickness is very small, even a plain weave will allow considerable deformation, but a satin weave is preferred nevertheless.

## 4.4 Fiber selection

Selection of a proper fiber for the fiber composite has to be done with several key requirements in mind:

1. The thickness of the fiber has to be low while the ultimate strain has to be high, this allows for a high packing efficiency of the inflatable structure. This is explained by looking at a folded fiber. The fiber can be bent the most when the radius of the bend can be as small as possible. At the bend, the part of the fiber in the "outer curve" is put under tension and the part of the fiber in the "inner curve" is put under compression. The thicker the fiber, the larger the strain at the outer curve of the bend at the same bend radius. A too large strain results in fiber failure. Thus, a fiber is required with a high strain/thickness ratio. The higher that ratio, the smaller the bend radius can be and therefore the better the fiber can be folded.
2. The fiber has to be able to withstand several fold/unfold cycles without breaking or severe deformation at the fold.
3. The density of the fiber has to be low in order to achieve a low composite density and therefore a low composite mass.
4. The fiber has to exhibit a very low amount of creep, this reduces the number and severity of permanent wrinkles (creases) when the inflatable structure is deployed after having been folded for over 1 year.
5. The fiber has to have a large temperature range.

The following table depicts several of the more common industrial fibers and their main properties [Michigan Technological University, 2007]:

| | Density ($gcm^{-3}$) | Longitudinal Tensile Modulus $E_1$ (GPa) | Transverse Tensile Modulus $E_2$ (GPa) | Poisson's ratio $\nu_{12}$ | Shear Modulus $G_{12}$ (GPa) | Longitudinal Tensile Strength $\sigma$ (MPa) | Longitudinal Thermal Expansion $\alpha_1$ ($10^{-6}$ $K^{-1}$) | Transverse Thermal Expansion $\alpha_2$ ($10^{-6}$ $K^{-1}$) | Heat Resistance °C | Cost $/kg |
|---|---|---|---|---|---|---|---|---|---|---|
| Glass | 2.45 | 71 | 71 | 0.22 | 30 | 3500 | 5 | 5 | | 0.70 |
| PBT | 1.58 | 320 | | | | 3100 | | | | 15.00 |
| Kevlar (49)<br>Kevlar (29) | 1.47 | 154<br>61 | 4.2 | 0.35 | 2.9 | 2800 | -4 | 54 | 550<br>450 | 4.50 |
| PE (Spectra)<br>PE (Dyneema) | 0.97<br>0.975 | 66-124[1]<br>115 | | | | 2300-3250[2]<br>3500 | -<br>-12 | | 150 | 12.00 |
| PBO Zylon AS<br>PBO Zylon HM | 1.54<br>1.56 | 180<br>270 | | | | 5800 | -6 | | 650 | 15.00 |
| Graphite (AS) | 1.75 | 224 | 14 | 0.2 | 14 | 2100 | -1 | 10 | | 7.00 |
| Graphite (HMS) | 1.94 | 385 | 6.3 | 0.2 | 7.7 | 1750 | -1 | 10 | | 8.00 |
| Boron | 2.45 | 420 | 420 | 0.2 | 170 | 3500 | 5 | 5 | | 54.00 |
| SiC | 3.2 | 406 | 406 | 0.2 | 169 | 3395 | 5.2 | 5.2 | | 75.00 |
| Saffil (5%$SiO_2$-$Al_2O_3$) | 3.3 | 300 | 300 | 0.2 | 126 | 1500 | 5.2 | 5.2 | | 2.50 |
| $Al_2O_3$ | 3.9 | 385 | 385 | 0.3 | 154 | 1400 | 8.5 | 8.5 | | 25.00 |

[1]Spectra 900 E=66-73GPa; Spectra 1000 E=98-113GPa; Spectra 2000 E=113-124GPa
[2]Spectra 900 $\sigma$=2.1-2.6GPa; Spectra 1000 $\sigma$=2.9-3.25GPa; Spectra 2000 $\sigma$=2.9-3.5GPa
PBT = Poly(p-phenylene-2,6-benzobisthiazole)
PE = Gel Spun ultra high molecular weight polyEthylene (Spectra®,Dyneema®)
PEN = polyEthylene Napthalate (Pentex®
PBO = Poly(p-phenylene-2,6-benzobisoxazole)

*Table 6 Selection of industrial fibers and their main properties*

In the above table, the ultimate strain of the fibers is not listed, but it is easily computed by dividing the longitudinal tensile strength of the fiber by its longitudinal tensile modulus. Doing this and setting a lower limit for the strain of 3% leads to the following shortlist:

1. Glass fiber (4.9%)
2. Kevlar 29 (3.5%)
3. Spectra 900 (3.5%)
4. Dyneema (3.0%)
5. Zylon AS (3.22%)
6. Vectran (4.5%) [Fette, 2004]

The last entry above, Vectran, is not listed in table 6. It is a liquid crystal polymer (LCP) fiber and is known to have very good creep properties [Fette, 2004].

Unfortunately, both PE fibers (Spectra and Dyneema) and Vectran have a maximum operating temperature of 150°C [Neil Pride Sails, 2007] [Fette, 2004]. In addition, the PE fibers also exhibit poor creep properties [Neil Pride Sails, 2007].
In subsection 4.2, it is indicated that cyanate ester resin systems require temperatures of ~120°C or even ~180°C to cure. Since the temperature of the iDod cannot be controlled exactly, it is not unlikely that the temperature of the inflatable structure will reach a temperature of 150°C when a curing temperature of ~120°C is required. Therefore, PE fibers and Vectran fibers are unsuited for the current application. However, when it can be proven that the temperature of the inflatable structure will remain well below 150°C, Vectran is a promising option.

After rejection of the above fibers, glass fiber, Kevlar, and Zylon are the remaining options. These options are extended by also considering quartz fibers and other aramid fibers besides Kevlar (Twaron and Technora).

The next figure shows the results for four fold/unfold cycles for glass fiber, carbon fiber, Kevlar, and Zylon (PBO) [Defoort, 2006]:

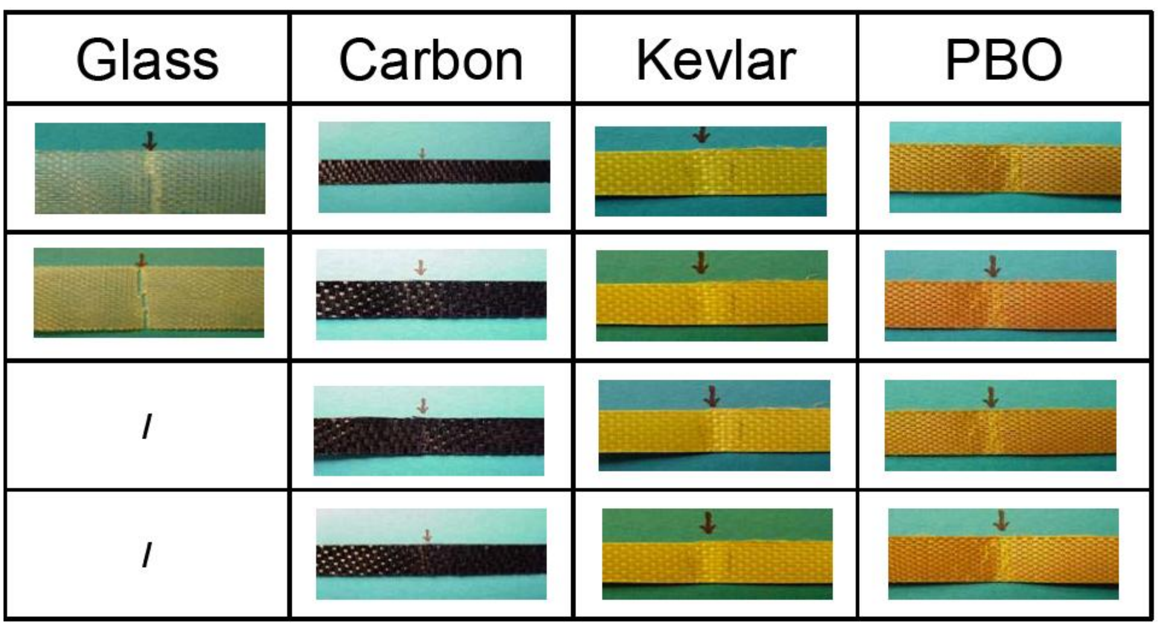


*Figure 7 Results for four fold/unfold cycles for various fibers*

It is clear that glass fiber is very sensitive to folding and is therefore rejected as an option. Although being similar to glass fiber, quartz fiber is listed in [Defoort, 2006] as being less sensitive to folding and as being very flexible. Therefore, quartz fiber is still an option.

When looking at the available fiber thicknesses, Zylon and Twaron are the thickest fibers of the remaining options with a minimum “thickness” (linear density) of 278 dtex for Zylon [Toyobo, 2007] and 420 dtex for Twaron [Teijin Twaron, 2006]. Kevlar 29 and Kevlar 49 are available in 220 dtex and 215 dtex respectively [DuPont]. Technora is available from 110 dtex [Wilms-Floet, 2007]. Quartz fiber, Astroquartz II (type 300 1/0), is available with a linear density of 165 dtex [JPS, 2007] (In the source, the linear density of type 300 2/0 is referred to as 15000 yd/lb. Type 300 1/0 has half the number of filaments of type 300 2/0 (120 versus 240), which results in 30000 yd/lb. This is equal to 60.48 m/g. Thus, 10000 m weighs 10000/60.48 = 165 g, which is also the linear density).

According to [Defoort, 2006], Aramid fibers have medium flexibility, Zylon fibers have high flexibility, and Quartz fibers have very high flexibility. According to the same source, all three fibers are not especially sensitive to folding.

The next table summarizes the properties of the three remaining fibers.

| | **Astroquartz II** | **Technora** | **Zylon** |
|---|---|---|---|
| **Stiffness [GPa]** | 72 | 82 | 180 |
| **Smallest linear density [dtex]** | 165 | 110 | 278 |
| **Density [g/cm$^3$]** | 2.2 | 1.39 | 1.54 |
| **Elongation [%]** | 5.0 | 4.1 | 3.2 |
| **Flexibility** | Very high | Medium | High |
| **Thermal stability** | High | High | High |
| **UV** | Transparent | Not transparent, weakly resistant | Transparency to be confirmed, weakly resistant |
| **CTE [ppm]** | 0.54 | -6 | -6 |
| **Availability** | Medium | Good | Medium |

*Table 7 Properties of selected fibers [Defoort, 2006] [Wilms-Floet, 2007] [JPS, 2007] [Michigan Technological University, 2007]*

Attractive about Technora and Zylon is their negative CTE, which will reduce the CTE of the composite they are part of. Zylon also offers a very high stiffness compared to the other two options. However, due to its thickness and medium availability, Zylon is considered too be a less good candidate than Astroquartz II and Technora.

Choosing between Technora and Astroquartz II is difficult. Looking at their linear density and at their density, it is concluded that the thickness of those fibers is roughly equal: Although the linear density of Astroquartz II is a factor 1.5 higher than that of Technora, its density is a factor 1.58 higher. It will therefore occupy only 1.5/1.58·100% = 94% of the volume that is required by the Technora fiber and is thus slightly thinner. The elongation, flexibility, and UV resistance of Astroquartz II is also better, but Technora has a better CTE and better availability. Also, the low density of Technora will result in a low density for the composite.

Since density is important for the weight of the composite and since a good availability is important for a short development process, Technora is selected as the fiber of choice. Yet, quartz fiber remains a good alternative option.

It is noted that the tensile modulus of Twaron and Technora is measured in a different way than for Kevlar [Wilms-Floet, 2007]. For Kevlar, the modulus is measured “bone-dry-finish-free”, meaning that all water and finish has been removed from the fiber. For Twaron and Technora, this is not the case, resulting in lower measured tensile moduli. When a correction is applied for this, roughly the same tensile moduli are obtained as for Kevlar. Therefore, it is from now on assumed that the stiffness of Technora is similar to that of Kevlar 29 (the Kevlar type that resembles Technora the most), which is 100 GPa [DuPont].

According to [JPS, 2007], the thinnest available Astroquartz II weave has a thickness of 0.075 m and an areal weight of 68 g/m$^2$. No Technora weaves have been found, but information from [Hexcel, 2007] and [Ten Cate Advanced Composites, 2007] indicates that 215 dtex aramid fiber weaves have a thickness between 0.08 and 0.12 mm.
For now, due to lack of sufficient data, it is assumed that a 110 dtex Technora weave has a weight of 45 g (1.39/2.2 · 68) and a thickness of 0.07 mm (calculated in the next subsection).

Lastly, it is noted that aramid fiber is known to have poor resistance against UV-radiation [Neil Pride Sails, 2007]. Although it is initially protected against this radiation by the outer layer of foil (see figure 3) and the resin in which it is embedded, this protection may not last for 25 years in space. Therefore, when there is genuine concern that a significant amount of aramid fiber will be exposed to UV-radiation sometime during the lifetime of the iDod, its UV-resistance can possibly be increased by coating the fiber. This is discussed in more detail in subsection 5.2.2. The influence of UV-radiation on a fiber composite with Technora (or Kevlar) fibers and its impact on the design of the iDod is left TBD.

## 4.5 Composite proposition

Using the information from the preceding subsections, a fiber composite proposition is made. It is proposed to use a prepreg with a 0°/90° Technora weave of 215 dtex and a cyanate ester resin. For transport, the prepreg is covered with PE foil to prevent the material on the roll from sticking together:

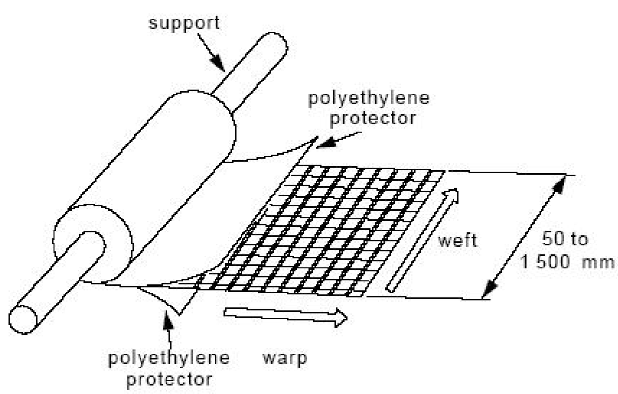


*Figure 8 Fiber composite prepreg [Hexcel, 2005]*

Using a prepreg moves one production step from the customer to the supplier, saving time for the customer. For clarity it is noted that only one ply of material is used.

In a fiber composite, the properties of the composite are optimal for a certain fiber volume content ($v_f$) and a certain matrix volume content ($v_m$). For an aramid/epoxy composite, the figure below indicates that $v_f$ = 0.45 and $v_m$ = 0.50.

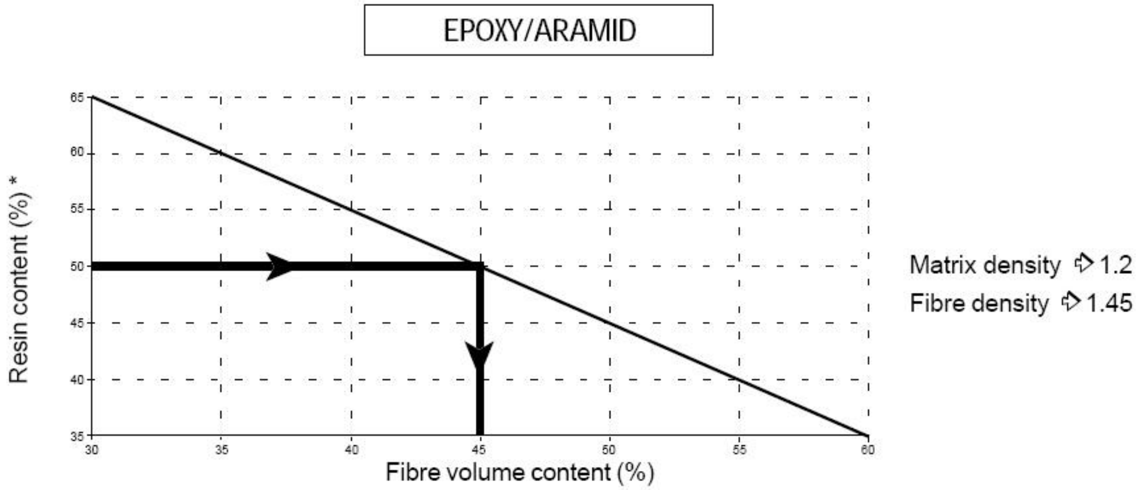


*Figure 9 Optimum volume contents for an aramid/epoxy composite [Hexcel, 2005]*

The resin content and the fiber volume content in the figure above don't add up to 100%. A possible cause for this is that voids have been taken into account. Voids are bubbles of air that are trapped in the resin and as such reduce the fraction of resin present in the total material volume.

The thickness of the cured ply ($t_{ply}$, in hundredths of millimeters) is determined with the following formula [Hexcel, 2005]:

$$t_{ply} = \frac{w_f}{10\rho_f v_f} \left[\frac{1}{100}\text{mm}\right]$$

In the formula, $w_f$ denotes the areal weight of the fiber weave (g/m$^2$) and $\rho_f$ denotes the density of the fiber (g/cm$^3$).

The density of the composite ($\rho_{comp}$) is determined using the rule of mixtures:

$$\rho_{comp} = v_f \rho_f + v_m \rho_m$$

Where $\rho_f$ is the density of the fibers and $\rho_m$ is the density of the matrix. The in-plane Young's modulus (E) of the composite in x-direction ($E_x$) and in y-direction ($E_y$) can also be determined using the rule of mixtures (parallel model, assuming equal strain in the matrix and the fiber). Since only one 0°/90° ply is used, $E_x = E_y$.

$$E_f v_f + E_m v_m = E_x = E_y$$

Where $E_f$ is the Young's modulus of the fibers and $E_m$ is the Young's modulus of the matrix. The CTE of the composite is determined in the same manner, assuming equal strain in the matrix and the fiber:

$$CTE_f v_f + CTE_m v_m = CTE_x = CTE_y$$

The next table summarizes the properties of the matrix and the fiber discussed earlier in this section which are required to determine the ply thickness, the composite density, the composite Young's modulus, and the composite CTE.

| | Matrix | Fiber |
|---|---|---|
| Density [g/cm$^3$] | 1.2 | 1.39 |
| Young's modulus [GPa] | 3.5 | 100 |
| CTE [ppm/K] | 55 | -6 |
| Volume fraction [%] | 50 | 45 |

*Table 8 Matrix and fiber properties*

Below, the calculations are performed to determine the properties of the composite:

$$t_{ply} = \frac{w_f}{10\rho_f v_f} = \frac{45}{10 \cdot 1.39 \cdot 0.45} = 7.19 \left[\frac{1}{100}\text{mm}\right] \approx 0.07 \text{ mm}$$

$$\rho_{comp} = v_f \rho_f + v_m \rho_m = 0.45 \cdot 1.39 + 0.50 \cdot 1.2 = 1.23 \text{ g/cm}^3$$

$$E_x = E_y = E_f v_f + E_m v_m = 100 \cdot 0.45 + 3.5 \cdot 0.5 = 46.75 \text{ GPa}$$

$$CTE_x = CTE_y = CTE_f v_f + CTE_m v_m = -6 \cdot 0.45 + 55 \cdot 0.5 = 24.8 \text{ ppm/K}$$

The most important conclusion that is drawn from the above calculations is that the CTE of the composite is relatively high compared to the CTE of Upilex-S. The CTE of Upilex-25S is listed in table 4 as being 12 ppm/K, this is half of that of the composite.
Using a composite is justified in [Maessen, iDod.TN.007] for its added stiffness. There, it is also indicated that using a composite offers the possibility of reducing the CTE of the complete structure to a very low value. This is beneficial with respect to thermal cycling and consequential micro cracking of coatings. Clearly, a reduction in CTE cannot be achieved using this particular composite. In fact, the CTE of the structure will be increased! The increase in stiffness compared to Upilex-S is a factor 5 (46.75 GPa versus 9.121 GPa (at room temperature)).

The density of the composite with 5% of its volume consisting out of voids is lower than the density assumed in [Maessen, iDod.DD.001], which is 1.3 g/cm$^3$. When no voids are present, the density is 1.29 g/cm$^3$.

# 5 COATING

Coatings have to be applied on the inflatable structure of the iDod to give it the correct thermo-optical properties and to provide protection against the hostile low Earth orbit environment. The selected thermal coating is discussed in subsection 5.2.1, while the selected protective coatings are discussed in subsection 5.2.2.

## 5.1 Thermal coating

In [Maessen, iDod.TN.011], a thermal coating proposition is made. This coating consists of vapor deposited aluminum (VDA) and $SiO_2$ on a Kapton substrate (at the time of writing that document, Kapton was assumed to be the membrane material). The $SiO_2$ is only required for protection against the space environment (see subsection 5.2.1).
Since no detailed thermal analysis has yet been made, it is for now assumed that VDA is a proper thermal coating for the structure. Nice to know is that Upilex can be ordered with a VDA coating [UBE Industries, 2007]. The properties of VDA are assumed to be similar to pure aluminum. Thus, its density is 2.70 g/cm$^3$ and its CTE at room temperature is 24 ppm/K [Matweb, 2007].

## 5.2 Protective coating

Since the low Earth orbit environment is very hostile for virtually all materials, some form of protection has to be applied for the materials used on the iDod. For the iDod, only protective coatings can be used since they require a minimal amount of mass and volume. Protective coatings for the polyimide foil and for the aramid fiber are discussed in the coming subsections.

### *5.2.1 Foil*

Polyimide foil, although being very resilient, is known to quickly wither away when exposed to the low Earth orbit environment. It is constantly battered with atomic oxygen, radiation (ultraviolet and x-ray), charged particles (electrons and protons), and MMOD (micro-meteoroids and orbital debris). Various coatings can be applied to form a barrier between the polyimide material and space. Crucial in the performance of a coating are its [Raja Reddy, 1995]:

- *Continuity*: It has to cover the substrate for 100%. If not, parts of the substrate will be unprotected.
- *Porosity*: When the coating exhibits relatively large pores, small particles can still penetrate the coating.
- *Degree of adhesion*: The coating has to adhere strongly to the substrate to prevent parts of the coating to release from the substrate at some point in the lifetime of the structure.
- *Durability*: The coating has to be resilient to the space environment.
- *Coefficient of thermal expansion (CTE)*: Due to thermal cycling, cracks can develop in the coating when its CTE is markedly different from that of the substrate. This results in parts of the substrate to be unprotected.

Inorganic coatings ($SiO_2$, $Al_2O_3$, ITO, $SnO_2$, etc.) are more or less the accepted standard for coating (metallized) polymer films. Due to their high oxygen-content they do not react well with atomic oxygen, which is beneficial. Silica, $SiO_2$, is a coating with good overall properties and is recommended in [Dever, 2002]. Downside of an inorganic coating is that it is relatively brittle, which will lead to the formation of cracks due to thermal cycling. To prevent this, it can be mixed with 5-10 mass% PTFE (Teflon) for more flexibility [Dever, 2002][Raja Reddy, 1995]. The thickness of a $SiO_2$ coating is usually around 1000Å. Its CTE is as low as 0.55 ppm/K and its density is 2.20 g/cm$^3$ [Wikipedia, 2007]. $SiO_2$ coatings on Upilex-S can be readily ordered.

The CTE of PTFE is 135 ppm/K [Boedeker Plastics, 2007]. When mixed with $SiO_2$, the CTE of the combination is, using the rule of mixtures, 7-14 ppm/K for 5-10% PTFE content (the density of PTFE (2.16 g/cm$^3$) is very close to the density of $SiO_2$ (2.20 g/cm$^3$), thus mass content translates 1:1 with volume content, which allows calculation of the CTE directly from the mass contents). This is comparable with the CTE of Upilex-25S, which is 12 ppm/K, and therefore advantageous with respect to thermal cycling.

Alternatively, polysiloxane coatings can be used instead of $SiO_2$. The chemical formula for siloxane is $R_2SiO$ with R being an organic group. Upon contact with atomic oxygen, $SiO_2$ is formed on the surface of the coating. Cracking or spalling (chips of coating falling off) of this upper layer results in a fresh layer of polysiloxane material being exposed. How this type of coating performs with respect to $SiO_2$ remains TBC, but is expected to be similar.

Information from [Vance, 1989] indicates that the erosion rate for siloxanes is one or two magnitudes less than for polyimide materials. Erosion rates for inorganic compounds such as $SiO_2$ are even three orders of magnitude less than for polyimide materials.

Although not likely to be used, it is noted that there exists the possibility to use polymer films that are more resistant to atomic oxygen than standard polyimide films. These films protect themselves by means of self-sacrifice: they form a layer of protective $SiO_2$ when exposed to

atomic oxygen. One such example is Kapton AOR (Atomic Oxygen Resistant) [Vance, 1989]. However, it is unclear whether this material is still available. This is left TBD.
Another, more recent, example is POSS Kapton polyimide (POSS = Polyhedral Oligomeric Silsesquioxane) [Tomczak, 2005]. This polyimide film is obtained by mixing polysiloxane with polyimide copolymer. Like Kapton AOR, it forms a layer of $SiO_2$ on its surface upon reaction with atomic oxygen. In [Tomczak, 2005], POSS polyimide is shown to exhibit up to 2 orders of magnitude less erosion yield than Kapton H (in case of 25 weight % POSS) upon exposure to atomic oxygen. Unfortunately, it being a recent and mainly American development, POSS polyimide is not regarded to be a useable material for the near future.

For now, 1000Å thick $SiO_2$ is selected as protective coating for the inflatable structure. Its selection is mainly driven by the possibility to purchase Upilex-S foil with this coating already applied by the foil manufacturer, UBE Industries. When possible, a small content of PTFE is desired in the coating for CTE compatibility with the Upilex foil.

### *5.2.2 Fiber*

As discussed in section 4.4, aramid fibers have poor resistance against UV radiation. This resistance can be enhanced by applying a special coating to the fiber before it is woven. Coating of aramid fibers is done by companies like Fiber-Line International. Not much information regarding the coating has been obtained, but on their website Fiber-Line states [Fiber-Line, 2007]: "*Fiber-Line's® formulations start with an UV resistant polymeric binder compatible with the high strength fiber and combines synergistic HALS (hindered amine light stabilizers) and organic UV inhibitors. Carbon black pigment performs the best in UV resistance; however other colors are available upon request".*
However, a discussion held with Danny Wlims-Floet, Sales Manager Composites of Teijin Twaron, gives reason to be skeptic regarding the above statement. According to him, in-house tests by Teijin Twaron and other companies showed that Technora fibers with carbon black pigmentation did not have better UV-resistance than uncoated fibers! Also, the UV resistance of Technora is similar to Twaron and Kevlar.
Thus, coating fibers should not be expected to provide dramatic improvement in UV resistance!

Furthermore, it has to be kept in mind that coatings influence the adherence of the fiber to the matrix. Therefore, they have to be applied with care to ensure satisfactory composite performance.

Although it is not expected, the aramid fibers can be exposed to atomic oxygen at some point in the lifetime of the iDod. Information from [Raja Reddy, 1995] indicates that aramid fibers have roughly the same reactivity coefficient (or erosion yield, $cm^3$/atom) as polyimide material. Kevlar 29 has a reactivity of $1.1\text{-}1.5 \cdot 10^{-24}$ $cm^3$/ atom, close to Upilex-S, while Kevlar 49 has a significantly higher reactivity of $4.0 \cdot 10^{-24}$ $cm^3$/atom, which is close to Kapton. For a fiber composite, the reactivity coefficient is comparable.

# 6 CONCLUSIONS & RECOMMENDATIONS

The storage device for the inflatable structure is selected to be made from aluminum 6061-T6. Reason for this is that this type of aluminum is standard in CubeSats.
The foil material for the inflatable structure is selected to be a polyimide material called Upilex-S. Reasons for its selection are the wide temperature regime in which it can be used and its resilience against the space environment.
The rigidizing material for the inflatable structure is a thermally cured fiber composite. The resin is a cyanate ester and the fiber is woven in a 0°/90° satin weave. Based on its low density and good availability, Technora (an aramid) is selected as the fiber type.
Vapor deposited aluminum (VDA) will serve as thermo-optical coating on the Upilex-S foil in order for the inflatable structure to obtain a sufficiently high temperature to allow curing of the cyanate resin.
A layer of 1000Å thick $SiO_2$ will serve as protective coating for the Upilex-S foil. This coating is widely used in spacecraft and mainly provides protection against atomic oxygen. It is

preferred to mix a small amount of PTFE (5-10%) with the $SiO_2$ for increased coating flexibility and a coating CTE that is close to the CTE of Upilex-S. This reduces the amount and severity of cracks forming in the coating due to thermal cycling.

The next table summarizes the values for the density and the CTE at room temperature for the selected materials. These properties are deemed to be the most important overall material properties for the iDod.

| | **Material** | **Density [g/cm$^3$]** | **CTE [ppm/K]** |
|---|---|---|---|
| **Storage device** | Aluminum 6061-T6 | 2.70 | 24 |
| **Inflatable structure** | Upilex-S | 1.47 | 12 |
| | Technora/cyanate composite | 1.23 | 25 |
| | VDA | 2.70 | 24 |
| | $SiO_2$ | 2.20 | 0.55 |
| | 90% $SiO_2$ + 10% PTFE | 2.20 | 14 |

*Table 9 Density and CTE of selected materials*

Based on its CTE mismatch with Upilex-S, it is recommended to get rid of the fiber composite when this is allowed by the stiffness requirements for the inflatable structure. Consequentially, the VDA coating is no longer needed since a high temperature doesn't have to be achieved anymore, removing another material causing CTE mismatch. Removing the composite also results in far less difficulties with respect to manufacturing and will reduce the mass and volume of the inflatable structure.

## 7 FURTHER WORK

Unless new important information becomes available, no further work on this topic is foreseen during this thesis.

## REFERENCES


1. About, Inc., *A Brief History of Kevlar,* http://composite.about.com/od/aboutcompositesplastics/l/aa050597.htm, Viewed February 2007.

2. Advanced Composites Group, *Low Temperature Moulding*, http://www.advanced-composites.com/what-we-do/aerospace/low-temperature-moulding/, Viewed March 2007.

3. ATK, *Advanced Materials*, http://www.atk.com/internationalproducts/interprod_advancedmaterials.asp, Viewed March 2007.

4. Bernasconi, M.C., *Material Aspects for Gossamer Structures: Thin-Film Options*, presentation at the 3rd European Workshop on Inflatable Space Structures, ESA ESTEC, Noordwijk (NL), 10-12 October 2006.

5. Boedeker Plastics, Inc., *PTFE Specifications*, http://www.boedeker.com/ptfe_p.htm, Viewed March 2007.

6. Bousquet, P.W., et. al*., De-orbiting Microscope spacecraft by drag enhancement,* IAC-06-B6.4.5.

7. Cytec Engineered Materials, *CYCOM® 5575-1 RTM,* Datasheet, 16 May 2002.

8. Defoort, B., et. al., *Sub $T_g$ Rigidization of Gossamer Structures*, Presentation on the 3rd European workshop on inflatable space structures, ESA ESTEC, Noordwijk (NL), 10-12 October, 2006.

9. Dever, J. et. al., *Exposure of Polymer Film Thermal Control Materials on the Materials International Space Station Experiment (MISSE)*, NASA/TM 2002-211363, February 2002.

10. DuPont™, *Kapton® HN Polyimide film,* Technical Data Sheet, March 2006.

11. DuPont™, *Products and Properties of Kevlar®*, Kevlar pdf datasheet obtained by e-mail.

12. Fette, R.B., Sovinski, M.F., *Vectran Fiber Time-Dependent Behaviour and Additional Static Loading Properties*, NASA/TM-2004-212773, Greenbelt (USA), December 2004.

13. Fiber-Line®, *UV Resistant Fibers*, http://www.fiber-lineinc.com/index.php?id=18, Viewed February 2007.

14. Fiberset Inc, *Glossary Of Composite Terms,* http://www.fiberset.com/html/glossary/glos_f.htm, 3 September 1999.

15. Groh, K.K. de et.al., *MISSE PEACE Polymers Atomic Oxygen Erosion Results*, NASA/TM-2006-214482, November 2006.

16. Groot, B.C.H. de, *Inflatable Gravity Gradient Boom System Development*, Delfi-1 SLR 142-149, Faculty of Aerospace Engineering, Delft University of Technology, June 2003.

17. Hexcel, Fabrics - *Aramid and High Performance Data Sheets,* http://www.hexcel.com/Products/Downloads/Fabrics+Data+Sheets.htm?map=P2&t=Aramid+and+High+Performance+Data+Sheets, Viewed February 2007.

18. Hexcel, Prepreg Data Sheets, http://www.hexcel.com/Products/Downloads/Prepreg%20Data%20Sheets/, Viewed February 2007.

19. Hexcel, Prepreg Technology, Informative datasheet, March 2005.

20. Iwata, M., et. al., *Measurement and Evaluation of Thermal Control Material with Polyimide for Space Use,* AIAA-3733-332, Journal of Spacecraft and Rockets, Vol. 38, No. 4, July-August 2001.

21. Jenkins, C.H.M., *Gossamer Spacecraft: Membrane and Inflatable Structures and Technology for Space Applications*, AIAA, Reston (USA), 2001.

22. JPS Composite Materials, *Product Manual,* http://www.jpsglass.com/jps_product_manual.pdf, Downloaded March 2007.

23. Lefevre, Y-M, *Inflatable Structure Technology: Promising Solutions for Spacecraft Applications,* First European Workshop on Inflatable Space Structures, ESTEC, Noordwijk (NL), 21-22 May 2002.

24. Maessen, D.C., *iDod attitude stability analysis,* iDod document iDod.TN.009, Version 1.0, Faculty of Aerospace Engineering, Delft University of Technology, 16 January 2007.

25. Maessen, D.C., *iDod inflatable structure conceptual design trade-off,* iDod document iDod.TO.001, Version 1.0, Faculty of Aerospace Engineering, Delft University of Technology, 11 January 2007.

26. Maessen, D.C., *iDod rigidization,* iDod document iDod.TN.007, Draft, Faculty of Aerospace Engineering, Delft University of Technology, 16 January 2007.

27. Maessen, D.C., *iDod storage device*, iDod document iDod.DD.002, Draft, Faculty of Aerospace Engineering, Delft University of Technology, Not yet published at time of writing of this report.

28. Maessen, D.C., *Straw man concept design description,* iDod document iDod.DD.001, Draft, Faculty of Aerospace Engineering, Delft University of Technology, 25 September 2006.

29. Maessen, D.C., *Thermal design,* iDod document iDod.TN.011, Version 1.0, Faculty of Aerospace Engineering, Delft University of Technology, 29 January 2007.

30. MatWeb, *Aluminum*, http://www.matweb.com/search/SpecificMaterial.asp?bassnum=AMEAl00 Viewed March 2007.

31. MatWeb, *Aluminum 5052-H32*, http://www.matweb.com/search/SpecificMaterial.asp?bassnum=MA5052H32 Viewed January 2007.

32. MatWeb, *Aluminum 6061-T6; 6061-T651*, http://www.matweb.com/search/SpecificMaterial.asp?bassnum=MA6061T6 Viewed February 2007.

33. MatWeb, *UBE Upilex-25S (25 micron) Polyimide Film*, http://www.matweb.com/search/SpecificMaterial.asp?bassnum=PUBE235 Viewed February 2007.

34. Michigan Technological University, *Properties of Selected Fibres and Matrices,* http://www.mse.mtu.edu/~drjohn/my4150/props.html, Viewed February 2007.

35. Myslinski, P.J., *Analysis of cyanate ester resins and graphite fabric for use in resin film infusion processing*, Faculty of the Virginia Polytechnic Institute and State University, Blacksburg (USA), December 1997.

36. Neil Pride Sails, *Fabric Lexicon, A Lexicon of Today's Fibers,* http://sailingsource.com/neilpryde/sailcloth/lexicon.htm, Viewed February 2007.

37. Polymer abbreviations, http://www.rit.edu/~axlsch/classes/schm703/Abbreviations.pdf, Viewed February 2007.

38. Pumpkin, Inc., *CubeSat Kit*, http://www.cubesatkit.com/ Viewed January 2007.

39. Raja Reddy, M., *Review: Effect of low earth orbit atomic oxygen on spacecraft materials*, Journal of Materials Science, No. 30, pg 281-307, Chapman & Hall, 1995.

40. Semprimoschnig, C.O.A. et al, *Assessing The Limits Of Commercially Available Polyimides,* First European Workshop on Inflatable Space Structures, ESTEC, Noordwijk (NL), 21-22 May 2002.

41. Smithsonian/NASA ADS, *Fiberite 954: cyanate ester systems*, Abstract, http://adsabs.harvard.edu/abs/1992SPIE.1690..288A, Viewed February 2007.

42. Teijin Twaron, *Main physical properties of Twaron & Technora,* received by e-mail on 27 February 2007.

43. Teijin Twaron, *Technora Data Sheet*, April 2002, received by e-mail on 27 February 2007.

44. Teijin Twaron, *Twaron Data Sheet*, February 2006, received by e-mail on 27 February 2007.

45. Ten Cate Advanced Composites, *Standaard weefseloverzicht,* received by e-mail from Harm Albers on 16 January 2007.

46. Ten Cate Advanced Composites USA (Bryte Technologies), *EX-1515 Resin System,* Technical Datasheet, January 2007.

47. The Composites Store, *Popular Weave Styles,* http://www.cstsales.com/weave_styles.html, Viewed February 2007.

48. Tomczak, S.J., et. al., *Properties and Improved Space Survivability of POSS (Polyhedral Oligomeric Silsesquioxane) Polyimides*, Materials Research Society Symposium Proceedings, Volume 851, 2005.

49. Toyobo, *Zylon, Products*, http://www.toyobo.co.jp/e/seihin/kc/pbo/menu/fra_menu_en.htm, Viewed March 2007.

50. UBE Europe GmbH, *Upilex-RN*, Datasheet, Düsseldorf (GE), 3 November 2005.

51. UBE Europe GmbH, *Upilex-S*, Datasheet, Düsseldorf (GE), 3 November 2005.

52. UBE Industries, Ltd., *Upilex films*, http://www.upilex.jp/e_tcm.html, Viewed February 2007

53. UBE Industries, Ltd., *Upilex-R Thermal Control Films*, Data Sheet TCF-R-000, Revision A, 6 September 2002.

54. UBE Industries, Ltd., *Upilex-S Thermal Control Films*, Data Sheet TCF-S-000, Revision A, 6 September 2002.

55. Vance, D.A., et. al., *Atomic-oxygen-resistant polymer for use in the low Earth orbit,* Lockheed Missiles & Space Company, Inc., R&D Division, Palo Alto (USA), 1989.

56. Wilms-Floet, D., e-mail exchange in which is outlined why the measured linear modulus of fibers with different dtex values varies and in which is explained how the linear modulus is measured at Teijin Twaron and DuPont respectively, e-mail received on 1 March 2007.

57. Wilms-Floet, D., Technora datasheet (Excel), received on 12 March 2007.

58. Wikipedia, *Bisphenol-A*, http://en.wikipedia.org/wiki/Bisphenol-A, 22 February 2007.

59. Wikipedia, *Epichlorohydrin*, http://en.wikipedia.org/wiki/Epichlorohydrin, 12 February 2007.

60. Wikipedia, *Epoxy*, http://en.wikipedia.org/wiki/Epoxy, 21 February 2007.

61. Wikipedia, *Fused quartz*, http://en.wikipedia.org/wiki/Fused_silica, 13 February 2007.

62. YLA Advanced Composite Materials, *Resin Systems*, http://www.ylainc.com/yla_products/product_list.php?name=other_resin_systems&showcategory=1&cat1=Epoxy&cat2=Cyanate&cat3=HighTemp&cat4=Other&cat5=Film&cat6=Microply&cat7=Compression, Viewed February 2007.

# Thermal design

## SUMMARY

For the inflatable structure of the iDod, it is investigated what type of coating is required for it to achieve average equilibrium temperatures between 100°C and 200°C. This is done for extreme cases using a single node model of the inflatable structure. The high temperatures are required to allow chemical rigidization of the inflatable structure by means of thermal curing of a thermoset resin.

The results indicate that a coating with an absorption/emission coefficient ($\alpha/\varepsilon$) ratio between 2.2 and 7.1 is required to reach an average temperature of 100°C. A ratio of 2 to 5 is deemed obtainable and therefore this average temperature can be reached. Metallic coatings are considered good coating candidates. A ratio between 6 and 18.8 is required for a temperature of 200°C and is considered to be infeasible.

It is recommended to use a resin with a low curing temperature. It is further recommended to perform a more detailed transient thermal analysis in the future. This allows for selection of the optimal places to position the thermal coating on the structure and will provide an estimate for the time that is required to fully cure the resin.

The influence of heating due to friction with the Earth's atmosphere is found to be not of importance above ~200 km altitude.

## KEYWORDS

Coating, temperature, inflatable structure

## DISTRIBUTION

| | Name | | Company / Institution |
|---|---|---|---|
| 1 | E.D. van Breukelen | Customer | ISIS B.V. |
| 2 | B.T.C. Zandbergen | Project supervisor | TU Delft |

## APPROVAL

| | Name | Company / Institution | Date | Signature |
|---|---|---|---|---|
| *Written* | D.C. Maessen | TU Delft | 3/21/2007 | |
| *Checked* | | | | |
| *Approved* | | | | |

## REVISION RECORD

| Issue | Date | Total pages | Affected pages | Brief description of change |
|---|---|---|---|---|
| Draft | 1/16/2007 | 12 | | |
| Version1.0 | 1/29/2007 | 31 | 1 | Summary extended |
| | | | 4 | Design requirements section added |
| | | | 4 | Symbol $c_p$ replaced by c in first formula |
| | | | 5 | Value for solar constant changed to 1371 ± 5 W/m$^2$ |
| | | | 5 | Explanation for $\alpha_{ir} = \varepsilon_{ir}$ changed |
| | | | 6 | Value for Earth infrared radiation energy at the Earth's surface changed to 237 ± 21 W/m$^2$. $S_{ir}$ changed to 177 ± 15.7 W/m$^2$ |
| | | | 6 | Value for albedo coefficient changed to 0.30 ± 0.05 |
| | | | 6 | Values for F from figure 2 now only regarded as indication |
| | | | 7 | Subsection 3.2 partially changed |
| | | | 7,8 | Subsection 4.1 added |
| | | | 8-17 | Subsection 4.2 greatly changed |
| | | | 18-20 | Subsection 4.4 expanded |
| | | | 21 | Units for aerodynamic heat flux made more clear in caption for table 7 |
| | | | 21,22 | Thermal testing section added |
| | | | 24-31 | Appendices with Matlab codes added |
| Version 1.1 | 3/14/2007 | 32 | 20 | Coating proposition added |
| | | | 23 | Added that a detailed thermal analysis also needs to take into account the effects caused by a temperature gradient over the tubes |
| | | | 23 | Recommendation added to check influence of change in optical properties with time |
| Version 1.2 | 3/21/2007 | 34 | 1 | Summary changed |
| | | | 4 | Changed subsection 3.2 into section 2 |
| | | | 5 | Adapted section 3 |
| | | | 8 | Changed title of section 5 |
| | | | 8 | Indicated that method used is advised by Aldert Kamp |
| | | | 8-14 | Changed subsection 5.2 |
| | | | 14 | Changed contents of subsection 5.2.3 |
| | | | 16 | Removed temperatures in figure 10 |
| | | | 18 | Inserted an example calculation to show that aerodynamic heating is not important. |
| | | | 18 | Indicated in subsection 8.1 why rigidization has to occur within a few orbits |
| | | | 20 | Added that a more advanced thermal model should be time-dependent and should be able to provide the temperature distribution over the entire inflatable structure |
| | | | 22-26 | Added appendix A |
| | | | Many | Minor textual changes |

## LIST OF TBD'S AND TBC'S

| TBD / TBC | Paragraph | Subject | Due date | Action by |
|---|---|---|---|---|
| TBD | Section 2 | Necessity of rigidization | TBD | TBD |
| TBD | Section 4 | Temperature tubes iDod | TBD | TBD |
| TBD | Section 4 | Precise coatings | TBD | TBD |
| TBD | Section 6 | Curing time resin | TBD | TBD |
| TBD | Section 6 | Qualification temperature range iDod | TBD | TBD |

## TABLE OF CONTENTS

# 1 INTRODUCTION

For any space structure, the thermal design is an important part of the complete design. Space inflatables are no exception to that. In case of the iDod, the temperature of the inflatable structure can only be controlled by using coatings.

This document deals with the selection of the proper coating type(s) for the inflatable structure of the iDod. Selection of the preferred type of coating is done based on four different single node computations of the average equilibrium temperature of the inflatable structure.
Since a single node computation provides only a very rough indication of the attainable temperature, no real coating selection is made. Instead, it is indicated which ratio $\alpha/\varepsilon$ (energy absorption / energy emission) is preferred for the coating(s) and an interesting coating option is proposed.
The influence of the CubeSat on the obtained temperatures is not taken into account.

Section 2 describes the geometry of the inflatable structure. The design requirement that dictates the thermal design is shortly discussed in section 3. Section 4 introduces the terminology and equations required to calculate equilibrium temperatures in section 5 and to make a coating selection in section 6. The influence of aerodynamic heating is shortly discussed in section 7. Thermal testing is briefly treated in section 8.

# 2 INFLATABLE STRUCTURE GEOMETRY

The thermal behavior of the inflatable structure to a large extent depends on its geometry. This can be seen in the equation for the equilibrium temperature in section 4, where four different projected areas are present. The relative size of these projected areas (in combination with their coating) determines how much energy is received or rejected. The inflatable structure of the iDod looks as follows:

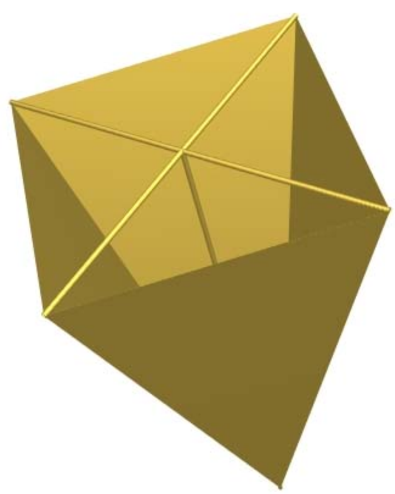

*Figure 1 Inflatable structure iDod*

From [Maessen, iDod.TO.001], the following dimensional properties are obtained. The height of the structure is 50 cm and the length of one side of the base of the pyramid is 56.12 cm. The triangular membranes at the sides of the structure have all got a surface area of ~1625 $cm^2$. The surface area of the open square (the base of the pyramid) is 3150 $cm^2$. Therefore, the amount of area that radiates energy away from the structure ($A_{out}$) is assumed to be $4*0.1625 + 0.315 \approx 1\ m^2$.

# 3 DESIGN REQUIREMENT

The inflatable structure of the iDod is rigidized by means of thermal curing [Maessen, iDod.TN.007]. For thermal curing, the temperature of the object to be rigidized has to be at least 120°C [Cadogan, 2001].
It is investigated what type of thermal coating is required for the inflatable structure to reach a minimum equilibrium temperature of 100°C and a maximum equilibrium temperature of 200°C. The maximum is set to 200°C to limit thermal gradients.

# 4 MODEL BUILDUP

A single-node model is the simplest model that can be applied to investigate the thermal behavior of an object. In this section, the general equation for the energy balance of an object is rewritten to yield an equation with which the steady state equilibrium temperature of a single-node object can be determined.

The temperature of an object can only be calculated when it is known how much energy enters and leaves the object. When Q represents a certain amount of energy, then the energy balance of an object can be written as [Noomen, 2001]:

$$\Delta Q = mc\frac{dT}{dt} = Q_{\text{in}} + Q_{\text{intern}} - Q_{\text{out}}$$

Where m denotes the mass of the object, c denotes its specific heat (a measure for the amount of energy that is required to increase the object's temperature), dT denotes a change in temperature, and dt denotes a change in time. $Q_{intern}$ indicates the amount of internal heat generated by the object.

In the current case, only the steady state temperature is of importance. Thus, $\Delta Q = 0$. In addition, there is no internal heat generation. This reduces the first equation to:

$$Q_{\text{in}} = Q_{\text{out}}$$

The heat transport between the CubeSat and the inflatable structure is for now neglected. Only radiation from the Sun and Earth are considered as energy sources (radiation from space is also neglected).
Energy from the Earth comes in two forms: albedo radiation (sunlight reflected by the Earth's surface) and infrared radiation. To distinguish between the three energy sources in the coming equations, energy from the Sun is given the suffix S, albedo radiation is given the suffix a, and infrared radiation is given the suffix ir. The energy balance is now written as:

$$Q_{\text{S}} + Q_a + Q_{ir} = Q_{\text{out}}$$

The individual terms of the above equation are determined as follows. First, the energy from the Sun is computed using the following equation [Noomen, 2001]:

$$Q_S = \alpha_S A_S S_0$$

Where the absorption coefficient $\alpha_S$ indicates the fraction of the energy absorbed by the material ($0<\alpha<1$), $A_S$ is the projected surface area that receives the energy from the Sun and $S_0$ is the solar energy per square meter in the vicinity of Earth (the well-known solar constant, ~1371 ± 5 W/m$^2$ [Fortescue, 1995]). The equation for albedo radiation is very similar [Noomen, 2001]:

$$Q_a = \alpha_a A_a S_a$$

Where $S_a$ is the amount of albedo radiation received. The amount of albedo radiation received depends on the albedo coefficient of Earth (a) and on the view factor F between the satellite and Earth (0<F<1), which leads to [Noomen, 2001]:

$$Q_a = \alpha_a A_a a F S_0$$

The equation for infrared radiation is built up exactly like the equation for albedo radiation [Noomen, 2001]:

$$Q_{ir} = \alpha_{ir} A_{ir} S_{ir}$$

The equation for the outgoing energy is [Noomen, 2001]:

$$Q_{out} = \varepsilon_{ir} A_{out} \sigma T^4$$

Where $\varepsilon_{ir}$ is the emission coefficient ($0<\varepsilon_{ir}<1$), $\sigma$ is Stefan Boltzmann's constant (5.67051E-8 $Wm^{-2}K^{-4}$), and T is the temperature of the object.

Kirchhoff's Law for diffuse radiation states that the infrared absorption coefficient and the infrared emission coefficient for the satellite material are the same since the Earth and the satellite have approximately the same temperature [Noomen, 2001]. Therefore, $\alpha_{ir} = \varepsilon_{ir} = \varepsilon$. Furthermore, $\alpha_a = \alpha_S = \alpha$. These simplifications lead to the following equation for the energy balance:

$$T = \left[ \frac{\alpha A_S S_0 + \alpha A_a a F S_0 + \varepsilon A_{ir} S_{ir}}{\varepsilon A_{out} \sigma} \right]^{1/4}$$

The amount of infrared energy produced by Earth is ~237 ± 21 $W/m^2$ at the Earth's surface [Noomen, 2001]. At an altitude h, this energy density reduces to [Noomen, 2001]:

$$S_{ir}(h) = (237 \pm 21) \left( \frac{R_E}{R_E + h} \right)^2$$

With $R_E$ equal to the mean radius of the Earth (6378 km). For h = 1000 km, $S_{ir}$ is equal to 177 ± 15.7 $W/m^2$. According to [Wertz, 1999], the albedo coefficient (a) is 0.30 ± 0.05 for Earth.

The value for the view factor F depends on the altitude of the satellite and on the angle of the satellite's local vertical with the rays of the Sun [Fortescue, 1995]. This bearing angle, $\beta$, is defined as shown below:

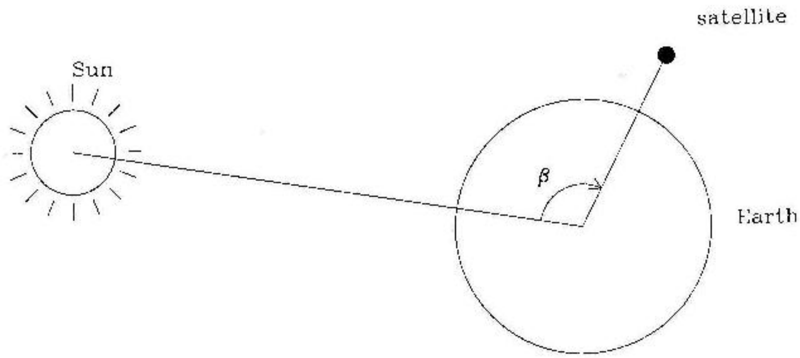


*Figure 2 Definition of the bearing angle $\beta$ [Noomen,2001]*

The variation in view factor for a satellite, taking into account shadowed area on Earth, is depicted below:

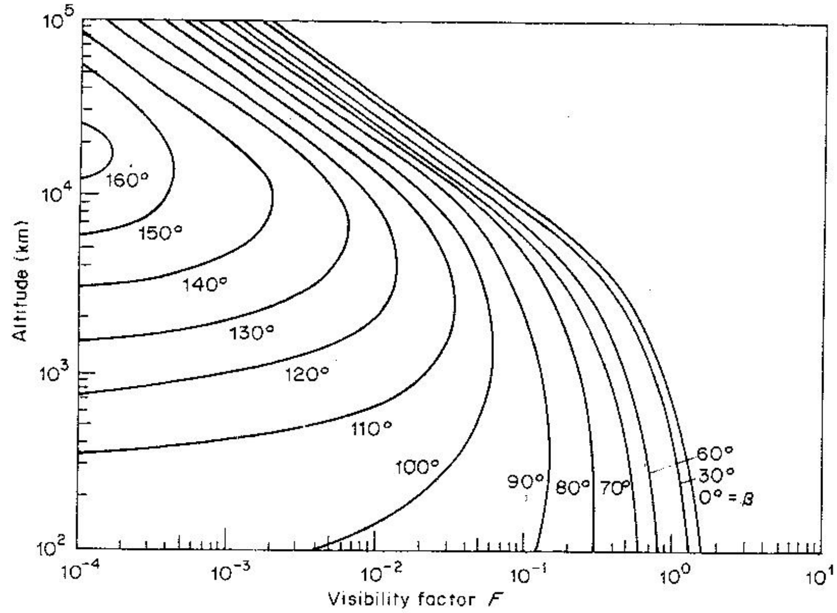


*Figure 3 Variation in F with altitude and$\beta$ for a satellite [Fortescue, 1995]*

Note that in figure 3 the maximum possible view factor is larger than 1, something which by definition is impossible (it is unknown what calculation causes this in the figure)! Furthermore, it is not clear for which satellite geometry this figure holds (likely to be a sphere or a flat plate). Therefore, this figure only serves as an indication between which values the view factor can vary for different altitudes and bearing angles.

# 5 EQUILIBRIUM TEMPERATURES

In the current section, first the method used to determine the equilibrium temperature of the inflatable structure is described. In subsection 5.2, two different cases are treated. For each case, the range of $\alpha$-$\varepsilon$ combinations that lead to the desired range of equilibrium temperatures (100°C-200°C) is determined. In subsection 5.3, based on the results of subsection 5.2, the desired thermal properties of the entire inflatable structure are derived.

## 5.1 Method for determining equilibrium temperatures

The equilibrium temperature of a single node structure in orbit around Earth can be calculated using the formula that has been derived earlier in section 4:

$$T = \left[ \frac{\alpha A_S S_0 + \alpha A_a a F S_0 + \varepsilon A_{ir} S_{ir}}{\varepsilon A_{out} \sigma} \right]^{1/4}$$

However, the areas and energies present in the above formula need not be constant over a complete orbit. In fact, they never are.

Two standard methods can now be applied to determine the temperature of the structure using the previous formula. One method is described in [Wertz, 1999]. In this method, the steady state temperature of the structure is determined in case it is in constant eclipse (no solar radiation $\Rightarrow$ $S_0 = 0$) or when it constantly bathes in sunlight (maximum amount of energy received). Using this method, the theoretical minimum and maximum steady state temperatures of the object are determined. However, the difference between these temperatures can be huge (> 100K) and both temperatures will almost never come to pass in reality (exception: dawn-dusk orbit, see subsection 4.2). Therefore, this method is considered to be too unrealistic to give a proper indication of the attainable temperatures.
The other method, the method that will be approximately applied here, is described in [Fortescue, 1995]. There, a weighted average of the amount of energy received during one orbit is used to determine an average equilibrium temperature. As it is described in [Fortescue, 1995], it is an extension to the method described in [Wertz, 1999]. Again both extreme temperatures are determined, but now, depending on the percentage of the orbital period spent in eclipse, a new weighted average temperature is determined. Thus, when the maximum and minimum temperatures have been determined to be for instance 200K and 350K respectively and when 30% of the orbital period is spent in eclipse, the weighted average equilibrium temperature is:

$$T_{\text{average}} = 0.30 T_{\text{cold}} + 0.70 T_{\text{hot}} = 0.30 \cdot 200 + 0.70 \cdot 350 = 305K$$

However, the method from [Fortescue, 1995] neglects the fact that the contribution of infrared radiation is constant during one orbit (for constant orbit height). To take this into account, the method applied here will use the average amount of energy received during one orbit instead of weighted temperatures. This leads to multiplication of $S_0$ with one minus the percentage of time spent in eclipse ($S_0 * (1 - t_{eclipse}/t_{orbit})$). For a circular orbit with an altitude of 1000 km, the orbit period is 105.12 minutes and the maximum time spent in eclipse is 34.94 minutes [Wertz, 1999], which leads to a multiplication of $S_0$ with ~2/3.

The method applied here will be called the “average energy method” and is used in the coming subsection. This method is advised to use by Aldert Kamp of the section Astrodynamics & Satellite Systems of this faculty.

## 5.2 Limit cases

This subsection treats two limit cases (“hot” and “cold”) in which the average energy method is applied to determine the range of $\alpha$-$\varepsilon$ combinations required to obtain equilibrium temperatures between 100°C and 200°C.

The “hot” case is an orbit in which the satellite is never in eclipse (a so-called dawn-dusk orbit). The angle between the orbital plane and the ecliptic plane (the plane containing the mean orbit of the Earth around the Sun) is then 90° and the satellite is positioned directly over Earth’s terminator. The “cold” case is an orbit with a maximum amount of time spent in eclipse. The orbital plane then lies within the ecliptic plane. The next figure schematically depicts both cases.

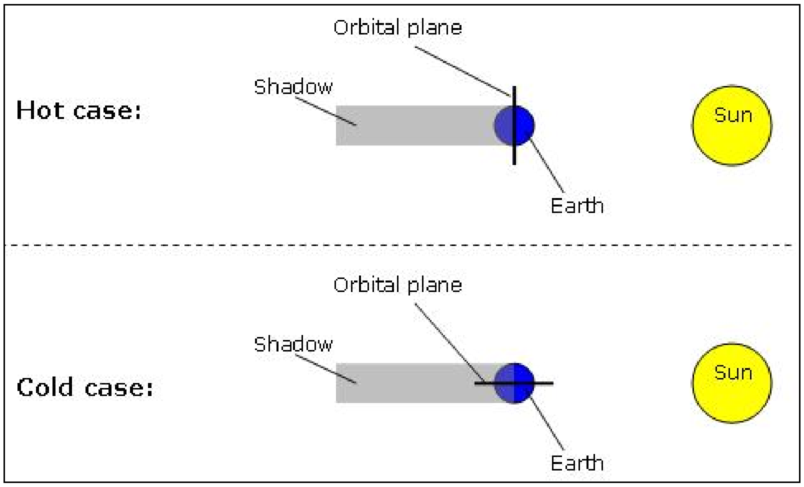


*Figure 4 Hot and cold cases*

The average amount of infrared energy received from Earth is constant during an orbit and therefore $S_{ir}$ is always 177 ± 15.7 W/m$^2$, see section 4. For the "hot" case $S_{ir}$ is assumed equal to 192.7 W/m$^2$, while it is assumed equal to 161.3 W/m$^2$ for the "cold" case.
Since the solar constant varies by a very small amount (< 0.5%, see section 4) $S_0$ is taken equal to 1371 W/m$^2$ for the hot case. For the cold case, $S_0$ is multiplied by 2/3, leading to 914 W/m$^2$.
The albedo coefficient for the hot case is taken to be its maximum value of 0.35, see section 4. For the cold case, it is taken to be 0.25.

For each case a range of average equilibrium temperature is determined using Matlab. The results are presented in the next subsections. In the last subsection, conclusions are drawn.

### 5.2.1 Case 1 (hot case)

In this case, the area receiving solar radiation is maximal and is equal to 0.315 m$^2$ over the entire orbit. This means the base of the pyramid structure is always facing the Sun. Then, a skewed side of the pyramid faces Earth. Zooming in:

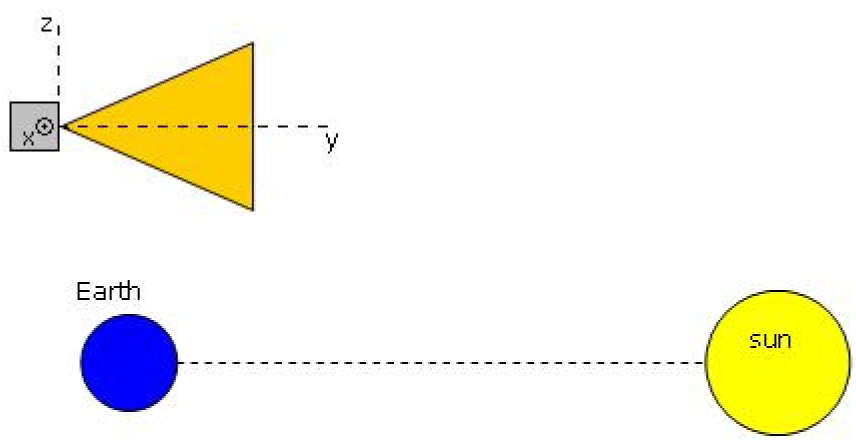


*Figure 5 Orientation for case 1.1*

Since the base of the pyramid must be facing the Sun, no rotation around the x- or z-axis is allowed. However, a rotation around the y-axis is allowed. When exactly one side of the pyramid is facing Earth, the projected area for this side is minimal and equal to (using information from section 2):

$$A_{side,projected} = A_{side}\cos\left[\operatorname{atan}\left(\frac{\frac{1}{2}width}{height}\right)\right] = 1625\cos\left[\operatorname{atan}\left(\frac{\frac{1}{2}56.12}{50}\right)\right] = 1417\ \text{cm}^2$$

The maximum projected area occurs when the diagonal of the base of the pyramid is the base of the projected side. Then, the projected area is $\sqrt{2}\cdot A_{side,projected}$ = 2004 cm$^2$. Since this is the "hot" case, the maximum projected area of the side is used since this leads to the highest temperature.

The view factor for the side of the pyramid facing Earth is taken equal to the view factor of a plate at a distance (h) of 1000 km from a sphere with a radius (R) of 6378 km. Then, according to [Fortescue, 1995] the following approximate formula can be used to determine the view factor:

$$F = \frac{\cos\lambda}{(1+H)^2} \text{ if } \lambda + \sin^{-1}\left(\frac{1}{1+H}\right) < \frac{\pi}{2}$$

Where H=h/R and $\lambda$ is defined as the angle between the surface normal of the plate and the line connecting the centers of the two bodies. The angle $\lambda$ is assumed to be 0°, which leads to:

$$F = \frac{\cos\lambda}{(1+H)^2} = \frac{\cos 0^\circ}{\left(1+\frac{1000}{6378}\right)^2} = 0.747$$

However, as seen from the satellite, exactly one half of the Earth is shaded, which leads to a view factor of 0.374.

Now, all variables except $\alpha$ and $\varepsilon$ have been determined:

| Variable | Value | Unit |
|---|---|---|
| $A_a$ | 0.2004 | m$^2$ |
| $A_{ir}$ | 0.2004 | m$^2$ |
| $A_S$ | 0.315 | m$^2$ |
| $A_{out}$ | 1 | m$^2$ |
| a | 0.35 | - |
| F | 0.374 | - |
| $S_0$ | 1371 | W/m$^2$ |
| $S_{ir}$ | 192.7 | W/m$^2$ |

*Table 1 Variables for case 1*

The value for $A_{out}$ is obtained from section 2. The formula for the temperature now becomes:

$$T = \left[\frac{\alpha\cdot 0.315\cdot 1371 + \alpha\cdot 0.2004\cdot 0.35\cdot 0.374\cdot 1371 + \varepsilon\cdot 0.2004\cdot 192.7}{\varepsilon\cdot 1\cdot 5.67051\cdot 10^{-8}}\right]^{1/4}$$

For 0 < $\alpha$ < 1 and 0 < $\varepsilon$ < 0.5, the Matlab results are:

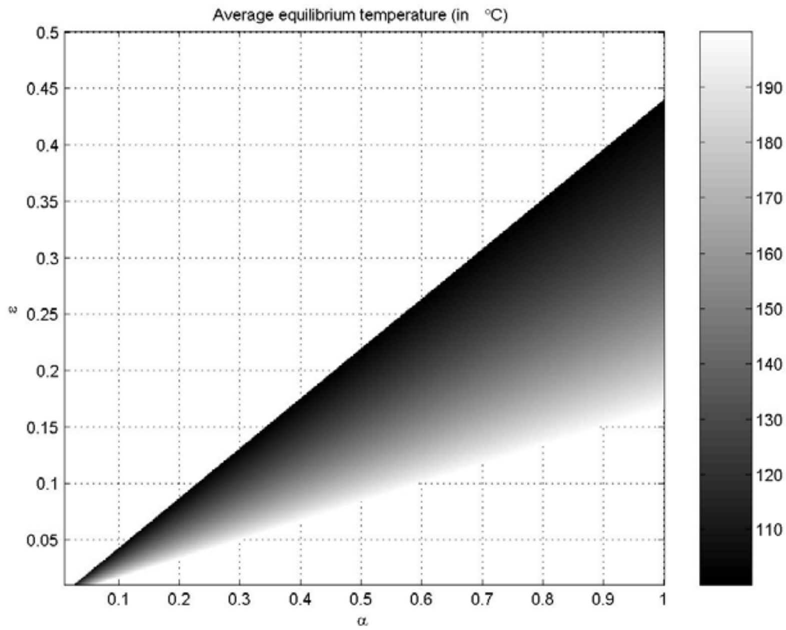


*Figure 6 Temperatures for case 1*

The above figure shows that in this case 2 < α/ε < 6 for the temperature of the inflatable to be between 100°C and 200°C.

In the following calculation, the Matlab result for α = 0.5 and ε = 0.15, which is 136.576°C, is checked:

$$T_{\text{case 1}} = \left[\frac{\alpha A_S S_0 + \alpha A_a a F S_0 + \varepsilon A_{ir} S_{ir}}{\varepsilon A_{out} \sigma}\right]^{1/4} - 273.15 =$$

$$= \left[\frac{0.5 \cdot 0.315 \cdot 1371 + 0.5 \cdot 0.2004 \cdot 0.35 \cdot 0.374 \cdot 1371 + 0.15 \cdot 0.2004 \cdot 192.7}{0.15 \cdot 1 \cdot 5.67051 \cdot 10^{-8}}\right]^{1/4} - 273.15 =$$

$$= \left[\frac{215.9325 + 17.9823 + 5.7926}{8.505765 \cdot 10^{-9}}\right]^{1/4} - 273.15 =$$

$$= 136.575^{\circ} C$$

Since the two temperatures match, the Matlab program is working correctly.

### *5.2.2 Case 2 (cold case)*

In this case, it is assumed that the smallest possible projected area of the pyramid structure is always facing towards the Sun. This has to be a skewed side of the pyramid, thus $A_S$ = 0.1417 m$^2$. A complicating factor now is that the projected area facing the Earth cannot be kept constant for the assumed orbit. It can vary between the extreme areas of 0.1417 m$^2$ and 0.315 m$^2$. The next figure illustrates this.

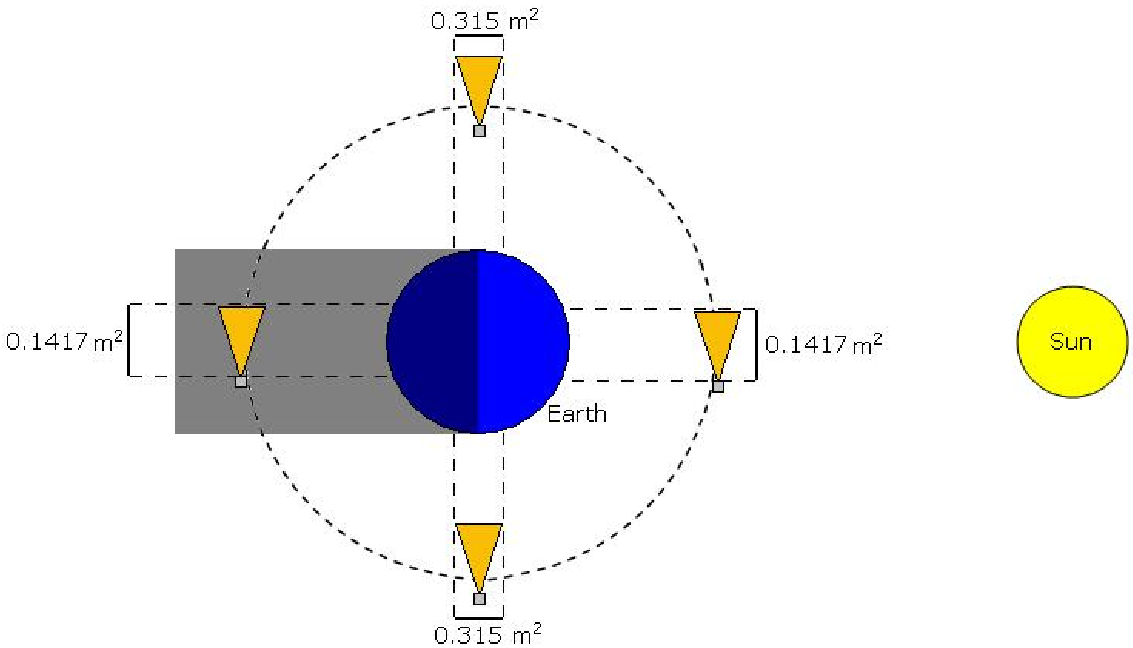


*Figure 7 Orientation of the satellite at four places in its orbit for case 2*

The projected surface area facing Earth will vary in a sine-line fashion between 0.1417 $m^2$ and 0.315 $m^2$. For simplicity, the average value between these extremes, 0.22835 $m^2$, is assumed for $A_{ir}$ and $A_a$.

The view factor will also vary for this case. For the four satellite positions depicted in the previous figure, the view factors are (starting at the top, going clockwise): 0.747, 0.374, 0.747, and 0. An average value for the view factor therefore has to be assumed. The figure is a bit misleading, since the view factor will be 0 during 1/3$^{rd}$ of the satellite orbit (in eclipse). In the figure, this period looks much shorter. The approach now taken is as follows. Since the solar constant will be multiplied by 2/3 for this case, eclipse is already taken into account for albedo radiation. Thus, the part of the orbit in which the view factor is 0 does not have to be taken into account for determination of the average view factor. Then, the view factor varies between 0 and 0.747 in a sine-like manner and the average value of 0.374 is chosen for the view factor in the calculations.

The variables are now:

| **Variable** | **Value** | **Unit** |
|---|---|---|
| $A_a$ | 0.22835 | $m^2$ |
| $A_{ir}$ | 0.22835 | $m^2$ |
| $A_S$ | 0.1417 | $m^2$ |
| $A_{out}$ | 1 | $m^2$ |
| a | 0.25 | - |
| F | 0.374 | - |
| $S_0$ | 1371 | $W/m^2$ |
| $S_{ir}$ | 161.3 | $W/m^2$ |

*Table 2 Variables for case 2*

The formula for the temperature is now:

$$T = \left[ \frac{\alpha \cdot 0.1417 \cdot \frac{2}{3} \cdot 1371 + \alpha \cdot 0.22835 \cdot 0.25 \cdot 0.374 \cdot \frac{2}{3} \cdot 1371 + \varepsilon \cdot 0.22835 \cdot 161.3}{\varepsilon \cdot 1 \cdot 5.67051 \cdot 10^{-8}} \right]^{1/4}$$

For $0 < \alpha < 1$ and $0 < \varepsilon < 0.2$, the Matlab results are:

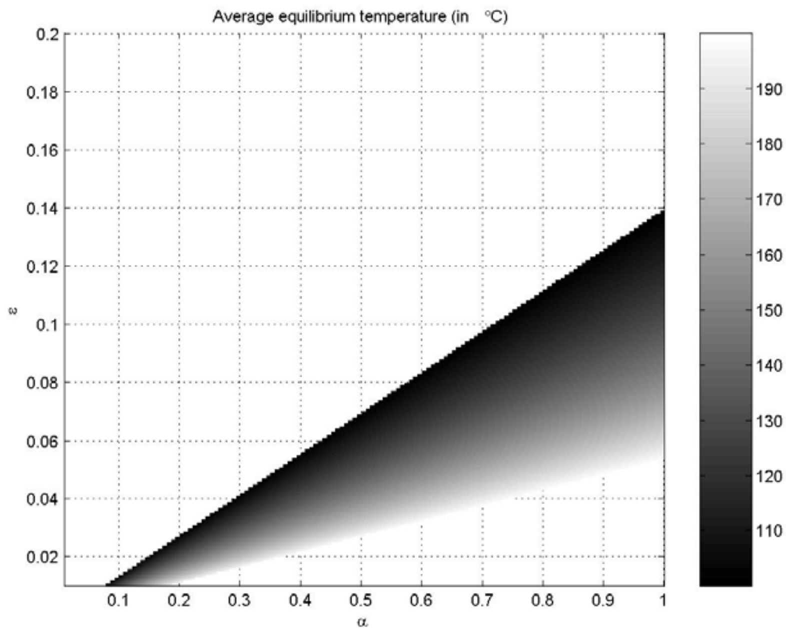


*Figure 8 Temperatures for case 2*

Now, the $\alpha/\varepsilon$ ratio has to be in between 7 and 18 to obtain the desired temperature range.

The Matlab result for $\alpha = 0.6$ and $\varepsilon = 0.05$ is 150.417°C. The analytical result is:

$$T_{\text{case 2}} = \left[ \frac{\alpha A_S S_0 + \alpha A_a aFS_0 + \varepsilon A_{ir} S_{ir}}{\varepsilon A_{out} \sigma} \right]^{1/4} - 273.15 =$$

$$= \left[ \frac{0.6 \cdot 0.1417 \cdot \frac{2}{3} \cdot 1371 + 0.6 \cdot 0.22835 \cdot 0.25 \cdot 0.374 \cdot \frac{2}{3} \cdot 1371 + 0.05 \cdot 0.22835 \cdot 161.3}{0.05 \cdot 1 \cdot 5.67051 \cdot 10^{-8}} \right]^{1/4} - 273.15 =$$

$$= \left[ \frac{77.7083 + 11.7087 + 1.8416}{2.83526 \cdot 10^{-9}} \right]^{1/4} - 273.15 =$$

$$= 150.415^{\circ} C$$

Since the two temperatures match, the Matlab program is working correctly.

### 5.2.3 Conclusions

First of all, it is noted that the foregoing analyses are not considered to be very detailed. The actual structure is relatively complex, which can result in parts of the structure achieving temperatures that are very different from the temperatures computed here. This is especially true for the parts of interest, the inflatable tubes, since reflections of energy inside the pyramid can influence temperature distributions considerably.

In appendix A, two more cases are considered: a “hot cold” case and a “cold hot” case. These are intermediate cases whose results have to lay in between those obtained in the limit cases. The results of those cases are also provided here, leading to the following designations for the four cases:

Case 1.1 Hot case from subsection 5.2.1
Case 1.2 Cold hot case from appendix A
Case 2.1 Hot cold case from appendix A
Case 2.2 Cold case from subsection 5.2.2

The resulting $\alpha/\varepsilon$ ratios for the four cases are summarized in the next table.

| Case | $\alpha/\varepsilon$ ratio for T = 100°C | $\alpha/\varepsilon$ ratio for T = 200°C |
|---|---|---|
| 1.1 | 2.2 | 6.0 |
| 1.2 | 5.1 | 13.2 |
| 2.1 | 3.4 | 8.9 |
| 2.2 | 7.1 | 18.8 |

*Table 3 Results for the four cases*

The results clearly show that the coating applied on those parts of the structure required to be hot has to have a high $\alpha/\varepsilon$ ratio. For the structure to become much warmer than 100°C, the $\alpha/\varepsilon$ ratio needs to be very high, something which does not look feasible (see table 6 in subsection 4.4).

The next table depicts the average temperatures achieved for all cases for three different ratios of $\alpha/\varepsilon$:

| | Case 1.1 | Case 1.2 | Case 2.1 | Case 2.2 |
|---|---|---|---|---|
| $\alpha/\varepsilon$ = 2 | 89 | 25 | 57 | 4 |
| $\alpha/\varepsilon$ = 5 | 179 | 99 | 138 | 70 |
| $\alpha/\varepsilon$ = 8 | 235 | 144 | 188 | 111 |

*Table 4 Temperature in °C for the four cases for three ratios of $\alpha/\varepsilon$*

The results in table 4 show that orientation is more important for temperature than the type of orbit. Furthermore, due to a different orientation, the achieved temperature in a certain orbit can vary many tens of degrees Celsius. Since the orientation of the spacecraft with deployed iDod cannot be controlled passively at this altitude (see [Maessen, iDod.TN.009]), this complicates the thermal design.

To be certain that a high enough temperature is reached in all situations to cure the resin, a $\alpha/\varepsilon$ ratio of 8 is required. However, then the temperature can become very high for certain cases and achieving a $\alpha/\varepsilon$ ratio of 8 is not considered feasible. A ratio of 2 to 5 is regarded to be feasible. Therefore, a resin with a relatively low curing temperature is advised to be used for thermal curing.

## 5.3 Coating characteristics for complete inflatable structure

The main conclusion reached in the previous subsection can be further detailed in order for the inflatable tubes to receive as much energy as possible. Starting with the inflatable tubes, their temperature can be made high and uniform when the outside and inside of the tubes are coated as follows:

- Outside: $\alpha/\varepsilon > 1$, this leads to much energy absorption.
- Inside: $\varepsilon$ high, this results in a more uniform temperature distribution of the tubes in case of long illumination of only one side of the structure. Black Kapton is a good candidate for this function (any pigmented polyimide will do).

The membranes should be designed such that a maximum amount of heat is channeled towards the inside of the pyramid:

- Outside (facing space): $\alpha/\varepsilon > 1$, this leads to a high membrane temperature.
- Inside (facing the interior of the inflatable structure): $\alpha$ low (which means much reflection) and $\varepsilon$ high $\Rightarrow$ $\alpha/\varepsilon < 1$. The high amount of reflection in combination with the high amount of energy emitted results in much energy being channeled towards the inflatable tubes.

The above is summarized in the following cross-section of the inflatable structure:

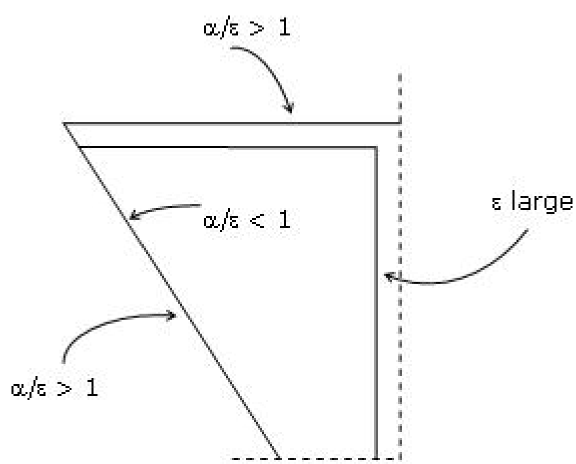


*Figure 9 Coating characteristics for inflatable structure*

A more detailed thermal analysis is required to assess the attainable temperature of this more complex structure for various coating combinations.

# 6 COATING PROPOSITIONS

On the next page, some examples of thermal coatings and their properties are shown.

| Surface | Absorptance $\alpha$ | Emittance $\varepsilon$ | $\alpha/\varepsilon$ |
|---|---|---|---|
| Gold plate on Al 7075 | 0.3 | 0.03 | 10.0 |
| Polished aluminium | 0.35 | 0.04 | 8.75 |
| Polished beryllium | 0.4 | 0.05 | 8.0 |
| Gold on aluminium | 0.26 | 0.03 | 6.5 |
| Polished stainless steel | 0.5 | 0.13 | 3.85 |
| Polished copper | 0.28 | 0.13 | 2.2 |
| Grafoil | 0.66 | 0.34 | 1.9 |
| Vapour-blasted stainless steel | 0.6 | 0.33 | 1.8 |
| Gold/Kapton/aluminium | 0.53 | 0.42 | 1.26 |
| Epoxy black paint | 0.95 | 0.85 | 1.12 |
| Acrylic black paint | 0.97 | 0.91 | 1.07 |
| Silicone white paint | 0.19 | 0.88 | 0.22 |
| —after 3 years' u.v. irradiation | 0.39 | 0.88 | 0.44 |
| Silicate white paint | 0.14 | 0.94 | 0.15 |
| —after 3 years' u.v. irradiation | 0.27 | 0.94 | 0.29 |
| Silicon solar cell, bare | 0.82 | 0.64 | 1.3 |
| Silicon solar cell, silica cover | 0.82 | 0.81 | 1.0 |
| Silicon solar cell, silica cover, blue filter | 0.78 | 0.81 | 0.96 |
| Silicon solar cell, silica cover, red filter | 0.7 | 0.81 | 0.86 |
| Kapton (5 mil)/aluminium | 0.48 | 0.81 | 0.6 |
| $In_2O_3$/Kapton/aluminium | 0.4 | 0.71 | 0.56 |
| Quartz fabric/tape | 0.19 | 0.6 | 0.3 |
| OSR (quartz mirror) silvered Teflon | 0.08 | 0.81 | 0.1 |
| FEP (5 mil)/silver | 0.11 | 0.8 | 0.14 |
| FEP (2 mil)/silver | 0.05 | 0.62 | 0.08 |

*Table 5 Various coatings and their thermal properties [Fortescue, 1995]*

The next figure from [Poinas, 2004] schematically depicts what kind of coating is required to obtain a certain $\alpha/\varepsilon$ ratio.

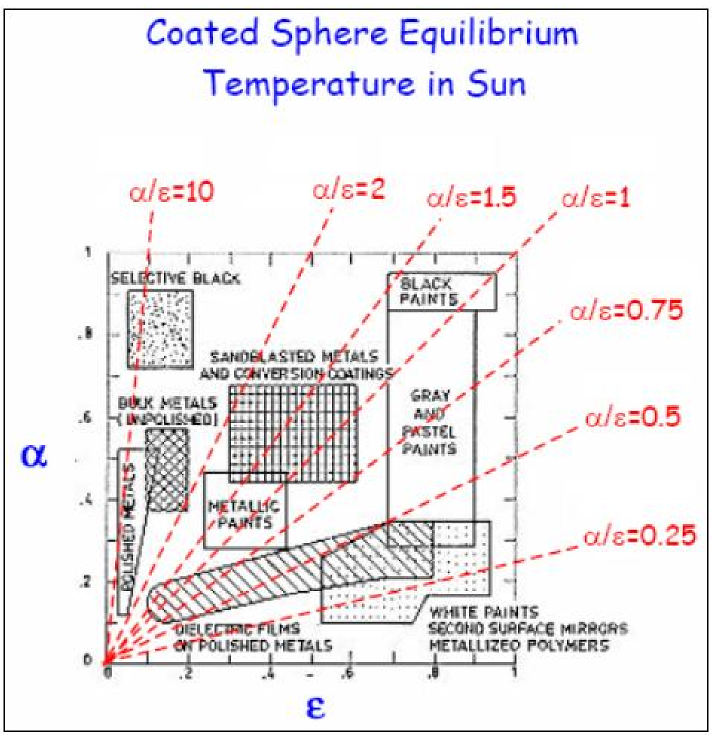


*Figure 10 Coating types required for different $\alpha/\varepsilon$ ratios [adapted from Poinas, 2004]*

The previous table and figure indicate that metallic or “selective black” coatings are required to obtain a high $\alpha/\varepsilon$ ratio. Based on this information, two preliminary coating options are proposed here.

## 6.1 Proposition 1

For the membranes, the proposed coating is vapor deposited aluminum (VDA) with on top of that a coating of $SiO_x$ on the outside of the membrane and only $SiO_x$ on the inside of the membrane:

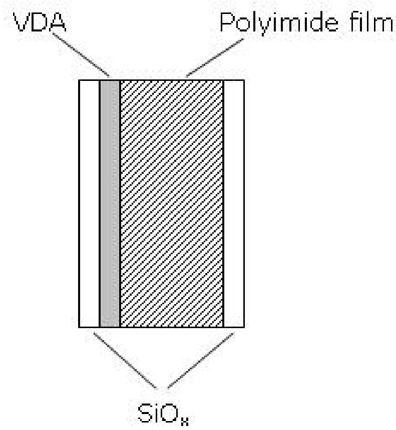


*Figure 11 Proposed membrane coating*

The layer of $SiO_x$ functions as the prime protective atomic oxygen barrier and is transparent. The VDA serves as a coating with a high $\alpha/\varepsilon$ for the outside of the membrane, while the combination of the semi-transparent polyimide film with VDA acts as a coating with a small $\alpha/\varepsilon$ for the inside of the membrane. A similar coating is also used on the membranes of the de-orbit device for the French Microscope spacecraft [Bousquet, 2006].
This coating has as a bonus that the radar signature of the spacecraft becomes much larger once the iDod is inflated. This is a cheap and fast way to assess whether or not the iDod has deployed once it should have.

Although Upilex-S is chosen in [Maessen, iDod.TN.008] as membrane material, the coating proposition here uses Kapton as membrane material since at the time of writing this proposition (version 1.0 of this document) no material choice had been made yet.

According to [Scialdone, 1992], for VDA coated Kapton with a 1000Å thick $SiO_x$ coating, $\alpha$ = 0.155 and $\varepsilon$ = 0.025 (no exposure to the space environment), which leads to $\alpha/\varepsilon$ = 6.2. After exposure to the space environment (10 months at 400 km altitude), $\alpha/\varepsilon$ = 5.5 ($\alpha$ = 0.127 and $\varepsilon$ = 0.023). Thus, the side of the membrane facing space has indeed got a high $\alpha/\varepsilon$ ratio.
According to [K&K Associates], 1 mil (25 $\mu$m) of Kapton with aluminum backing results in $\alpha/\varepsilon$ = 0.57 ($\alpha$ = 0.38 and $\varepsilon$ = 0.67). Thus, the side of the membrane facing the inside of the inflatable structure has got a low $\alpha/\varepsilon$ ratio (although perhaps not as low as desired).

It is noted that the coating properties from [Scialdone, 1992] are suspected to be the properties in case no wrinkles are present in the material. In the case of wrinkled material, the surface properties of the material change and with that, its emissivity coefficient.

For the inflatable tubes, a logical choice would now be to also apply a coating of $SiO_x$ and VDA on the outside of the tubes.

## 6.2 Proposition 2

Another option is to leave out the VDA layer on the membrane and to use transparent Upilex membranes with a coating of $SiO_x$ on both sides. The coating for the inflatable tubes is left unchanged. The advantage of this option is the direct illumination of the tubes irrespective of their orientation with respect to the sun. The downside is that there is much less increase in radar signature and there is no funneling of heat towards the tubes. Since no thermal analysis has been performed for this option, it is TBD whether the tubes can get hot enough using this coating.

# 7 AERODYNAMIC HEATING

Besides radiation, friction with the atmosphere is also a source of heat for the satellite. The next table provides the aerodynamic heat flux for satellites with a circular or modestly eccentric orbit.

| Altitude | Aerodynamic heat flux ($W/m^2$ h) Circular orbit | Eccentric orbit ($e = 0.13$) |
|---|---|---|
| 100 | 170 000 | 17 000 |
| 150 | 1300 | 130 |
| 200 | 160 | 16 |
| 250 | 39 | 3.9 |
| 300 | 15 | 1.5 |
| 350 | 7 | 0.7 |
| 400 | 3.7 | 0.4 |
| 450 | 2.2 | 0.2 |
| 500 | 1.2 | 0.1 |

*Table 6 Aerodynamic heating of Earth satellites in $Wm^{-2}h$ [Fortescue, 1995]*

For the current spacecraft, the worst case orbit is assumed, which is a circular one. This will not be far from the truth, since it will slowly spiral towards Earth from a circular starting orbit [Maessen, iDod.DD.001]. The table clearly shows that heating of the spacecraft due to friction with the atmosphere only is important below an altitude of ~100 km. At 150 km, the amount of power received in one hour is approximately equal to the power received from the Sun during one hour:

Aerodynamic heating $\Rightarrow 1300 \ \frac{\mathrm{Wh}}{\mathrm{m}^2} = 4.68 \cdot 10^6 \ \frac{\mathrm{Ws}}{\mathrm{m}^2}$

Solar radiation $\Rightarrow 1371 \ \frac{\mathrm{W}}{\mathrm{m}^2} \cdot 3600 \ \mathrm{s} = 4.94 \cdot 10^6 \ \frac{\mathrm{Ws}}{\mathrm{m}^2}$

Since the spacecraft will de-orbit rapidly once it is below an altitude of 200 km, even without iDod, the aerodynamic heat flux is not important for the thermal design of the inflatable structure.

# 8 TESTING

Thermal testing of the inflatable structure is required to verify the design and construction of the structure. The most important tests required for the inflatable structure are outlined in the coming subsections.

Although not treated in detail here, it is noted that development tests can be required to gain important knowledge about individual parts of the structure at an early stage of the design.

## 8.1 Rigidization testing

In case rigidization of the inflatable tubes by means of thermal cure is required, a very important part of the thermal design is to ensure that the thermoset resin in the inflatable tubes attains the required temperature (or higher). In addition, the temperature has to be kept at or above the required temperature for a prolonged amount of time (~½ hour per orbit) to ensure proper curing of the thermoset resin within a few (< 10) orbital revolutions. Otherwise, in case there is a leak in the inflatable structure, all inflation gas might escape before sufficient rigidization is achieved to guarantee sufficient structural stiffness. Thus, it has at least to be tested whether or not the inflatable tubes rigidize within the specified amount of time (TBD) when subjected to the expected radiation energies. To make it more realistic, this test can be performed in a fashion similar to a thermal cycling test where temperatures are increased and decreased in a cyclic pattern.

## 8.2 Acceptance and qualification testing

Naturally, it has to be tested whether or not the structure can actually withstand the temperatures is it expected to reach. For instance, parts with different coefficients of thermal expansion (CTE) can restrain each other's expansion or contraction under influence of temperature. This leads to stresses in the area where the parts meet and can lead to failure of a part. In addition, adhesives can loose their desired properties when heated above or below a certain temperature. They can for instance become brittle at low temperatures or, in case of thermoplastic adhesives, become very viscous at high temperatures.
For the iDod, the interface between the inflatable structure and the stowage canister is a good example of a critical point with respect to CTE and adhesive properties.

Testing solely for the temperature range predicted by thermal models is not enough. This range has to be broadened, as is indicated in the next figure.

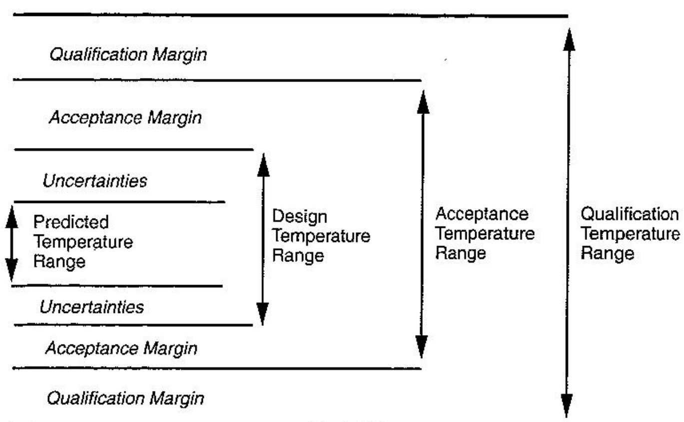


*Figure 12 Temperature range definitions [Wertz, 1999]*

According to [Wertz, 1999], the design temperature range is usually 5-7°C wider than the predicted temperature range at the final analysis campaign (in the preliminary design definition analysis, the predicted range is usually widened by 15°C). This temperature range is often the required temperature range and can be regarded as a buffer against uncertainties in the thermal models.
The acceptance temperature range is usually 5°C wider than the design temperature range. Testing in this range is usually performed to identify material defects or bad workmanship. Components have to pass a test at this level in order to be allowed as flight hardware.
The qualification temperature range is generally 10°C wider than the design temperature range at which components must function in orbit. It is the extreme temperature range for which a part is guaranteed to operate with the required performance and reliability. Tests performed at this level are mainly meant to identify any weakness in the thermal design.

Thus, it has to be tested whether or not the structure can actually cope with temperatures 10°C above or below its design temperature range. In case of the iDod, this range might even be broadened further since the thermal environments it can encounter can be very different since it is meant to be applied on many CubeSats. When it can be proven that the iDod functions properly for a wide range of temperatures, the amount of eventual modifications (these might be required for a certain mission) to the baseline design can be kept to a minimum (from a thermal design point of view). How wide the qualification temperature range has to be for the iDod is left TBD.

Testing the range of temperatures the structure has to withstand can be done by means of a solar balance test or a thermal vacuum test. Both tests are conducted in a vacuum chamber with nitrogen-cooled walls to simulate deep space. The solar balance test simulates space conditions the most accurately, since there a special light source is used to simulate solar radiation. Both tests make use of infrared lamps or even thermal heaters to influence the temperature of the test-object. Next to testing the object's performance, these tests are also used to validate the thermal model(s) of the object.

A (vacuum) thermal cycling test is also required for the iDod. As the name already implies, during this test the structure is subjected to many (1000) cycles of subsequent heating and cooling at a prescribed rate (°C/min.). Next to verifying workmanship, the test will give vital information about the behavior of the structure's protective coating. Due to the many cycles, the coating may crack at various places, exposing unprotected material to the space environment (the main cause of concern here is erosion due to atomic oxygen). When many cracks are formed as a result of the test, the coating is likely not to be adequate and measures have to be taken to improve the protection.

# 9 CONCLUSIONS & RECOMMENDATIONS

From the foregoing, it is concluded that it is possible to achieve a high temperature for the inflatable tubes of the iDod. Whether this temperature is high enough to allow chemical rigidization of the inflatable tubes by means of heat (requiring a temperature of ~120°C) needs to be confirmed by more detailed analysis. It is therefore recommended to construct a model with which a time-dependent temperature distribution for the complete inflatable structure can be obtained. This way, the time per orbit in which the temperature of the inflatable struts is high enough for proper curing of the resin can be estimated. It will also allow for selection of the optimum places to position the thermo-optical coating. In the detailed analysis, it has also to be checked whether there will be a significant temperature gradient over the tubes. When this gradient is too steep, the resulting strains can lead to severe bending of a tube and possibly to failure of the inflatable structure.

Aerodynamic heating is not a heat source that needs to be considered during the remainder of the design of the iDod.

It is recommended to verify the thermal properties of the selected coating before and after folding of the structure. Then, the effects of wrinkles in the surface on the values for $\alpha$ and $\varepsilon$ can be taken into account. Presently some work on how to determine $\varepsilon$ is performed by the master students M. Mostert and R. Tijsterman in the chair of System Integration Space.

It is further recommended to verify or to determine the change in the thermo-optical properties of possible coatings due to ageing. This change can cause the average temperature of the structure to increase or decrease over time. When possible, a decrease is desired since this will result in less severe thermal cycling effects.

# 10 FURTHER WORK

Due to time constraints, it is not foreseen that any more work is performed on this topic during this thesis. However, when the design of the iDod is continued, a much more detailed thermal model of at least the inflatable structure is required.

## REFERENCES


1. Bousquet, P.W., et. al., *De-orbiting Microscope spacecraft by drag enhancement*, IAC paper IAC-06-B6.4.5, 2006.

2. Cadogan, D.P. and Scarborough, S.E., *Rigidizable materials for use in Gossamer Space Inflatable Structures*, AIAA paper 2001-1417, 42nd AIAA/ASME/ASCE/AHS/ASC Structures, Structural Dynamics, and Materials Conference & Exhibit, AIAA Gossamer Spacecraft Forum, Seattle (USA), 16-19 April 2001.

3. Fortescue, P. and Stark, J., *Spacecraft Systems Engineering*, Second Edition, John Wiley & Sons Ltd., Chichester (UK), 1995.

4. K&K Associates, *The Thermal Connection*, www.tak2000.com/data/finish.htm, viewed January 2007.

5. Maessen, D.C., *iDod attitude stability analysis*, iDod document iDod.TN.009, Version 1.0, Faculty of Aerospace Engineering, Delft University of Technology, 16 January 2007.

6. Maessen, D.C., *iDod inflatable structure conceptual design trade-off,* iDod document iDod.TO.001, Version 1.0, Faculty of Aerospace Engineering, Delft University of Technology, January 2007.

7. Maessen, D.C., *iDod rigidization,* iDod document iDod.TN.007, Draft, Faculty of Aerospace Engineering, Delft University of Technology, 16 January 2007.

8. Maessen, D.C., *iDod Straw man concept design description,* iDod document iDod.DD.001, Faculty of Aerospace Engineering, Delft University of Technology, September 2006.

9. Maessen, D.C., *Material selection,* iDod document iDod.TN.008, Version 1.0, Faculty of Aerospace Engineering, Delft University of Technology, 13 March 2007.

10. Noomen, R., *Lecture Notes ae3-808 (Introduction Space Technology III), Part 2: Thermal Control*, Version 2.0a, Delft University Press, October 2001.

11. Poinas, P., *Satellite Thermal Control Engineering*, Presentation for “SME 2004”, http://esamultimedia.esa.int/docs/industry/SME/2004-Training/M&P/09_Materials_&_Means_Thermal_Control.pdf, 25 June 2004.

12. Scialdone, J.J. and Clatterbuck, C.H., *Four Space Application Material coatings on the Long-Duration Exposure Flight*, NASA Technical Memorandum 104574, Goddard Space Flight Center, Greenbelt (USA), November 1992.

13. Wertz, J.R., Larson, W.J., *Space Mission Analysis and Design*, Third Edition, Kluwer Academic Publishers, Dordrecht (NL), 1999.

## APPENDIX A: INTERMEDIATE THERMAL CASES

In subsection 5.2, two extreme cases are analyzed to determine the $\alpha/\varepsilon$ ratios required to reach average equilibrium temperatures between 100°C and 200°C. Here, two more cases are considered to determine the influence of the orientation of the satellite on its temperature.

In the first case of subsection 5.2, the hot case, the satellite is never in eclipse and receives a maximum amount of power from the Sun and Earth. In the second case, the cold case, the eclipse length is maximal and the amount of power received is minimal.
For the first new case the satellite is never in eclipse, but now receives a minimal amount of power. The second new case has a maximum eclipse length, but the satellite now receives a maximum amount of power.

The four cases are now named as follows:

| | |
|---|---|
| Case 1.1 | Hot case from subsection 5.2.1 |
| Case 1.2 | Cold hot case (first new case) |
| Case 2.1 | Hot cold case (second new case) |
| Case 2.2 | Cold case from subsection 5.2.2 |

**Case 1.2 (cold hot case)**

In this case, the projected area receiving solar radiation is minimal and is equal to 0.1417 $m^2$ over the entire orbit. This means exactly one skewed side of the pyramid structure is always facing the Sun. Zooming in:


*Figure 13 Orientation for case 1.2*

Since a skewed side of the pyramid has to face the Sun continuously, only a rotation around the z-axis is permitted in the above figure. When this rotation is performed, the minimal projected area receiving infrared and albedo radiation from Earth is exactly one skewed side of the pyramid and thus 0.1417 $m^2$.

The albedo coefficient is here taken to be the minimal value of 0.25, see section 4. The view factor is the same as in case 1.1, which is 0.374. The reader is referred to subsection 5.2.1 for the calculation of the view factor. The infrared energy received is also set to the lowest value; see section 4, being 161.3 $W/m^2$.

The variables for this case are thus:

| Variable | Value | Unit |
|---|---|---|
| $A_a$ | 0.1417 | $m^2$ |
| $A_{ir}$ | 0.1417 | $m^2$ |
| $A_S$ | 0.1417 | $m^2$ |
| $A_{out}$ | 1 | $m^2$ |
| a | 0.25 | - |
| F | 0.374 | - |
| $S_{0,av}$ | 1371 | $W/m^2$ |
| $S_{ir,av}$ | 161.3 | $W/m^2$ |

*Table 7 Variables for case 1.2*

The value for $A_{out}$ is obtained from section 2. The formula for the equilibrium temperature from section 4 now becomes:

$$T = \left[ \frac{\alpha \cdot 0.1417 \cdot 1371 + \alpha \cdot 0.1417 \cdot 0.25 \cdot 0.374 \cdot 1371 + \varepsilon \cdot 0.1417 \cdot 161.3}{\varepsilon \cdot 1 \cdot 5.67051 \cdot 10^{-8}} \right]^{1/4}$$

For $0 < \alpha < 1$ and $0 < \varepsilon < 0.25$, the Matlab results are:

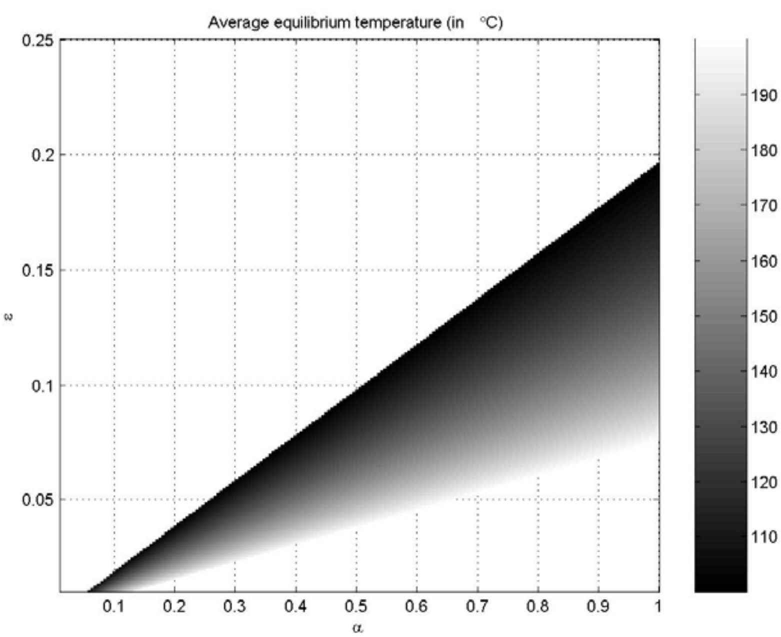


*Figure 14 Temperatures for case 1.2*

The result indicate that a $\alpha/\varepsilon$ ratio of 5 to 12 is required to obtain temperatures between 100°C and 200°C.

A check is performed to determine whether the Matlab results are what they should be. The Matlab result for $\alpha$ = 0.8 and $\varepsilon$ = 0.1 is 144.320°C. The analytical result is:

$$T_{\text{case 1.2}} = \left[\frac{\alpha A_S S_0 + \alpha A_a a F S_0 + \varepsilon A_{ir} S_{ir}}{\varepsilon A_{out} \sigma}\right]^{1/4} - 273.15 =$$

$$= \left[\frac{0.8 \cdot 0.1417 \cdot 1371 + 0.8 \cdot 0.1417 \cdot 0.25 \cdot 0.374 \cdot 1371 + 0.1 \cdot 0.1417 \cdot 161.3}{0.1 \cdot 1 \cdot 5.67051 \cdot 10^{-8}}\right]^{1/4} - 273.15 =$$

$$= \left[\frac{155.4166 + 14.5314 + 2.2856}{5.67051 \cdot 10^{-9}}\right]^{1/4} - 273.15 =$$

$$= 144.319^{\circ} C$$

Since the two temperatures match, the Matlab program is working correctly.

**Case 2.1 (hot cold case)**

In this case, it is assumed that the largest possible projected area of the pyramid structure is always facing towards the Sun. This has to be the base of the pyramid, thus $A_s$ = 0.315 m$^2$. A complicating factor now is that the projected area facing the Earth cannot be kept constant for the assumed orbit. It can vary between the extreme areas of 0.1417 m$^2$ and 0.315 m$^2$. The next figure illustrates this.

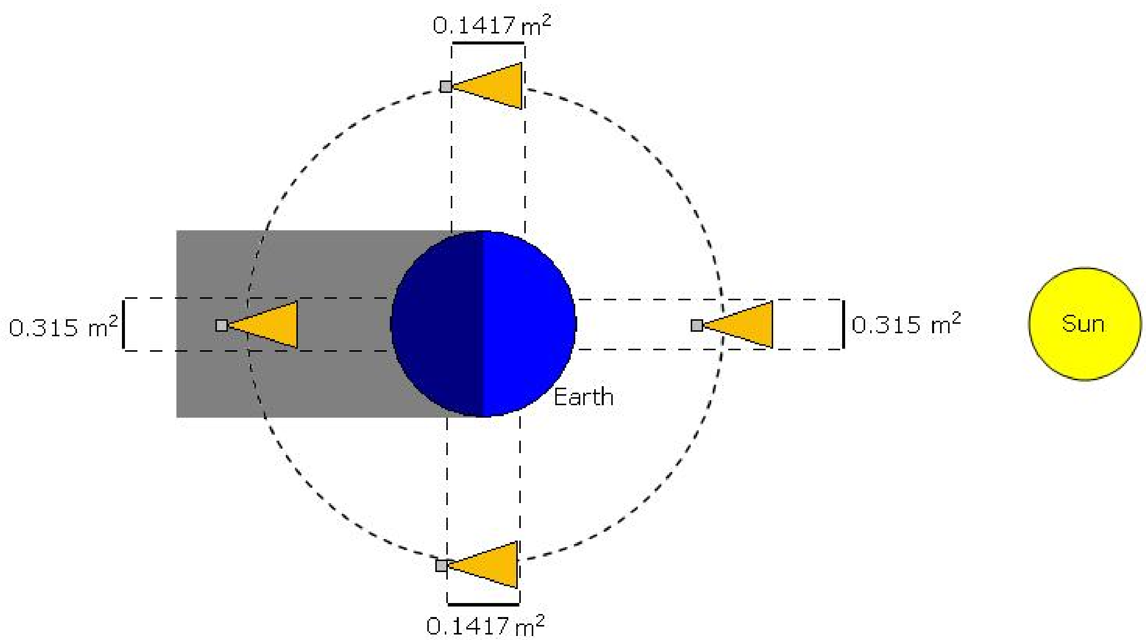


*Figure 15 Orientation of the satellite at four places in its orbit for case 2.1*

The projected surface area facing Earth will vary in a sine-line fashion between 0.1417 m$^2$ and 0.315 m$^2$. For simplicity, the average value between these extremes, 0.22835 m$^2$, is assumed for $A_{ir}$ and $A_a$.

The view factor will also vary for this case. For the four satellite positions depicted in the previous figure, the view factors are (starting at the top, going clockwise): 0.374, 0.747, 0.374, and 0. An average value for the view factor therefore has to be assumed. The figure is a bit misleading, since the view factor will be 0 during 1/3$^{rd}$ of the satellite orbit (in eclipse). In

the figure, this period looks much shorter. The approach now taken is as follows. Since the solar constant will be multiplied by 2/3 for this case, eclipse is already taken into account for albedo radiation. Thus, the part of the orbit in which the view factor is 0 does not have to be taken into account for determination of the average view factor. Then, the view factor varies between 0 and 0.747 in a sine-like manner and the average value of 0.374 is chosen for the view factor in the calculations.
Since this is a “hot” subcase, the albedo coefficient is assumed to be equal to 0.35, see section 4.

The variables for this case are now:

| Variable | Value | Unit |
|---|---|---|
| $A_a$ | 0.22835 | $m^2$ |
| $A_{ir}$ | 0.22835 | $m^2$ |
| $A_S$ | 0.315 | $m^2$ |
| $A_{out}$ | 1 | $m^2$ |
| a | 0.35 | - |
| F | 0.374 | - |
| $S_0$ | 1371 | $W/m^2$ |
| $S_{ir}$ | 192.7 | $W/m^2$ |

*Table 8 Variables for case 2.1*

The formula for the temperature now becomes:

$$T = \left[ \frac{\alpha \cdot 0.315 \cdot \frac{2}{3} \cdot 1371 + \alpha \cdot 0.22835 \cdot 0.35 \cdot 0.374 \cdot \frac{2}{3} \cdot 1371 + \varepsilon \cdot 0.22835 \cdot 192.7}{\varepsilon \cdot 1 \cdot 5.67051 \cdot 10^{-8}} \right]^{1/4}$$

For 0 < $\alpha$ < 1 and 0 < $\varepsilon$ < 0.35, the Matlab results are:

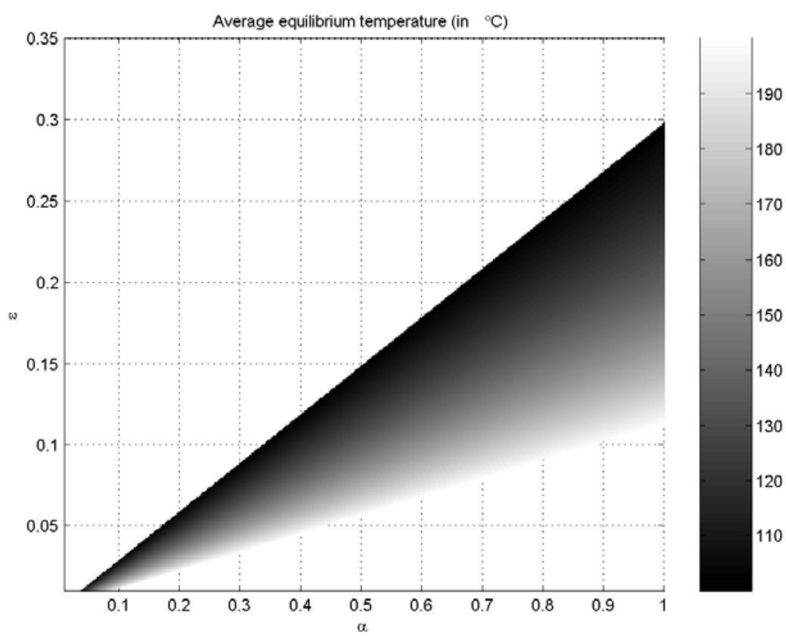


*Figure 16 Temperatures for case 2.1*

For the above figure it is derived that the $\alpha/\varepsilon$ ratio has to be in between 3.5 and 9 to obtain the desired temperature range.

The Matlab result for $\alpha$ = 0.6 and $\varepsilon$ = 0.1 is 156.671°C. The analytical result is:

$$T_{\text{case 2.1}} = \left[ \frac{\alpha A_S S_0 + \alpha A_a a F S_0 + \varepsilon A_{ir} S_{ir}}{\varepsilon A_{out} \sigma} \right]^{1/4} - 273.15 =$$

$$= \left[ \frac{0.6 \cdot 0.315 \cdot \frac{2}{3} \cdot 1371 + 0.6 \cdot 0.22835 \cdot 0.35 \cdot 0.374 \cdot \frac{2}{3} \cdot 1371 + 0.1 \cdot 0.22835 \cdot 192.7}{0.1 \cdot 1 \cdot 5.67051 \cdot 10^{-8}} \right]^{1/4} - 273.15 =$$

$$= \left[ \frac{172.746 + 16.3922 + 4.4003}{5.67051 \cdot 10^{-9}} \right]^{1/4} - 273.15 =$$

$$= 156.670^{\circ} C$$

Since the two temperatures match, the Matlab program is working correctly.

## APPENDIX B: MATLAB CODE CASE 1.1

```
%Average equilibrium temperature for case 1.1 ("hot hot" case)
%Created: 24 January 2007
%Author: D.C. Maessen

clear all;
clc;
warning off MATLAB:divideByZero;

%Constants:
As = 0.315;                 %[m^2]      Surface area exposed to solar radiation
Aa = 0.2004;                %[m^2]      Surface area exposed to albedo radiation
Air = 0.2004;               %[m^2]      Surface area exposed to infrared radiation
Aout = 1;                   %[m^2]      Surface area that emits radiation
So = 1371;                  %[W/m^2]     Solar constant (1371 W/m^2)
a = 0.35;                   %[-]       Albedo coefficient (0.30 plus or minus 0.05)
F = 0.374;                  %[-]       View factor satellite-Earth
sigma = 5.67051E-8;         %[W/m^2/K^4]   Stefan Boltzmann's constant
Re = 6378;                  %[km]       Radius Earth
h = 1000;                   %[km]       Satellite orbit height
Sir = 258*(Re/(Re+h))^2;    %[W/m^2]     Infrared energy per square meter at distance
h for Earth's surface (237+21 W/m^2)

%Stepsize
step = 0.001;

%Range for alpha and epsilon
ALPHA=[0.01:step:1];
EPSILON=[0.01:step:0.5];

% ALPHA=[0.5];
% EPSILON=[0.15];

%Create a grid
[alpha,epsilon]=meshgrid(ALPHA,EPSILON);

%Temperature calculation (in degrees Celsius!)
T = ((alpha*As*So+alpha*Aa*a*F*So+epsilon*Air*Sir)./(epsilon*Aout*sigma)).^(1/4) -
273.15;

%Set every temperature which is smaller than 100 degrees Celsius or larger than 200 degrees
Celsius to NaN
i = find(T<100);
T(i)=NaN;
j = find(T>200);
T(j)=NaN;


%Plot the result

% surf(alpha,epsilon,T);title('Average equilibrium temperature (in
\circC)');xlabel('\alpha');ylabel('\epsilon');zlabel('temperature [\circC]')
% view(0,90)
% % xlim([0.01 1.01]);ylim([0.01 1.01]);
% % shading flat
% shading interp
```

```
% colorbar

pcolor(alpha,epsilon,T);title('Average equilibrium temperature (in
\circC)');xlabel('\alpha');ylabel('\epsilon');zlabel('temperature [\circC]')
colormap(gray)
shading interp
colorbar
grid
```

## APPENDIX C: MATLAB CODE FOR CASE 1.2

```
%Average equilibrium temperature for case 1.2 ("cold hot" case)
%Created: 24 January 2007
%Author: D.C. Maessen

clear all;
clc;
warning off MATLAB:divideByZero;

%Constants:
As = 0.1417;                %[m^2]      Surface area exposed to solar radiation
Aa = 0.1417;                %[m^2]      Surface area exposed to albedo radiation
Air = 0.1417;               %[m^2]      Surface area exposed to infrared radiation
Aout = 1;                   %[m^2]      Surface area that emits radiation
So = 1371;                  %[W/m^2]    Solar constant (1371 W/m^2)
a = 0.25;                   %[-]        Albedo coefficient (0.30 plus or minus 0.05)
F = 0.374;                  %[-]        View factor satellite-Earth
sigma = 5.67051E-8;         %[W/m^2/K^4]    Stefan Boltzmann's constant
Re = 6378;                  %[km]       Radius Earth
h = 1000;                   %[km]       Satellite orbit height
Sir = 216*(Re/(Re+h))^2;    %[W/m^2]    Infrared energy per square meter at distance
h for Earth's surface (237-21 W/m^2)

%Stepsize
step = 0.001;

%Range for alpha and epsilon
ALPHA=[0.01:step:1];
EPSILON=[0.01:step:0.25];

% ALPHA=[0.8];
% EPSILON=[0.1];

%Create a grid
[alpha,epsilon]=meshgrid(ALPHA,EPSILON);

%Temperature calculation (in degrees Celsius!)
T = ((alpha*As*So+alpha*Aa*a*F*So+epsilon*Air*Sir)./(epsilon*Aout*sigma)).^(1/4) -
273.15;

%Set every temperature which is smaller than 100 degrees Celsius or larger than 200 degrees
Celsius to NaN
i = find(T<100);
T(i)=NaN;
j = find(T>200);
T(j)=NaN;


%Plot the result

% surf(alpha,epsilon,T);title('Average equilibrium temperature (in
\circC)');xlabel('\alpha');ylabel('\epsilon');zlabel('temperature [\circC]')
% view(0,90)
% % xlim([0.01 1.01]);ylim([0.01 1.01]);
% % shading flat
% shading interp
```

```
% colorbar

pcolor(alpha,epsilon,T);title('Average equilibrium temperature (in
\circC)');xlabel('\alpha');ylabel('\epsilon');zlabel('temperature [\circC]')
colormap(gray)
shading interp
colorbar
grid
```

## APPENDIX D: MATLAB CODE FOR CASE 2.1

```
%Average equilibrium temperature for case 2.1 ("hot cold" case)
%Created: 24 January 2007
%Author: D.C. Maessen

clear all;
clc;
warning off MATLAB:divideByZero;

%Constants:
As = 0.315;                 %[m^2]      Surface area exposed to solar radiation
Aa = 0.22835;               %[m^2]      Surface area exposed to albedo radiation
Air = 0.22835;              %[m^2]      Surface area exposed to infrared radiation
Aout = 1;                   %[m^2]      Surface area that emits radiation
So = 914;                   %[W/m^2]    Solar constant (2/3*1371 W/m^2)
a = 0.35;                   %[-]        Albedo coefficient (0.30 plus or minus 0.05)
F = 0.374;                  %[-]        View factor satellite-Earth
sigma = 5.67051E-8;         %[W/m^2/K^4]  Stefan Boltzmann's constant
Re = 6378;                  %[km]       Radius Earth
h = 1000;                   %[km]       Satellite orbit height
Sir = 258*(Re/(Re+h))^2;    %[W/m^2]    Infrared energy per square meter at distance
h for Earth's surface (237+21 W/m^2)

%Stepsize
step = 0.001;

%Range for alpha and epsilon
ALPHA=[0.01:step:1];
EPSILON=[0.01:step:0.35];

% ALPHA=[0.6];
% EPSILON=[0.1];

%Create a grid
[alpha,epsilon]=meshgrid(ALPHA,EPSILON);

%Temperature calculation (in degrees Celsius!)
T = ((alpha*As*So+alpha*Aa*a*F*So+epsilon*Air*Sir)./(epsilon*Aout*sigma)).^(1/4) -
273.15;

%Set every temperature which is smaller than 100 degrees Celsius or larger than 200 degrees
Celsius to NaN
i = find(T<100);
T(i)=NaN;
j = find(T>200);
T(j)=NaN;


%Plot the result

% surf(alpha,epsilon,T);title('Average equilibrium temperature (in
\circC)');xlabel('\alpha');ylabel('\epsilon');zlabel('temperature [\circC]')
% view(0,90)
% % xlim([0.01 1.01]);ylim([0.01 1.01]);
% % shading flat
% shading interp
```

```
% colorbar

pcolor(alpha,epsilon,T);title('Average equilibrium temperature (in
\circC)');xlabel('\alpha');ylabel('\epsilon');zlabel('temperature [\circC]')
colormap(gray)
shading interp
colorbar
grid
```

## APPENDIX E: MATLAB CODE FOR CASE 2.2

```
%Average equilibrium temperature for case 2.2 ("cold cold" case)
%Created: 24 January 2007
%Author: D.C. Maessen

clear all;
clc;
warning off MATLAB:divideByZero;

%Constants:
As = 0.1417;                %[m^2]      Surface area exposed to solar radiation
Aa = 0.22835;               %[m^2]      Surface area exposed to albedo radiation
Air = 0.22835;              %[m^2]      Surface area exposed to infrared radiation
Aout = 1;                   %[m^2]      Surface area that emits radiation
So = 914;                   %[W/m^2]    Solar constant (2/3*1371 W/m^2)
a = 0.25;                   %[-]        Albedo coefficient (0.30 plus or minus 0.05)
F = 0.374;                  %[-]        View factor satellite-Earth
sigma = 5.67051E-8;         %[W/m^2/K^4]  Stefan Boltzmann's constant
Re = 6378;                  %[km]       Radius Earth
h = 1000;                   %[km]       Satellite orbit height
Sir = 216*(Re/(Re+h))^2;    %[W/m^2]    Infrared energy per square meter at distance
h for Earth's surface (237-21 W/m^2)

%Stepsize
step = 0.001;

%Range for alpha and epsilon
ALPHA=[0.01:step:1];
EPSILON=[0.01:step:0.2];

% ALPHA=[0.6];
% EPSILON=[0.05];

%Create a grid
[alpha,epsilon]=meshgrid(ALPHA,EPSILON);

%Temperature calculation (in degrees Celsius!)
T = ((alpha*As*So+alpha*Aa*a*F*So+epsilon*Air*Sir)./(epsilon*Aout*sigma)).^(1/4) -
273.15;

%Set every temperature which is smaller than 100 degrees Celsius or larger than 200 degrees
Celsius to NaN
i = find(T<100);
T(i)=NaN;
j = find(T>200);
T(j)=NaN;


%Plot the result

% surf(alpha,epsilon,T);title('Average equilibrium temperature (in
\circC)');xlabel('\alpha');ylabel('\epsilon');zlabel('temperature [\circC]')
% view(0,90)
% % xlim([0.01 1.01]);ylim([0.01 1.01]);
% % shading flat
% shading interp
```

```
% colorbar

pcolor(alpha,epsilon,T);title('Average equilibrium temperature (in
\circC)');xlabel('\alpha');ylabel('\epsilon');zlabel('temperature [\circC]')
colormap(gray)
shading interp
colorbar
grid
```

# iDod storage device

## SUMMARY

In this document, a design is made for the storage device for the inflatable structure of the iDod such that it fits inside a CubeSat.

Two options for mounting of the storage device have been considered: mounting it on a printed circuit board in the CubeSat or integrating it in the top panel of the CubeSat. The latter option is considered to be more practical and is therefore selected. This results in dimensions of 83x83x15 $mm^3$ for the storage device itself with flanges that act as the remainder of the top panel extending to 100x100 mm. The mass of the complete storage device is 40 grams while the mass without flanges and moveable lid is ~23 grams.

## KEYWORDS

Storage device, integration, mounting

## DISTRIBUTION

| | Name | | Company / Institution |
|---|---|---|---|
| 1 | E.D. van Breukelen | Customer | ISIS B.V. |
| 2 | B.T.C. Zandbergen | Project supervisor | TU Delft |

## APPROVAL

| | Name | Company / Institution | Date | Signature |
|---|---|---|---|---|
| *Written* | D.C. Maessen | TU Delft | 4/2/2007 | |
| *Checked* | | | | |
| *Approved* | | | | |

## REVISION RECORD

| Issue | Date | Total pages | Affected pages | Brief description of change |
|---|---|---|---|---|
| Draft | 3/20/2007 | 20 | | |
| Version 1.0 | 3/27/2007 | 21 | 3 | Added requirements section and moved some content of other sections into this section |
| | | | 4, 10 | Indicated commonality of design with Delfi-$C^3$ |
| | | | 8 | Added subsection 3.3 |
| | | | 10 | Volume of deployment confirmation switch indicated |
| | | | 11 | Subsection 4.5 expanded |
| | | | 11, 12 | Subsection 4.6 (design summary) added |
| | | | 12-14 | Moved technical drawings from appendix B to subsection 4.7 |
| | | | 15 | Section 6 expanded |
| | | | many | Small textual changes |
| Version 1.1 | 3/29/2007 | 22 | 11 | Subsection 4.3 added |
| Version 1.2 | 4/2/2007 | 24 | 12, 13 | Subsection 4.4 added |

## LIST OF TBD'S AND TBC'S

| TBD / TBC | Paragraph | Subject | Due date | Action by |
|---|---|---|---|---|
| TBD | Section 2 | Folding method inflatable structure | TBD | TBD |
| TBD | Subsection 4.3 | Rotation angle lid during deployment inflatable | TBD | TBD |
| TBD | Subsection 4.4 | Placement CGG | TBD | TBD |
| TBD | Subsection 4.7 | Effect of storage device on temperature solar cells | TBD | TBD |
| TBD | Appendix A | Responses due to vibrations | TBD | TBD |

## TABLE OF CONTENTS

# 1 INTRODUCTION

Since the inflatable structure of the iDod has to be folded prior to deployment and has to be separated from the various items inside the CubeSat, it needs to be stored in a storage device.

The requirements for this storage device are lined out in section 2. Section 3 deals with the integration of the storage device into a standard CubeSat structure and selection of a manner to mount the storage device onto a CubeSat. The detailed design of the storage device is discussed in section 4.

Appendix A treats the loads on the CubeSat structure resulting from mounting the iDod on it.

# 2 REQUIREMENTS

Firstly, the storage device has to fit inside a 10x10x10 $cm^3$ cube such as the one depicted below.

*Figure 1 Standard 1-unit CubeSat chassis [Pumpkin, 2007]*

In [van Breukelen, 2007], it is stated that the difference in mass of a CubeSat with iDod should be less than 100 grams from the same CubeSat without iDod. Furthermore, its volume should be less or equal to 104 $cm^3$.

The height of the storage device should be minimal in order to leave a practically sized volume available for other CubeSat components.

A so-called cool gas generator (CGG) from TNO is to be used to inflate the inflatable structure.

The CubeSat and the storage device have to be able to survive the loads imposed on them during launch. The maximum acceleration a CubeSat is subjected to during launch is assumed to be equal to that of the DNEPR launcher, which is a launcher that has already been used to launch CubeSats (in July 2006, but the launch failed). According to the user's guide [ISC Kosmotras, 2001], the maximum lateral acceleration of the vehicle is 8 g. In the user's guide also a safety factor of 1.3 on top of this acceleration is advised, which results in an acceleration of 10.4 g. This acceleration is rounded off to 10 g for easy calculation.

# 3 INTEGRATION OPTIONS

In CubeSats, mass and volume are extremely restricted. Therefore, when designing a CubeSat component both the mass and volume have to be taken into account, but also the integration of the component. Designing a component without integration in mind will almost certainly result in issues even though its mass and volume may be within budget. Its dimensions can be such that it is extremely impractical to use it on a CubeSat or it may be impossible to mount it. Therefore, integration is as important a design issue for the iDod storage device as is its mass and volume.

In many CubeSats, the internal configuration is such that several PCBs are stacked above each other and held in place using threaded rods (3M size). This is illustrated in the next picture where the internal configuration of CanX-1 is shown:

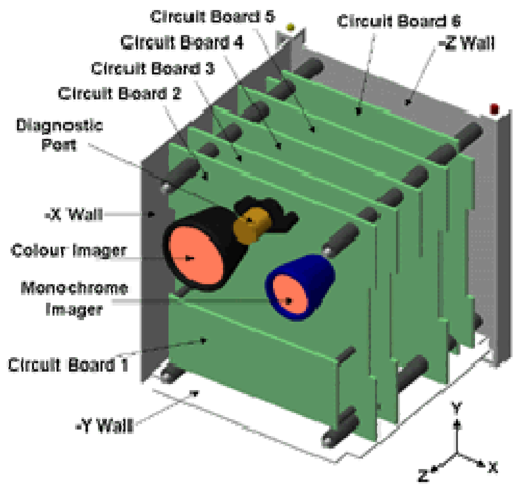


*Figure 2 Stacked PCBs [University of Toronto, 2007]*

Other configurations are also possible, but often there will be one or several PCBs that are positioned such as the ones in the figure above. Thus, the height of the storage device cannot be too large or otherwise it will cause interference problems with one or more PCBs.

In CubeSats, the standard PCB size is 90x96 mm. This PCB size is also used in Delfi-$C^3$. PCBs are often PC/104 modules and utilize PC/104 connectors. Using these connectors allows the PCBs to be stacked on top of each other with a rigid connection (stackthrough) that serves as the satellite bus.

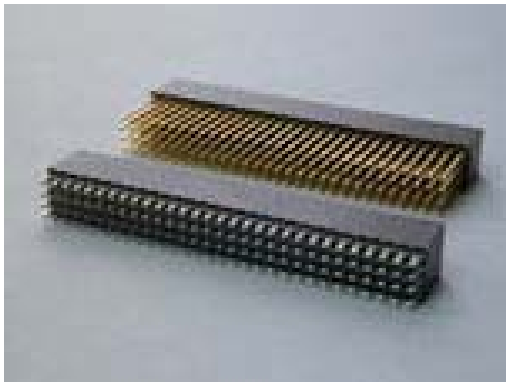

*Figure 3 PC/104 connectors [Emulation Technology, 2007]*

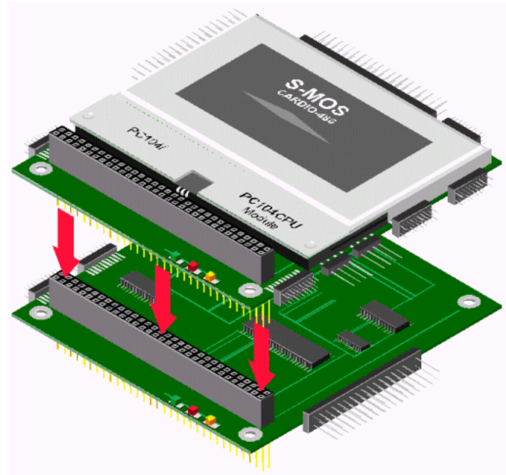


*Figure 4 Stacking PC/104 modules [Answers.com, 2007]*

For mounting the storage device to the CubeSat structure, there are two obvious options:

- Mounting on a PCB
- Integration in a side panel (assumed to be the top panel)

In the first case, a large section of the panel directly above the storage device has to be removed to allow the lid of the container to be opened.

The different mounting options have an impact on the loads exerted on the structure of the CubeSat. In appendix A, these loads are assessed and it is concluded that with respect to the resulting loads, both mounting options are possible. It is noted that responses due to vibrations are not taken into account and remain TBD.

## 3.1 Mounting on a PCB

When the storage device is mounted on a PCB, it has to stay clear of threaded rods, standoffs, and the stackthrough connector. This results in the layout depicted in figure 5 (top view). The hashed area is the area that is available for the storage device.

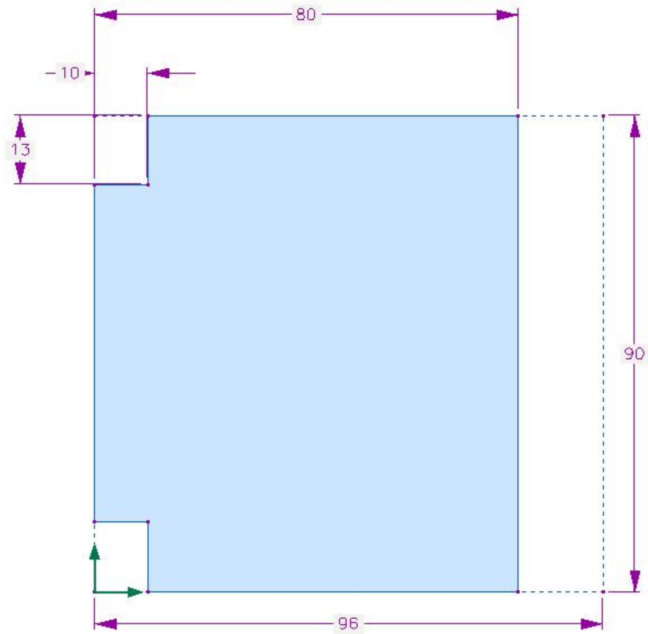


*Figure 5 Top view of container envelope (hashed) over PC104 envelope (dotted lines)*

With a ground area of approximately 90x80 mm, the height of the storage device needs to be 15 mm in order to obtain a volume close to 100 $cm^3$ (104 $cm^3$).

Below, several views are presented of a conceptual storage device mounted on a PCB. The blue rectangles are solar cells (8x3 cm) and the double row of very small holes is holes for the PC/104 connector.

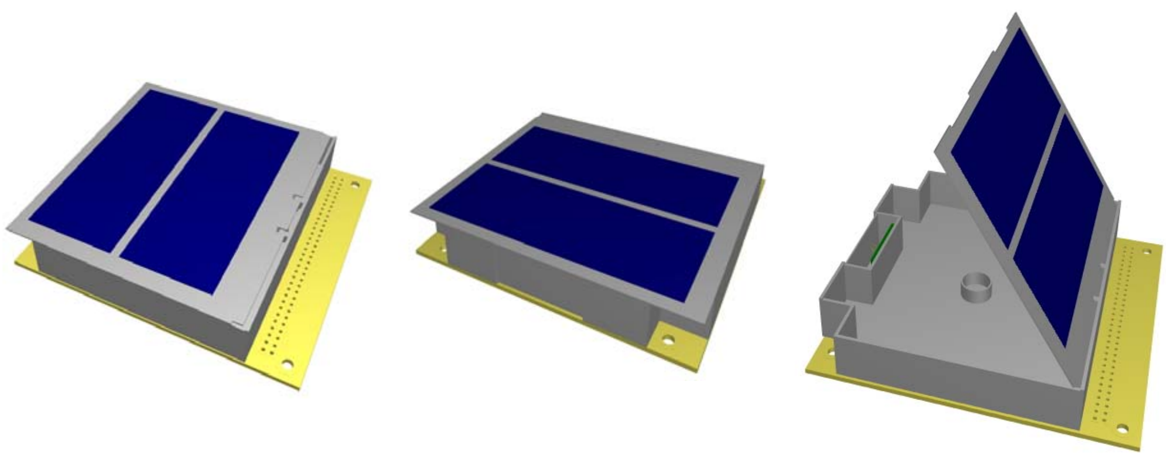

*Figure 6 Storage device mounted on a PCB*

The middle and right pictures above show why the hashed area in figure 5 is not perfectly rectangular, but has two small corners removed: this is necessary to allow room for the threaded rods that are stuck through the PCB.

## 3.2 Integration in top panel

Instead of mounting the storage device onto a PCB, it can also be integrated into the top panel of the CubeSat. The great advantage here is that the iDod almost becomes a plug-and-play system for the CubeSat integrator. It is not entirely plug-and-play because the on-board computer of the CubeSat needs to be fitted with extra software to handle the iDod system.

The only thing the integrator needs to ensure structurally is that the bottom of the storage device has enough clearance with the uppermost PCB inside the CubeSat. How much this clearance should be depends on the specific CubeSat and has to be determined by the integrator. A determining factor in this is the thermal balance of the satellite which will be different for a CubeSat with iDod from a CubeSat without iDod.

In this case, the envelope of the storage device can be 83x83x15 $mm^3$, giving a total available volume of ~103 $cm^3$. The width of the storage device needs to be 83 mm since CubeSats are normally built up out of a frame with ribs having a thickness of maximally 8.5 mm. The width of the frame is 100 mm and thus the minimal spacing between the ribs is $100 - 2 \cdot 8.5 = 83$ mm.

The next picture shows the ground plane of the storage device projected over a standard PCB. From the picture it is clear that there is virtually no room for items on the PCB that can be positioned next to the storage device. Thus, they all have to be below the storage device. A PC/104 connector is often the object with the most height on a PCB. Therefore, the clearance between the upper PCB and the bottom of the storage device has to be minimally the height of a PC/104 connector which is 11.05 mm [PC/104 Embedded Consortium, 2003].

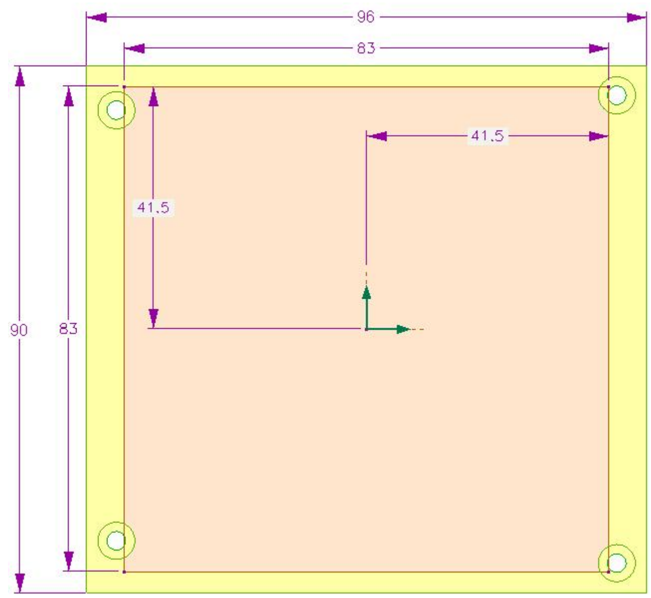


*Figure 7 Top view of container envelope*

Below, a conceptual design for a storage device integrated into the top panel is depicted. The flanges on the storage device are left 100x100 mm. This way, cutouts and holes can be made in the flanges by the customer as he sees fit.

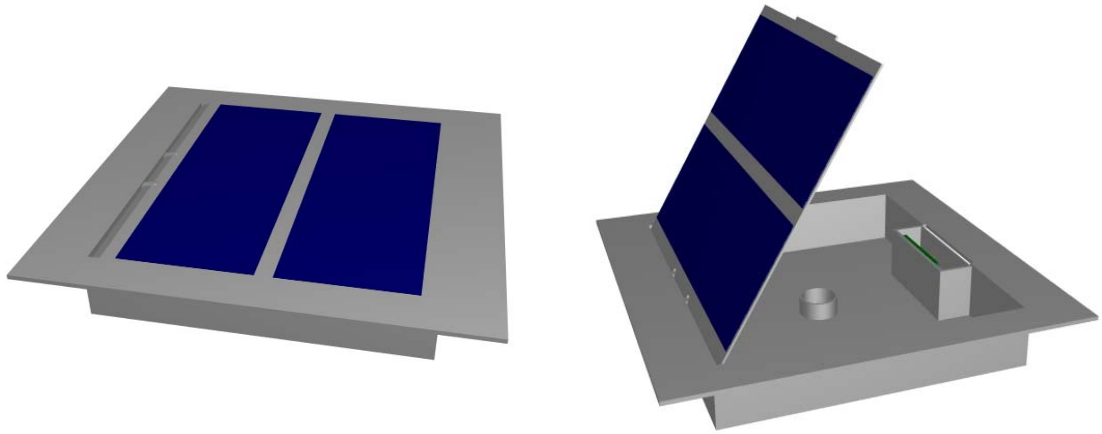

*Figure 8 Storage device integrated in top panel*

## 3.3 Selection

The option to mount the storage device onto a PCB has several noticeable disadvantages:

- The top panel of the CubeSat has to be adapted (section cut out)
- The storage device has to be aligned precisely with the gap in the top panel (very small gaps are desired to minimize radiation influence on the electronics). Thus, either the stacked PCBs have to be positioned very carefully or the storage device has to be mounted on its PCB when the top panel is already in place (the storage device is then lowered through the hole in the top panel onto its PCB).
- The container has several corners that are impractical for folding of the inflatable structure; it is very difficult to utilize the available volume maximally in this way.

The first two downsides are important for the CubeSat integrator; these will cost him both in time and money. The last downside is important for the supplier of the iDod since not being able to use all available volume results in a smaller maximum size for the inflatable structure and thus a smaller starting altitude and smaller potential market.

When the storage device is integrated into the top panel of the CubeSat, the loads resulting from the high acceleration are directly fed into the frame of the CubeSat. This is a more desirable load case than in case the storage device is mounted onto a PCB. Then, the loads are fed into the frame via a shear panel which is by definition not meant to handle out-of-plane loads. Generally, the frame of a 1-unit CubeSat consists out of L-shaped strips of aluminum located at the ribs of the cube. Assuming their wall thickness is 1 mm and that their flanges are 8.5 mm high, the results from the analysis in Appendix A indicate that these L-sections are more than stiff and strong enough to handle the load caused by the storage device and the acceleration of 10 g.

In light of the above, integrating the storage device into the top panel of the CubeSat is the preferred method.

# 4 DETAILED DESIGN

On the next page, pictures of the storage device selected in subsection 3.3 are shown. The flanges on the storage device are not shown because they obstruct the view of some items.

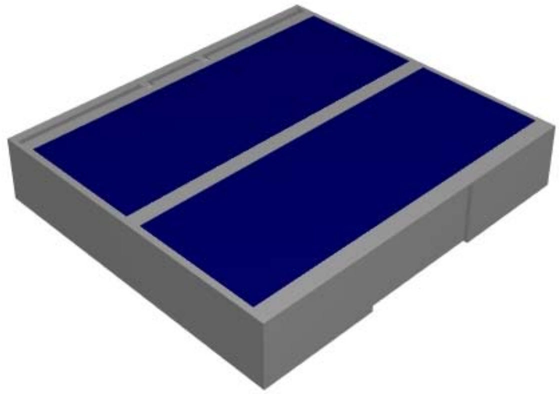

*Figure 9 Storage device closed*

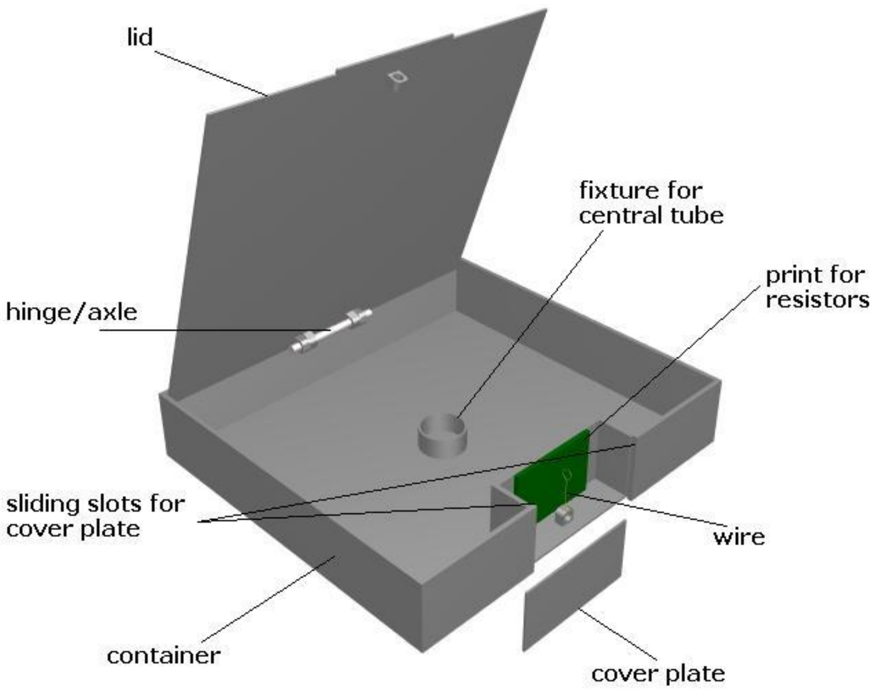


*Figure 10 Storage device opened*

The function of the various items indicated in the above figure is treated in the coming subsections.

## 4.1 Material selection

The storage device is made out of aluminum 6061-T6. Reason for this is that standard CubeSat chassis are made out of a combination of aluminum 6061-T6 and aluminum 5052-H32 [Pumpkin, 2007]. These two types of aluminum have very similar coefficients of thermal expansion (CTE). The density of aluminum 6061-T6 is 2.7 g/cc and its CTE is 23.6 μm/m/K (linear 68°F (= 20°C)) [MatWeb, 2007].

## 4.2 Hold down and release mechanism

At the present time, it is assumed that the inflatable structure is deployed once a lid covering the iDod has been opened. This lid is held down by means of a wire (for instance Dyneema or some other type of polyethylene fiber) which is melted through once the deployment

command is given. Melting through of the wire is achieved by heating up a resistor which is in contact with the wire. The lid is allowed to rotate around a thin aluminum axle. Opening of the lid is achieved by means of two helical torsion springs positioned on the axle (for redundancy, in case one spring cold welds to the axle).
The method of using torsion springs and melting a wire using resistors is also used on Delfi-$C^3$ to deploy antennas (developed by Richard van den Eikhoff) and solar panels. Therefore, much knowledge about this mechanism is available at the faculty. This will greatly speed up the development of this system.

Correct deployment of the lid can be confirmed by means of a switch that is either opened or closed once the panel has reached the required amount of rotation. The switch is not indicated in the above picture. Its dimensions are unknown and for now it is assumed that it occupies a volume of 4 $cm^3$ [Maessen, iDod.TN.010]. If required, the maximum rotation angle can be enforced by hard stops or plungers. Allowing the lid to rotate more than 90° is beneficial to ensure maximum clearance for the inflatable structure. Protruding elements like antennas could even be forced out of the way by the lid.
The reason for choosing a single lid over for instance two lids is simple: less moving parts and therefore less chance of (partial) failure. Less parts also has the benefit of less mass and volume.

The restraining wire is attached to the lid and the bottom of the container by pulling it through two small brackets and making either a knot or by melting the wire such that the ends can be pressed against other parts of the wire and allowed to cool down to form a strong bond. It is expected that attachment using melting will require some practicing and fine-tuning to prevent the wire from melting through. After the wire has been attached, a cover plate is slid in front of the wire and the resistor through sliding slots in the wall of the container. The function of the cover plate is to protect the fragile wire and resistor during handling of the storage device.

The printed circuit board (PCB) on which the resistor is mounted is made from standard FR-4 PCB laminate (FR stands for Flame Retardant, type 4 means woven glass reinforced epoxy resin) [AirBorn Electronics, 2007]. This material is standard for CubeSats [Pumpkin, 2007] and is also used on Delfi-$C^3$. For redundancy, it can be opted to install two resistors instead of one. The second resistor then acts as a backup if the main resistor fails. The restraining wire can then be attached such that it runs between the resistors in an S-shape, ensuring it always makes contact with both resistors. Of course, care has to be taken that the wire does not exert a too large pulling force on the wires with which the lower resistor is attached to the PCB, see the next figure.

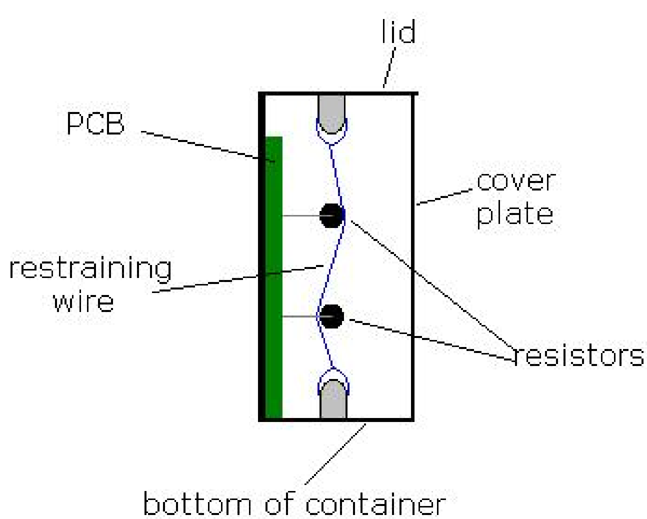


*Figure 11 Placement of resistors and restraining wire*

## 4.3 Required rotation angle lid

The lid of the storage device has to rotate enough to prevent it from coming into contact with a membrane of the inflatable structure. The next figure depicts the required rotation angle if the length of the central tube of the inflatable is 50 cm and the length of the spokes is 40 cm.

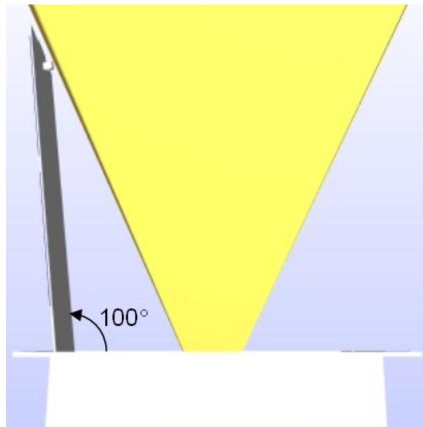


*Figure 12 Lid rotated 100°*

A rotation angle of at least 100° is thus required once the inflatable is deployed.

However, when the inflatable is being deployed, it requires more volume than when it is fully deployed. This is due to the deployment of the spokes, which rotate away from a position close to the central tube to their end position [Maessen, iDod.TN.006].

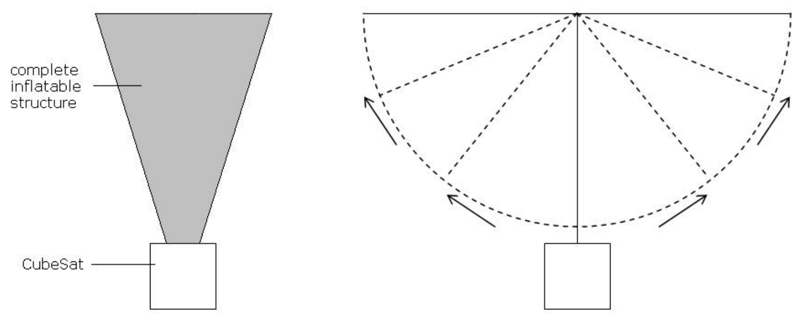


*Figure 13 Deployment scheme inflatable structure [Maessen, iDod.TN.006]*

In this case, a rotation of at least 140° is required to prevent a membrane from coming into contact with the lid.
Whether it is really necessary to prevent the membrane from coming into contact with the lid is TBD by means of tests. When the membrane cannot get stuck behind something it will simply slide along the surface of the lid. However, at the end of the lid, there is a small bracket present that is used to attach the Dyneema wire to. This bracket may pose problems.

## 4.4 CGG placement

The CGG used to inflate the inflatable structure is described in [Maessen, iDod.TN.006]. Although small, 18 mm long and a maximum diameter of 8 mm, its size is still considerable for the iDod. There are three options for the placement of the CGG.

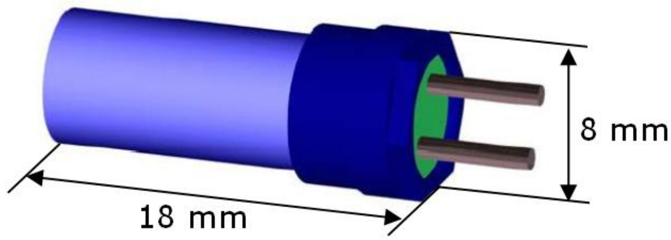


*Figure 14 CGG with dimensions [adapted from Maessen, iDod.TN.006]*

The first option is to screw the CGG into the fixture for the inflatable structure. This is the best integration option for the CGG itself. There is only one possible place for a leak (the screwing thread) and the mass and volume required for the fixture are minimal. But with this option, the CGG is either in the way of a membrane or of an inflatable tube of the inflatable when the inflatable is stowed.
Another option is to position the CGG under the hinge for the lid of the storage device. Then, a small tube is required to transport the inflation gas to the inflatable tubes. This option increases the possible number of leaks by two: at the connection of the tube with the CGG and at the connection of the tube with the fixture. The required mass and volume are also higher than for the previous option due to the use of a tube and due to the requirement for a separate fixture for the CGG. The advantage is that the CGG is likely to be less in the way than for the previous option.
The last option is to use a CCG with a different shape that fits inside the fixture for the inflatable tubes. Whether this is possible volume-wise is TBD. This option implies a new CGG design that has to be tested and validated just for this application. In other words: it is expensive. There are also possible issues with the velocity of the gas jet that impinges on the tube material of the inflatable. This is discussed in more detail in [Maessen, iDod.TN.006].

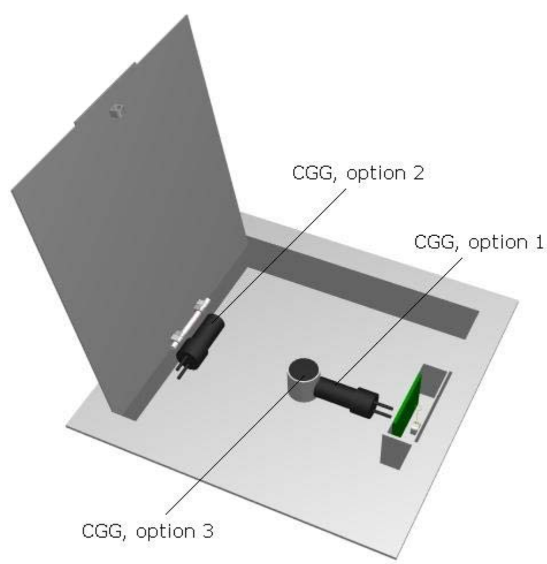


*Figure 15 CGG placement options*

There is no perfect placement option for the CGG. Folding tests will have to point out which placement option is the most favorable one.

## 4.5 Mass and volume

The wall thickness of the lid and the bottom of the container is 0.5 mm. The thickness of the vertical sides of the storage device is 1 mm.

As already indicated in subsection 3.2, the volume occupied by the selected storage device is ~103 $cm^3$. The volume available for the inflatable structure is somewhat smaller due to the presence of the fixture for the central tube (∅ = 10 mm, height = 10 mm), the CGG (1 $cm^3$), the deployment confirmation switch (4 cc), and the volume reserved for the hold down and release mechanism (30x10x15 $mm^3$). This leaves a volume of 79 $cm^3$ for the inflatable structure.

The mass of the complete storage device is determined using the CAD program used to draw the storage device and amounts to ~40 g when only the aluminum parts are taken into account. However, the mass of the flanges and the lid are not taken into account for the mass of the storage device since they function as the top panel of the CubeSat and are therefore normally also present on a CubeSat. Without the flanges and the lid, the storage device weighs ~23 g.

## 4.6 Manufacturing

The storage device is created by milling its exact shape from a block of extruded aluminum 6061-T6. Extruded aluminum 6061-T6 can be purchased in rods from various suppliers. Milling allows the wall thickness to be easily made to specifications. Milling also allows variation of the wall thickness at different places when this proves to be necessary. Using sheet metal, varying the wall thickness is cumbersome and expensive. Although milling is not a cheap production method in itself, its major advantage is that only one production step is required.
If sheet metal is used it needs to be bended and the corners need to be joined by welding (not preferred, it changes the material properties locally and is difficult for aluminum) or by using extra L-strips of material at the corners. This is labor-intensive and therefore expensive.

## 4.7 Solar cells

Since CubeSats are normally completely covered with solar cells to maximize the available power, it is very likely that the lid of the storage device will also be equipped with solar cells. This has already been implicitly assumed in the preceding subsections.

The solar cells are assumed to be 80x30 mm large. Therefore, only two will fit on the storage device. The solar cells are assumed to be connected in series and the solar cells need to be grounded. This results in a total of 3 wires that have to run from the lid of the storage device to the container and further on into the CubeSat. The wires to be used for this are likely to be AWG28 (American Wire Gauge) wires or similar.
The wires can run down to the storage device via a gap present between the lid and the vertical wall of the storage device at the hinge side of the lid. This gap is required to allow the lid to rotate more than 45° upward. The wires have to be ~3 mm longer than required at the gap in order to have enough length when the lid is rotated 90° upward. This extra length of wire needs to be free to move when required.

The presence of the storage device under the solar cells will cause the solar cells to have a different temperature than when the storage device is not present. How the storage device affects the temperature of the solar cells and how this affects their performance is left TBD.

## 4.8 Design summary

The storage device is depicted in figures 8, 9, 10, and 15. Its main design features are:

1. It is integrated into the top panel of the CubeSat
2. It has a lid that hinges on one side to allow deployment of the inflatable structure; the lid has to rotate at least 100° to prevent it from coming into contact with a membrane of the inflatable once it has been deployed
3. The dimensions of the container of the storage device are 83x83x15 $mm^3$
4. 1 mm thick flanges extend from the container to form a 100x100 $mm^2$ square and function as the remainder of the top panel

5. The container and flanges of the storage device are made by milling a block of 6061-T6 aluminum into the correct shape. The lid is made from 0.5 mm thick 6061-T6 aluminum sheet
6. The mass of the complete storage device is ~40 grams; the mass of the container is ~23 grams
7. The lid opens by means of a torsion spring and is held down by a Dyneema wire which is melted through using resistors once the lid needs to be opened
8. A CGG is used to inflate the inflatable structure and is positioned inside the storage device. The exact placement of the CGG is TBD.
9. Solar cells can be mounted on the lid to provide the CubeSat with power
10. The container features a fixture to which the inflatable structure can be attached.

## 4.9 Technical drawings

The next pages depict technical drawings of the lid and of the container of the storage device.

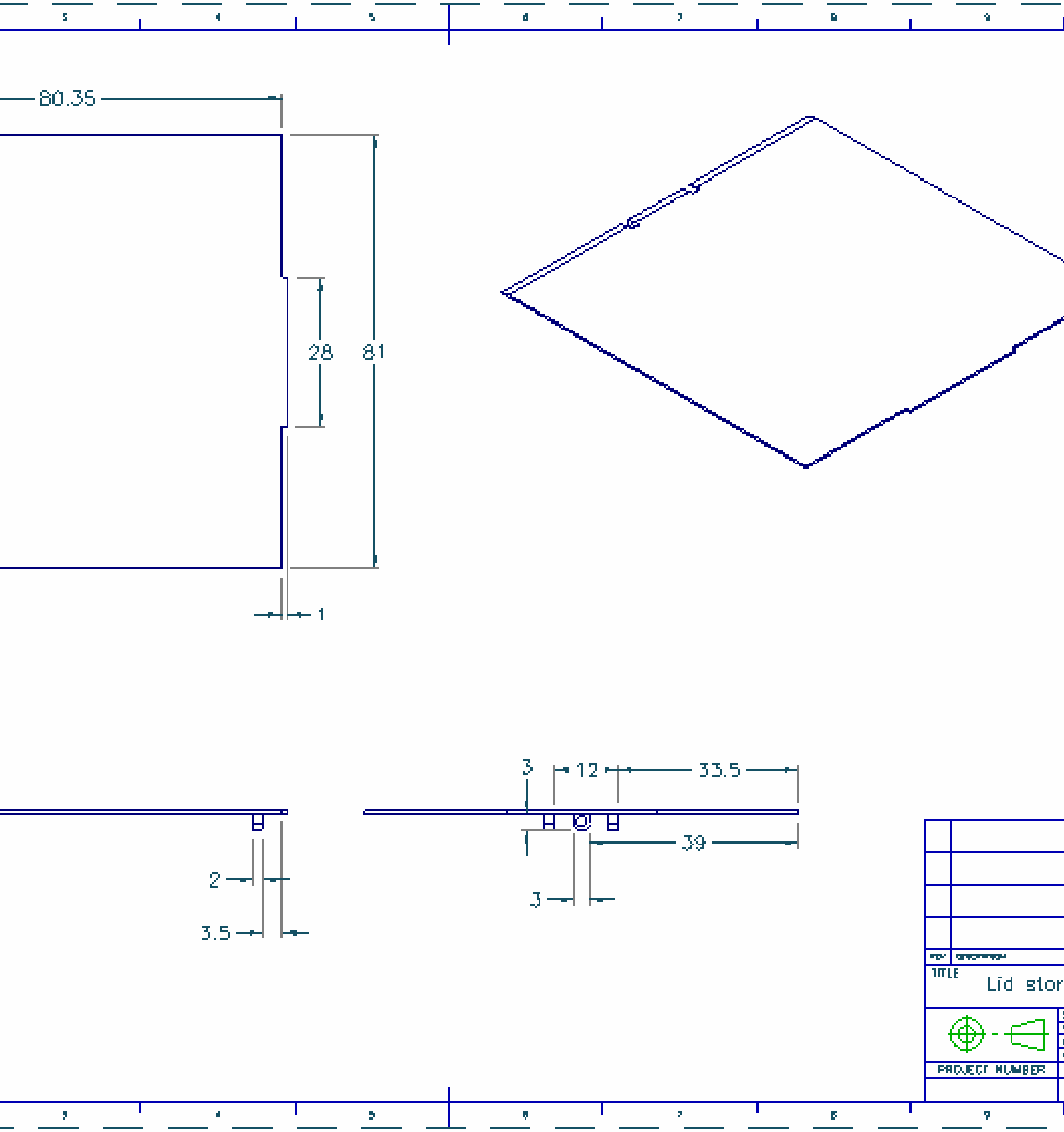
80.35
28
81
1
3
12
33.5
39
2
3.5
3
TITLE
Lid stor
PROJECT NUMBER

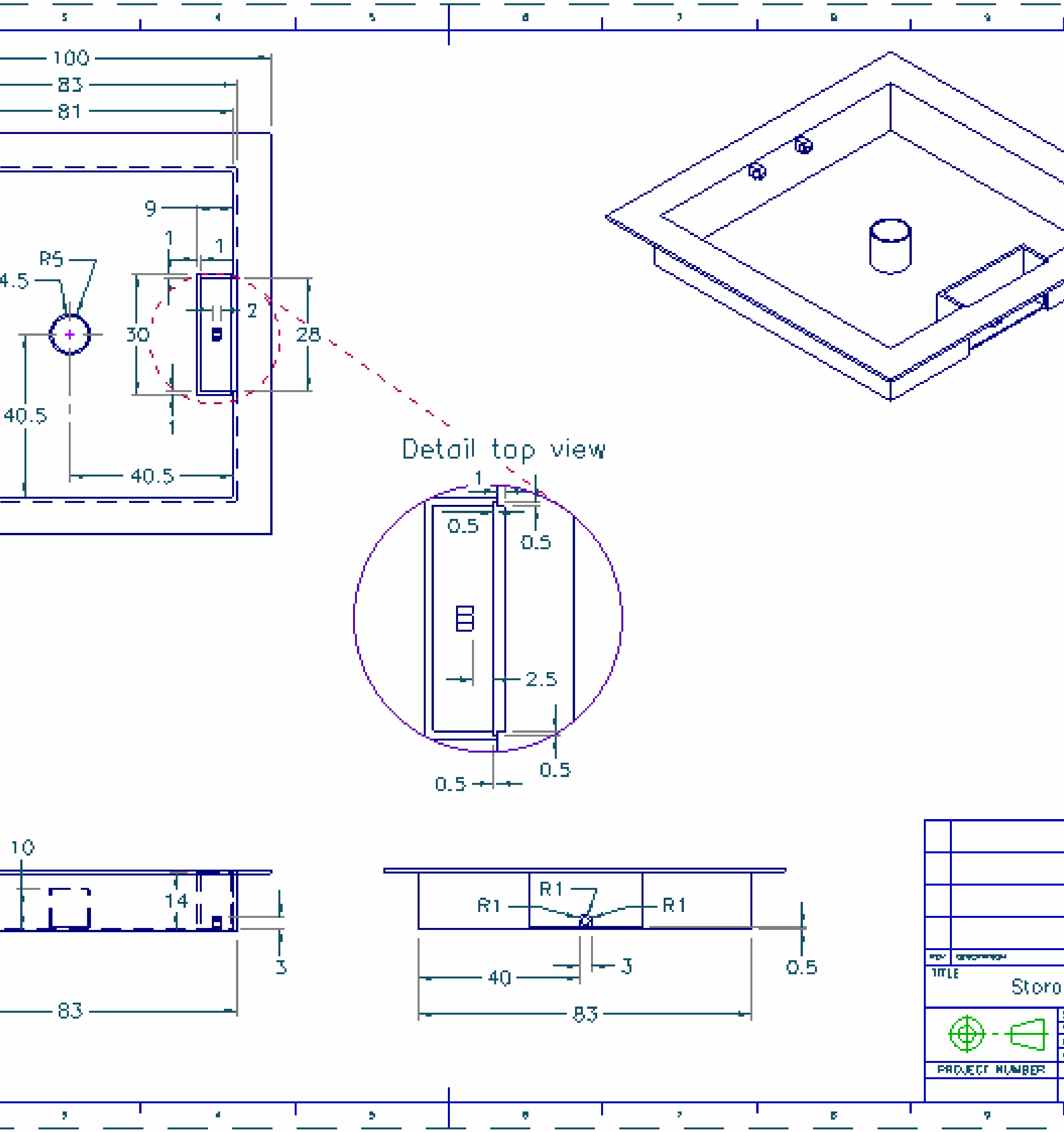
100
83
81
9
1
1
R5
4.5
2
30
28
40.5
40.5
Detail top view
1
0.5
0.5
2.5
0.5
0.5
10
14
3
83
R1
R1
R1
40
3
0.5
83
TITLE
Storo
PROJECT NUMBER

# 5 CONCLUSIONS & RECOMMENDATIONS

In the preceding sections, it is chosen to integrate the storage device into the top panel of the CubeSat. This removes issues with alignment and results in more advantageous dimensions of the storage device for folding of the inflatable structure. It also results in a favorable loading of the CubeSat frame during launch.

The volume available for the inflatable structure is ~79 $cm^3$ and the mass of the container of the storage device is ~23 g. The complete storage device weighs ~40 g, but the flanges and the lid are not taken into account for its mass since they act as top panel of the CubeSat and as such do not 'add' mass to a CubeSat when the iDod is used on it.

It is recommended look more closely at the hold down and release mechanism in the remainder of the design. The volume allocated to it is an educated guess and should be optimized. The same goes for the cool gas generator used to inflate the inflatable structure.

# 6 FURTHER WORK

The precise integration of the CGG into the storage device has to be dealt with in a later stage of the design. In addition, the required wall thicknesses and dimensions of components have to be determined exactly. The incorporation of solar cells on the lid of the storage device has to be looked at in more detail. Thermal effects also have to be determined for the solar cells. The influence of vibrations on the structure of the storage device and the CubeSat has to be assessed as well as the influence of vibrations on the hold down and release mechanism.

## REFERENCES

1. AirBorn Electronics, *FR-4 PCB Laminate*, http://www.airborn.com.au/method/fr4pcb.html, Viewed March 2007.

2. Answers.com, *PC/104,* http://www.answers.com/topic/pc-104, Viewed March 2007.

3. Breukelen, E.D. van, *Top Level Requirements for inflatable De-orbit device (iDod)*, iDod document ISIS.iDod.REQ, Revision 1.3, Delft, 17 March 2007.

4. Emulation Technology, Inc., *PC/104 and PC/104+ Connectors & Hardware*, http://www.emulation.com/173/, Viewed March 2007.

5. Gere, J.M., Timoshenko, S.P., *Mechanics of MATERIALS*, Fourth SI Edition, Stanley Thornes (Publishers) Ltd, Cheltenham (UK), 1999.

6. Hartog, J.P. Den, *Sterkteleer*, Het Spectrum, Utrecht/Antwerpen, 1967.

7. Hexcel, Prepreg Technology, Informative datasheet, March 2005.

8. ISC Kosmotras, *Space Launch System DNEPR User's Guide*, Issue 2, November 2001.

9. Maessen, D.C., *iDod mass and volume breakdown*, iDod document iDod.TN.010, Draft, Faculty of Aerospace Engineering, Delft University of Technology, 19 January 2007.

10. Maessen, D.C., *iDod stowage and deployment*, iDod document iDod.TN.006, Draft, Faculty of Aerospace Engineering, Delft University of Technology, 28 March 2007.

11. MatWeb, *AISI 1005 Steel*, http://www.matweb.com/search/SpecificMaterial.asp?bassnum=M1005A Viewed March 2007.

12. MatWeb, *Aluminum 5052-H32*, http://www.matweb.com/search/SpecificMaterial.asp?bassnum=MA5052H32 Viewed January 2007.

13. MatWeb, *Aluminum 6061-T6; 6061-T651*, http://www.matweb.com/search/SpecificMaterial.asp?bassnum=MA6061T6 Viewed February 2007.

14. MatWeb, *E-glass fiber, Generic*, http://www.matweb.com/search/SpecificMaterial.asp?bassnum=CGF004 Viewed March 2007.

15. MatWeb, *Epoxy,Cast, Unreinforced*, http://www.matweb.com/search/SpecificMaterial.asp?bassnum=O1700 Viewed March 2007.

16. PC/104 Embedded Consortium, *PC/104 Specification*, Version 2.5, November 2003.

17. PowerStream, *Wire Gauge and Current Limits*, http://www.powerstream.com/Wire_Size.htm, Viewed March 2007.

18. Pumpkin, Inc., *CubeSat Kit*, http://www.cubesatkit.com/ Viewed January 2007.

19. University of Toronto, *CanX-1*, http://www.utias-sfl.net/nanosatellites/CanX1/CanX1System.html, Viewed March 2007.

20. Wijker, J.J., *Spacecraft Structures*, Lecture notes, Delft University Press, September 2004.

## APPENDIX A: LOADS RESULTING FROM MOUNTING ON A PCB

Different ways of mounting the storage device on a CubeSat results in different loads being exerted on the CubeSat structure. This appendix treats the loads and reactions due to these loads for the option discussed in section 3.1: mounting the storage device onto a PCB. Responses due to vibrations are not taken into account in the calculations and remain TBD.

As already mentioned in section 2, the acceleration of the CubeSat during launch is assumed to be 10g.

It is noted that it is assumed that the CubeSat is positioned such in the launcher that the ground plane of the storage device is perpendicular to the launch acceleration.

Mounting the storage device onto a PCB will result in the PCB and the threaded rods to be subjected to relatively high launch loads. These loads are also transmitted to the side panel onto which the threaded rods are connected. Being a shear panel, this side panel is not supposed to carry high out-of-plane loads. In this subsection it is checked whether the loads caused by the storage device can be handled by the PCB, the threaded rods, and the panel onto which the threaded rods are connected.

Figure 14 depicts a schematic representation of the storage device mounted on a PCB.

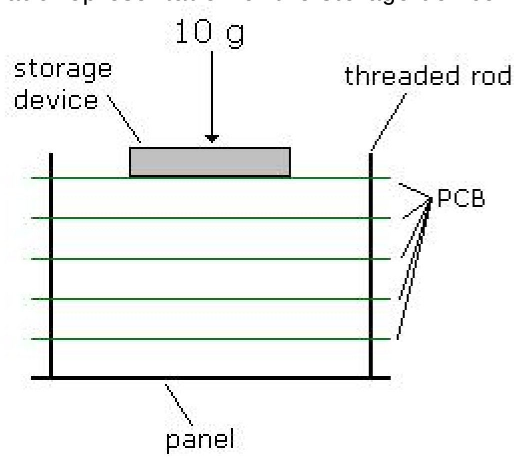


*Figure 16 Launch load acting on storage device*

The width of the PCB (between the threaded rods) is assumed to be 90 mm, its height is assumed to be 1 mm. The panel on which the threaded rods are mounted is assumed to have the same dimensions as the PCBs. The load caused by the storage device and the acceleration is assumed to be a concentrated load acting halfway the PCB. The vertical spacing between the PCBs is assumed to be 15 mm.

The PCBs are assumed to be made out of an E-glass/epoxy composite (GFRP) with the fibers in 0°/90° direction. The panel is assumed to be made out of aluminum and the threaded rods are assumed to be made out of steel. Approximate values for the Young's modulus of these materials are given in the next table.

| Material | Young's Modulus [GPa] |
|---|---|
| E-glass | 72 |
| Epoxy | 3 |
| Aluminum | 70 |
| Steel | 200 |

*Table 1 Young's modulus for various materials [MatWeb, 2007]*

Using the rule of mixtures, the Young's modulus of the PCB is determined to be 37 GPa (½·72 + ½·3).

The moments of inertia for the PCB, the panel, and the threaded rods are determined using formulas from [Gere, 1999]. The PCB and the panel are assumed to have a width b of 90 mm and a height h of 1 mm, the threaded rod is assumed to have a circular cross section with a diameter d of 3 mm:

$$I_{PCB} = I_{panel} = \frac{1}{12}bh^3 = \frac{1}{12}\cdot 0.09\cdot 0.001^3 = 7.5\cdot 10^{-12}\ \text{m}^4$$

$$I_{\text{threaded rod}} = \frac{1}{64}\pi d^4 = \frac{1}{64}\pi\cdot 0.003^4 = 3.976\cdot 10^{-12}$$

To determine the deflections of the PCB and the side panel due to the storage device, the myosotis formulae (vergeet-mij-nietjes) are used:

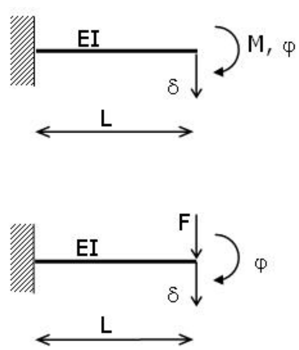


$$\delta = \frac{ML^2}{2EI} \qquad \varphi = \frac{ML}{EI}$$

$$\delta = \frac{FL^3}{3EI} \qquad \varphi = \frac{FL^2}{2EI}$$

*Figure 17 Myotosis formulae [Wijker, 2004]*

First, the deflection at the center of the PCB on which the storage device is mounted is determined. The PCB is assumed to be clamped at both sides by the threaded rods and loaded by a concentrated load F at its center. This is not a perfect model for the real situation, but it will give a good indication of the deflection that can be expected. The deflection is determined in the following way. The deflection angle at the center of the PCB is zero, thus the deflection at the center can be modeled as is depicted in the next figure:

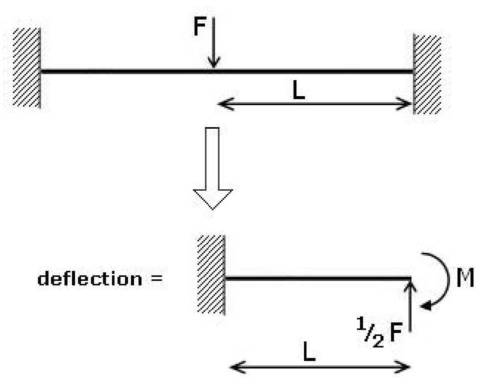


*Figure 18 Deflection at the center of the PCB*

In the above picture, ½F and M are the reactions at the clamped side due to the load F. The reaction moment M is unknown, but it is known that the rotation at the clamped edge is equal to 0°, therefore:

$$\varphi = \frac{F/_{2}L^2}{2EI} - \frac{ML}{EI} = 0 \Rightarrow M = \frac{1}{4}FL$$

Since the complete iDod weighs 100 grams, an acceleration of 10g results in the load F to be equal to 10 N. The distance L is equal to 45 mm. The deflection at the center of the PCB now becomes:

$$\delta_{PCB} = \frac{ML^2}{2E_{GFRP}I_{PCB}} - \frac{\frac{1}{2}FL^3}{3E_{GFRP}I_{PCB}} = \frac{\frac{1}{4}FL^3}{2E_{GFRP}I_{PCB}} - \frac{\frac{1}{2}FL^3}{3E_{GFRP}I_{PCB}} = \frac{1}{24}\frac{FL^3}{E_{GFRP}I_{PCB}} =$$
$$= \frac{1}{24}\frac{10\cdot 0.045^3}{37\cdot 10^9\cdot 7.5\cdot 10^{-12}} = 1.37\cdot 10^{-4}\text{ m} = 0.14\text{ mm}$$

When assuming that the PCB stretches and deforms into a v-shape, this deflection results in the distance L to become 45.000218 mm instead of 45 mm ($\sqrt{(45^2+0.14^2)}$). The strain, $\varepsilon$, is then:

$$\varepsilon = \frac{\Delta L}{L} = \frac{0.000218}{45} = 4.84\cdot 10^{-6}$$

Knowing that $E_{GFRP}$ = 37 GPa, this leads to a stress of 0.18 MPa due to the stretching of the PCB. This stress is negligible when looking at the maximum tensile stress GFRP can withstand: ~600 MPa [Hexcel, 2005].

The stress in the PCB at the location of the threaded rods is determined using the flexure formula [Gere, 1999] times three to incorporate stress concentrations around the holes for the threaded rods. In the next calculation, the symbol e is the maximum distance from the neutral line at the cross section of the PCB (its value is 0.5 mm):

$$\sigma = 3\frac{Me}{I_{PCB}} = 3\frac{(10\cdot 0.05)\cdot 0.0005}{7.5\cdot 10^{-12}} = 100\text{ MPa}$$

In the upper part of the PCB this is a tensile stress, while at the lower side of the PCB this stress is a compressive stress. According to [Hexcel, 2005], standard GFRP should be able to cope with a stress of ~600 MPa in tension and a stress of ~550 MPa for compression. Both stresses are a factor 5 to 6 above the calculated (concentrated) stress. Thus, the PCB will be able to handle this load.

The threaded rod is loaded in compression. Therefore, buckling is the most likely failure mode. Since the threaded rods are constrained by the PCBs and since the PCBs are 15 mm apart, the length of the threaded rod that has to be considered is 15 mm. The length/diameter ratio of a threaded rod is 15/3 = 5, which is considerable. Therefore, the threaded rod is likely to fail with respect to Euler buckling. When the length L of the rod is 15 mm and when it is assumed to have a pinned-pinned connection, then the Euler buckling load is [Wijker, 2004]:

$$F_E = \frac{\pi^2 E_{\text{steel}} I_{\text{threaded rod}}}{L^2} = \frac{\pi^2\cdot 200\cdot 10^9\cdot 3.976\cdot 10^{-12}}{0.015^2} = 34881\text{ N} \gg 10\text{ N}$$

Thus, the threaded rods will not buckle due to this load. Even when the length of the threaded rod is 100 mm, the buckling load is still 785N, which is much higher than the actual load.

Determination of the deflection of the side panel (onto which the threaded rods are connected) at its center is done in a way similar to that used for the PCB. The complication now is that there are two off-center loads with a magnitude of ½F present. Again the panel is split at its center and assumed to be clamped there. Due to the load of ½F, there is a reaction force R and a reaction moment M present at the wall:

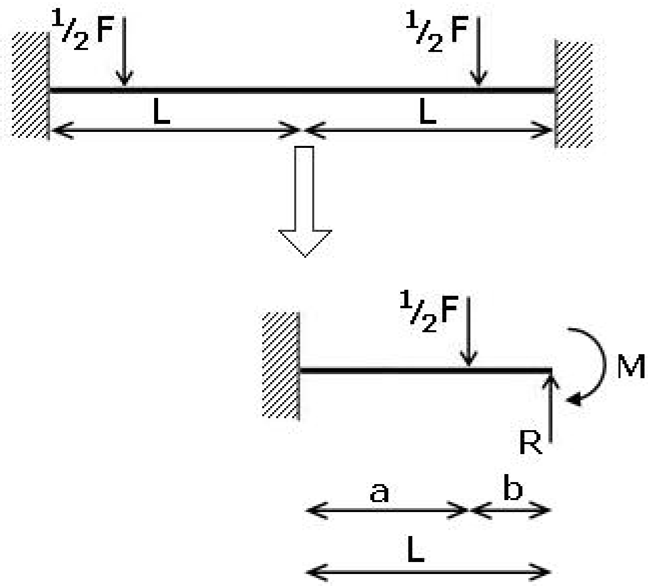


*Figure 19 Method used to determine panel deflection*

The dimensions in the above figure are: L = 50 mm, a = 45 mm, and b = 5 mm. According to [Den Hartog, 1967] for a clamped-clamped beam with a load ½F applied at an arbitrary location, the following applies at the clamped locations:

$$\delta = \frac{\frac{1}{2}Fa^3}{3EI} + \frac{\frac{1}{2}Fa^2b}{2EI} + \frac{ML^2}{2EI} - \frac{RL^3}{3EI} = 0$$

$$\varphi = \frac{\frac{1}{2}Fa^2}{2EI} + \frac{ML}{EI} - \frac{RL^2}{2EI} = 0$$

In this case, $\delta \neq 0$ and R = ½F:

$$\delta = \frac{\frac{1}{2}Fa^3}{3EI} + \frac{\frac{1}{2}Fa^2b}{2EI} + \frac{ML^2}{2EI} - \frac{\frac{1}{2}FL^3}{3EI}$$

$$\varphi = \frac{\frac{1}{2}Fa^2}{2EI} + \frac{ML}{EI} - \frac{\frac{1}{2}FL^2}{2EI} = 0$$

The reaction moment M is determined as follows:

$$\frac{\frac{1}{2}Fa^2}{2EI}+\frac{ML}{EI}-\frac{\frac{1}{2}FL^2}{2EI}=0$$

$$\frac{1}{4}Fa^2-\frac{1}{4}FL^2=-ML$$

$$M=\frac{\frac{1}{4}Fa^2-\frac{1}{4}FL^2}{-L}=-\frac{F\left(a^2-L^2\right)}{4L}=-\frac{10\left(0.045^2-0.05^2\right)}{4\cdot 0.05}=0.02375\text{ Nm}$$

Now the deflection at the right wall can be determined:

$$\delta=\frac{\frac{1}{2}Fa^3}{3EI}+\frac{\frac{1}{2}Fa^2b}{2EI}+\frac{ML^2}{2EI}-\frac{\frac{1}{2}FL^3}{3EI}$$

$$\delta=\frac{Fa^3}{6EI}+\frac{Fa^2b}{4EI}+\frac{ML^2}{2EI}-\frac{FL^3}{6EI}=\frac{2Fa^3+3Fa^2b+6ML^2-2FL^2}{12EI}=\frac{F\left(2a^3+3a^2b-2L^3\right)+6ML^2}{12EI}=$$

$$=\frac{10\left(2\cdot 0.045^3+3\cdot 0.045^2\cdot 0.005-2\cdot 0.05^3\right)+6\cdot 0.02375\cdot 0.05^2}{12\cdot 70\cdot 10^9\cdot 7.5\cdot 10^{-12}}=$$

$$=-2.78\cdot 10^{-6}\text{ m}=-2.78\cdot 10^{-3}\text{ mm}$$

The deflection at the right wall is negative, which means that it bends upward relative to the center of the panel. Thus, the center of the panel will deflect $2.78\cdot 10^{-3}$ mm downward. The stresses caused by this deflection are negligible.

Of course the panel is not only loaded by the storage device through the threaded rods. It is also loaded by other PCBs and the threaded rods themselves. When an exaggerated load of 1kg is assumed instead of just 100 g, the force F is 10 times higher (100 N). Then, the reaction moment M and the reaction force R are also ten times higher. This all leads to the deflection becoming ten times higher, which is ~0.03 mm. This is still very small (almost five times less than for the PCB) and therefore the load on the panel is considered not to be a problem.

From the foregoing, it is concluded that mounting the storage device onto a PCB will not result in overly large loads on any structural item of the CubeSat if the storage device is mounted such that its ground plane is perpendicular to the launch acceleration.

# iDod

## *Development of a generic inflatable de-orbit device for CubeSats*

Part 2 of 2

D.C. Maessen

9-5-2007

Design and Production of Composite Structures
Space Systems Engineering

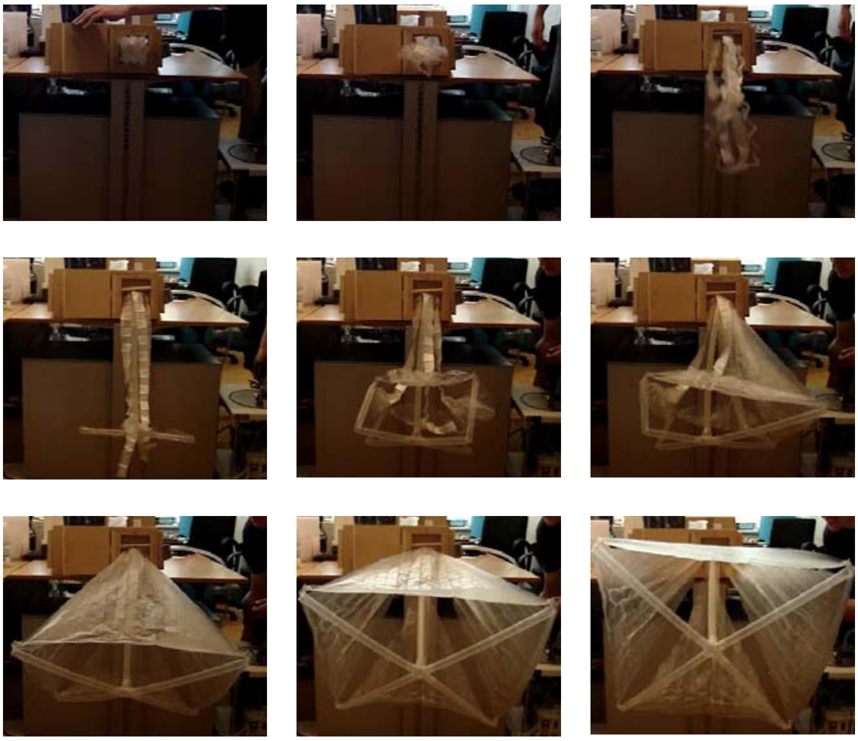

Faculty of Aerospace Engineering

Delft University of Technology

# TABLE OF CONTENTS

# iDod stowage and deployment

## SUMMARY

The stowage and deployment of the inflatable structure of the iDod is analyzed. A cool gas generator delivers nitrogen gas for inflation. Depending on the temperature of the inflatable, the pressure inside the structure is between 0.59 and 1.07 bar.

Several methods to fold tubes and membranes are discussed and the most promising methods are selected to be used for the inflatable. For tubes, this is z-folding. For the membranes, these are map folding and interleaved folding (a modification of map folding). These are the most basic folding techniques and are selected because of the geometry and small dimensions of the inflatable structure and the storage device.

A breadboard model of the inflatable structure is stowed and deployed from a mockup storage device using two different folding schemes. A folding scheme where the membranes are folded using interleaved folding gives the best results with respect to packaging and deployment. During the tests, a packing efficiency of 16% is achieved. Based on this result, a packing efficiency of 20-25% is considered achievable.

## KEYWORDS

Stowage, deployment, storage device, inflatable structure, cool gas generator, packing efficiency

## DISTRIBUTION

| | Name | | Company / Institution |
|---|---|---|---|
| 1 | E.D. van Breukelen | Customer | ISIS B.V. |
| 2 | O.K. Bergsma | Project supervisor | TU Delft |

## APPROVAL

| | Name | Company / Institution | Date | Signature |
|---|---|---|---|---|
| *Written* | D.C. Maessen | TU Delft | 4/19/2007 | |
| *Checked* | | | | |
| *Approved* | | | | |

## REVISION RECORD

| Issue | Date | Total pages | Affected pages | Brief description of change |
|---|---|---|---|---|
| Draft | 3/28/2007 | 36 | | |
| Version 1.0 | 4/11/2007 | 36 | 28, 29 | Inserted subsection 5.3 |
| Version 1.1 | 4/19/2007 | 43 | 1 | Achievable packing efficiency added to summary |
| | | | 6 | Determined that all gas is produced in exactly 1 second |
| | | | 7 | Updated table 1 |
| | | | 29-35 | Inserted subsections 5.4 and 5.5 |
| | | | 43 | Inserted appendix C |

## LIST OF TBD'S AND TBC'S

| TBD / TBC | Paragraph | Subject | Due date | Action by |
|---|---|---|---|---|
| TBD | Subsection 2.2 | Strength of adhesives at high temperature | TBD | TBD |
| TBC | Subsection 2.3 | Power of CubeSat battery is sufficient to ignite CGG | TBD | E.D. van Breukelen |
| TBD | Subsection 2.3 | Puncturing of tube foil due to fast gas jet | TBD | TBD |
| TBD | Subsection 3.1 | Gas jet velocity of CGG | TBD | TBD |
| TBD | Subsection 4.2.5 | Membrane folding using Miura-ori pattern | TBD | TBD |
| TBD | Subsection 5.2.3 | Deployment envelope second method smaller than for first method? | TBD | TBD |
| TBD | Subsection 5.5 | Stiffening of membrane edges to prevent curling | TBD | TBD |

## TABLE OF CONTENTS

# 1 INTRODUCTION

The iDod requires an inflatable structure in order to increase the frontal surface area of the satellite and hence reduce it ballistic coefficient [van Breukelen, 2007]. This structure needs to be stowed and deployed using inflation gas.

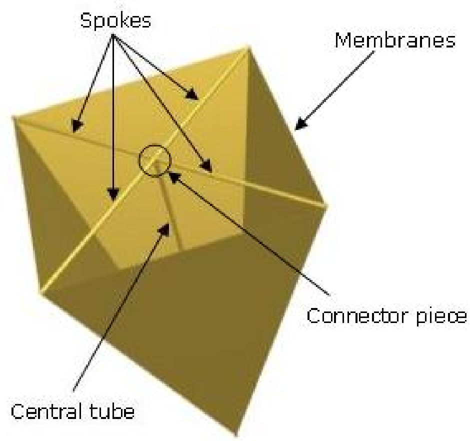


*Figure 1 Inflatable structure of the iDod*

Section 2 discusses the requirements imposed on the inflation system and on the stowage and deployment of the inflatable structure. Section 3 discusses the inflation system and its consequences for the pressure obtained in the inflatable structure. Section 4 treats and selects possible options for folding of the inflatable tubes and the membranes of the inflatable structure. The hold down and release mechanism is also briefly discussed. Section 5 treats several attempts to fold and deploy a breadboard model of the inflatable structure. Section 6 provides the most important conclusions and recommendations.

# 2 REQUIREMENTS

Subsection 2.1 treats the requirements for the inflation system. Subsection 2.2 treats the requirements for the inflatable structure.

## 2.1 Inflation system

From [Jenkins, 2001], several standard requirements for the inflation gas are obtained:

1. Low molecular weight
2. Noncondensing within the anticipated range of operating pressures and temperatures (either in the structure or in the supply system)
3. Nonreactive with structural elements (unless rigidization is meant to be initiated by means of reaction of the structure with the inflation gas)

For the gas supply, the following requirements are imposed:

1. Low volume
2. Low mass
3. Reliable
4. Controllable
5. Provide enough inflation gas to obtain a pressure of at least 0.2 bar in the inflatable structure

### 2.2 Inflatable structure

On the inflatable structure of the iDod, three requirements are imposed with respect to stowage and deployment:

1. Fit inside the storage device (83x83x15 mm$^3$)
2. Controlled deployment (preferred)
3. Small deployment envelope

It is realized that controlled deployment of the inflatable structure is likely to be impossible due to its size and complex shape. Therefore, a controlled deployment is preferred, not required.

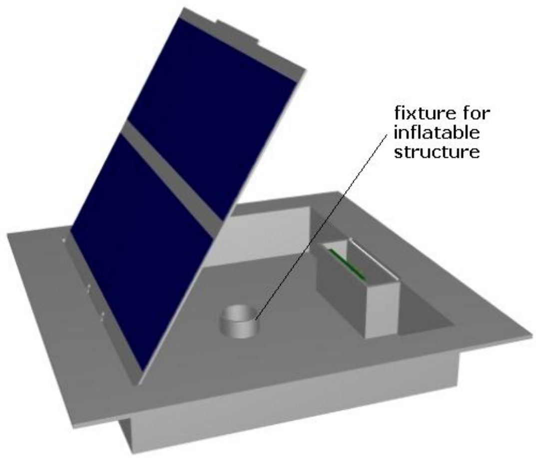


*Figure 2 Storage device for the iDod*

## 3 INFLATION SYSTEM

The inflatable structure of the iDod of course requires inflation gas. The current section discusses the storage and delivery of the gas using a so-called cool gas generator (CGG) and the pressure obtained in the inflatable structure using a CGG.

### 3.1 Gas storage and delivery using a CGG

For the iDod, the system to store and deliver the inflation gas is extremely simple: it consists out of a single item called a cool gas generator (CGG). This system has been the preferred system since the start of the design. Therefore, no other system is analyzed (some alternatives are treated briefly).

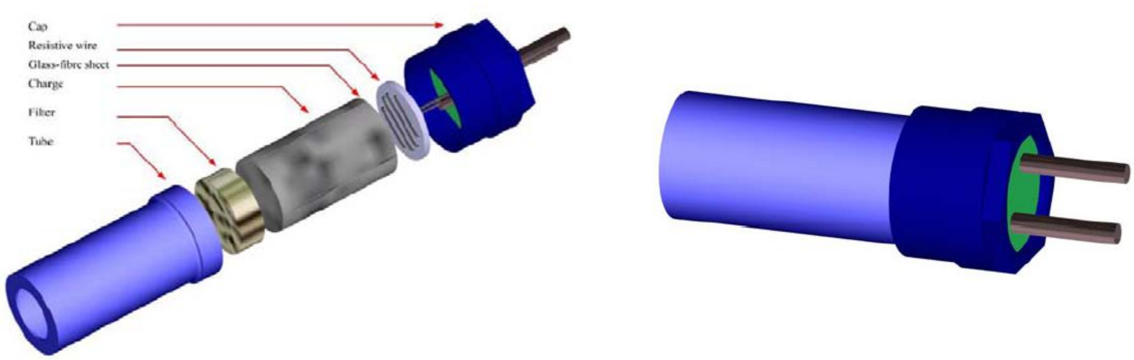


*Figure 3 Exploded view (left) and an assembled view (right) of a CGG using a resistance wire for ignition [Boscher, 2007]*

In the standard design, a solid substance (the charge) is stored in a casing of titanium (TiAl6V4 [Boscher, 2007]) and rapidly decomposes into gas upon ignition of a pyrotechnical device. This poses a problem since no pyrotechnics are allowed on CubeSats [Rackemann, 2006 (report)]. The solution is to ignite the charge using a resistance wire. Currently, 13 W of power during 2 seconds is required for ignition using a resistance wire [e-mail Laurens van Vliet, appendix C]. It is assumed that the battery of the CubeSat can deliver this amount of power (TBC). Otherwise, a small battery can be installed in the storage device to supply the required power.

The CGG can be screwed into the side of the fixture for the inflatable structure, deleting the need for a gas distribution system.

*Figure 4 Twelve CGGs mounted together [Bradford Engineering, 2006]*

CGGs are available that produce pure nitrogen gas. This gas fulfills the first three requirements of subsection 2.1: it has a low molecular weight (28 g/mol), is noncondensing within the anticipated range of operating pressures and temperatures (see subsection 3.2 and figure 5), and it is nonreactive with the iDod materials. Thus, this gas is selected as inflation gas.

Since the CGG technology is space qualified [Bradford Engineering, 2006] and since no gas distribution system is required, this system is very reliable. The delivery of the inflation gas can be controlled to some extend by modifying the shape of the charge in the CGG. This influences the amount of gas produced per unit of time (gas production with a pill-shaped grain is faster than for a slender cylinder-shaped grain). However, the gas will be delivered in one shot when one CGG is used. This cannot be changed.

The downside of using a very small CGG is that all inflation gas is produced in a second: Table 1 shows that the mass flow is 0.15 g/s and that the amount of gas produced is 0.12 normal liters ($1.2 \cdot 10^{-4}$ $m^3$). With a molecular weight for $N_2$ of 28 g/mol, this mass flow is equal to $5.36 \cdot 10^{-3}$ mol/s. Using the ideal gas law [Maessen, iDod.TN.003] it is derived that 0.12 normal liters is equal to $5.36 \cdot 10^{-3}$ mol:

$$pV = nR_aT \quad \Rightarrow \quad n = \frac{pV}{R_aT} = \frac{1.013 \cdot 10^5 \cdot 1.2 \cdot 10^{-4}}{8.3145 \cdot 273} = 5.36 \cdot 10^{-3} \text{ moles}$$

Where p is pressure [Pa], V is volume [$m^3$], n is the number of moles inside the volume [mol], $R_a$ is the Universal gas constant equaling 8.3145 J/mol/K and T is the temperature of the gas [K]. Thus, all gas is produced in just one second. This raises concern about the velocity of the gas jet since it might be high enough to puncture the material of the inflatable structure. Whether this is really so needs to be verified and remains TBD.

When the gas jet is too fast, two options remain: reduce the velocity of the gas jet by artificial means or use another means of inflating the inflatable structure.

Reducing the velocity can be done by placing a plate in front of the gas jet: The gas jet impacts on the plate, thereby loosing much energy, and is forced to flow around it at a reduced velocity. Or, the gas can be forced to travel through a porous material, thereby also loosing much speed. Both methods are illustrated in figure 6.

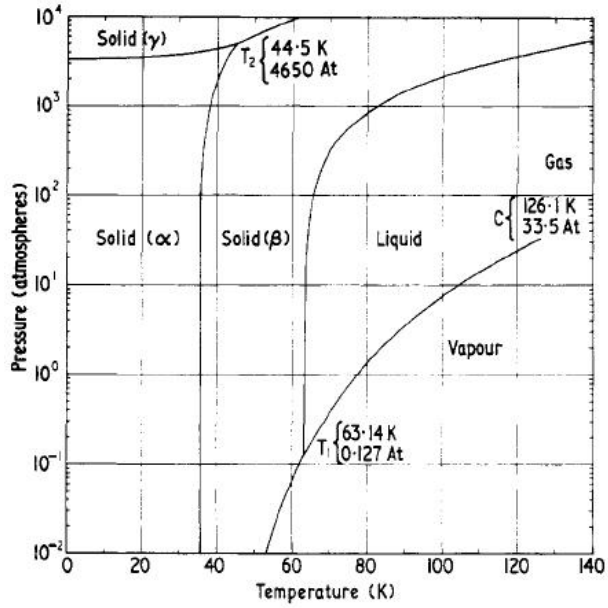


*Figure 5 Phase diagram nitrogen [Wray]*

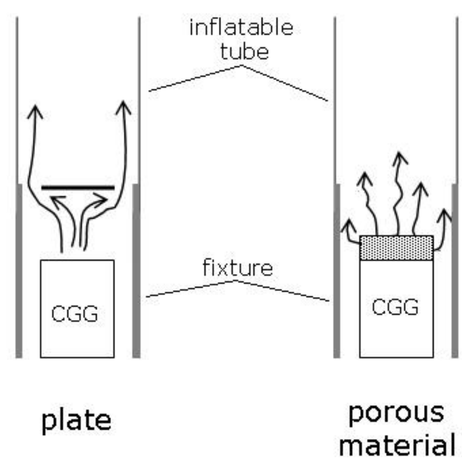


*Figure 6 Ways to reduce the velocity of the gas jet*

| | |
|---|---|
| **Mass [g]** | 3 |
| **Dimensions [mm]** | ∅ = 8 mm, length = 18 mm |
| **$N_2$ output [normal liters]** | 0.12 |
| **Mass flow [g/s]** | 0.15 |
| **Gas jet velocity [m/s]** | TBD |
| **Power requirement [Ws]** | 26 (13 W during 2 seconds) |

*Table 1 Properties CGG [Boscher, 2007] [e-mail Laurens van Vliet, appendix C]*

When for some reason a CGG is not found to be adequate for the current application, the inflatable structure can also be inflated using a sublimating powder [de Groot, 2003]. The

principle is very simple: due to a low pressure and high temperature, the powder sublimes into a gas. This has also been used in the famous ECHO balloons made by NASA in the 1960s. Downside to this option is that the achievable pressures are only $10^{-5}$ to $10^{-6}$ bar [Freeland, 1998].
Due to the very low achievable pressures, the previous option is not very attractive. An option that is attractive is to decompose a powder endothermically by heating it using a resistance wire such that a gas is formed. This way, the amount of gas produced can be controlled simply by the total amount of powder or by adding heat for a longer or shorter amount of time to the powder. An example calculation in appendix B for $MgCO_3$ (decomposition temperature ~500°C) shows that only 0.2 g of $MgCO_3$ is required to provide 0.045 normal liters of $CO_2$ (g). Using a 5 W resistance wire, it then takes 47 seconds (assuming 100% efficiency) to produce all the gas. It is noted that this is only an example and more research into this method should be performed if this method is preferred over using a CGG.

Compared to a conventional pressure vessel, a CGG uses about six times less volume to store the same amount of gas [Rackmann, 2006 (presentation)], depending on the pressure used in the pressure vessel, while requiring about the same amount of mass.

## 3.2 Internal pressure and structural consequences

In [Maessen, iDod.TN.003], the required amount of inflation gas is determined for the straw man concept of the iDod in case a pressure of 0.2 bar has to be achieved. Using the same calculations, the required amount of inflation gas to achieve the same pressure for the current concept is determined.

In [Maessen, iDod.TO.001], the total length and diameter of the inflatable tubes is equal to 209 cm and 1 cm respectively. In the same document, it is indicated that the size estimate for the inflatable structure is wrong and the obtained mass and material volume are multiplied by a factor 1.5 to compensate for this.
By increasing the length of the four “spokes” of the inflatable structure (see figure 1) by 10 cm and the length of the central tube by 15 cm, the mass of the complete structure becomes roughly a factor 1.5 higher. Then, the total length of the tubes is 264 cm. The internal volume of the tubes is then 207.34 $cm^3$ ($2.07 \cdot 10^{-4}$ $m^3$).

The anticipated temperature range of the inflatable structure is very large: 0°C till +225°C. The lower temperature is estimated to be the temperature of the CubeSat upon initiation of the deployment, which is likely be done when the satellite is heated by the Sun (due to the higher temperature, the inflatable will be more flexible and will therefore deploy more easily). The upper temperature is the highest possible average temperature of the inflatable structure, 180°C [Maessen, iDod.TN.011], multiplied by a (somewhat arbitrary) factor of 1.25 to obtain a maximum temperature.

Rewriting the ideal gas law allows calculation of the required amount of moles to achieve a pressure of 0.2 bar (20000 Pa) at a temperature of 273K [Maessen, iDod.TN.003]:

$$n = \frac{pV}{R_a T} = \frac{20000 \cdot 2.07 \cdot 10^{-4}}{8.3145 \cdot 273} = 1.83 \cdot 10^{-3} \text{ moles}$$

In “normal liters”, this is (using T = 273 K and p = $1.013*10^5$ Pa as standard conditions):

$$pV = nR_a T \Rightarrow V = \frac{nR_a T}{p} = \frac{1.83 \cdot 10^{-3} * 8.3145 * 273}{1.013 \cdot 10^5} =$$
$$= 4.09 * 10^{-5}\ m^3 = 0.041 \text{ normal liters}$$

The smallest CGG currently available at TNO delivers 0.12 normal liters of gas (see table 1). This CGG thus delivers about 293% of the nominally required amount of gas and will result in a pressure of 0.59 bar at 273K. At 498K (225°C), the pressure is 1.07 bar. This is much higher than required, but is not likely to lead to structural problems since the hoop stress in the inflatable tubes with this pressure is [Gere, 1999]:

$$\sigma = \frac{pr}{t} = \frac{107000 \cdot 0.005}{0.0001} = 5.35 \cdot 10^{6}\ \mathrm{Pa} = 5.35\ \mathrm{MPa}$$

In the formula, p is the pressure, r is the radius of the tubes (0.5 cm), t is the wall thickness of the tubes (assumed to be 0.1 mm), and $\sigma$ is the stress.
In [Maessen, iDod.TN.008], Upilex-S is selected as foil material for the inflatable tubes. Its maximum tensile stress at 300°C is 294 MPa [UBE Europe, 2005], which is much higher than the stress occurring due to the pressure. Therefore, although delivering much more gas than required, a CGG is allowed to be used for gas supply from a material point of view. In fact, a high pressure is advantageous for removing wrinkles in the structure.

Whether the adhesives used to construct the tubes and the tubular structure are strong enough to handle this pressure at 225°C needs to be confirmed by testing and remains TBD. Based on the foregoing, the force that the adhesive used to construct the tubes needs to withstand at 498K can already be determined by calculating the tension force in the wall of the tubes due to the internal pressure. In the below picture, F is the force in the wall, p is the pressure, and r is the radius of the tube.

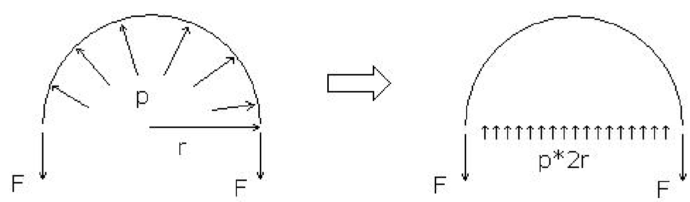


*Figure 7 Determination of pressure force in tube wall*

The above leads to:

$$2pr = 2F \quad \Rightarrow \quad F = pr = 1.07 \cdot 10^{5} \cdot 0.005 = 535\ \mathrm{N/m}$$

Thus, the adhesive needs to have a minimal strength of 535 N/m at 498K.

# 4 STOWAGE AND DEPLOYMENT

For deployment of a structure in space there are two keywords: *passive* and *control*. Passive implies that there is no active system like a motor and sensors working together to influence the deployment (envelope) of the structure. Control implies that the structure will deploy in a predictable manner. Both keywords are always sought after when a structure needs to be deployed in space since incorporating this in the design reduces the amount of possible failures. No example is known of an inflatable structure that is actively controlled during deployment, which indicates that the deployment of inflatable structures is either passively controlled or not controlled at all.

Inflatable structures can be stowed in many ways; the one more efficient than the other, but doing this such that the deployment of the structure is completely predictable and therefore controlled poses considerable challenges.

The next subsection discusses a number of possible ways to stow a tubular structure and the effect of the stowage method on the deployment of the structure. Subsection 4.2 discusses means to fold membranes. Subsection 4.3 briefly discusses the hold down and release mechanism that is selected to ensure proper stowage and release of the inflatable structure of the iDod.

## 4.1 Tube folding

Stowage and deployment are inseparable: the way the tubes of the inflatable structure are folded determines the way the structure is deployed. However, the best way to stow a structure can very well lead to a poor deployment and vice versa. Here, stowage volume is critical and is therefore deemed more important than deployment.
A literature survey of the most common folding methods in use today for tubes has been performed and the methods found in this study are briefly treated in the coming subsections. The first four methods are also described in [de Groot, 2003] and parts of that description are also used here.

### *4.1.1 Z-fold*

The z-fold is the most simple deployment method, but very practical. It can be used in two ways: removing all air from the inflatable, compress it together and fold it like one would fold a piece of paper or by folding it like an accordion.

The first way results in very high package factors (or packing efficiency; defined as the ratio between inherent material volume of the inflatable and the volume of the stowed package. The package factor of the accordion-style is somewhat less high, mainly due to the common use of a spring to initiate deployment before inflation gas is introduced into the structure.

The main drawback of this method is that there is no control over the deployment, resulting in a chaotic movement of the deploying boom. Another disadvantage is that residual air left in the boom can inflate the boom ahead of schedule through expansion. Also, stored elastic energy due to packing can deploy the boom ahead of schedule.

The following figure schematically depicts deployment of an accordion-style folded boom.

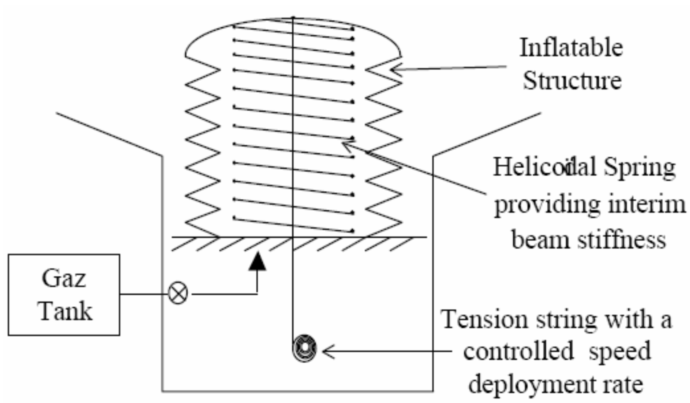


*Figure 8 Z-folding using a spring [Lefevre, 2002]*

### *4.1.2 Roll-up*

The roll-up method is widely used for deploying tubes and struts in space. Commonly, the tube is rolled onto a spool and held in place by a retardation method. Pressurizing the tube from the other end pulls it from the spool and through the collar which provides directional deployment control. An example of the roll-up method is shown below.

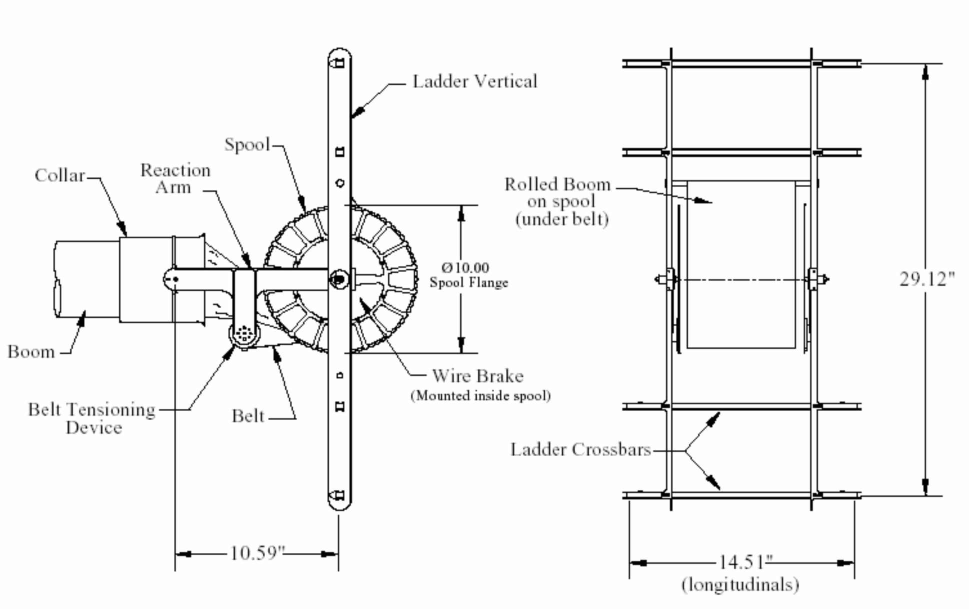


*Figure 9 Roll-up method [Sapna, 2000]*

Retardation methods for the roll-up device can be divided into two categories: systems along the entire length of the boom and systems at the spool.
A method along the length of the boom is the use of Velcro peel flaps. The flaps are peeled from each other during deployment and thereby provide retardation and thus control over the deployment rate. Velcro however, can peel imperfectly and cause impulse forces to act on the tube, resulting in unwanted deployment dynamics. Flat constant force springs (similar to tape measures) embedded in the wall of the tube are another possibility of a method along the length of the boom. The spring force is overcome via inflation and the tube is rolled out. The result is a smooth and predictable deployment. A negative attribute of this method is the residual spring force present in the boom after deployment. This imposes extra structural (stiffness) requirements on the boom. Also, the achieved packaging ratio is less than that of some other methods due to the mechanism used.

Both methods of retardation along the length of the boom add mass to the tube itself. Several methods to provide retardation at the spool, preventing a mass increase of the tube, have been developed. The wire brake, see the figure below, is an example and works by rolling a metal rod from one spool to another, thereby deforming the rod and thus dissipating energy in the form of heat.

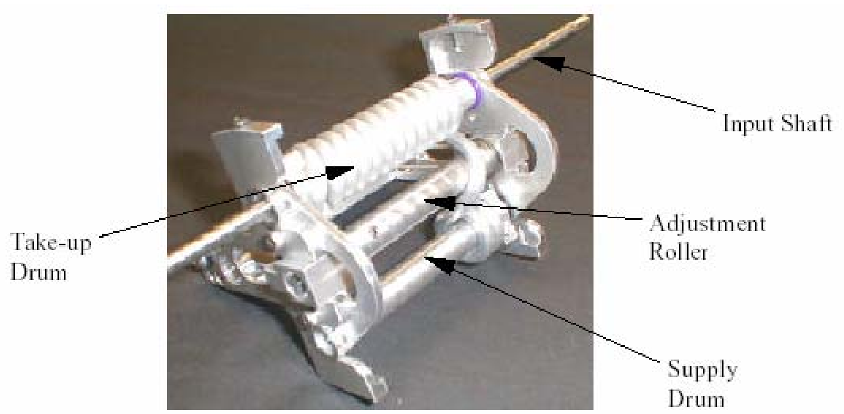


*Figure 10 wire brake mechanism (inside spool) [Sapna, 2000]*

The wire brake system is a promising method but it is difficult to dimension correctly due to temperature effects. Another possibility is the use of an eddy current damper. This is in essence a metal block or plate attached to and rotates with the spool and moves through a permanent magnet. This causes currents in the metal and thus a Lorenz force opposing the movement.

The retardation methods, which are placed at the spool, cannot prevent inflation of the tube around the spool. An elastic belt is therefore part of the mechanism shown in figure 9. This belt exerts pressure on the rolled tube, thereby preventing inflation around the spool. The application of pressure by the belt results in friction being generated between the belt and the tube during deployment. This friction can be used as a method of retardation.

For the current inflatable structure, a spool with a mechanism will not be practical due the restrictions in mass, volume, and shape of the inflatable. Then, the roll-up method degrades into the “dumb” party favor roll-up method. However, the packaging efficiency for this method will be high and the deployment is sort of controlled since a tube rolled up like a party favor will not bend sideways during deployment. In addition, the extra stiffness at the joint line of the tube can be used to further limit movement of the tube to some degree.

#### *4.1.3 Compartmentalization*

The concept of compartmentalization is the division of an inflatable boom into several sequential chambers. These chambers are inflated one by one and thus control over the deployment is achieved. This principle is shown in figure 11.

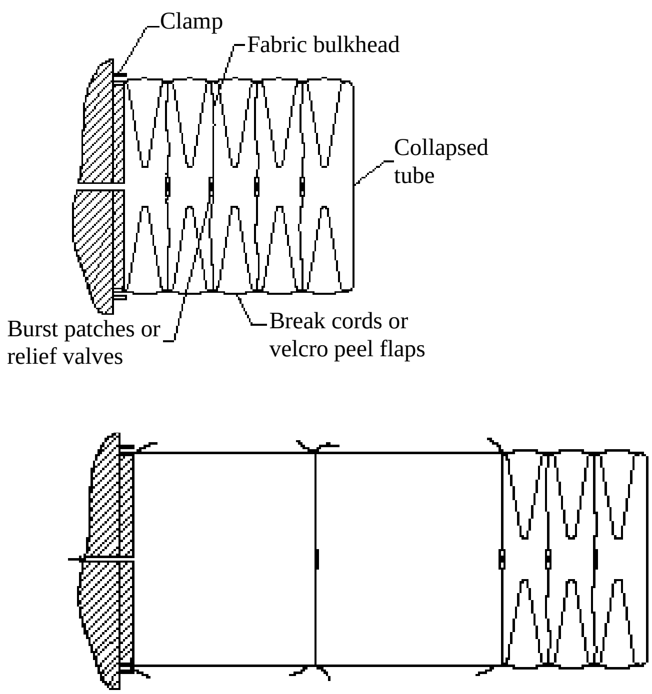


*Figure 11 Compartmentalization method [Cadogan, 1998, 1999]*

As with the z-fold and party favor method, high packaging efficiencies can be achieved using this method. Controlling, in this case staging, the inflation is achieved by using a retardation method. For this method there are several options possible. Burst disks or pressure relief valves can be placed in between the chambers. They burst or respectively open when the correct inflation pressure is achieved in the first chamber, after which the second chamber is inflated. Burst disks have to be replaced after each inflation test and the valves result in a slightly lower pressure in consecutive chambers. Another option is to allow only a small opening or orifice between the chambers, which restricts the gas flow between them. Disadvantage of this method is that chambers can pressurize ahead of schedule.

All the above methods to provide retardation require components to be placed inside the boom, making production extremely difficult for a 1 cm diameter tube.
The internal retardation methods can be augmented by external methods. Examples of these are the use of Velcro peel flaps and break cords. Both can be applied on the current inflatable structure, but result in cumbersome production and testing. When not absolutely required, it is advised not to use these methods. This implies that compartmentalization as a whole is not advised to be used for the iDod unless absolutely necessary.

### 4.1.4 Columnation

The columnation method allows an inflatable tube to extend linearly. An example of this method is presented in figure 12. The inflatable tube is drawn over a mandrel and stored behind it. Inflation of the tube takes place by letting gas flow through the centre of the mandrel. This results in an axial pressure load on the end of the tube. This load translates into a longitudinal stress in the membrane wall, which pulls the tube over and off the mandrel. Seals are present on the mandrel to act as pressure barrier to prevent inflation of the tube behind the mandrel and as a method of retardation by applying friction. This friction controls the longitudinal stress and thereby the deployment rate and the rigidity of the structure during deployment. The packaging efficiency for this method is less than that of the z-fold method, the roll-up method (party favor), and the compartmentalization method due to the need for a mandrel.

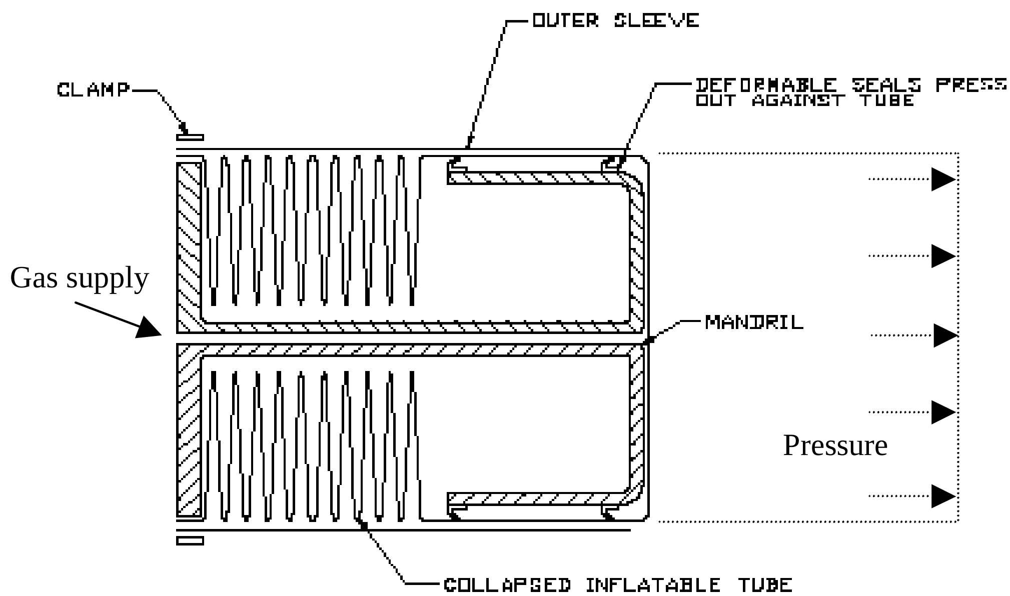


*Figure 12 Columnation method [Cadogan, 1999]*

The current method is considered to be impossible to apply on the current structure, since then a tube of ~0.5 m length has to be collapsed to a height of less than 15 mm (the height of the storage device). The space in which the tube has to be collapsed is simply way too small; one can't even get a finger inside that space!

### 4.1.5 TADECS

TADECS is an abbreviation for Tetragonal Accordion Deployment Control System, patented by ASTRIUM Space Transportation [Bousquet, 2006]. This method is very similar to the columnation method, but instead of a mandrel, use is made of a so-called “petal” (Greek for leaf). In addition, a special tetragonal accordion folding pattern is used to fold the boom [Le Couls, 2006].

*Figure 13 Tetragonal accordion folding pattern [Le Couls, 2006]*

The petal consists out of four flexible lamellas of which two are always restraining a fold. Using a spring system, the petal compresses the folds, ensuring a small package. Pressure is released into the boom via the hollow "stalk" of the petal. This pressure forces tube upwards and the folds are forced over the petal one by one in a smooth manner. The spring forces the petal downward once a fold has cleared the petal.

*Figure 14 From left to right: folded boom, petal, petal inside folded boom [Le Couls, 2006][Bousquet, 2006]*

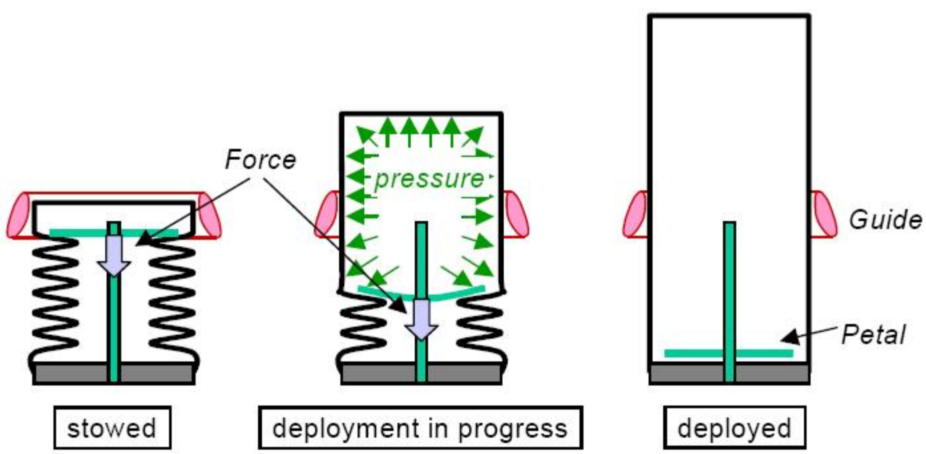


*Figure 15 TADECS deployment scheme [Le Couls, 2006]*

Although it is a very elegant and controlled way to deploy a boom, this method is not suited for the current application. This is caused by requirement that one needs to be able to put a hand inside the boom to create the intricate folding pattern. Clearly, doing this is impossible for the iDod.

#### 4.1.6 Telescopic deployment

All previously discussed methods to stow and deploy an inflatable boom required the use of intricate devices to ensure a controlled deployment. The current method does not.

This is done by using a conical boom instead of a boom with a constant radius. Such a boom can be packed using folds that are concentric about the boom axis. When inflation gas is introduced at the base of the boom, the concentric packaging ensures a straight and smooth deployment.

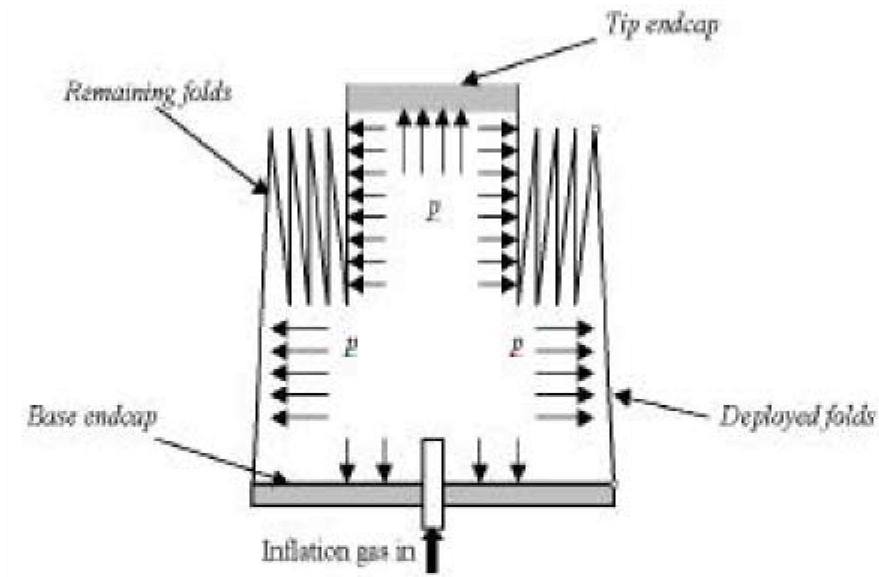


*Figure 16 Conical inflation scheme [Lichodziejewski, 2003]*

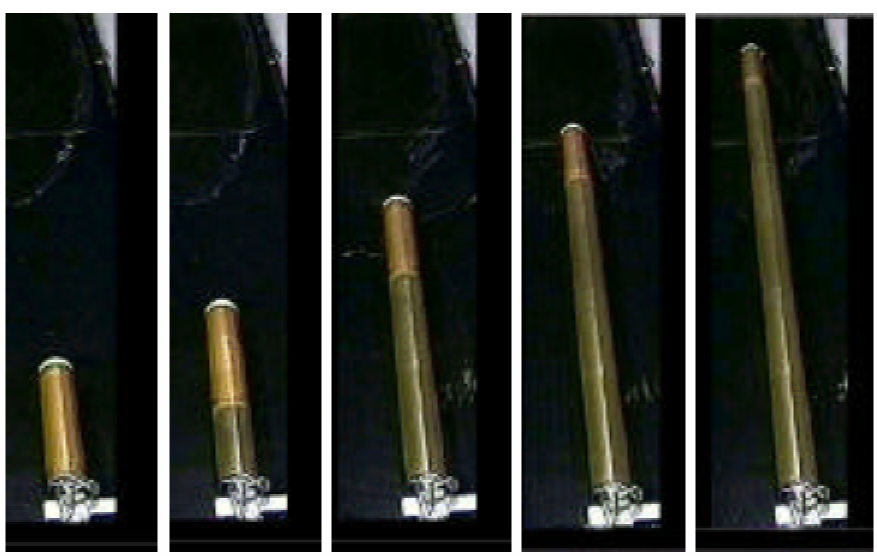

*Figure 17 Deployment [Lichodziejewski, 2003]*

Unfortunately, this technique cannot be used for the current structure because of mass, volume and size issues:

When the ~50 cm long central tube of the inflatable structure is to be stowed in this fashion, it has to obtain a stowed height of ~1 cm (see section 1). Thus, it needs to have 50 folds of 1 cm height. When the wall thickness of the tube is 0.1 mm, then every fold reduces the internal diameter at the base of the tube by 0.2 mm. Stowing the central tube using 50 folds then requires the base of the tube to have a diameter of 2 cm when the tip of the tube has a diameter of 1 cm (considered to be the smallest practical diameter). However, this example calculation assumes a packaging efficiency of 100%, which in reality does not occur. A packaging efficiency of 33% is more realistic, which means that every fold reduces the internal diameter at the base of the tube by 0.6 mm. This leads to a diameter at the base of 4 cm. The total material area of the conical tube is then ~393 $cm^2$, while it is just ~157 $cm^2$ for the straight tube. This means that the mass of the conical tube is 2.5 times higher than that of the straight tube. In addition, a volume of ~12.5 $cm^3$ is required to stow the conical tube, while a straight tube would require a stowed volume of ~4.7 $cm^3$ when assuming a packaging efficiency of 33% (again a factor 2.5).
Next to mass and volume, there is also a purely practical reason why this option is not suited for the current application: It turns out that it is extremely difficult to fold a tube with a very small diameter in this manner. Fingers become very crude, clumsy tools and creating nice, straight folds is next to impossible. One would have to design and produce special tools to make this folding scheme possible and then it would only be useful for the central tube, not for the spokes. This is not worth the effort.

#### *4.1.7 Tube folding pattern selection*

The foregoing discussion leads to the selection of just three methods that can be used to stow the tubes of the inflatable structure:

1. Z-fold
2. Roll-up
3. Compartmentalization

Of these three, compartmentalization is the least attractive one due to its cumbersomeness. Roll-up will be difficult to apply for the spokes, since they are restrained by the membranes. This is not the case for the z-fold method and therefore, the z-fold is the most practical way to stow the inflatable tubes.

### 4.2 Membrane folding

Next to tubes, the inflatable structure also consists out of thin membranes spanned between the tubes (see figure 1). For the membranes, several folding patterns might be applicable [Bernasconi, 2006]:

1. Letter folding
2. Map folding
3. Interleaved folding (modified map folding)
4. Miura-ori

The next subsections treat these folding patterns briefly.

Note: In the next subsections, drawings are presented for the folding patterns. In these drawings, dotted lines mark concave folds (the material is folded upward, creating a V-shape) and full lines mark convex folds (the material is folded downward, creating a /\-shape).

#### *4.2.1 Letter folding*

With letter folding, the membrane is first folded about its center line. Then, the resulting folded membrane is folded about its current center line, perpendicular to the previous center line. This operation is continued until the desired package size is obtained.
The membrane unfolds in an alternating pattern with the deployment direction alternating per fold. Two deployment directions occur, with the directions being perpendicular to each other.

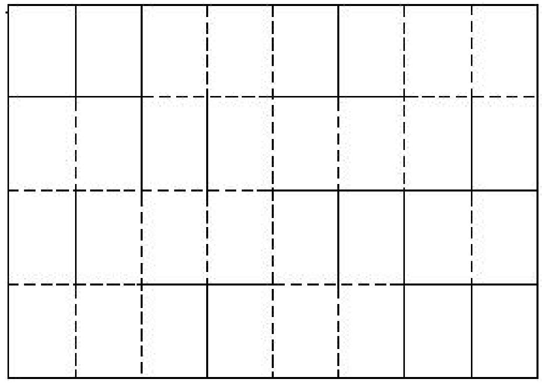

*Figure 18 Letter folding [adapted from Pellegrino, 2001]*

#### *4.2.2 Map folding*

Here, the membrane is first folded in a zig-zag pattern. This results in a strip with the desired width, but still with the full length of the starting shape. The length of the strip is then reduced using again a zig-zag pattern.
Upon unfolding, the membrane opens first in one, and then in the other direction.

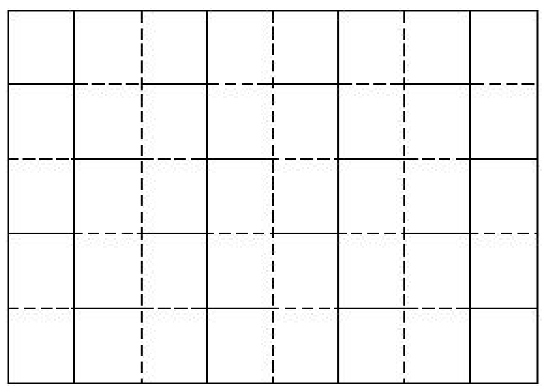

*Figure 19 Map folding [adapted from Pellegrino, 2001]*

#### *4.2.3 Interleaved folding*

Interleaved folding is a modification to map folding. According to [Bernasconi, 2006]: *"One folds the sheet in a zig-zag pattern, but "misses a step" in the middle of the sheet, interleaving segments from the one membrane half with those from the opposite half, forming a ladder-like pattern in a partially unfolded state."* Again, a strip with the desired width is formed and its length can be reduced by another pattern of zig-zag folds.
The membrane opens first in one, then in the other direction.

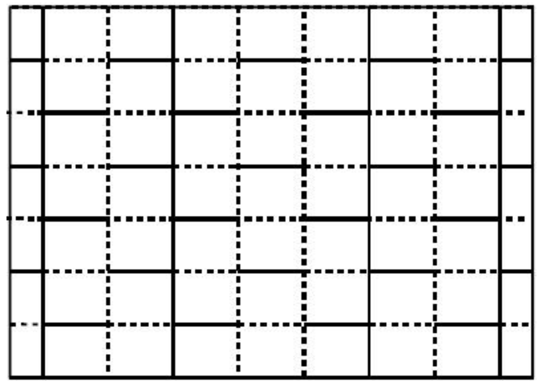

*Figure 20 Interleaved folding [Bernasconi, 2006]*

#### *4.2.4 Miura-ori*

All previously discussed membrane folding methods can be described as sequential methods where the deployment in one direction follows after deployment in the other direction. The Miura-ori method (named after its inventor) however is a synchronous method, meaning that the membrane unfolds in two directions at the same time.

The Miura-ori method is a modification to map folding. The difference is that the “vertical” fold lines do not follow a straight line, but zig-zag at angles of $\pm\ \alpha$ to the vertical [Bernasconi, 2006].

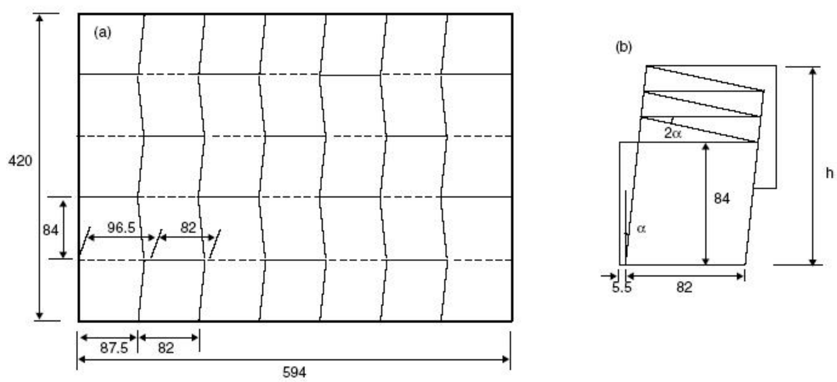


*Figure 21 Miura-ori for A2 paper [adapted from Pellegrino, 2001]*

Unclear in the above figure is that the vertical folds alternate between being convex and concave. Below, the complete folding sequence for this method is depicted.

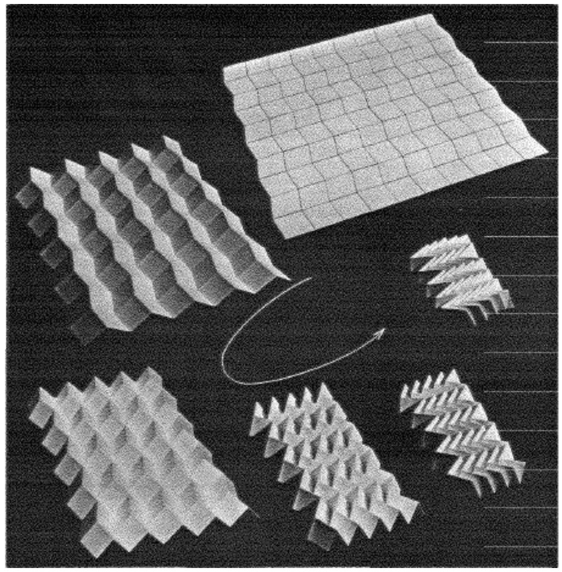

*Figure 22 Miura-ori folding pattern [Pellegrino, 2001]*

#### 4.2.5 Membrane folding pattern selection

Due to the complex shape of the inflatable structure, letter folding cannot be applied. Folding and unfolding of the membrane in this manner cannot be done without hindering the deployment of the spokes of the inflatable structure. In addition, letter folding leads to folds within folds within folds (etc.), resulting in a thick package with the first folds being extremely stretched and no room for the last folds.

The Miura-ori method can be applied to fold the membranes, but is very time-consuming. Due to time constraints, this folding method is not attempted and left TBD.

Map folding and interleaved folding can be applied and are treated in section 5.

### 4.3 Hold down and release mechanism

Keeping the inflatable structure stowed inside the storage device is accomplished by forcing it to stay packed under a moveable lid (see figure 2). Keeping this lid closed and opening it in due time can be done in a number of ways:

- using explosive bolts
- melting through a restraining wire using resistors
- removing a pin (or something similar)
- opening a clamp
- using electromagnets
- melt a substance like wax or paraffin in which some kind of hook is held down

Removing the restraint on the lid allows the lid to be opened by means of (for instance) torsion springs.

Removing a pin or opening a clamp can be accomplished either by using a motor or by using one of the other restraining methods, which is an unwanted complication of the system and also adds mass and volume.
Electromagnets have the obvious downside of requiring power when operated and it is not known how these can be used in such a way that they only require power when the lid needs to be opened. Using them will thus be very inefficient with respect to power.

Explosive bolts and melting of a substance both have the downside of creating extra space debris larger than 10 μm, something not allowed by the European code of conduct for space debris mitigation [Anselmo, 2004].
The only remaining option is to melt through a wire. This option has three important advantages:

1. This mechanism is used on Delfi-$C^3$, which is currently being developed at this faculty. Therefore, much knowledge about this system is already available.
2. No objects larger than 10 micron are released into space.
3. Low mass and volume.

A logical material choice for the wire is polyethylene (PE). This materials melts at a temperature of ~150°C [Wikipedia, 2007] and is sold as high performance wire by DSM in The Netherlands under the trade name Dyneema. It is also used on Delfi-$C^3$.
This mechanism is already incorporated into the storage device shown in section 1 where it is located inside a special “box” to prevent the wire from coming into contact with the inflatable structure. In the box, the top of the printed circuit board (green) on which the resistors are mounted can be seen.

# 5 PRACTICAL RESULTS

Putting theory into practice is difficult for space deployable structures due to the lack of gravity in space. Deployment testing on Earth must therefore be done in loading conditions different than those under which the structure has to function in space or the influence of gravity on the deployment of the structure has to be removed (gravity offloading). For inflatables, this is usually done in either of two ways: using wires and counterweights (see the figure below) or by deployment on water (figure 17).

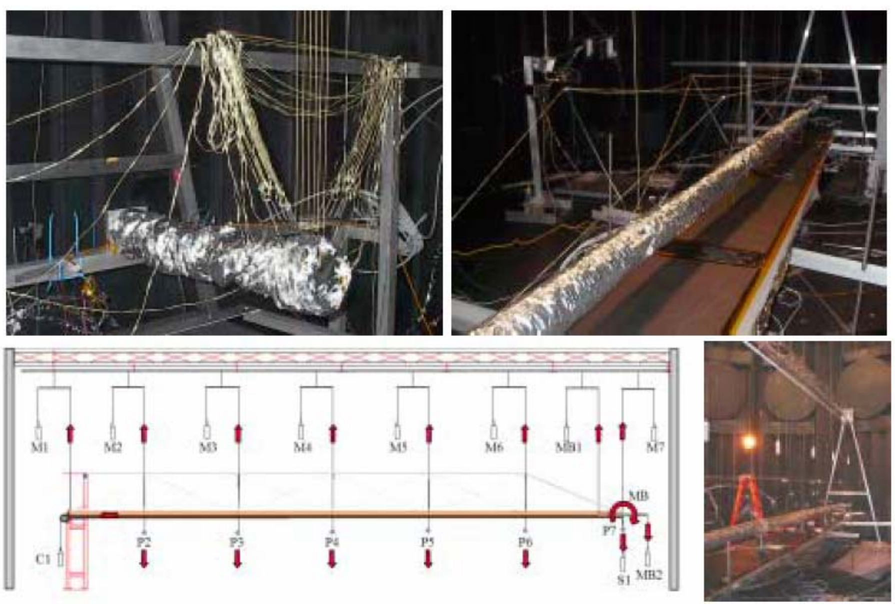


*Figure 23 Gravity offloading using wires and counterweights [Lichodziejewski, 2004]*

Deployment of the current inflatable on water is impossible due to its complex shape. Gravity offloading using wires and counterweights can be done, but it is very difficult to remove undesired forces imposed on the structure by the wires. Furthermore, the structure deploys very rapidly, giving the gravity offloading device virtually no time to adjust before deployment is complete. It is therefore expected that gravity offloading using wires and counterweights will provide unrealistic test data unless deployment is performed extremely slowly.

Because of the reasons discussed above and because of time constraints, gravity offloading is not used. However, it is possible to determine with a high degree of confidence how the structure will deploy in zero-g by filming the deployment and studying the deployment frame-by-frame.
The next subsections treat several attempts to fold and deploy a breadboard model of the inflatable structure from a 140x150x18 $mm^3$ container. This container is deliberately made larger than the designed container since the goal is to explore possible folding methods for the inflatable and to select the most promising one. After the most promising one has been chosen, the container is successively made smaller until it becomes impossible to store the inflatable inside the container. Then, the packing efficiency for the breadboard model is known and can be extrapolated to the packing efficiency for the designed inflatable.

## 5.1 Method 1: z-folding and map folding

In the first attempt to fold a breadboard model if the inflatable, the inflatable tubes are all z-folded while the membranes are map folded.

### *5.1.1 Folding description*

A step by step description of the method applied is given below:

1. Attach the membranes to the central tube using tape
2. Attach the membranes to the spokes using tape
3. Attach the structure to the fixture using a hose clamp
4. Evacuate air from the tubes
5. Fold the membranes using the map folding pattern until one long strip with the desired width is created
6. Reduce the length of the strip using zig-zag folds until the end of the spoke is situated in a corner of the storage device
7. Use z-folding to reduce the length of the spokes until they fit between the fixture and the corner.
8. Use z-folding to fold the central tube over the width of the storage device.
9. Position the section where all tubes come together between two spokes where the central tube is not located.

A hand pump is used to evacuate air from the tubes and to insert air into the tubes. Removing all air from the spokes is difficult since the vacuum is created first inside the central tube, which is then compressed by the outside air pressure, preventing any remaining air from being evacuated from the spokes. In addition, the tubular structure is far from leak-tight at the connector piece (the second version of the tubular structure is used, this version has some prominent leaks) and as a result air can enter the tubes after the initial air has been evacuated.
The leaks result in a non-optimal compression of the tubes and thus in a non-optimal packaging efficiency. However, it is still possible to fold the entire inflatable such that it fits within the container with relative ease.

The next figure shows the folding scheme for the membranes. It starts with a triangular membrane being zig-zag folded until a long strip with the desired width is created. Then, the parts of the membrane sticking out of the container are zig-zag folded to fit inside the container such that the spoke end is approximately halfway the container width. This scheme is repeated for the next membrane with as complicating factor that one end of the second membrane is connected to the end of the already mentioned spoke. When the second membrane is folded into a strip, the end connected to the spoke is folded inside the container and the spoke end is positioned in a corner and lies top of the folded membranes.

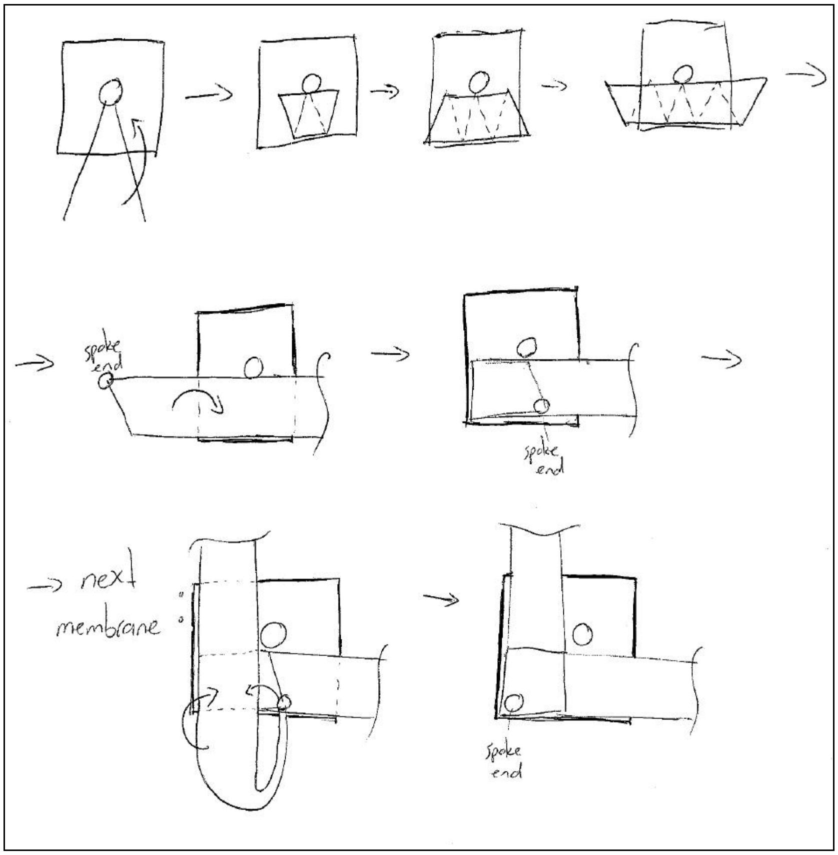


*Figure 24 Membrane folding scheme for first method*

Once all membranes have been folded, the result is as follows:

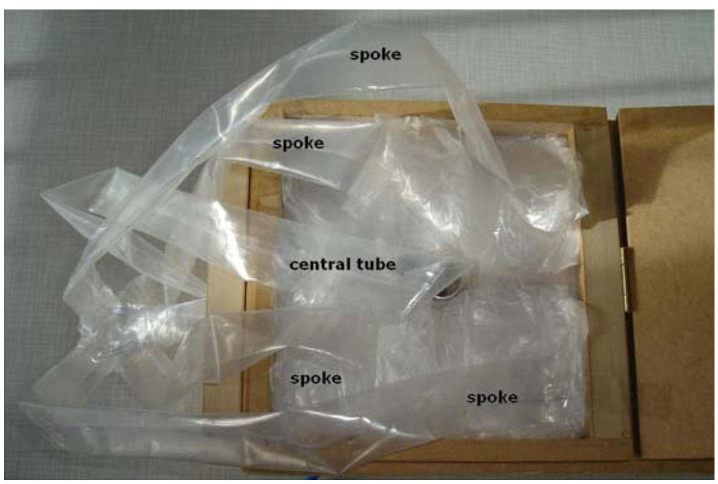


*Figure 25 Membranes folded*

Now, the spokes and the central tube are zig-zag folded such that the spokes span the distance between the fixture and the corners of the container and the central tube spans the width of the container. The connector piece for the spokes and the central tube is placed next to the central tube in between two spokes.

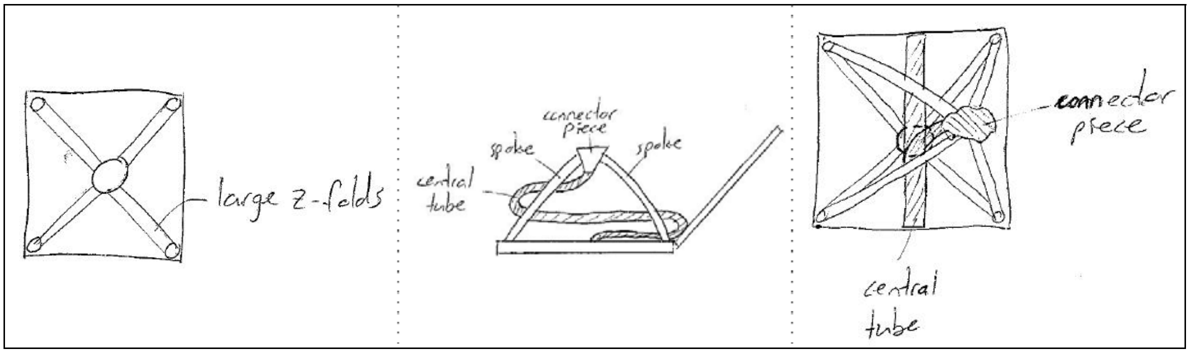


*Figure 26 From left to right: positioning of the spokes, folding of the central tube, positioning of the connector piece*

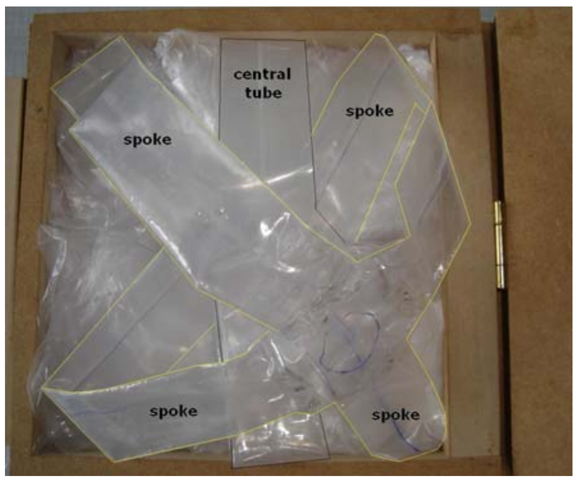


*Figure 27 Tubes folded*

#### *5.1.2 Deployment*

Below, several frames of the deployment movie for this method are presented. The inflatable deploys horizontally. This has two reasons:

1. Due to the many leaks, deploying the inflatable upward against gravity is not possible with the pressure provided by a hand pump.
2. Having all tubes visible when the membranes are deployed is much more easy this way than when the inflatable is deployed upward. Then, a camera has to be installed above the inflatable in order for all tubes to be visible.

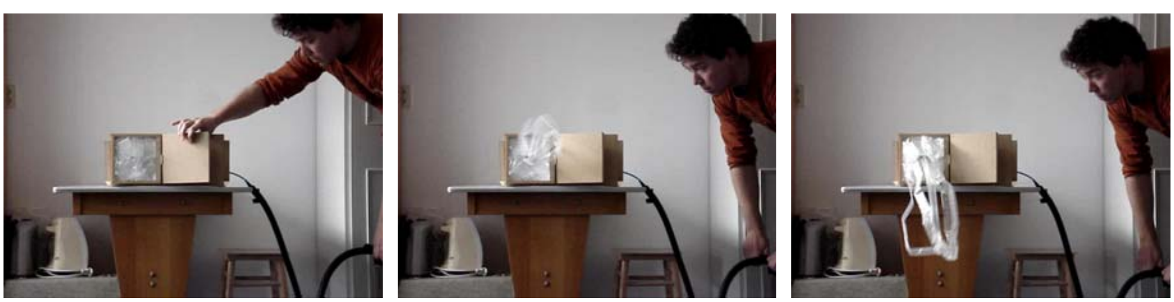

**1** **2** **3**

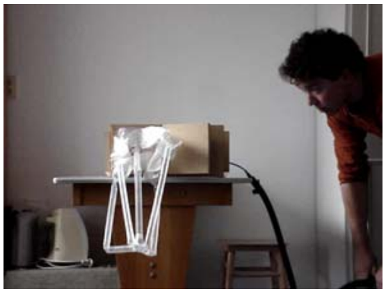
4


5


6


7

Due to the combined effect of gravity and leaks, the inflatable hangs towards the ground. This effect was underestimated and therefore part of the inflatable is missing in the seventh frame.

#### *5.1.3 Results*

Packing factor

The inflatable structure has been successfully folded into a volume of 140x150x18 mm$^3$. Part of this volume is used by the fixture (∅ = 20 mm, height = 13 mm) and by the hose clamp (mainly the screw (∅ = 8 mm, length = 20 mm)). Thus, the volume available for the inflatable is:

$$V_{\text{available}} = V_{\text{container}} - V_{\text{fixture}} - V_{\text{clamp}} =$$
$$= \left(140 \cdot 150 \cdot 18\right) - \left(\frac{1}{4}\pi \cdot 20^2 \cdot 13\right) - \left(\frac{1}{4}\pi \cdot 10^2 \cdot 20\right) = 378000 - 4084 - 1571 \approx 372500 \text{ mm}^3$$

The tubes of the inflatable are made from 90 μm thick polyethylene foil [Maessen, iDod.CM.001]. The tubes have a diameter of 20 mm and the total tube length is ~2100 mm [Maessen, iDod.CM.004]. Their total material volume is then 11875 mm$^3$. The membranes are made from 20 μm thick foil and each membrane is a triangle with a base of 650 mm and a height of 700 mm. The total material volume for four membranes is then 18200 mm$^3$. The connector piece for the tubes is also made from 90 μm thick polyethylene foil and has a material volume of ~530 mm$^3$ [Maessen, iDod.CM.002].

$$V_{\text{inflatable}} = V_{\text{tubes}} + V_{\text{connector piece}} + V_{\text{membranes}} =$$
$$= \left(\pi \cdot 20 \cdot 2100 \cdot 0.09\right) + 530 + 4\left(\frac{1}{2} \cdot 650 \cdot 700 \cdot 0.02\right) = 11875 + 530 + 18200 \approx 30500 \text{ mm}^3$$

The achieved packing efficiency, η, is thus: $\eta = \frac{V_{\text{inflatable}}}{V_{\text{available}}} \cdot 100\% = \frac{30500}{372500} \cdot 100\% = 8.2\%$

The packing factor is defined as 1/η and is thus equal to 12.2.

General comments

Stowing the inflatable inside the container is not very difficult. There is still ample of unused volume. The membranes fold into very small packages while the much thicker tubes require a lot more space. This is partly due to the residual air left in the tubes. The connector piece is difficult to stow efficiently due to its shape and due to the thick adhesive present at the point where tubes are connected to it.

On the left side of figure 27, only a membrane is stored halfway the container and no tube. This leads to a large amount of unused volume there, which is not efficient. However, in the real storage device (see figure 2), that is exactly the position of the hold down and release mechanism. Thus, not using that volume is actually not that bad, since in the real storage device, this volume is not available.

The way in which the membranes are folded results in a relatively thick package of membrane material at the corners of the container. Since the spokes are also positioned at the corners of the container, this is not very handy. It is better to leave as much space available at the corners for the spokes and to concentrate the membrane material around the center of the container. This will result in a higher achievable packing efficiency.

The deployment of the inflatable is fast (~5 seconds) and quite good. The central tube deploys without much movement from left to right, which is caused by the longitudinal folds present in the tube. The central tube also does not move much up or down, which is of course due to the pull of gravity, but also due to the restriction of its movement by the spokes. After the central tube has fully deployed in frame 4, the spokes rapidly swing into their intended position in frames 5 and 6 once the pressure is high enough to overcome the last large fold present in them (this fold is clearly visible in frame 4 for the left spoke).
The membranes deploy in two separate motions, which is of course dictated by the manner in which they are folded. First, they are unfolded sideways to form long strips again. Then, as the spokes inflate, they rapidly unfold perpendicular to the previous unfolding action into triangles. When the spokes are inflated, the membranes are pulled taut violently. Should they come into contact with protruding elements on the CubeSat at this moment, they are likely to tear.

The next figure schematically depicts the deployment envelope for the inflatable in two phases: the inflation phase of the central tube and the inflation phase of the spokes. The envelope required for the inflation phase of the central tube is triangular due to the sideway movement of the central tube. The spokes require a quarter of a circle with a radius equal to their length for deployment. The membranes do not deploy in a circular manner, but in order to be sure they don't hit any protruding elements of the CubeSat, it is safest not to allow any elements to be present inside an imaginary half sphere formed by the deployment envelope of the spokes.

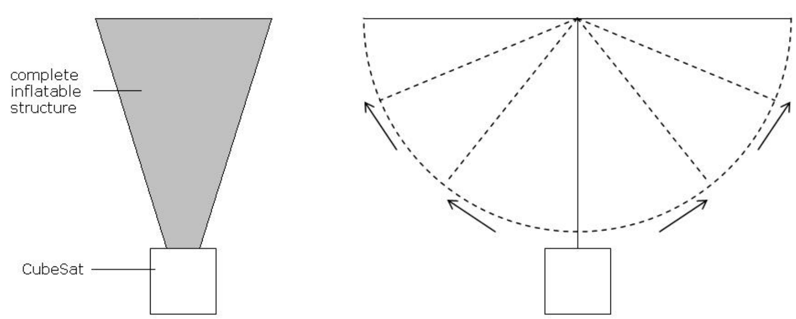


*Figure 28 Deployment envelope for first method*

## 5.2 Method 2: z-folding and interleaved folding

In this second attempt to fold a breadboard model if the inflatable, the inflatable tubes are all z-folded while the membranes are interleaved folded.

### 5.2.1 Folding description

A step by step description of the method applied is given below. An important difference with the first method is that the membranes are attached to the spokes once the membranes have been folded, not prior to folding!

1. Attach the membranes to the central tube using tape
2. Attach the central tube to the fixture using a hose clamp
3. Remove of the supports of the mock up storage device
4. Fold the membranes using the interleaved folding pattern
5. Attach the membranes to the spokes using tape
6. Use z-folding to reduce the length of the spokes until they fit between the fixture and the corner.
7. Use z-folding to fold the central tube over the width of the storage device.
8. Position the section where all tubes come together between two spokes where the central tube is not located.
9. Close the storage device and reattach the supports

Due to the removal of the supports of the mock up storage device to ease folding of the membranes, it was impossible to evacuate air from the tubes before folding them since the air tube could not be connected to its fixture at the bottom of the storage device. However, folding the tubes to fit inside the container was still possible and some air was forced out by hand while folding the tubes.

The next figure shows the folding scheme for the membranes. It starts with a triangular membrane being reduced in width by folding the corners first inward using a large fold and then outward using a smaller fold. The corners of the membrane are kept free to allow attachment of the spokes to them at a later stage. When folding the left corner, some material is folded over material that was folded inward for the right corner. It can be argued whether this is an interleaved fold or a map fold, but here it has been chosen to call it an interleaved fold.
Once the width of the membrane is reduced, the membrane is zig-zag folded until it fits inside the container. Now, the corners are folded inward, which results in a rectangular package.
This is done for all membranes, resulting in four rectangular packages touching each other at their corners.
Now, the corners of the membranes are folded back and attached to the spoke ends.
From this point on, folding of the structure is exactly the same as for the first method.

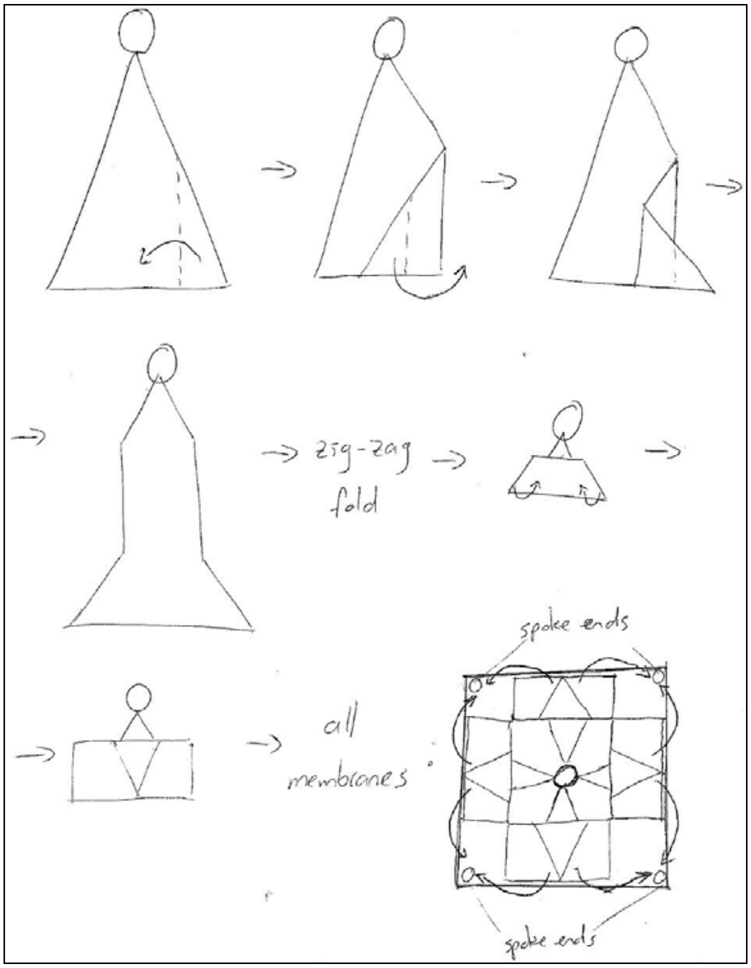


*Figure 29 Membrane folding scheme for second method*

#### 5.2.2 Deployment

Several frames of the deployment movie for this method are depicted below. Since this deployment was carried out in the evening, the resulting images are quite dark and have been made brighter and more contrasting.

**1** **2** **3**

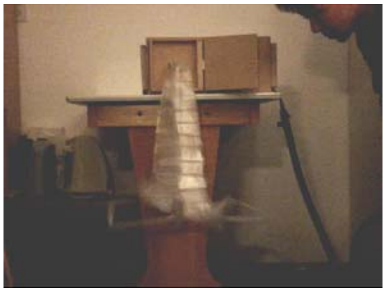
4


5


6


7

Due to the residual air left in the tubes, the inflatable unfolds before pressure can be applied using the hand pump. This results in the structure to fall towards the ground and inflation starts after the central tube has full deployed.

#### *5.2.3 Results*

<u>Packing factor</u>

Since the size of the storage device and the size of the inflatable haven't changed from those of the previous method, the packing factor is still 12.2.

<u>General comments</u>

Stowing the inflatable inside the container is not very difficult even with the residual air left inside the tubes. A great advantage of this method over the previous method is that the corners of the container are almost free of membrane material. This leaves much room free for the spokes.

Since deployment of the inflatable did not go according to plan, there is not very much that can be said about it other than that the deployment of all parts of the structure went smoothly once air was introduced inside the tubes. The membranes seem to restrict the deployment envelope of the spokes since the membranes must first deploy in length-direction and then in width-direction. This results in a smaller deployment envelope than for the first method, but since the test did not go according to plan, this is still TBD.

### 5.3 Method to remove all air from the inflatable tubes

As already mentioned in subsection 5.1.1, removing all air from the spokes is difficult since the central tube collapses upon applying the vacuum, preventing air present in the spokes to be removed. This problem is solved as follows:

1. Insert a thick-walled hose into the central tube up to just under the connector piece. Such hoses are available at the composites laboratory at this faculty and are normally used to create a vacuum when producing a fiber composite part by vacuum bagging.

2. Wrap tape around the central tube at the end of the hose to close off the gap between the inner wall of the central tube and the outer wall of the hose.
3. Connect a vacuum pump to the hose and remove the air from the spokes and the hose.
4. When the air is removed from the spokes, tightly roll up one spoke and assure it stays rolled up by wrapping tape around it.
5. Again remove the air in the three non-rolled spokes.
6. Roll up a second spoke and assure it stays rolled up.
7. Repeat the above process until all spokes have been rolled up.
8. Remove the hose from the central tube.
9. Attach the central tube to the fixture using tape instead of a hose clamp. A hose clamp does not result in an air-tight connection and the screw mechanism of the hose clamp is relatively bulky.
10. Remove the remaining air from the connector piece and the central tube.

Now, virtually all air has been removed from the tubular structure and it can be folded compactly.

*Figure 30 Spokes rolled up after air has been removed*

## 5.4 Stowage and deployment from 255 cm$^3$ volume

The internal volume of the mockup storage device used in subsections 5.1 and 5.2 is now reduced using wooden blocks to a volume of 11.5x12.3x1.8 cm$^3$.

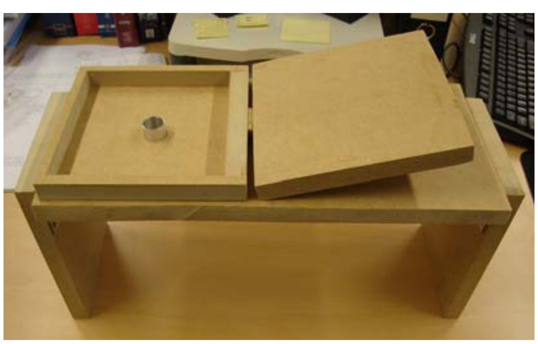

*Figure 31 Mockup storage device*

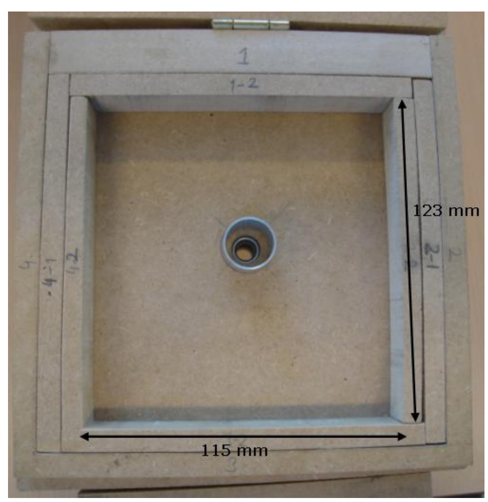


*Figure 32 Stowage volume reduced to 115x123x18 mm$^3$*

The membranes are attached to the bottom of the container using tape. Attachment to the spokes is now achieved using the loop and slit method described in [Maessen, iDod.CM.005].

The membranes are folded using the interleaved folding method, the tubes are folded using the z-folding technique and the air inside the tubes is evacuated in the manner described in subsection 5.3. For this test, version 3 of the tubular structure is used.

Determination of the available volume is performed in the same manner as in subsection 5.1.3, but now no hose clamp needs to be subtracted since the central tube is now attached to its fixture using tape:

$$V_{\text{available}} = V_{\text{container}} - V_{\text{fixture}} = $$
$$= \left(115\cdot123\cdot18\right) - \left(\frac{1}{4}\pi\cdot20^2\cdot13\right) = 254610 - 4084 = 250526 \text{ mm}^3$$

The material volume of the inflatable ($V_{\text{inflatable}}$) is still 30500 mm$^3$. The achieved packing efficiency, $\eta$, is thus now:

$$\eta = \frac{V_{\text{inflatable}}}{V_{\text{available}}}\cdot100\% = \frac{30500}{250526}\cdot100\% = 12.2\%$$

The packing factor is defined as $1/\eta$ and is thus equal to 8.2.

The next figure shows on the left the central tube taped to the fixture and the membranes taped to the bottom of the storage device. On the right, a membrane draped over a wooden plank is shown. This wooden plank is level with the upper face of the walls of the storage device and aids in folding the membrane by allowing the membrane to be laid completely horizontal instead of a section having to be laid on the tabletop and a section 'hanging in the air' between the tabletop and the storage device. Now, no awkward vertical folding has to be performed once the membrane needs to be folded near the storage device.

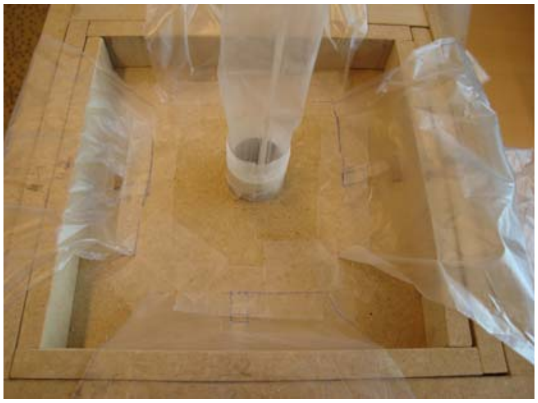

*Figure 33 Central tube and membranes taped to the storage device (left) and wooden plank used to aid folding of the membranes (right)*

Using a thin ruler, straight and well-defined folds are made in the membranes and the membranes are folded into packages of 3 cm wide and 6 to 8 cm long (the length wasn't cared for too much yet). Figure 34 shows all four membranes packed and kept in place by steel blocks.

*Figure 34 Membranes folded*

The central tube is folded like in the previous methods, but the connector piece is now laid on top of the fixture instead of between two spokes. This fits only just under the lid, but it is much better than the previous method since the spokes and the connector piece are folded much more easily and efficiently:

*Figure 35 Central tube and connector piece folded into position*

Now, the membranes are connected to the ends of the spokes and the spokes are folded zig-zag style. Connecting the membranes to the spokes is cumbersome, but possible. It is strongly recommended to mark the membranes and the spokes before folding to prevent connecting the wrong membrane to the wrong spoke! This can easily happen when the connector piece is slightly rotated when folded and almost did happen during this test.

*Figure 36 Complete inflatable structure folded*

Deployment of the inflatable during this test is very since the mass flow of the vacuum pump used to inflate the tube is not as high as the mass flow of the hand pump used earlier. The deployment test did not go as planned since during deployment, one spoke got stuck behind an air hose and had to be released manually. This is a good example of something that can also happen in space. In addition, one spoke-membrane connection failed. Whether this was due simply because it was overlooked or because the T-shape slipped out of the slits is unknown. In any case, the T-shapes and slits have to be reinforced with an extra layer of tape to make them stiffer and more durable because it does not take much effort to disconnect the membrane from the spoke once the T-shape has been folded several times.

Frames of the deployment test are shown below. During the first 8 frames, everything is going as it should. At frame 9, the inflatable wants to rise upward, but cannot do this since it gets stuck behind a hose. The cameraman (the author) rushes to get the structure clear from the hose in frame 10. In frame 11, the structure is clear. Frame 12 shows one membrane being attached to only one spoke. Frame 13 shows the inflatable sagging towards the ground due to the failure of one tube seal caused by leaving the pump on far too long which resulted in a too high pressure (no pressure-relief valve was used). This seal was easily re-made after the test.

**1** **2** **3**

**4** **5** **6**


7

8

9

10

11

12
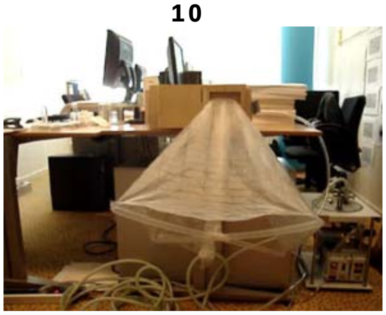
13

### 5.5 Stowage and deployment from 189 cm$^3$ volume

After the successful stowage of the structure in the previous test, the internal volume of the storage device is further reduced to 10x10.5x1.8 cm$^3$. The same structure as in subsection 5.4 is folded and deployed from this volume. The achieved packing efficiency, $\eta$, is now:

$$\eta = \frac{V_{\text{inflatable}}}{V_{\text{available}}} \cdot 100\% = \frac{30500}{189000} \cdot 100\% = 16.1\%$$

The packing factor is thus equal to 6.2.

The membranes are now folded into 3x3 cm squares. This results in more volume being available to stow the spokes. The height of the membrane package of course increases, but this height is far less than 15 mm (between 5 and 10 mm). Creating the squares is not very difficult, but it is time consuming (it takes ±½ hour to fold one membrane). Contrary to the previous test, the attachment points of the membranes (up to the slits) are deliberately positioned such that they stick out of the square during folding (like the little triangles at the sides of the folded membrane in figure 29). This helps enormously when connecting the membranes to the spokes. This begins to get difficult due to the small volume and the relatively large tubes (their diameter is twice the designed diameter). The connection points at the membranes have been stiffened and reinforced with an extra layer of tape. With respect to height, everything fits easily inside the available volume.


*Figure 37 Membranes folded in 3x3 cm squares (left) and complete structure folded (right)*

During this test, the deployment of the inflatable went as desired. In frame 4 it is visible that a piece of wood used to create the smaller volume has fallen against the fixture of the central tube. This resulted in the membrane there being pushed against the fixture. However, no negative effects on the deployment due to this have been observed.


During the third and fourth deployment tests, it is observed that the membranes tend to curl at their edges after having been handled several times. This is an undesired effect and it is

TBD whether engineering models need to have stiffened membrane edges to prevent this effect from occurring.

# 6 CONCLUSIONS & RECOMMENDATIONS

When using a CGG to inflate the inflatable structure of the iDod, the pressure inside the inflatable is between 0.59 and 1.07 bar, depending on the temperature of the inflatable. This is three to five times as much as the pressure that has been assumed to be required at the start of the design [Maessen, iDod.DD.001], but is not expected to lead to structural problems. In fact, it will aid in removing wrinkles and creases formed in the inflatable during stowage.

First folding results for a breadboard inflatable structure have been obtained. The packing efficiency obtained thus far is ~16%. Up till now, it has been assumed a packing efficiency of 33% (packing factor of 3) is possible. After having performed four deployment tests, this assumption is deemed very optimistic and it is doubted this efficiency will be reached eventually. A packing efficiency of 20-25% is more realistic with 20% being certainly possible and 25% being likely to be possible.

It is strongly recommended to perform more tests on breadboards to obtain additional information regarding the packing efficiency and the deployment envelope for the inflatable structure. Preferably, deployment tests should be performed in a zero-g environment (parabolic flight) with engineering models of the structures in a later stage of the design. These tests can then be used as qualification and verification tests.

# REFERENCES

1. Anselmo, et. al., *European Code of Conduct for Space Debris Mitigation*, Issue 1.0, 28 June 2004.

2. Bernasconi, M.C., *Folding Patterns for Gossamers' Building Blocks, A Primer*, presentation, 3rd European Workshop on Inflatable Space Structures, ESA ESTEC, Noordwijk (NL), 10-12 October 2006.

3. Boscher, J., *Micropropulsion system – Engineering model, Design Review,* TNO Defense, Security, and Safety, Rijswijk, The Netherlands (NL), 4 January 2007.

4. Bousquet, P.W., et. al., *De-orbiting Microscope spacecraft by drag enhancement*, IAC paper IAC-06-B6.4.5, 2006.

5. Bradford Engineering, *Solid Propellant Cool Gas Generator*, datasheet, Heerle (NL), September 2006.

6. Breukelen, E.D. van, *Top Level Requirements for inflatable De-orbit device (iDod)*, iDod document ISIS.iDod.REQ, Revision 1.3, Delft, 17 March 2007.

7. Cadogan, D.P. and Grahne, M.S., *Deployment control mechanisms for inflatable space structures*. 33rd Aerospace Mechanisms Conference, May 1999.

8. Cadogan, D.P., et al., *Inflatable space structures: A new paradigm for space structure design*. IAF paper 98-I-.1.02, 49th International Astronautical Congress, Melbourne (Australia), Sept/Okt 1998.

9. Freeland, R.E., et. al, *Inflatable Deployable Space Structures: Technology Summary*, IAF paper IAF-98-I.5.01, 1998.

10. Gere, J.M. and Timoshenko, S.P., *Mechanics of MATERIALS*, Fourth SI Edition, Stanley Thornes (Publishers) Ltd, Cheltenham (UK), 1999.

11. Groot, B.C.H. de, *IGGB system: component concept selection*, Delfi-1 Technical Note DELFI.1.TN.41118.02, Faculty of Aerospace Engineering, Delft University of Technology, 4 June 2003.

12. Jenkins, C.H.M., *Gossamer Spacecraft: Membrane and Inflatable Structures and Technology for Space Applications*, AIAA, Reston (USA), 2001.

13. Kunze, A., Kröplin.B, *Comparison of construction methods for inflatable truss structures,* First European Workshop on Inflatable Space Structures, ESTEC, Noordwijk (NL), 21-22 May 2002.

14. Le Couls, O., et. al., *Aluminum Laminate Technology for Micro-Satellite Deorbiting Aerobrake System*, presentation, 3rd European Workshop on Inflatable Space Structures, ESA ESTEC, Noordwijk (NL), 10-12 October 2006.

15. Lefevre, Y-M, *Inflatable Structure Technology: Promising Solutions for Spacecraft Applications,* First European Workshop on Inflatable Space Structures, ESTEC, Noordwijk (NL), 21-22 May 2002.

16. Lichodziejewski, D., et. al., *Bringing an Effective Solar Sail Design Toward TLR 6*, AIAA paper 2003-4659, 2003.

17. Lichodziejewski, D., et. al., *Development and ground testing of a compactly stowed scalable inflatably deployed solar sail*, AIAA paper 2004-1507, 2004.

18. Maessen, D.C., *Connecting tubes to a connector piece*, iDod document iDod.CM.004, Draft, Faculty of Aerospace Engineering, Delft University of Technology, 3 March 2007.

19. Maessen, D.C., *Connector piece design and construction*, iDod document iDod.CM.002, Draft, Faculty of Aerospace Engineering, Delft University of Technology, 3 March 2007.

20. Maessen, D.C., *Creating flexible tubes*, iDod document iDod.CM.001, Draft, Faculty of Aerospace Engineering, Delft University of Technology, 3 March 2007.

21. Maessen, D.C., *iDod inflatable structure conceptual design trade-off*, iDod document iDod.TO.001, Version 1.1, Faculty of Aerospace Engineering, Delft University of Technology, 28 February 2007.

22. Maessen, D.C., *iDod storage device*, iDod document iDod.DD.002, Draft, Faculty of Aerospace Engineering, Delft University of Technology, 20 March 2007.

23. Maessen, D.C., *iDod Straw man concept design description,* iDod document iDod.DD.001, Faculty of Aerospace Engineering, Delft University of Technology, September 2006.

24. Maessen, D.C., *Material selection*, iDod document iDod.TN.008, Version 1.0, Faculty of Aerospace Engineering, Delft University of Technology, 13 March 2007.

25. Maessen, D.C., *Membrane attachment*, iDod document iDod.CM.005, Draft, Faculty of Aerospace Engineering, Delft University of Technology, 12 April 2007.

26. Maessen, D.C., *Required amount of inflation gas for tripod*, iDod document iDod.TN.003, Version 1.0, Faculty of Aerospace Engineering, Delft University of Technology, 5 October 2006.

27. Maessen, D.C., *Thermal design*, iDod document iDod.TN.011, Version 1.2, Faculty of Aerospace Engineering, Delft University of Technology, 21 March 2007.

28. Pellegrino, S. and Vincent, J.F.V., *Deployable Structures*, Springer, Vienna, Austria, pp 59-76, 2001. Web source: http://www.bath.ac.uk/mech-eng/biomimetics/FoldMembrane.PDF

29. Rackemann, N., *Design and Development of a Propulsion System for a Cubesat*, presentation, TNO Defense, Security, and Safety, 27 March 2006.

30. Rackemann, N., *Design and Development of a Propulsion System for a Cubesat*, Master Thesis report, Technical University of Berlin, Germany, 30 March 2006.

31. Sapna, G.H. and Folke, J.L., *Inflatable boom controlled deployment mechanism for the inflatable sunshield in space (ISIS) flight experiment*. 34th Aerospace Mechanisms Conference, May 2000.

32. Thomas, J.C. et al, *Experimental study and modeling of highly inflated fabric beams,* First European Workshop on Inflatable Space Structures, ESTEC, Noordwijk (NL), 21-22 May 2002.

*33.* UBE Europe GmbH, *Upilex-S*, Datasheet, Düsseldorf (GE), 3 November 2005.

*34.* Wikipedia, *Ultra high molecular weight polyethylene*, http://en.wikipedia.org/wiki/Dyneema, Viewed March 2007.

35. Wray, E.M., *Real phase diagrams,* Thttp://ej.iop.org/links/rTxj1ltUA/6AuzJx3X2xGsp-7cav5vpA/pev7i4p243.pdf, Viewed March 2007.

# APPENDIX A: NOTES OF CONVERSATION WITH LAURENS VAN VLIET

**Conversation with Eddie van Breukelen and Laurens van Vliet at ISIS (27-11-2006)**

Mail van Eddie voorafgaand aan gesprek:

```
Beste Laurens en Daan,

Bij deze de beloofde 'agenda'-mail

Voor vanmiddag heb ik een zaaltje afgeschreven bij ons op kantoor aan
de
Rotterdamseweg 145

Onderwerpen om te bespreken voor deze formele kick-off lijken me:
- resultaten Daans afstudeerwerk totnogtoe (Daan, neem je ook je
modelletjes mee?)
- bespreking beantwoording kennisvraag:
"Kennisvraag:
Zoals besproken in ons gesprek van 20 juli 2006, vraagt ISIS voor de
kleine EZ-Innovatievoucher 25 uur kennisoverdracht met betrekking tot
de
werking en de toepassing van de koude gasgeneratortechnologie in het te
ontwikkelen inflatable de-Orbit device. Dit in de vorm van geschreven
en
mondeling advies bij de ontwikkeling van een conceptueel ontwerp en een
ontwikkelingsmodel. "
- laten we gezamenlijk proberen te komen tot een opzetje voor het
geschreven deel van het advies
- hoe gaan we om met de formele 'houdbaarheidsdatum' op de
EZ-innovatievoucher?
- laten we iets afspreken over hoe en in hoeverre Laurens voor
mondeling
advies advies beschikbaar kan zijn bij Daans afstudeerwerk tot zijn
afstudeerdatum.

Tot straks en met vriendelijke groet,

Eddie
```

Aantekeningen gesprek:

- Bij TNO is een afstudeerder bezig met de doorontwikkeling van hun cold gas thruster, hij zou ook iets moeten doen aan de ontwikkeling van de ontsteker van de CGG.
- De eigenschappen van de ontsteker zijn nog vrij onbekend, de bovengrens van de ontsteektijd is 20 sec op 12 Watt voor het geval een gloeidraad wordt gebrukt. Tijd en wattage kunnen teruggebracht worden door een pyro-achtige ontsteker te gebruiken (bijvoorbeeld door de gloeidraad in te smeren met een ontvlambaar goedje). Dit kost wel ontwikkelingstijd en het is nog onduidelijk wanneer iets als ‘pyro’ beschouwd wordt. Pyrosystemen zijn officieel namelijk niet toegestaan in CubeSats. Met pyrosystemen is bliksem ook een issue, omdat de benodigde stroomsterkte voor ontsteking laag is en dus eventueel door een blikseminslag op of in de buurt van het lanceerplatform gegenereerd kan worden. Eddie weet echter van een CubeSat-team dat wel pyro-achtige systemen gebruikt (ze zijn wel hun eigen launch-broker, dus het is voor hen makkelijker om zo’n systemen toe te laten op de raket), **Eddie gaat dan**

**ook uitzoeken hoe zij met de (certificerings)problemen rond pyro's zijn omgesprongen**.

- X-POD / P-POD zou soort kooi van Faraday moeten zijn. Volgens Eddie heeft Delfi-$C^3$ vandaag een X-POD onvangen. Die zou eventueel misschien gebruikt kunnen worden om dit te testen i.v.m. risico bliksem voor pyro.
- Er wordt voorlopig ervan uitgegaan dat de benodigde power voor de ontsteking van de CGG geleverd wordt door de batterij van de CubeSat (batterij is vrij standaard in CubeSats, hoewel bijv. Delfi-$C^3$ er geen gebruikt). **De ondergrens van het beschikbare vermogen van zo'n batterij wordt uitgezocht door Eddie.**
- Op dit moment wordt niet verwacht dat er een safe/arm schakelaar nodig is voor de CGG, omdat CubeSats tijdens de lancering sowieso uitgeschakeld zijn (worden geactiveerd tijdens deployment door een simpele switch).

- Huidige kleinste maat CGG is 0.3 gram, deze maat gaat ook gebruikt worden voor MicroNed.
- $\varnothing_{inwendig}$ ~ 6 mm, wanddikte ~ 1 mm => $\varnothing_{totaal}$ ~ 7 mm. L/D ~ 3 => L ~ 18 mm => L = 20 mm.

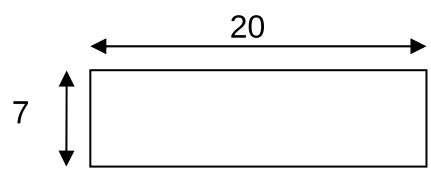


- $\rho_{grain}$ ~ 1000 kg/m$^3$ , $\rho_{total}$ ~ 1500 kg/m$^3$ (1.5 g/cc)
- CGG kan ook dikker en korter gemaakt worden zodat hij niet hoeft te liggen, maar bijvoorbeeld rechtop in de opblaasbare buis kan staan. Brandtijd wordt dan wel korter met als gevolg een hogere uitstroomsnelheid. Mogelijk gevolg: gat in buis door grote gas-snelheid. Twee oplossingen: plaat voor uitstroomopening zetten om stroming af te remmen (die moet dan om de plaat heen) of een poreus materiaal voor de opening plaatsen:

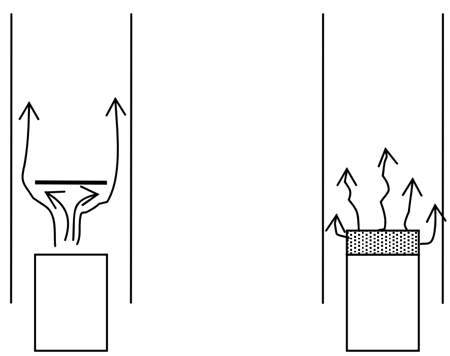

plaat poreus

- Gebruik geen connector om draden aan CGG vast te maken, soldeer ze eraan vast en maak ze op goede lengte (connector is ~ 0.5 gram, niet veel minder dan de CGG zelf!)
- Vastmaken CGG aan structuur op 2 manieren: met schroefdraad of met kabelklem.
- Temperatuur casing kan misschien 200°C worden (kan minder zijn, nog onduidelijk voor dit formaat CGG) => eventueel probleem door opwarmen folie/composiet.

# APPENDIX B: MEMO LAURENS VAN VLIET TO E.D. VAN BREUKELEN (28-11-2006)

Eddie,

Naar aanleiding van onze meeting, d.d. 27 november 2006, hierbij een kort overzicht van de besproken onderwerpen en resultaten van uitzoekwerk wat ik daarna heb gedaan. Het is gezien de beperkte omvang van de opdracht niet de bedoeling dat dit memorandum een compleet overzicht geeft van alle details.

Voor het toepassen van de koelgasgeneratortechnologie op de schaal die nodig is voor de opblaasbare structuur is het nog nodig dat er een ontsteker ontwikkeld moet worden die gasgeneratoren op de benodigde schaal veilig en betrouwbaar kan ontsteken. De ESA standaard initiator (ESI) is veel te groot voor de huidige toepassing. De massa van de ESI zonder connector is al 12 gram en de afmetingen zijn ongeveer 28 mm lang bij een maximale diameter van 16 mm. Recent heeft TNO een ontsteker getest, die nog niet uit ontwikkeld is, die qua orde grootte geschikt zou zijn voor de huidige toepassing, echter is de benodigde energie nog erg groot voor toepassing aan boord van een gemiddelde cube-sat. De conclusie is dat de benodigde energie voor de ontsteker omlaag moet, maar het is nog onduidelijk hoeveel. In principe is de benodigde energie met enkele ordes omlaag te brengen door gebruik te maken van een energetische boosterlading in de gasgenerator. Het onderscheid met pyrotechniek wordt daardoor echter kleiner en is mogelijk ongewenst voor de toepassing op cube-sats. Afgesproken is dat ISIS bij gebruikers gaat informeren wat er op dit gebied acceptabel is.

Voor het huidige ontwerp van de opblaasstructuur is een nominaal gasvolume nodig van ongeveer 0.045 normaal liter (normaal liter bij 1 bar en 273K). Tijdens de bespreking gingen we er vanuit dat de gasgeneratoren die recent bij TNO zijn getest met Nico Rackemann bijna 1 op 1 geschikt zouden zijn voor de opblaasstructuur. Berekeningen met huidige input geven echter aan dat zelfs deze gasgeneratoren een factor 3 te groot zijn. Nog kleinere gasgenerator zijn in principe wel mogelijk, echter komt daarmee tevens ook de gewenste brandduur van liefst enkele seconden zeer sterk in gevaar.

Omdat het benodigde gasvolume maar zo klein is en dus ook de benodigde gasgeneratoren ook ben ik op een ander idee gekomen. Dit idee is het volgende:
Als je nou een stof neemt die endotherm bij lage temperatuur kan ontleden en daarbij een gas vormt en je deze stof opwarmt met een gloeidraad, zou dit dan op deze schaal een goed alternatief zijn voor onze gasgeneratoren?

Ik zal even een voorbeeld geven met magnesium carbonaat ($MgCO_3$):
- $MgCO_3$ ontleedt bij ongeveer 500°C in MgO(s) en $CO_2$(g)
- Voor decompositie van $MgCO_3$ is 117 kJ/mol aan thermische energie nodig.
- Om 0.045 normaal liter gas te krijgen is $2*10^{-3}$ mol $CO_2$ nodig
- $2*10^{-3}$ mol x 117 kJ/mol is 234 J
- Molaire massa van $MgCO_3$ is 84 gram/mol
- Om $2*10^{-3}$ mol $CO_2$ te krijgen heb je $2*10^{-3}$ *84 = 0.168 gram $MgCO_3$ nodig.
- Neem een 5 Watt gloeidraad en plaats die in een buisje met 0.2 gram $MgCO_3$. Dan duurt het in totaal (even 100% efficiency aangenomen) ongeveer 47 seconden voordat alle $MgCO_3$ is ontleedt.
- Met een moderne Li-ion batterij is de benodigde energie op te slaan in een halve gram batterij massa, echter om het benodigde vermogen te leveren zal hij wat groter moeten zijn.

- Omdat de massa van het gas zo klein is zal een temperatuur van enkele honderden graden zeer snel worden gereduceerd in de omliggende structuur en geen negatieve effecten hebben op de inflatable structuur
- Een extra voordeel kan zijn dat er een overmaat aan vaste stof worden meegenomen, waarbij de ontleding kan worden gestopt indien een geschikte druk in de inflatable stuctuur is behaald. Desgewenst kan bij een lange uithardingstijd van de stuctuur nog achteraf wat gas bijgeproduceerd worden door weer energie aan de gloeidraad toe te voegen.

Bovenstaande geeft aan dat het idee van het ontleden van een stof theoretisch haalbaar moet zijn en op deze schaal. Er zal echter mee geëxperimenteerd moeten worden wat de geschikte praktische oplossing zou kunnen zijn. Het voordeel is dat deze experimenten door studenten kunnen worden uitgevoerd en dat de experimenten op de TU kunnen worden gedaan. TNO zou een dergelijk onderzoek ook kunnen uitvoeren en/of begeleiden.

Ik heb wat tijd besteed aan het zoeken naar mogelijk andere geschikte stoffen dan magnesium carbonaat, het blijkt echter dat het selecteren uit het grote aantal mogelijkheden niet eenvoudig is en veel uren gaat kosten.
Er zijn allerlei criteria die je in overweging moet nemen en een goede trade-off valt buiten het budget van het huidige project.
Een aantal mogelijke criteria zijn:

- Decompositie temperatuur in de range van 100-500°C, maar liefst wel zo dicht mogelijk bij de 100°C. (Niet lager dan 100°C i.v.m. operationele temperatuur range)
- Smelt temperatuur > 100°C (i.v.m. levensduur is het beter geen vloeistoffen in het operationele temperatuurgebied te gebruiken)
- Dichtheid > 1 g/cc ?? om een compact systeem te houden
- Welke gassen mogen wel en welke niet gevormd worden?
- In ieder geval geen gassen die onder de condities in de inflatable structuur gaan condenseren! (Welke temperatuur range kunnen we verwachten?)
- Geen giftige of gevaarlijke stoffen

MgCO3 heeft een wat hoge ontledingstemperatuur, maar is een veilige stof en CO2 is tussen -50°C en +50°C waarschijnlijk goed te gebruiken, wanneer de temperatuurrange in de inflatable structuur groter wordt dan is $CO_2$ al gauw minder geschikt.

Conclusies:

- Met de huidige schatting van het benodigde gasvolume wordt het toepassen van de koudgasgeneratortechnologie niet meer triviaal.
- Waarschijnlijk wordt het erg lastig om brandtijden van veel langer dan 1 seconde te halen, bij het gewenste gasvolume.
- Voordat de koudgasgeneratortechnologie kan worden toegepast zal er nog een ontstekingmechanisme moeten worden uitontwikkeld en gekwalificeerd. Dit zal voor een deel al gebeuren binnen MicroNed, mogelijk is een deel hiervan direct toepasbaar voor het de-orbit device.
- Een alternatief zou kunnen zijn om het de-orbit device zo aan te passen dat het één op één compatible is met de gasgenerator die onder MicroNed wordt ontwikkeld.
- Het idee om een stof thermisch te laten ontleden lijkt op de huidige schaal een geschikt alternatief en het advies is om hier eens wat mee te gaan experimenteren om de haalbaarheid te onderzoeken.
- De grote voordelen zouden zijn:

- Experimenten kunnen door studenten gedaan worden
- Experimenten kunnen op de TUD worden gedaan
- Absoluut geen pyrotechniek
- Het gecombineerde idee met een de-orbit device is mogelijk patentwaardig

Laurens van Vliet

## APPENDIX C: E-MAIL WITH PROPERTIES CGG

**E-mail from Laurens van Vliet to D.C. Maessen and E.D. van Breukelen (4/16/2007):**

Daan,

Ik heb zo goed als mogelijk de tabel ingevuld.

| | |
|---|---|
| **Mass [g]** | 3 |
| **Dimensions [mm]** | 8x23 |
| **$N_2$ output [normal liters]** | 0.12 |
| **Mass flow [g/s]** | 0.15 |
| **Velocity gas jet [m/s]** | * |
| **Power requirements** | 13 Watt during 2 seconds** |

*) de snelheid van de gas jet hangt van heel veel details af. In het algemeen expandeer je in eerste instantie naar vacuum en zal de gas snelheid per definitie heel hoog zijn (welke bron je dan ook zou gebruiken).
**) dit is de huidige stand van zaken

Ik hoop dat je hiermee uit de voeten kan.

Vriendelijke groeten,

Laurens

# iDod preliminary design description

## SUMMARY

The current document provides a description of the final version of the preliminary design of the iDod system. The system consists out of two major components: a storage device and an inflatable pyramid-shaped structure. The outer dimensions of the storage device are 83x83x15 $mm^3$ and it has flanges which enable it to function like and replace a standard CubeSat side panel.
Currently, a packing efficiency of 20% is considered feasible for the inflatable. This leads to a height of 40 cm and a diameter of the base of the inflatable of 60 cm. With these dimensions, the iDod system is capable of de-orbiting a 1-unit CubeSat from 910 km altitude. The total iDod mass is 94 grams and its volume is 103 $cm^3$, respectively 9.4% and 10.3% of the total CubeSat mass and volume.

It is recommended to determine whether rigidization of the inflatable using a fiber composite is really required. This depends on the risk the customer is willing to take with respect to impact of micrometeoroids and orbital debris. If the structure is to be rigidized, then it has to be determined whether the inflatable tubes can attain the required curing temperature of 120°C under space conditions by means of a more detailed simulation and physical tests.
It is also recommended to perform a more detailed analysis of the attitude and of the orbit evolution of a CubeSat with deployed inflatable. This has to be focused on the unstable part of the de-orbit trajectory since it is yet unclear what the influence of solar radiation pressure is on both features in this section of the de-orbit phase.
A further recommendation is to determine the exact packing efficiency obtainable for the inflatable structure. This drives the de-orbit performance of the system and at the moment, a conservative 20% is assumed based on results obtained with breadboard structures.
Finally, it is recommended to perform deployment tests using gravity offloading or, preferably, in a zero-g environment (parabolic flight). This gives more insight into the deployment behavior of the inflatable and into its deployment envelope.

## KEYWORDS

iDod, CubeSat, inflatable structure, storage device, stowage, deployment

## DISTRIBUTION

| | Name | | Company/ Institution |
|---|---|---|---|
| 1 | E.D. van Breukelen | Customer | ISIS B.V. |
| 2 | B.T.C. Zandbergen | Project supervisor | TU Delft |
| 3 | O.K. Bergsma | Project supervisor | TU Delft |

## APPROVAL

| | Name | Company/ Institution | Date | Signature |
|---|---|---|---|---|
| *Written* | D.C. Maessen | TU Delft | 5/3/2007 | |
| *Checked* | | | | |
| *Approved* | | | | |

## REVISION RECORD

| Issue | Date | Total pages | Affected pages | Brief description of change |
|---|---|---|---|---|
| Draft | 4/23/2007 | 26 | | |
| Version 0.1 | 4/25/2007 | 26 | 1, 25 | – Added that the obtainable curing temperature should be determined by more detailed analysis and physical tests<br>– Added recommendation about attitude and orbit evolution analysis |
| Version 1.0 | 5/3/2007 | 24 | 5, 15 | Removed section 2 (top level requirements) and subsection 4.2.2 (deployment); both are superfluous |
| | | | 6 | Added that the choice for rigidization depends on the risk the customer is willing to take |
| | | | 10 | Changed maximum starting altitude from 915 km to 910 km |
| | | | 10 | Removed last two paragraphs (superfluous) from subsection 2.4 |
| | | | 11 | Removed superfluous explanation for selection of fiber and weave type |
| | | | 12 | Removed superfluous items:<br>– explanation for the selection of a flexible connector piece over a rigid one<br>– explanation for the choice to integrate the storage device into the top panel of the CubeSat<br>– paragraph highlighting commonality of selected hold down and release mechanism with Delfi-$C^3$ |
| | | | 12, 14 | Changed title of section 4 and subsection 4.2 |
| | | | 14, 15 | Removed superfluous discussion of advantages of selected membrane attachment method |
| | | | 15 | Removed superfluous explanation of folding method membranes and tubes and removed figure 18 showing the folding method for the membranes |
| | | | 15 | Inserted a new figure 18 clarifying the membrane attachment method in more detail |
| | | | 15,16,17 | Added section 5 |

## LIST OF TBD'S AND TBC'S

| TBD / TBC | Paragraph | Subject | Due date | Action by |
|---|---|---|---|---|
| TBD | Section 1 | Deployment sensor system | TBD | TBD |
| TBD | Section 1 | Tubing inflation system | TBD | TBD |
| TBD | Section 1 | Small items like fixtures and cabling | TBD | TBD |
| TBD | Subsection 2.1 | Required stiffness inflatable structure | TBD | TBD |
| TBD | Subsection 2.1 | Need for rigidization of the inflatable structure / risk of | TBD | TBD |

| | | | | |
|---|---|---|---|---|
| | | impact with micrometeoroid | | |
| TBD | Subsection 2.2 | Availability of 90% $SiO_2$ + 10% PTFE coating for Upilex-S foil | TBD | TBD |
| TBD | Subsection 3.1 | Strength of adhesive at expected operating temperature iDod | TBD | TBD |
| TBD | Subsection 3.1 | Application of VDA coating on membranes | TBD | TBD |
| TBD | Subsection 3.1 | Position of the fiber composite layer on the inflatable structure | TBD | TBD |
| TBD | Subsection 4.1 | Position CGG | TBD | TBD |

## TABLE OF CONTENTS

# 1 INTRODUCTION

This document describes the preliminary design of the iDod. Its main function is to decelerate a satellite in such a way that the satellite loses altitude and eventually burns up in the Earth's atmosphere. This de-orbit maneuver has to be completed within 25 years after the operational life of the satellite has ended [van Breukelen, 2007]. This deceleration is to be accomplished by inflating a structure that increases the frontal surface area of the satellite in the direction of flight. This leads to a larger drag force on the satellite and hence a decrease in the velocity of the satellite, which in turn results in a decrease in altitude. The inflation gas has to be delivered by a so-called cold gas generator (CGG), provided by TNO.

The required size of the iDod structure varies with satellite mass and initial altitude. Therefore, a baseline design of the iDod is made that can be adapted such that it can be applied on non-baseline satellites in non-baseline orbits. The baseline satellite for the iDod is a 1-unit CubeSat with a size of 10x10x10 $cm^3$ and a mass of 1.0 kg. The baseline orbit has the following characteristics [van Breukelen, 2006]:

| | |
|---|---|
| **Orbit height [km]** | 1000 |
| **Eccentricity [-]** | 0 |
| **Inclination [°]** | 90 |
| **Orbit epoch** | 1 July 2007 |

*Table 1 iDod baseline orbit characteristics*

The orbit epoch is set at 1 July 2007 since at this date the solar activity is minimal. During solar minimum, the activity of the Sun is relatively low, which results in less heating (and thus expansion) of the Earth's atmosphere and hence a lower density at a certain altitude. This leads to less drag and thus a longer de-orbit time.

An important design parameter for the iDod is the ballistic coefficient ($C_B$) of the satellite [Wertz, 1999]. This is a measure for how susceptive the satellite is to aerodynamic drag. A low ballistic coefficient indicates high susceptibility and therefore faster orbit decay than a high ballistic coefficient.
To determine the required ballistic coefficient, the frontal surface area, the mass, and the drag coefficient of the satellite have to be known. The mass is set at 1 kg and the drag coefficient ($C_D$) is set at 2.0 [van Breukelen, 2006]. The value 2.0 for the $C_D$ is a standard estimate (values are usually in the range 1.5 – 2.5). The iDod provides an average frontal surface area S of 0.15 $m^2$ (see subsection 3.4), which results in a ballistic coefficient equal to [Wertz, 1999]:

$$C_B = \frac{m}{C_D S} = \frac{1}{2*0.15} = 3.33\ kg/m^2$$

In comparison, the average ballistic coefficient of a standard 1-unit cubesat is 33.33 $kg/m^2$. The difference between the two ballistic coefficients is also roughly the difference in de-orbit time. Thus, when the inflatable structure is used, the satellite will de-orbit ~10 (33.33/3.33) times faster than the satellite without inflatable structure.

The next figure presents a breakdown of the complete iDod system. Items in a thick-lined box have been designed and are discussed further on in this document. Other items like the deployment sensor system and the tubing for the inflation system are still TBD.

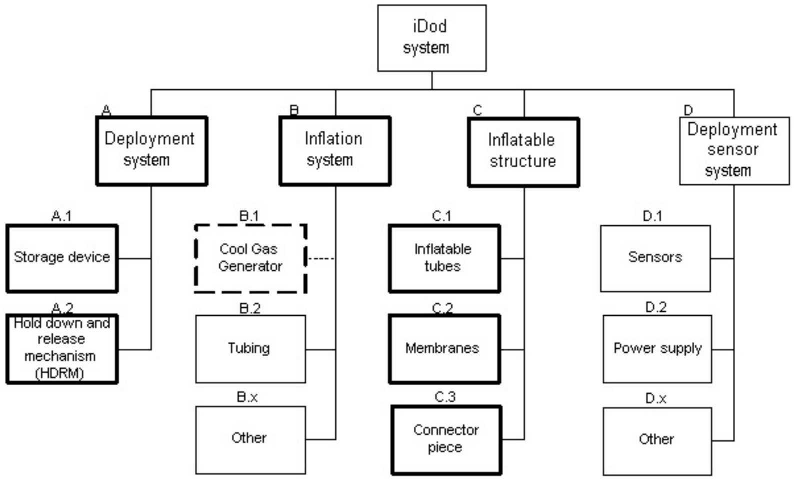


*Figure 1 iDod system breakdown*

Item B.1, the cool gas generator (CGG), is an off the shelf item supplied by TNO. Therefore, no design is made for the CGG, but its influence on the design is taken into account. This is indicated using a dashed box with thick lines.
Items dubbed “Other” are small components like fixtures and cabling. These are TBD in a more detailed design.

Section 2 discusses the overall properties and performance of the iDod system. The inflatable structure is discussed in detail in section 3. Section 4 deals with the storage of the inflatable structure. Section 5 lists all iDod components and their dimensions and mass. Section 6 lists the conclusions and recommendations following from the preliminary design phase.

# 2 IDOD OVERALL PROPERTIES

The current chapter treats the overall properties of the iDod system. Subsection 2.1 discusses the buildup and dimensions of the most important system components. Subsection 2.2 lists the selected materials and their most important properties. Subsection 2.3 presents the mass and volume budgets for the complete system. Lastly, subsection 2.4 treats the de-orbit performance of the designed system.

## 2.1 Buildup and dimensions

The iDod consists out of two major items: a storage device and an inflatable structure. The inflatable is stored inside the storage device and inflated using a CGG at the appropriate moment. Before the inflatable is deployed, a lid on the storage device is released and rotated to allow deployment of the inflatable.

The geometry and buildup for the inflatable is selected in [Maessen, iDod.TO.001]. There, a square pyramid-shape with one central tube and four ‘spokes’ is determined to be the best of several concepts.

The dimensions for the inflatable are determined in appendix A. This is done based on a conservative estimate for the expected packing efficiency for the inflatable of 20% [Maessen, iDod.TN.006]) and clearance with protruding satellite elements. This leads to a spoke length of 30 cm and a central tube length of 40 cm.

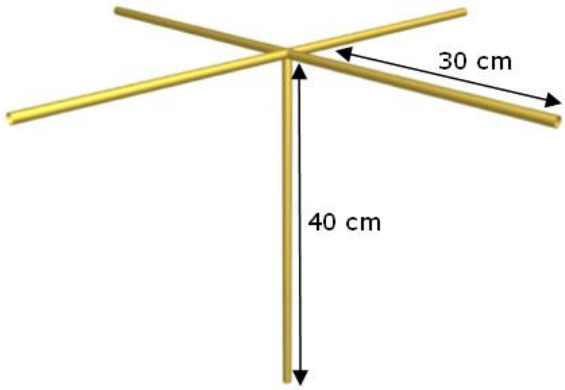


*Figure 2 Tubular structure with dimensions*

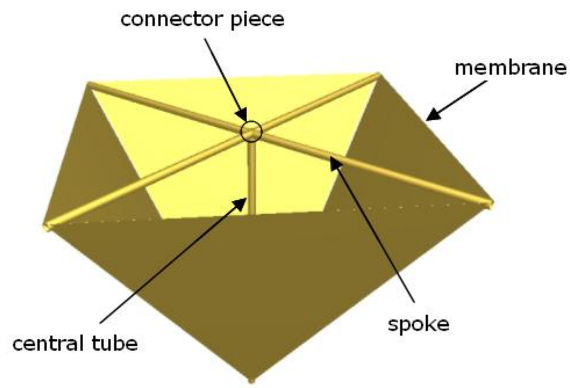


*Figure 3 Complete inflatable structure*

After deployment, the inflatable tubes are rigidized by thermal cure of a thermosetting fiber reinforced resin embedded in the tubes. The reason for rigidizing the tubes is the increased stiffness of the structure compared to a non-rigidized structure with the same wall thickness. However, whether rigidization is really necessary is still TBD. Rigidization is namely only required when the stiffness of the inflatable tubes is insufficient to guarantee structural integrity during the 25 year long de-orbit maneuver. The required stiffness is also TBD. In [Maessen, iDod.TN.007] it is concluded that rigidization of the inflatable tubes of the iDod is only required when the risk (the probability times the impact of the result!) of impacts of micrometeoroids and orbital debris on the inflatable tubes is considered by the customer to be too high. This risk is still TBD and it is up to the customer to decide whether rigidization should be performed once the risk is known.

The storage device is depicted below. The external dimensions of the 'box' are 83x83x15 $mm^3$. The flanges extend the width to 100x100 $mm^2$. The flanges and the lid of the storage device replace a standard CubeSat side panel and allow the storage device to be integrated into the CubeSat structure in the same manner as a normal side panel. The CubeSat integrator can cut or drill away pieces of the flanges to suit his needs. The storage device is discussed in more detail in subsection 4.1.

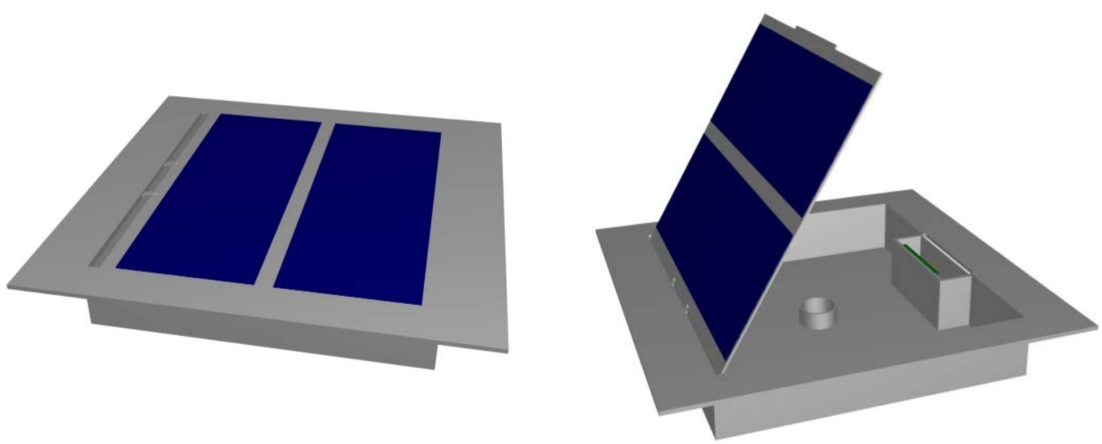

*Figure 4 iDod storage device*

The next figures show the inflatable deployed from the storage device, demonstrating the massive difference in deployed and stowed volume, and the inflatable attached to a CubeSat.

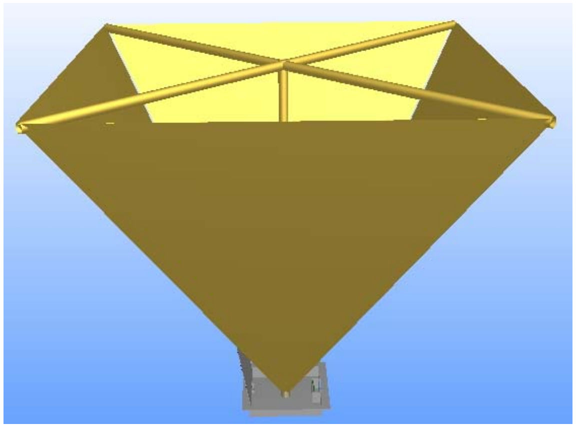

*Figure 5 Inflatable deployed from storage device*

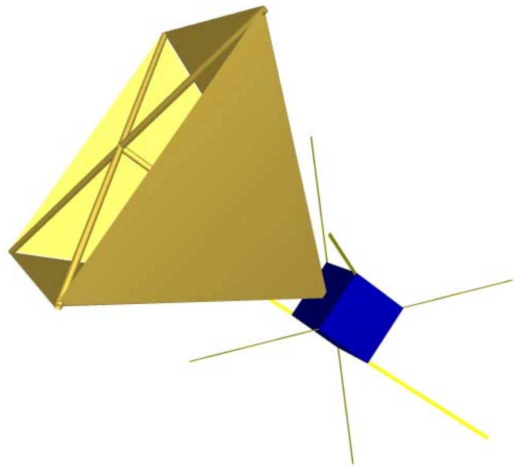

*Figure 6 Deployed inflatable attached to 1-unit CubeSat*

## 2.2 Materials

The main materials for the iDod system are selected in [Maessen, iDod.TN.008]. The table below lists the selected materials. Note that lowermost cell in the second column lists two similar coating materials: $SiO_2$ and 90% $SiO_2$ + 10% PTFE. This is done to indicate that $SiO_2$ is selected, but that 90% $SiO_2$ + 10% PTFE is preferred since it offers better overall properties. However, it is to be determined (TBD) whether the preferred coating is available since Upilex-S is normally coated with pure $SiO_2$. VDA stands for vapor deposited aluminum.

| | **Material** | **Function** |
|---|---|---|
| **Storage device** | Aluminum 6061-T6 | Define storage volume and provide space environment protection |
| **Inflatable structure** | Upilex-S | Foil material tubes and membranes |
| | Technora/cyanate composite | Tube rigidizing material |
| | VDA | Thermo-optical coating |
| | $SiO_2$<br>90% $SiO_2$ + 10% PTFE | Protective coating |

*Table 2 Materials selected for the iDod system*

The next table lists the values for the density and the coefficient of thermal expansion (CTE) at room temperature for the selected materials. These are deemed the most important properties for the overall system design.

| | **Material** | **Density [g/cm$^3$]** | **CTE [ppm/K]** |
|---|---|---|---|
| **Storage device** | Aluminum 6061-T6 | 2.70 | 24 |
| **Inflatable structure** | Upilex-S | 1.47 | 12 |
| | Technora/cyanate composite | 1.23 | 25 |
| | VDA | 2.70 | 24 |
| | $SiO_2$ | 2.20 | 0.55 |
| | 90% $SiO_2$ + 10% PTFE | 2.20 | 14 |

*Table 3 Density and CTE of selected materials [Maessen, iDod.TN.008]*

## 2.3 Mass and volume budgets

With exception of the inflatable structure, the mass and volume of all iDod components is the same as in [Maessen, iDod.TN.010].

The total system volume is 103 $cm^3$ including a contingency of 4 $cm^3$ on the volume of the stowed inflatable structure, see figure 7.

The mass of the total system is 94 grams including contingencies, see figure 8. Without the flanges and the lid, which replace the standard side panel, the mass is 77 grams. The mass difference between a CubeSat with iDod and a CubeSat without iDod is 69.5 grams since the mass of the flanges and the lid combined is 7.5 grams less than a standard side panel [Maessen, iDod.TN.010).

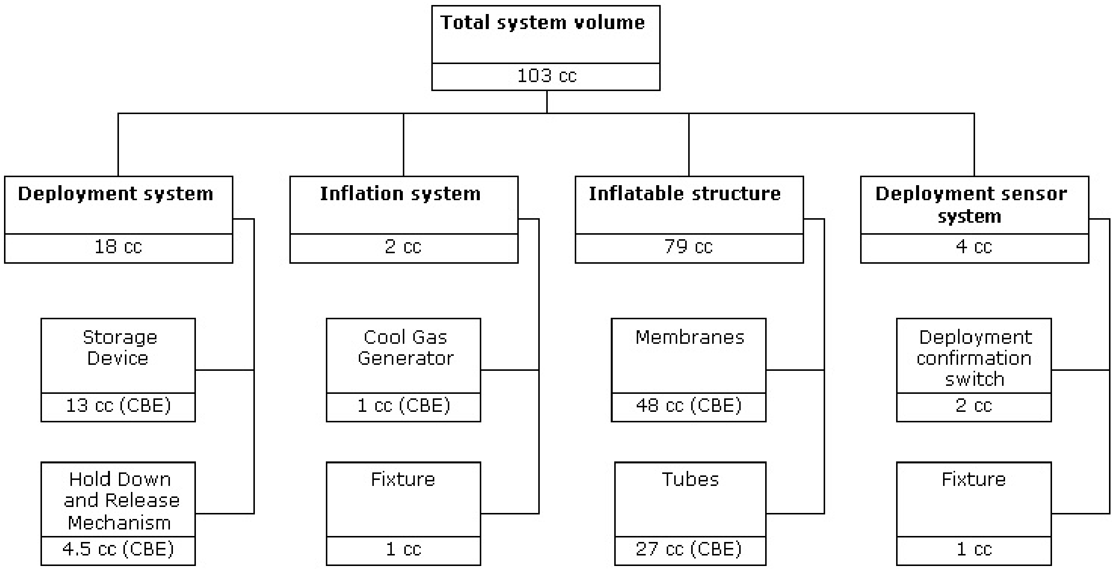


*Figure 7 iDod system volume breakdown*

The term CBE in figures 7 and 8 is short for current best estimate.

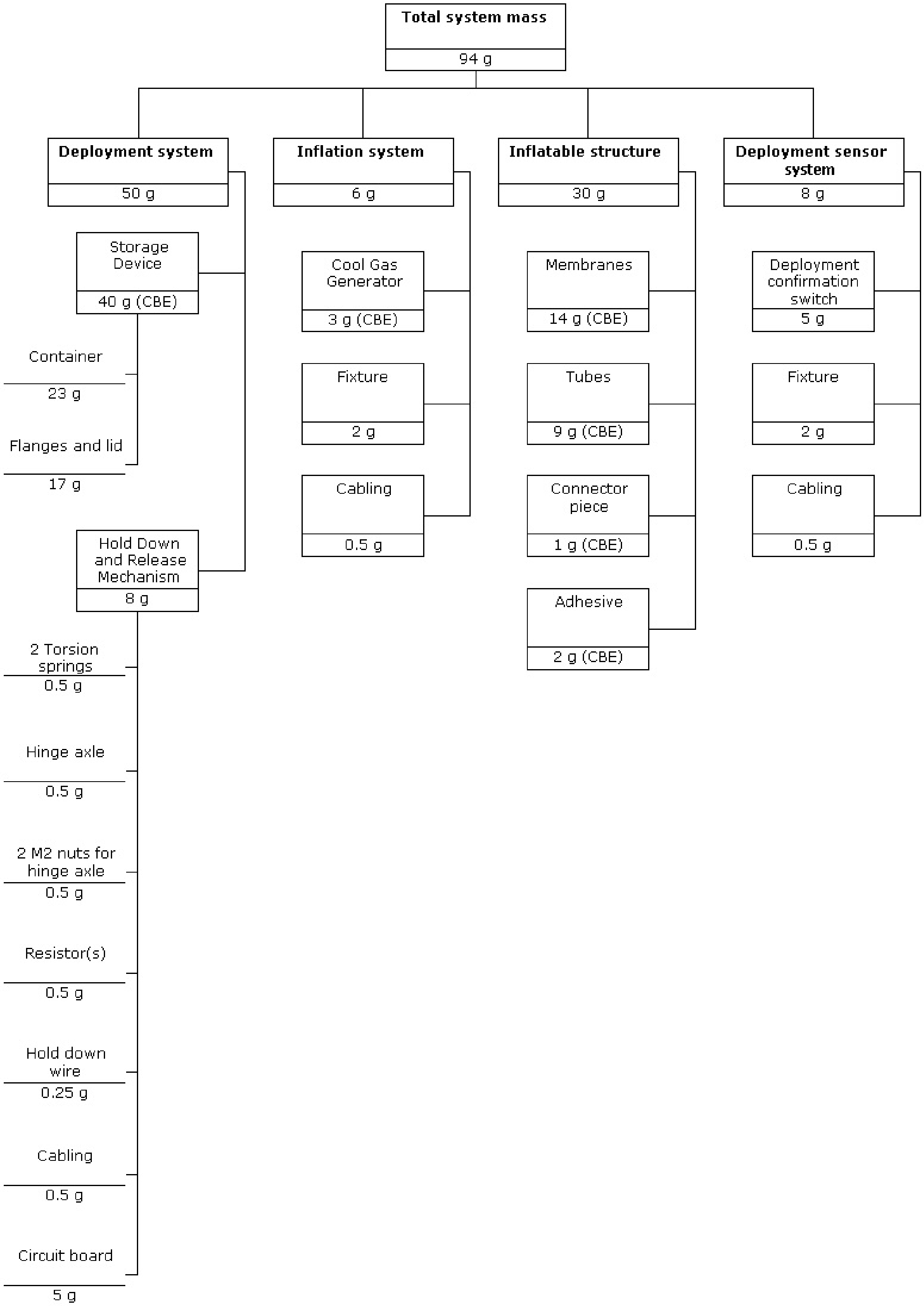


*Figure 8 iDod system mass breakdown*

### 2.4 De-orbit performance

In section 2 it is indicated that the satellite with deployed inflatable cannot be passively stabilized above an altitude of 450-650 km. Therefore, it is assumed that the orientation of the satellite is random above this altitude. Then, the average frontal surface area of the inflatable structure has to be equal to the desired frontal surface area.

In appendix A, the achievable average frontal surface area that can be delivered by the iDod is determined in case the packing efficiency of the inflatable structure is 20%. The result is a frontal surface area of 1500 $cm^2$ when the central tube of the inflatable is 40 cm long and the spokes of the inflatable are 30 cm long.

In [van Breukelen, 2006], the required frontal surface area to de-orbit a satellite within 25 years from a certain altitude is determined for several starting altitudes. This information is used to construct a graph of the required frontal surface area at a given starting altitude:

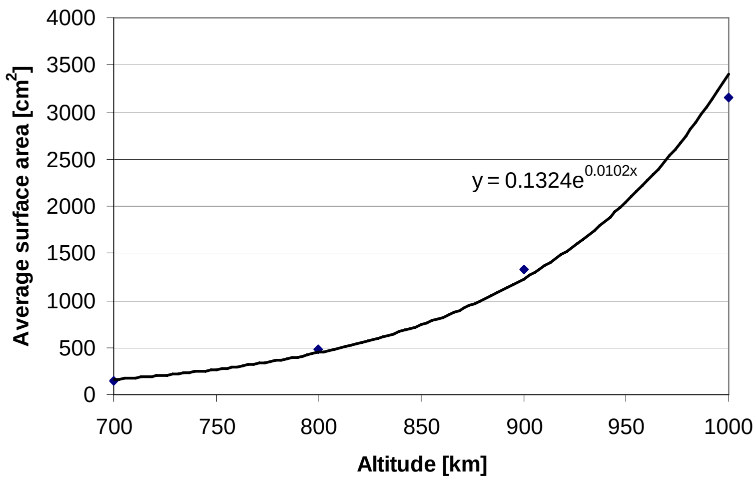


*Figure 9 Required frontal surface area for given starting altitude*

A frontal surface area of 1500 $cm^2$ leads to a starting altitude of ~910 km. Thus, with the current design, a 1-unit CubeSat can be de-orbited within 25 years from an altitude of 910 km.

## 3 INFLATABLE STRUCTURE

The overall geometry and buildup of the inflatable structure has already been discussed in subsection 2.1 and is therefore not treated here. Subsection 3.1 treats the inflatable tubes and the membranes in a bit more detail. Subsection 3.2 treats the connector piece that is required at the junction of all five inflatable tubes (see figure 3).

### 3.1 Tubes and membranes

The tubes of the inflatable have a diameter of 10 mm and consist out of three layers of material: two layers of Upilex-S foil and one layer of woven fiber composite material for structural stiffness. The inner layer of foil acts as gas retention layer and also prevents the tacky fiber composite from sticking to itself when folded. The outer layer of foil acts as restraining layer and as substrate for the required thermo-optical coating (VDA) and the protective coating ($SiO_2$).
The function of the thermo-optical coating is to heat up the tubes sufficiently, above 120°C, to allow curing of the cyanate resin of the fiber composite. For this, the coating needs to have an absorption/emission ($\alpha/\varepsilon$) ratio of 2.2 to 7.1, depending on the satellite orientation and orbit [Maessen, iDod.TN.011]. This is achievable using VDA.

The fibers used in the fiber composite are Technora fibers, a type of aramid fiber. The fibers are woven into a so-called 4H satin weave [Maessen, iDod.TN.008].

Figure 10 shows a cross-section of the inflatable tubes with the fiber composite layer embedded between the layers of foil. However, as discussed in appendix B, there are more ways in which the inflatable structure can be stiffened. For now, the current option is adopted, but selection of the final stiffening method using a fiber composite (if required) remains TBD.

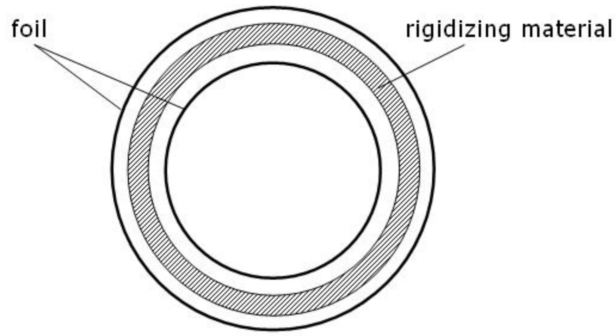


*Figure 10 Baseline tube cross-section [Maessen, iDod.TN.008]*

The spokes are preferred to be sealed at their end in such a way that a flat tube end is created [Maessen, iDod.CM.005]. This eases membrane attachment to the spokes, discussed in subsection 4.2.1.

The internal volume of the inflatable tubes is 126 $cm^3$. The CGG used to inflate the tubes delivers 0.12 normal liters of nitrogen gas [Maessen, iDod.TN.006]. Using the same calculations as in [Maessen, iDod.TN.006], this leads to an internal pressure of 0.97–1.76 bar for a temperature of 0–225°C. This is larger than the baseline pressure of 0.2 bar, but the tube material can easily handle the resulting stress of 8.8 MPa. Whether the adhesive used to seal the tubes can handle the occurring stress is TBD. If it can't, another option is to inflate the inflatable using a sublimating powder as discussed in [Maessen, iDod.TN.006].

The membranes consist out of one layer of Upilex-S foil. In [Maessen, iDod.TN.011], the membranes are selected to be coated by $SiO_2$ on both sides. Whether the membranes also need a VDA coating to aid in heating up the inflatable tubes (by means of radiating their heat towards the tubes) is left TBD using a more sophisticated thermal model than the one used in [Maessen, iDod.TN.011].

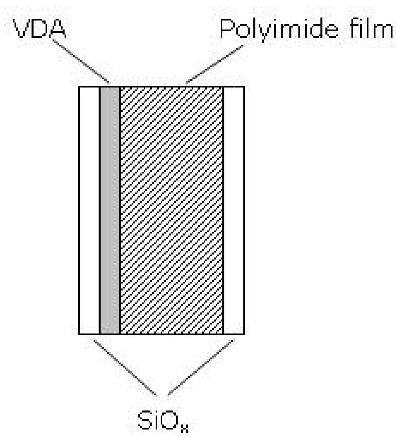


*Figure 11 Proposed membrane coating (the VDA layer is optional) [Maessen, iDod.TN.011]*

### 3.2 Connector piece

At the position where the five inflatable tubes meet, an airtight connection is required. This connection is selected to be flexible and not rigid.

The layout and a constructed connector piece for five 20 mm diameter tubes are shown in the next figure. The dimensions are in millimeters and it is noted that the 20 mm circle in the layout is not a hole but drawn on the connector piece foil to act as an alignment aid during assembly. For 10 mm diameter tubes, the dimensions of the connector piece are all halved.

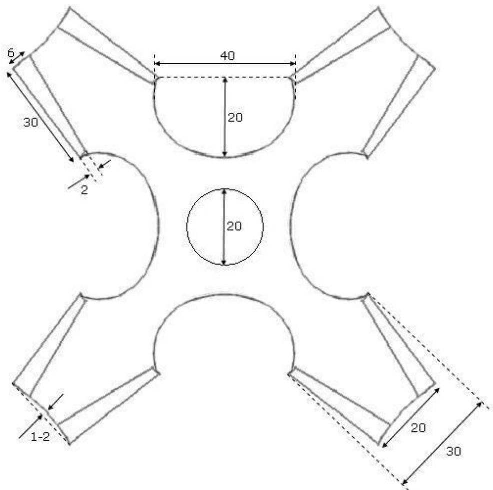


*Figure 12 Connector piece for 20 mm diameter tubes [Maessen, iDod.CM.002]*

## 4 STORAGE

The inflatable structure of the iDod is stored in a storage device. The design of this storage device is outlined in subsection 4.1. Deployment of the inflatable structure follows after opening a lid on the storage device and introduction of gas into the inflatable tubes. Subsection 4.2 treats the stowage of the inflatable inside the storage device and the obtained packing efficiency.

### 4.1 Storage device

In [Maessen, iDod.DD.002] it is chosen to integrate the storage device for the inflatable structure into the top panel of the CubeSat.

The wall thickness of the walls of the storage device and of the flanges is 1 mm, the wall thickness of the lid and bottom is 0.5 mm.

The inflatable structure is deployed once a lid on the storage device is opened. This lid is held down by means of a Dyneema (polyethylene) wire which is melted through once the deployment command is given. Melting through of the wire is achieved by heating up a resistor which is in contact with the wire. The lid is allowed to rotate around a thin aluminum axle. Opening of the lid is achieved by means of two helical torsion springs positioned on the axle.

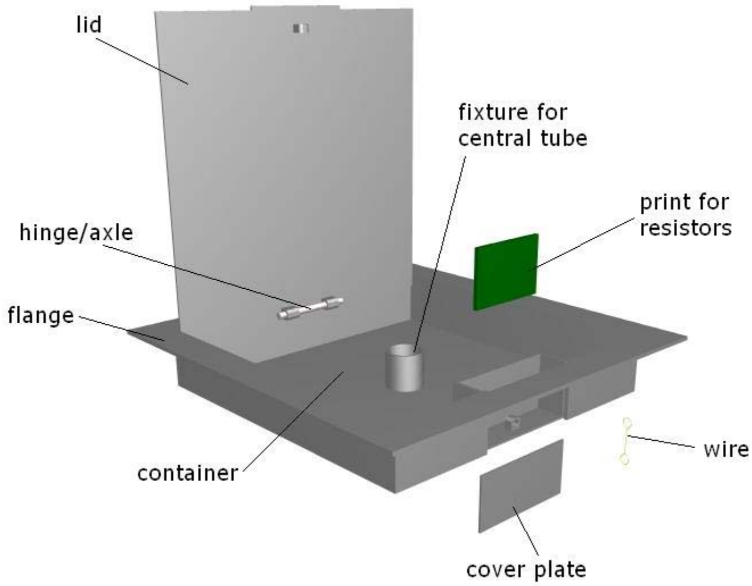


*Figure 13 Exploded view of the storage device*

Correct deployment of the lid is confirmed by means of a switch that is either opened or closed once the panel has reached the required amount of rotation.

A CGG is used to deliver the gas required to inflate the inflatable structure. The placement of the CGG is still TBD, but the most likely placement option for it is option 2 (against a wall) indicated in figure 15.

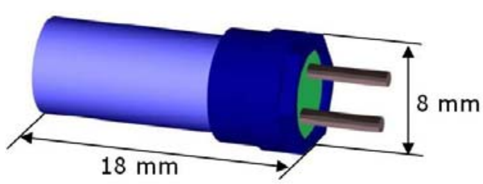


*Figure 14 CGG with dimensions [Maessen, iDod.DD.002]*

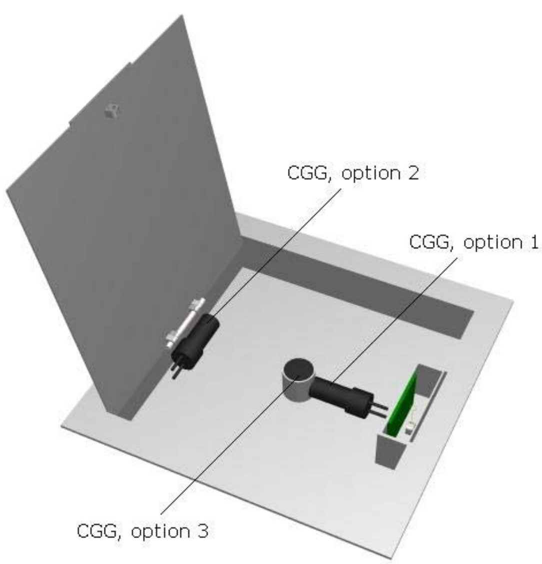


*Figure 15 CGG placement options [Maessen, iDod.DD.002]*

Solar cells can be mounted on top of the lid of the storage device to generate power for the CubeSat.

## 4.2 Packing efficiency

Below, a breadboard model of the inflatable tubular structure with 20 mm diameter tubes, a central tube length of 50 cm, and a spoke length of 40 cm is depicted. On the right side, one membrane is attached to the breadboard model.

*Figure 16 Breadboard model (version 3) of the inflatable structure without (left) and with (right) a membrane attached to it*

The membranes are attached to the spokes and the bottom of the storage device using a loop and slit method discussed in [Maessen, iDod.CM.005].

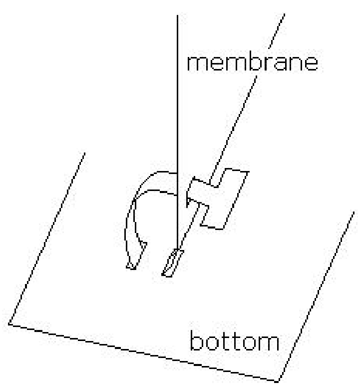


*Figure 17 Membrane attachment to the bottom of the storage device using the loop and slit method [Maessen, iDod.CM.005]. Note the T-shape of the material used to form the loop.*

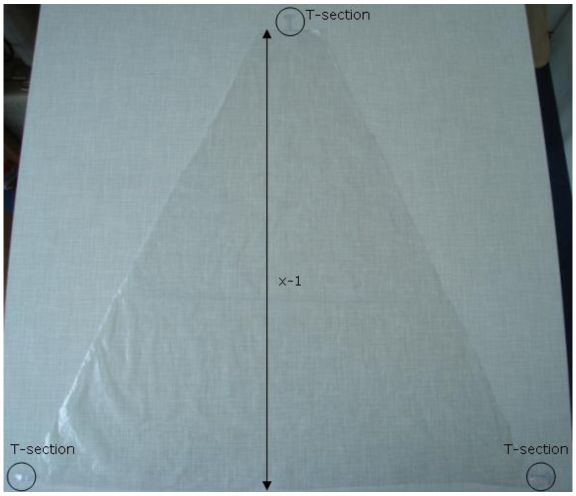


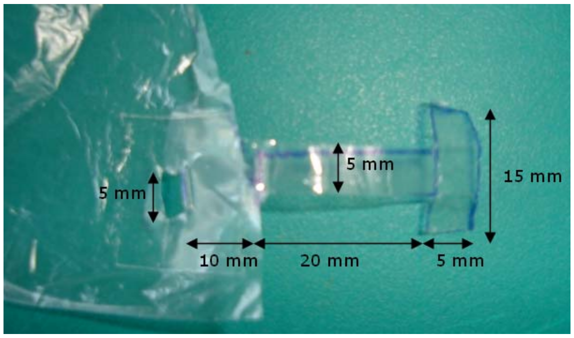


*Figure 18 Membrane with the positions of the T-sections used for the loop and slit method indicated (left, ignore the x-1) and close up of a T-section and a slit with dimensions in mm (right) [Maessen, iDod.CM.005]*

The membranes are folded using an interleaved folding pattern, which is discussed in [Maessen, iDod.TN.006]. The result is shown on the left side of figure 19. After the membranes have been folded, the spokes are connected to the membranes and all the inflatable tubes are zig-zag folded, which is also described in [Maessen, iDod.TN.006]. The final result is depicted on the right side of figure 18.
In this manner, a packing efficiency of 16% has been obtained during tests. Based on this result, a packing efficiency of 20-25% (packing factor of 5 to 4) is considered possible.


*Figure 19 Membranes folded in 3x3 cm squares (left) and complete structure folded (right) [Maessen, iDod.TN.006]*

## 5 IDOD COMPONENTS LIST

The current section lists the components required to assemble the preliminary iDod system. The documents in which these dimensions are determined or in which the method is described with which the dimensions listed here have been determined are also listed.

| Component | Dimensions | Mass [g] | Count | Reference | Comment |
|---|---|---|---|---|---|
| Container storage device | Outer dimensions 83x83x15 mm$^3$ Wall thickness bottom 0.5 mm Wall thickness sides and flanges 1 mm | 31 | 1 | iDod.DD.002 | |
| Lid storage device | ~ 81x80.35x0.5 mm$^3$ | 9 | 1 | iDod.DD.002 | |
| Torsion spring | TBD | 0.25 | 2 | iDod.TN.010 | Mass is educated guess |
| Hinge axle | Diameter = 2 mm Length = 22 mm | 0.5 | 1 | iDod.TN.010 | Mass is educated guess |
| M2 nut | Inner diameter = 2 mm | 0.25 | 2 | iDod.TN.010 | Mass is educated guess |
| Dyneema wire | TBD | 0.25 | 1 | iDod.TN.010 | Mass is educated guess |
| Resistor | TBD | 0.5 | 1 or 2 (TBD) | iDod.TN.010 | Mass is educated guess, no resistor selected yet |
| Print resistor | TBD | 5 | 1 | iDod.TN.010 | Mass is educated guess |
| Wiring print resistor | TBD | 0.5 | 1 | iDod.TN.010 | Mass is educated guess |
| | | | | | |
| Cool Gas Generator (CGG) | Max. diameter = 8 mm Length = 18 mm | 3 | 1 | iDod.TN.006 | Length is without connector pins! |
| Tubing CGG | TBD | TBD | TBD | iDod.TN.006 | TBD whether tubing is really required |
| Print CGG | TBD | TBD | TBD | - | TBD whether print is really required |
| Fixture CGG | TBD | 2 | 1 | iDod.TN.010 | Mass is educated guess |
| Wiring CGG | TBD | 0.5 | 1 | iDod.TN.010 | Mass is educated guess |
| | | | | | |
| Central tube Upilex-S foil | Thickness = 25 μm Length ≈ 420 mm Diameter = 10 mm | ~0.6 | 2 | iDod.CM.001 iDod.DD.003 | |
| Central tube fiber composite | Thickness = 70 μm Length ≈ 420 mm Diameter = 10 mm | ~1.3 | 1 | iDod.CM.001 iDod.DD.003 | |
| Spoke Upilex-S foil | Thickness = 25 μm Length ≈ 320 mm Diameter = 10 mm | ~0.4 | 8 | iDod.CM.001 iDod.DD.003 | |
| Spoke fiber composite | Thickness = 70 μm Length ≈ 320 mm Diameter = 10 mm | ~1.1 | 4 | iDod.CM.001 iDod.DD.003 | |
| Connector piece Upilex-S foil | Thickness = 25 μm Surface area ~29 cm$^2$ | ~0.1 | 2 | iDod.CM.002 | See figure 12 for dimensions (divide by 2!) |
| Connector piece fiber composite | Thickness = 70 μm Surface area ~29 cm$^2$ | ~0.3 | 1 | iDod.CM.002 | See figure 12 for dimensions (divide by 2!) |
| Adhesive | - | 2 | 2 types | iDod.CM.002 iDod.CM.004 | Adhesive for flight models TBD. Currently, Dow Corning HM-2510 Assembly Sealant and RUPLO 100K-S CA-adhesive are used. |

| Component | Dimensions | Mass [g] | Count | Reference | Comment |
|---|---|---|---|---|---|
| Membrane Upilex-S foil, triangular sheet | Thickness = 25 μm<br>Width base = 425 mm<br>Height ≈ 450 mm | ~3.5 | 4 | iDod.TO.001<br>iDod.DD.003 | Width of membrane near storage device ~5 cm |
| | | | | | |
| Deployment confirmation switch (DCS) | TBD | 5 | 1 | iDod.TN.010 | Mass is educated guess |
| Fixture DCS | TBD | 2 | 1 | iDod.TN.010 | Mass is educated guess |
| Print DCS | TBD | TBD | TBD | - | TBD whether print is really required |
| Wiring DCS | TBD | 0.5 | 1 | iDod.TN.010 | Mass is educated guess |

*Table 4 iDod system component list*

## 6 CONCLUSIONS & RECOMMENDATIONS

De-orbiting a 1-unit CubeSat from 1000 km altitude, a top level requirement [van Breukelen, 2007], is not possible using the iDod. A de-orbit from 910 km is possible with a total iDod mass of 94 grams and a total iDod volume of 103 $cm^3$.

At this point, most of the design for the inflatable structure has been performed. This is not the case for the items inside the storage device. The inflation system, the deployment sensor system, and the hold down and release mechanism all still have to be designed in more detail.

For further development of the iDod system, it is recommended to first determine whether rigidization of the inflatable using a fiber composite is really required. This depends on the risk the customer is willing to take with respect to impact of micrometeoroids and orbital debris. If the structure is to be rigidized, then it has to be determined whether the inflatable tubes can attain the required curing temperature of 120°C under space conditions by means of a more detailed simulation and physical tests.

It is recommended to perform a more detailed analysis of the attitude and of the orbit evolution of a CubeSat with deployed inflatable. This has to be focused on the unstable part of the de-orbit trajectory since it is yet unclear what the influence of solar radiation pressure is on both features in this section of the de-orbit phase.

It is further recommended to determine the exact packing efficiency obtainable for the inflatable structure. This drives the de-orbit performance of the system and at the moment, a conservative 20% is assumed based on results obtained with breadboard structures.

It is also recommended to perform deployment tests using gravity offloading or, preferably, in a zero-g environment (parabolic flight). This gives more insight into the deployment behavior of the inflatable and into its deployment envelope.

## REFERENCES

1. Breukelen, E.D. van, *Determination of scenario for iDod baseline conceptual design and range of required inflatable drag surface sizes*, iDod document ISIS[1].iDod.TN.002, issue 1.1, Delft, 12 July 2006.

2. Breukelen, E.D. van, *Top Level Requirements for inflatable De-orbit device (iDod)*, iDod document ISIS[1].iDod.REQ, Revision 1.3, Delft, 17 March 2007.

3. Gere, J.M., Timoshenko, S.P., *Mechanics of Materials,* Fourth SI edition, Stanley Thornes (Publishers) Ltd., Cheltenham (UK), 1999.

4. Maessen, D.C., *Connector piece design and construction,* iDod document iDod.CM.002, Draft, Faculty of Aerospace Engineering, Delft University of Technology, 2 March 2007.

5. Maessen, D.C., *iDod attitude stability analysis,* iDod document iDod.TN.009, Version 1.0, Faculty of Aerospace Engineering, Delft University of Technology, 16 January 2007.

6. Maessen, D.C., *iDod inflatable structure conceptual design trade-off,* iDod document iDod.TO.001, Version 1.1, Faculty of Aerospace Engineering, Delft University of Technology, 28 February 2007.

7. Maessen, D.C., *iDod mass and volume breakdown,* iDod document iDod.TN.010, Version 1.1, Faculty of Aerospace Engineering, Delft University of Technology, 19 April 2007.

8. Maessen, D.C., *iDod storage device,* iDod document iDod.DD.002, Version 1.2, Faculty of Aerospace Engineering, Delft University of Technology, 2 April 2007.

9. Maessen, D.C., *iDod stowage and deployment,* iDod document iDod.TN.006, Version 1.1, Faculty of Aerospace Engineering, Delft University of Technology, 19 April 2007.

10. Maessen, D.C., *iDod Straw man concept design description,* iDod document iDod.DD.001, Faculty of Aerospace Engineering, Delft University of Technology, 25 September 2006.

11. Maessen, D.C., *Effects of atomic oxygen on space inflatable materials,* iDod document iDod.TN.001, Version 1.0, Faculty of Aerospace Engineering, Delft University of Technology, 2 October 2006.

12. Maessen, D.C., *Material selection,* iDod document iDod.TN.008, Version 1.0, Faculty of Aerospace Engineering, Delft University of Technology, 13 March 2007.

13. Maessen, D.C., *Membrane attachment,* iDod document iDod.CM.005, Draft, Faculty of Aerospace Engineering, Delft University of Technology, 12 April 2007.

14. Maessen, D.C., *Simplified load case to assess the importance of structural strength,* iDod document iDod.TN.004, Version 1.0, Faculty of Aerospace Engineering, Delft University of Technology, 9 October 2006.

15. Maessen, D.C., *Thermal design,* iDod document iDod.TN.011, Version 1.2, Faculty of Aerospace Engineering, Delft University of Technology, 21 March 2007.

16. Weisstein, E.W., *Square Pyramid*, From Mathworld—A Wolfram Web Resource, http://mathworld.wolfram.com/SquarePyramid.html , Last modified on 10 February 2006.

17. Wertz, J.R., Larson, W.J., *Space Mission Analysis and Design*, Third Edition, Kluwer Academic Publishers, Dordrecht (NL), 1999.

## APPENDIX A: DETERMINATION OF AVERAGE FRONTAL SURFACE AREA INFLATABLE STRUCTURE

Since the attitude of the CubeSat with deployed inflatable structure is not stable above an altitude of 450-650 km (depending on solar activity) [Maessen, iDod.TN.009], its frontal surface area is not constant. It is assumed that the orientation of the satellite is random above this altitude. Therefore, the average frontal surface area of the inflatable structure has to be equal to the desired frontal surface area.

Determination of the average frontal surface area of the inflatable by an analytical approach is complicated due to shadowing effects that have to be taken into account. This is discussed in [Maessen, iDod.TO.001]. Instead, the average frontal surface area is determined graphically by creating 2D images of a 3D CAD drawing of the inflatable structure using several freeware programs. The 3D CAD drawing is rotated over a number of angles around two perpendicular axes. Each rotation results in a different 2D image. By determining the ratio of pixels representing the inflatable versus all the pixels in the entire image and knowing the area the entire image represents, the frontal surface area of the inflatable for one particular orientation is obtained. Doing this for many orientations results in an average frontal surface area for a random orientation.

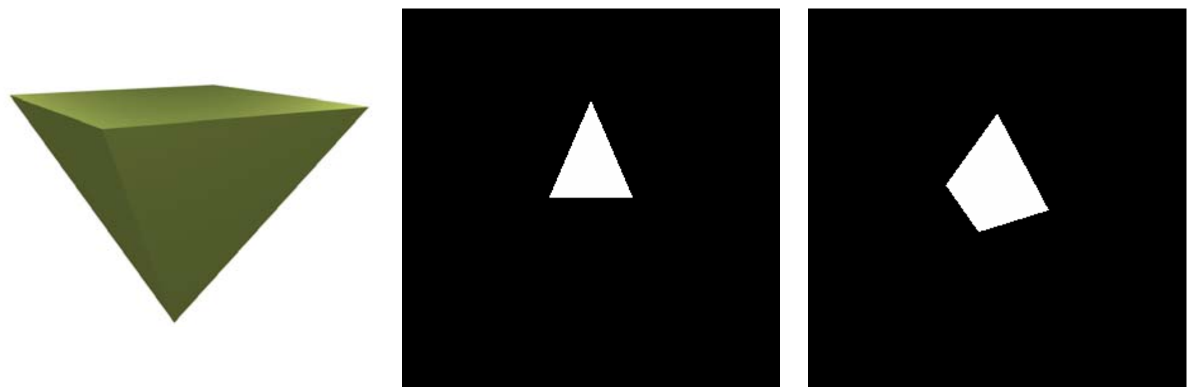

*Figure 20 3D rendering and 2D projections of a fake inflatable with a central tube length of 40 cm and a spoke length of 30 cm*

Before the frontal surface area is determined, the allowable dimensions of the inflatable need to be determined. The volume budget in [Maessen, iDod.TN.010] indicates that 79 $cm^3$ of volume is available to stow the inflatable. In [Maessen, iDod.TN.006], it is estimated that a packing efficiency of 20-25% is achievable for the inflatable. A conservative packing efficiency of 20% then leads to an allowed material volume for the inflatable of $0.2 \cdot 79 \approx 16$ $cm^3$.

The inflatable is built up out of tubes, four spokes and a central tube, and thin membranes. The tubes have a diameter of 1 cm and consist out of three layers of material: a layer of Upilex-S foil, a layer of Technora/cyanate composite, and again a layer of Upilex-S foil [Maessen, iDod.TN.008]. The Upilex-S foil is 25 μm thick while the composite is 70 μm thick.

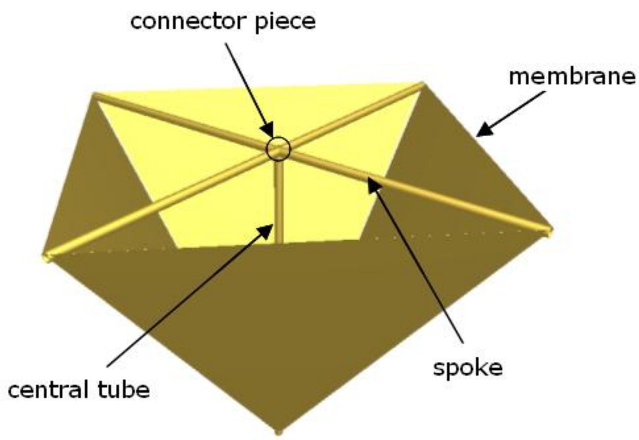


*Figure 21 Inflatable structure*

The material volume of the tubes is determined as follows. The cross-sectional area of the tubes is [Gere, 1999]:

$$A_{\text{cross}} = 2\pi rt = 2\pi \cdot 0.5 \cdot \left(0.007 + 2 \cdot 0.0025\right) = 0.0377\ \text{cm}^2$$

In the formula, t is the wall thickness of the tube and r is the radius of the tube. The material volume of the tubes is then simply the total length of all tubes combined times the cross-sectional area.

The material volume of the membranes is the total membrane area times the membrane thickness of 25 $\mu$m. The membranes have a triangular shape and act as the sides of the pyramid-shaped inflatable. The definition for the height (h) of the pyramid is graphically shown in the next figure. The edges of the base of the pyramid have length "a", the sides of the pyramid have a *slant height* "s", and the skewed edges of the pyramid have an *edge length* "e".

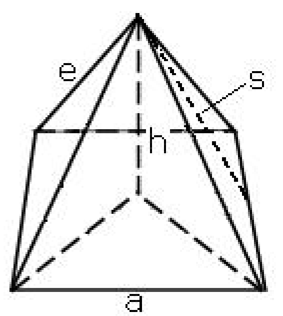


*Figure 22 Pyramid with length definitions*

The area of a membrane is equal to:

$$A_{\text{membrane}} = \frac{1}{2}as$$

The slant height s is determined with the next formula from [Weisstein, 2006]:

$$s = \sqrt{h^2 + \frac{1}{4}a^2}$$

The height of the pyramid is equal to the length of the central tube of the inflatable. The length of a spoke of the inflatable is equal to ½√2·a. Thus, for a given central tube and spoke length, the membrane volume can be determined. Using Excel, several combinations of central tube length and spoke length are found that result in a total material volume of just under 16 $cm^3$:

| | **Central tube length [cm]** | **Spoke length [cm]** | **Total tube volume [$cm^3$]** | **Membrane area [$cm^2$]** | **Total membrane volume [$cm^3$]** | **Total material volume [$cm^3$]** |
|---|---|---|---|---|---|---|
| **Option 1** | 30 | 34.5 | 6.3 | 943 | 9.4 | 15.8 |
| **Option 2** | 35 | 32.25 | 6.2 | 953 | 9.5 | 15.7 |
| **Option 3** | 40 | 30 | 6.0 | 960 | 9.6 | 15.6 |

*Table 5 Options for inflatable structure*

The most important difference between the above options is the surface area of the base of the pyramid. This varies between 1800 $cm^2$ for option 3 and 2381 $cm^2$ for option 1 and is the dominant area when determining the average frontal surface area.

For the three options, the average frontal surface area is 1750 $cm^2$ for option 1, 1625 $cm^2$ for option 2, and 1500 $cm^2$ for option 3.
It is noted that these estimations can be up to 4% smaller than the real average frontal surface area of the inflatables. This discrepancy is found by determining the average frontal surface area of two differently sized cubes (100 mm ribs and 200 mm ribs) when they are rotated around a single axis and comparing it with the analytical result for both cubes. The graphical estimation gives average frontal surface areas of 12445 $mm^2$ and 49172 $mm^2$ for cubes with 100 mm ribs and 200 mm ribs respectively. The analytical result is 14142 $mm^2$ and 50930 $mm^2$. Thus, the estimated average areas are 97.7% and 96.5% of the real areas. Hence, a discrepancy of 4% between the estimated and the real value is possible.

A large frontal surface area is desired and therefore option 1 is preferred. However, this option has the drawback of a larger *half angle* than the other options. The half angle is the angle between the line perpendicular to the upper face of the CubeSat and one side of the pyramid. The definition for the half angle is graphically shown in the next figure.

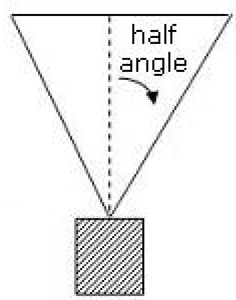


*Figure 23 Half angle*

The half angle $\theta$ is computed using the following equation:

$$\theta = a\cos\left(\frac{h}{s}\right) = a\cos\left(\frac{h}{\sqrt{h^2+\frac{1}{4}a^2}}\right) = a\cos\left(\frac{h}{\sqrt{h^2+\frac{1}{4}\left(\sqrt{2}b\right)^2}}\right) = a\cos\left(\frac{h}{\sqrt{h^2+\frac{1}{2}b^2}}\right)$$

In the formula, b denotes the length of the spokes. For option 1, the half angle is 39.1°. For option 2, the half angle is 33.1°. For option 3, the half angle is 27.9°. The half angle for the inflatable selected in [Maessen, iDod.TO.001] was 29.3°, which was part of the reason for selecting that option. Thus, the current option should have a half angle close to 29.3°. This leads to the selection of option 3 and thus to an average frontal surface area of 1500 $cm^2$.

## APPENDIX B: ALTERNATIVE FIBER COMPOSITE PLACEMENT OPTIONS

A fiber composite is embedded in the inflatable tubes of the iDod and is required to stiffen the inflatable structure such that it will retain its overall shape during the complete de-orbit maneuver. Whether the structure needs to be stiffened using a fiber composite or whether this can be done by using thicker foil material is still TBD, but for now it is assumed that a fiber composite layer is required.

However, stiffening of the structure can be done in more ways than this baseline method. Below, a list of options for stiffening the inflatable is shown, demonstrating that more options are possible. Note that here no choice is made for the final fiber composite placement, this is left TBD. The current section only serves to show that there are other options besides the baseline option and that choosing the baseline option without considering other options is premature.

1. Around the entire circumference and entire length of all tubes and the connector piece (baseline)
2. Only around the entire circumference and entire length of the central tube
3. Use (a) long strip(s)/chord(s) over the length of the tubes
4. Use fiber composite rings along the length of the tubes (this reduces the length of the non-reinforced part of the tubes, which is advantageous with respect to buckling)
5. Spiral a strip/chord of fiber composite along the length of the tubes
6. Position the fiber composite at the edges of the membranes, forming a rigid frame and drawing away loads from the tubes
7. Use a fiber composite ‘chord’ running along the spokes and between the membranes (the chord is not connected to the membranes), this also forms a rigid frame.

The next figure shows the options when using one or several strips of fiber composite instead of wrapping the fiber composite around the entire tube circumference.

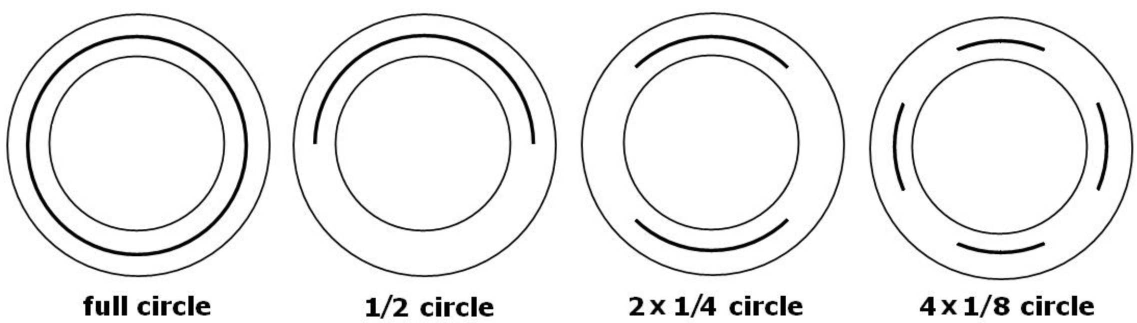


*Figure 24 Options for fiber composite layer in tube cross-section*

Instead of strips of fiber composite, chords can be used to stiffen the inflatable tubes. This leads to a huge mass decrease, but may of course also lead to problems. Discussing these problems is beyond the scope of this report. The next figure indicates which mass difference is likely to be obtained by using several straight chords along the length of a tube instead of using the baseline option.

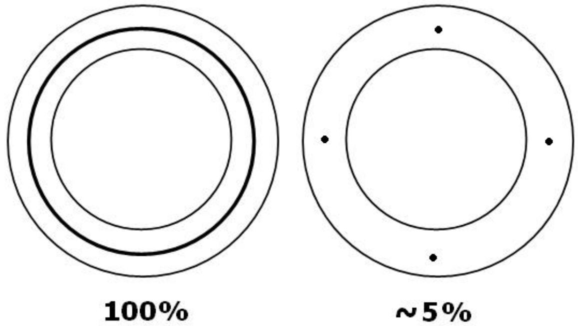


*Figure 25 Mass difference when using several chords along the length of a tube*

Besides using long straight strips or chords, also rings and a spiraled strip/chord can be used to stiffen the inflatable tubes:

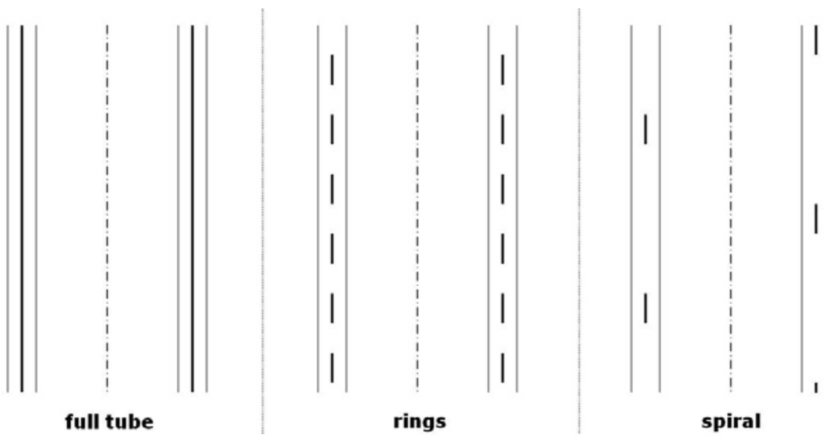


*Figure 26 Options for fiber composite layer along tube length*

Below, the two “frame” options (options 6 and 7) are shown. The thick red lines indicate the position of the composite.

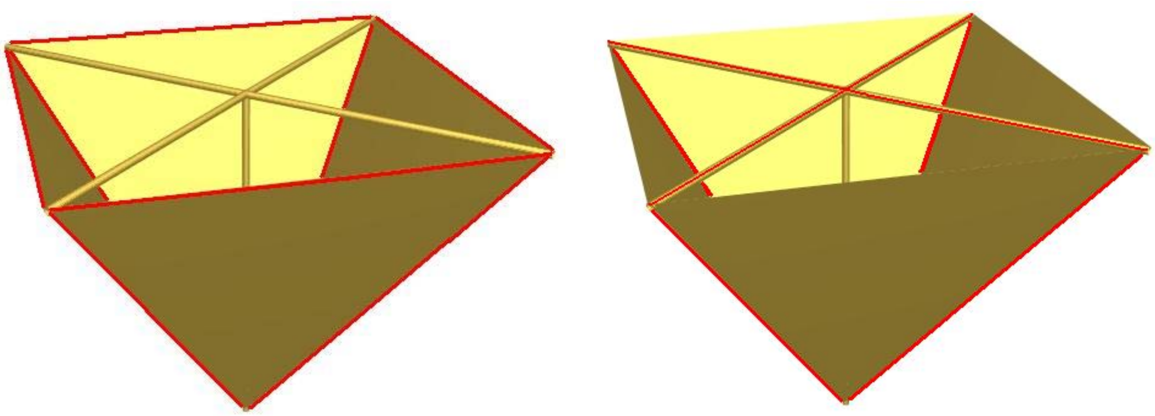

*Figure 27 Fiber composite along the edges of the membranes (left) and chords along the pyramidal structure (right)*

# Required amount of inflation gas for tripod

## Introduction

In this document, it is determined how much inflation gas is required to inflate the straw man concept of the iDod. This number is expressed in "normal liters", the gas volume in liters at sea level conditions. This is typically done for cool gas generators (CGGs).

## Work done

*Nominal amount of inflation gas*

The required amount of moles of inflation gas, assumed to be $GN_2$ (gaseous nitrogen), is determined using the ideal gas law [de Groot, 2003, Delfi-1 SLR 146]:

$$pV = nR_aT$$

Where p is pressure [Pa], V is volume [$m^3$], n is the number of moles inside the volume [mol], $R_a$ is the Universal gas constant equaling 8.3145 J/mol/K and T is the temperature of the gas [K]. This equation can be rewritten as follows:

$$n = \frac{pV}{R_aT}$$

The inflation volume for the iDod is [Maessen, 2006]:

$$\begin{aligned} V &= 3V_{strut} + V_{tube,ballute} = 3*L*\pi r^2 + 2\pi R*\pi r^2 = \pi r^2\left(3L + 2\pi R\right) = \\ &= \pi*0.005^2\left(3*0.5 + 2\pi*0.3167\right) = \\ &= 2.74*10^{-4}\ m^3 \end{aligned}$$

The maximum amount of inflation gas is needed when the temperature of the gas is minimal because the inflation pressure (0.2 bar, [Maessen, 2006]) and the volume are constant. Since no thermal analysis has been performed, a minimum temperature $T_{min}$=250 K is assumed. The inflation pressure and minimum temperature need to be determined more precisely in a later stage of the design for a better prediction of the required amount of inflation gas. Using the assumed values results in the following amount of inflation gas:

$$n = n_{T\min} = \frac{p_iV_{iDod}}{R_aT_{\min}} = \frac{20000\cdot 2.74\cdot 10^{-4}}{8.3145\cdot 250} = 2.637\cdot 10^{-3} \text{ moles}$$

In "normal liters", this is (using T = 273 K and p = $1.013*10^5$ Pa as standard conditions):

$$\begin{aligned} pV = nR_aT \Rightarrow V = \frac{nR_aT}{p} &= \frac{2.637\cdot 10^{-3}*8.3145*273}{1.013\cdot 10^5} = \\ &= 5.91*10^{-5}\ m^3 = 0.059 \text{ normal liters} \end{aligned}$$

The smallest CGG currently available at TNO delivers 0.12 normal liters of gas (using a 0.3 $cm^3$ grain). This CGG thus delivers about 203% of the nominally required amount of gas.

*Sensitivity analysis*

The required amount of inflation gas is determined for an ambient temperature range of 200 K to 300 K (20% above and below nominal) and an inflation pressure range of 0.16 bar to 0.24 bar (also 20% above and below nominal). The following is the result:

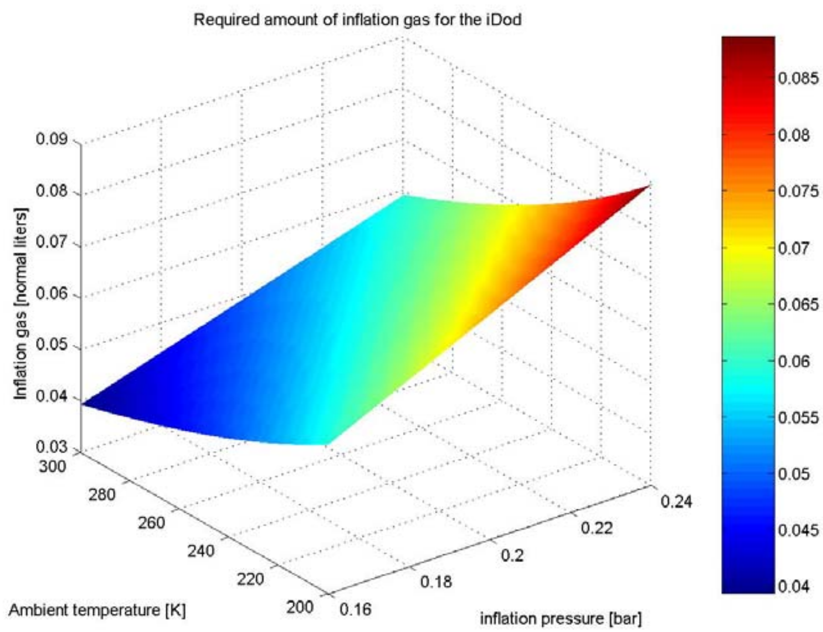


*Figure 1 Amount of inflation gas required as function of inflation pressure and ambient temperature*

A high ambient temperature and low inflation pressure result in the lowest amount of required inflation gas (0.0394 normal liters, 33.3% below nominal). A low temperature and a high pressure result in the largest amount of inflation gas (0.0886 normal liters, 49.9% above nominal).

Since it is likely the volume of the inflatable structure changes in the course of the design, it is investigated how a change in volume affects the required amount of inflation gas at the four extremes of the above figure. The next table presents the required amount of normal liters of inflation gas for eight specific situations. Between brackets it is indicated in percentages how much this amount is above or below the nominal value of 0.059 normal liters.

| | **20% smaller volume** | **20% larger volume** |
|---|---|---|
| **High pressure, high temperature** | 0.0473 (-20%) | 0.0709 (+20%) |
| **High pressure, low temperature** | 0.0709 (+20%) | 0.1063 (+80%) |
| **Low pressure, high temperature** | 0.0315 (-47%) | 0.0473 (-20%) |
| **Low pressure, low temperature** | 0.0473 (-20%) | 0.0709 (+20%) |

*Table 1 Required amount of inflation gas (normal liters) for varying volume*

From the preceding table and figure it is clear that to reduce the required amount of inflation gas, it is necessary to have a low inflation pressure and a high ambient temperature. High inflation pressures should be avoided irrespective of the ambient temperature.
Furthermore, the change in the required amount of inflation gas is proportional to the change in volume, temperature, or pressure. Thus, no large variations in the required amount of inflation gas will occur when no large variations are made in the variables that drive the required amount of inflation gas.

*Uncertainties*

In the forgoing analyses, several effects have not been taken into account. These are:

- Compressibility (the gas used is a non-ideal gas)
- Permeability
- Leaks

All above effects are manageable. The first effect has only got a minute influence on the amount of gas required for these conditions. Permeability can be controlled by choosing a suitable gas retention layer for the inflatable structure. This effect is not expected to change the required amount of inflation gas by more than 1 or 2% since the inflatable structure will be rigidized within a few hours after deployment [Maessen, 2006]. At that point, gas leakage it not important anymore.

The main issue here is leaks caused by non-perfect seals or holes in the inflatable structure. The allowable leak rate is determined as follows:

In the worst-case scenario assumed in this document, the inflatable structure has a volume 20% larger than nominal, an inflation pressure 20% higher than nominal and is inflated at a temperature 20% lower than nominal. Then, 0.1063 normal liters of inflation gas are required to properly inflate the structure (see table 1). As said earlier, the smallest CGG available delivers 0.12 normal liters of gas. Thus, there is: 0.12 – 0.1063 = 0.0137 normal liters of inflation gas "spare" when this small CGG is used. In the time between initial inflation and full rigidization, gas loss has to be kept within certain bounds. After rigidization, gas loss is not important anymore for this mission. The allowable leak rate now depends on the time it takes to fully rigidize the structure. When rigidization takes for instance one hour, the allowable (volume) leak rate ($Q_v$) is:

$$Q_v = \frac{\text{spare gas}}{\text{rigidization time}} = \frac{0.0137}{1*60*60} = 3.81*10^{-6} \text{ normal liters/s} =$$
$$= 3.81*10^{-3} \text{ sccs } GN_2$$

The term "sccs" stands for standard cubic centimeters per second.
In [Zandbergen, 2006] it is mentioned that a typical allowed volume leak rate for chemical propulsion systems is $1*10^{-6}$ sccs GHe (gaseous helium) at tens of bars of pressure. This translates to $1.12*10^{-6}$ $GN_2$ [Zandbergen, 2006], which is roughly a factor 3000 less than computed above. Therefore, it is concluded that the current volume leak rate is attainable without major difficulties. However, it has to be kept in mind that the allowable leak rate is inversely proportional to the rigidization time. Therefore, long rigidization times (> 5 hours) have to be avoided whenever possible.

*Testing*

To check whether the leak rate determined above can really be attained, a test for leak rate has to be performed. If the measured leak rate is larger than allowed, either a larger CGG is required or the design of the inflatable structure needs to be changed (construction or rigidization method). In addition, an inflation test can also be used to determine whether the chosen inflation pressure is high enough to remove all major wrinkles from the inflatable structure and whether it is allowed to reduce the inflation pressure in order to save gas. Inflation tests can be used for other purposes as well, but these are beyond the scope of this technical note.

Measuring the leak rate is likely to be easiest by measuring the change in internal pressure of the structure over a certain time span. This pressure needs to be determined anyway to determine the pressure required to inflate the structure properly. Schematically, this is performed as follows:

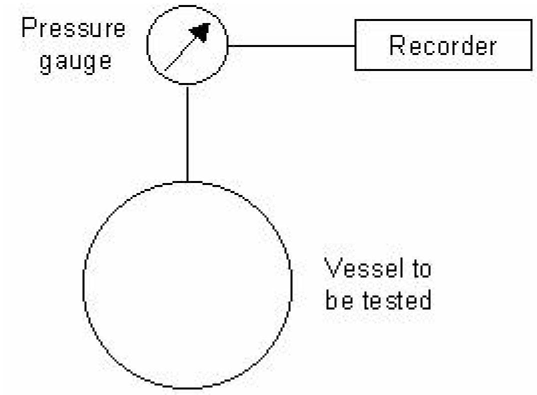


*Figure 2 Leakage test [Zandbergen, 2006]*

When the internal volume of the structure does not change significantly during the test, the measured pressure drop is a measure for the gas mass lost ($\Delta m_g$) [Zandbergen, 2006]:

$$\Delta m_g = \frac{V}{R}\left[\frac{p}{ZT} - \frac{p_i}{Z_i T_i}\right]$$

In the above formula, “Z” is the compressibility factor of the gas used, “R” is the specific gas constant for the gas under consideration and the subscript “i” indicates initial conditions. Assuming “Z” is equal to 1 and that the temperature (T) remains constant gives:

$$\Delta m_g = \frac{V}{R}\left[\frac{p}{ZT} - \frac{p_i}{Z_i T_i}\right] = \frac{V}{RT}\Delta p$$

The molar leak rate ($Q_m$) per second is determined by dividing the result of the above equation by the time span t (in seconds) and the molecular weight (M, [kg/mol]) of the inflation gas ($GN_2$):

$$Q_m = \frac{\Delta m_g}{Mt} = \frac{V}{R/M\, Tt}\Delta p = \frac{V}{R_a Tt}\Delta p \qquad \text{[mol/s]}$$

One mol corresponds to 22.414 liters of gas at a pressure of 1013 mbar and a temperature of 0°C [Zandbergen, 2006]. To determine the correct volume leak rate “$Q_v$” from the molar leak rate “$Q_m$”, a correction has to be made to allow for measurement conditions that are not equal to the standard conditions of 1013 mbar and 0°C:

$$Q_v = \frac{T_{actual}}{T_{std}}\frac{p_{actual}}{p_{std}} Q_m * 22.414 == \frac{T_{actual}}{T_{std}}\frac{p_{actual}}{p_{std}}\frac{22.414V}{R_a Tt}\Delta p = \{T = T_{actual}\} =$$
$$= \frac{p_{actual}}{p_{std}}\frac{22.414V}{R_a T_{std} t}\Delta p$$

For example, when the measured pressure drop is 5000 Pa over a time span of 1 hour (3600 seconds) and the actual barometric pressure is by chance equal to the standard barometric pressure, then:

$$Q_v = \frac{p_{actual}}{p_{std}} \frac{22.414V}{R_a T_{std} t} \Delta p = 1 * \frac{22.414 * 2.74 * 10^{-4}}{8.3145 * 273 * 3600} 5000 = 3.76 * 10^{-6} \text{ normal liter/s} =$$
$$= 3.76 * 10^{-3} \text{ sccs}$$

However, the leak rate in space is different from the leak rate on Earth when the leak rate on Earth is determined at ambient pressure conditions.
When the internal pressure in a pressure vessel is above 0.01 mbar, there will be a viscous flow present at the leak [Leak detection]. Here, the pressure is certainly above 0.01 mbar and therefore the flow at a leak will be viscous. A viscous flow can be either turbulent or laminar. Large leaks and high pressure differences will lead to turbulent flow in a leak and are easy to find. Therefore, they are not of interest. Small leaks result in a laminar flow. Then, the following applies [Leak detection]:

$$\frac{Q_{v,Earth}}{p_{Earth,1}^2 - p_{Earth,2}^2} = \frac{Q_{v,space}}{p_{space,1}^2 - p_{space,2}^2}$$

The subscripts 1 and 2 indicate internal and external pressure respectively. Thus, the volume leak rate changes with the square of the pressure difference. Filling in numbers (in bars) gives the following:

$$\frac{Q_{v,Earth}}{1.2^2 - 1^2} = \frac{Q_{v,space}}{0.2^2 - 0^2} \quad \Rightarrow \quad \frac{Q_{v,Earth}}{Q_{v,space}} = \frac{0.44}{0.04} = 11$$

This indicates that the leak rate in a test on Earth under ambient pressure is in this case 11 times higher than the leak rate in space. Thus, with the previously determined allowed leak rate of $3.81*10^{-3}$ sccs $GN_2$ in space, the allowed leak rate on Earth under ambient pressure can be $4.19*10^{-2}$ sccs $GN_2$.

## Conclusions & recommendations

Under the assumed conditions, the nominally required amount of inflation gas for the straw man concept of the iDod is ~0.059 normal liters. This can be delivered by the smallest available CGG at TNO, which has a capacity of 0.12 normal liters.
When volume, inflation pressure and ambient temperature are all varied by plus or minus 20%, the required amount of inflation gas varies between 47% below nominal and 80% above nominal.

A test for leak rate has to be performed for the inflatable structure. This can be done by measuring the reduction in internal pressure over a certain time span. However, it has to be kept in mind that when this test is performed under ambient pressure conditions, the allowable leak rate is 11 times larger than the one determined for space conditions (which is a good thing).

It is recommended to avoid high inflation pressures. Having a low inflation pressure will always reduce the required amount of inflation gas irrespective of inflation volume and ambient temperature.

The allowable leak rate depends upon rigidization time in an inversely proportional linear manner. Thus, short rigidization times lead to larger allowable leak rates. It is therefore recommended to strive for a short rigidization time, since then the required gas-tightness of the structure is attainable without too much effort.

Further work

The required amount of inflation gas needs to be determined more accurately at a later stage in the design when more information is available regarding the dimensions, inflation pressure, and ambient temperature of the iDod.

The allowable leak rate needs to be determined when the rigidization method and rigidization time is known.

Inputs and outputs

The inputs and outputs are presented in the below table:

| **Inputs** | **Outputs** |
|---|---|
| Inflation pressure of 0.2 bar (assumed) | Nominal required amount of inflation gas is 0.059 normal liters |
| Ambient temperature of 250 K (assumed) | |
| Dimensions inflatable structure | Required amount of inflation gas varies between -47% and +80% with respect to the nominal value when all variables are varied with plus or minus 20% |
| Capacity smallest available CGG (0.12 normal liters) | |
| Rigidization time (1 hour, assumed) | |
| | Allowable leak rate is $3.81*10^{-3}$ sccs $GN_2$ for 1 hour rigidization time under worst-case conditions |
| | |

*Table 2 Inputs and outputs*

Changes to the previous version

With respect to the previously released version, several important changes have been incorporated into this document:

- The standard conditions have been changed to 273 K and 1013 mbar instead of 300 K and 1000 mbar. This has been done since it is anticipated TNO also uses these values for their standard conditions. If this is the case, no conversion has to be applied between the values for the required amount of inflation gas obtained here and the values used by TNO to indicate the capacity of their CGGs.
- A sensitivity analysis for the required amount of inflation gas has been added.
- Several uncertainties that influence the required amount of inflation gas have been added.
- An allowable leak rate has been determined for the inflatable structure.
- A “testing” section, an “inputs and outputs” section, and the current section have been added.

References

1. Groot, B.C.H. de, *Inflatable Gravity Gradient Boom System Development*, Delfi-1 documents SLR 142-149, Faculty of Aerospace Engineering, Delft University of Technology, June 2003.

2. Leak detection, *The flow of gases in leaks,* http://www.leakdetection-technology.com/ , viewed October 2006.

3. Maessen, D.C., *Straw man concept design description,* iDod document iDod.DD.001, Faculty of Aerospace Engineering, Delft University of Technology, September 2006.

*4.* Zandbergen, B.T.C., *Leak analysis fundamentals*, internal document, Faculty of Aerospace Engineering, Delft University of Technology, August 2006.

# Effects of atomic oxygen (AO) on space inflatable materials

## Introduction

Atomic oxygen is the dominant gaseous species in the low Earth orbit space environment. It is produced by the photo-dissociation of molecular oxygen by energetic photons in the Vacuum Ultra-Violet (VUV) range (100 ~ 200 nm). Due to the very long mean free path length in LEO, ~$10^4$ m, the probability of re-association of these atoms is very low. Because of the high orbital velocity of spacecraft, incident AO impinges on a satellite with a kinetic energy of about 4 to 5 eV and with flux values as high as $10^{14}$ to $10^{15}$ atoms/cm$^2$/s. This can cause significant erosion of polymer material. In addition, AO has been observed to alter optical and thermal properties of polymers (including paints, thin films, and composites) [Jenkins, 2001, Ch 8].

This document assesses the threat AO poses to the structural integrity of the iDod. This is done by determining the surface erosion of pristine Kapton under the conditions the iDod encounters during its life. This is done via a method described in chapter 8 of [Wertz, 1999], via a method described in chapter 8 of [Jenkins, 2001], and by making use of ESA's internet tool SPENVIS (Space Environment Information System).
The reason for using three different methods is that no tool can accurately predict the erosion due to AO. This way, a more solid estimate of the erosion can be made.

## Work done

*General information*

The erosion depth of pristine Kapton can be determined when the orbit decay rate of the spacecraft is known. At columns 37 and 38 in the back cover of [Wertz, 1999] a rough orbit lifetime estimate for a spacecraft with ballistic coefficient $C_B$ = 50 kg/m$^2$ is provided. For the cubesat-iDod combination, $C_B$ = 1.587 kg/m$^2$ [Maessen, 2006, iDod.DD.001]. Thus, the values found in [Wertz, 1999] need to be multiplied with 1.587/50 to obtain the decay rate of the current spacecraft. A nice coincidence is that $C_B$ = 50 kg/m$^2$ is also the ballistic coefficient for a one unit CubeSat (assuming $C_d$ = 2.0).

Below, the estimated orbit lifetimes are depicted.

| | **Estimated orbit lifetime [days]** | | | |
|---|---|---|---|---|
| | **Solar minimum** | | **Solar maximum** | |
| **Alt. [km]** | **$C_B$ = 50 kg/m$^2$** | **$C_B$ = 1.587 kg/m$^2$** | **$C_B$ = 50 kg/m$^2$** | **$C_B$ = 1.587 kg/m$^2$** |
| 100 | 0.06 | 0.002 | 0.06 | 0.002 |
| 200 | 1.65 | 0.05 | 1.03 | 0.03 |
| 300 | 49.9 | 1.58 | 11.0 | 0.35 |
| 400 | 552.2 | 17.5 | 77.4 | 2.46 |
| 500 | 1205 | 38.3 | 801 | 25.4 |
| 600 | 3430 | 109 | 2580 | 81.9 |
| 700 | 13400 | 425 | 12600 | 400 |
| 800 | 42000 | 1333 | 41000 | 1302 |
| 900 | 128000 | 4063 | 127000 | 4032 |
| 1000 | 341000 | 10825 | 340000 | 10794 |

*Table 1 Orbit lifetime estimation*

According to the values in the previous table, the time to de-orbit for the cubesat with deployed iDod when starting at a 1000 km high orbit is about 29.5 years. Using STK 7, this is 25 years [van Breukelen, 2006, ISIS[1].iDod.TN.002]. The lifetime estimation of STK 7 is regarded to be more accurate than that of [Wertz, 1999]. However, the latter estimation is used in the three analyses since it takes a lot of time to determine the time spent in a certain orbit range using STK 7 and only a rough estimation of the erosion needs to be obtained.

From table 1 it can be deduced how long the satellite with deployed iDod spends in a particular altitude range:

| | **Solar minimum** | **Solar maximum** |
|---|---|---|
| **Alt. range [km]** | **Time spent in altitude range [days]** | **Time spent in altitude range [days]** |
| 200-300 | 1.5 | - |
| 300-400 | 15.92 | 2 |
| 400-500 | 20.8 | 22.9 |
| 500-600 | 70.7 | 56.5 |
| 600-700 | 316 | 318 |
| 700-800 | 908 | 902 |
| 800-900 | 2730 | 2730 |
| 900-1000 | 6762 | 6762 |

*Table 2 Time spent in altitude range for satellite with deployed iDod*

The angle of incidence of the AO with respect to the object affects the magnitude of erosion which is suffered in a certain time span. The incidence angle ($\theta$) is defined as follows:

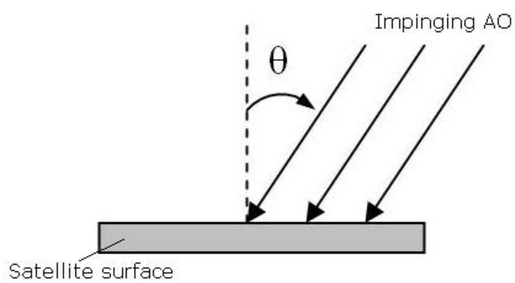


*Figure 1 Incidence angle definition*

Less damage occurs for larger angles and the damage decreases in a cosine-like curve for increasing incidence angle. For all three analyses it is assumed that the AO impinges on the iDod head-on (in ram direction) and will thus cause maximum erosion.

*Method from [Wertz, 1999]*

In chapter 8 of [Wertz, 1999], a method is presented with which the erosion depth of pristine Kapton can be estimated. There, it is said that Kapton erodes at a rate of approximately 2.8 $\mu$m for every $10^{24}$ atoms/m$^2$ of atomic oxygen fluence. The fluence F over a time interval T is there given as:

$$F = \rho_N VT \quad (1)$$

Where $\rho_N$ is the number density of AO and V is the satellite velocity.

For a particular circular orbit, V is easily determined using the table in the back cover of [Wertz, 1999]. For a certain orbit range, V is taken as the orbital velocity at the average orbit height. Thus, for the range 600-700 km, the velocity for a 650 km high orbit is selected. The time interval T spent in a certain orbit range is equal to the time indicated in table 2 for that orbit range. The number density of AO is obtained from [SPENVIS, 2001] where the atmosphere model MSISE-90 is used to model the Earth's atmosphere at various conditions:

| Altitude [km] | AO number density at solar minimum [$m^{-3}$] | AO number density at solar maximum [$m^{-3}$] |
|---|---|---|
| 100 | $6.58*10^{17}$ | $1.10*10^{18}$ |
| 200 | $2.80*10^{15}$ | $1.49*10^{16}$ |
| 300 | $2.24*10^{14}$ | $4.29*10^{15}$ |
| 400 | $2.00*10^{13}$ | $1.48*10^{15}$ |
| 500 | $1.91*10^{12}$ | $5.38*10^{14}$ |
| 600 | $1.95*10^{11}$ | $2.01*10^{14}$ |
| 700 | $2.13*10^{10}$ | $7.76*10^{13}$ |
| 800 | $2.48*10^{9}$ | $3.07*10^{13}$ |
| 900 | $3.06*10^{8}$ | $1.24*10^{13}$ |
| 1000 | $3.50*10^{7}$ | $5.00*10^{12}$ |

*Table 3 AO number densities*

The entries at 1000 km altitude are not listed in [SPENVIS, 2001], but added by the author (educated guesses). The number densities at intermediate altitudes (150 km, 250 km, etc.) are obtained by fitting an exponential curve through the data points from table 3:

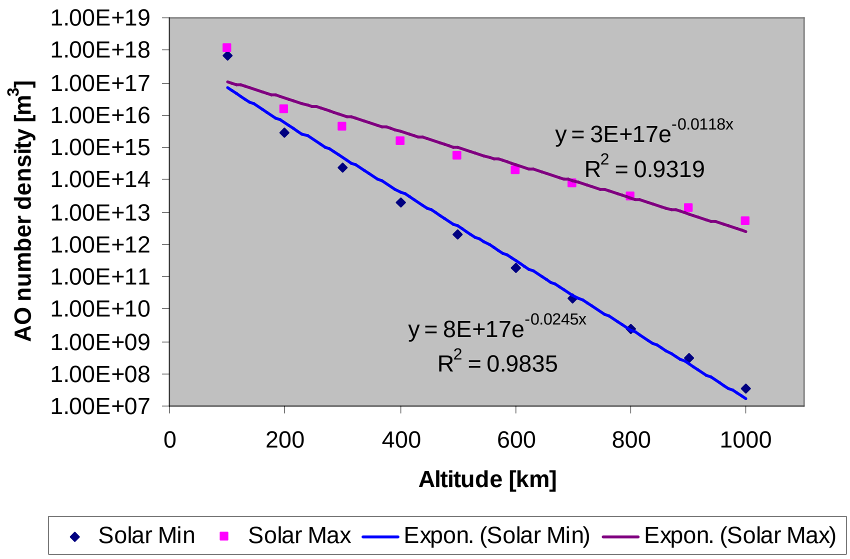


*Figure 2 AO number density variation*

The number densities obtained in this way are used as the number densities for the various altitude ranges. Now, the AO fluence for each altitude range is determined (the range 100-200 km is omitted since the time spent in that range is negligible):

| | Solar minimum | Solar maximum |
|---|---|---|
| Alt. range [km] | AO fluence [atoms/$m^2$] | AO fluence [atoms/$m^2$] |
| 200-300 | $1.76*10^{24}$ | 0 |
| 300-400 | $1.60*10^{24}$ | $6.42*10^{24}$ |
| 400-500 | $1.79*10^{23}$ | $2.24*10^{25}$ |
| 500-600 | $5.21*10^{22}$ | $1.69*10^{25}$ |
| 600-700 | $2.00*10^{22}$ | $2.90*10^{25}$ |
| 700-800 | $4.91*10^{21}$ | $2.51*10^{25}$ |
| 800-900 | $1.27*10^{21}$ | $2.32*10^{25}$ |
| 900-1000 | $2.69*10^{20}$ | $1.75*10^{25}$ |
| Total | $3.62*10^{24}$ | $1.40*10^{26}$ |

*Table 4 AO fluence*

Using equation (1), the amount of Kapton erosion is now:

| **Condition** | **Erosion depth [μm]** |
|---|---|
| Solar minimum | 10 |
| Solar maximum | 393 |

*Table 5 Kapton erosion depth using the method from [Wertz, 1999]*

Both values are extreme values that will never occur in real life. The main reason for this is that during 25 years, the sun will experience two solar cycles (one cycle lasts about 11 years) in which its intensity varies between its maximum and its minimum value in a sine-like wave.

The spacecraft will thus never experience only solar minimum or solar maximum conditions during its lifetime, as is assumed here. Therefore, the actual erosion will be somewhere in between the values obtained using this method. For that value, the root-mean-square (RMS) value is taken. This statistical value is often used to denote the magnitude of a varying quantity. This variation commonly is a sine-like wave. The RMS is determined as follows:

$$x_{RMS} = \sqrt{\frac{1}{N}\sum_{i=1}^{N} x_i^2} = \sqrt{\frac{x_1^2 + x_2^2 + ... + x_N^2}{N}} \quad (2)$$

The only values known in this case are the two values from table 2. Inserting these values into the above equation yields an RMS value of 278 μm. Thus, the RMS erosion depth for pristine Kapton using [Wertz, 1999] is 278 μm.

*Method from [Jenkins, 2001]*

The parameter $\gamma^*$ has been proposed to estimate the erosion yield for hydrocarbon polymers [Jenkins, 2001, Ch 8]:

$$\gamma^* = \frac{M^* N_T}{\rho\left(N_C - N_O\right)} = \frac{M^* \gamma}{\rho} \quad (3)$$

In the above formula, $N_T$, $N_C$, and $N_O$ represent the total number of atoms, the number of carbon atoms, and the number of oxygen atoms in the polymer repeat unit respectively. M* is the average atomic weight of the polymer repeat unit and $\rho$ is equal to the polymer density. The ratio $M^*/\rho$ is about constant for most polymers and $\gamma$, the chemical structure parameter, can be easily determined when the repeat unit of the polymer is known.

The standard erosion yield parameter R is given by [Jenkins, 2001, Ch 8]:

$$R = \frac{M}{AF} \quad (4)$$

The symbol M indicates mass loss (g), A is the exposed area ($m^2$), and F is the atomic oxygen fluence (atoms/$cm^2$). Dividing the above equation by $\rho$ yields the commonly used erosion yield parameter $R_e$ ($cm^3$/atom):

$$R_e = \frac{R}{\rho} \quad (5)$$

It is desired to use a material for which $R_e$ is small. The relationship between $R_e$ and $\gamma$ is nearly linear, which indicates that polymers with a low value for $\gamma$ will in general erode less fast than polymers with a high value for $\gamma$.

In figure 3 a nomogram from [Jenkins, 2001, Ch 8] is provided with which the erosion depth (thickness loss) for a certain polymer due to AO impingement can be estimated for a certain orbit and a certain time span. Note: this nomogram is only valid for *standard* atmospheric conditions, not for conditions during solar minimum or solar maximum!
The figure works as follows: suppose a satellite at an altitude of 350 km has a lifetime of ~400 days. This combination yields a certain point on the nomogram. This point lies on a line for which the AO fluence is constant and equal to $10^{22}$ atoms/cm$^2$ (solid line). This solid line crosses the dotted lines for constant erosion yield parameter $R_e$ at certain points. For the unknown material used in the example, $R_e = 0.1*10^{-24}$ cm$^3$/atoms. The cross point of the correct solid and dotted line now indicates the total erosion depth of the material in $\mu$m. In this case, the expected erosion depth after 400 days is 10 $\mu$m when assuming head-on impingement.
In [Jenkins, 2001], it is not mentioned that figure 3 is valid for standard atmospheric conditions. However, this can be determined using equation (1) by filling in the numbers valid for the above example. This will yield a required AO particle density of $3.76*10^{14}$ atoms/m$^3$. This is a close match to the AO particle density found in table 7-2(b) of [SPENVIS, 2001], which is valid for mean atmospheric conditions. There, for an altitude of 340 km, the AO particle density is listed as $3.53*10^{14}$ atoms/m$^3$ (350 km is not listed in the table).

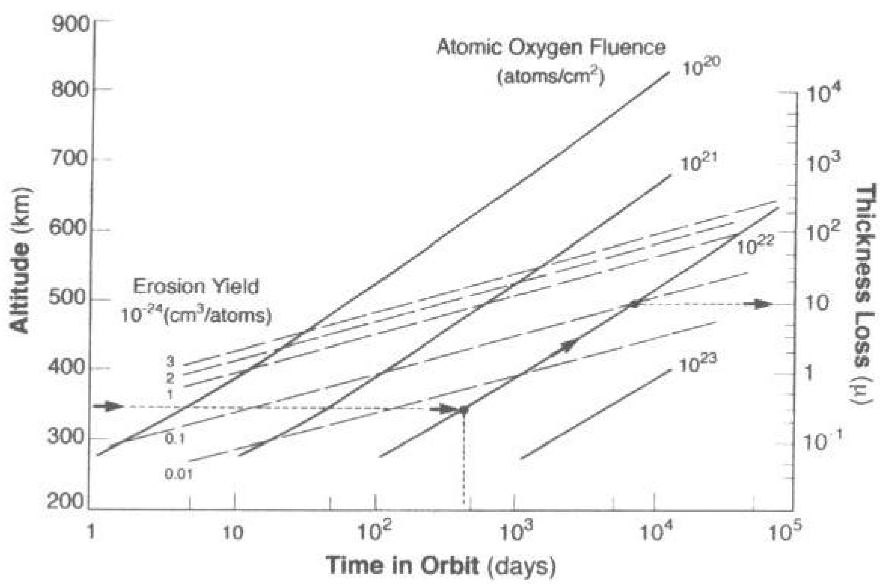


*Figure 3 Nomogram for estimating material erosion depth*

Using the previous figure, the erosion depth for pristine Kapton can be estimated (for pristine Kapton, $R_e = 3.0*10^{-24}$ g/atom [Jenkins, 2001, pg 289 and Reddy, 1995, table VII]). However, the orbit decay rate for standard atmospheric conditions cannot be readily obtained from [Wertz, 1999]. A quick way around this problem is to use the orbit decay data for solar minimum and solar maximum conditions in table 2 and to determine the erosion depth for both conditions. The erosion depth for standard atmospheric conditions will then lie in between the obtained values.

| | **Solar minimum** | | **Solar maximum** | |
|---|---|---|---|---|
| **Alt. range [km]** | **Time spent in altitude range [days]** | **Erosion depth [μm]** | **Time spent in altitude range [days]** | **Erosion depth [μm]** |
| 200-300 | 1.5 | 5 | - | - |
| 300-400 | 15.92 | 10 | 2 | 1.5 |
| 400-500 | 20.8 | 2 | 22.9 | 2 |
| 500-600 | 70.7 | 2 | 56.5 | 1 |
| 600-700 | 316 | 2 | 318 | 1.5 |
| 700-800 | 908 | 2 | 902 | 2 |
| 800-900 | 2730 | 0.8 | 2730 | 0.8 |
| 900-1000 | 6762 | 0.5 | 6762 | 0.5 |
| **Total** | | **~25** | | **~10** |

*Table 6 Material loss estimation using method from [Jenkins, 2001]*

The current method indicates that the material loss will lie in between 10 and 25 μm assuming standard atmospheric conditions. However, the accuracy of this method is far from good: one has to read off values from a logarithmically scaled figure and the effects of the variation in solar activity are not taken into account. Since solar maximum conditions have a large effect on the erosion depth of a material (see previous method), it is believed that the current method results in an underestimation of the erosion depth due to AO.

Taking into account the difficulty in reading off correct values on a logarithmic scale, the material losses found are multiplied by a factor 2. On top of this factor, another factor 2 is taken into account for the influence of solar maximum conditions. This leads to values of 40 μm and 100 μm. Since standard atmospheric conditions are assumed, the average of the two values is taken. Then, the erosion depth using [Jenkins, 2001] is 70 μm.

*SPENVIS*

The internet tool SPENVIS (www.SPENVIS.oma.be) is an official ESA tool that allows users to make use of various space environment models for specific analyses.

With SPENVIS also the erosion of various materials due to AO impingement can be determined. For the determination of AO erosion depths, the tool works as follows: First, a certain satellite orbit and the duration of that orbit need to be specified. The orbit is then simulated using an orbit simulator. Next, the conditions the satellite is subjected to need to be indicated. These entail the solar activity, the particles under consideration (in this case only AO) and the orientation of the satellite. In addition, the material under investigation has to be selected from a list or has to be specified manually. These conditions are then applied to the selected orbit and various outputs are generated.

Unfortunately, it is not possible to let SPENVIS calculate the complete orbit decay of the satellite taking into account varying solar activity. Thus, a similar approach as the one for the method from [Wertz, 1999] has to be adopted: the orbit decay trajectory is divided up into several distinct parts and for each part the erosion depth for either solar maximum or solar minimum conditions is determined.

However, the approach used here is in several ways different than that of the other methods:

1. Since an orbit simulator is used, it is possible to let the specified orbits be elliptical and not circular as with the other methods. This way, the influence of the exponential decay in the density of the atmosphere is better taken into account. Thus, for the range 900-1000 km, the orbit is not specified as a circular orbit at 950 km, but as an elliptical orbit with its perigee at 900 km and its apogee at 1000 km.
2. The orbit simulator also allows the user to specify the orientation of the orbit in space, this has a significant impact on the results of the simulation, as will be discussed further on.

3. The amount of solar activity has to be specified manually. Based on that, SPENVIS calculates the atmospheric conditions. With the other methods, the atmospheric conditions are readily obtained from literature. Thus, choosing the wrong values for the parameters that indicate the amount of solar activity can result in conditions other than desired. With the other methods, this problem does not exist.

Before discussing the various actions performed and the results, first the settings that are valid for all simulations are provided:

- The orbit start date is always 1 Jan 2007 at 00:00:00 hrs
- The orbit inclination (angle with respect to the equatorial plane of the Earth) is 90°
- The starting true anomaly of the satellite (the satellite's angular position in the orbit) is 0°
- The wind model used is HWM93 (no other model is available)
- The atmospheric model used is NRLMSISE-00
- Thermal motion of particles is taken into account
- The orientation of the satellite is such that maximum erosion occurs. This is the case for a polar angle of 0° and for an azimuthal angle of 0°.
- The erosion depth of pristine Kapton is determined. The erosion yield for this material is selected to be $3.0*10^{-24}$ $cm^3$/atoms (SPENVIS also allows other erosion yields for Kapton).

The amount of solar activity needs to be specified by filling in values for three parameters.

- Previous day's solar 10.7 cm radio flux ($F_{10.7}$, [$Wm^{-2}Hz^{-1}$])
- 81 day average solar 10.7 cm radio flux
- Daily geomagnetic activity index (Ap, [2nT] (nT = nano-Tesla))

The solar 10.7 cm radio flux is a measure of the noise level generated by the sun at a wavelength of 10.7 cm at the Earth's orbit. This index is strongly correlated to the number of sunspots on the sun and therefore an excellent measure for the amount of the solar activity. The daily geomagnetic index is a measure for the average level of geomagnetic activity over the Earth for a given day. It is influenced by the measure of solar activity. The variation in the $F_{10.7}$ index since 1975 is obtained from [BGS]:

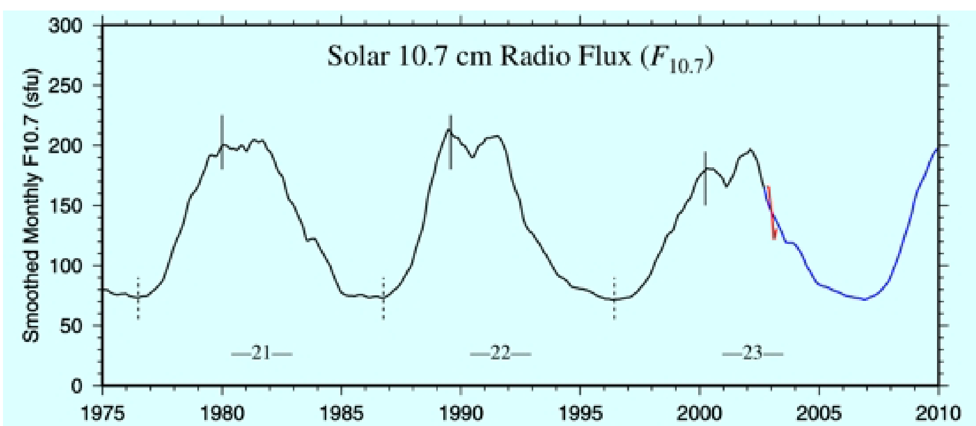


*Figure 4 Solar 10.7 cm radio flux since 1975 [BGS]*

On the vertical axis, the $F_{10.7}$ index has units [sfu], which stands for solar flux unit (= $1*10^{22}$ $Wm^{-2}Hz^{-1}$).

The variation of the Ap index since 1991 is obtained from [SEC] and put into Excel to produce figure 5 ([SEC] only provides a list of numbers). From the same source, also the $F_{10.7}$ index is obtained, which is also inserted into the figure in order to visualize the relationship between the two parameters:

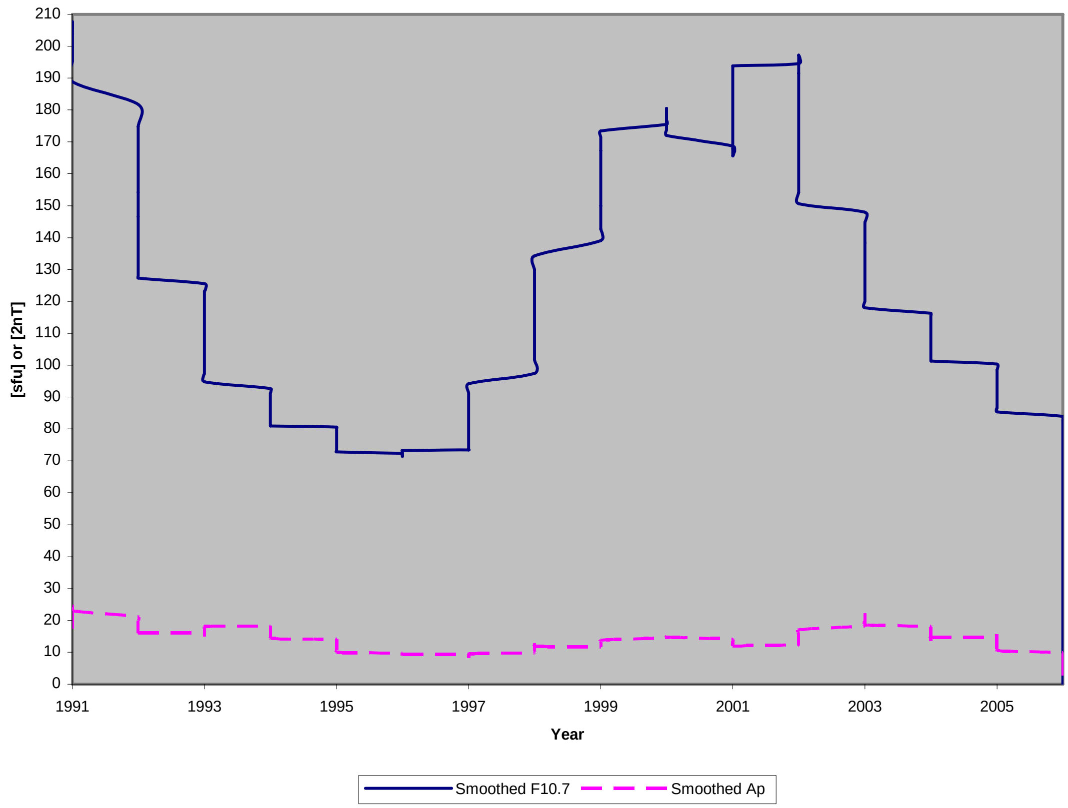


*Figure 5 Smoothed $F_{10.7}$ and Ap indices from [SEC]*

The figure shows that the solar activity influences the Earth's geomagnetic index: low solar activity results in low values for Ap and high solar activity results in high values for Ap. The value for Ap more or less varies between 10 and 20 [2nT].

Using the information from figures 4 and 5, the following values are used to indicate solar maximum or solar minimum conditions:

Solar maximum:

| | |
|---|---|
| Previous day's $F_{10.7}$ [$10^{22}$ $Wm^{-2}Hz^{-1}$] | 210.0 |
| 81 day average $F_{10.7}$ [$10^{22}$ $Wm^{-2}Hz^{-1}$] | 190.0 |
| Ap [2nT] | 20.0 |

Solar minimum:

| | |
|---|---|
| Previous day's $F_{10.7}$ [$10^{22}$ $Wm^{-2}Hz^{-1}$] | 70.0 |
| 81 day average $F_{10.7}$ [$10^{22}$ $Wm^{-2}Hz^{-1}$] | 80.0 |
| Ap [2nT] | 10.0 |

As indicated earlier, the orientation of the satellite's orbit influences the amount of erosion experienced. This orientation is defined by specifying two angles (see also figure 6):

- Right Ascension of the Ascending Node (RAAN or $\Omega$). This is the angle between the ascending node of the orbit and the line from the center of the Earth towards the vernal equinox point (point in the orbit of the Earth indicating the beginning of spring).
- Argument of perigee ($\omega$). This is the angle between the ascending node and the semi major axis of the orbit.

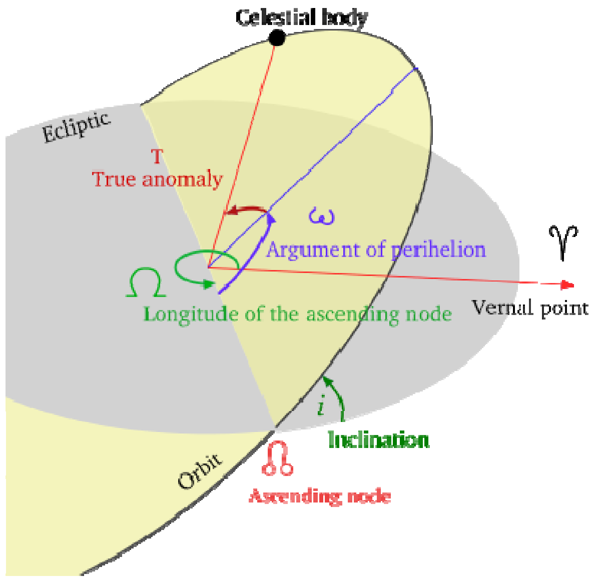


*Figure 6 Definition of orbital elements [Wikipedia]*

A sensitivity analysis has been performed in order to determine the variation in AO fluence as function of Ω and ω. This has been done for an elliptic orbit with an altitude range of 900-1000 km for in a time period of 6762 days (other altitude ranges produce similar effects). The AO fluence has been chosen as output since this number is independent of material choice. However, it is directly proportional to erosion depth and thus a good measure for the severity of the conditions in that particular orbit. The results are depicted in figures 7 and 8.

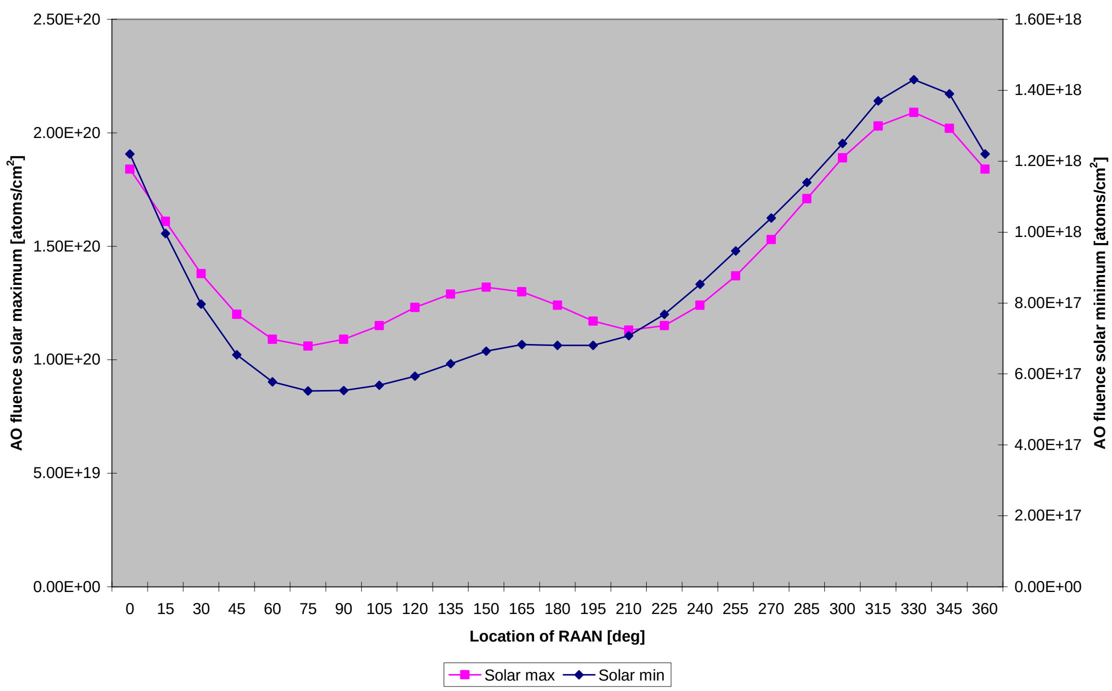


*Figure 7 Variation in AO fluence as function of position of Ω (ω = 0°)*

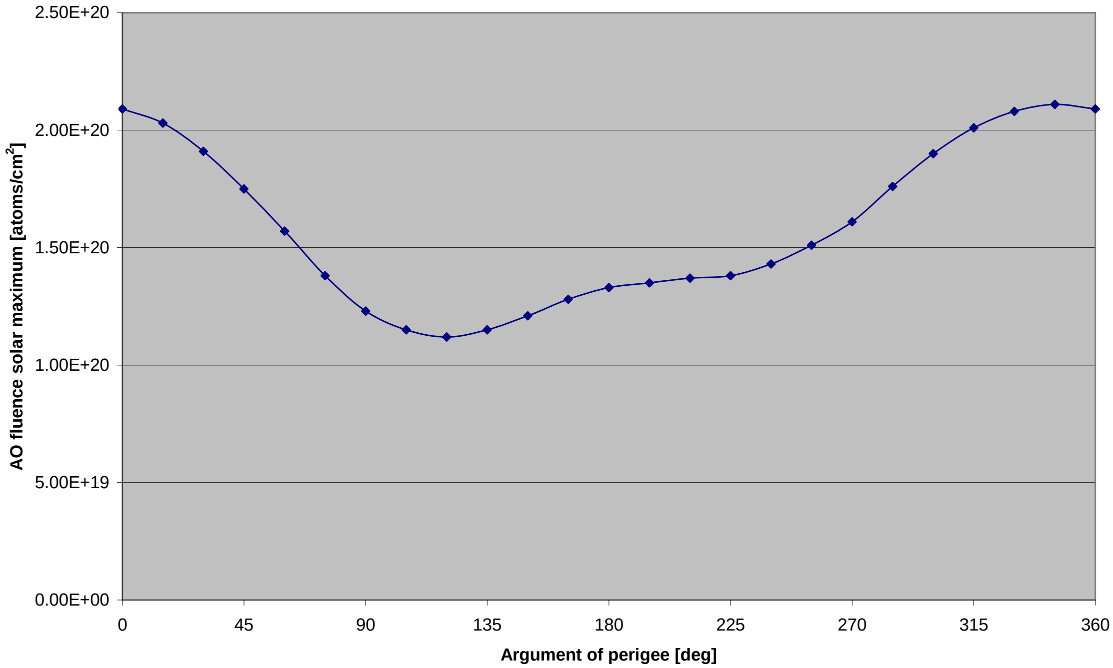


*Figure 8 Variation in AO fluence during solar maximum as function of position of $\omega$ ($\Omega$ = 330°)*

Figure 8 has been created using the position of Ω from figure 7 for which maximum AO fluence occurs (330°). For both figures, the AO fluence varies roughly by a factor of two, depending on the orientation of the orbit. However, one cannot "add" the two figures together to create positions for which the difference in AO fluence is a factor 4. For both figures, the maximum and minimum AO fluence is roughly the same. In addition, the maximum and minimum AO fluence values occur at the same points for solar maximum and solar minimum conditions.

From figures 7 and 8, it is concluded that for maximum AO fluence, the position of the orbit should be such that Ω = 330° and ω = 345°. For minimum AO fluence, the position should be such that Ω = 75° and ω = 120°.
In order to obtain an upper bound for the erosion depth estimation, both solar maximum conditions and maximum AO fluence have to be simulated. For the lower bound, both solar minimum conditions and minimum AO fluence have to be simulated. This has been done and the results of the simulations are depicted in tables 7 and 8. It is noted that the obtained erosion depth is valid for pristine Kapton.

| **Perigee height [km]** | **Apogee height [km]** | **Time in orbit [days]** | **Front fluence [atoms/m$^2$]** | **Front ersosion depth [μm]** |
|---|---|---|---|---|
| 900 | 1000 | 6762 | $2.11*10^{24}$ | 6.32 |
| 800 | 900 | 2730 | $2.44*10^{24}$ | 7.33 |
| 700 | 800 | 902 | $2.40*10^{24}$ | 7.21 |
| 600 | 700 | 318 | $2.63*10^{24}$ | 7.88 |
| 500 | 600 | 56.5 | $1.51*10^{24}$ | 4.53 |
| 400 | 500 | 22.9 | $2.09*10^{24}$ | 6.27 |
| 300 | 400 | 2 | $6.73*10^{23}$ | 2.02 |
| 200 | 300 | - | 0 | 0 |
| **Total** | | | **$1.39*10^{25}$** | **~41.5** |

*Table 7 Erosion depth determination for solar maximum conditions*

Compared to the results of the first method from [Wertz, 1999], the resulting AO fluence and erosion depth is one order of magnitude smaller ($1.40*10^{26}$ atoms/m$^2$ and 393 μm using [Wertz, 1999])!

| Perigee height [km] | Apogee height [km] | Time in orbit [days] | Front fluence [atoms/m$^2$] | Front ersosion depth [$\mu$m] |
|---|---|---|---|---|
| 900 | 1000 | 6762 | $4.36*10^{21}$ | $1.31*10^{-2}$ |
| 800 | 900 | 2730 | $9.48*10^{21}$ | $2.84*10^{-2}$ |
| 700 | 800 | 908 | $1.86*10^{22}$ | $5.57*10^{-2}$ |
| 600 | 700 | 316 | $4.20*10^{22}$ | $1.26*10^{-1}$ |
| 500 | 600 | 70.7 | $6.76*10^{22}$ | $2.03*10^{-1}$ |
| 400 | 500 | 20.8 | $1.59*10^{23}$ | $4.77*10^{-1}$ |
| 300 | 400 | 15.92 | $1.08*10^{24}$ | 3.25 |
| 200 | 300 | 1.5 | $1.04*10^{24}$ | 3.12 |
| **Total** | | | **$2.42*10^{24}$** | **~7.3** |

*Table 8 Erosion depth determination for solar minimum conditions*

Compared to the results of the first method from [Wertz, 1999], the resulting AO fluence and erosion depth are about the same now ($3.62*10^{24}$ atoms/m$^2$ and 10 $\mu$m using [Wertz,1999]).

Taking the RMS average the resulting estimate for the erosion depth using this method is 29.8 $\mu$m.

## Conclusions & recommendations

Even though three different methods have been used to estimate the erosion depth of pristine Kapton due to AO impingement, no method has been found to be satisfying. No method is able to take orbital decay to due aerodynamic drag and/or variation in solar activity into account. Therefore, the errors for all methods are larger than desired.

The average values for the erosion depth are widely different for all methods used: 278, 70 and 29.8 $\mu$m respectively. From these values it is clear that, when using pristine Kapton, a relatively thick layer of material, 30 $\mu$m at least, is required in order to prevent the structure from falling apart during the de-orbit phase.

A positive observation is that during solar minimum conditions, only significant erosion starts to occur below ~500 km altitude.

For now, the worst-case erosion depth estimate is taken as the real erosion depth when using pristine Kapton as structural material. This depth is 278 $\mu$m, which leads to a required Kapton thickness of ~280 $\mu$m.
Using information from [Maessen,2006, iDod.TN.005], this thickness leads to a Kapton weight of >200 g for the straw man concept. This is far above the maximum allowable total system weight of 84 g [van Breukelen, 2006, ISIS.iDod.REQ]. Thus, another material has to be used or a coating has to be applied on the Kapton foil in order to reduce the material erosion due to AO impingement by at least a factor 10. These materials and coatings are readily available and it has to be investigated which option (other material or a coating) results in the best performance.

AO impingement is not the only mechanism known to cause material erosion; other sources of material erosion are UV radiation, space radiation, charged particles, and micrometeoroids and orbital debris (MOD). It is recommended that the (combined) effects of these other mechanisms are also studied in order to obtain more knowledge about their severity with respect to AO impingement and to obtain a better estimate for the total material erosion during the life of the iDod.

## Further work

It has to be investigated which materials and/or coatings have got erosion rates that are at least a factor 10 better than that of pristine Kapton.

More information should be obtained regarding the combined effects of UV radiation and AO on polyimide materials. In addition, the effects of space radiation, charged particles, and micrometeoroids and orbital debris (MOD) on polyimides have to be investigated.

When possible, a better method has to be used in a later stage of the design to estimate the erosion of materials due to AO impingement.

## Inputs and outputs

The inputs and outputs are presented in the below table:

| **Inputs** | **Outputs** |
|---|---|
| Material investigated is pristine Kapton | Average erosion depth due to AO impingement using:<br>• Method from [Wertz, 1999]: 278 μm<br>• Method from [Jenkins, 2001]: 70 μm<br>• SPENVIS: 30 μm |
| De-orbit maneuver takes ~29.5 years | |
| Starting altitude is 1000 km | |
| Orbit inclination is 90° | |
| Head-on AO impingement | |
| Solar maximum and solar minimum conditions are taken into account | |

*Table 9 Inputs and outputs*

## Changes to the previous version

With respect to the previously released version, several important changes have been incorporated into this document:

- Two new methods to determine the erosion depth have been added (method from [Wertz, 1999] and SPENVIS
- An average (RMS) value for the erosion depth is used as final result instead of upper and lower boundaries.
- The angle of incidence of impinging AO has been properly defined
- The figure from [Jenkins, 2001] (figure 3) has been identified to only be valid for average solar activity. This has been taken into account in the final erosion depth estimation for this method. Furthermore, inaccuracies in reading off correct erosion depth values from this figure have also been taken into account for the determination of the final erosion depth value for this method.
- The "conclusions and recommendations" section has been thoroughly revised.
- An "inputs and outputs" section and the current section have been added.

## References

1. Breukelen, E.D. van, *Determination of scenario for iDod baseline conceptual design and range of required inflatable drag surface sizes*. ISIS internal document ISIS[1].iDod.TN.002, July 2006.

2. Breukelen, E.D. van, *Top Level Requirements for inflatable De-orbit device (iDod)*. ISIS internal document ISIS.iDod.REQ, Draft, July 2006.

3. British Geological Survey, *Predicting Space Weather at BGS,* http://www.geomag.bgs.ac.uk/spweather/bgs_predicting.html , viewed September 2006.

4. Jenkins, C.H.M., *Gossamer Spacecraft: Membrane and Inflatable Structures and Technology for Space Applications*, AIAA, Reston (USA), 2001.

5. Maessen, D.C., *Straw man concept design description,* iDod document iDod.DD.001, Faculty of Aerospace Engineering, Delft University of Technology, September 2006.

6. Maessen, D.C., *Tripod mass estimate,* iDod document iDod.TN.005, Faculty of Aerospace Engineering, Delft University of Technology, September 2006.

7. Reddy, M., *Effect of low earth orbit atomic oxygen on spacecraft materials,* Journal of Materials Science, 1995, pp. 281-307.

8. Space Environment Center, *Recent Solar Indices*, http://www.sec.noaa.gov/ftpdir/weekly/RecentIndices.txt (last update 6 September 2006), viewed September 2006.

9. SPENVIS, *The neutral Earth atmosphere,* http://www.spenvis.oma.be/spenvis/ecss/ecss07/ecss07.html (last update 17 April 2001), viewed September 2006.

10. Wertz, J.R., Larson, W.J., *Space Mission Analysis and Design*, Third Edition, Kluwer Academic Publishers, Dordrecht (NL), 1999.

11. Wikipedia, *Orbital elements,* http://en.wikipedia.org/wiki/Orbital_parameters (Last update 28 August 2006), viewed September 2006.

# Connector piece design and construction


## SUMMARY

Two flexible connector piece prototypes are developed; one made from polyethylene foil, and one from silicone rubber. Both connector pieces can be constructed in a satisfactory manner.

The silicone connector piece proves to be far more heavy and voluminous than the connector piece made from foil. Therefore, it is decided to use the foil connector piece for further development of the inflatable structure of the iDod.



## KEYWORDS

Connector piece, polyethylene, silicone


## DISTRIBUTION

| | Name | | Company / Institution |
|---|---|---|---|
| 1 | E.D. van Breukelen | Customer | ISIS B.V. |
| 2 | O.K. Bergsma | Project supervisor | TU Delft |

## APPROVAL

| | Name | Company / Institution | Date | Signature |
|---|---|---|---|---|
| *Written* | D.C. Maessen | TU Delft | 3/2/2007 | |
| *Checked* | | | | |
| *Approved* | | | | |

## REVISION RECORD

| Issue | Date | Total pages | Affected pages | Brief description of change |
|---|---|---|---|---|
| Draft | 3/2/2007 | 18 | | |
| | | | | |

## LIST OF TBD'S AND TBC'S

| TBD/TBC | Paragraph | Subject | Due date | Action by |
|---|---|---|---|---|
| TBD | Section 5 | Proper application of composite to connector piece | ?? | ?? |
| | | | | |
| | | | | |

## TABLE OF CONTENTS

# 1 INTODRUCTION

The current document treats the design and construction of two connector piece prototypes. The connector piece's function is to provide an airtight, flexible connection. This is to be done at the point where five inflatable tubes of the inflatable structure of the hybrid pyramid version of the iDod meet:

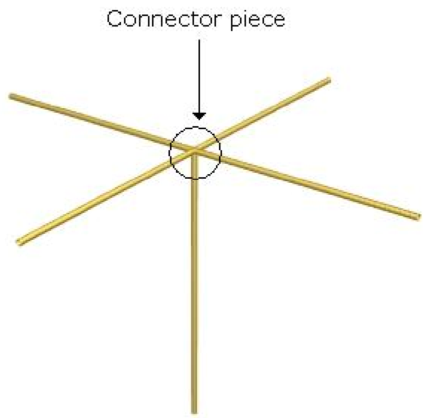


*Figure 1 Connector piece position*

A description of the hybrid pyramid concept can be found in [Maessen, iDod.TO.001].

One prototype is made from foil; the other is made from silicone rubber. The foil connector piece is treated in section 2. The silicone connector piece is treated in section 3.

# 2 FOIL CONNECTOR PIECE

The current section treats the development and production of a connector piece made from foil. Subsection 2.1 deals with the initial development, while subsection 2.2 deals with the construction of a PE (polyethylene) connector piece using adhesive (RUPLO CA-adhesive 100-S and 1500-S).

## 2.1 Foil connector development

For the initial development, use is made of PET (polyethylene terephthalate) foil coated on one side with PE (supplier: Hakapak, Eindhoven (NL)). This foil was readily available at the faculty.

The goal of the development is to design and construct a connector piece that connects five tubes of 20 mm diameter at right angles. During this initial development, the flaps of the connector piece are connected to each other using double sided tape (3M). For the later PE connector pieces, the flaps are bonded together using adhesive.

The development of the connector piece starts with a design from [Bernasconi, 1999] for four tubes at right angles and is gradually changed and improved into the final connector piece. This gradual development is discussed in the coming subsections.

### *2.1.1 Original connector*

The starting point for the connector piece is one from [Bernasconi, 1991] for four tubes at right angles. This connector is shown in the next three figures. The connector piece is created by attaching side 1 to side 6, side 2 to side 3, and side 4 to side 5 (see figure 2).

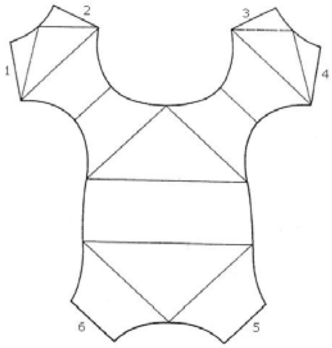


Figure 2 Connector piece layout [Bernasconi, 1991]

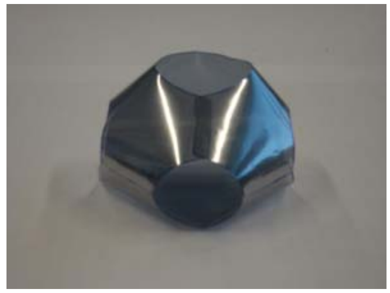

Figure 3 Front view original connector

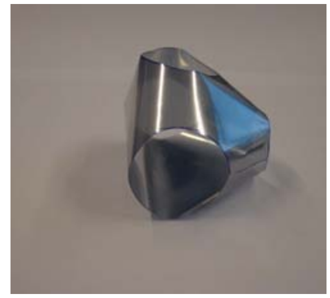

Figure 4 Side view original connector

### *2.1.2 Connector version 1*

Version 1 of the connector piece is created by mirroring the top part of the original connector in a horizontal line. Now, five tubes can be connected to each other.

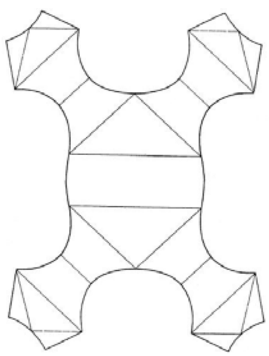

Figure 5 Layout connector piece version 1

Figure 6 Top view version 1

Figure 7 3D view version 1

However, there are some obvious flaws for this connector: Note that the diameters of the holes are not the same for the new connector piece. Referring to figure 6, the central hole is smaller than the upper and lower holes, which in turn are smaller than the left and right holes (not really visible as such in the picture itself). In addition, the four holes for the “spokes” are not at the same height. This is visible in figure 7 where two holes are supported and the other two holes are ‘floating’ in the air.

### *2.1.3 Connector version 2*

After creating version 1, it was realized that the length of the sides of the connector piece determine the circumference of the four “spoke” holes. This is indicated by the thick lines in the next figure:

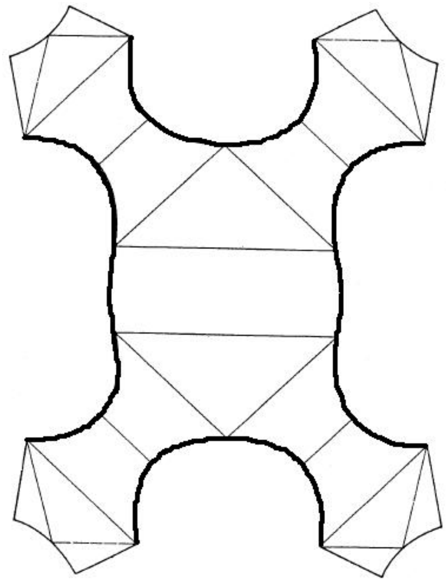

*Figure 8 "Spoke" holes circumference indicated for connector piece version 1*

Several changes are now made in version 2 with respect to version 1: the flaps are broadened to increase the diameter of the top hole (which was a bit too small) and the length and width of the central section is reduced and made equal to obtain equally sized “spoke” holes.

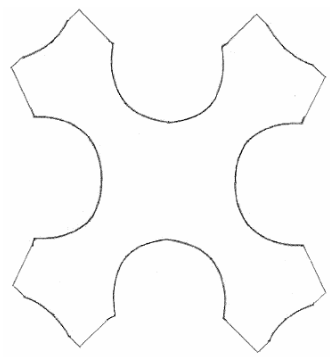

*Figure 9 Layout connector piece version 2*

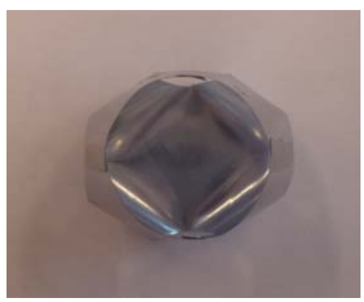

*Figure 10 Top view version 2*

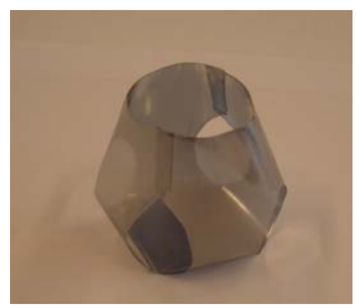

*Figure 11 3D view version 2*

For this version, the spoke-holes are now roughly equal in size and no holes are “floating” in the air anymore. However, the flaps were made too wide, which resulted in the hole for the central tube being too large.

### 2.1.4 Connector version 3

In the third version, the length of the flaps is increased and the width of the flaps is reduced to roughly the original width. The reason for increasing the length of the flaps is provided in subsection 2.1.5.

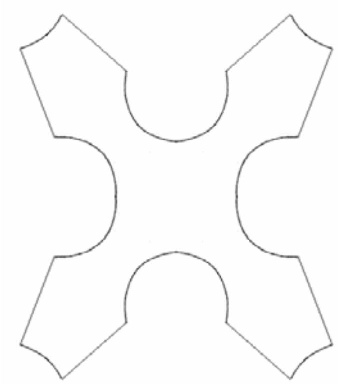

Figure 12 Layout connector piece version 3

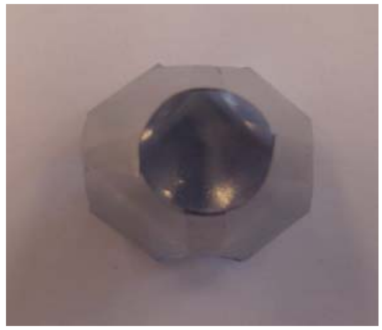

Figure 13 Top view version 3

Figure 14 3D view version 3

Due to a drawing error, increasing the length of the flaps unfortunately resulted in the flaps having a ‘short’ and a ‘long’ side. This is clearly visible in figure 12. This led to the holes that are created by bonding two ‘short’ sides together, to be not as round as the other holes. At the point where the two flaps are joined, the lines of the hole meet at a ~90° angle:

Figure 15 Sharp edged hole

This error is corrected in version 4. Furthermore, the central hole of version 3 is a bit too small (∅ ≈ 15 mm) and is corrected in version 4 by making the flaps at tiny bit broader at their end.

### 2.1.5 Connector version 4

This connector piece is made completely symmetrical. For this, imagine that the layout of connector version 3 is divided into eight parts (each 45° ‘wide’). Now, the part of the connector layout which lies in the first of these half quadrants is mirrored multiple times to create the new layout. That part is also made wider since the flap is otherwise far too slender. In addition, the half circles from which the spoke holes are created are made rounder near the flap to obtain more round holes for the spokes. The edges that overlap and are bonded together are also indicated.

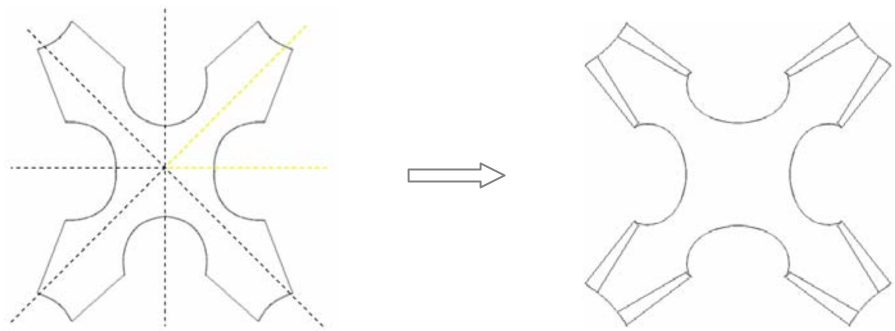

*Figure 16 From connector piece version 3 to version 4*

The dimensions (in mm) of the final connector piece are indicated below:

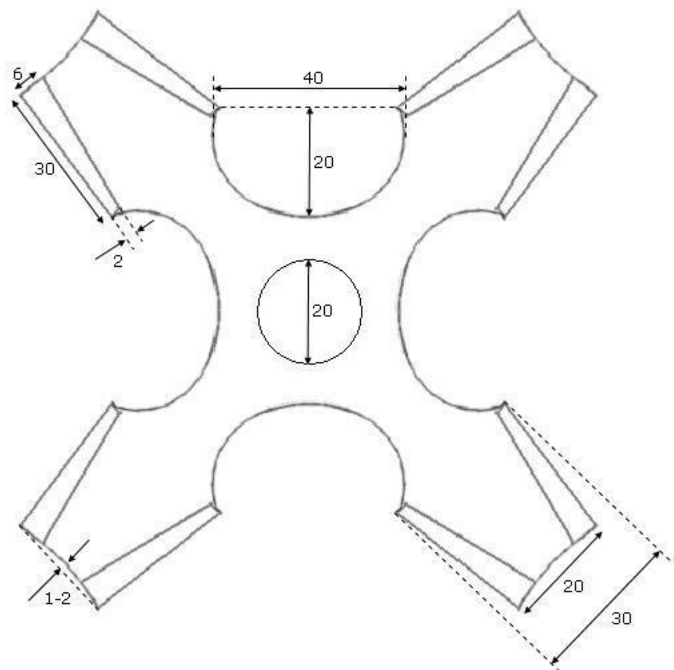


*Figure 17 Connector piece version 4 with dimensions*

The circle in the middle is used as an alignment aid when attaching the central tube to the connector piece (see [Maessen, iDod.CM.004]). A top view and a 3D view of this version are depicted below.

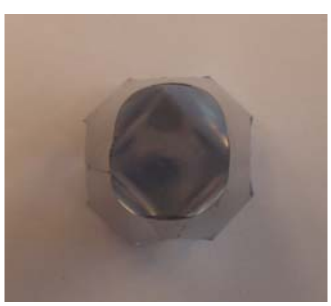

*Figure 18 Top view version 4*

*Figure 19 3D view version 4*

The angles of the sides of the connector are roughly 10° off vertical. At the time of developing the connector piece, it was thought that having such a small angle eases the connection of the

spokes to the connector piece and also helps in creating an angle close to 90° between the spokes and the central strut.
After connecting the inflatable tubes to the connector piece further on in the development, the first argument proved to be false: Since a rather broad band of adhesive is used to connect a tube to the connector piece, the small angle of the sides is irrelevant since the adhesive easily covers both a part of the tube and a part of the connector piece.
The second argument also proved to be incorrect. Due to the production method chosen (see [Maessen, iDod.CM.004]), the angle between the spokes and the central tube is always close to 90° (except in the case of production errors).

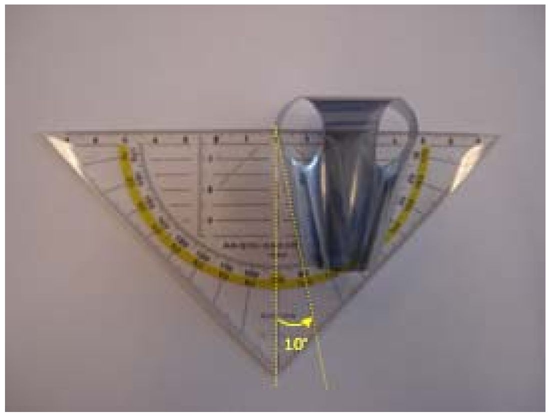


*Figure 20 Angle of a side of connector version 4*

Why then is it important to have such long flaps that result in small angles? As it turns out, the length of the flaps is useful when a connector piece for 10 mm diameter tubes needs to be created. Then, one's fingers are approximately as wide as a connector piece flap is long (it is assumed the current connector piece is then simply made 50% smaller). Fingers then become very crude tools to construct a connector piece and when the flaps are even shorter than now, producing a proper connector piece will be a very difficult and irritating job.
Thus, the relatively long flaps are not necessary to facilitate a proper orientation of the "spokes", but for creating the connector piece itself.

Lastly, all connector piece versions are captured in one view:

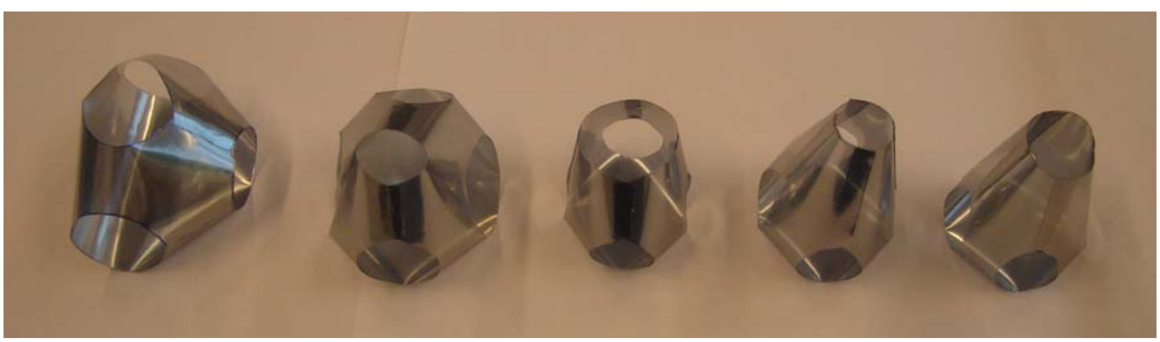

*Figure 21 Connector piece evolution*

## 2.2 PE connector piece construction using adhesive

Since the inflatable tubes are made from PE (see [iDod.CM.001]), the developed connector piece is also made from PE instead of PET/PE. Adhesive testing, described in iDod.CM.003, resulted in the selection of RUPLO CA-adhesives 100K-S and 1500-S (CA = cyano-acrylate) as promising candidates for adhesion of the bonds of the connector piece. Since these adhesives were officially expired, new adhesives were ordered. But, the 100K-S variant was no longer available and instead a variant called 100-S is used. No apparent differences between the two variants were noticed. Two connector pieces were constructed using the 100-S variant and two other connector pieces were constructed using the 1500-S variant.

Bonding the flaps of the connector piece together using adhesive without some means of holding the flaps in the correct position is impossible. Therefore, tape is used to connect the flaps to each other. Call the flaps “flap 1” and “flap 2” and let flap 2 be on the outside of the bond. Now do the following: Apply tape on the outside *and* inside of the bond. Also, make sure that the tape covers the bond from spoke hole to central hole. This way, the complete bond surface is pressed together by the tape. If this is not done, often the edges of the bond near the holes will not be in contact, preventing a good seal from being formed. Although these edges are very likely to be filled with adhesive once the tubes are connected to the connector piece, bonding them together lower the risk of peeling a part of the bond loose by accident.

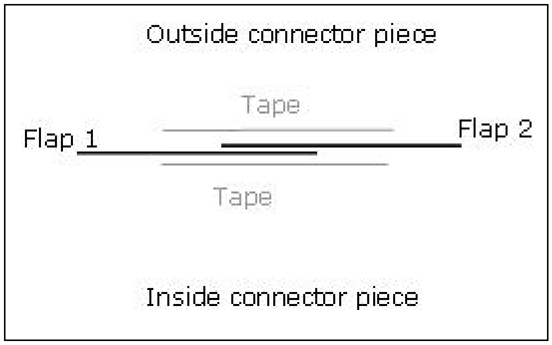


*Figure 22 Tape on two sides of a bond*

Now, the tape on the outside of the connector can be peeled of flap 1 (don’t peel it of flap 2!) such that primer and adhesive can be applied on the faces to be bonded together while the connection between the flaps is maintained by the tape at the inside of the connector piece. After application of the adhesive, the bond can be restored by attaching the peeled-of piece of tape again to flap 1.

When the adhesive has cured sufficiently (the day after the adhesive has been applied), remove the tape on the inside of the connector piece using a tweezers (“pincet”) and a small pincer (“tang”). Doing this by hand is close to impossible and you risk damaging the connector piece. First, peel a small flap of tape loose near the central hole of the connector piece (for this, the thin tweezers is the most useful tool). Then, using the pincer (since it has much grip), remove the tape by pulling it loose while sticking the pincer through a spoke hole. This way, the tape is easily peeled of the foil. Removing the tape on the outside of the connector piece is easy.

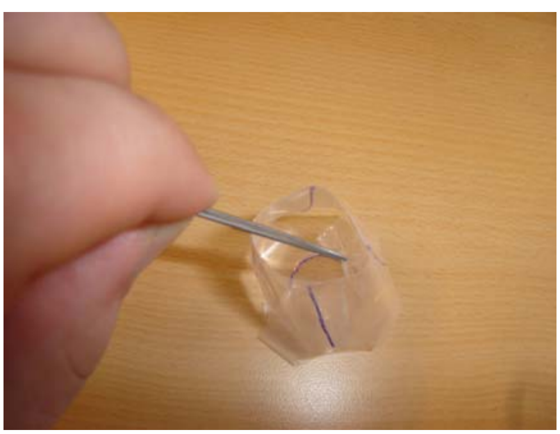

*Figure 23 Using the tweezers*

*Figure 24 Using the pincer*

The connector pieces created have got, as desired, flexible bonds. However, two bonds (one using 100-S and one using 1500-S) were not wetted properly by adhesive or primer and about 1 cm of bond length was not bonded at those bonds. Fortunately, applying primer and adhesive a second time at the two failed bonds resulted in a satisfactory bond. Thus, it is possible to 'repair' bonds that are not bonded over their entire length.

The bonds created using the 100-S variant are more flexible than those created with the 1500-S variant. Therefore, future connector pieces will all be made using RUPLO CA-adhesive 100-S.

The weight of a completed connector piece is measured to be 0.5 $\pm$ 0.05 g (the measurement is accurate up to 0.01 g, but connector pieces can be slightly smaller/larger and the mass of the adhesive used can be slightly larger/smaller).
The thickness of the PE foil is 0.09 $\pm$ 0.01 mm while the total surface area of a connector piece is measured to be 59 $\pm$ 1 $cm^2$. The volume of a connector piece then lies between 0.464 $cm^3$ and 0.600 $cm^3$.
Since these are the weight and volume of a connector piece for 20 mm tubes, the weight and volume of a PE connector piece for 10 mm tubes is estimated to be 0.25 g and 0.27 $cm^3$ respectively.


*Figure 25 Four adhesively bonded connector pieces*

# 3 SILICONE CONNECTOR PIECE

The other option for a connector piece is to create it from silicone rubber. The advantage here is that a well-defined and easy connection can be made. The disadvantage is that the silicone connector is much thicker than the foil version, which leads to a mass and volume penalty.

## 3.1 Mold options

The mold for the connector piece can either be made out of one wax piece or by using five metal rods that can be assembled and disassembled.

The wax mold has the advantage that it does not need to be taken apart once the silicone connector piece has been made and the mold needs to be removed from the product. To remove the mold from the connector piece, the entire part can be heated in an oven. This causes the wax to melt and flow away, resulting in a mold-free connector piece. This is the well-known lost-wax method. The obvious disadvantage is that every new connector piece requires a new wax mold, which is relatively costly due to the small number of connector pieces required.

Contrary to the wax mold, the metal mold can be used indefinitely to create connector pieces. The disadvantage is that the mold needs to be detachable in order to be able to separate the mold from the product. Furthermore, the rods need to be shaped preferably such that a smooth transition is created at the point where all the rods meet in order to reduce undesired stresses in the connector piece once pressurized. However, this is not possible when the mold has to be detachable as well. Instead, clay can be used to smoothen out any corners. The clay can easily be removed after the metal rods have been removed from the connector piece.

Since circumstances allowed the metal mould to be manufactured free of charge and in a short time, this option has been chosen. The mold is depicted below.

*Figure 26 Metal mold*

The central block of material is made from aluminum and is roughly 20x20x15 mm. Three holes are drilled through and through the block and treaded to create M5-sized holes. The edges of the block were smoothed by sanding them such that a smooth transition between the tubes and the central block is created. This smooth transition eases removal of the central block after production of the connector piece.
The five rods are made from steel and are 50 mm long and 20 mm in diameter. Holes are drilled through the entire length of the rods (not treaded!) to allow an M5 bolt to be pushed through.
Every rod is connected to the central block using a 60 mm long M5 bolt. For the spokes, these bolts are too long to allow them to be screwed fully against the rod (they will hit each other at the center of the aluminum block). Therefore, nuts are used to reduce the distance the bolts can be screwed into the aluminum block. For the upper rod this is not necessary since the other four bolts can't obstruct its bolt anymore.

The dimension of the sides of the central block (20x15 mm) result in a surface area that is slightly smaller than that of a rod (300 mm$^2$ versus 314 mm$^2$). Thus, it is in principle possible to pull the central block out of the connector piece without rupturing the rubber. Having smooth corners is now also helpful in preventing large stresses to occur in the corners when the central block is wriggled out.

## 3.2 Connector piece construction

Construction of the connector is treated in four steps. These are the creation of the silicone rubber, the preparation of the metal mold, the application of the rubber to the mold, and finally the removal of the mold from the connector piece. They will all be treated in the coming subsections. Subsection 3.2.5 treats the final result and ways to improve the production process.

### 3.2.1 Creating the silicone rubber

The silicone connector piece is made from Dow Corning “Silastic M” RTV silicone rubber (supplier: Fatol Mulder, Hengelo (NL)). This type of silicone rubber is normally in stock at the composites laboratory of the faculty (ask Marc van Dongen). The rubber is created by mixing two components together in a mixture ratio (by weight) of 10:1 (base : curing agent). The base color is beige; the curing agent’s color is blue. The base is very viscous (0.13 Pa·s), almost a paste, which makes it difficult to pour. The curing agent is very fluid (0.0055 Pa·s), almost like water (0.001 Pa·s).

Creation of the rubber is performed as follows: Mix the base and the curing agent in a 10:1 ratio. Mix very well!! If not mixed properly, part of the rubber is much weaker than the rest. When this rubber is used to create a part of the connector piece, this part will tear much sooner than other parts, especially at corners. After mixing, remove any trapped air with a vacuum oven. Be careful, removing the air will create a quick and large rise in fluid level (which drops off very quickly once the air is removed)! When your bucket is not high enough or when the pressure in the oven is not increased it will spill, wasting a large part of costly silicone rubber.

After creation, the rubber is a thick fluid. The fluid becomes more viscous over time and after ~2 hours it is already too viscous to be useable anymore. Total curing time for the rubber is 24h.

*Figure 27 Recently mixed silicone rubber*

### 3.2.2 Preparing the metal mold

After the mold is screwed together, it is covered with a thin layer of wax to ease removal of the metal parts after creation of the connector piece. Then, clay is applied to the mold at places with sharp corners to increase the bend radius there (Pelikan plastilin clay was used, but ordinary play-doh would also be fine). This reduces the chances of rupturing the silicone there. The clay is easily removed from the connector piece after removal of the steel mold since it does not stick to either the metal mold or to the silicone.

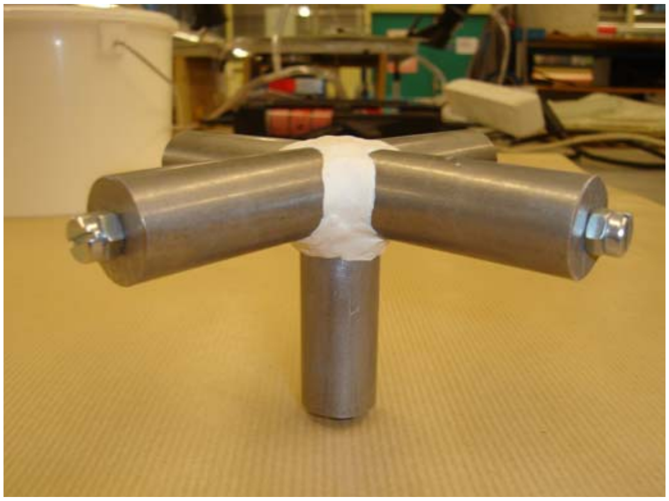

*Figure 28 Mold with clay*

### *3.2.3 Applying rubber to the mold*

First, the mold is dipped into the rubber, resulting in a very thin layer of rubber adhering to the mold. The work piece is then laid on four wooden blocks such that only the ends of the bolts rest on the blocks.
Applying more rubber with a brush or spatula increases the wall thickness and thus reduces the chance of rupturing the connector piece when removing the mold. Obtaining an equal wall thickness everywhere is virtually impossible when doing this, but is not very important for a prototype.

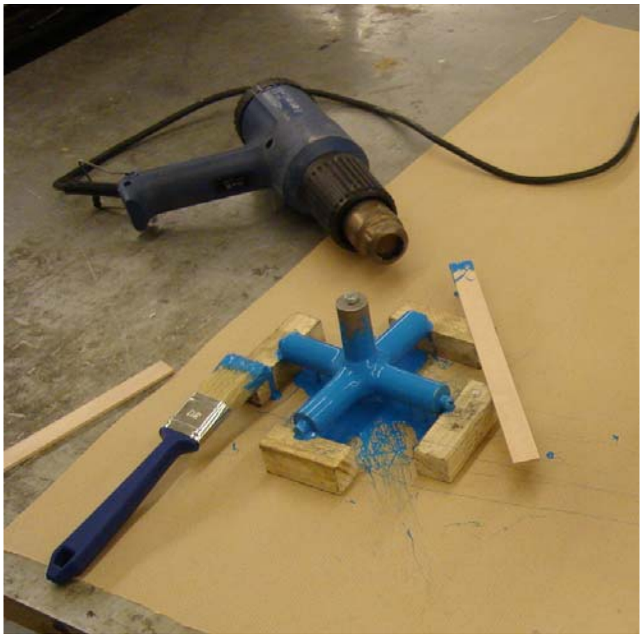

*Figure 29 Creation of the connector piece*

When the silicone is still relatively fluid, gravity will pull it towards the ground. This results in a small wall thickness at the top of structure. Increasing the wall thickness there is only possible by applying more rubber there with a brush or spatula from time to time. Since the rubber slowly becomes more viscous over time, this tactic works especially well at a later stage of the creation.

Since higher temperatures speed up the hardening of the rubber, a blow-drier was used to try to reduce the amount of silicone dripping from the mold. However, the blow-drier did not help much and it is likely to be easier to wait with applying rubber to the mold until the rubber has reached a proper amount of viscosity (it should of course not be too viscous, otherwise it is impossible to apply it properly to the mold anymore).

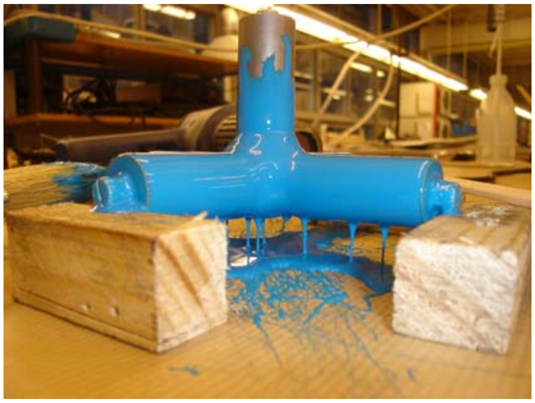

*Figure 30 Rubber very fluid*

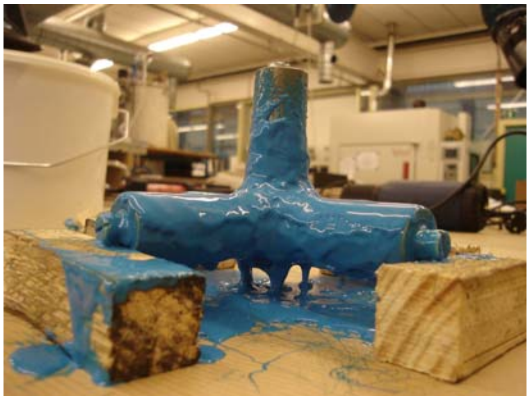

*Figure 31 Rubber very viscous*

### *3.2.4 Removing the mold*

Removal of the mold is surprisingly easy. First, the silicone at the ends of the tubes has to be cut and removed. Then, the central rod and three spoke rods can be removed. First, the bolt with which they are fastened has to be removed. Then, it is possible to fold the silicone tube in which the rod is positioned, back towards the center of the connector piece (see figure 33). Doing this greatly decreases the amount of friction that opposes the rod from being pulled out. After that, the rod can be pulled out with little effort.

*Figure 32 Silicone at the ends of the rods removed*

*Figure 33 Tube rolled back*

After having removed four rods, the last rod has to be removed together with the central block. Thus, now the bolt should *not* be removed. The central block is removed with the last rod since then the connector piece can stretch more than when the other rods are still in place. This reduces the chances of rupturing it.
When pulling out the rod and the block, a large amount of clay will remain inside the connector piece. Since it does not stick to the rubber, it is easily removed.

*Figure 34 Last rod and central block still in connector piece*

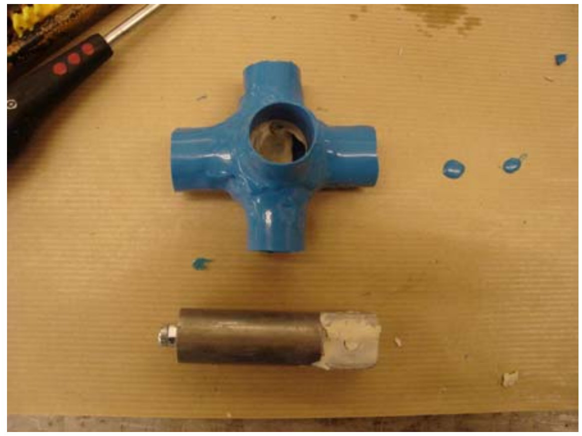

*Figure 35 Rod and block removed*

### 3.2.5 Final result and ways to improve the production

Result

A top view and a bottom view of the connector piece are presented in figures 36 and 37.
In the top view it looks like some tubes are not straight. This is not the case; the tubes are straight and well aligned. It is an optical illusion caused by the tubes not having been cut off at 90° angles.
The bottom view clearly shows the less than perfect outer surface finish caused by the dripping of the silicone during production.

*Figure 36 Top view connector piece*

*Figure 37 Bottom view connector piece*

The variation in wall thickness is shown in figure 38. This is in part caused by the dripping of the silicone and in part caused by manually applying more silicone.

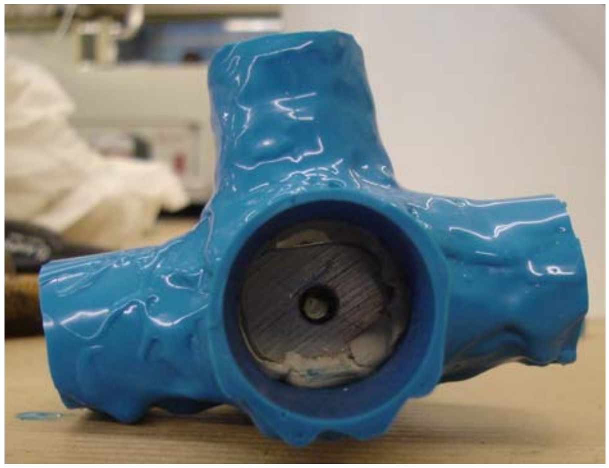

*Figure 38 Variation in wall thickness*

The measured weight of this prototype is 17.17 ± 0.01 g, the measured volume is 13 ± 1 cc. From this it follows that the density lies between 1.2257 g/cc and 1.4317 g/cc. The density claimed by Dow Corning is 1.29 g/cc, which is almost halfway the range determined. Since the volume measurement performed on the connector piece is quite crude (measured using a measuring cup with a scale of 25 cc per step), the density is taken equal to the claimed density of 1.29 g/cc. From this follows a volume for the connector piece of ~13 cc.

Based on the above, the volume and weight of a silicone connector piece for 10 mm diameter tubes is estimated to be 5 cc and 6.5 g respectively. The volume and weight are not divided by two compared to the connector piece created since the wall thickness can be more uniform and smaller than achieved here. Therefore, a volume of 5 cc seems more appropriate than a volume of 6.5 cc. With a density of 1.3 g/cc the resulting weight is 6.5 g.

<u>Possible improvements</u>

When the same technique is used in future to create a silicone connector piece, the following is advised:

- Use threaded rods and nuts instead of bolts to screw the spokes to the central part. Then, it is easier to position the work piece such that it can rest on an object (no need for exact placement). In addition, the item can be easily picked off the resting object (now, the bolt ends were covered in silicone and were sticking to the wooden blocks).
- Increase the height of the resting object. The work piece can then be turned upside down, allowing the bottom to be reachable with brush or spatula. In addition, the liquid silicone is now pulled towards central rod, not away from it. Turning the work piece over several times will improve its outer surface finish.

An even better improvement of the production process is possible by using a positive and a negative mould between which the silicone can be poured (similar to casting). Then, there are no problems with silicone dripping to the ground and the wall thickness around the connector piece can be adjusted at will (the wall thickness at the corners can for instance be increased). A pitfall for this manner of production is the possibility of trapping air inside the connector piece, which will weaken it.
When a metal mold is used for further production, the central aluminum block can be made superfluous by shaping the spoke rods such that they fit around the central rod. For this, two spokes need to have half a circle milled away at one end (see figure 40) with a radius equal to that of the central rod. For the other two spoke rods, this has to be done twice at the same end, but the second time perpendicular to the first time. The result is depicted in figure 41. By doing this, those spokes fits around the central rod and the spoke rods from figure 40. Important to realize is that for the first two spokes, about 3 mm of material needs to be

removed at the pointed ends since this material will otherwise block the holes on the central rod from the bolts needed to fasten the last two spokes.

*Figure 39 Central rod*

*Figure 40 Spoke 1*

*Figure 41 spoke 2*

Figure 42 presents an exploded view of the assembly of all the rods.

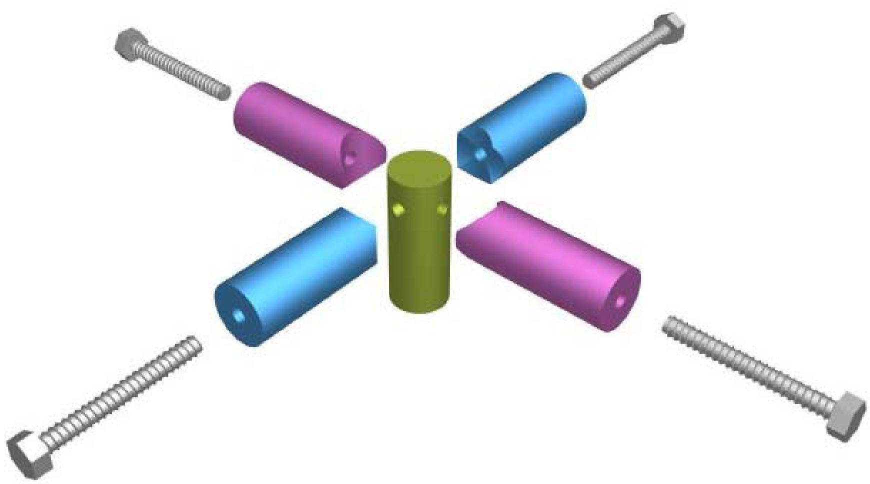

*Figure 42 Exploded view of the assembly*

Instead of using a metallic mold, a wax mold is of course also applicable. By using a wax mold, there is no chance of tearing the silicone rubber when removing the mold since the mold is melted away. Thus, the wall thickness of the connector piece can be made even smaller when using a wax mold. Yet, using a wax mold will be more expensive than using a metal mold since every new connector piece will require a new mold. With a very small batch size, this is relatively expensive.

## 4 CONCLUSIONS & RECOMMENDATIONS

Both types of connector piece can be constructed to yield a satisfactory performance (flexible and able to connect five flexible tubes), but the foil connector is much smaller and lighter than the silicone connector. For the 10 mm tube variants, the foil connector is estimated to be a factor 26 lighter and a factor 18 less voluminous than the silicone option. Although the silicone connector piece ensures good alignment of the inflatable tubes, its (relatively) huge mass and volume penalty makes it unsuitable for the current application. Thus, the foil connector piece is used in the remainder of the development.

When shape accuracy is a driving requirement and when the mass and volume budgets are less restricted, a connector piece similar to the silicone one is preferred over a foil connector piece.

Silicone rubber is inherently difficult to bond. However, it does retain its properties over a large temperature range, which is advantageous for space applications. Therefore, it is recommended to investigate other types of rubber that do not have severe bonding issues and which also retain their properties over broad temperature range (-50°C - 150°C). With respect to the temperature range, interesting options are neoprene, butyl, EPDM, Hypalon®, and Viton®.

# 5 FURTHER WORK

No further connector piece development is foreseen for the remainder of this thesis. When a fiber reinforced composite is used to rigidize the inflatable structure, it is logical to also rigidize the connector piece. How the composite should be applied to obtain a proper connector piece is left TBD in a later stage of this development.

# REFERENCES


1. Bernasconi, M.C., et al, *Inflatable foldable structure and method of manufacturing foldable structures,* United States Patent 5044579, 3 September 1991.

2. Dow Corning Corporation, *Silastic® M RTV silicone rubber base,* Material Safety Data Sheet, Midland (USA), 28 August 2006.

3. Dow Corning Corporation, *Silastic® M RTV silicone rubber curing agent,* Material Safety Data Sheet, Midland (USA), 28 January 2002.

4. Maessen, D.C., *iDod inflatable structure conceptual design trade-off,* iDod document iDod.TO.001, Version 1.0, Faculty of Aerospace Engineering, Delft University of Technology, 11 January 2007.

# Creating flexible tubes


## SUMMARY

A method is described in which LD-PE (low density polyethylene) foil is heat-sealed to create slender flexible tubes. Heat sealing is preferred over using adhesives since the technique is fast an accurate, which is ideal for prototyping. However, it is believed that future tubes need to be created using adhesives since plastics likely to be used in space are not (or very difficult) heat sealable.



## KEYWORDS

Heat seal, adhesive, PE, bond


## DISTRIBUTION

| | Name | | Company / Institution |
|---|---|---|---|
| 1 | E.D. van Breukelen | Customer | ISIS B.V. |
| 2 | O.K. Bergsma | Project supervisor | TU Delft |

## APPROVAL

| | Name | Company / Institution | Date | Signature |
|---|---|---|---|---|
| *Written* | D.C. Maessen | TU Delft | 4/10/2007 | |
| *Checked* | | | | |
| *Approved* | | | | |

## REVISION RECORD

| Issue | Date | Total pages | Affected pages | Brief description of change |
|---|---|---|---|---|
| Draft | 3/2/2007 | 8 | | |
| Version 0.1 | 4/10/2007 | 8 | 8 | Removed section 6 (Further work) |

## LIST OF TBD'S AND TBC'S

| TBD/TBC | Paragraph | Subject | Due date | Action by |
|---|---|---|---|---|
| TBD | 4.3 | Will tape or liquid adhesive result in a better bond? | TBD | TBD |
| | | | | |
| | | | | |

## TABLE OF CONTENTS

# 1 INTODRUCTION

The current document outlines the creation of flexible, inflatable tubes made from LD-PE (low density polyethylene) foil. LD-PE was chosen as tube material because it was readily available and low cost. The PE tubes are created by heat sealing two ends of a strip of PE foil together. The reasons for using heat sealing and the production process are discussed in sections 2 and 3. However, this bonding technique is believed not to be useable using the 'real' iDod materials. Therefore, another way of creating the bond needs to be developed. This is discussed in section 4.

# 2 WHY HEAT SEALING

Next to PE being difficult to bond using adhesives, there are intrinsic advantages of this method over bonding the ends together using adhesive:

1. Heat sealing is fast, the bond is created in a matter of seconds.
2. No chance of bonding the tube to the mold.
3. The bond is flexible.
4. The seam is only 3 mm wide.
5. The seam is always straight.

For prototype work, especially the first argument is important since it allows fast production and therefore more time to for instance design the required connector piece and the manner in which the tubes are connected to it.
When using an adhesive, full curing of a bond can take up to a day, depending of course on the type of adhesive used. In addition, a pre-treatment of the material is often required when using adhesives, adding more time to the process.

When using adhesive, bonding the tube to the mold can be avoided by ensuring no adhesive comes in contact with the mold or by ensuring the adhesive is incompatible with the mold (it can't stick to the mold).
However, the first option requires either very careful application of the adhesive or using something like masking tape to prevent the adhesive from coming in contact with the mold when the adhesive is being applied. Both methods are very time consuming.
Ensuring incompatibleness of the adhesive and the mold requires either a "special" mold material or a "special" adhesive. Since plastic foils are inherently difficult to bond, the second alternative is not very attractive since it reduces the already limited number of adhesives than can be used. The first alternative is more attractive, but requires a possibly uncommon material to be acquired and perhaps worked into the correct shape.
All of the above problems are non-existent with heat sealing since then a simple wooden or metallic mold can be used without problems.

The third argument is naturally very important for structures that need to be very flexible and is always guaranteed when using heat sealing. For adhesives, this might not be the case since they often are not required to be very flexible. Thus, not all adhesives that are compatible with the foil material will be flexible enough for this application. This possibly further limits the number of adhesives that can be used.

For prototype work, the fourth and fifth arguments in themselves are not very important. However, both arguments amplify the first argument since no time consuming measures need to be taken to ensure a thin, straight seam. Creating a 3 mm wide, straight seam using adhesive is *not* a trivial matter.

# 3 CONSTRUCTION

Construction of the tubes is performed in the following steps. After description of each step, a picture is presented to clarify the description of that particular step.

1. <u>Create a mold with the proper circumference.</u> The shape of the circumference is in principle unimportant, but the heat seal device used requires a mold with little height. Here, a piece of thin wood is used.

2. <u>Cut a piece of foil with the correct dimensions.</u> The length of the foil has to be equal to the desired tube length; the width has to be at least slightly more than the circumference of the eventual tube since some overlap is required for the bond. In the below picture, the width of the foil is more than required and two small flaps are visible. The function of these two extras is explained in steps 3 and 4.

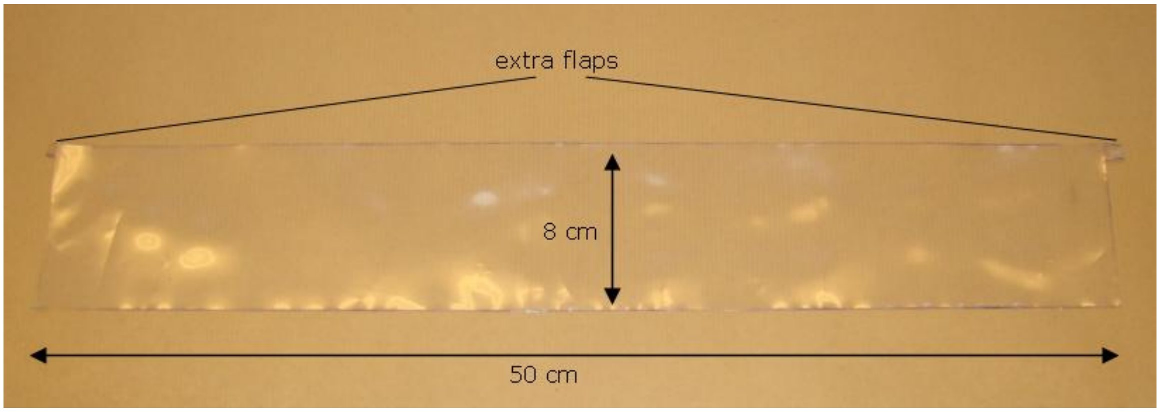


*Figure 1 Piece of foil required to create a 50 cm long, 20 mm diameter tube*

3. <u>Wrap the foil around the mold and fasten it at both ends to the mold using tape.</u> Allowing the width of the foil to be substantially more than absolutely necessary allows for pulling the foil tight around the mold along the entire tube length, resulting in a more uniform tube diameter and straight tube. The longer the tube, the more important this becomes. Tape can be used at several places along the length of the tube as a temporary fastener to ensure the foil stays in the required shape. After creation of the seam, the excess foil can easily be cut away. Fastening the foil to the ends of the mold ensures that the foil cannot move (twist) around the mold. It also removes the need to keep the foil in the correct shape by hand when the mold-tube combination is positioned above the heat seal wire. *Do not attach the foil halfway to the mold, since then it becomes almost impossible to remove the tube from the mold after creation.*

*Figure 2 End of tube wrapped around mold*

4. Create the heat seal. Using a foot-operated heat seal device (Adion Elektro Sealmaster 580), the heat seal is created. Operating the device by foot allows the operator to use both hands to position the work piece. Unfortunately, the wire that is heated and allows for creation of the seal is facing upward. Therefore, the seam that is to be created needs to face downward and is blocked from view. By having two small flaps extending at both ends of the tube, the position of the piece of foil at the 'inside' of the seam can still be known. Using the flaps to outline the correct position of the work piece, it is not difficult to position it such that a straight bond with minimal material overlap is created. The upper arm of the heat seal device is forced down by the operator by pressing down his foot. Once a sufficiently strong contact is made between the upper arm and the work piece, a buzzing noise sounds, indicating that the seal is being created. After several seconds, the buzzing sound stops and heating of the wire is stopped. The operator needs to keep applying pressure for several seconds more after the sound has stopped to allow for the bond to cool and settle. After than, the upper arm of the device can be released and the work piece can be removed.

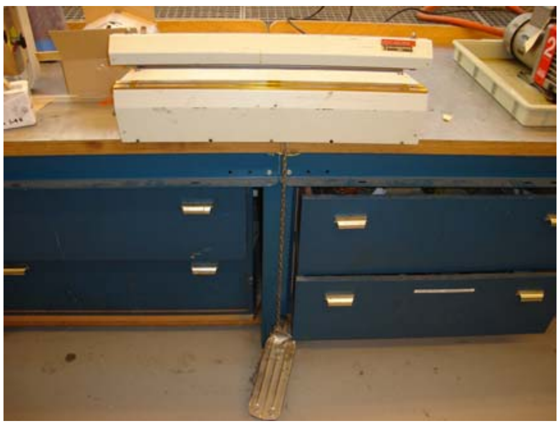

*Figure 3 Heat seal device*

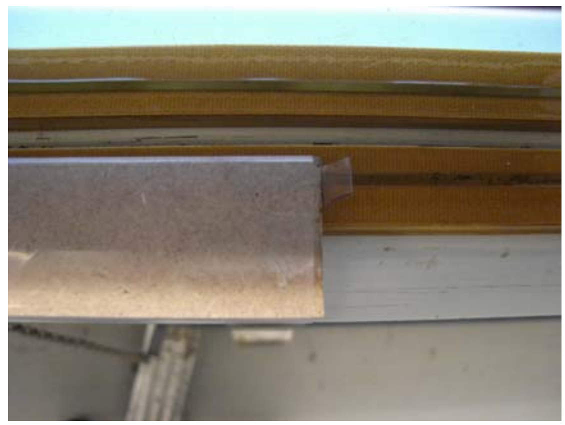

*Figure 4 Positioning the tube over the wire*

5. Remove the tube from the mold. Removal of the tube is accomplished by first removing all the tape and then pulling the mold out of the tube. Often, the tube sticks to the mold at several places, preventing removal of the mold. This can be overcome by forcing the heat sealed bond off the mold by pulling on the extra flap of foil. After that, this flap can be cut away using a knife or scissors and lastly the mold can be pulled/pushed out of the tube.

*Figure 5 Heat seal (white line at the bottom of the tube)*

*Figure 6 Cutting away the extra flap of foil*

A completed tube is depicted below.

*Figure 7 Completed tube*

Noticeable are two 'kinks' near the center and at three quarters of the length of the tube. These are formed as a result of first attaching the flap of foil with a small piece of tape at the middle of the tube. Then, the flap is attached to the left and right of the middle with two more pieces of tape for each direction. However, attaching the flap at the middle of the tube with a piece of tape results in a slight stretching of the foil. This causes the flap to become slightly rectangular instead of straight (see the right picture in figure 8). Trying to get the flap straight again results in excess material at some points, causing the 'kinks' in the finished tube.

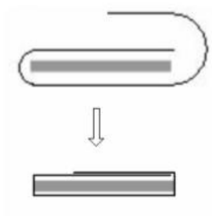

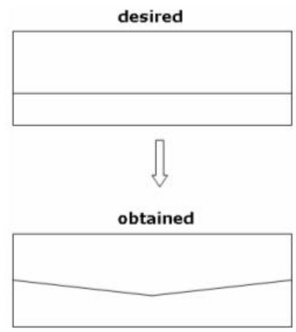


*Figure 8 Wrapping the foil around the mold (left) and the exaggerated shape of the flap once wrapped around the mold (right)*

The mass of a 49.5 cm long tube ($\pm$ 0.1 cm) is measured to be 2.639 $\pm$ 0.0001 g. Therefore, the tube mass per meter tube length is 5.33 $\pm$ 0.01 g. The thickness of the PE foil is measured to be 0.09 $\pm$ 0.01 mm. Thus, the material volume per meter tube length is 5.65 $\pm$ 0.63 $cm^3$.

# 4 NEXT DEVELOPMENT STEPS

The current section will treat a method for tube construction which is believed to remove the 'kinks' created in the current tubes. In addition, a change in tube material from PE to PET (polyethylene terephthalate) is discussed. Subsection 4.3 will treat tube construction using adhesives.

## 4.1 Removing the kinks in the tubes

Creating 'kinks' in the tubes is thought to be avoidable when the flap of foil is not attached using several small pieces of tape, but using one large piece of tape over the entire length of the tube. Although this is not trivial to do for one person, it should result in the same amount of tension being applied over the entire length of the tube, removing the cause of the kinks.

It is also believed that wrapping the foil around a 2 cm diameter rod to create the desired circumference will help in preventing kinks from forming because the foil doesn't have to be stretched around several sharp edges. After the foil has been wrapped around the rod and fixed to itself, it can be removed from the rod and slid over a rectangular mold (which does not necessarily have to have a circumference equal to the one of the tube!) and be heat sealed.

### 4.2 Changing from PE to PET

When working with plastics, one is confronted with a dilemma: All heat sealable plastics are hard to bond using adhesives, but all "easy" to bond plastics are hard to heat seal. There are also plastics which perform 'average' for both techniques, but plastics with this property are not preferred since they lead to problems for both techniques.

As said earlier, the main reason for choosing heat sealable PE is the fast tube creation possible and the fact that the material is readily available at this faculty. However, connecting the tubes to the connector piece and creating the PE connector piece itself becomes problematic since these connections are difficult to heat seal properly (especially the tube-connector piece connection) and PE is hard to bond using adhesives.

Although PE is hard to bond using adhesives, some adhesives have been found which are adequate for the current application [Maessen, iDod.CM.003]. Even if they are not likely to be the adhesives that can be used for eventual flight models, they do allow for functional demonstration of the inflatable structure. Since this is the current goal, they are adequate for now.

However, it is very likely that the tube material for the flight models is not going to be PE, but some other type of polymeric material. Chances are high that this type of polymer is difficult or even impossible to heat seal and therefore everything needs to be bonded using adhesives. Then, also the tubes need to be created using adhesives. Finding out how proper tubes need to be created using "space-resistant" material is believed to be costly since the material itself is very costly.
Therefore, it is advised to use PET foil for this. PET is a cheap plastic that is relatively easy to bond, which implies there are many adhesives available that meet the requirements. Using some of the experience gained with creating heat sealed tubes, creating PET tubes is thought not to be very hard.

### 4.3 Creating tubes using adhesives

Creating a tube using initially liquid adhesives can be done in the following manner. Wrap foil around a rod with the proper diameter. Attach tape over the entire length of the foil at the 'beginning' of the foil such that the 'sticky' side of the tape is facing away from the rod and that half of the tape is bare. The foil that is subsequently wrapped over the rod can now be attached to the bare tape. This way, a bond is created at the inside of the tube. Now, the remaining flap of foil can be pulled upward such that a small 'gutter' is formed at the place where the tape and the ends of the foil meet. Now, adhesive can be applied over the entire length of the gutter. Once the adhesive has been applied, the flap is attached to the other foil and the adhesive is left to harden.

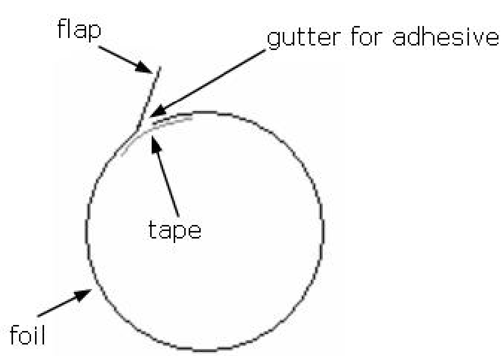


*Figure 9 Tube creation with adhesive*

Downside to this method is that some tape is left at the inside of the bond and will be difficult to remove for 1 cm diameter tubes. However, this can also be a positive aspect since the bond is now redundant (in flight models, space-qualified tape would then have to be used). A positive aspect about this method is that a straight seam is created without the risk of gluing the tube to the rod.

Tubes can also be created using tapes. Using pressure-sensitive tape, tubes can be created using the method discussed earlier in this subsection but without the liquid adhesive. For redundancy, tape can also be applied at the outside of the bond.
Tape can also be used to create a bond using hot melt adhesive. The tape with the adhesive is laid over the bond and by using a hot iron, the adhesive is melted. According to [Grossman, 1990], such a bond is stronger than a bond created with pressure-sensitive tape.

Whether tape is better than liquid adhesive or vice versa remains TBD. When using tape, the seam is likely to be stiffer than when using liquid adhesive and the structure will be a bit heavier. On the other hand, tape is relatively easy to work with and does not 'flow' like liquid adhesive (possibly resulting in an irregular bond).
With respect to air tightness, it is believed that careful selection of tape will give the same results as liquid adhesive.

# 5 CONCLUSIONS & RECOMMENDATIONS

Constructing flexible tubes by heat sealing LD-PE is fast and accurate and therefore ideal for prototyping.

However, since it is believed that flight models of the iDod will consist out of materials which do not lend themselves well to heat sealing, proper construction of tubes using adhesives needs to be learned in the future. A material which lends itself well for this is PET.

# REFERENCES

1. Grossman, G., Williams, G., *Inflatable Concentrators for Solar Propulsion and Dynamic Space Power*, Journal of Solar Energy Engineering, Volume 112 / 229, November 1990.

2. Maessen, D.C., *PE adhesives testing,* iDod document iDod.CM.003, Draft, Faculty of Aerospace Engineering, Delft University of Technology, 2 March 2007.

# Connecting tubes to a connector piece

## SUMMARY

It is described how five flexible tubes are currently attached to a flexible connector piece in a leak-tight manner. Two possible methods to improve the production are discussed. A two-step approach is recommended as future production method.

## KEYWORDS

Connector piece, flexible tubes, jig, adhesive

## DISTRIBUTION

| | Name | | Company / Institution |
|---|---|---|---|
| 1 | E.D. van Breukelen | Customer | ISIS B.V. |
| 2 | O.K. Bergsma | Project supervisor | TU Delft |

## APPROVAL

| | Name | Company / Institution | Date | Signature |
|---|---|---|---|---|
| *Written* | D.C. Maessen | TU Delft | 4/11/2007 | |
| *Checked* | | | | |
| *Approved* | | | | |

## REVISION RECORD

| Issue | Date | Total pages | Affected pages | Brief description of change |
|---|---|---|---|---|
| Draft | 3/2/2007 | 9 | | |
| Version 0.1 | 4/11/2007 | 9 | 1 | Added in the summary that a two-step production approach is recommended to be used in the future |
| | | | 8 | Sentence under figure 10: replaced “rather” by “very”<br>Sentence under figure 11: replaced “one rod” by “at least one rod” |
| | | | 9 | Second improved production method from section 5 recommended as future production method |
| | | | 9 | Removed section 7 (Further work) |

## LIST OF TBD’S AND TBC’S

| TBD/TBC | Paragraph | Subject | Due date | Action by |
|---|---|---|---|---|
| | | | | |
| | | | | |
| | | | | |

## TABLE OF CONTENTS

# 1 INTODRUCTION

After having created flexible tubes [Maessen, iDod.CM.001] and a flexible connector piece [Maessen, iDod.CM.002] out of polyethylene (PE) foil and having selected proper adhesives [Maessen, iDod.CM.003] to bond PE foil, the inflatable structure of the iDod can be constructed. That structure is pyramid shaped with thin foil membranes acting as the sides of the pyramid and an inflatable tubular structure that looks as follows:

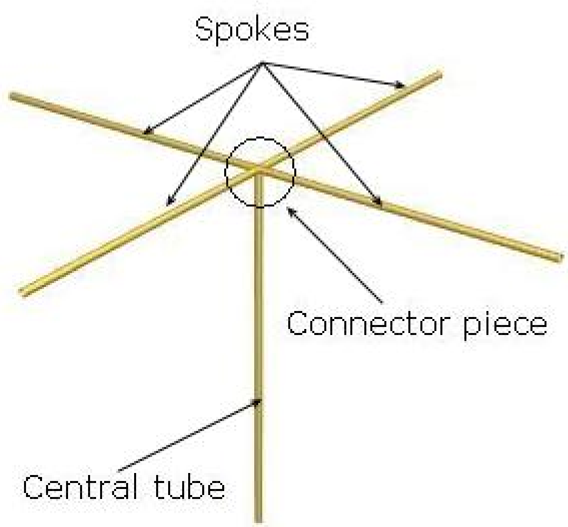


*Figure 1 Inflatable tubes*

The breadboard construction of this tubular structure is discussed in the next sections. First, section 2 deals with the jig used for the construction of the tubular structure using a PE foil connector piece. Sections 3 and 4 treat the creation of the tubular structure using a connector piece made out of PE foil and the creation of part of the tubular structure using a connector piece made out of silicone rubber respectively. Section 5 discusses a production method with which the alignment of the inflatable tubes can be improved.

# 2 JIG

The jig used in the production of the tubular structure with the foil connector piece is made from 18 mm thick MDF wood. The next figure shows the jig with a partial tubular structure already on it.

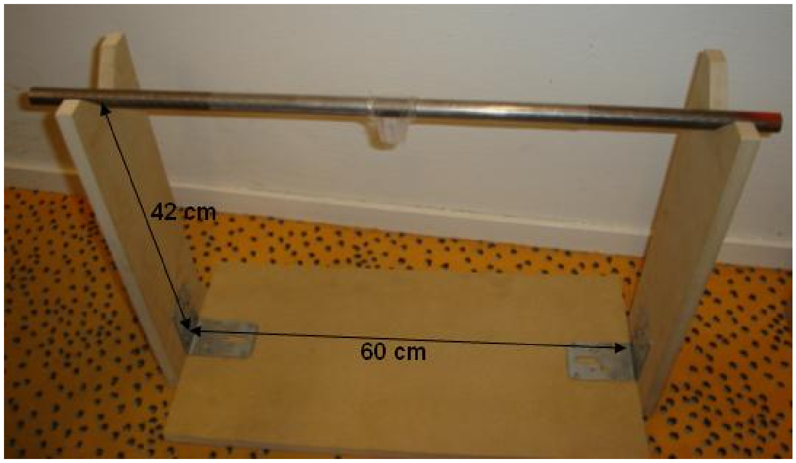


*Figure 2 Jig*

A steel rod of 20 mm diameter and ~75 cm length is used to provide a stiff support for the flexible tubes that are to be attached to the connector piece. The internal width of the jig is 60 cm, while the clearance between the bottom plate and the steel rod is 42 cm. This clearance is required for the spokes of the inflatable structure, which are 40 cm long.

In figure 2, the steel rod is 'blunt' at both ends. However, while attaching the first two tubes to the connector piece, it was realized that making one end of the rod pointed eases sliding a tube over the rod and inserting it inside a hole of the connector piece. Therefore, one end was sharpened such that the diameter there was reduced from 20 mm to 5 mm over a distance of 50 mm.

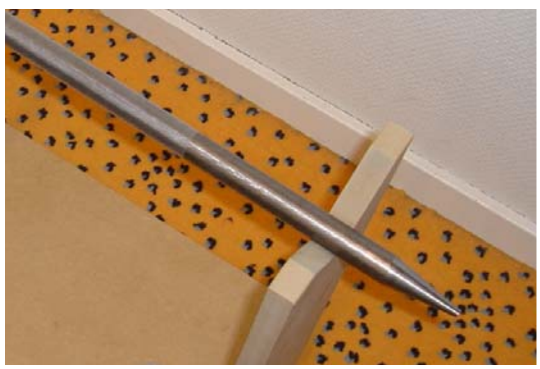

*Figure 3 One end of the rod sharpened*

## 3 FOIL CONNECTOR PIECE

Attaching the flexible tubes to the foil connector piece is performed in several steps. It is best to attach the central tube after the spokes have been attached. This way, when attaching the spokes, the connector piece is not deformed by the weight of the central tube. Even though being small, this deformation will lead to misalignment of the spokes once the assembly is removed from the steel rod.
Attaching the spokes to the connector piece can be done two at a time, but for best accuracy it is better to do it one at a time. Since the silicone adhesive used to create the connection provides a strong bond after a few minutes, it is easily possible to connect a second spoke to the connector piece (aligned with the first spoke) only a few minutes after the first spoke has been attached. After attaching the second spoke, it is wise to let the adhesive fully cure (which takes two days) before attaching the spokes perpendicular to the two spokes already attached to the connector piece.

The steps undertaken are as follows:

1. Slide a tube over the steel rod and let it stick out at the pointed end of the rod. Deform the end that sticks out and insert it into a hole of the connector piece.
2. Now slide the tube and connector piece over the rod until the connector piece is about halfway.
3. Fix the end of the tube and the bottom of the connector piece to the steel rod using tape such that they cannot move relative to one another when applying the adhesive.
4. Apply Dow Corning HM-2510 silicone adhesive at the position where the tube and the connector piece meet. When one rotates the rod around its central axis, the glue gun can be held in the same position while applying the adhesive.
5. Let the adhesive cure for a few minutes.
6. Remove the assembly from the rod and repeat the same process for a second spoke that is aligned with the first spoke.
7. Let the adhesive cure for two days.
8. Remove the assembly and attach the second pair of spokes. <u>Beware</u>*: gravity results in the already attached tubes to sag towards the ground when they are not supported! This results in deformation of the connector piece and in misalignment of the two new spokes*. Supporting the already attached tubes at their end removes the issue with sagging, but creates the inconvenience that the steel rod cannot be rotated anymore when applying the adhesive. Thus, applying the adhesive now has to be performed in two steps: first, apply the adhesive on half the connection, flip the assembly upside down and apply adhesive on the other half of the connection. Repeat this procedure for the last spoke.
9. Let the assembly cure again for two days.
10. To attach the central tube to the assembly, first remove the assembly from the steel rod. Then, attach double sided tape to the 'blunt' end of the rod.
11. Slide the central tube over the rod and insert it into the connector piece at the blunt end of the rod. Then, slide the assembly backwards such that the inside of the bottom of the connector piece is pressed against the double sided tape. This way, the connector piece cannot move relative to the rod. The circle drawn earlier at the center of the connector piece (see [Maessen, iDod.CM.002]) should now line up with the edge of the rod to ensure proper alignment of the tubes.
12. Align the assembly such that the spokes are horizontal and vertical and support the horizontal spokes at their end to prevent sagging. Again, apply the adhesive in two steps and let it cure for two days.

*Figure 4 Version 1*

*Figure 5 Version 2*

*Figure 6 Version 3*

The total mass for a version with 20 mm diameter tubes, 40 cm long spokes, and a 50 cm long central tube has been determined to be 14.52 ± 0.001 g. The total tube length for this version is measured to be 210.2 ± 0.5 cm, which leads to a total tube mass of 11.204 ± 0.05 g (using the tube mass per meter from [Maessen, iDod.CM.001], 5.33 ± 0.01 g). The mass of the connector piece is 0.5 ± 0.05 g [Maessen, iDod.CM.002]. From these three known masses, the total mass of the silicone adhesive for this version is deduced to be 2.82 ± 0.1 g.

# 4 SILICONE CONNECTOR PIECE

Since it is decided in [Maessen, iDod.CM.002] to use the foil connector piece instead of the silicone connector piece for further development, no complete tubular structure is made with the silicone connector piece. However, since silicone rubber is prone to be hard to adhesively bond, it is attempted to do this using the RUPLO CA-adhesives already tested for PE foil [Maessen, iDod.CM.003].

Two PE tubes are bonded to the silicone connector piece. One is bonded using the 100-S variant and the other is bonded using the 1500S variant. The surface of the connector piece is pretreated with the same primer used to pretreat the PE tubes.
The result of this test is positive for both types of adhesive: both bonds perform well in tension while their performance with respect to peel is passable (the performance with respect to peel is not very important since the connection will not be loaded with a peel force during folding or deployment).

The test also resulted in a surprising result with respect to alignment: The tubes are not perfectly aligned! This is surprising since this connector piece is designed such that misalignment is theoretically impossible!

The most probable cause for the misalignment is the misalignment of the holes drilled into the steel rods used for production of the silicone connector piece (see [Maessen, iDod.CM.002]). It could be seen that for some rods, one end of the hole was slightly misaligned with the central axis of the rod. When screwing the rods with misaligned holes against the central square block, this results in a small misalignment of the rod and therefore a small misalignment of the tubular features of the connector piece. This was not recognized during production of the connector piece. At the outside, this internal misalignment is not visible. In addition, the central block can also have been not perfectly square, resulting in misalignment of the rods.

*Figure 7 Two tubes bonded to the silicone connector piece*

*Figure 8 Tubes not aligned*

Two more observations were done when attaching the tubes to the connector piece.
Firstly, the internal diameter of the tubes is equal to the internal diameter of the tubular features on the connector piece (both are created using a 20 mm diameter mold). It was assumed that the small thickness of the tubes would not cause this to result in any problems and the tubes would snuggly fit inside the connector piece. This proved not to be the case and for both tubes, there is some excess material that is folded inward and not connected to the wall of the tubular feature in which the tube is inserted. It is noted however, that this is not the case for the entire length of the bond. The folds are located near the center of the connector piece, not at the ends of the tubular features (there, the tube connects to the tubular feature over its entire circumference). The equal internal dimensions are also likely to be the cause that inserting the tube into the connector piece is accompanied by a considerable amount of friction.
Secondly, although being a minor issue, it noted that it is difficult to determine how far a tube has been inserted into the connector piece without means to verify this. One way would be to draw a circle on the tube at the place where that circle should align with the end of the tubular structure. Now, it cannot be verified how far the tube has been inserted since there are no reference points present.

# 5 IMPROVED PRODUCTION METHOD

For improved alignment of the tubes, a jig consisting out of five rods can be used. When this is done, all tubes can be connected to the connector piece at the same time and all tubes are prevented from sagging towards the ground.
Connecting these rods such that they can be disconnected once the tubular structure has been created is however problematic. Connecting the rods for the spokes to the rod for the central tube seems to be the most logical way. When using a screwed connection (screw a M4 bolt into one end of a spoke rod, glue the bolt to the rod, cut off the head of the bolt and screw the rod with bolt to the central rod), one runs into problems.

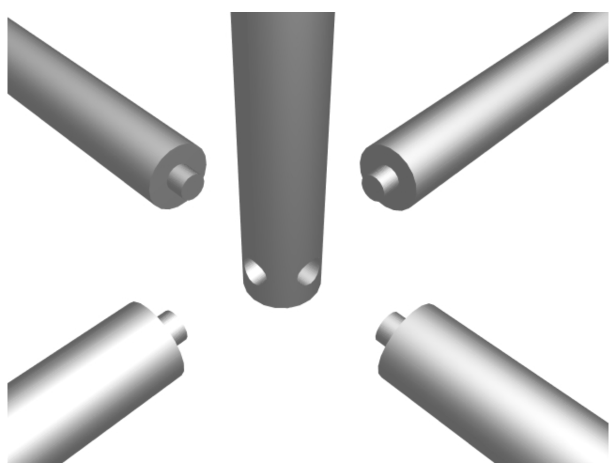

*Figure 9 Screwing spoke rods to the central rod*

With 10 mm diameter rods, the amount of ‘flesh’ available in the central rod to screw four bolts in is only 3 mm per bolt. Screwing in the bolts any further will lead to the bolts hitting each other. Reducing the diameter of the bolts alleviates this problem slightly, but not much (the gain is 0.5 mm per bolt). It is doubted that such a connection will result in a satisfying stiffness of the jig.
Increasing the amount of flesh for the bolts improves the connection and can be done in the manner depicted in the next figure. There, the central tube is shown. It is hollow and a pointed rod is inserted into it. At the bottom of the central tube, four slightly sloped blocks are present that are pushed out of the central tube by the pointed rod. The pointed rod and the blocks have threaded holes in them that line up when the rod hits a hard stop. The blocks can be connected to each other by for instance a thin elastic band which forces the blocks back to

their original position when the pointed rod is removed, allowing the tube to be retracted out of the connector piece.

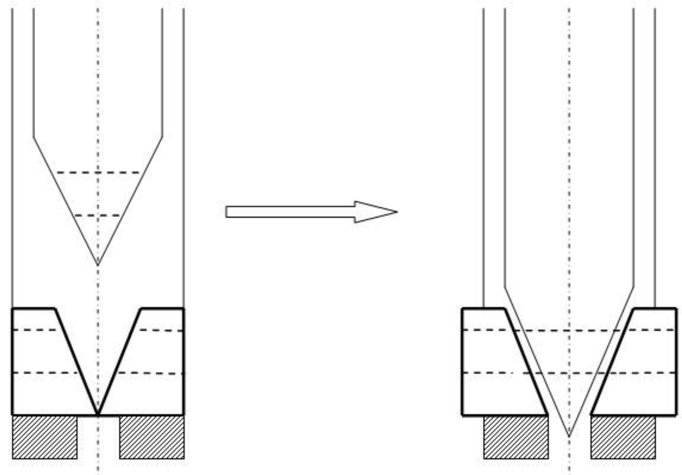

*Figure 10 Hollow central tube with blocks that can be pushed out*

The method described above is very complicated. The difficulty with the central tube can be prevented when the production is done in two steps. First, all the spokes are attached to the connector piece using one long rod and two smaller rods that can be connected and disconnected by screwing the smaller rods into a hole in the middle of the long rod. Milling away some material at the location of the hole in the long rod such that the small rods fit snugly in the created depression will improve the stiffness of the connection. After attaching the spoke tubes to the connector piece, the smaller rods are removed and the long rod is rotated 90°. This allows attachment of another rod over which the central tube is positioned and attached to the connector piece.

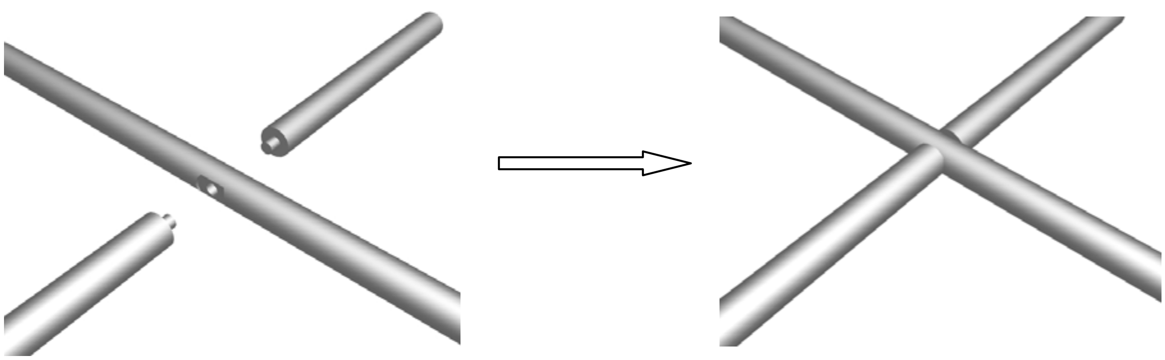

*Figure 11 Second option for improved production*

For both production methods, it is handy when it is possible to rotate at least one rod around its central axis. Then, the adhesive can be applied in one go instead of in two separate steps. Using a jig similar to the one already in use will allow this. Supports can be used to prevent rotation of the assembly when this is not desired.

# 6 CONCLUSIONS & RECOMMENDATIONS

Constructing five tubes to a flexible connector piece in a leak-tight manner is possible. Attaching the tubes such that they are approximately orientated at right angle to each other is also possible using the current production method. However, this can only be done when during the production great care is taken not to deform the connector piece when attaching new tubes.

Improving the production method of the tubular structure is possible and is recommended for future structures. It will improve the alignment of the inflatable tubes with respect to each other and the overall shape of the complete inflatable structure. The two-step approach described in section 5 is preferred over the approach using five rods since it requires a less complicated jig and the connection of the rods is guaranteed not to cause major difficulties.

## REFERENCES

1. Maessen, D.C., *Connector piece design and construction,* iDod document iDod.CM.002, Draft, Faculty of Aerospace Engineering, Delft University of Technology, 2 March 2007.

2. Maessen, D.C., *Creating flexible tubes,* iDod document iDod.CM.001, Draft, Faculty of Aerospace Engineering, Delft University of Technology, 2 March 2007.

3. Maessen, D.C., *PE adhesives testing,* iDod document iDod.CM.003, Draft, Faculty of Aerospace Engineering, Delft University of Technology, 2 March 2007.

# PE adhesives testing

## SUMMARY

Different types of adhesive are tested for their ability to create a bond on low density polyethylene (LDPE) foil. For perpendicular surfaces with a flexible bond, the Dow Corning HM-2510 Assembly Sealant is the best option. For flexible lap joints, the RUPLO 100K-S CA-adhesive is the best option.

## KEYWORDS

Adhesive, PE foil, silicone, methylmethacrylate, cyanoacrylate

## DISTRIBUTION

| | Name | | Company/ Institution |
|---|---|---|---|
| 1 | E.D. van Breukelen | Customer | ISIS B.V. |
| 2 | O.K. Bergsma | Project supervisor | TU Delft |

## APPROVAL

| | Name | Company/ Institution | Date | Signature |
|---|---|---|---|---|
| *Written* | D.C. Maessen | TU Delft | 4/10/2007 | |
| *Checked* | | | | |
| *Approved* | | | | |

## REVISION RECORD

| Issue | Date | Total pages | Affected pages | Brief description of change |
|---|---|---|---|---|
| Draft | 3/2/2007 | 12 | | |
| Version 0.1 | 4/10/2007 | 12 | 4 | Added addendum about sanding and degreasing |
| | | | 9 | Added source for melting temperature LDPE |
| | | | 11 | Added that the type of adhesive for materials other than LDPE is TBD |

## LIST OF TBD'S AND TBC'S

| TBD/TBC | Paragraph | Subject | Due date | Action by |
|---|---|---|---|---|
| TBD | Section 4 | Type of adhesive for materials other than LDPE | TBD | TBD |
| | | | | |
| | | | | |

## TABLE OF CONTENTS

# 1 INTODRUCTION

Low density polyethylene (LDPE) is difficult to adhesively bond due to its low surface energy (caused by the absence of polar groups in the molecule which determine the bonding quality). Therefore, different adhesives need to be tested to find out whether it can be bonded satisfactorily. An adhesive needs to be found to allow construction of a flexible PE connector piece as well as an adhesive to allow for the creation of tube-connector piece joints.

The tests described in this document are performed using strips of PE foil (2x3 cm). One strip is laid partially over another strip to form a lap joint and the adhesive at the joint is allowed to cure for one or two days at normal room conditions.
In one test, a connector piece and a tube were used instead of strips. This is the first test and is described in subsection 2.1.

The following adhesives are tested and are described in the coming sections:

- Bison Poly Max MS Polymer
- Dow Corning HM-2510 Assembly Sealant
- PLEXUS MA310
- RUPLO TA 610
- RUPLO CA-adhesive 100K-S, 1500S, and 1500S-D-5

The first two adhesives are tested for the tube-connector piece interface. The other adhesives are tested for the connector piece bonds.

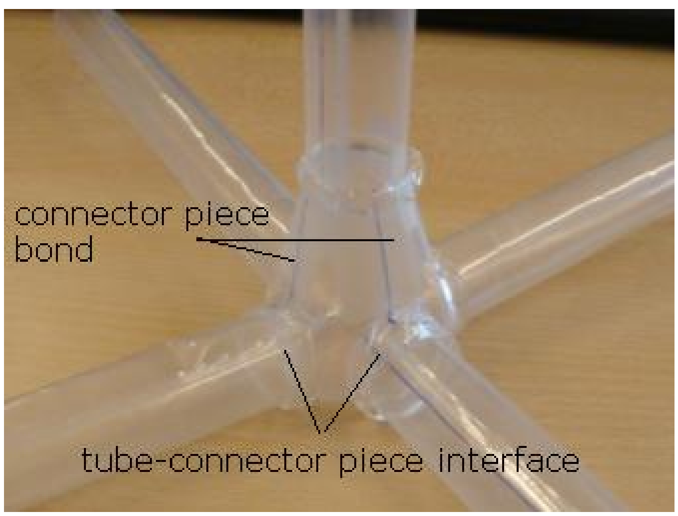


*Table 1 Bonds eventually to be created using the adhesives to be tested*

# 2 TUBE-CONNECTOR PIECE INTERFACE ADHESIVES

For the tube-connector piece interface, the surfaces that need to be bonded are almost perpendicular to each other. Then, a thin adhesive is not appropriate since a gap needs to be filled. Therefore, silicone adhesives are tested since they are thick, remain flexible, and are known to be able to bond “difficult” surfaces.

## 2.1 Bison Poly Max MS Polymer

The first adhesive tested is Bison Poly Max MS polymer (MS = Modified Silicone). This adhesive is readily available at the local D.I.Y. (Do It Yourself) shop. The adhesive fully cures under influence of moisture in two to three days.

Being the first adhesive to be tested, it is enthusiastically tried to immediately construct a connector piece with it and to connect a tube to the connector piece. On hindsight, testing the adhesive by trying to bond two simple pieces of foil would have been a better and simpler approach.

### 2.1.1 Pretreatment

The pretreatment consists out of roughening up the bond area using P80 sanding paper for 10 seconds. After that, the surface is degreased using ethanol. *Addendum: it is better to degrease first, then roughen up the surface, and then clear the surface. This way, no grease can be rubbed in the material!*
After the sanding, it is observed that the thin foil is deformed and its thickness greatly reduced at the areas that have been sanded (there are even places where the foil has been completely sanded away). Obviously, this is *not* desired and a lesson for the coming tests.

### 2.1.2 Adhesive application

The adhesive is dispensed from its container in a thick line onto a metal plate. A spatula is used to apply some of this adhesive onto the bond surfaces. Next to the adhesive, the connector piece is held together using tape. The tube and the connector piece are only held together by the adhesive.
No stiff support is utilized to ensure a proper shape of the foil when applying the adhesive. Since the adhesive is relatively thick and needs to be applied with some force, the absence of any support results in unwanted deformation of the foil. The reduced thickness of the foil due to the sanding adds to this problem. This is also a good lesson for further tests.

### 2.1.3 Results

After three days of curing the created bonds are tested by trying to pull them apart manually. This is achieved with little to no effort. Therefore, it is concluded that this type of adhesive cannot be used with the current materials and (an)other adhesive(s) need(s) to be tested.

The following figure shows the result for this test. The milky white areas are the areas that have been sanded. The rough looking areas are places where adhesive has been applied (clearly visible at the tube-connector piece interface). Striking is the contrast between the untreated surface at the right side of the tube and the surfaces that have been sanded or where adhesive is applied.

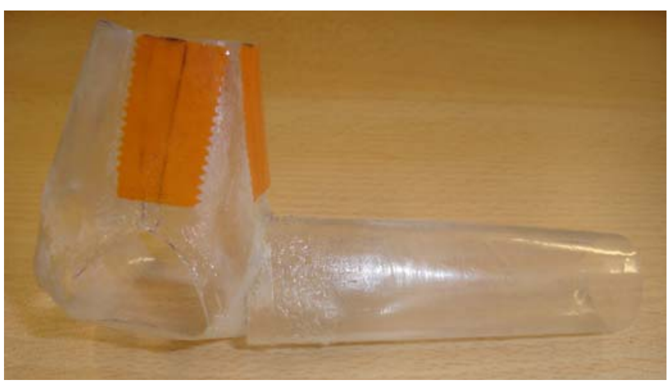

*Figure 1 Result of Bison Poly Max MS Polymer*

## 2.2 Dow Corning HM-2510 assembly sealant

The Dow Corning HM-2510 Assembly Sealant is a colorless hot melt silicone adhesive, advised to use for the tube-connector piece interface by Richard Klein (MAVOM, Alphen a.d. Rijn (NL)). “Hot melt” implies that the adhesive needs to be heated (in this case to 120°C) before it is hot and therefore viscous enough to be applied. For heating and application of the glue, a Steinel “PurGlue 50” electronic cordless cartridge glue gun is used. The adhesive is a thermoplastic, which implies that it hardens when it cools down, and cures under influence of moisture in 2 days. However, it remains slightly sticky for a long period of time after that period. The adhesive is dispensed in a thick line (± 4 mm wide and high).

*Figure 2 Steinel PurGlue 50*

*Figure 3 Cartridge of HM-2510*

The main characteristics of the adhesive are summarized in the next table [Dow Corning Corporation, 2006 and 2007]:

| | |
|---|---|
| **Color** | Water clear |
| **Durometer – Shore A** | 47 Shore A |
| **Dynamic Viscosity (@ 120°C)** | 1050 Poise |
| **Elongation at break** | 760% |
| **Green Strength** | Instant<br>5 psi (0.03 MPa) @ 15 min<br>6 psi (0.04 MPa) @ 60 min |
| **Nonvolatile Content** | >98.5% |
| **Open time** | 15 min |
| **Pot life** | 1440 min |
| **Room temperature cure** | 2 days |
| **Shelf life** | 12 months |
| **Specific gravity @ 25°C (uncured)** | 1.07 |
| **Service temperature range** | -45°C - 150°C |
| **Tensile strength** | 390 psi (2.7 MPa) |
| **Modulus at 50% elongation** | 38 psi (0.26 MPa) |

*Table 2 Characteristics Dow Corning HM-2510*

In the above table, two terms need to be explained. First, the term “Durometer”: the durometer is a standard instrument used to measure the hardness of rubbers and rubber-like materials. Shore A is a durometer scale for soft rubbers or plastics. There are 12 scales for the durometer; each scale has a range of 0-100 with 100 indicating a harder material on that scale [Wikipedia, 2006].

The “green strength” is the strength of the bond before the adhesive has fully cured. The green strength is closely related to the fixture time (the amount of time before bonded parts can be handled). For this type of adhesive, the fixture time is very short (minutes), but it is safer to wait a day or two before handling the product. Otherwise you might misalign it since the adhesive is not fully cured yet.

### 2.2.1 Pretreatment

The experiences gained from the previous test have led to testing the current adhesive for a number of different pretreatments. The pretreatments are described below.

- *None*. The PE foil is only cleaned using isopropanol.
- *5 sec sanding with P80 sanding paper*. After sanding, the foil is cleaned using isopropanol.
- *5 sec sanding with P120 sanding paper*. After sanding, the foil is cleaned using isopropanol.
- *5 sec sanding with P180 sanding paper*. After sanding, the foil is cleaned using isopropanol.
- *10 min UV/Ozone*. First, the foil is cleaned using isopropanol. Then, the foil is laid under an UV radiation source (wavelengths of 184.9 nm and 253.7 nm, 80 W vapor Heraeus Noble light NNIQ120 [Oosterom, 2005]) in an enclosed area. The UV radiation source is readily available at the adhesion institute of this university. The enclosed area allows formation and containment of ozone under the influence of the UV radiation. The ozone and UV radiation oxidize the surface of the foil, increasing the surface energy. The black light needs to warm up for 5 minutes. After that period, the foil can be laid close to it and the black light needs to be turned on for another 10 minutes to allow full oxidation of the foil surface. After this treatment, the foil surface retains its new properties for approximately 1 hr.
- *5 sec sanding with P120 sanding paper and 10 min UV/Ozone*. First, the amount of surface area is increased by means of sanding. Then, the surface is cleaned using isopropanol. Lastly, the foil is laid under the black light for 10 minutes.
- *20 sec corona discharge.* First, the foil is cleaned using isopropanol. Then, the foil is treated using a corona discharge for 20 seconds, increasing its surface energy. The corona discharge is created using a TIGRES Corona gun CKG with a TIGRES power supply of 50 Hz. The corona gun consists out of two metal electrode bars that are 15 mm apart. Between the electrodes, a 50 kHz corona discharge is ignited. Compressed air flow in-between the electrodes, forcing the discharge towards the substrate in the form of a cone with a parabolic base [Oosterom, 2005]. The corona gun is readily available at the adhesion institute of this university.

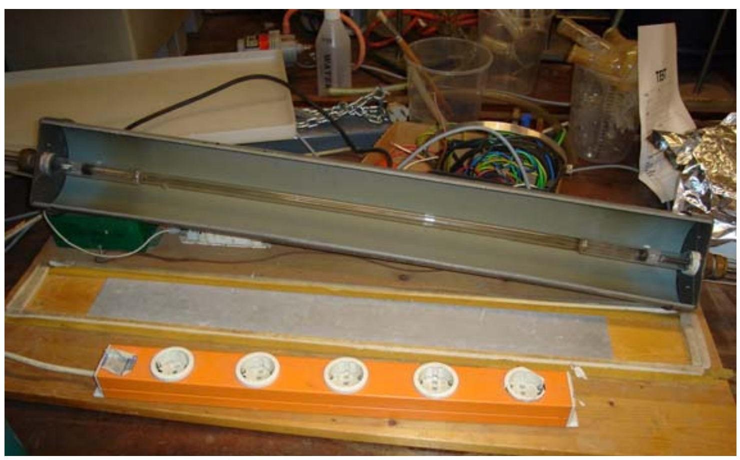

*Figure 4 UV radiation source*

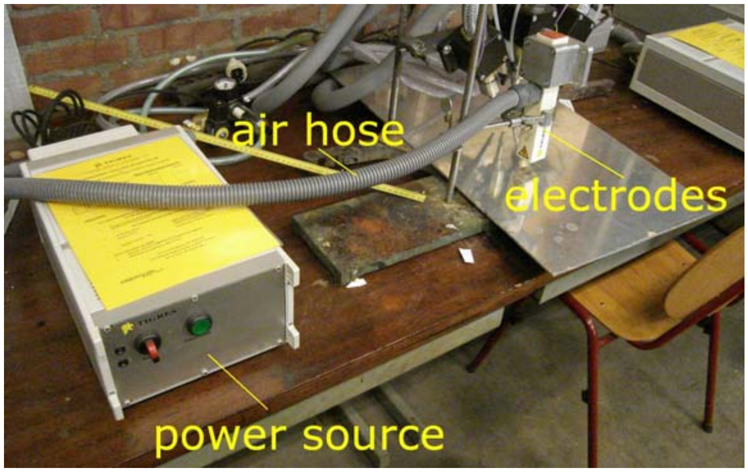


*Figure 5 TIGRES corona gun*

#### *2.2.2 Adhesive application*

The adhesive is applied directly from the gun onto one piece of foil. The other piece of foil is then laid on the adhesive and pressed down.
Since the adhesive has a high temperature and since LDPE has a melting point of 120°C, especially the second piece of foil tends to shrink and curl slightly when it comes in contact with the adhesive. This can be prevented by waiting with application of the adhesive 10 to 20 seconds after it has been removed from its heat source. The adhesive has now cooled slightly, which reduces the amount of deformation of the foil, but is also more viscous, which makes it more difficult to create a relatively thin bond line. For the tube-connector piece connection, this problem is less apparent since the adhesive is applied on top of the foil, which prevents deformation to a large extent.

#### *2.2.3 Results*

The results of the tests with the different pretreatments are summarized in the next table. For each pretreatment, 3 test samples are prepared unless otherwise stated. The precise strength of the bond is not determined; it is only tested whether the bond holds when it is pulled taut manually.

| **Pretreatment** | **Adhesion** | **Remarks** |
|---|---|---|
| 3x none | Good | |
| 3x P80 | Good | Sanding causes weakening of PE foil |
| 6x P120 | Good | Quality first 3 samples was poor, therefore 3 extra samples have been made. Cause of the poor quality is the high temperature of the adhesive. |
| | | Sanding causes weakening of PE foil |
| 6x P180 | Good | Quality first 3 samples was poor, therefore 3 extra samples have been made. Cause of the poor quality is the high temperature of the adhesive. |
| | | Sanding causes weakening of PE foil |
| 3x UV/ozon | Good | |
| 3x P120 + UV/ozon | Good | Sanding causes weakening of PE foil |
| 3x Corona discharge | Good | |
| 2x P120 + Corona | Good | The sanded samples have got the tendency to curl over during the corona treatment when the corona discharge comes close to the edge of the foil. This is probably caused by heating of the samples due to the discharge or due to the discharge hitting and heating the aluminum plate under the sample, which in turn heats the sample |

| | | |
|---|---|---|
| | | from underneath. Because there is less material present at the sanded area, it will heat up strongly there. This causes it to almost melt locally and curl upward. Some pieces of foil were unusable because of that. |
| | | Sanding causes weakening of PE foil |

*Table 3 Results HM-2510*

The results of the tests show that the current adhesive can be used to bond PE. It can even be used without application of cumbersome pretreatments like UV/ozone and corona discharge. Sanding of the surface is not advised since it weakens the material and does not improve the bond quality. When the samples are pulled taut manually, the sanded samples have the tendency to fail at the foil at a much smaller force than all other samples.

Pretreatments like UV/ozone and corona discharge are meant to ensure proper bonding for a prolonged amount of time, something that is not required for breadboarding. Furthermore, these pretreatments are cumbersome compared to simple degreasing. Therefore, it is decided to use this adhesive for the tube-connector piece interface and the only pretreatment that will be applied is degreasing of the bond surface.

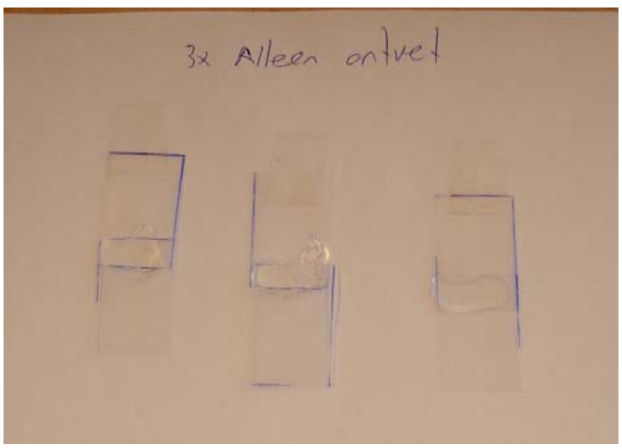


*Figure 6 Samples that have only been cleaned using isopropanol*

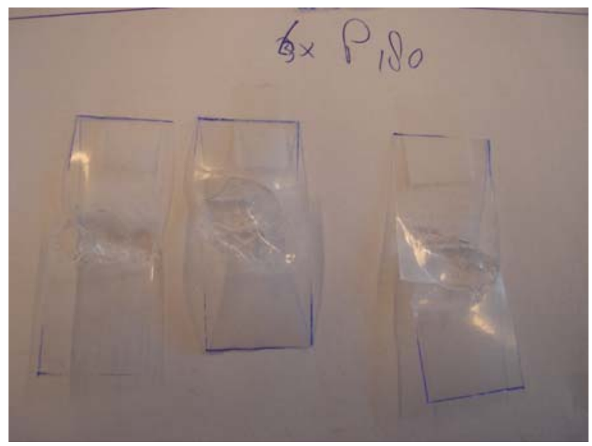

*Figure 7 Zoomed in on three deformed samples*

# 3 CONNECTOR PIECE BOND ADHESIVES

For the connector piece, thin and flexible bonds need to be created. Two sorts of adhesive are tested, namely methylmethacrylate adhesives and cyanoacrylate adhesives.

## 3.1 Methylmethacrylate adhesives

Methylmethacrylate adhesives are two-component adhesives that cure via an exothermic reaction between the two components. Two variants are tested: the PLEXUS MA310 and the RUPLO TA 610. For both variants, the samples are cleaned using ethanol before the adhesive is applied.

### *3.1.1 PLEXUS MA310*

This adhesive was readily available at the adhesion institute, but can also be acquired via for instance MAVOM. A special dispenser is required to mix the two components in the correct proportion (1:1 ratio), but this was also readily available.
Despite having an exothermic reaction, the adhesive is tested since it is one of the few adhesives available that are recommended for PE.

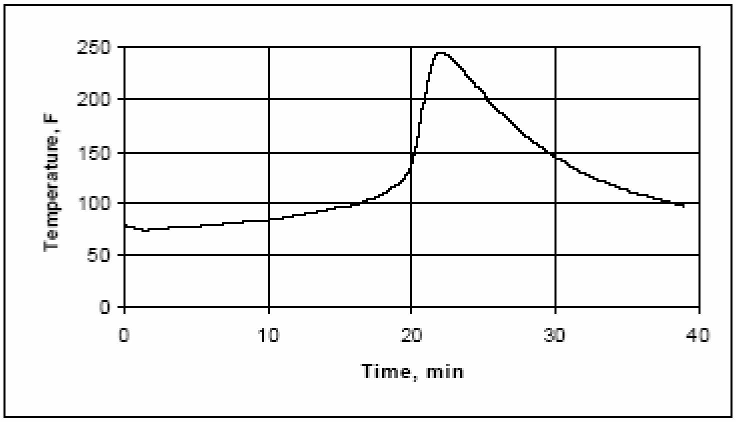


*Figure 8 Exothermic curve for MA310 at 75°F (24°C) (10 grams) [ITW PLEXUS, 2005]*

The above figure indicates that the exothermic reaction of the adhesive has a peak temperature of ~250°F, which is 120°C, for 10 grams of adhesive. Coincidentally, this is equal to the melting temperature of LDPE [Wikipedia, 2007].

The tests performed with this adhesive result in strong bonds between the strips of foil. However, the bond is relatively thick and there are two major drawbacks: The mass of the adhesive applied on the samples is less than a gram, but the heat developed in the reaction is still high enough to cause severe wrinkling of the foil. Next to the wrinkling of the foil, the adhesive that comes into contact with air becomes brittle and therefore the bond is no longer flexible. The combination of the two effects leads to the conclusion that this type of adhesive is not suited for the current application.

*Figure 9 Deformed MA310 samples*

#### *3.1.2 RUPLO TA 610*

This adhesive is different to the previous one in that the two components do not need to be mixed prior to application to the bond surface. One component needs to be applied on one bond surface and the other component on the other bond surface. The ratio between the two components is thus not important. Placing the two surfaces against each other results in the two components to react and form a bond. Both components are very viscous. The hardener is applied to the foil using a thin brush that is incorporated into the lid of the bottle. The adhesive is dispensed on a metal plate and then applied to the foil using a toothpick; the adhesive is a bit more viscous than the hardener.

The exothermic reaction is less severe for this type of adhesive than for the MA310, but the upper piece of foil still tends to curl upward. This is counteracted by holding it down using a piece of tape.

The result for this adhesive is not very good. Although the bond is flexible and rather thin, the strength of the bond is not very high in tension and the peel strength is very poor. The cyanoacrylate adhesives of the next subsection perform better overall.

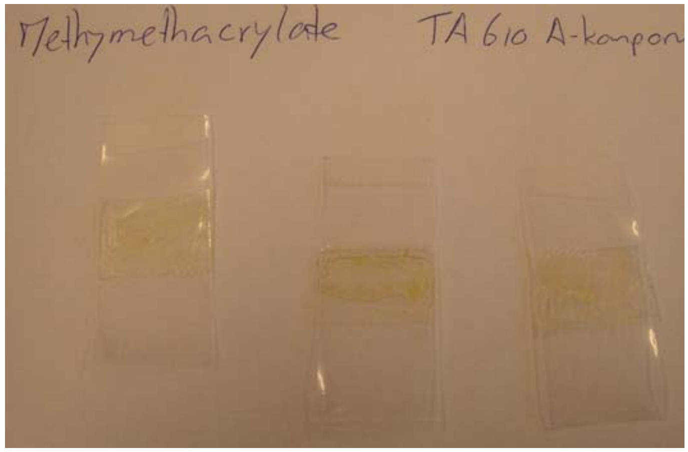


*Figure 10 Three TA610 samples*

## 3.2 Cyanoacrylate adhesives

The cyanoacrylate (CA) adhesives are supplied by RUPLO (Ten Boer, NL). A PE/PP primer is required to pretreat the surface and is also supplied by RUPLO. The CA-adhesives and the primer were readily available at the adhesion institute. The available adhesives had already passed their expiration date, but some were found adequate for testing. These are the three types described in the next subsections.

*Figure 11 The three different CA-adhesives*

### *3.2.1 RUPLO 1500S*

This adhesive has a relatively low viscosity. The adhesive is directly applied to one piece of foil (one drop is sufficient) and the other piece of foil is laid on top of the first one.

Just as with the MA310, the adhesive that hardens while in contact with air becomes brittle. However, there is no exothermic reaction and the created bond is very thin. When care is taken to ensure no adhesive is exposed to air, the bond is also very flexible. The tensile strength of the bond is very good, but the peel strength is poor. The peel strength is however much better than that of the TA610.

#### *3.2.2 RUPLO 1500S-D-5*

The results for this adhesive are similar to those for the 1500S variant.

#### *3.2.3 RUPLO 100K-S*

This type is similar to the previous two, with the only difference being its very low viscosity. The results are also similar, but the flexibility of the bond is larger than that of the 1500S variants.

Because this variant results in a very thin, flexible bond and can be applied in the correct dosage using for instance a toothpick, it is selected to be used for the bonds of the connector piece.

*Figure 12 Two 100K-S samples*

## 4 CONCLUSIONS & RECOMMENDATIONS

For the tube-connector piece interface, the Dow Corning HM-2510 Assembly Sealant is regarded to be adequate for breadboarding. The same applies for the RUPLO 100K-S cyanoacrylate adhesive.

Both adhesives have one drawback. The HM-2510 remains slightly sticky after is has fully cured. Thus, when iDod breadboard structures are folded, surfaces folded against the silicone adhesive will stick to the adhesive. The 100K-S has poor peel strength, but this problem is alleviated by the fact that the edges of the bonds of the connector piece are covered in silicone sealant when the tubes are attached to the connector piece. Therefore, once the tubular structure is assembled, there is little chance of peel forces occurring that can open the bond.

The two adhesives selected are not recommended for use in iDod structures made from other materials than PE. For that, better performing adhesives are likely to be available. Which ones those are is TBD.

## 5 FURTHER WORK

No further testing of adhesives on LDPE is foreseen.

## REFERENCES

1. Dow Corning Corporation, *Dow Corning HM-2510 Assembly Sealant*, Product Information, 17 April 2006.

2. Dow Corning Corporation, *Dow Corning HM-2510 Assembly Sealant-clear,* http://www.dowcorning.com/applications/search/products/Details.aspx?prod=04061592&type=PROD, viewed February 2007.

3. Dow Corning Corporation, *Dow Corning HM-2510 Assembly Sealant-clear,* Material Safety Data Sheet, Version 1.3, Midland (USA), 14 December 2006.

4. ITW PLEXUS, *MA310,* Technical Data Sheet, Revision 5, January 2005.

5. Oosterom, R. et. al., *Adhesion Performance of UHMWPE after different surface modification techniques,* Elsevier, Medical Engineering & Physics, 7 July 2005.

6. RUPLO lijmtechniek, *Safety Data Sheet activator nr 100,* product code: 0173009, Ten Boer (NL), 22 January 2003.

7. RUPLO lijmtechniek, *Safety Data Sheet cyanoacrylaatlijm,* product code: 0152003, Ten Boer (NL), 22 January 2003.

8. RUPLO lijmtechniek, *Safety Data Sheet Primer PE/PP,* product code: 0173001, Ten Boer (NL), 30 July 2003.

9. RUPLO lijmtechniek, *Safety Data Sheet TA 610,* Version 5, Ten Boer (NL), 24 January 2003.

10. RUPLO lijmtechniek, *Safety Data Sheet TA 610 verharder,* Version 2, Ten Boer (NL), 14 April 2000.

11. Wikipedia, *Low density polyethylene*, http://en.wikipedia.org/wiki/LDPE, 11 March 2007.

12. Wikipedia, *Shore durometer,* http://en.wikipedia.org/wiki/Durometer, 4 December 2006.

# Membrane attachment

## SUMMARY

Methods to attach the membranes of the inflatable structure to the inflatable tubes and to the storage device are explored. At the tubes, the shape of the tube end (flat or circular) complicates attachment, but does not influence the choice for the best attachment method.

A method in which a T-shaped piece of membrane material is pulled through a slit at the tube end and looped back through a slit in the membrane is selected as the best method for the membrane-tube connection. This way, the connection does not require any adhesive, is highly flexible to reduce thermal cycling stresses, and offers easy detachment and reattachment.
At the storage device, the same method is used, but now the T-shape is looped through two slits in the bottom of the storage device and through a slit in the membrane.

## KEYWORDS

Membrane, inflatable tube, seal, connection

## DISTRIBUTION

| | Name | | Company/ Institution |
|---|---|---|---|
| 1 | E.D. van Breukelen | Customer | ISIS B.V. |
| 2 | O.K. Bergsma | Project supervisor | TU Delft |

## APPROVAL

| | Name | Company/ Institution | Date | Signature |
|---|---|---|---|---|
| *Written* | D.C. Maessen | TU Delft | 4/12/2007 | |
| *Checked* | | | | |
| *Approved* | | | | |

## REVISION RECORD

| Issue | Date | Total pages | Affected pages | Brief description of change |
|---|---|---|---|---|
| Draft | 4/12/2007 | 21 | | |
| | | | | |

## LIST OF TBD'S AND TBC'S

| TBD/TBC | Paragraph | Subject | Due date | Action by |
|---|---|---|---|---|
| TBD | Subsection 6.1 | Peel strength adhesive | TBD | TBD |
| | | | | |
| | | | | |

## TABLE OF CONTENTS

# 1 INTRODUCTION

The inflatable structure of the iDod consists out of inflatable tubes and membranes. These have to be connected to each other in a certain manner. Near the CubeSat the membranes can also be connected to the CubeSat body instead of to an inflatable tube.

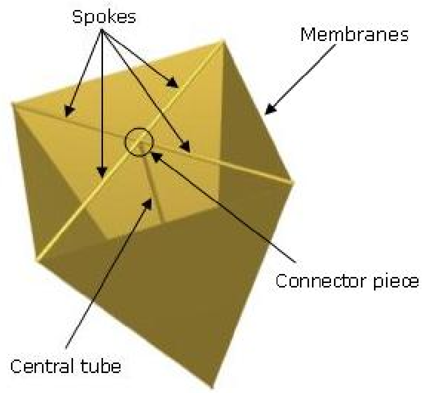


*Figure 1 Inflatable structure of the iDod*

The way the membranes are attached to the tubes depends on the method used to seal the tubes at their end in order to make them leak tight. Section 2 discusses the requirements imposed on the seal method for the tubes and the attachment method of the membranes. Sections 3 and 4 discuss the various options for sealing the tubes and connecting the membranes to the tubes respectively. Section 5 discusses the options for the attachment of the membranes near the storage device. In section 6 the best options are selected. Practical results for the attachment methods selected in section 6 are described in section 7. Section 8 discusses the most important conclusions and recommendations.

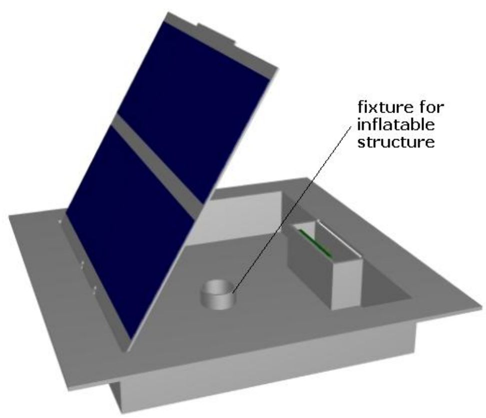


*Figure 2 Storage device for inflatable structure [Maessen, iDod.TN.006]*

# 2 REQUIREMENTS

The method used to seal the inflatable tubes is preferred to require no rigid parts. A solution with rigid parts will be heavier and more voluminous than a solution without rigid parts. In addition, the packing efficiency for the tubes will be higher and mismatches in the coefficient of thermal expansion of different materials are avoided.

The method used to attach the membranes either to the inflatable tubes or to the storage device is required to incorporate:

- Low mass and volume
- Flexibility to prevent stresses resulting from thermal cycling
- Maximum clearance between the membranes and the lid of the storage device

Furthermore, the attachment method is preferred to be redundant and preferred to not require any adhesive. The last preference follows from the method in which the inflatable is stowed. This method has not been determined yet, but it is likely that the membranes and the inflatable tubes will be separately folded and only connected to each other when everything has been folded. If adhesive is used for the connection, the inflatable can only be inflated once. This is obviously expensive in both time and material. In addition, when the adhesive is not properly selected and fails in space sometime during its 25 year long service life, the connection is lost. When no adhesive is used, such a failure can only occur when material erodes away and when that happens, a bond using adhesive will also fail.

# 3 SEAL METHODS FOR INFLATABLE TUBES

A number of possible concepts to seal a cylindrical tube are shown below:

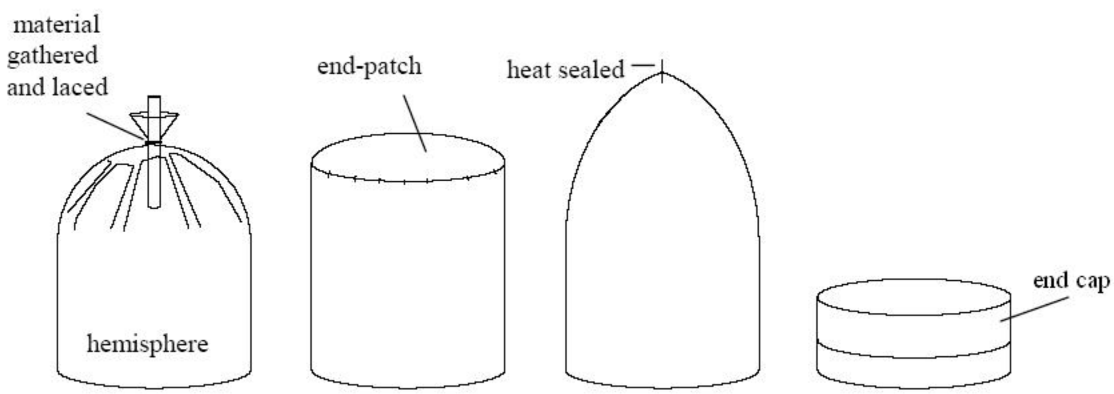


*Figure 3 Sealing methods for inflatable tubes [adapted from Kunze, 2002]*

The methods can be divided into two sorts: methods resulting in a flat tube end and methods resulting in a circular tube end.

## 3.1 Flat tube end

In figure 3, only one method is shown that results in a flat tube end: heat sealing. This is the manner in which the polyethylene tubes of the current breadboard inflatables are sealed:

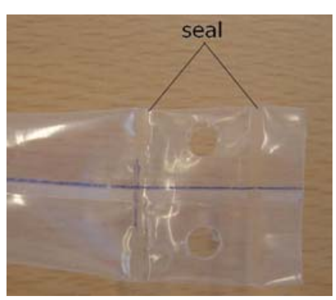


*Figure 4 Current seal method*

The two holes between the seals are for a hole-hole connection, which is treated in subsection 4.1.1. The seal at the right is not required, but helps in holding the tube material close together.

## 3.2 Circular tube end

Three sealing methods from figure 3 result in a circular tube end: gathering and lacing material, an end patch, or an end cap.

Gathering and lacing material around a rod can be applied when the tube material is very thin. Lacing of the material can be done using adhesive.

The end patch method uses a circular piece of foil with many flaps as the end patch. The flaps are bent and consecutively bonded to the inside of the tube.

The rigid end cap is slid in or over the tube after which the tube is bonded to the flanges of the end cap. This method is very similar to the end patch method with the difference being the presence of a continuous flange instead of many flaps.

# 4 MEMBRANE ATTACHMENT TO THE INFLATABLE TUBES

As mentioned earlier, attachment of the membranes to the inflatable tubes depends on the manner in which the tubes are sealed. Therefore, this section is divided into two subsections. The first subsection treats attachment methods in case the tube end is flat. The second subsection treats attachment methods in case the tube end is circular.

## 4.1 Flat tube end

This is the way the tubes are currently closed at their end. If this method is used, at least four ways of attaching the membranes to the tubes are possible:

1. *hole-hole*; connect two holes together
2. *adhesion*; bond the membrane and tube together using adhesive
3. *loop*; use a fiber or a strip of foil to form a loop and connect the loop with holes in the tube and the membrane
4. *slit in membrane*; make a small cut in the membrane and slide the membrane over the tube

The last method can be performed in two ways, as will be explained later. Also, the third and fourth method can be combined into a hybrid method. The above list is not claimed to be complete and neither are the options in the list claimed to be the best ones. All above options are treated in the next subsections. Note that all connections are made behind the seal in the tube (like in figure 4 for the hole-hole connection)!

### *4.1.1 Hole-hole*

The hole-hole method is schematically shown in the next figure. Holes are made in the tube and the membrane. The hole in the membrane has an opening, allowing the tube material to be inserted in that hole. When this has been done, the opening is closed using the reinforcement material (grey areas) that is already required to strengthen the area next to the holes. The reinforcements are simply extra foil material.

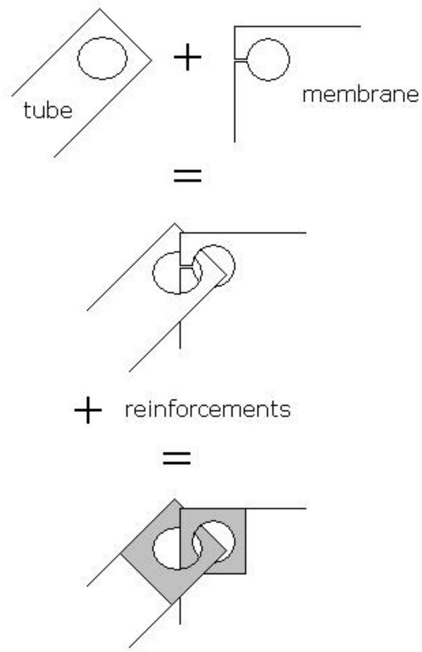


*Figure 5 hole-hole attachment method*

#### *4.1.2 Adhesion*

The adhesion method is schematically shown in the next figure. At the end of a tube, a long strip of material is present. At the corner of the membrane, two thin flaps of material are made. At the middle of the picture, the strip of material of the tube is wrapped around the tube. The outermost flap of the membrane is folded inward and bent 90°. The other flap is also bent 90°. At the bottom of the picture, a front view of the connection of one tube and two membranes is shown. The membrane material is grey while the tube material is black. The two flaps of the membrane are positioned above each other.

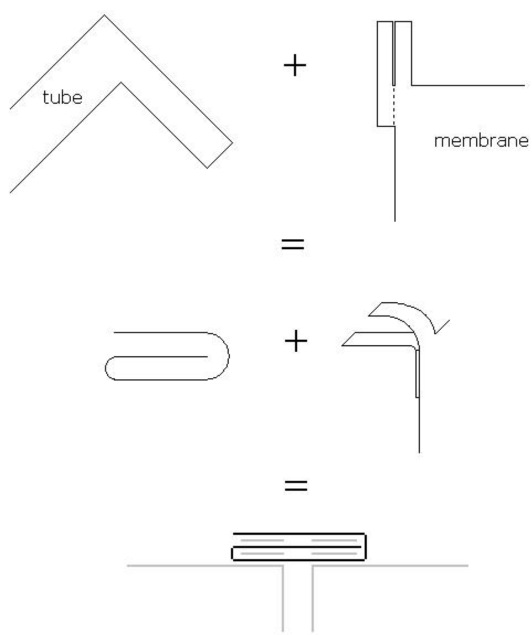


*Figure 6 Adhesion method*

This method is quite intricate, but the advantage is that the connection is redundant. The membrane can also be bonded to the tube end using a single lap joint, but then the connection is not redundant.

It is noted that instead of liquid adhesive, double sided tape can of course also be used.

#### *4.1.3 Loop*

In this method, holes are made in the tube and in the membrane. These holes are connected to each other using foil material or some sort of fiber formed into a loop. The method is graphically depicted in the figure below. Reinforcements are used around the holes and at the place where the loop needs to be closed if membrane material is used for the loop.

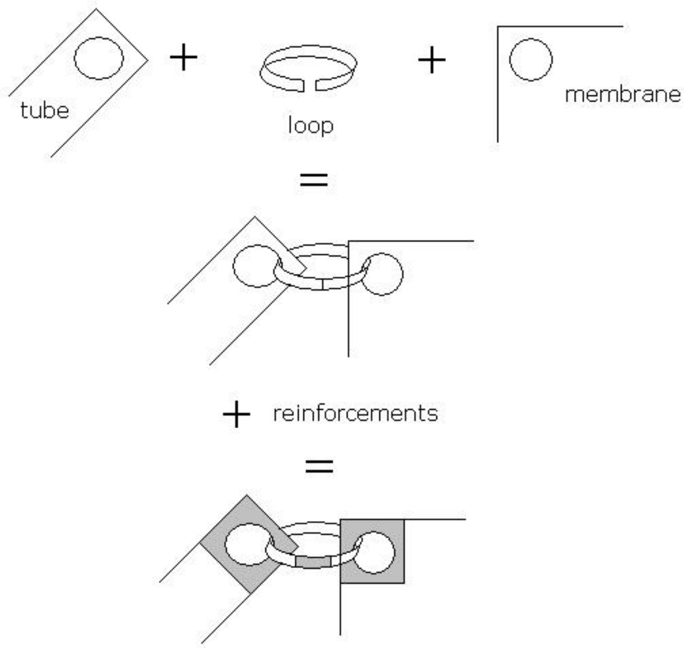


*Figure 7 loop method*

#### *4.1.4 Slit in membranes*

The next figure depicts the current method. A rectangular slit is made at the corner of the membrane and the membrane is slid over the rectangular end of the tube. The slit in the membrane is reinforced with extra material. Two stops at both sides of the membrane prevent it from sliding over the tube. These stops can be several layers of foil material bonded to the tube or even thick adhesive

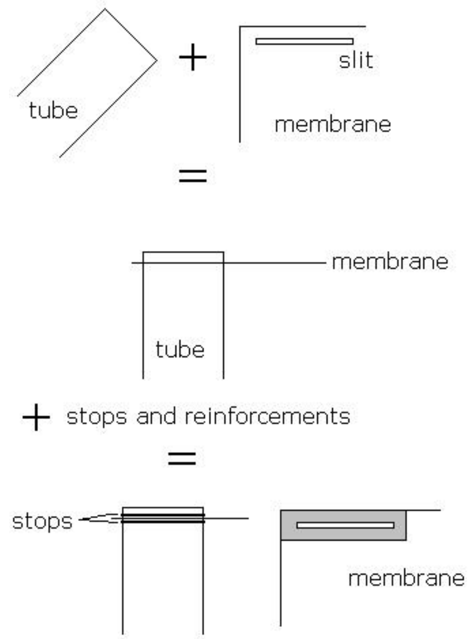


*Figure 8 Slit method*

#### *4.1.5 Alternative slit in membranes*

Alternatively, the slit in the membrane can be made smaller than the width of the rectangular part of the tube. With cuts at the end of the tube, a T-shape is created with the vertical bar of the T slightly less wide than the slit in the membrane. Folding the horizontal bar of the T allows the membrane to be hooked behind the T:

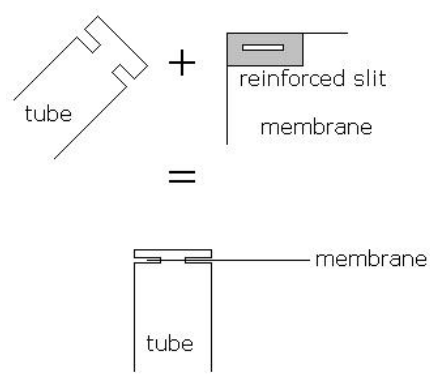


*Figure 9 Alternative slit method*

#### *4.1.6 Loop and slit*

The previous method can also be performed using a slit in the tube end and a slit and T-shape for the membrane. The T-shaped membrane end is pulled through the slit in the tube and through the slit in the membrane itself, forming a loop.

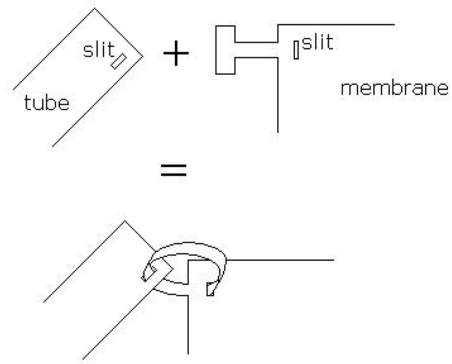


*Figure 10 Alternative slit method with T-shape at membrane*

## 4.2 Circular tube end

When the tube end is circular, attaching a membrane to a tube is somewhat more involved than when the tube end is flat. Three methods can be applied (again, these methods are not the only ones!):

1. adhesion
2. hole in membranes
3. load sleeve

### *4.2.1 Adhesion*

Using adhesive (or double sided tape), the membrane can either be bonded to the end cap or end patch (when used) using a simple lap joint or a strip of membrane material can be wrapped around the tube and bonded to the tube using adhesive.

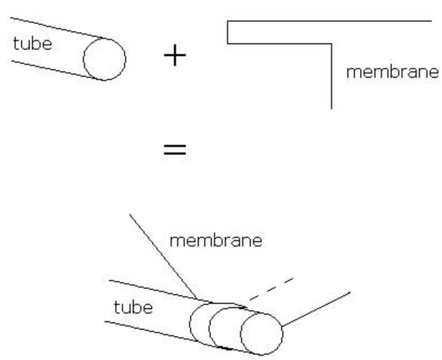


*Figure 11 Adhesion method for circular tube end*

### *4.2.2 Hole in membranes*

This method is similar to the method described in subsection 4.1.4 but now a circular hole is made in the membrane instead of a rectangular one.

### *4.2.3 Load sleeve*

Figure 11 shows a load sleeve around a cylindrical tube. A small flange is used to connect items to the load sleeve. This flange is flat and therefore all methods discussed in subsection 4.1 can be used to attach the membrane to the flange!

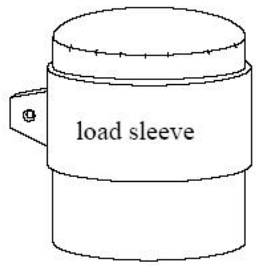


*Figure 12 Load sleeve [adapted from Kunze, 2002]*

The load sleeve can be made from foil material that is wrapped around the tube and bonded to it. The flange can be made by bonding two pieces of foil together or by using the alternative slit method from subsection 4.1.5.

# 5 MEMBRANE ATTACHMENT NEAR THE STORAGE DEVICE

Near the storage device, there are two options for attachment of the membranes:

1. to the central tube
2. to the storage device

## 5.1 Attachment to the central tube

When the membrane is attached to the central tube, three methods can be applied:

1. adhesion
2. hole in the membrane (like in subsections 4.1.4 and 4.2.2)
3. load sleeve with four flanges

The methods are too obvious to describe in detail. For the load sleeve method it is noted that the flanges are now perpendicular to the flange in figure 12.

## 5.2 Attachment to the storage device

The membranes can be attached either to the walls or to the bottom of the storage device. In both cases, bonding the membranes to the storage device using adhesive or double sided tape is the most obvious method.

Alternatively, when the membrane is attached to the bottom of the storage device it can also be fixed without bonding it to the storage device. This is similar to the loop and slit method of subsection 4.1.6. Instead of through a slit in a tube, the T-section is now pulled through two slits at the bottom of the storage device and through a slit in the membrane itself. This connection can even be made redundant by using two T-sections per membrane.

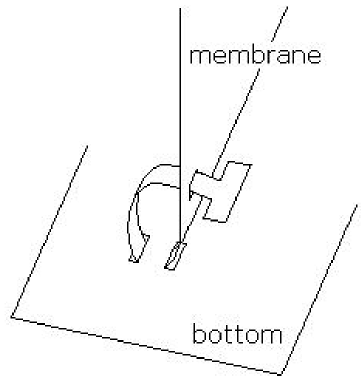


*Figure 13 Attaching the membrane to the bottom of the storage device using slits*

This method cannot be used at the walls of the storage device since the membrane material pulled through the walls can come into contact with the frame of the CubeSat upon insertion of the storage device into the CubeSat structure. The obvious risk there is that the membrane material can be damaged or even cut through.

# 6 METHOD SELECTION

In the current section the up- and downsides of the methods discussed in sections 3, 4, and 5 are treated and the best method of that section is selected.

## 6.1 Seal method inflatable tubes

In [Maessen, iDod.TN.008] Upilex-S foil is chosen as tube and membrane material. This material is not heat sealable and therefore the method which is used to close the tubes of the breadboard models of the inflatable cannot be used for flight models.
However, adhesive can also be used to create a flat tube end. The problem now is that the adhesive is loaded with a peel force once the tube is inflated. This is the worst manner in which a glued bond can be loaded. Yet, this method is by far the easiest and fastest method available and is preferred over all other methods. It remains TBD by testing whether or not this closing method can be applied to flight models of the inflatable.
Silicone sealant is a good candidate for this kind of bond since it is relatively thick compared to other liquid adhesives and will therefore result in a better seal near the fold lines created when pressing the tube end together.

A problem with the preferred sealing method is that the line where the tubes are sealed has very low stiffness and behaves like a hinge. Currently, the seal line is in the same plane as the spokes of the inflatable. This can result in the situation depicted in the next figure where the material behind the seal is deflected towards the CubeSat.

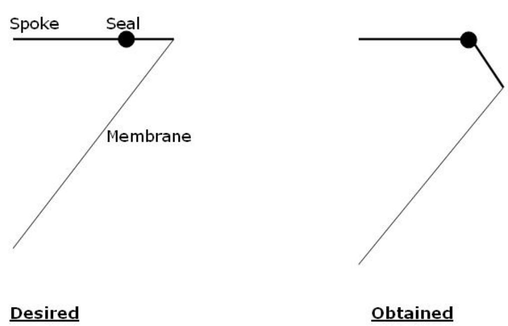


*Figure 14 Tube seal acting as hinge*

Luckily there is a very simple solution for this: rotate the seal line 90° such that it runs parallel to the central tube.

When a flat seal cannot be constructed, an end patch is preferred as sealing method. It is realized that the edges between the flaps necessary to bond the patch to the tube are an invitation to leaks, but this can be solved by laying a ring of silicone sealant over the edge of the tube, thereby closing the leaks.

A rigid end cap is not preferred for reasons already treated in section 2.

## 6.2 Membrane attachment to the inflatable tubes

The preferred seal method for the tubes is the one resulting in a flat tube end. The following table lists the (dis)advantages of the membrane attachment methods now available for various criteria.

| | **Hole-hole** | **Adhesion** | **Loop** | **Slit** | **Alternative slit** | **Loop and slit** |
|---|---|---|---|---|---|---|
| **Detachable** | Yes, but material has to be cut and re-joined | No | Yes, but material has to be cut and re-joined | Yes, but material has to be cut and re-joined | Yes | Yes |
| **Redundant** | No | Yes | No | No | No | No |
| **Flexibility** | Medium | Low | High | Medium | Medium | High |

*Table 1 (Dis)advantages membrane attachment methods*

The mass of the connection types is not included in the above table since this will be similar for all methods. The hole-hole, loop, and slit methods are detachable, but this requires making a cut somewhere and closing this cut again when a new connection needs to be made.

The loop and slit method is the preferred method due to its high flexibility and due to its easy detachability.

In case a flat tube end is not possible, a load sleeve combined with a loop and slit connection is preferred. This is due to the same advantages it offers as the loop and slit method in case of a flat tube end.

## 6.3 Membrane attachment at the storage device

When choosing between membrane attachment to the central tube or to the storage device itself, two additional complications have to be taken into account:

1. clearance with the lid of the storage device
2. clearance with the cool gas generator (CGG)

The next figure shows the required rotation angle of the lid of the storage device when the membranes are attached to the central tube.

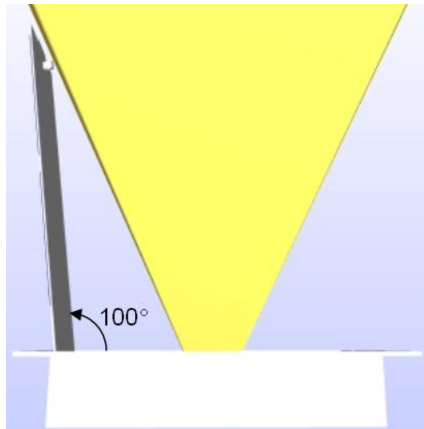


*Figure 15 Lid rotated 100° [Maessen, iDod.DD.002]*

When the membranes are connected to the bottom of the storage device, the required rotation angle of the lid will be larger. Connecting the membranes to the walls of the storage device results in serious problems at the wall where the lid hinges.

The CCG, used to provide the inflation gas for the inflatable, creates difficulties when the membrane is attached to the bottom of the storage device. This is outlined in [Maessen, idod.DD.002]. Three placement options for the CGG are shown in the figure below. Option 3 is the preferred option, but it is unlikely that this option is possible. With respect to leaks, option 1, where the CGG is screwed into the side of the fixture, is preferred. With respect to folding of the inflatable, option 2 is preferred. No placement choice for the CGG has been made yet. Note that in option 1, the CGG can be positioned everywhere around the fixture.

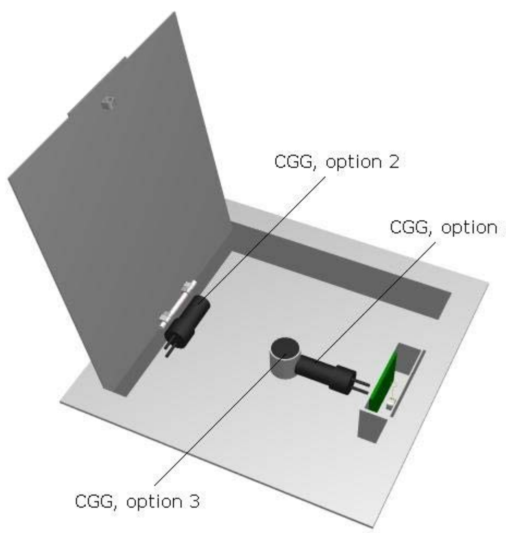


*Figure 16 CGG placement options [Maessen, iDod.DD.002]*

When option 1 is chosen for the CGG placement, attaching the membranes to the bottom of the storage device is problematic when the CGG is positioned as in figure 16. Then, attachment to the central tube using a load sleeve with four flanges and the loop and slit method is regarded to be the best option. This way, all membranes are attached in the same manner and no clearance issues between the membrane attachment points and the CGG can arise. In addition, the membranes will have more clearance with the lid than in case they are attached to the bottom of the storage device. The downside of this option is that a load sleeve (extra material) has to be used and that this load sleeve has to be bonded to the central tube.

However, currently it is expected that the CGG will be positioned as in option 2 since this greatly eases folding of the membranes. Then, attaching the membranes to the bottom of the storage device using the loop and slit attachment method becomes attractive since it can be implemented in a redundant style as already indicated in subsection 5.2. A possible downside to this attachment option is the limited working volume available to loop the T-section through the slit in the membrane. A pincer or a tweezers might have to be used in that case.

Choosing between the load sleeve option and the connection to the bottom of the storage device is difficult on beforehand. Folding tests with these connections have to point out which option is the better one. These tests are described in the next section.

# 7 PRACTICAL RESULTS

The next two subsections treat the practical results obtained for attachment of the membranes to the inflatable tubes as well as attachment of the membranes at the storage device. Subsection 7.3 lists the conclusions drawn from the practical results.

## 7.1 Membrane attachment to the inflatable tubes

Creating the membranes and attaching them to the inflatable tubes using the loop and slit method is done as follows:

1. Make a triangular cardboard mould. The base is 60 cm wide and the width is 70 cm.

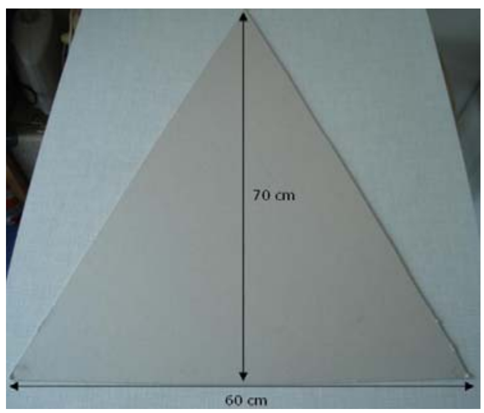


*Figure 17 Membrane mould with dimensions*

2. Use this mould to cut out a membrane with these dimensions. At the base of the triangle, create a 5x4 cm strip at both corners. These strips are used later on to create the T-sections. As membrane material, ordinary garbage bag foil (transparent, 20 μm thick) is used.
3. Position the ends of the spokes to which the membrane is to be connected at the corners with the strips. Mark the point at which the slit in a spoke overlaps the membrane material. This point must lie halfway the vertical bar of the T in the T-section that is created next.
4. Draw the T-section on the membrane material. Make the vertical bar of the T 20 mm long with a width of 5 mm. Make the horizontal bar 15 mm wide with a height of 5 mm. Draw the slit in the membrane material 10 mm under the T-section.
5. Apply tape on the drawing of the T-section and the slit. This reinforces and stiffens them. Then, cut out the slit and the T-section. Note: cutting out the T-section and the slit *before* applying tape is far more tedious!!

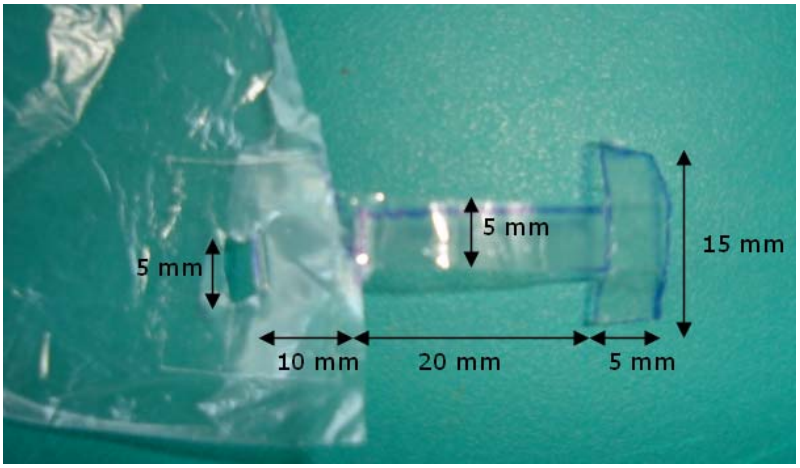


*Figure 18 T-section and slit at a membrane corner*

6. Connect the membrane and the spokes to each other using the loop and slit method.
7. Measure the distance, called x, from the middle of the base of the triangular membrane to its attachment point (whether this attachment point is a load sleeve flange or the bottom of the storage device is irrelevant). This distance is less than 70 cm and therefore the point will lie on the membrane. The attachment point lies halfway the vertical bar of the new T-section that now has to be created!
8. Remove the membrane from the spokes to facilitate the drawing and cutting to be done for the next attachment point.
9. Draw the T-section and the slit in the membrane required for the new attachment point and strengthen them using tape. Also, draw a horizontal line at the base of the T-shape.
10. Cut the membrane along the horizontal line (at a distance of x-1 cm from the base of the membrane) and the T-section.
11. Attach the membrane to the spokes and to the new connection point using the loop and slit method.
12. Repeat this method for all membranes.

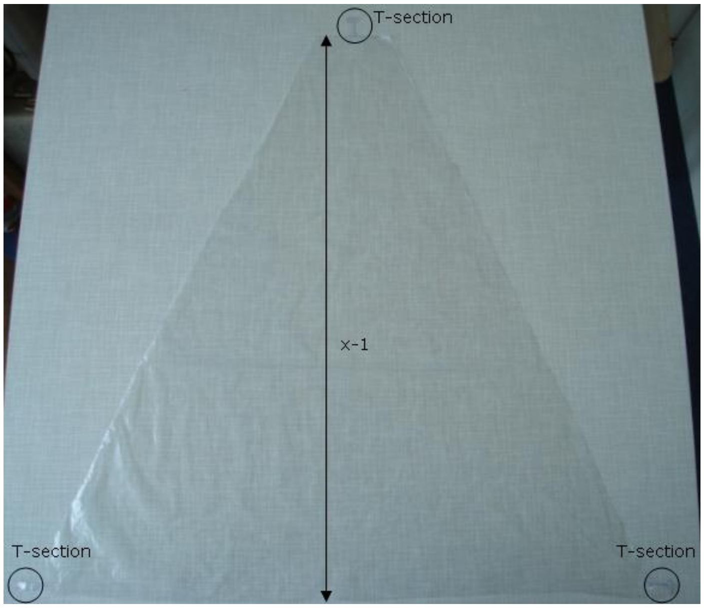


*Figure 19 Final membrane shape*

## 7.2 Membrane attachment at the storage device

Subsections 7.2.1 and 7.2.2 will discuss the membrane attachment to the storage device using two different methods.

### *7.2.1 Attachment to a load sleeve*

A load sleeve with four flanges can be constructed in the following manner:

1. Cut about 20 mm of tube from a self-made 20 mm diameter PE tube. This is the first part of the load sleeve.
2. Make four cuts in the small tube. Make them ~10 mm deep and 90° apart. The four flaps created in this manner are to be the flanges of the load sleeve.
3. Create a 40 mm diameter circle from PE foil with a 20 mm diameter hole in the middle.
4. Slide the small tube and the thick ring over another 20 mm diameter tube. Use the ring to bend the flaps in the small tube such that they are perpendicular to the larger tube. The ring and the small tube are now pressed against each other and their centerlines overlap. Connect the flaps and parts of the ring together using tape.
5. Remove the now connected ring and small tube from the large tube and also attach the ring to the inside of the small tube using tape.
6. Cut away those parts of the ring not overlapping a flap of the small tube. The load sleeve with four flanges has now been created.

*Figure 20 Finished load sleeve with flanges*

7. Make small slits in the flanges with a width of 5 mm.
8. Slide the load sleeve over the central tube of the inflatable structure such that the flanges are ~1 cm removed from the base of the central tube.
9. Connect the membranes to the flanges of the load sleeve using the loop and slit method.

*Figure 21 Load sleeve attached to the central tube and connected to one membrane*

*Figure 22 Membrane pulled into a curved shape by gravity*

*Figure 23 All membranes attached to the inflatable tubes, front view (left) and top view (right)*

Before the inflatable structure is attached to the storage device, the connections between the membranes and the spokes are removed. This eases folding of the structure. The central tube is attached to the fixture of the storage device using tape, resulting in the following:

*Figure 24 Central tube connected to fixture of breadboard storage device*

The flanges of the load sleeve a positioned ~1 cm above the bottom of the storage device. One membrane is now folded using the interleaved folding pattern discussed in [Maessen, iDod.TN.006]. The result is shown below.

*Figure 25 Folding results. From left to right: right corner of membrane folded, membrane folded into long rectangle, final stowed configuration*

The final stowed membrane is 7 cm wide, 3 cm deep, and 0.5 to 1 cm high depending on how strongly it is compressed. With a membrane thickness of 20 μm, this result in a packing efficiency of 20 to 40% (packing factor of 2.5 to 5).

Folding of the membrane does not present any special difficulties due to the used attachment method. The flanges of the load sleeve pose no difficulty when folding the membrane. Attachment of the central tube to its fixture does not pose serious issues with respect to accessibility of the connection, although the absence of the load sleeve would ease things considerably.
When folding the long rectangular membrane, it is difficult to keep the membrane taut and the longitudinal folds in place. When this is not done, membrane material piles up in front of material that has already been folded. From a packing efficiency point of view, this is not a big issue, but in the process many undesired wrinkles are introduced in the membrane material.

These wrinkles can have a detrimental effect on the protective coating of the membrane since the coating can crack at those places.

#### *7.2.2 Attachment to the bottom of the storage device*

Although planned, this test is not performed since while performing the previous test, it was realized that the results of this method will be a copy of the results obtained in the previous subsection. Folding of the membrane will be exactly the same and even when a CGG is in the way the membrane can be draped on top of it when it is fully folded (since the folded package was about 0.5 cm thick in the previous subsection, the combined height of the membrane and the CGG will be less than 14 mm, which is the available height). During folding, the presence of the CGG will not complicate the folding process in any way. When a CGG is present, attachment of the membrane to the storage device will be more tedious, but the attachment to the storage device using the previous method is also a bit tedious.

### 7.3 Conclusions

The attachment method chosen for the membrane-spoke connection works satisfactorily: the connection is easily made and unmade while it is highly unlikely to fail under normal circumstances.

Attachment of the membranes at the storage device will be easiest when they are attached to the bottom of the storage device using the loop and slit method. This way, no load sleeve with flanges is required, obviously saving mass and volume and easing attachment of the central tube to its fixture. The position of the CGG does not play a significant role in this choice.

## 8 CONCLUSIONS & RECOMMENDATIONS

The ends of the inflatable tubes are preferred to be sealed in such a way that a flat tube end is created. When this cannot be done in a leak tight manner, and end patch is preferred to be used. In both cases a good adhesive candidate to close potential leaks is silicone sealant.

When the tube ends are flat, the loop and slit method is selected for the membrane-tube connection. When the tube ends are circular a load sleeve combined with the loop and slit method is selected for the membrane-tube connection. This method offers high joint flexibility, easy detachment and reattachment, and does not require adhesive.

The connection method for the membranes near the storage device is selected to be attachment to the bottom of the storage device using the loop and slit method.

It is recommended to perform leak tests on tubes sealed with adhesive at operating temperatures to assess the leak tightness of the seal.

## REFERENCES

1. Kunze, A. and Kröplin, B., *Comparison of construction methods for inflatable truss structures*, presentation, 1st European Wrkshop on Inflatable Space Structures, ESA ESTEC, Noordwijk, The Netherlands, 21-22 May 2002.

2. Maessen, D.C., *iDod storage device,* iDod document iDod.DD.002, Version 1.2, Faculty of Aerospace Engineering, Delft University of Technology, 2 April 2007.

3. Maessen, D.C., *iDod stowage and deployment,* iDod document iDod.TN.006, Version 1.0, Faculty of Aerospace Engineering, Delft University of Technology, 11 April 2007.

4. Maessen, D.C., *Material selection,* iDod document iDod.TN.008, Version 1.0, Faculty of Aerospace Engineering, Delft University of Technology, 13 March 2007.

# Misalignments inflatable structure

## SUMMARY

The current document discusses theoretical misalignments that can occur in the inflatable structure of the iDod. For two breadboards of the tubular structure of the inflatable the misalignments are measured. The measurements indicate that the 2 cm diameter tubes of the prototypes are on average ~3° off their desired centerline.
The effect of misalignments of this magnitude on the surface area of the membranes and the base of the pyramid-shaped inflatable is determined. It is concluded that the effect of the misalignments on these two areas is insignificant and will thus influence the average frontal surface area of the inflatable marginally. Thus, misalignments will not cause a deviation in the expected de-orbit time of the CubeSat with deployed iDod.

It is recommended to keep the deviations in flight models below 3° and preferably below 1° since then the membranes of the inflatable can all have the same dimension, which eases production.

## KEYWORDS

Misalignment, inflatable, tubes, membranes, de-orbit

## DISTRIBUTION

| | Name | | Company/ Institution |
|---|---|---|---|
| 1 | E.D. van Breukelen | Customer | ISIS B.V. |
| 2 | O.K. Bergsma | Project supervisor | TU Delft |

## APPROVAL

| | Name | Company/ Institution | Date | Signature |
|---|---|---|---|---|
| *Written* | D.C. Maessen | TU Delft | 3/30/2007 | |
| *Checked* | | | | |
| *Approved* | | | | |

## REVISION RECORD

| Issue | Date | Total pages | Affected pages | Brief description of change |
|---|---|---|---|---|
| Draft | 3/30/2007 | 19 | | |
| | | | | |

## LIST OF TBD'S AND TBC'S

| TBD/TBC | Paragraph | Subject | Due date | Action by |
|---|---|---|---|---|
| | | | | |
| | | | | |
| | | | | |

## TABLE OF CONTENTS

# 1 INTRODUCTION

Structural misalignments (or defects) will cause the inflatable structure of the iDod to deviate from its designed pyramid shape. This in turn will influence the de-orbit time for the satellite since this depends on the average frontal surface area of the inflatable.

The current document discusses in section 2 which misalignments can occur in theory. Section 3 discusses which misalignments have been measured for two prototypes. The consequences of misalignments on the average frontal surface area of the inflatable structure of the iDod are treated in section 4. Conclusions and recommendations are given in section 5.

# 2 THEORETICAL MISALIGNMENTS

The inflatable structure of the iDod is shown below. The areas where misalignments can occur are indicated in the picture.

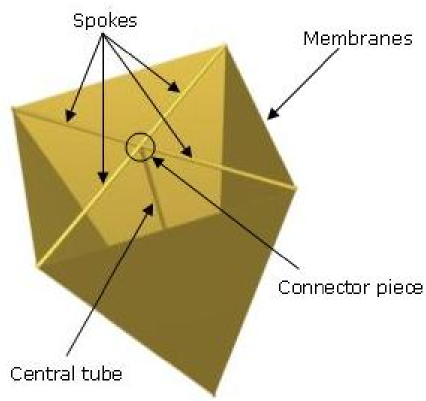


*Figure 1 Misalignment areas*

The coming subsections each treat the possible misalignments that can present themselves in the areas indicated above. It is assumed that components other than the misaligned ones are not adjusted to these misalignments. This will cause internal stresses and deformations. The magnitude of these is not treated.

## 2.1 Central tube

With respect to the central tube, three misalignments can occur:

1. Position of the central tube with respect to the geometric center of the CubeSat.
2. Central tube not straight.
3. Length of the central tube not according to specifications

### *2.1.1 Central tube position*

The position of the central tube affects the shape of the inflatable structure as well as the dynamic behavior of the complete satellite. However, the dynamics of the satellite are not of interest here and are therefore not treated.
In case the membranes of the inflatable structure do not meet at the root of the central tube, but are attached near the sides of the CubeSat, the following is the result in case the central tube is not positioned correctly (not to scale!):

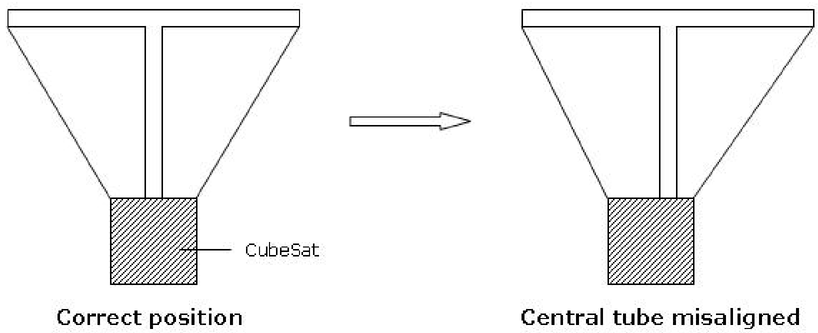


*Figure 2 Central tube misaligned*

Note that although the membranes in the above picture are depicted as a single line, this line in reality represents the edge of two membranes! In the entire document, reference will be made to just one of these membranes. For the other membrane, the result is exactly the same.

When the central tube is misaligned badly (right picture in figure 2), the membrane at the right side has to stretch in order to compensate for the extra distance it has to span. However, since the membrane is likely to be made out of material that does not stretch easily (a relatively large force is required to stretch it), there will be a tensile stress in the membrane. This tensile stress in the membrane results in a compressive force on the spokes as is depicted in the figure below. In the figure, the arrows with thick heads are the 'starting' forces and the arrows with the thin heads are the forces resulting form the 'starting' forces.

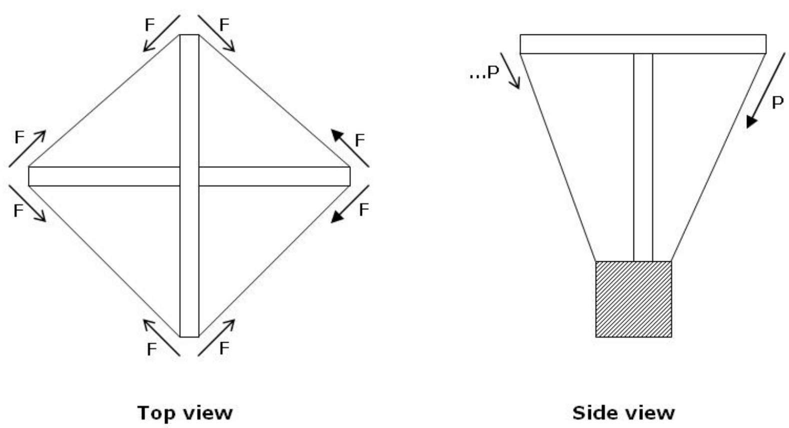


*Figure 3 Compressive forces on the spokes due to misalignment of central tube*

The vertical forces, when large enough, will result in the spokes to bend towards the CubeSat.

In the figure above, the vertical force on the right spoke is larger than the vertical force on the left spoke. This results in a clockwise moment on the end of the central tube, bending it towards the right. The next figure depicts the deformation in an exaggerated way. The left spoke is assumed not to be deformed, but it is rotated upward due to the deformation of the central tube.

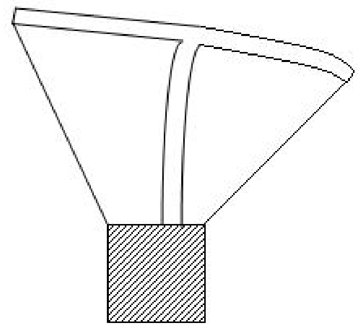

*Figure 4 Central tube misalignment result*

In case the membranes are attached to the central tube itself (not likely) or to the fixture of the central tube, a misalignment of the position of the central tube will have no consequence for the shape of the inflatable.

### *2.1.2 Straightness central tube*

When the central tube is not perfectly straight, the result is the same as for a misalignment of the central tube. The difference now is that connecting the membranes to the (fixture of the) central tube now also results in a deformation.

### *2.1.3 Length central tube*

The length of the central tube is important in that it contributes to the average frontal surface area of the satellite. For instance, when the central tube is too short, the membranes are not stretched fully, resulting in a smaller than desired average frontal surface area when the satellite is at a too high altitude to be passively stabilized by aerodynamic drag. The shape of the membranes will largely be determined by the creases (permanent wrinkles) present in the material. When the altitude is low enough for the satellite to be passively stabilized, the frontal surface area will be large enough since now the area of the ground plane of the pyramid is important and that area is not affected.

When the central tube is too long, the required frontal surface area is also not obtained since the required area of the ground plane of the pyramid is not achieved: All membranes are put under tension. Consequentially, either the membranes will stretch or the spokes will bend, depending on what requires the least effort. When the spokes are bent, the required area of the ground plane of the pyramid is not achieved.

When the membranes are not stretched, the central tube is loaded in compression, which can result in buckling of the central tube and failure of the complete inflatable structure. Of course, bending a spoke can also result in buckling of that spoke. Buckling of, say, the left spoke in figure 5 will result in reducing the forces acting on that side of the inflatable. This leads to the inflatable to bend to the right. Buckling of a spoke is a more 'favorable' failure mode than buckling of the central tube since the frontal surface area 'lost' by buckling of the spoke is compensated for by the area still present at the membrane opposite to the buckled spoke. This is not the case when the central tube buckles.

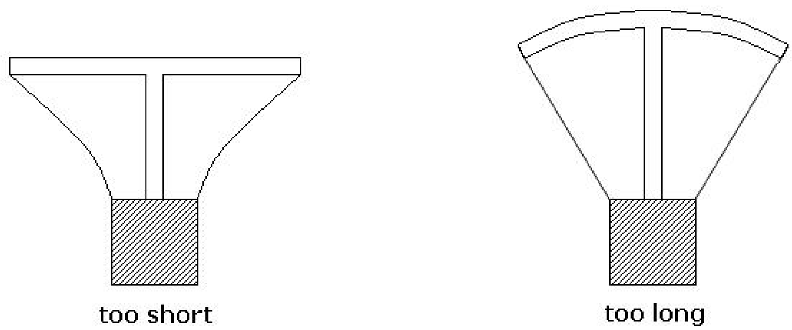


*Figure 5 Central tube too short (left) or too long (right)*

### 2.2 Connector piece

For the connector piece, there is one defect that will cause misalignment. This occurs when the connector piece is not mounted straight/parallel to the central tube.

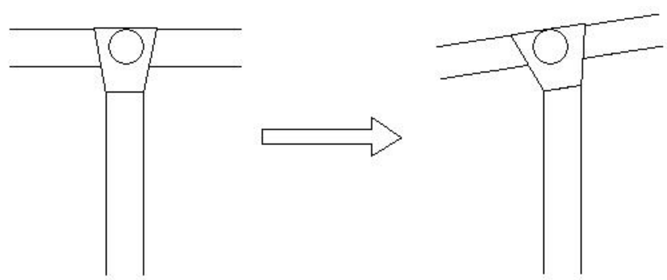

*Figure 6 Connector piece not mounted straight onto the central tube*

The result of the error depicted above is that the membrane at the left side of the connector piece will be slack, while the membrane at the right side of the connector piece will be pulled taut. Pulling the right membrane taut results either in stretching of the membrane or in bending of the spoke. This is illustrated in the next figure.

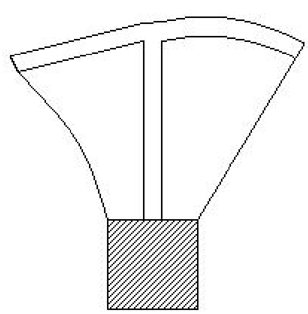

*Figure 7 Result of misalignment connector piece*

A tensile stress the right membrane also results in compressive forces acting on the spokes, just like in the case with the misaligned central tube of subsection 2.1.1. Therefore, these two situations are very similar.

### 2.3 Spokes

With respect to the spokes, three errors can occur:

1. Spokes not perpendicular to each other.
2. Spokes not perpendicular to the central tube.

3. Length of the spokes not according to specifications.

The first two errors can be caused either by the spokes not being perfectly straight or by improper connection of the spokes to the connector piece.

### *2.3.1 Spokes not perpendicular to each other*

When the spokes are not perpendicular to each other, they form a non-perfect cross. Spokes between which an angle of less than 90° is present result in the membrane between them to (initially) be somewhat slack. When the angle is larger than 90°, a tensile stress is caused in the membrane between the spokes. This results in the spokes to be forced towards each other.

Figure 8 depicts a situation where the spokes are far from perpendicular to each other. The membrane in the 'second quadrant' is initially slack because the angle between the spokes to which it is attached is less than 90°. No 'corrective' forces are present there. The other three membranes are pulled taut since the angles between the other spokes are more than 90°. The force acting on the spokes in the 'first quadrant', P, is smaller than the other forces since the angle between the spokes is less removed from 90°.

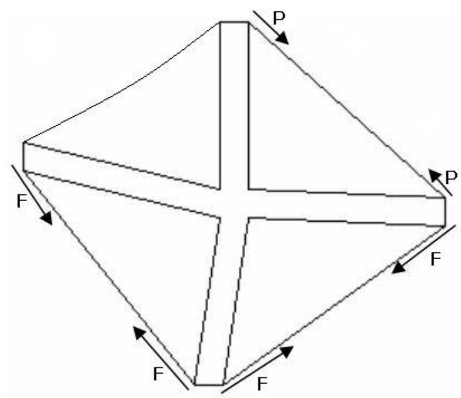


*Figure 8 Forces acting on the spokes when the spokes are not perpendicular to each other (initial situation)*

The forces on the spokes will, after the initial situation, cause all membranes to be pulled taut. The spokes will be bent in the direction of the largest forces. In the case above this means that the left and right spoke are bent downward. The lower spoke will not bend to the left or right since the forces acting on it cancel each other in horizontal direction.
The spokes are also loaded in compression (axially), which can lead to buckling (in extreme cases).

### *2.3.2 Spokes not perpendicular to the central tube*

In this case, the spokes are not all in the same plane. Thus, a situation like in subsection 2.2 can occur where one spoke points upward and another one points downward. Alternatively, all tubes can point 'upward' (away from the CubeSat), resulting in a situation similar to that of the too long central tube of subsection 2.1.3: The spokes will be forced to bend towards the CubeSat. In case all spokes point 'downward' (toward the CubeSat), the situation is similar to the case of the too short central tube in subsection 2.1.3. Only now the surface area of the ground plane of the pyramid is not equal to the desired area.

### *2.3.3 Length of the spokes*

When the spokes are too short, the membranes are slack and will therefore not provide the required surface area. This is similar to the previous case where all spokes point downward.

When the spokes are too long, the membranes are pulled taut which forces the spokes to bend towards the CubeSat. The result is similar to that of subsection 2.1.3 where the central tube is too long.

### 2.4 Membranes

With the membranes, two possible causes for errors are present: wrong dimensions or a faulty positioning of the attachment point of the membrane on the CubeSat.
The second error translates directly into a wrong width or a wrong height (or both) of the membrane at the position of the spokes. That is, the spokes are forced to bend (when the membrane is too small, not when it is too large!) Thus, only the first error is considered.

From a frontal area point of view, too large membranes are of course not a problem. Too small membranes result in a too small average frontal surface area and are therefore to be avoided.

Structurally, a too small width of the membranes at the location of the spokes results in the same situation as discussed in subsection 2.3.1 where the spokes are not perpendicular to each other. When the membranes are not long enough, the spokes are forced downward, which is structurally similar as the situation in subsection 2.1.3 where the central tube is too long.

## 3 OBSERVED MISALIGNMENTS

The current section treats the misalignments in the tubular structure of the inflatable. The next four figures depict misalignments present in the second breadboard model of the tubular structure.

*Figure 9 Central tube not straight*

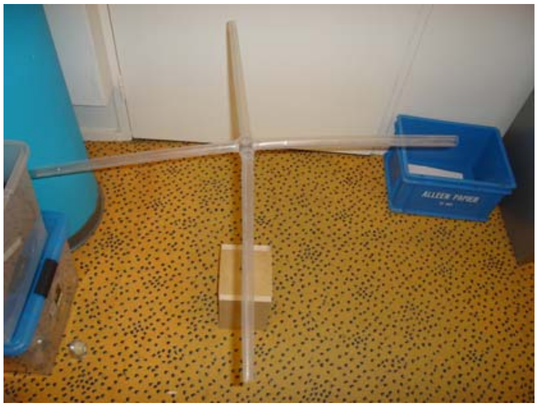

*Figure 10 Spokes not aligned*

*Figure 11 Misalignment central tube*

*Figure 12 Misalignment central tube (rotated 90°)*

From figures 11 and 12, it is clear that the misalignment of the central tube is quite severe for this particular model. This is mainly caused by production errors resulting from a lack of experience on how to assemble the structure properly. For the third model, the misalignments are already much smaller (see subsection 4.2) while the basic production method has not changed.

Subsection 3.1 treats the misalignments observed for the spokes in the second and third breadboard models. Subsection 3.2 treats the misalignments observed for the central tube.

## 3.1 Spoke misalignment

As discussed in subsection 2.3, spokes can have three different errors. Of these, an error in their length larger than a few millimeters is considered very improbable in engineering models and thus not considered here.

### *3.1.1 Perpendicularity between spokes*

The perpendicularity between the spokes is determined by measuring the offset of the center of the end of one spoke from the centerline of the spoke that is supposed to be parallel with it. For the 2nd prototype, the spokes are measured to be ± 15 mm and ± 25 mm off. For the 3rd prototype, the spokes are ± 15 mm and ± 0 mm off. The following pictures show the measured offsets.

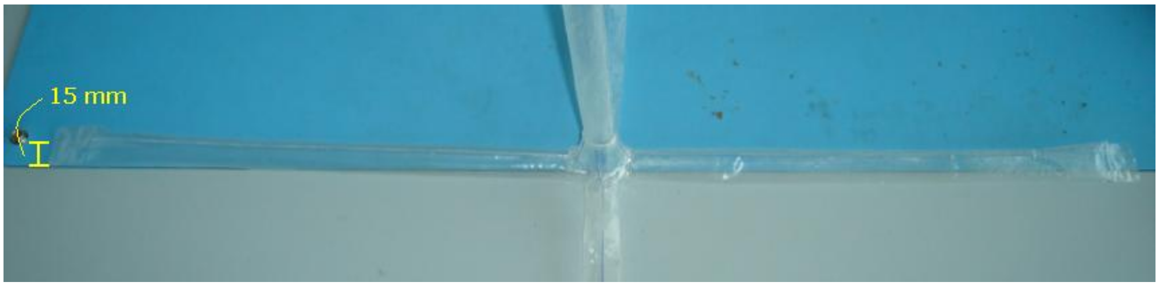


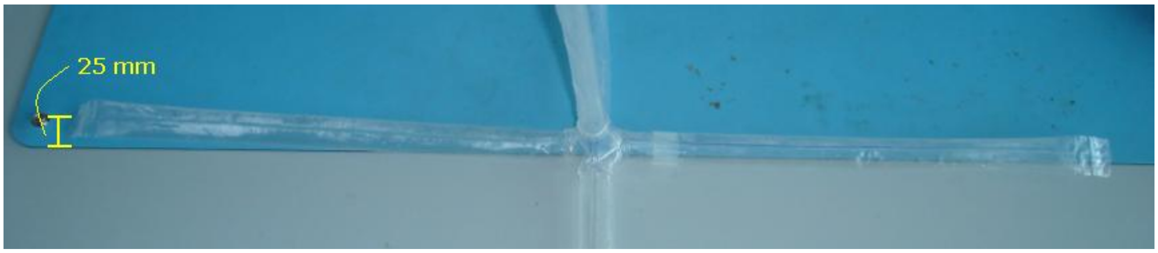

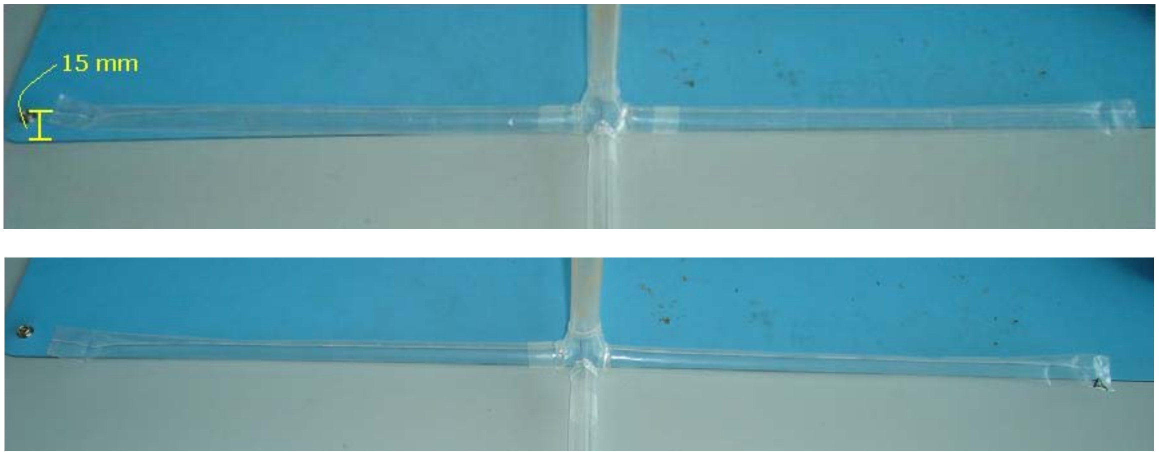


*Figure 13 Misalignments between the spokes. The two uppermost pictures are from the second prototype; the other two pictures are from the third prototype*

With a spoke length of 400 mm, the largest error, 25 mm, leads to a maximum measured deflection angle of 3.5°.

#### *3.1.2 Perpendicularity with respect to central tube*

Measuring the perpendicularity of the spokes with respect to the central tube is difficult if not impossible due to gravity. When the spokes are unsupported, they will sag towards the ground, making a measurement of their true deflection impossible. When they are supported, they will all be in the same plane, also making a deflection measurement impossible. Therefore, only an estimation of their deflection relative to the central tube is given. Based on the results for their misalignment with respect to each other, they are estimated to have a deflection at their end of 20 mm at most. With a length of 400 mm, this results in a deflection angle of 3°.

### 3.2 Central tube misalignment

As with the spokes, the error in the length of the central tube is considered to be insignificant and is therefore not considered. The error in the position of the central tube cannot be determined since it is not mounted to the storage device. Yet, this error will be extremely small (< 0.1 mm) since the fixture for the central tube will be an integral part of the storage device, which is precision milled from a block of aluminum [Maessen, iDod.DD.002].

The only misalignment that can be determined is the straightness of the central tube. Like with the spokes, this is determined by measuring the offset of the end of the central tube with respect to the desired centerline. For the 2$^{nd}$ prototype, the central tube is ± 65 mm and ± 70 mm off. For the 3$^{rd}$ prototype, the central tube is ± 10 mm and ± 20 mm off.

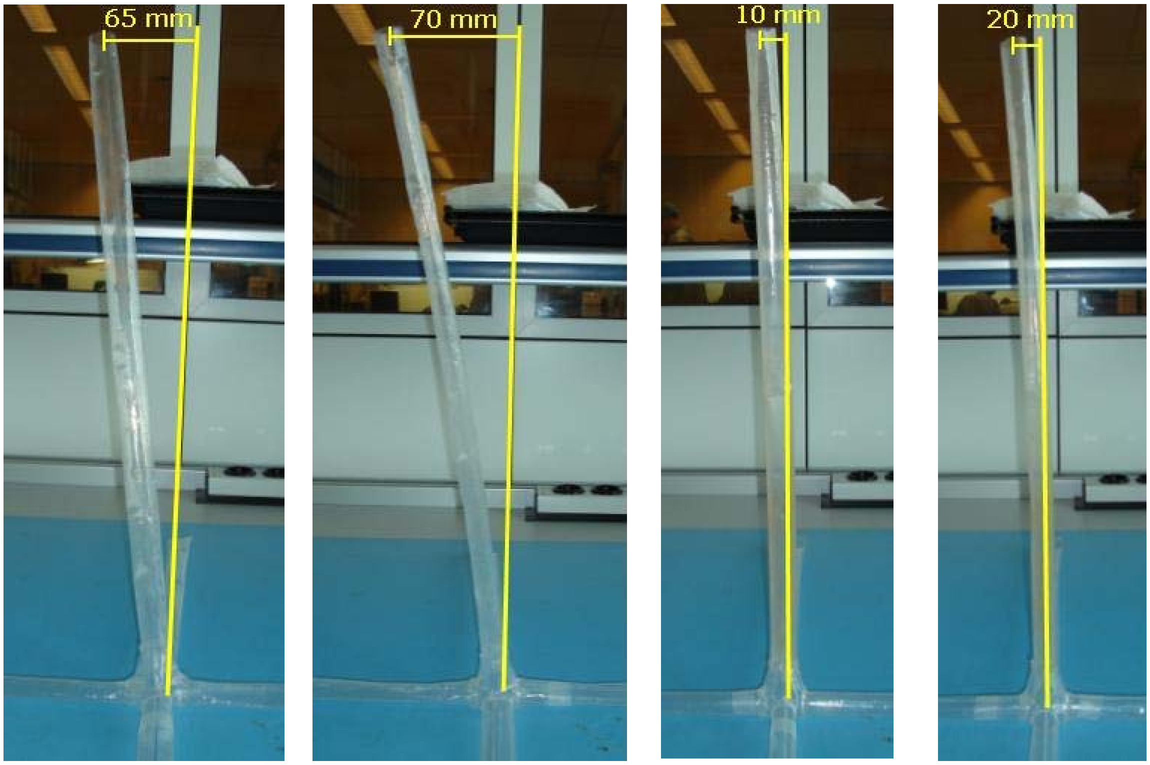


*Figure 14 Misalignments central tubes. The two pictures on the left are from the second prototype; the two pictures on the right are from the third prototype*

The largest error is 70 mm for a tube length of 500 mm, which translates into an angle of 8°. However, the largest measured error for the 3rd prototype is just 2.5°. As already discussed in the beginning of this section, the misalignment for the 2nd prototype is caused by a lack of experience. Therefore, the misalignment measured for the 3rd prototype is taken to be the misalignment that can be expected.

# 4 MISALIGNMENT CONSEQUENCES

Misalignment of components of the inflatable structure has two important consequences:

1. failure to meet the required average frontal surface area,
2. structural failure of the inflatable when the misalignments are too severe.

The second consequence indirectly also results in a failure to meet the required average frontal surface area.

Many misalignments in section 2 have a similar effect, namely the spokes being pulled towards the CubeSat (all three cases of subsection 2.1, case 2.2, case 2.3.2, case 2.3.3, and case 2.4 when the membranes are not long enough). Therefore, the chance of that effect occurring is relatively high.

Due to misalignments, undesired internal stresses will be present in the inflatable if the dimensions of the membranes are not adapted to these misalignments. The obvious way to prevent these stresses from occurring is to adapt the dimensions of each membrane to the measured misalignments. This will result in a deviation from the desired shape of the inflatable, but since the expected misalignments are small the deviation will also be small.

In this section, estimations will be given for the surface area of the base and the membranes of the inflatable structure due to the following misalignments:

1. Spokes not perpendicular to each other
2. Spokes rotated 3° upward (away from the CubeSat) or downward
3. Central tube not straight

The calculations with which the new areas are determined can be found in Appendix A.

For easy reference, the definition of some terms and the value for some lengths and areas as designed are given below.

The height (h) of the pyramid is graphically shown in the next figure. The edges of the base of the pyramid have length "a", the half diagonal of the base has length "b", the sides of the pyramid have a *slant height* "s", and the skewed edges of the pyramid have an *edge length* "e".

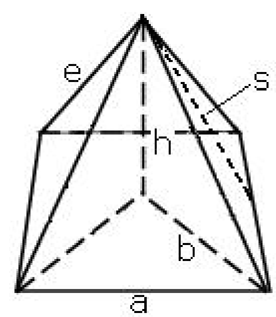


*Figure 15 Pyramid with length definitions*

Using the (wrong) dimensions of the inflatable derived in [Maessen, iDod.TO.001], the various lengths and surfaces are:

| | |
|---|---|
| **a [cm]** | 56.12 |
| **b [cm]** | 39.69 |
| **e [cm]** | 63.84 |
| **h [cm]** | 50 |
| **s [cm]** | 57.34 |
| **$A_{base}$ [$cm^2$]** | 3150 |
| **$A_{membrane}$ [$cm^2$]** | 1609 |

*Table 1 Lengths and surface areas inflatable as designed*

## 4.1 Spokes not perpendicular to each other

When the spokes are not perpendicular to each other, nothing changes in the total area of the inflatable.

On average the distance between the spoke ends (a) is still the designed 56.12 cm since the distance that is lost between one pair of spokes is gained for another pair of spokes. Therefore, the area of the base of the pyramid is still 3150 $cm^2$.
The total area of the membranes also does not change for the same reason as why the area of the base does not change.

## 4.2 Spokes rotated 3° upward or downward

For the area of the base of the pyramid, it does not matter whether the spokes are rotated upward or downward, for both cases the new area is 99.73% compared with the designed area.

Compared to the design, the area of the membranes is 102.07% when the spokes are rotated upward and 97.61% when the spokes are rotated downward.

Obviously, an upward rotation of the spokes is beneficial for the average frontal surface area of the inflatable, but this comes at the cost of more membrane area and thus more mass and volume.

### 4.3 Central tube not straight

In this case, the area of the base of the pyramid obviously does not change. In addition, just as in subsection 4.1, the deflections of the spokes caused by the curvature of the central tube will on average not lead to a change in total membrane surface area.

### 4.4 Conclusion

The expected misalignments will not cause any significant change in the average frontal surface area of the inflatable structure.
But, when for instance the central tube is not straight, the structure will not be symmetrical any more since the membranes are different in size. It is now possible that the structure will attain an attitude of least resistance, leading to a slower than desired de-orbit time. However, since the measured misalignments are small considering that only two (almost) full scale prototypes have been made thus far, the misalignments to be expected on flight models will be even smaller. Therefore, it is considered very improbable that the inflatable will attain an attitude of least resistance in space. Even when it does attain such an attitude, the increase in de-orbit time will not be measurable since it will be relatively small and due to the influence of many other variables on the de-orbit time (atmospheric density, solar radiation pressure, drag coefficient, etc.).

## 5 CONCLUSIONS & RECOMMENDATIONS

Misalignments are unavoidable for the inflatable structure of the iDod, but are expected to be so small that their influence on the de-orbit performance of the iDod is insignificant.

For two prototypes of the inflatable structure, offset angles of ~3° between the tubes and their desired centerline have been measured. For engineering models, these angles are expected to be smaller due to better production techniques and more experience.

Measuring the perpendicularity between the spokes and the central tube of the inflatable structure is difficult due to gravity. This has to be done in a zero-g (parabolic flight) environment, but doing this at all is not expected to be necessary since the deviation from the desired situation will be small.

It is recommended that for flight models of the inflatable structure, the deviation between the desired centerline of the inflatable tubes and the real centerline is kept below 3° and preferably below 1°. This will ease the construction of the membranes since they can all have the same dimensions. If this deviation is to be achieved, it is imperative that the inflatable tubes are as straight as possible, which is not trivial for tubes with a diameter of 1 cm and a length of ~50 cm.

## REFERENCES

1. Breukelen, E.D. van, Top Level Requirements for inflatable De-orbit device (*iDod)*, iDod document ISIS.iDod.REQ, Revision 1.3, Delft, 17 March 2007.

2. Gere, J.M., Timoshenko, S.P., *Mechanics of MATERIALS*, Fourth SI Edition, Stanley Thornes (Publishers) Ltd, Cheltenham (UK), 1999.

3. Maessen, D.C., *iDod Straw man concept design description,* iDod document iDod.DD.001, Version 1.0, Faculty of Aerospace Engineering, Delft University of Technology, 25 September 2006.

4. Maessen, D.C., *iDod storage device,* iDod document iDod.DD.002, Version 1.0, Faculty of Aerospace Engineering, Delft University of Technology, 27 March 2007.

5. Maessen, D.C., *iDod stowage and deployment,* iDod document iDod.TN.006, Draft, Faculty of Aerospace Engineering, Delft University of Technology, 28 March 2007.

6. Maessen, D.C., *Material selection,* iDod document iDod.TN.008, Version 1.0, Faculty of Aerospace Engineering, Delft University of Technology, 13 March 2007.

7. Maessen, D.C., *iDod inflatable structure conceptual design trade-off,* iDod document iDod.TO.001, Version 1.1, Faculty of Aerospace Engineering, Delft University of Technology, 28 February 2007.

8. UBE Europe, *Upilex-S*, datasheet, 3 November 2005.

9. Veldman, S.L., *Design and Analysis Methodologies for Inflated Beams*, Ph.D. dissertation, Faculty of Aerospace Engineering, Delft University of Technology (NL), Delft University Press, 2005.

10. Weisstein, E.W., *Triangle Area*, http://mathworld.wolfram.com/TriangleArea.html, 31 October 2005.

11. Weisstein, E.W., *Triangle*, http://mathworld.wolfram.com/Triangle.html, 25 October 2005.

12. Wertz, J.R., Larson, W.J., *Space Mission Analysis and Design*, Third Edition, Kluwer Academic Publishers, Dordrecht (NL), 1999.

13. Wijker, J.J., *Spacecraft Structures*, Lecture notes, Delft University Press, September 2004.

## APPENDIX A: NEW VALUES FOR AREAS DUE TO MISALIGNMENTS

Due to misalignments in the tubular structure of the inflatable, the shape of the inflatable will deviate from the designed shape. Here, it is determined what the new areas of the membranes and the base of the pyramid-shaped inflatable will become due to the following misalignments in the tubular structure:

1. Spokes not perpendicular to each other
2. Spokes rotated 3° upward (away from the CubeSat) or downward
3. Central tube not straight

The height (h) of the pyramid is graphically shown in the next figure. The edges of the base of the pyramid have length “a”, the half diagonal of the base has length “b”, the sides of the pyramid have a *slant height* “s”, and the skewed edges of the pyramid have an *edge length* “e”.

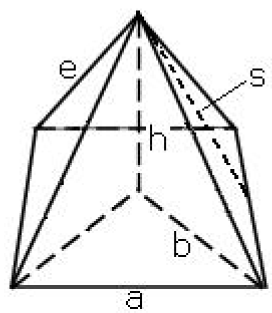


The slant height, edge length, and membrane area are determined using the following formulas from [Maessen, iDod.TO.001]:

$$s = \sqrt{h^2 + \frac{1}{4}a^2}$$

$$e = \sqrt{h^2 + \frac{1}{2}a^2}$$

$$A_{\text{membrane}} = \frac{1}{2}as$$

Using the (wrong) dimensions of the inflatable derived in [Maessen, iDod.TO.001], the various lengths and surfaces are:

| | |
|---|---|
| **a [cm]** | 56.12 |
| **b [cm]** | 39.69 |
| **e [cm]** | 63.84 |
| **h [cm]** | 50 |
| **s [cm]** | 57.34 |
| **$A_{base}$ [$cm^2$]** | 3150 |
| **$A_{membrane}$ [$cm^2$]** | 1609.01 |

**Spokes not perpendicular**

When the spokes are not perpendicular to each other, nothing changes in the total area of the inflatable. On average the distance between the spoke ends (a) is still the designed 56.12 cm since the distance that is lost between one pair of spokes is gained for another pair of spokes. Therefore, the area of the base of the pyramid is still 3150 cm$^2$.

The total area of the membranes also does not change for the same reason as why the area of the base does not change.

**Spokes rotated upward 3°**

When all spokes are rotated 3° upward, the projected surface area of the base is changed. Since a spoke is rotated, length b changes for the projected surface area into a virtual length b' which is equal to:

$$b' = b\cos\left(3^\circ\right) = 39.69 \cdot \cos\left(3^\circ\right) = 39.63 \text{ cm}$$

Since b changes, the length a has to change too. The new value for a is a':

$$a' = 2b'\cos\left(45^\circ\right) = 2 \cdot 39.63 \cdot \cos\left(45^\circ\right) = 56.05 \text{ cm}$$

The new base area then is:

$$A_{\text{base}} = \left(a'\right)^2 = 56.05^2 = 3141.37 \text{ cm}^2$$

The new area of the base is: (3150/3141.37)·100% = 99.73% of the designed area.

The membrane area changes too. The slant height s becomes s'. Using the cosine rule, the value for s' can be determined:

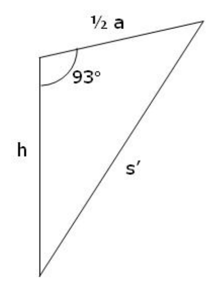


$$s' = \sqrt{h^2 + \left(\frac{1}{2}a\right)^2 - 2\left(\frac{1}{2}a\right)h\cos\left(93^\circ\right)} = \sqrt{50^2 + 28.06^2 - 2 \cdot 50 \cdot 28.06 \cdot \cos\left(93^\circ\right)} = 58.60 \text{ cm}$$

The new membrane area is:

$$A_{\text{membrane}} = \frac{1}{2}a's' = \frac{1}{2} \cdot 56.05 \cdot 58.60 = 1642.30 \text{ cm}^2$$

This area is: (1642.30/1609.01)·100% = 102.07% compared to the designed area.

**Spokes rotated downward 3°**

The area of the base is again 99.73% compared to the designed area.

The slant height now becomes smaller since the angle between a spoke and the central tube is not 93°, but 87°. The new slant height is called s'':

$$s'' = \sqrt{h^2 + \left(\frac{1}{2}a\right)^2 - 2\left(\frac{1}{2}a\right)h\cos\left(87^\circ\right)} = \sqrt{50^2 + 28.06^2 - 2\cdot 50\cdot 28.06\cdot\cos\left(87^\circ\right)} = 56.04\ \text{cm}$$

The new membrane area is:

$$A_{\text{membrane}} = \frac{1}{2}a's'' = \frac{1}{2}\cdot 56.05\cdot 56.04 = 1570.50\ \text{cm}^2$$

This area is: (1570.50/1609.01)·100% = 97.61% compared to the designed area.

**Central tube not straight**

In this case, the area of the base obviously does not change.

The new areas of the membranes depend on the curvature of the central tube. Knowing the displacement with respect to the desired centerline, as performed in subsection 3.2, is not enough. The angle of the end of the central tube with respect to the horizontal also needs to be known.

For the 3rd prototype, the deflection of a spoke at its end due to the curvature of the central tube is measured to be ~50 mm. This translates in an angle of ~7 degrees with respect to the horizontal. It is now assumed that the curvature of the central tube and two parallel spokes are in the same plane. The other two spokes are assumed to be perfectly perpendicular to the central tube and will not be deflected due to the curvature of the central tube. When the deflected spokes are themselves also 3 degrees off the desired centerline, the total deflection angle for these spokes can be as much as ~10 degrees or ~70 mm. Then, two membranes will get one corner to be 70 mm higher than designed and the two other membranes will both get a corner 70 mm lower than designed. Graphically:

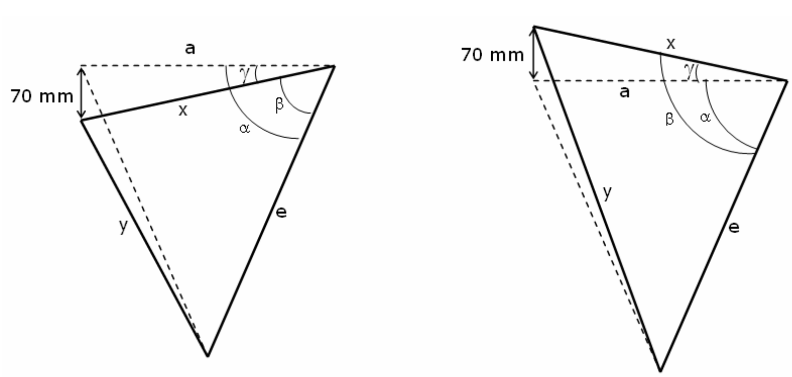


Corner lower

When one corner is lower than designed, the angle $\alpha$ is equal to:

$$\alpha = \operatorname{acos}\left(\frac{\frac{1}{2}a}{e}\right) = \operatorname{acos}\left(\frac{\frac{1}{2}\cdot 56.12}{63.84}\right) = 63.92^\circ$$

The length of side x is:

$$x = \sqrt{a^2 + 7^2} = \sqrt{56.12^2 + 7^2} = 56.56 \text{ cm}$$

Using this value, the angle $\gamma$ can be determined:

$$\gamma = \operatorname{acos}\left(\frac{a}{x}\right) = \operatorname{acos}\left(\frac{56.12}{56.56}\right) = 7.11^\circ$$

With angles $\alpha$ and $\gamma$ known, angle $\beta$ can be easily calculated:

$$\beta = \alpha - \gamma = 63.92^\circ - 7.11^\circ = 56.81^\circ$$

Since the height of the triangle is as yet unknown, the standard formula to determine the surface area of the triangle cannot be used. From [Weisstein, 2005] it is obtained that the area of a triangle can also be determined when the length of two sides and the value for one angle are known. Using the definitions for the sides and the angles depicted below, the area can be obtained using the following formula:

$$A_{\text{membrane}} = \frac{1}{2} bc \sin A$$

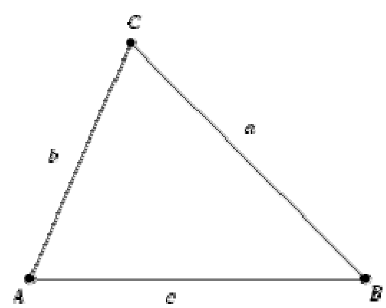


Using the values for x, e, and $\beta$, the new membrane area is obtained without knowing the height of the triangle:

$$A_{\text{membrane}} = \frac{1}{2} xe \sin\beta = \frac{1}{2}\cdot 56.56 \cdot 63.84 \cdot \sin\left(56.81^\circ\right) = 1510.79 \text{ m}^2$$

This new area is: (1510.79/1609.01)·100% = 93.90% compared to the designed area.

<u>Corner higher</u>

The only difference in the calculations for this case compared to the previous case is that now $\beta = \alpha + \gamma$:

$$\beta = \alpha + \gamma = 63.92^\circ + 7.11^\circ = 71.03^\circ$$

The new membrane area is:

$$A_{\text{membrane}} = \frac{1}{2} xe \sin\beta = \frac{1}{2} \cdot 56.56 \cdot 63.84 \cdot \sin\left(71.03^{\circ}\right) = 1707.23 \text{ m}^2$$

The new area is: (1707.23/1609.01)·100% = 106.10% compared to the designed area.

Conclusion

When looking at the result for both cases (93.90% and 106.10%), it is concluded that on average there is no difference in average membrane area compared to the designed area for this case!

# iDod mass and volume breakdown


## SUMMARY

The masses and volumes of the major components of the iDod system are allocated in a top down approach. System masses and volumes not fully utilized indicate the presence of some margin on the requirements.

The mass requirement for the iDod is met, the volume requirement is not. This indicates that the inflatable structure has to be reduced in size, which results in a starting altitude lower than 1000 km.

It is recommended to determine the achievable packing factor and the exact required size of the inflatable. This aids in a better determination of the mass and volume of the inflatable structure.



## KEYWORDS

mass, volume


## DISTRIBUTION

| | Name | | Company/ Institution |
|---|---|---|---|
| 1 | E.D. van Breukelen | Customer | ISIS B.V. |
| 2 | B.T.C. Zandbergen | Project supervisor | TU Delft |
| 3 | O.K. Bergsma | Project supervisor | TU Delft |

## APPROVAL

| | Name | Company/ Institution | Date | Signature |
|---|---|---|---|---|
| *Written* | D.C. Maessen | TU Delft | 4/5/2007 | |
| *Checked* | | | | |
| *Approved* | | | | |

## REVISION RECORD

| Issue | Date | Total pages | Affected pages | Brief description of change |
|---|---|---|---|---|
| Draft | 1/19/2007 | 6 | | |
| Version 1.0 | 4/5/2007 | 8 | 1 | Summary changed |
| | | | 4 | New figure inserted and old figure replaced by an updated figure |
| | | | 6 | – Total system mass increased from 100 g to 117 g<br>– Mass allocated to inflatable structure increased from 55 to 56 g<br>– Adhesive mass reduced from 10 to 2 g<br>– Mass allocated to deployment system increased from 32 to 48 g<br>– Mass allocated to complete storage device increased from 32 to 48 g |
| | | | 7 | – Total system volume increased from 104 cc to 135 cc<br>– Deployment system volume increased from 12 cc to 18 cc<br>– Inflation system volume reduced from 4 cc to 2 cc<br>– Inflatable structure volume increased from 84 cc to 111 cc |
| | | | 8 | Volume conclusion changed |
| Version 1.1 | 4/19/2007 | 8 | 5, 6, 8 | Mass CGG changed from 1.8 to 3 grams. |

## LIST OF TBD'S AND TBC'S

| TBD / TBC | Paragraph | Subject | Due date | Action by |
|---|---|---|---|---|
| TBD | Section 3 | Required size inflatable | TBD | TBD |
| TBD | Section 3 | Packing factor inflatable | TBD | TBD |
| | | | | |

## TABLE OF CONTENTS

# 1 INTRODUCTION

In this document, the mass and volume for the major subsystems and components of the iDod is assigned in a top-down manner. Components for which the mass and volume has already been determined (current best estimate, CBE), are naturally assigned this mass and volume.

# 2 MASS AND VOLUME ALLOCATION

The breakdown of the iDod system is presented below:

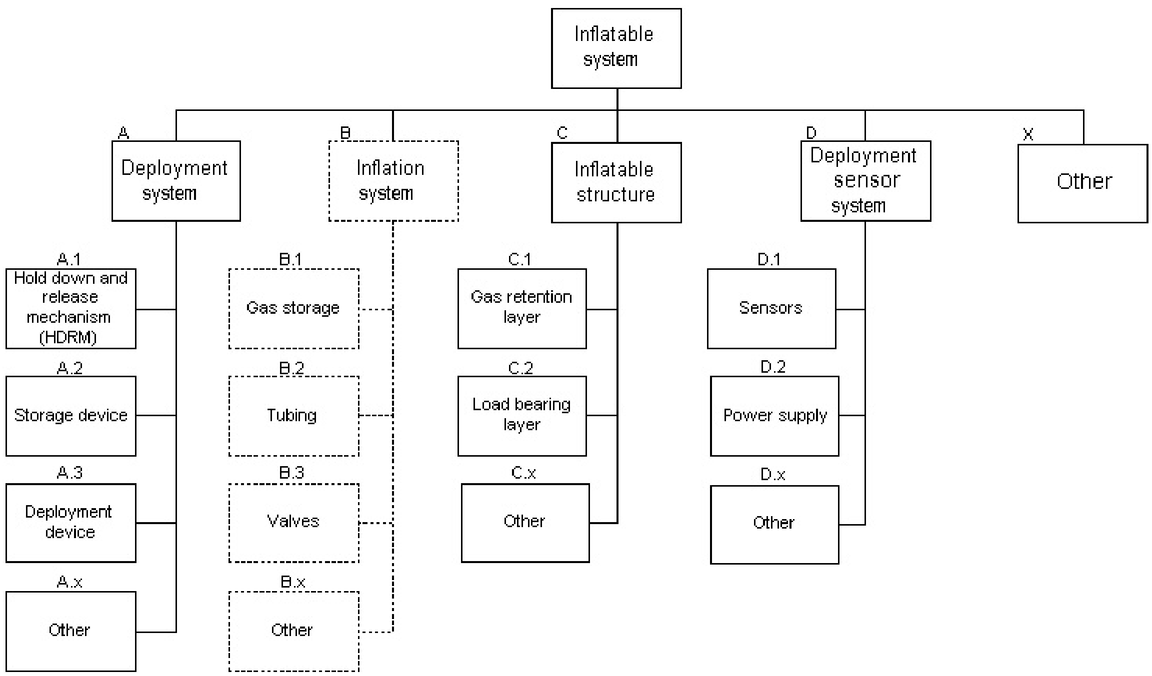


*Figure 1 iDod system breakdown [Maessen, iDod.DD.001]*

The upcoming mass and volume breakdown is loosely based on the above system breakdown.

## 2.1 Important information

The storage device for the iDod is a container of approximately 83x83x15 $mm^3$ [Maessen, iDod.DD.002]. It is made out of aluminum 6061-T6.

At the present time, the inflatable structure is deployed once a lid covering the container has been opened. This lid is held down by means of a Dyneema wire which is melted through once the deployment command is given. Melting through of the wire is achieved by heating up a resistor which is in contact with the wire. The lid is allowed to rotate around an aluminum axle. Opening of the panel is achieved by means of two helical torsion springs positioned on the axle (for redundancy, in case one spring cold welds to the axle). A picture of the storage device is shown on the next page.

As described in [Maessen, iDod.DD.002], the storage device is integrated into the top panel of the CubeSat. Therefore, there are flanges present at the sides of the storage device that function as part of the top panel.

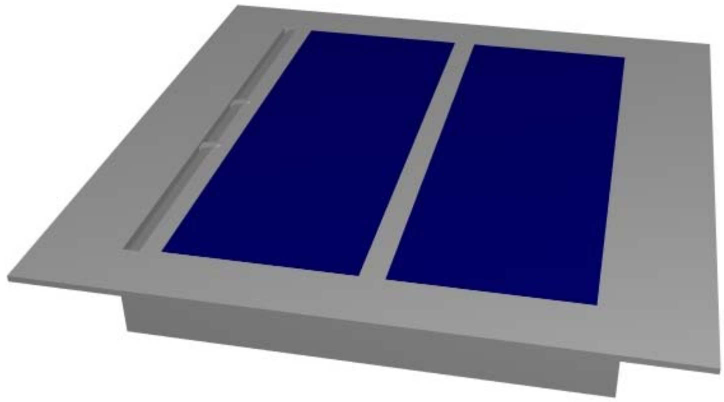

*Figure 2 Closed storage device with solar cells*

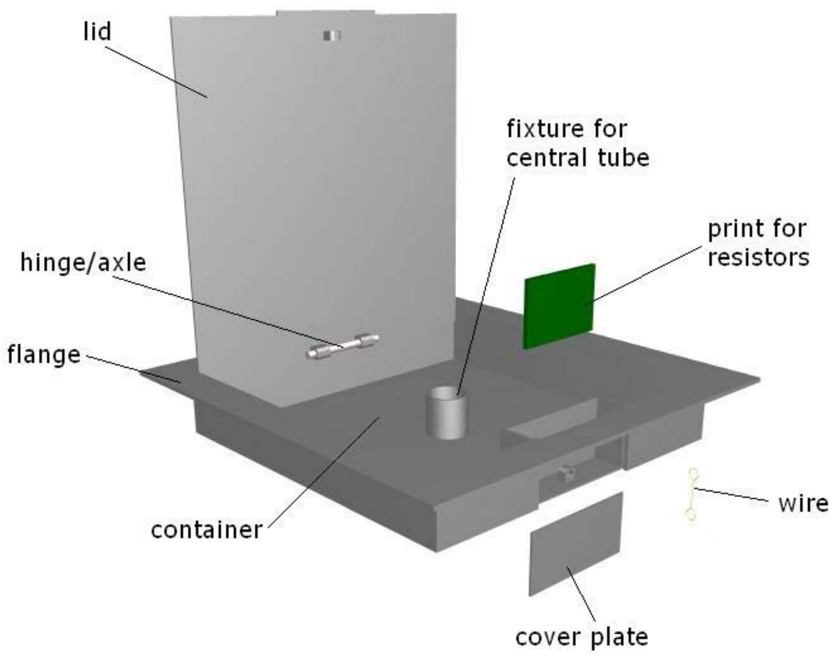


*Figure 3 Opened storage device*

Correct deployment of the lid can be confirmed by means of a switch that is either opened or closed once the panel has reached the required amount of rotation.

The difference in mass of a CubeSat without iDod and the complete iDod system shall be no more than 100 g [van Breukelen, 2007]. Since the iDod replaces a standard panel of the CubeSat, this is the same as stating that the mass difference between a standard CubeSat panel and the complete iDod system shall be no more than 100 g. Since the standard thickness of a top panel is roughly 1 mm and since the thickness of the flanges and the lid of the storage device are 1 mm and 0.5 mm respectively, the weight of these items almost cancels out. In fact, the part of the iDod replacing a standard top panel is even ~7.5 g lighter than a standard top panel. Therefore, the total mass available for the remaining structure is 107.5 g.

It is further noted that solar cells, if applied on the lid, are also not taken into account for the iDod system mass or volume. The reason for this is that the solar cells are regarded to be part of the power subsystem of the satellite, not of the iDod subsystem. Furthermore, the thermal finish on the outside of the iDod is also not regarded as being part of the iDod system, but as being part of the satellite thermal subsystem.

## 2.2 Mass allocation

Figure 4 provides the mass budget for the complete iDod system. It is noted that the total mass of all the components of a system combined is sometimes less than the mass allocated to that system. This is regarded as a sort of contingency. It also shows that staying below the required 107.5 grams is possible with the information available at this stage of the design: When the flanges and the lid of the storage device are not taken into account, the total mass of the iDod system amounts to 99 grams.

In [Maessen, iDod.DD.002] it is determined that the mass of the complete storage device amounts to 40 g when only the aluminum parts are taken into account. Without the flanges and the lid, the storage device weighs 23 g. The mass of the hold down and release mechanism components is an educated guess based on information obtained from [Frutos Pastor, 2005].

No official datasheets are available for the Cool Gas Generator that is to be used. In [Maessen, iDod.TN.006] it is stated that the mass of a CGG is equal to 3 grams. The mass of the fixture is an educated guess.

As is decided in [Maessen, iDod.TN.008], the inflatable tubes of the inflatable structure have a Technora/cyanate layer of 0.07 mm thickness and two layers of 25 $\mu$m thick Upilex-S foil. The membranes also exist out of 25 $\mu$m thick Upilex-S foil. The mass of the inflatable tubes and the mass of the membranes of the inflatable structure is the current best estimate (CBE) for those components. The method to determine the CBE is discussed in [Maessen, iDod.TO.001]. Due to the selection of materials different than in [Maessen, iDod.TO.001], the mass of the various parts of the inflatable structure is different than is calculated there. With the current materials, the CBE for the membrane mass is 36 g and the CBE for the tubes is 17 g. It is noted that for both masses a factor of 1.5 is taken into account as a contingency for the non-exact determination of the correct size of the inflatable structure, as discussed in [Maessen, iDod.TO.001].
The mass allocated to the adhesive for the inflatable structure is 2 g. This is based on the mass measured for the silicone adhesive required to construct a 1:1 version of the inflatable structure with 20 mm diameter PE tubes [Maessen, iDod.CM.004]. This mass was $2.82 \pm 0.1$ g. In case of 10 mm diameter tubes, only half of that is needed, which results in ~1.5 g (the circumference of the tubes is halved, thus only half of the adhesive is required). Since it is expected that a flight model will utilize a different type of adhesive, which can be heavier than the current adhesive, a conservative 2 g is allocated for the adhesive.
With a mass for the connector piece of the inflatable of 1 gram [Maessen, iDod.CM.002], the total mass for the inflatable structure then adds up to 56 g.

For the deployment sensor system, all masses are educated guesses.

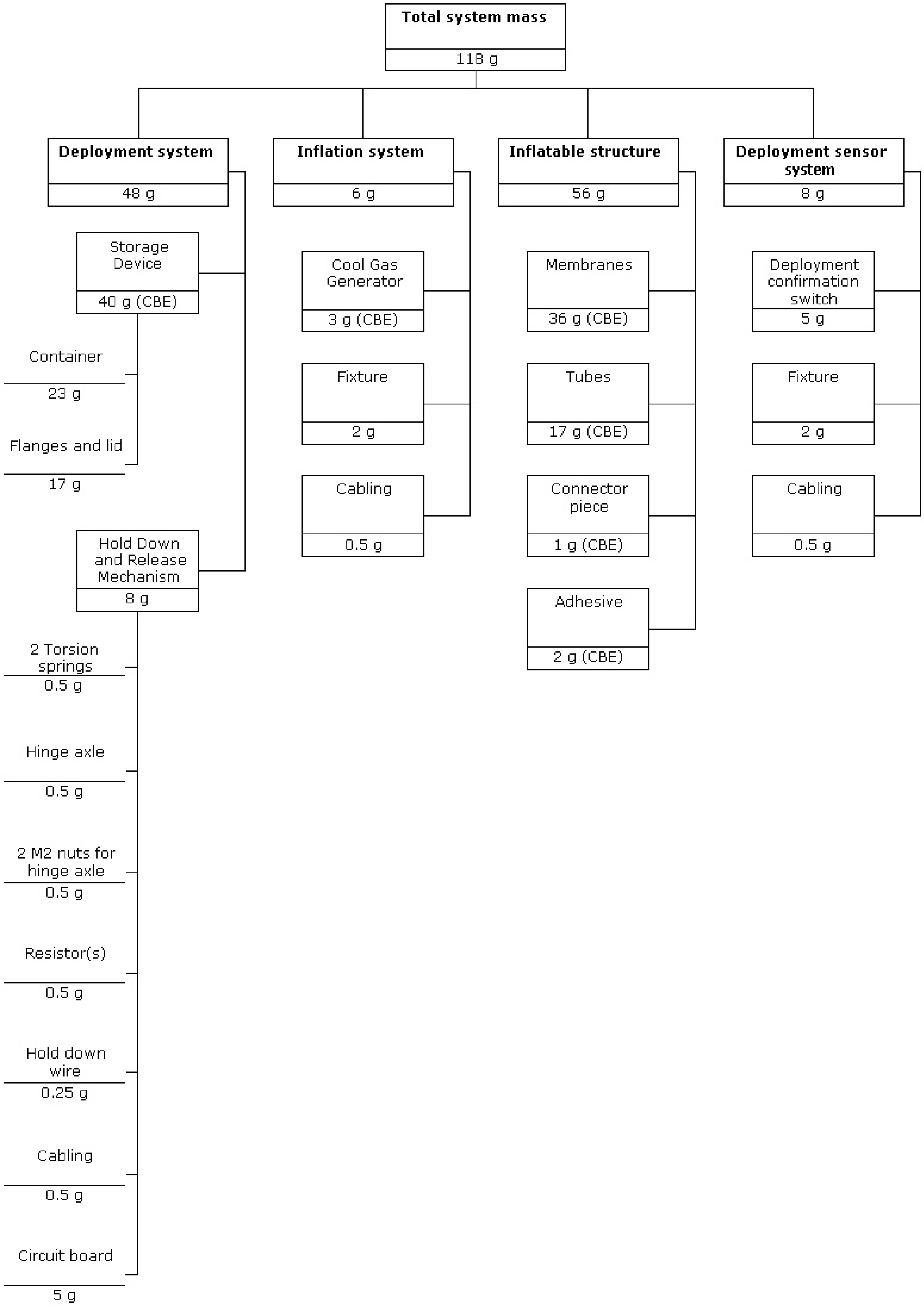


*Figure 4 System mass breakdown*

Note that the mass contingencies for the subsystems in figure 4 are very small: the maximum contingency is 13% for the inflation system. No contingency is taken on the mass of the inflatable structure.

## 2.3 Volume allocation

The total system volume available for the iDod is equal to 103 $cm^3$ [Maessen, iDod.DD.002]. In the current volume allocation, cabling volume is not taken into account. As with the mass breakdown, not the total amount of available volume is allocated to some of the subsystems. The breakdown is depicted in figure 5.

The walls, lid, and fixture of the storage device of the iDod require in total 12.65 $cm^3$ of volume (the flanges are not taken into account). This is rounded off to 13 $cm^3$. The hold down and release mechanism currently requires 4.5 cc of volume (3x1.5x1 $cm^3$).

The Cool Gas Generator that is to be used has a maximum diameter of 8 mm and a length of 18 mm [Maessen, iDod.TN.006]. This results in a volume of 0.9 $cm^3$, which is rounded off to 1 $cm^3$. The volume of the fixture, 1 $cm^3$, is an educated guess.

The stowed volume of the inflatable tubes and the mass of the membranes of the inflatable structure is the current best estimate (CBE) for those components. The method to determine the CBE is discussed in [Maessen, iDod.TO.001]. Like with the mass estimate, the materials chosen for the inflatable have turned out to be different than those assumed in [Maessen, iDod.TO.001]. With the new materials, the stowed volume (assuming a packing factor of 3) of the membranes is 73 cc and the stowed volume of the tubes is 38 cc (for both volumes, again a margin of 1.5 is applied on the calculated volume).

The volume for the components of the deployment sensor system is an educated guess.

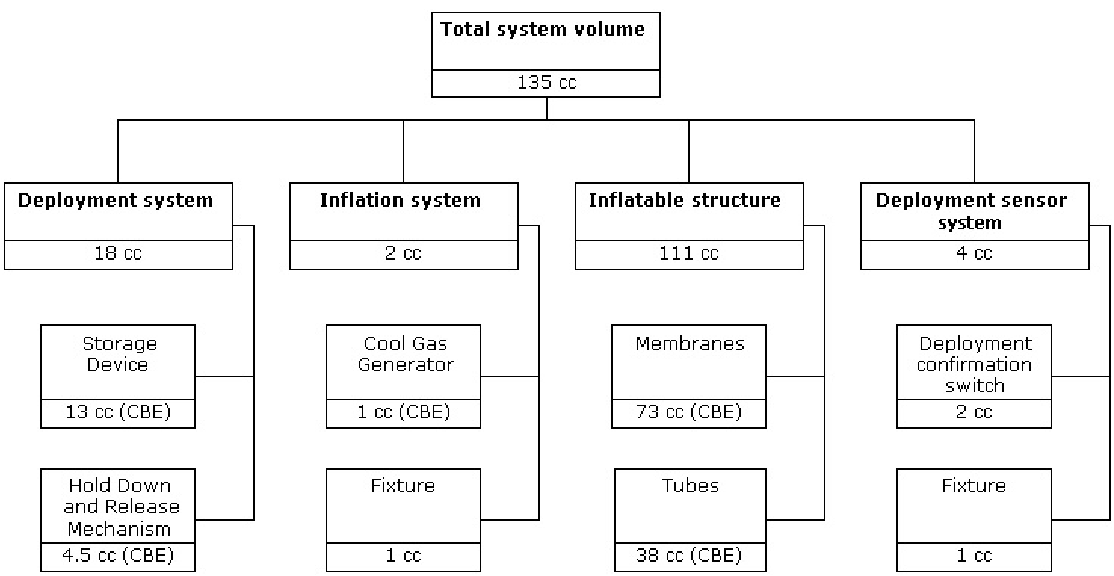


*Figure 5 System volume breakdown*

The breakdown shows that staying within the available 103 $cm^3$ is not possible; the total system volume is 31% higher. There is some contingency in the obtained volume, but even without this contingency, the difference is still 29.6%.

# 3 CONCLUSIONS & RECOMMENDATIONS

The mass breakdown indicates some margin with respect to the requirements. The current mass difference between a standard CubeSat panel and the iDod system is 99 grams while 107.5 grams is allowed.

The volume breakdown shows that the volume required for the present iDod system is 135 $cm^3$. The total amount of volume available is 103, which means that the complete iDod system requires too much volume. Based on this information, the inflatable structure has to be reduced in size which translates into a starting altitude for the CubeSat lower than 1000 km.

It is strongly recommended to determine the required size of the inflatable structure properly using a software program currently under development by E.D. van Breukelen. Now, a rather large margin of 1.5 is taken on top of the wrongly determined size in [Maessen, iDod.TO.001].

It is further strongly recommended to determine the ratio stowed volume/material volume (the packing factor) of the inflatable by testing. In [Maessen, iDod.TO.001] the ratio was assumed to be 3, but only testing can prove whether that assumption was correct. Determining the ratio removes the uncertainty regarding the amount of volume the inflatable structure will occupy.

# 4 FURTHER WORK

As the design of the iDod matures, it is expected that this document will be updated to reflect the knowledge about the mass and volume of the system gained over time.

# REFERENCES


1. Breukelen, E.D. van, Top Level Requirements for inflatable De-orbit device (*iDod)*, iDod document ISIS.iDod.REQ, Revision 1.3, Delft, 17 March 2007.

2. Maessen, D.C., *Connecting tubes to a connector piece,* iDod document iDod.CM.004, Draft, Faculty of Aerospace Engineering, Delft University of Technology, 2 March 2007.

3. Maessen, D.C., *Connector piece design and construction,* iDod document iDod.CM.002, Draft, Faculty of Aerospace Engineering, Delft University of Technology, 2 March 2007.

4. Maessen, D.C., *iDod inflatable structure conceptual design trade-off,* iDod document iDod.TO.001, Version 1.0, Faculty of Aerospace Engineering, Delft University of Technology, 28 February 2007.

5. Maessen, D.C., *iDod storage device,* iDod document iDod.DD.002, Version 1.2, Faculty of Aerospace Engineering, Delft University of Technology, 2 April 2007.

6. Maessen, D.C., *iDod stowage and deployment,* iDod document iDod.TN.006, Version 1.1, Faculty of Aerospace Engineering, Delft University of Technology, 19 April 2007.

7. Maessen, D.C., *iDod Straw man concept design description,* iDod document iDod.DD.001, Draft, Faculty of Aerospace Engineering, Delft University of Technology, September 2006.

8. Maessen, D.C., *Material selection,* iDod document iDod.TN.008, Version 1.0, Faculty of Aerospace Engineering, Delft University of Technology, 13 March 2007.

9. Frutos Pastor, A. and Eikhoff, R. van den, *Small Spacecraft Mass Budget System*, Mass budget system for Delfi-$C^3$, Version 2.6, Faculty of Aerospace Engineering, Delft University of Technology, 14 December 2005.

# Determination of external forces on the iDod

## Introduction

In order to determine whether the iDod can handle all the external forces it is subjected to, these forces first need to be determined. The determination of these forces is performed here. Assumptions regarding the dimensions of the inflatable structure can be found in [Maessen, 2006].

## Work done

From [Wertz, 1999, pg 206], several external forces (accelerations) acting on certain parts of a satellite can be determined. These are aerodynamic drag, gravity gradient and centrifugal force. The last force is actually a fictional force, caused by using a rotational reference frame:

| Source | x-direction (velocity) | y-direction (orbit normal) | z-direction (nadir) |
|---|---|---|---|
| Aerodynamic drag | $\ddot{x} = \frac{1}{2}\frac{C_d A}{m}\rho a^2 \omega^2$ | $\ddot{y} = 0$ | $\ddot{z} = 0$ |
| Gravity gradient | $\ddot{x} = -x\omega^2$ | $\ddot{y} = -y\omega^2$ | $\ddot{z} = 2z\omega^2$ |
| Centrifugal | $\ddot{x} = x\omega^2$ | $\ddot{y} = 0$ | $\ddot{z} = z\omega^2$ |

*Table 1 Velocity-dependent forces acting on the satellite*

In the above table, $\omega$ is the orbital angular velocity of the satellite, a is the semi-major axis of the orbit, and x, y, and z are the distances of the masses of interest from the spacecraft center of mass (COM). The three foregoing forces are all dependent on the orbital angular velocity of the satellite. This is not the case for the fourth external force discussed in this document: the solar radiation pressure force. The force due to solar radiation pressure is provided further on in this document.

In the coming sections, the satellite can have two different orientations with respect to its velocity vector. The first one is the desired orientation with the large membrane of the iDod perpendicular to the velocity vector of the satellite, see figure 1. In the second orientation, the large membrane of the iDod is parallel to the velocity vector of the satellite (see figure 2). In [Wertz, 1999], the direction of flight is assumed to be the x-axis. To avoid confusion with the formulas given, that particular convention is also adopted here. This implies that, in this document, the coordinate system for the satellite changes with changing orientation.

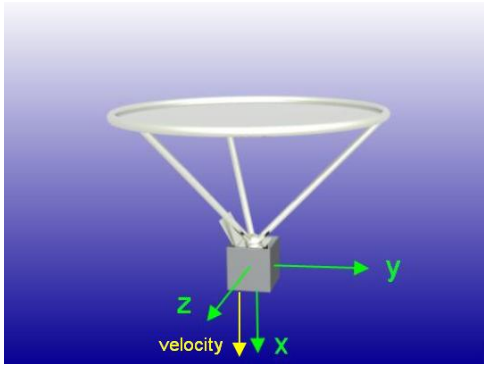


*Figure 1 Membrane perpendicular to velocity vector*

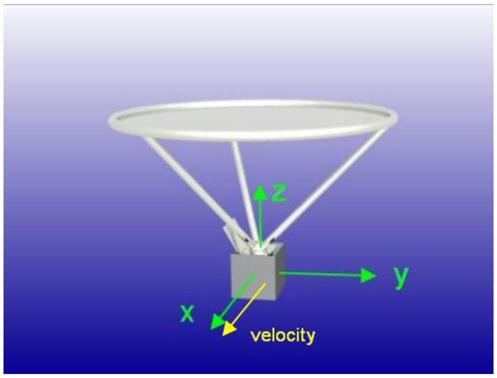


*Figure 2 Membrane parallel to velocity vector*

*Aerodynamic drag*

First, the force due to aerodynamic drag is evaluated. This force is proportional to the frontal surface and mass of the object considered and only acts in the direction of flight. With the iDod deployed, the complete satellite can be regarded to consist out of two objects: the original cubesat and the iDod. The maximum deceleration experienced by both objects occurs at the orbit with maximum atmospheric density during solar maximum. Of course, this is the lowest orbit attained and is for now assumed to be at a height of 200 km. The orientation of the satellite is now as indicated in figure 1. The mass of the iDod is assumed to be 0.05 kg. The deceleration of both objects is now determined (the values for $\rho$, a, and $\omega$ are copied from [Wertz, 1999]):

$$\ddot{x}_{cubesat} = \frac{1}{2}\frac{C_d A_{cubesat}}{m_{cubesat}}\rho_{200}a_{200}^2\omega_{200}^2 = \frac{1}{2}\frac{2*0.01}{0.95}3.52*10^{-10}*6578000^2*\left(1.1833*10^{-3}\right)^2 =$$
$$= 2.245*10^{-4}\ \text{m/s}^2$$

$$\ddot{x}_{iDod} = \frac{1}{2}\frac{C_d A_{iDod}}{m_{iDod}}\rho_{200}a_{200}^2\omega_{200}^2 = \frac{1}{2}\frac{2*0.315}{0.05}3.52*10^{-10}*6578000^2*\left(1.1833*10^{-3}\right)^2 =$$
$$= 0.134365 = 1343.65*10^{-4}\ \text{m/s}^2$$

Now, the force on both objects can be easily determined:

$$F_{cubesat} = m_{cubesat}\ddot{x}_{cubesat} = 0.95*2.245*10^{-4} = 2.133*10^{-4}\ \text{N}$$

$$F_{iDod} = m_{iDod}\ddot{x}_{iDod} = 0.05*1343.65*10^{-4} = 67.183*10^{-4}\ \text{N}$$

Since the iDod experiences a larger force than the CubeSat, it is concluded that one strut joining the two objects is loaded in tension with a force equal to $6.5*10^{-3}$ N. For the tripod, this results in forces of ~$2*10^{-3}$ N in the struts.

*Gravity gradient and centrifugal*

When the satellite is having the desired attitude (see figure 1), no net force is present on the iDod in either direction! This is due to the perfect symmetry of the structure with respect to the z- and y-axes. In the direction of the x-axis, the forces induced by the centrifugal effect and the gravity gradient cancel each other.

When the orientation of the satellite is such that the struts of the iDod are more or less parallel to the gravity vector (see figure 2), there is a small acceleration present in z-direction of magnitude $3z\omega^2$. This orientation should only be present at the beginning of life of the iDod, thus at an altitude of 1000 km. The tensional force on one strut is now (assuming a mass of 0.05 kg, a strut length of 0.5 m, and neglecting the angle of the strut):

$$F_{strut} = \frac{m_{iDod}*3z\omega^2}{3} = \frac{0.05*3*0.5*\left(9.96*10^{-4}\right)^2}{3} = 2.5*10^{-8}\ \text{N}$$

Although the mass of the iDod and the length of the struts are not exactly known, it is clear that the force on the struts caused by aerodynamic drag is five orders of magnitude larger than the force determined here.

*Solar radiation pressure*

The force due to solar radiation pressure can be determined using the following formula [Wertz, 1999, pg 366]:

$$F_{solar} = \frac{F_s}{c} A\left(1+q\right)\cos\left(i\right)$$

Where $F_s$ is the solar constant (1367 W/m$^2$), c is the speed of light, A is the surface area, q is the reflectance factor (between 0 and 1, here taken to be 0.6) and i is the angle of incidence of the sun (assumed to be 0°). When the satellite has got an orientation as indicated in figure 1, the force on one strut is now approximately (neglecting the angle of the strut):

$$F_{strut} = \frac{F_{solar}}{3} = \frac{\frac{F_s}{c} A\left(1+q\right)\cos\left(i\right)}{3} = \frac{\frac{F_s}{c}\left(A_{iDod} - A_{cubesat}\right)\left(1+q\right)\cos\left(i\right)}{3} =$$

$$= \frac{\frac{1367}{3.0*10^8}\left(0.315-0.01\right)\left(1+0.6\right)\cos\left(0\right)}{3} = 7.4*10^{-7} N$$

This force is obviously much smaller than the previously determined aerodynamic force at 200 km altitude.

*Loads on Earth*

Next to the external forces encountered in space, the inflatable structure of the iDod is also subjected to loads on Earth. These loads are:

- Handling loads
- Test loads
- Launch loads

Since the inflatable structure is folded and supported during launch, it is not expected to carry any significant loads during that phase of its life. However, vibrations during launch can lead to degradation of surface coatings of folded structures. This is generally caused by sliding and scuffing of the folded surfaces [Jenkins, 2001]. Although not being a real load on the inflatable structure, this effect has to be taken into consideration in its design.

Handling loads are, at this stage of the design, expected only to be present during production and eventual testing of the inflatable structure. The satellite-integrator is not expected to be allowed to deploy the flight model in order to minimize the risk of puncturing the fragile structure and to prevent premature rigidization (in the case of chemical rigidization). Thus, handling loads will only be present in a controlled environment and will therefore be low. How low they will be is impossible to predict and to specify. However, they will certainly be higher than 1 N, which is already a factor 1000 larger than the largest force encountered in space (which is aerodynamic drag). Since the structure will be treated with extreme care, it is expected the handling loads will not exceed 10 N.

External loads on the inflatable structure during tests on Earth will be caused by gravity. Assuming no gravity-offloading is applied on the inflatable structure during tests and assuming horizontal deployment, the tensile force in one strut is determined as follows.

In figure 3, a schematic representation of the forces acting on the inflatable structure is presented. Here, the structure is assumed to be composed out of a single thin walled circular beam (length "L" = 0.5 m, radius "r" = 5 mm, thickness "t" = 0.25 mm, mass "$m_{beam}$" = 0.01 kg) and a point mass ("$m_{tip}$" = 0.04 kg, representing the large membrane). The beam is clamped to a rigid support. The gravitational acceleration acts on the structure as a distributed load. This distributed load can be replaced by two point loads $F_1$ and $F_2$ on half the length of the beam and the point mass respectively. These loads are calculated by multiplying the mass of the component with the gravitational acceleration of 9.81 m/s$^2$. The loads will result in a reaction force R and a reaction moment M.

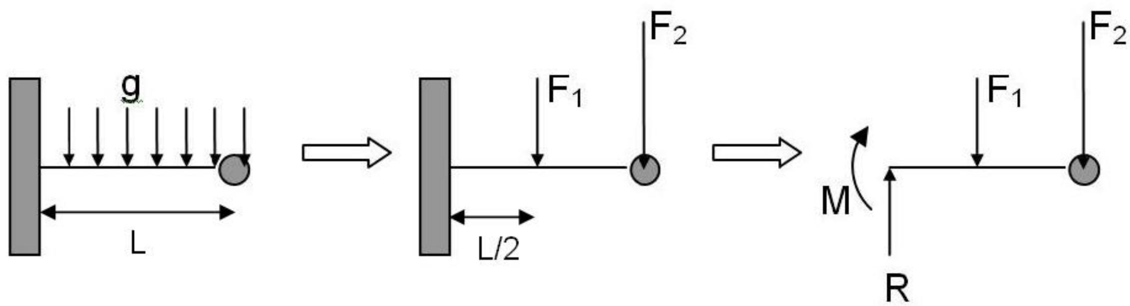


*Figure 3 Schematic representation of forces acting on inflatable structure during test*

$$F_1 = m_{beam} g = 0.01*9.81 = 9.81*10^{-2} N$$
$$F_1 = m_{tip} g = 0.04*9.81 = 3.92*10^{-1} N$$

$$R = F_1 + F_2 = 4.9*10^{-1} N$$
$$M = \frac{L}{2} F_1 + L F_2 = 2.2*10^{-1} Nm$$

The moment M creates tensile and compressive forces in the beam. A first approximation for the magnitude of these forces is to assume the moment is generated by a force couple:

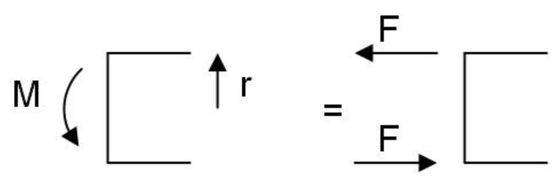


*Figure 4 Replacing of moment by a force couple*

The resulting tensile and compressive forces are now equal to:

$$M = 2Fr \quad \Rightarrow \quad F = \frac{M}{2r} = \frac{2.2*10^{-1}}{2*5*10^{-3}} = 22.1N$$

Remembering that the inflatable structure has got three struts instead of one, the tensile force in one strut is then ~9N (assuming as strut angle of 35° with respect to the horizontal).

Conclusions

The aerodynamic drag is the largest external force present in space and amounts to roughly 6.5*10$^{-3}$ N at an altitude of 200 km. The tension force in a strut will then be roughly 2*10$^{-3}$ N.

On Earth, the largest external force present is either the gravitational load on the inflatable structure during testing or the handling load. Both are not expected to be larger than 10 N. However, it is clear that these forces are much larger than the external forces present in space and thus drive the design of the inflatable structure in this respect.

## Further work

The external forces acting on the structure on Earth need to be determined more accurately before production and testing are commenced.

The external forces acting on the structure in space need to be analyzed in more detail when attitude stability and the amount of deceleration need to be determined accurately.
From a structural integrity point of view, this only needs to be done when concerns arise about the degradation of the materials used for the inflatable structure after prolonged exposure to the space environment.

When a coating is applied on the material of the inflatable structure, it has to be determined to what point this coating will degrade due to scuffing and sliding of the folded package during launch.

## Inputs and outputs

The inputs and outputs are presented in the below table:

| **Inputs** | **Outputs** |
|---|---|
| Acceleration levels of masses due to external influences in space | Largest external force in space is aerodynamic drag at 200 km altitude, this results in a tension force in the struts of ~$2*10^{-3}$ N. |
| Assumed masses and dimensions of a 1-unit CubeSat and the inflatable structure | |
| Force due to solar radiation pressure | Largest external forces on Earth are either handling loads or the gravitational load during tests, both loads are expected to result in a maximum force of ~10 N. |
| Gravitational force on deployed inflatable structure on Earth | |

*Table 2 Inputs and outputs*

## Changes to the previous version

With respect to the previously released version, several important changes have been incorporated into this document:

- External forces acting on the inflatable structure on Earth have been added and discussed
- A definition of the orientation of the satellite in space has been added
- The force due to solar radiation pressure has been re-calculated since the solar constant was erroneously taken equal to 1.367 W/m$^2$ while its correct value is 1367 W/m$^2$. The resulting force is now a factor 1000 larger, but still not nearly as large as the aerodynamic force at 200 km altitude.
- An “inputs and outputs” section and the current section have been added.

## References

*1.* Jenkins, C.H.M., *Gossamer Spacecraft: Membrane and Inflatable Structures and Technology for Space Applications*, AIAA, Reston (USA), 2001.

2. Maessen, D.C., *iDod Straw man concept design description,* iDod document iDod.DD.001, Faculty of Aerospace Engineering, Delft University of Technology, September 2006.

3. Wertz, J.R., Larson, W.J., *Space Mission Analysis and Design*, Third Edition, Kluwer Academic Publishers, Dordrecht (NL), 1999.

## Simplified load case to assess the importance of structural strength

Introduction

To asses whether structural strength is important in the design of the iDod an exceptional load case is introduced. The iDod is at this stage of the design a tripod structure, but for this load case it is assumed that, for some reason, two of the struts do not take up any load. Thus, only one strut has to carry all the loads. This strut is *not* pressurized any more.

A strut consists out of two layers of Kapton HN and one layer of fiber/epoxy composite [Maessen, 2006, iDod.DD.001]. However, *the composite is now assumed to take up none of the loads*. When it turns out that even for this case the required thickness of the Kapton HN is less than 100 μm, it is clear that the strength of the structure is relatively unimportant in the design.

Kapton HN is a general-purpose all-polyimide film commonly used in spacecraft applications. The temperature range in which it can be used is wide: -269°C until +400°C. Main advantage of this type of film is that it retains a good balance of properties over this temperature range [DuPont]. Furthermore, the film has very low permeability which makes it suitable as a gas retention layer.

Work done

*Determination of required Kapton thickness*

The largest force acting on the iDod structure is the aerodynamic force at an altitude of 200 km at solar maximum conditions. This force is equal to ~$6.5*10^{-3}$ N [Maessen, 2006, iDod.TN.002]. The base (the large circular plate) of the iDod is assumed to be infinitely stiff. Furthermore, it is assumed that the material behaves linearly. A graphical representation of the situation:

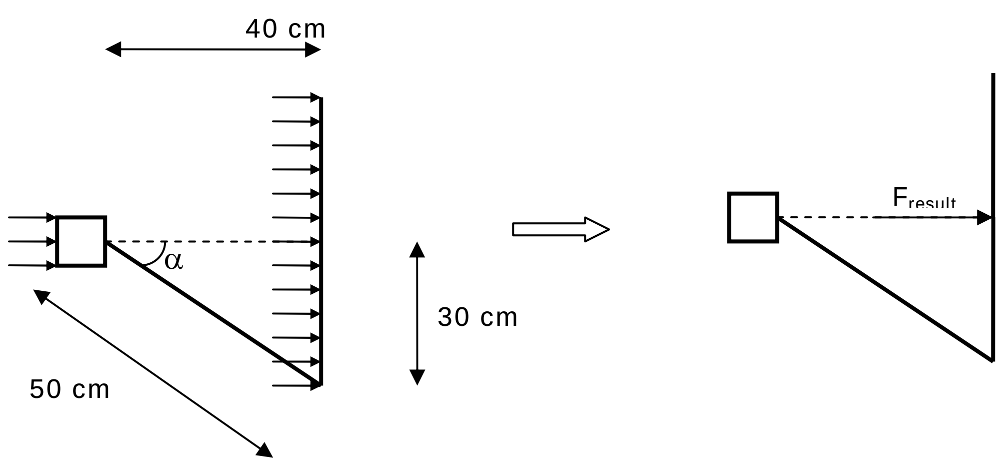


Some important parameters used in the calculations:

| Parameter | Value | Comments |
|---|---|---|
| Strut radius | 5 mm | Deemed the minimal workable dimension |
| Strut length | 500 mm | TBC |
| Ballute radius | 300 mm | Actually 316.7 mm |
| Poisson's ratio | 0.34 | Poisson's ratio of Kapton HN |
| Kapton HN 3% yield stress | 41 MPa | At 200°C, conservative number |
| Kapton HN Young's modulus | 2.0 GPa | At 200°C, conservative number |

*Table 1 Parameters*

Instead of the ultimate stress, the yield stress is taken as the failure stress for the Kapton. The reason for this is that the material behavior of Kapton up to its yield point is almost linear, a thing that cannot be said about its behavior at higher stress levels [Dupont]. Thus, standard analytical equations can be applied to this problem. Furthermore, the yield point is a more conservative failure point than the ultimate stress.

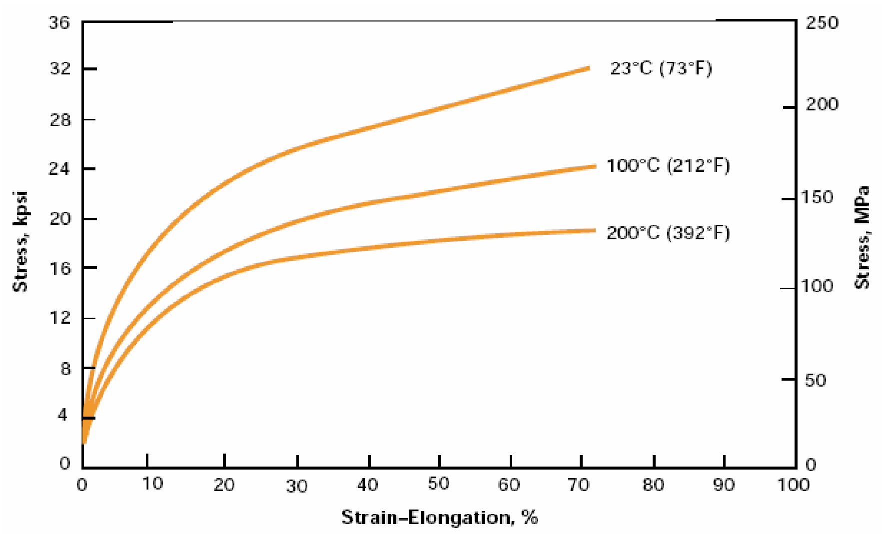


*Figure 1 Tensile stress-strain curves for 25 $\mu m$ thick Kapton HN film [Dupont]*

Due to the force $F_{result}$ the strut will experience a tension force, a compression force and will deflect to some extent. In order to be able to cope with these "phenomena", the Kapton HN requires a certain thickness. The next table provides the required Kapton HN thickness for the various phenomena encountered in this load case. Actually, only the first two phenomena in the table are strength-related. The third phenomenon is related to the elastic instability of the strut and the last two phenomena are related to the stiffness of the structure.

| **Phenomenon** | **Formula** | **Source** | **Kapton HN thickness [$\mu$m]** |
|---|---|---|---|
| Tension force due to $F_{result}$ | $\sigma = \frac{F}{A}$ | [Gere, 1999] | 0.004 |
| Tension due to moment | $\sigma = \frac{My}{I}$ | [Gere, 1999] | 0.48 |
| Flexural buckling due to moment | $M = \frac{2\sqrt{2}}{9}\frac{\pi Ert^2}{\sqrt{1-\upsilon^2}}$ | [Veldman, 2005] | 12 |
| Deflection due to moment (5 mm) | $\delta = \frac{ML^2}{2EI}$ | [Ashby, 2005] | 50 |
| Rotation due to moment (1°) | $\theta = \frac{ML}{EI}$ | [Ashby, 2005] | 57 |

*Table 2 Required Kapton HN thickness for various phenomena*

The symbols in the table represent:

| | | |
|---|---|---|
| $\sigma$ | stress | [N/m$^2$] |
| F | force | [N] |
| A | cross-sectional area | [m$^2$] |
| M | moment | [Nm] |

| | | |
|---|---|---|
| y | distance from the central axis of the strut to its outer edge | [m] |
| E | Young's modulus of the material | [N/m$^2$] |
| r | strut radius | [m] |
| t | strut wall thickness | [m] |
| $\upsilon$ | Poisson's ratio Kapton | [-] |
| $\delta$ | deflection of the end of the strut | [m] |
| L | strut length | [m] |
| $\theta$ | strut rotation at the base of the strut | [degrees] |

For the first two phenomena, the Kapton will fail due to plastic deformation of the material. For the third phenomenon, failure is caused by wrinkling of the Kapton film. For the last two phenomena, it is not so much the material that fails, but failure is now considered as "not complying to the requirement" (5 mm deflection or 1° rotation). The allowed values for deflection and rotation are considered to be quite extreme for this structure. Therefore, it is satisfying to see that the required Kapton thickness for these extreme cases is relatively small.

Even when the strength and stiffness provided by the fiber/epoxy composite is not taken into account, the required Kapton HN thickness is small, even for this exceptional load case.

*Influence of material connections*

In the above analyses, the influence of material connections on the effective strength (or stiffness) of the structure has not been taken into account. In general, a connection point is a weak point in a structure and will therefore lead to premature structural failure if this effect is not taken into consideration for the structural calculations. However, this of course also depends on the specific load case under consideration.

It is likely that the connections for the inflatable structure will be made by gluing Kapton onto other pieces of Kapton (to make a tube out of a sheet of Kapton foil or to connect the struts to the base of the inflatable structure) or onto rigid connections to the CubeSat. The load then has to be transferred by the glue from one end of the connection to the other end via a shear force.

At this point in the design, it is unknown what type of connections will be used. Therefore, it is not possible to asses whether these connections will have any influence on the strength of the structure. For now, it is assumed that the connections result in a strength reduction of 50% for all strength-related phenomena considered in the previous section. Then, the required Kapton thicknesses become:

| **Phenomenon** | **Kapton HN thickness [$\mu$m]** |
|---|---|
| Tension force due to $F_{result}$ | 0.008 |
| Tension due to moment | 0.96 |

*Table 3 Required Kapton HN thickness for 50% strength reduction due to connections*

The required Kapton thicknesses for the two phenomena are still very small. For the three other phenomena considered, the connections will result in smaller required Kapton thicknesses since at the point of the connection extra material is present. For the stiffness-related phenomena this leads to a larger moment of inertia and thus in increased stiffness. For the flexural buckling phenomenon, the effect of the connection is difficult to asses since here the precise location of the connection is important: When the moment results in a compression force at the location of the connection, then the extra material will result in a larger required moment to initiate flexural buckling. When this is not the case, the extra material will have no significant effect.

*Testing*

From the foregoing analysis it is concluded that a full scale test for structural strength is not required.

When parts of the inflatable structure are created by bonding materials together, it is required to test the strength of the bond thus created in order to be certain the bond will not fail under the loads it is subjected to in space. This can be done by loading a test specimen in tension and to measure the force at which the bond fails. Once the extreme temperatures the inflatable structure is exposed to are known, bonds can be tested at these extreme temperatures to confirm their ability to carry the required load under those conditions.
Since the forces acting on the structure are very small, it is believed that the bonds will fail at loads much larger than those anticipated during the operational life of the structure, even at the most extreme temperatures encountered. Therefore, the tests are seen as absolute confirmation the bonds will hold and not as a critical point in the test phase of the design. Thus, the tests are part of validation of the design of the inflatable structure.

## Conclusions & recommendations

Based on the above results, it is concluded that a strut will easily be able to handle all the external loads it is subjected to in space. Therefore, structural strength is not deemed to be an important design parameter.

It is recommended to perform a test for bond strength at the extreme temperatures the structure is exposed to. This test is currently not regarded as being difficult to pass, but is required in order to validate the design.

## Further work

No further work on strength determination of the struts is foreseen. Tests for bond strength have to be performed in a later stage of the design.

## Inputs and outputs

The inputs and outputs are presented in the below table:

| **Inputs** | **Outputs** |
|---|---|
| Dimensions inflatable structure | Required Kapton thickness to provide minimum structural strength is ~1 $\mu$m when material connections are taken into account and the strength of the fiber/epoxy composite is neglected |
| Properties Kapton | |
| Influence of material connections | |
| | |
| | |

*Table 4 Inputs and outputs*

## Changes to the previous version

With respect to the previously released version, several important changes have been incorporated into this document:

- Relevant Kapton properties and material behavior have been added
- For each case treated, the corresponding failure mode has been added
- A symbol explanation has been added
- An “influence of material connections” section, a “testing” section, an “inputs and outputs” section and the current section have been added.

References


1. Ashby, M.F., *Materials Selection in Mechanical Design*, Third edition, Butterworth-Heinemann, Oxford (UK), 2005.

2. Dupont, *Summary of Kapton properties,* http://www2.dupont.com/Kapton/en_US/assets/downloads/pdf/summaryofprop.pdf . Viewed September 2006.

3. Gere, J.M., Timoshenko, S.P., *Mechanics of Materials,* Fourth SI edition, Stanley Thornes (Publishers) Ltd., Cheltenham (UK), 1999.

4. Maessen, D.C., *External forces on the iDod,* iDod document iDod.TN.002, Faculty of Aerospace Engineering, Delft University of Technology, September 2006.

5. Maessen, D.C., *Straw man concept design description,* iDod document iDod.DD.001, Faculty of Aerospace Engineering, Delft University of Technology, September 2006.

6. Veldman, S.L., *Design and Analysis Methodologies for Inflated Beams*, Ph.D. dissertation, Faculty of Aerospace Engineering, Delft University of Technology (NL), Delft University Press, 2005.

# Tripod mass estimate

## Introduction

In this document, a mass estimate is provided for the straw man concept of the iDod. The iDod is assumed to be a so-called tripod having a large circular base that is connected via three struts to the cubesat:

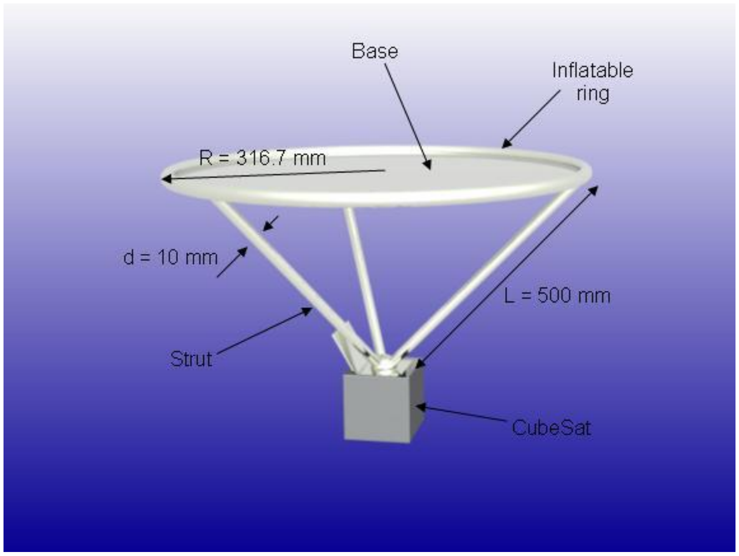


*Figure 1 iDod straw man concept [Maessen, 2006]*

The struts and the large inflatable ring consist out of three layers of material: two layers of Kapton HN foil and one layer of fiber/epoxy composite. The large circular foil at the base of the tripod consists out of one layer of Kapton HN.

## Work done

*Total area of material in the struts*

Three struts of length L = 500 mm and radius r = 5 mm:

$$A_{strut} = L * 2\pi r = 0.5 * 2\pi * 0.005 = 0.0157\ m^2$$

Two layers of Kapton HN per strut $\Rightarrow$ 6 layers of Kapton HN for the struts:

$$A_{Kapton,struts} = 6A_{strut} = 0.0942\ m^2$$

One layer of composite per strut $\Rightarrow$ 3 layers of composite for the struts:

$$A_{comp,struts} = 3A_{strut} = 0.0471\ m^2$$

*Total area of material in the inflatable ring*

The ring has a large radius R = 316.7 mm, and a small radius r = 5 mm:

$$A_{ring} = L*2\pi r = 2\pi R*2\pi r = 2\pi*0.3166506*2\pi*0.005 = 0.0625\ m^2$$

Two layers of Kapton HN:

$$A_{Kapton,tube} = 2A_{tube} = 0.1250\ m^2$$

One layer of composite:

$$A_{comp,tube} = A_{tube} = 0.0625\ m^2$$

*Total area of the circular foil at the base of the tripod*

The foil has a radius R = 316.7 mm. With this radius, it overlaps the inflatable ring, but this is allowed since extra material is required to attach the inflatable ring to the foil:

$$A_{film} = \pi R^2 = 0.315\ m^2$$

The film consists out of one layer of Kapton HN:

$$A_{Kapton,film} = A_{film} = 0.315\ m^2$$

*Bond overlap*

Next to the required connection between the circular foil and the inflatable ring, other bonds are also necessary. The Kapton foil of the struts and the inflatable ring needs to be bonded together in order to create a tubular structure. For this bond, a material overlap of 5 mm is foreseen. This is 16% of the circumference of an inflatable part and therefore also 16% of the area of an inflatable part. Furthermore, there need to be connections between the struts and the inflatable ring and between the struts and the CubeSat. These six connections are, for now, assumed to have the same circumferential area as a strut of 1 cm length ($\pi*10^{-4}$ $m^2$). These connections are further assumed to consist out of all three layers of material. This results in the following extra material area:

$$\begin{aligned} A_{Kapton,bond} &= 0.16*A_{Kapton,struts} + 0.16*A_{Kapton,tube} + 2*6*\pi*10^{-4} = \\ &= 0.16*0.0942 + 0.16*0.1250 + 2*6*\pi*10^{-4} = 0.0388\ m^2 \end{aligned}$$

$$A_{comp,bond} = 6*\pi*10^{-4} = 0.0019\ m^2$$

*Total area tripod*

Total Kapton HN area: $A_{Kapton} = 0.0942 + 0.1250 + 0.315 + 0.0388 = 0.573\ m^2$

Total composite area: $A_{comp} = 0.0471 + 0.0625 + 0.0019 = 0.112\ m^2$

*Mass determination*

The mass of Kapton HN is 1.42 g/$m^2$ per 1 $\mu$m thickness.

The thickness of the composite is for now taken from [de Groot, 2003] and is 0.25 mm, which results in $2.7875 \cdot 10^{-5}$ $m^3$ of composite volume. Again from [de Groot, 2003], the density of the composite (Kevlar/epoxy) is 1300 kg/$m^3$. The mass of the composite is thus 0.0362 kg or 36.2 grams.

The extra mass of bonding agent is for now not taken into account.

Depending on the chosen Kapton thickness, the total mass is (assuming using the same Kapton thickness everywhere):

| **Kapton thickness [μm]** | **Mass Kapton [g]** | **Total mass [g]** | **mass % Kapton** |
|---|---|---|---|
| 1 | 0.81 | 37.01 | 2.2 |
| 2 | 1.63 | 37.83 | 4.3 |
| 3 | 2.44 | 38.64 | 6.3 |
| 4 | 3.25 | 39.45 | 8.2 |
| 5 | 4.07 | 40.27 | 10.1 |
| 6 | 4.88 | 41.08 | 11.9 |
| 7 | 5.70 | 41.90 | 13.6 |
| 8 | 6.51 | 42.71 | 15.2 |
| 9 | 7.32 | 43.52 | 16.8 |
| 10 | 8.14 | 44.34 | 18.4 |
| 11 | 8.95 | 45.15 | 19.8 |
| 12 | 9.76 | 45.96 | 21.2 |
| 13 | 10.58 | 46.78 | 22.6 |
| 14 | 11.39 | 47.59 | 23.9 |
| 15 | 12.20 | 48.40 | 25.2 |
| 16 | 13.02 | 49.22 | 26.5 |
| 17 | 13.83 | 50.03 | 27.6 |
| 18 | 14.65 | 50.85 | 28.8 |
| 19 | 15.46 | 51.66 | 29.9 |
| 20 | 16.27 | 52.47 | 31.0 |
| 21 | 17.09 | 53.29 | 32.1 |
| 22 | 17.90 | 54.10 | 33.1 |
| 23 | 18.71 | 54.91 | 34.1 |
| 24 | 19.53 | 55.73 | 35.0 |
| 25 | 20.34 | 56.54 | 36.0 |
| 26 | 21.16 | 57.36 | 36.9 |
| 27 | 21.97 | 58.17 | 37.8 |
| 28 | 22.78 | 58.98 | 38.6 |
| 29 | 23.60 | 59.80 | 39.5 |
| 30 | 24.41 | 60.61 | 40.3 |

*Table 1 Influence of Kapton thickness on total mass*

Conclusion

For the tripod structure, a mass of 50 grams seems feasible. That requires a Kapton HN thickness of about 17 μm. This thickness is thought to be adequate when the Kapton is coated with protective material such as $SiO_2$ to prevent excessive material erosion in space. The mass can be further reduced by reducing the amount of fiber/epoxy composite in the structure or by selecting a lighter composite when this is allowed.

Further work

A better mass estimate has to be made in the future when the final iDod materials have been selected. Then, also the contribution of bonding agent to the mass of the structure has to be taken into account.

Inputs and outputs

The inputs and outputs are presented in the below table:

| **Inputs** | **Outputs** |
|---|---|
| Dimensions iDod straw man concept | Fiber/epoxy mass is estimated at 36.2 grams |
| Mass properties Kapton and fiber/epoxy composite | Every $\mu$m of Kapton adds 0.814 grams to the total mass of the structure (estimated) |

*Table 2 Inputs and outputs*

Changes to the previous version

With respect to the previously released version, several important changes have been incorporated into this document:

- A figure explaining the dimensions mentioned in the text has been added
- Material overlap at the location of connections has been added and taken into account for the mass determination
- An “inputs and outputs” section and the current section have been added.

References

1. Groot, B.C.H. de, *Inflatable Gravity Gradient Boom System Development*, Delfi-1 documents SLR 142-149, Faculty of Aerospace Engineering, Delft University of Technology, June 2003.

2. Maessen, D.C., *Straw man concept design description,* iDod document iDod.DD.001, Faculty of Aerospace Engineering, Delft University of Technology, September 2006.

# Comparison of baseline inflatables with final version

## SUMMARY

This document compares the final version of the inflatable structure of the iDod with the baseline designs of the inflatable structure used during most of the design phase. Proper sizing of the final design has been made possible by an updated estimate for the packing factor and an improved method to determine the average frontal surface area of the inflatable structure.

## KEYWORDS

Inflatable structure, properties

## DISTRIBUTION

| | Name | | Company / Institution |
|---|---|---|---|
| 1 | E.D. van Breukelen | Customer | ISIS B.V. |
| 2 | B.T.C. Zandbergen | Project supervisor | TU Delft |
| 3 | O.K. Bergsma | Project supervisor | TU Delft |

## APPROVAL

| | Name | Company / Institution | Date | Signature |
|---|---|---|---|---|
| *Written* | D.C. Maessen | TU Delft | 5/2/2007 | |
| *Checked* | | | | |
| *Approved* | | | | |

## REVISION RECORD

| Issue | Date | Total pages | Affected pages | Brief description of change |
|---|---|---|---|---|
| Draft | 4/23/2007 | 4 | | |
| Version 1.0 | 5/2/2007 | 5 | 1 | Changed title |
| | | | 3-5 | Rewritten section 2 |
| | | | 4 | Split table in section 2 into two separate tables |

## LIST OF TBD'S AND TBC'S

| TBD / TBC | Paragraph | Subject | Due date | Action by |
|---|---|---|---|---|
| | | | | |
| | | | | |
| | | | | |

## TABLE OF CONTENTS

# 1 INTRODUCTION

In [Maessen, iDod.DD.003], new dimensions for the inflatable structure of the iDod are presented. Up to that point, no proper determination of the average frontal surface area of the inflatable is made. In [Maessen, iDod.TO.001, v1.0], it is tried to do this using an analytical approach, but this method does not incorporate shadowing effects and to compensate for that, the mass and material volume of the inflatable designed there are multiplied at a later stage with a factor 1.5 [Maessen, iDod.TO.001, v1.1].
The method applied in [Maessen, iDod.DD.003] is applied at a too late stage to adapt all documents affected by this development. Instead, the current document is made in which the results for the 'baseline' inflatables as sized in [Maessen, iDod.TO.001, v1.0 and v1.1] are compared to the results of the final concept as sized in [Maessen, iDod.DD.003].

# 2 CONCEPT COMPARISON

The buildup of the inflatable structure of the iDod is shown below.

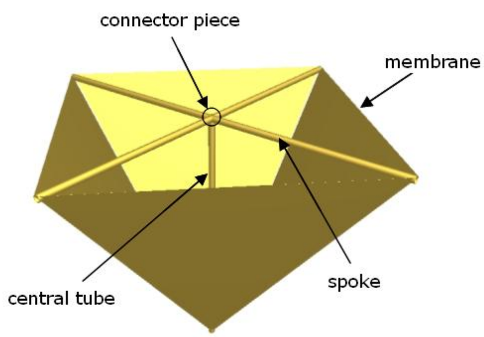


*Figure 1 Inflatable structure*

In [Maessen, iDod.TO.001, v1.0], the central tube length is determined to be 50 cm and the spoke length is determined to be 40 cm. This is the baseline concept. However, later on it is found out that these dimensions are determined wrongly. Thus, the actual average frontal surface area for this concept is smaller than the calculated 3150 $cm^2$. To compensate for this, the mass and material volume of the inflatable are multiplied in [Maessen, iDod.TO.001, v1.1] with a factor $k = 1.5$. This translates into a central tube length of 65 cm and a spoke length of 50 cm. This concept is here called the adapted baseline concept. By that time, the baseline concept has been used to determine the thermal properties of the final inflatable, to determine the pressure inside the inflatable tubes, and to size breadboard models of the inflatable structure. When the error in the dimensioning is found, only the obtained internal pressure of the tubes is adapted. For the final concept, the dimensions are determined accurately and also a new estimation for the packing factor is used.

Thus, three differently sized concepts are now discussed in various documents. To create some clarity, the next tables give an overview of the properties of these three concepts.
Table 1 shows how the first baseline concept initially grows in size into the adapted baseline concept. Yet, the average frontal surface areas, and therefore the de-orbit performance, of both concepts are listed to be equal. This is explained as follows: For the baseline concept the area is determined without taking into account shadowing effects. For the adapted baseline concept, shadowing is taken into account via a detour by multiplying the mass and material volume of the baseline concept with a factor $k = 1.5$. This leads to new dimensions and it is *assumed* at that stage that the average frontal surface area is indeed the required 3150 $cm^2$.

| | Baseline concept | Adapted baseline concept |
|---|---|---|
| **Document where described** | iDod.TO.001 | iDod.TO.001 |
| **Packing factor** | 3 | 3 |
| **Average frontal surface area [$cm^2$]** | 3150 (without shading) | 3150 (with shading) |
| **Maximum starting altitude [km]** | 1000 | 1000 |
| **Central tube length [cm]** | 50 | 65 |
| **Spoke length [cm]** | 40 | 50 |
| **Membrane area [$cm^2$]** | 1609 | 2616 |
| **Total material volume [$cm^3$]** | 22 | 32 |
| **Gas required for 0.2 bar internal pressure [normal liters]** | 0.032 | 0.041 |
| **Internal pressure using a Cool Gas Generator [bar]** | 0.74 @ 0°C<br>1.35 @ 225°C | 0.59 @ 0°C<br>1.07 @ 225°C |
| **Required adhesive strength [N/m]** | 675 @ 225°C | 535 @ 225°C |

*Table 1 Concept comparison for equal de-orbit performance*

The problem with the adapted baseline concept is that its (assumed) stowed volume, 96 $cm^3$, is larger than the available stowage volume of 79 $cm^3$ [iDod.DD.002]. In light of this problem, it is agreed with the customer to let go of the performance requirement and to keep the available stowage volume the same. Naturally, this indicates a reduction in size and therefore performance for the inflatable structure.
During the remainder of the design process, an improved method to determine the average frontal surface area of an object is conceived [Maessen, iDod.DD.003]. With this method it is possible to determine the average frontal surface areas of both baseline concepts accurately. The new method indicates an average frontal surface area of 2600 $cm^2$ for the baseline concept and 4150 $cm^2$ for the adapted baseline concept. Thus, increasing the mass and material volume with a factor k = 1.5 has lead to an actual area increase of k* = 1.6 for this geometrical object. To obtain an average frontal surface area of 3150 $cm^2$, the required area factor with which the baseline concept had to be multiplied is k* = 1.2.
Next to the improved area determination, the assumed packing factor of 3 is updated to 5 following tests performed in [Maessen, iDod.TN.006].

The new area determination method and the updated packing factor lead to a new, final, design for the inflatable. Table 2 shows how the baseline concept compares to this final concept.

| | Baseline concept | Final concept |
|---|---|---|
| **Document where described** | iDod.TO.001 | iDod.DD.003 |
| **Packing factor** | 3 | 5 |
| **Average frontal surface area [$cm^2$]** | 2600 | 1500 |
| **Maximum starting altitude [km]** | 970 | 915 |
| **Central tube length [cm]** | 50 | 40 |
| **Spoke length [cm]** | 40 | 30 |
| **Membrane area [$cm^2$]** | 1609 | 960 |
| **Total material volume [$cm^3$]** | 22 | 15 |
| **Gas required for 0.2 bar internal pressure [normal liters]** | 0.032 | 0.025 |
| **Internal pressure using a Cool Gas Generator [bar]** | 0.74 @ 0°C<br>1.35 @ 225°C | 0.97 @ 0°C<br>1.76 @ 225°C |
| **Required adhesive strength [N/m]** | 675 @ 225°C | 880 @ 225°C |

*Table 2 Concept comparison for equal stowed volume (shading effects taken into account)*

The main difference of the final concept with the other concepts is its reduced de-orbit performance. Main disadvantage is the higher pressure inside the inflatable tubes.

# 3 CONCLUSIONS & RECOMMENDATIONS

The final concept of the inflatable structure of the iDod is smaller than what has been assumed during most part of the design. Reasons for this are the new estimate for the packing factor, which has grown from 3 to 5, and accepting a reduced de-orbit performance. With this new size, other properties of the preliminary inflatable change as well.

For this particular geometrical concept, the average frontal surface area can be determined analytically without taking into account shadowing effects and by multiplying the result with a factor $1/k^* = 1/1.2 = 5/6$.

# REFERENCES


1. Maessen, D.C., *iDod inflatable structure conceptual design trade-off,* iDod document iDod.TO.001, Version 1.0, Faculty of Aerospace Engineering, Delft University of Technology, 11 January 2007.

2. Maessen, D.C., *iDod inflatable structure conceptual design trade-off,* iDod document iDod.TO.001, Version 1.1, Faculty of Aerospace Engineering, Delft University of Technology, 28 February 2007.

3. Maessen, D.C., *iDod preliminary design description,* iDod document iDod.DD.003, Draft, Faculty of Aerospace Engineering, Delft University of Technology, 23 April 2007.

4. Maessen, D.C., *iDod storage device*, iDod document iDod.DD.002, Version 1.2, Faculty of Aerospace Engineering, Delft University of Technology, 2 April 2007.

5. Maessen, D.C., *iDod stowage and deployment,* iDod document iDod.TN.006, Version 1.1, Faculty of Aerospace Engineering, Delft University of Technology, 19 April 2007.

6. Maessen, D.C., *Thermal design,* iDod document iDod.TN.011, Version 1.2, Faculty of Aerospace Engineering, Delft University of Technology, 21 March 2007.

# Design and Breadboard Production of an Inflatable De-Orbit Device for CubeSats

## Introduction

Small satellites are becoming more and more popular as an easy access to space. Due to growing concerns about space debris, debris mitigation guidelines for low Earth orbit and geostationary orbit have been proposed in a forum of space faring nations. For low Earth orbit the guideline is that satellites should not remain in orbit longer than their operational lifetime plus 25 years. Currently, these guidelines are more of a 'gentlemen's agreement', but that will change and small satellites (~ 1-5 kilograms) such as those based on the CubeSat standard will need some form of de-orbiting measure to comply if they want to use orbits with altitudes above approximately 700 km. Above this altitude, the natural lifetime of the orbit is longer than 25 years.

A de-orbiting system for this type of satellites will be designed which based on an inflatable device that can be deployed once the operational lifetime of the satellite expires. The inflatable device increases the frontal surface area thereby changing the ballistic coefficient of the satellite. This in turn increases the aerodynamic drag of the satellite and speeds up the satellite's orbit decay from years to months. Similar systems have been proposed in literature, but the new cold gas generator technology of TNO provides an opportunity to make a better system. Furthermore an alternative concept, the nanoTerminator™ with a passive electrodynamic tether has been developed by another company. This will be the reference system to

- at least equal de-orbit performance
- outperform on ease of integration and volume
- compare system mass to. This may be slightly higher if necessary

## Involved parties

- ISIS: E.D. van Breukelen MSc, Customer, Technical Support
- TNO – Defense, Security and Safety: ir. L. van Vliet, Cold Gas Generator Support (TBC)
- Delft University of Technology: ir. B.T.C. Zandbergen & dr. ir. O.K. Bergsma, Responsible Researchers

## Work to be performed

During the thesis, the following work shall be performed:

- Design of a compact, scalable inflatable de-orbit device for small satellites in low Earth orbit (LEO[1]) by means of increased aerodynamic drag, based on Cold Gas Generator technology. The system shall be compatible with the so-called CubeSat standard and shall enable these satellites to conform with proposed international regulations when the system is incorporated.
- Development and Production of a development model with which the functionality of the concept can be demonstrated
- Functional Performance Test of the deployment of the inflatable device.

[1] There is no commonly agreed upon definition for LEO orbits, but they are usually orbits with altitudes between 200 and 2000 km

A detailed design of the complete inflatable system (schematically depicted on the next page) will not be possible during the time that can be spent on the thesis (7 months). Therefore, the student shall have to concentrate on several subsystems. These will be the:

- deployment system
- inflatable structure

The deployment sensor system will be treated in less detail. This system might be required when (proper) deployment of the iDod cannot be confirmed using basic telemetry from the cubesat or via ground observations (radar or optical). The inflation system is in principle provided by TNO according to specifications generated during this thesis.

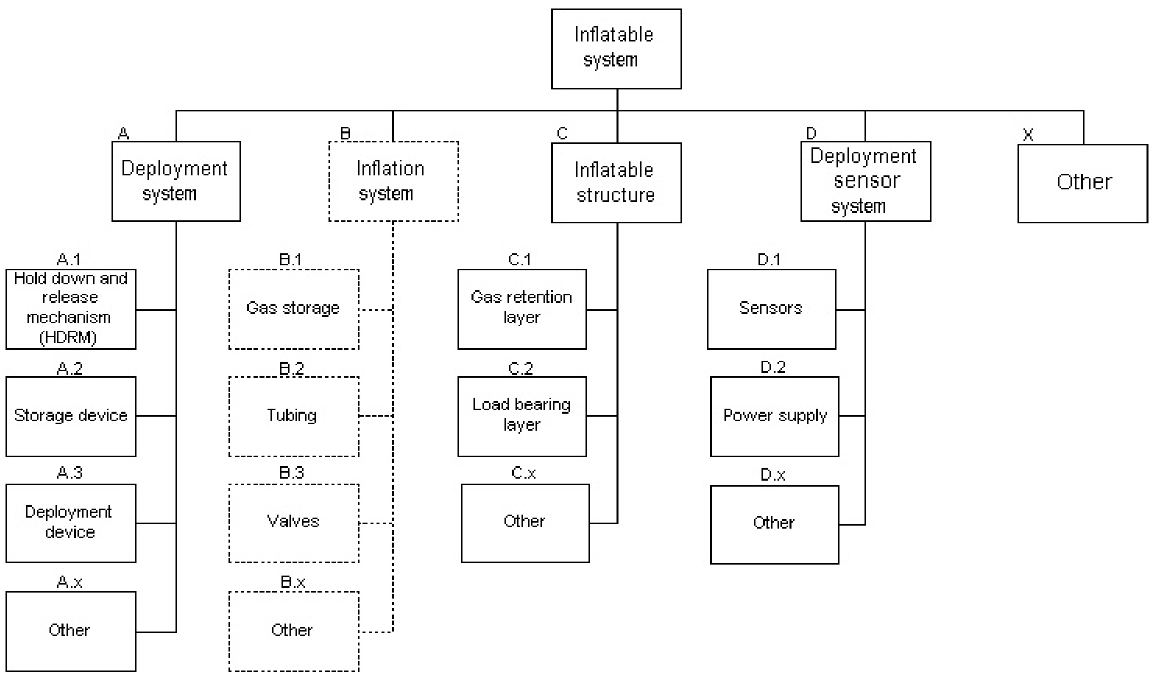


*Figure 1 Inflatable system breakdown*

## Deliverables

For the conceptual design phase, the proposed deliverables are:

- First design and development plan
- Design documentation:
    - First requirement specification (user and technical)
    - Conceptual designs (including trade-offs and selection criteria)
    - First Cold Gas Generator specifications for TNO
    - First Design Justification Files (including performance analysis)

For the detailed design phase, the proposed deliverables are:

- Complete design and development plan
- Design documentation:
    - Complete requirement specification (user and technical)
    - Detailed design (including a design in Pro-Desktop)
    - Cold Gas Generator specifications for TNO
    - All Design Justification Files (including performance analysis)
- Development model

    - Hardware
    - Documentation (technical drawings, manual and logbook)
- Test documentation
    - Test plan
    - Test report (including results, conclusions, and recommendations)
- Qualification plan

## Planning

The preliminary planning for the remainder of the thesis study is depicted on the next page.

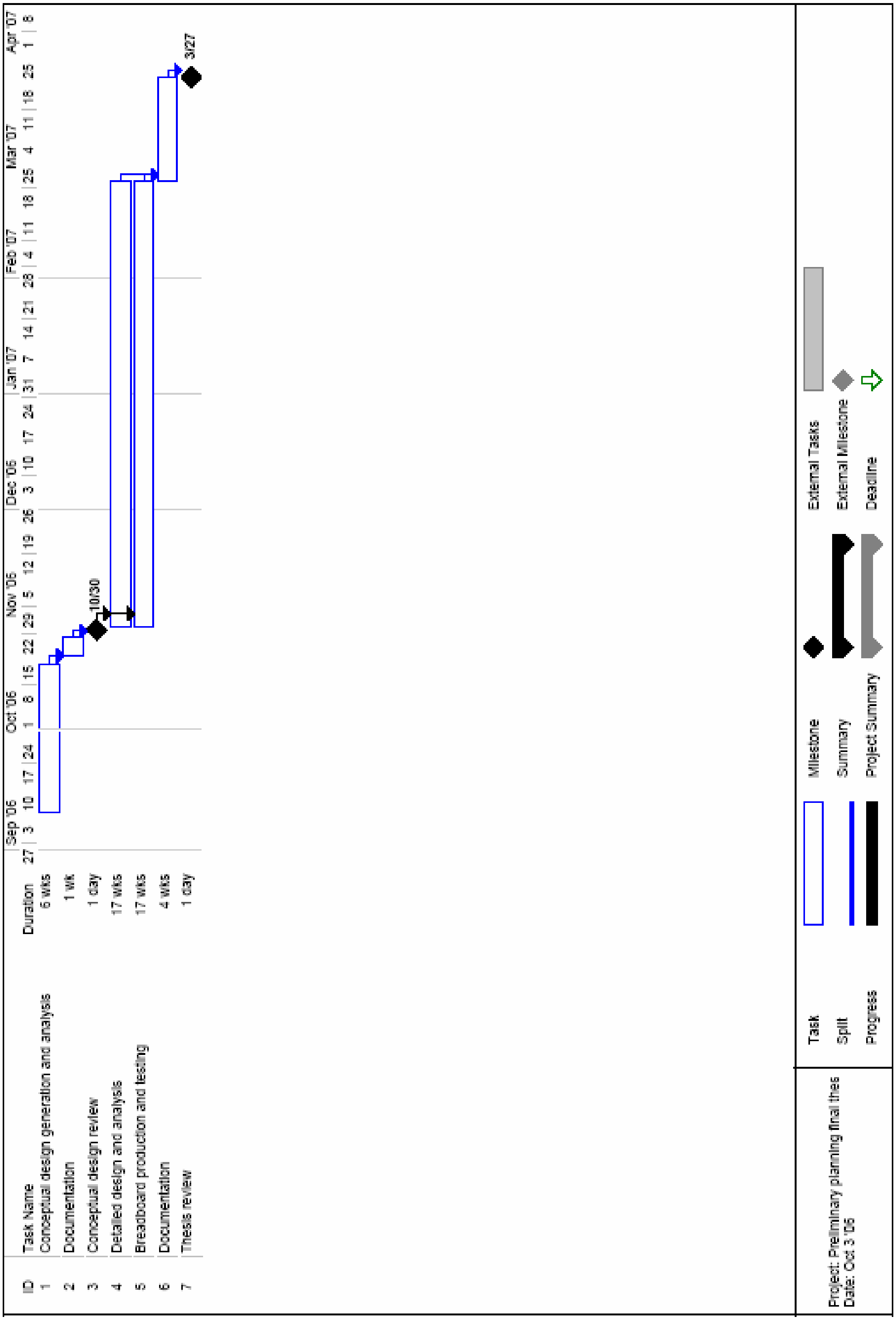
ID
Task Name
Duration
1 Conceptual design generation and analysis 6 wks
2 Documentation 1 wk
3 Conceptual design review 1 day
4 Detailed design and analysis 17 wks
5 Breadboard production and testing 17 wks
6 Documentation 4 wks
7 Thesis review 1 day
Sep '06
Oct '06
Nov '06
Dec '06
Jan '07
Feb '07
Mar '07
Apr '07
10/30
3/27
Project: Preliminary planning final thes
Date: Oct 3 '06
Task
Split
Progress
Milestone
Summary
Project Summary
External Tasks
External Milestone
Deadline